frontiers | Research Topics

Naturalistic neuroscience – towards a full cycle from lab to field

Edited by
Karen A. Mesce, Anna Lisa Stöckl, Susanne Hoffmann,
M. Jerome Beetz and Manu Madhav

Published in
Frontiers in Neural Circuits
Frontiers in Systems Neuroscience
Frontiers in Integrative Neuroscience

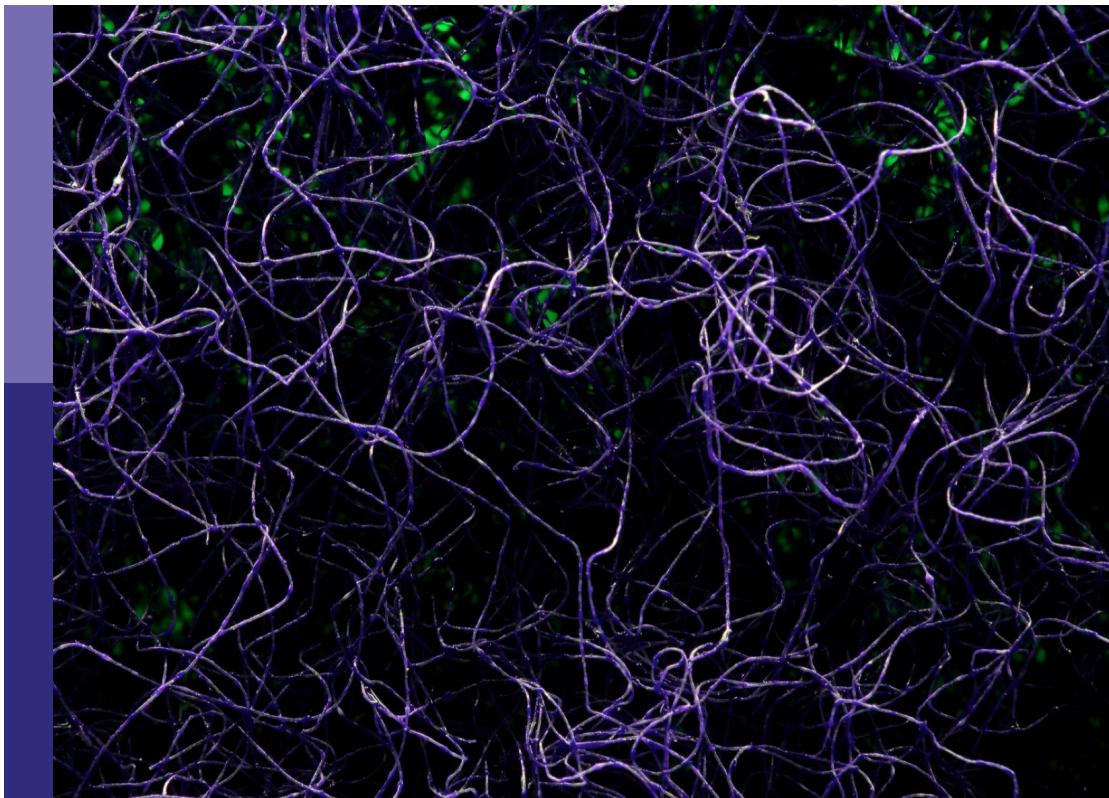

ISSN 1664-8714
ISBN 978-2-8325-3308-6
DOI 10.3389/978-2-8325-3308-6

About Frontiers

Frontiers is more than just an open access publisher of scholarly articles: it is a pioneering approach to the world of academia, radically improving the way scholarly research is managed. The grand vision of Frontiers is a world where all people have an equal opportunity to seek, share and generate knowledge. Frontiers provides immediate and permanent online open access to all its publications, but this alone is not enough to realize our grand goals.

Frontiers journal series

The Frontiers journal series is a multi-tier and interdisciplinary set of open-access, online journals, promising a paradigm shift from the current review, selection and dissemination processes in academic publishing. All Frontiers journals are driven by researchers for researchers; therefore, they constitute a service to the scholarly community. At the same time, the *Frontiers journal series* operates on a revolutionary invention, the tiered publishing system, initially addressing specific communities of scholars, and gradually climbing up to broader public understanding, thus serving the interests of the lay society, too.

Dedication to quality

Each Frontiers article is a landmark of the highest quality, thanks to genuinely collaborative interactions between authors and review editors, who include some of the world's best academicians. Research must be certified by peers before entering a stream of knowledge that may eventually reach the public - and shape society; therefore, Frontiers only applies the most rigorous and unbiased reviews. Frontiers revolutionizes research publishing by freely delivering the most outstanding research, evaluated with no bias from both the academic and social point of view. By applying the most advanced information technologies, Frontiers is catapulting scholarly publishing into a new generation.

What are Frontiers Research Topics?

Frontiers Research Topics are very popular trademarks of the *Frontiers journals series*: they are collections of at least ten articles, all centered on a particular subject. With their unique mix of varied contributions from Original Research to Review Articles, Frontiers Research Topics unify the most influential researchers, the latest key findings and historical advances in a hot research area.

Find out more on how to host your own Frontiers Research Topic or contribute to one as an author by contacting the Frontiers editorial office: frontiersin.org/about/contact

Naturalistic neuroscience – towards a full cycle from lab to field

Topic editors

Karen A. Mesce — University of Minnesota Twin Cities, United States
Anna Lisa Stöckl — University of Konstanz, Germany
Susanne Hoffmann — University of Minnesota Twin Cities, United States
M. Jerome Beetz — Julius Maximilian University of Würzburg, Germany
Manu Madhav — University of British Columbia, Canada

Citation

Mesce, K. A., Stöckl, A. L., Hoffmann, S., Beetz, M. J., Madhav, M., eds. (2023). *Naturalistic neuroscience – towards a full cycle from lab to field*. Lausanne: Frontiers Media SA. doi: 10.3389/978-2-8325-3308-6

Table of contents

frontiers | Frontiers in Neural Circuits

TYPE Editorial
PUBLISHED 08 August 2023
DOI 10.3389/fncir.2023.1251771

OPEN ACCESS

EDITED AND REVIEWED BY
Edward S. Ruthazer,
McGill University, Canada

*CORRESPONDENCE
Susanne Hoffmann
✉ shoffmann@orn.mpg.de

RECEIVED 02 July 2023
ACCEPTED 26 July 2023
PUBLISHED 08 August 2023

CITATION
Hoffmann S, Beetz MJ, Stöckl A and Mesce KA (2023) Editorial: Naturalistic neuroscience — Towards a full cycle from lab to field. *Front. Neural Circuits* 17:1251771. doi: 10.3389/fncir.2023.1251771

Editorial: Naturalistic neuroscience — Towards a full cycle from lab to field

Susanne Hoffmann[1,2]*, M. Jerome Beetz[3], Anna Stöckl[3,4] and Karen A. Mesce[5]

[1]Department of Behavioural Neurobiology, Max Planck Institute for Ornithology, Seewiesen, Germany, [2]Department of Behavioural Neurobiology, Max Planck Institute for Biological Intelligence, Seewiesen, Germany, [3]Department Zoology II, Julius Maximilian University of Würzburg, Würzburg, Germany, [4]Department of Neurobiology, University of Konstanz, Konstanz, Germany, [5]Department of Entomology, University of Minnesota, St. Paul, MN, United States

KEYWORDS

animal behavior, sensory system, motor control, brain, natural stimuli

Editorial on the Research Topic
Naturalistic neuroscience — Towards a full cycle from lab to field

Due to the flexible and adaptive nature of the nervous system and to the complexity of information the brain is constantly processing, it is extremely difficult to understand fully the neural mechanisms of behavior. Natural behavioral patterns are often the product of multidimensional integration of sensory information and internal state. To isolate specific features of this complexity under controlled experimental conditions, previous research has often reduced the dimensionality of parameters influencing a behavior. Such a simplified research design is undoubtedly very valuable for testing causal relationships between brain function and behavior. Now that a firm understanding of fundamental neural principles has been established, neuroscience is incorporating these principles into a more natural context in which they have evolved. In order to achieve an ecologically generalizable understanding of how the brain controls behavior, naturalistic contexts at biological, mental and social levels should be considered when designing neuroethological experiments. Recent technological developments, for example, encompassing virtual reality techniques (Madhav et al., 2022), now enable researchers to study the neural mechanisms of behavior under more naturalistic contexts. Within a naturalistic neuroscience framework (Figure 1), it was recently possible to uncover statistics in natural sensory information that match behavioral switches (Bigge et al., 2021), to facilitate the elucidation of how active flight modulates compass representation in the insect brain (Beetz et al., 2022), and even to record brain activity in vocally interacting wild birds that ranged completely free in their natural habitat (Hoffmann et al., 2019).

In this Research Topic, 12 articles highlight experimental approaches and technological advancements that consider natural contexts when investigating the neural bases of animal (including human) behavior, and take Naturalistic Neuroscience from the lab to the field. The Research Topic includes eight original research articles, one brief research report, three reviews, and one methods article.

One crucial aspect of naturalistic neuroscience is to successfully characterize the behavior of animals in the wild. Because wave-type electric fish continuously generate electric signals for navigation and social communication purposes, spatio-temporal properties of their electric signals can be used by researchers to localize and follow individual electric fish. In their methods article, Raab et al. introduce an improved algorithm for tracking wave-type electric fish. This algorithm, which is more robust against detection losses than previous

approaches, relies on the combined detection of individual-specific spatial and temporal characteristics of electric signals emitted by the fish. The authors successfully tracked individuals of *Apteronotus leptorhynchus* in their natural habitat demonstrating the relevance of their algorithm.

Using a similar approach, Givon et al. studied the spatial behavior of rivulated rabbitfish in their natural reef habitat to pave the way for future research on the neurobiology of free-range navigation. They triangulated the position of individual fish from acoustic recordings of sound signals emitted by tags implanted in the fish. Each individually tracked fish showed a fixed home range within which they perform repeated navigation behavior, which suggests that the neural basis of their navigation behavior could be investigated in natural settings in the near future.

On land, the neurobiology of navigation has been extensively studied in insects. Yilmaz et al. investigated the homing strategies of wild balbyter ants in South Africa to define their relative usage of landmarks and path integration during short distance navigation. The authors conclude that even when foraging in the close vicinity of their nest, balbyter ants benefit from path-integrated vectors to initially define their homing direction.

To study the neural mechanisms of insect navigation, Nguyen et al. recorded intracellularly from the brain of monarch butterflies while presenting different combinations of visual orientation cues. The authors concluded that central complex neurons integrate celestial and terrestrial information, and weigh them flexibly to allow a highly dynamic cue preference during navigation.

The insect's central complex represents a central hub for goal-directed behavior. By recording neural signals from actively hunting praying mantises Wosnitza et al. showed that central-complex neurons can flexibly switch between encoding the mantis's own movement and the movement of potential pray. This study not only demonstrates that the central complex is involved in hunting behavior, but also emphasizes that the insect's behavioral state strongly modulates the tuning of its neurons.

The neurobiology of acoustic behavior is another major research area in neuroethology. In their brief research report, Ferreiro et al. introduce a freely-moving search paradigm to study human auditory perception. Combining live position tracking with wireless sound stimulation, they reintroduced the natural interdependence of an individual's own locomotion and the sensory environment into a laboratory setting.

Avian systems have long been vital to understanding the neural substrates of acoustic-mediated behaviors. By inactivating the auditory brain area NC in female Bengalese finches, Lawley et al. demonstrate the importance of this nucleus for male song preference. Their study suggests the involvement of the female bird's NC in song evaluation and mate choice.

In their review article, Coleman et al. discuss recent findings from studies on sensory cues and motor patterning that are used by songbirds for vocal coordination during duet singing. The authors emphasize that acoustic cues from the respective duet partner are necessary to link the vocal pattern-generating circuit in the brain between two duetting individuals, and also showcase the challenges of recording neural activity in field-based settings.

Bats have also been instrumental in progressing the field of acoustic-mediated behaviors. With their study on the influence of behavioral state on vocal control, Luo et al. demonstrated that experimental conditions have a strong influence on the sound frequency adjustments that are performed by echolocating bats to match the frequency of emitted sounds to their auditory sensitivity. Pratt's roundleaf bats that were naturally flying, and conspecifics that were artificially moved on a pendulum, precisely compensated for motion-induced doppler shifts in returning echoes of their sonar emissions; stationary bats, however, that only listened to echo playbacks did not perform Doppler shift compensation.

How the auditory system of echolocating bats processes naturalistic echo information is reviewed by Beetz and Hechavarría. This review article mainly focuses on different behavioral contexts and their potential to influence the neural processing of echo information. Possible future directions for this area of research, within the framework of naturalistic neuroscience, are discussed at the end of the article.

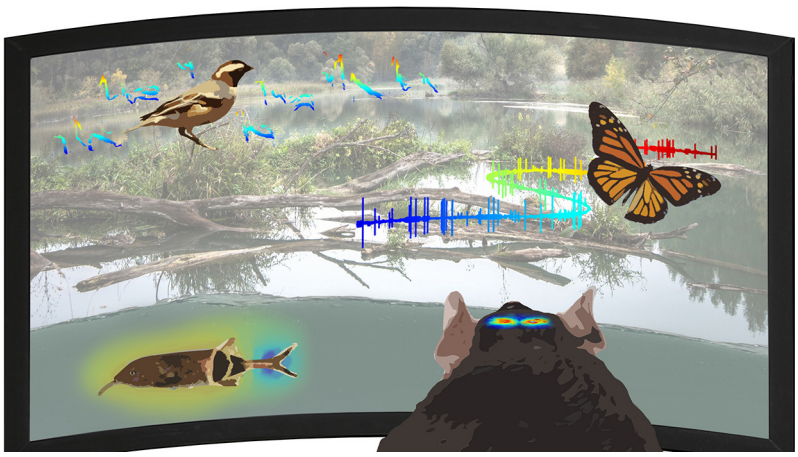

FIGURE 1
Naturalistic neuroscience - Toward a full cycle from lab to field.

A huge step in investigating neuroethological mechanisms was the development of biologgers, which are small devices that are carried by animals and record behavioral or physiological data. Gaidica and Dantzer introduce a new implantable biologger, which they designed to study the neurobiology of sleep. The device was tested in laboratory rats and captive squirrels, and showed great potential for long-term EEG recordings in freely behaving animals in laboratory and field-based settings.

Another indispensable technique for naturalistic neuroscientific research is virtual reality (VR), which allows subjects of study to interact with a completely controllable stimulus environment. In his review article, Thurley explains what we understand by VR and why VR is useful for neuroethological research, and describes the technical components needed for naturalistic VR. The review concludes with a discussion of the potential and limitations of VR for naturalistic neuroscience.

In conclusion, we provide a Research Topic of compelling research studies and reviews in our recent Research Topic Naturalistic Neuroscience, which highlight exciting advances in taking neuroscience to the natural context in which circuits and behaviors ultimately operate.

Author contributions

For the Research Topic, all authors generated a list of potential authors, invited their contributions and handled their manuscripts throughout the peer-review process. The initial draft of this editorial was written by SH and edited by all authors. All authors approved the submitted version of the editorial.

Conflict of interest

The authors declare that the research was conducted in the absence of any commercial or financial relationships that could be construed as a potential conflict of interest.

Publisher's note

References

Beetz, M. J., Kraus, C., Franzke, M., Dreyer, D., Strube-Bloss, M. F., Rössler, W., et al. (2022). Flight-induced compass representation in the monarch butterfly heading network. *Curr. Biol.* 32, 338–349, doi: 10.1016/j.cub.2021.11.009

Bigge, R., Pfefferle, M., Pfeiffer, K., and Stöckl, A. (2021). Natural image statistics in the dorsal and ventral visual field match a switch in flight behaviour of a hawkmoth. *Curr. Biol.* 31, R280–R281, doi: 10.1016/j.cub.2021.02.022

Hoffmann, S., Trost, L., Voigt, C., Leitner, S., Lemazina, A., Sagunsky, H., et al.. (2019). Duets recorded in the wild reveal that interindividually coordinated motor control enables cooperative behavior. *Nat Commun.* 10, 2577, doi: 10.1038/s41467-019-10593-3

Madhav, M. S., Jayakumar, R. P., Lashkari, S. G., Savelli, F., Blair, H. T., Knierim, J. J., et al. (2022). The Dome: a virtual reality apparatus for freely locomoting rodents. *J. Neurosci. Methods* 368, 109336, doi: 10.1016/j.jneumeth.2021.109336

frontiers | Frontiers in Neural Circuits

REVIEW
published: 18 May 2022
doi: 10.3389/fncir.2022.899370

Neural Processing of Naturalistic Echolocation Signals in Bats

M. Jerome Beetz[1]* *and Julio C. Hechavarría*[2]

[1] Zoology II, Biocenter, University of Würzburg, Würzburg, Germany, [2] Institute of Cell Biology and Neuroscience, Goethe University Frankfurt, Frankfurt, Germany

Echolocation behavior, a navigation strategy based on acoustic signals, allows scientists to explore neural processing of behaviorally relevant stimuli. For the purpose of orientation, bats broadcast echolocation calls and extract spatial information from the echoes. Because bats control call emission and thus the availability of spatial information, the behavioral relevance of these signals is undiscussable. While most neurophysiological studies, conducted in the past, used synthesized acoustic stimuli that mimic portions of the echolocation signals, recent progress has been made to understand how naturalistic echolocation signals are encoded in the bat brain. Here, we review how does stimulus history affect neural processing, how spatial information from multiple objects and how echolocation signals embedded in a naturalistic, noisy environment are processed in the bat brain. We end our review by discussing the huge potential that state-of-the-art recording techniques provide to gain a more complete picture on the neuroethology of echolocation behavior.

Keywords: biosonar, neural coding, naturalistic stimuli, bats, acoustic stream, neuroethology

OPEN ACCESS

Edited by:
Germán Sumbre,
École Normale Supérieure, France

Reviewed by:
Liora Las,
Weizmann Institute of Science, Israel
Angeles Salles,
University of Illinois Chicago, United States

***Correspondence:**
M. Jerome Beetz
jerome.beetz@uni-wuerzburg.de

Received: *18 March 2022*
Accepted: *21 April 2022*
Published: *18 May 2022*

Citation:
Beetz MJ and Hechavarría JC (2022) Neural Processing of Naturalistic Echolocation Signals in Bats. Front. Neural Circuits 16:899370. doi: 10.3389/fncir.2022.899370

INTRODUCTION

Bats acoustically orient by broadcasting echolocation sequences and extracting spatial information from echoes, a strategy referred to as echolocation behavior. The accessibility of naturalistic orientation signals makes the investigation of the neural underpinnings of echolocation behavior a promising field of research. Traditionally, electrophysiological studies are conducted by using synthesized echolocation signals that represent only portions of naturalistic echolocation signals (Dear and Suga, 1995; Kössl et al., 2015; Macías et al., 2020b). Hereby, both the call dynamics and the temporal context of acoustic signals, i.e., the organization of echolocation signals in sequences, has often been neglected. This is surprising when considering the substantial effects of stimulus rate on neural processing (O'Neill and Suga, 1982; Wong et al., 1992; Wu and Jen, 1996; Galazyuk et al., 2000; Smalling et al., 2001; Zhou and Jen, 2006; Macías et al., 2022). One possible reason why many scientists use synthesized acoustic stimuli instead of naturalistic echolocation signals is, besides from the fact that artificial stimuli are well controllable, the challenge of recording the echolocation signals immediately before they arrive at the bat's ears. To get along with that challenge, it is desirable to place a microphone close to the bats' ears (Hase et al., 2022), a complicated task when considering that commercially available recording devices are usually too heavy to be carried by bats. Therefore, some scientists adopted a pendulum paradigm that allows to place a bat together with acoustic recording devices in mass of a pendulum (Henson et al., 1982; Kobler et al., 1985; Gaioni et al., 1990; Fitzpatrick et al., 1991; Vater et al., 2003; Macías et al., 2016b; Beetz et al., 2021). During the forward swing, the bat broadcasts echolocation calls that are recorded together

with echoes by an ultrasound sensitive microphone. These acoustic signals can later be used as naturalistic echolocation signals presented to passively listening bats (Beetz et al., 2016a,b, 2017, 2018). Another approach, but leading to comparable acoustic recordings, is to train bats resting on a perch while mechanically approaching a target that the bat must ensonify (Macías et al., 2018). However, by far the most naturalistic and desirable approach is to record neural signals directly from echolocating bats (Kothari et al., 2018).

Before focusing on recent neurophysiological findings, the review gives a brief historical background on the discovery of echolocation behavior, and an overview on how echolocation information conveys spatial information. This is of particular importance when evaluating the stimulus design used for neural recordings. Later, the review focuses on four aspects that scientists should consider when investigating neural coding of naturalistic echolocation signals: (i) temporal context and dynamics of the stimulus; (ii) complex echolocation scenes composed of multiple objects or multi-reflective substrates; (iii) echolocation signals embedded in a naturalistic acoustic context; (iv) neural recordings from actively echolocating and flying bats.

BRIEF HISTORY OF BAT ECHOLOCATION

Observations on bat navigation date to the 18th century when Lazzaro Spallanzani described that bats with occluded eyes perform rapid flight maneuvers without colliding with surrounding obstacles (Dijkgraaf, 1960; Griffin, 2001). Subsequent experiments by Louis Jurine of Geneva demonstrate that bats use their auditory system for navigation because when the bats' ear canals were plugged, their navigational capabilities drastically dropped, and they collided with obstacles. Hahn (1908) conducted similar experiments and came to the same conclusions. Because scientists could not detect any sounds that the bats may use for orientation, it remained mysterious how the auditory system helps the bats to orient in darkness. Hartridge (1920) proposed that bats emit high frequency calls, inaudible to humans and that they extract spatial information from the echoes. Ironically, this hypothesis could not be tested until G. W. Pierce invented an ultrasound detector about two decades later and confirmed Hartridge's hypothesis together with Donald R. Griffin (Pierce and Griffin, 1938; Griffin, 1944, 1958). High frequency signals are spatially directed and their short wavelengths allow reflections off small targets, optimal to hunt for tiny insects (Boonman et al., 2013). The shortcoming of high frequency calls is that they rapidly attenuate with distance limiting the working range of echolocation to just a few meters (Grinnell and Griffin, 1958; Kick, 1982; Lawrence and Simmons, 1982b). To navigate over long distances, bats often use a combination of auditory and visual information (Williams and Williams, 1967, 1970; Boonman et al., 2013). In addition, a magnetic compass is discussed that assists bats to find their way over long-distance migrations (Holland et al., 2006, 2010; Wang et al., 2007b).

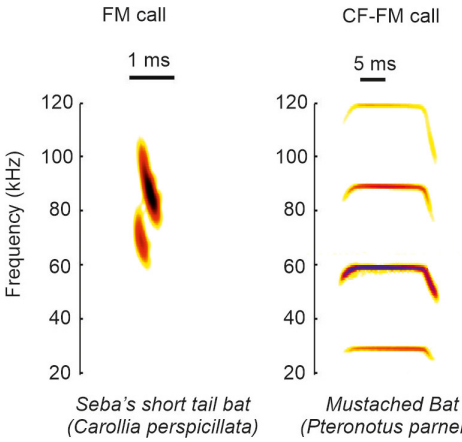

FIGURE 1 | Example calls of FM and CF-FM bats. The example spectrograms shown correspond to vocalization from the species *Carollia perspicillata* and *Pteronotus parnellii*.

ACOUSTIC PARAMETERS OF ECHOLOCATION SIGNALS

Based on the call structure, bats can be classified into species emitting frequency modulated calls (FM-bats) or a combination of constant frequency and frequency modulated call-components (CF-FM bats) (Neuweiler, 1990; Altringham, 2011; **Figure 1**). The FM covers a broad frequency range (Simmons and Young, 2010) and it is suited to analyze the object's position, structure, and shape (Simmons, 1973; Simmons et al., 1979; Simmons and Stein, 1980; Surlykke et al., 1993; Faure and Barclay, 1994; Jensen and Miller, 1999; Siemers and Schnitzler, 2004). The narrowband CF component lasts longer than the FM and some insectivorous bats use it to detect flying insects that cause amplitude and frequency modulations in the echoes (Neuweiler, 1990). The ecological diversity of bats is reflected in the acoustic call properties. Each bat species adopts different calls, and each individual can dynamically change different call portions (for review see Griffin and Novick (1955), Neuweiler (1989, 1990), Jones (1999), Schnitzler and Kalko (2001), Brinklov et al. (2010)). The dynamics in call design imply that there does not exist a unique call template for each species. Because each call may slightly differ from preceding calls, it is challenging to discuss the behavioral relevance from neurophysiological findings obtained with a single call template used as acoustic stimulus.

Not only the call variability may affect neural processing but also the sequence character of the emitted signals. Each echo represents an acoustic snapshot of the surrounding, comparable to a single frame of a movie. As with adding single frames at a certain rate to create movie scenes, the sequence character of emitted echolocation calls results in a smooth and quasi-continuous representation of the surroundings. By dynamically adjusting the call rate, bats control the spatial accuracy of their echolocation system. High spatial accuracy is important when bats navigate in highly cluttered or unfamiliar environments or when zooming into objects or prey (Kick, 1982;

Roverud and Grinnell, 1985a; Surlykke and Moss, 2000; Petrites et al., 2009; Hiryu et al., 2010; Barchi et al., 2013; Falk et al., 2014; Kothari et al., 2014; Sändig et al., 2014; Knowles et al., 2015; Wheeler et al., 2016; Beetz et al., 2019). Immediately before the catch, some bats reach call rates higher than 200 Hz (Griffin, 1953; Schnitzler et al., 1987; Jones and Rayner, 1988; Kalko and Schnitzler, 1989; Kalko, 1995). Taken together, the dynamics in call design and call rate may affect neural processing and must be carefully considered when investigating how naturalistic echolocation signals are processed in the bat brain.

WHAT SPATIAL INFORMATION IS CONVEYED BY ECHOES?

To conceptualize how echoes convey spatial information, we imagine a simplified scenario, where a frugivorous FM-bat detects a fruit tree. First, the bat localizes the tree relative to its current location. It computes the tree position along the horizontal axis (azimuth) by using binaural cues (Simmons et al., 1983; Obrist et al., 1993; Fuzessery, 1996; Firzlaff and Schuller, 2003). Echoes arrive earlier and with a higher intensity to the ipsilateral ear than to the contralateral ear (**Figure 2A**, *left column*). Because of the bat's small head size, inter-aural time differences may be too short and thus less relevant to decode the tree's azimuth position (Grothe and Park, 1998). With their fine frequency tuning, bats can also use inter-aural spectral differences to infer the tree's azimuthal position. To reach the contralateral ear, the echo passes the bat's head. This creates multiple echoes (Wotton et al., 1995; Aytekin et al., 2004) that partially overlap and thus creates spectral notches in the echo reaching the contralateral ear (**Figure 2A**, *middle column, see also Figure legend for details*). Spectral differences of echoes reaching the ipsi- and contralateral ear can be used to determine the azimuthal position of the echo source (Fuzessery, 1996; Aytekin et al., 2004). In addition to inter-aural parameters, bats can also use monaural spectral cues, i.e., the energy content at particular frequency bands to infer the object's azimuth (Bates et al., 2011; Wohlgemuth et al., 2016b; **Figure 2A**, *right column*).

To adjust the flight height and avoid collisions, the bat must know the tree's height. Due to the characteristic anatomy of the outer ear, echoes get reflected off ear parts in an elevation-dependent manner (Grinnell and Grinnell, 1965; Lawrence and Simmons, 1982a; Wotton et al., 1995; Firzlaff and Schuller, 2003; Aytekin et al., 2004; Chiu and Moss, 2007; Hoffmann et al., 2015). The position and number of spectral notches depend on the object's elevation (Fuzessery, 1996; Aytekin et al., 2004). With increasing elevation, the notch frequency increases (Wotton et al., 1995; Firzlaff and Schuller, 2003; Aytekin et al., 2004; Wohlgemuth et al., 2016b; **Figure 2B**). Behavioral studies in the FM-bat *Eptesicus fuscus* showed that they indeed use spectral notches for elevation processing (Wotton et al., 1996; Wotton and Simmons, 2000).

For distance processing, bats measure the delay between call emission and echo arrival, also referred as "echo delay" (**Figure 2C**) (Hartridge, 1945; Nordmark, 1960; Cahlander et al., 1964; Simmons, 1973, 1989). Because acoustic signals travel at an approximate constant speed, the echo delay increases with distance, 1 ms per 17 cm. Distance processing based on echo-delays only works until there is a detectable delay between call and echo. If the object is just a few centimeters away from the bat, call and echo temporally overlap and bats use spectral information, including notches arising from call-echo interferences to process the object's distance (Pye, 1960, 1961a,b). Neurons sensitive to spectral notches have been well described in the inferior colliculus and auditory cortex of the insectivorous FM-bat *Eptesicus fuscus* (Sanderson and Simmons, 2000, 2002). Along the same line of argument, if two objects are very close to each other, e.g., a fruit in front of clutter, then both objects create temporally overlapping echoes. Some neurons of the inferior colliculus of *E. fuscus* respond differently to objects associated with clutter than in the absence of clutter allowing a reliable sonar object discrimination in a cluttered environment (Allen et al., 2021).

Bats also determine the object's shape and texture with echo information. Here, they profit again from different strategies. One possibility is to scan object edges (Yovel et al., 2010) by using echo delay information (**Figure 2D**). Many bats living in cluttered environments often hover in front of objects (Griffin and Novick, 1955; Neuweiler, 1989, 1990; Schmidt et al., 2000; von Helversen and von Helversen, 2003). By keeping a constant object-distance and carefully pinpointing the sonar beam along object edges, bats can compute the object's shape. As soon as the sonar beam points off the object, the echolocation call hits an object in the background and the echo delay dramatically shifts to long delays. Note that while these ideas have been discussed extensively and they have strong theoretical support, whether the bats use echo delay information to infer the object's shape remains unclear. To date, most neural data have been obtained in head-restrained bats that were under anesthesia. To understand the purpose of hovering and especially its neuronal control, future studies should follow a more naturalistic approach by recording from vocalizing bats hovering in front of objects.

Objects spatially tightly embedded in highly cluttered backgrounds might result in delay differences of less than a millisecond, making object shape determination based on echo delay information challenging (Simmons et al., 1974; Simmons and Chen, 1989). Under these conditions, it might be easier for the bat to infer object shapes and textures with spectral information (Simmons et al., 1974, 1990, 1998; Simmons, 1989; Mogdans et al., 1993; Simon et al., 2006; **Figure 2E**). Neurophysiological studies demonstrate that subcortical and cortical neurons, indeed selectively respond to spectral notches (Sanderson and Simmons, 2002; Firzlaff et al., 2006; Macías et al., 2020a).

INFLUENCE OF THE TEMPORAL CONTEXT ON NEURAL PROCESSING

Neurons encoding object distances belong to one of the best described neuron types in bat research (Feng et al., 1978; O'Neill and Suga, 1979; Sullivan, 1982b; Fitzpatrick et al., 1993; Portfors and Wenstrup, 1999; Hagemann et al., 2011; Wenstrup and Portfors, 2011; Hechavarría and Kössl, 2014;

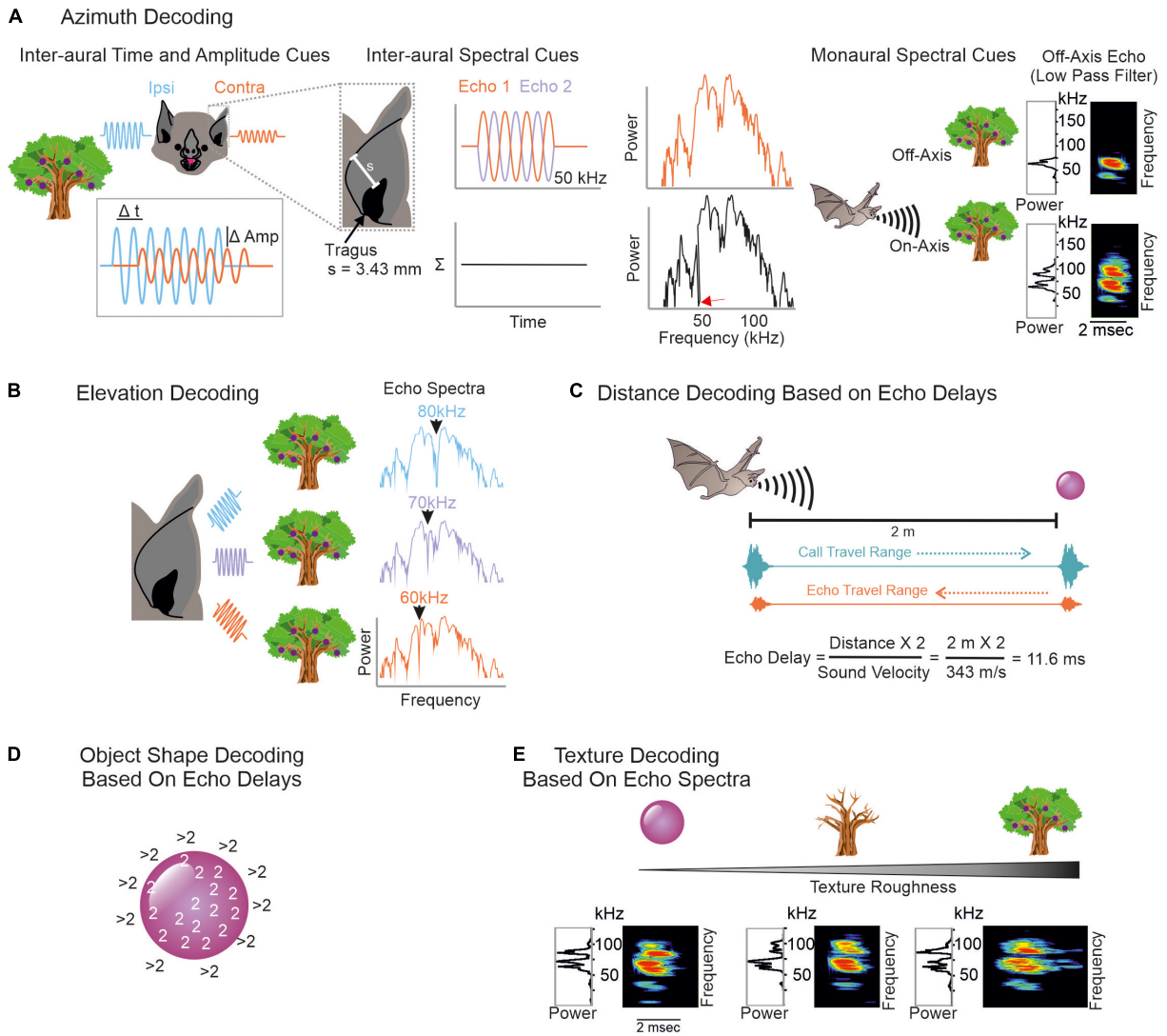

FIGURE 2 | Overview on decoding spatial information from echoes. **(A)** To infer an object's azimuth, bats can use inter-aural amplitude, time (*left*), and spectral cues (*middle*), but also monaural spectral cues (*right*). Ipsilateral echoes (*blue waves*) are higher in amplitude (*Amp*) and reach the ipsilateral ear earlier than the contralateral ear (*orange waves*). Contralateral echoes bypass the bat's head which creates spectral notches due to multiple reflections. To understand how spectral notches are generated, we assume that the echo gets reflected off the bat's pinna. This evokes a second echo that temporally overlaps with the first echo. By assuming a pinna-tragus distance of 3.43 mm and considering that the second echo travels back to the tragus, sound waves with a wavelength of 6.86 mm (or 50 kHz) are phase shifted by 180° between both echoes. This creates a spectral notch at 50 kHz (*red arrow* in black power spectrum). Based on characteristic spectral notches, contralateral echoes are discriminable from ipsilateral ones. Because of the frequency dependent directionality, echoes from off-axis objects mainly contain low frequency portions. Echoes from on-axis objects additionally contain high frequency portions (Surlykke et al., 2009a; Simmons, 2012, 2014; Wohlgemuth et al., 2016b). **(B)** Elevation decoding is based on elevation-dependent spectral-notches in the echoes. **(C)** Target distance is computed based on echo-delays. Both call and echo travel the distance between the bat and the object at sound velocity. This leads to distance-dependent echo delays to which combination-sensitive neurons in the auditory system of bats are tuned to. **(D)** To determine the object's shape, the edges can be scanned by computing echo-delays. As soon as the calls get reflected off objects in the background, the echo delays abruptly increase. **(E)** Texture roughness is determined by spectral cues like spectral notches.

Macías et al., 2016a). While being diffusely organized in the inferior colliculus, delay-tuned neurons of the auditory cortex are, in many bat species, topographically organized in a chronotopic map (for review see Kössl et al. (2014)). Neurons tuned to long echo-delays and thus encoding long target-distances are clustered in different cortical areas than neurons tuned to short echo-delays. When a bat approaches a target during flight, the echo delays progressively shorten (*Oscillogram* in **Figure 3**). By considering the chronotopic organization, it was discussed that an activity wave moves along a target-distance gradient in the cortex when the bat approaches a target (Hechavarría et al., 2013; Bartenstein et al., 2014; Kössl et al., 2014). This activity wave was experimentally confirmed by placing multi-electrode arrays along the target-distance gradient of an anesthetized frugivorous bat *Carollia perspicillata* and recording simultaneously from multiple neurons that were tuned

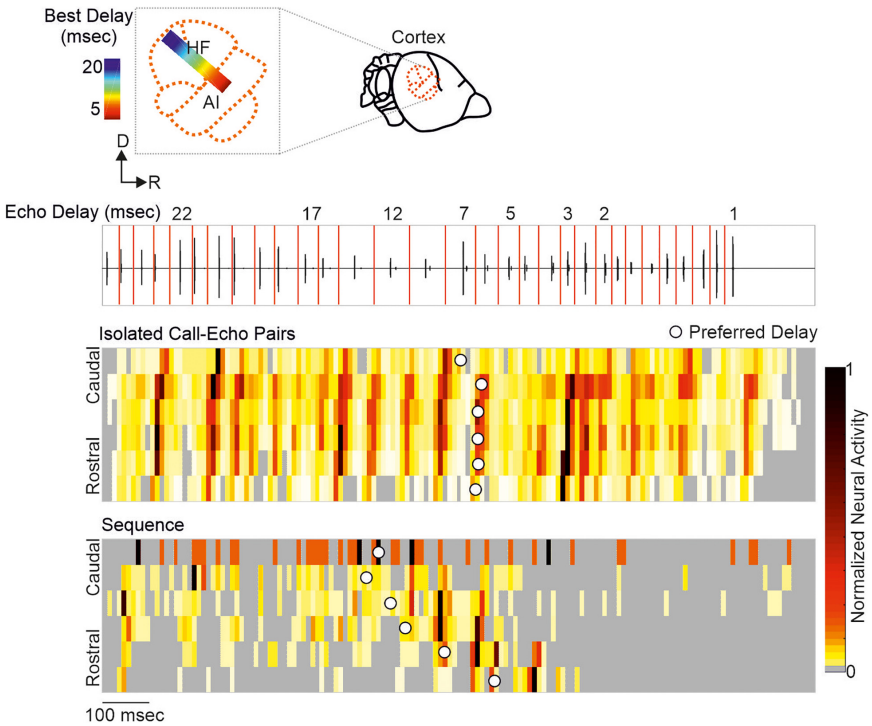

FIGURE 3 | A neural activity wave travels across the cortex when the bat is stimulated with a naturalistic echolocation sequence of an approach flight, but it is absent when presenting the same call-echo pairs in randomized order. Top: Schema of the chronotopic gradient of the auditory cortex in *Carollia perspicillata*. Neurons tuned to long delays (~ 20 ms) are clustered in caudal regions while short delays (~ 2 ms) are primarily processed in rostral regions of the cortex. Bottom: Oscillogram of the stimulus. Red vertical lines border the call-echo pairs. Heatmaps represent the neural activity of six simultaneously recorded units in response to temporally isolated call-echo pairs **(Top)** and to the naturalistic echolocation sequence **(Bottom)**. The naturalistic echolocation sequence contained the same acoustic information as the call-echo pairs that were played randomly with a 500 ms inter-stimulus interval. Only the temporal context, i.e., stimulus history and the stimulus rate differ between both stimulation protocols. Units are ordered along the rostro-caudal axis. Preferred echo delays, median time points of the neural responses of each unit are indicated as white dots. Data adapted from Beetz et al. (2016b).

to different echo delays (Beetz et al., 2016b). When the bats were stimulated with a naturalistic echolocation sequence of an approach flight, an activity wave moved from caudal to rostral cortex regions. Caudal neurons encoding long echo-delays respond stronger to the first half of the sequence while the neural activity propagated toward rostral neurons during the course of the sequence. Unexpectedly, this activity wave was absent when presenting the bats isolated call-echo pairs in a randomized order and with at least 500 ms of inter-stimulus interval (compare response to "Isolated Call-Echo Pairs" with response to "Sequence" in **Figure 3**). Although both stimulus protocols "Isolated Call-Echo Pairs" and "Sequence" contain the same echolocation information, they evoke totally different neural responses in the cortex. These different responses can be explained when considering the stimulus history and acoustic rates carried by the stimuli. The high acoustic rate represented in the naturalistic sequence evokes substantial neuronal suppression in the cortex. However, instead of completely silencing the cortex, the neurons partially recover from suppression at neuron-specific echo delays (Beetz et al., 2016b). Thus, cortical suppression in response to the echolocation sequence, renders an otherwise highly responsive cortex into a selective cortex that maps the distance information of an approach flight.

Although substantial effects of stimulus rate on tuning sharpness have been documented in former studies (O'Neill and Suga, 1982; Wong et al., 1992; Wu and Jen, 1996, 2006b; Galazyuk et al., 2000; Smalling et al., 2001; Jen et al., 2002; Zhou and Jen, 2006), delay tuning is commonly examined by using synthesized call-echo pairs as acoustic stimuli (Dear and Suga, 1995; Hagemann et al., 2010; Kössl et al., 2012, 2015; Hechavarría et al., 2013; Macías et al., 2016a, 2020b). These stimuli only mimic portions of the echolocation signals (**Figure 4A**) and are far beyond a naturalistic stimulus context (Sullivan, 1982b; Casseday and Covey, 1996; Galazyuk et al., 2005; Feng, 2011; Wenstrup et al., 2012; Hechavarría and Kössl, 2014; Suga, 2015). The current model on delay tuning in FM-bats was designed based on results obtained under artificial stimulus conditions. According to this model, each acoustic signal evokes an inhibition followed by a rebound excitation (**Figure 4B**). Hereby, the duration of inhibition depends on the signal amplitude. The higher the signal amplitude, the longer the inhibition and the longer the response latency, a phenomenon also referred to as paradoxical latency shift (PLS) which is widespread in delay-tuned neurons of FM-bats (Sullivan, 1982a,b; Berkowitz and Suga, 1989; Klug et al., 2000; Galazyuk and Feng, 2001; Galazyuk et al., 2005; Wang et al., 2007a;

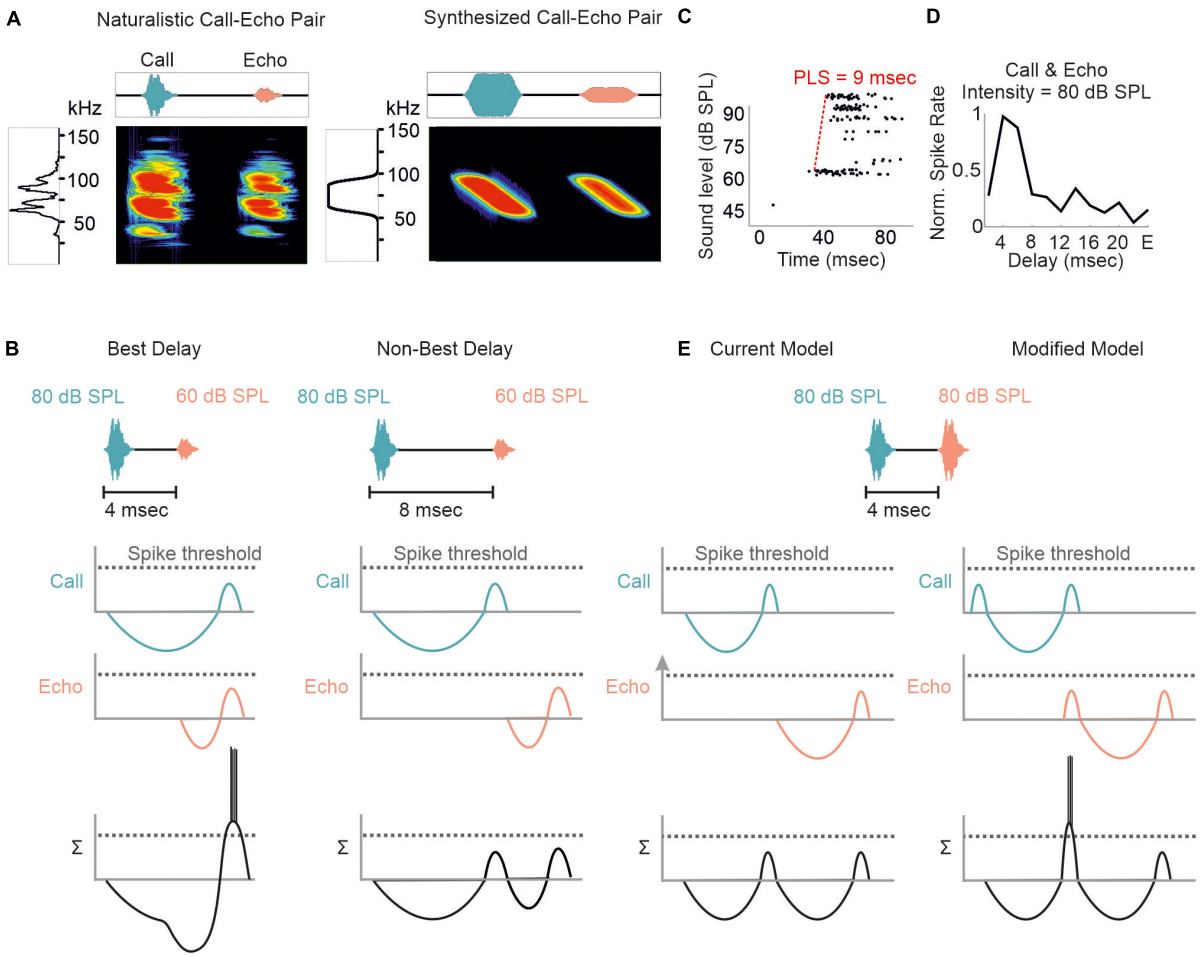

FIGURE 4 | Proposed models of delay tuning in FM-bats. **(A)** Oscillogram, spectrogram, and power spectrum of a naturalistic call-echo pair of *C. perspicillata* (*left*) and a synthesized call-echo pair (*right*). For simplicity the power spectrum represents the call only. **(B)** Proposed model of delay tuning in FM-bats. Post-synaptic responses of a delay-tuned neuron are schematically shown in response to the neuron's best delay (4 ms, *left*) and a non-best delay (8 ms, *right*). Post-synaptic inputs from call and echo are depicted in green and orange, respectively. The summed response (Σ) of the delay-tuned neuron is shown in black. Note that the neuron spikes only when the inhibitory rebounds from call and echo coincide. **(C)** Rate-level function of a cortical delay-tuned neuron showing a paradoxical latency shift (PLS) of about 9 ms. Each dot of the raster plot represents a spike **(D)** Delay-tuning curve from a cortical neuron of *C. perspicillata* that is sensitive to equally intense call and echo (80 dB SPL). **(E)** The current model of delay-tuning in FM-bats cannot explain delay tuning to equally intense call and echo (*left*). By adding an initial excitatory component, delay-tuning to equally intense call and echo can be explained (*right*). In the modified model, the post-inhibitory rebound from the call response coincides with the initial excitatory response to the echo, thus passing the spike threshold. Data shown in **(C)** are adapted from Hechavarría and Kössl (2014).

Ma and Suga, 2008; Feng, 2011; Hechavarría and Kössl, 2014). Since echolocation calls are more intense than echoes, delay-tuned neurons respond with longer latencies to calls than to echoes. If the amount of PLS is as long as the echo delay, then both subthreshold responses coincide and pass the spike threshold (*"Best Delay" column* in **Figure 4B**). Depending on the amount of PLS, different neurons have specific echo delays to which they respond best (Sullivan, 1982b; Berkowitz and Suga, 1989; Galazyuk et al., 2005; Feng, 2011; Hechavarría and Kössl, 2014). Despite the elegance of PLS, it does not fully explain the mechanisms underlying delay tuning in FM-bats. Some delay-tuned neurons show no PLS, and delay tuning can even be observed when call and echo are equally intense (Grinnell, 1963; Hechavarría and Kössl, 2014; Beetz et al., 2016b; **Figures 4C,D**). The latter cannot be explained with a PLS because excitatory rebounds from call and echo would never coincide ("*current model*" in **Figure 4E**). Based on results from extracellular recordings from lightly anesthetized and passively listening bats, we modified the current model of delay tuning. If a brief subthreshold excitation precedes the inhibition, ending up with two excitatory components (initial excitation and inhibitory rebound) and one inhibitory component evoked by each acoustic signal, then the inhibitory rebound in response to the call may coincide with the initial excitation in response to the echo ("*modified model*" in **Figure 4E**). This may explain delay tuning to equally intense acoustic signals and in absence of PLS. Unfortunately, no intracellular data from the auditory cortex of FM-bats exist to test the existence of a subthreshold initial

excitation. So far, all intracellular recordings in FM-bats focused on the inferior colliculus (Covey et al., 1996; Xie et al., 2007; Peterson et al., 2008; Voytenko and Galazyuk, 2008; Li et al., 2010). Importantly, many neurons from the auditory midbrain show an initial excitation followed by inhibition (Suga, 1964; Covey et al., 1996), a process mediated a process mediated by GABA (Jen et al., 2002; Zhou and Jen, 2002; Wu and Jen, 2006a,b). However, it is noteworthy that changes in signal duration can substantially change the post-synaptic potentials of a collicular neuron (Covey et al., 1996). The high post-synaptic dynamics induced by slight stimulus changes raises concerns about the transferability of post-synaptic potentials measured with artificial stimuli. To what extent delay-tuned neurons of the cortex show initial excitatory responses followed by inhibition and post-inhibitory rebounds and whether these response components contribute to the neural mechanisms of delay tuning awaits to be answered.

What is even more underexplored is how the temporal dynamics of excitation and inhibition influence the neural responses to naturalistic echolocation sequences in FM bats. At the level of the auditory midbrain, neural suppression in response to the echolocation sequence improves the neural tracking ability of acoustic signals by increasing the signal-to-noise ratio of the neural response (Beetz et al., 2017). While many collicular neurons are adapted to encode the time points of acoustic signals in an echolocation sequence (Sanderson and Simmons, 2005; Beetz et al., 2017; Macías et al., 2018), forward suppression vastly deteriorates this tracking ability at the cortex level (Bartenstein et al., 2014; Beetz et al., 2016b; **Figure 5A**). In contrast to *C. perspicillata* and *Phyllostomus discolor*, cortical suppression is weaker in the FM-bat *Tadarida brasiliensis* and some neurons well represent the time points of acoustic signals (Macías et al., 2022). Hereby, the spike timing precision increases with the stimulus rate and thus improves the neurons' tracking ability (Macías et al., 2022) similar to what has been found in the inferior colliculus of *C. perspicillata* (Beetz et al., 2017). In contrast to this, neural suppression in the inferior colliculus of *E. fuscus* is stronger than in *C. perspicillata*, resulting in some neurons selectively responding to particular call-echo pairs in a naturalistic echolocation sequence (Macías et al., 2018). Altogether, the degree and site of neural suppression can differ across bat species, an interesting comparative effect on processing echolocation sequences.

Regional differences in GABA-mediated inhibitions in the inferior colliculus and auditory cortex may explain the different suppression strength seen in the midbrain and cortex of *C. perspicillata*. While blocking GABA abolishes PLS and affects delay tuning in the inferior colliculus (Galazyuk and Feng, 2001; Feng, 2011), at cortical level, PLS and delay tuning are unaffected by GABA blockage (Hechavarría and Kössl, 2014; **Figure 5B**). At the cortex, GABA blockage has a strong effect on the response amplitude. Altogether, the data indicate that PLS seen at the cortex level is inherited from subcortical structures, like the inferior colliculus or the thalamus. Future work, especially from the thalamus is required to fully understand the role of GABA and PLS on delay tuning.

Most cortical delay-tuned neurons are more sensitive to faint than to intense acoustic signals (Hechavarría and Kössl, 2014; **Figure 5C**). Non-monotonic intensity rate functions are less abundant in the inferior colliculus (Yang et al., 1992; Park and Pollak, 1993, 1994) than in the cortex (Suga and Manabe, 1982; Measor et al., 2018). In the pallid bat, non-monotonicity is more pronounced when using broadband FM sweeps than pure tones. This indicates that non-monotonicity is accentuated from sideband inhibition through dynamic interactions of different frequency inputs (Measor et al., 2018). The current view is that inhibitory inputs in the mammalian cortex are more broadly tuned than excitatory inputs (Wehr and Zador, 2003; Tan et al., 2004) and that there is an unbalanced recruitment between excitation and inhibition with increasing intensity (Wu et al., 2006). Experiments on thalamocortical brain slices from mice demonstrated that non-monotonicity can arise through local cortical inhibition (de la Rocha et al., 2008). While these findings, together with a formulated model, explain non-monotonicity in response to simple acoustic stimuli, they do not explain how non-monotonicity contributes to processing complex acoustic streams (de la Rocha et al., 2008), like echolocation sequences. By considering the presence of non-monotonicity, we adapted our current model of delay tuning (initial excitation + inhibition + post-inhibitory rebound) for the neural responses to the naturalistic echolocation sequences. Because of relatively low suppression, collicular neurons respond to almost each acoustic signal of our sequence. However, at the neuron's best delay (6 ms in our example; **Figure 5D**) the post-inhibitory rebound from the call response coincides with the initial excitation of the echo response which results to a higher spike rate than non-optimal echo delays (blue arrowhead in **Figure 5D**). The very same echolocation sequence whose acoustic signals are well tracked by collicular neurons is totally differently encoded in the cortex. Here, massive suppression, in combination with non-monotonicity reduces the post-synaptic potentials induced by calls and echoes. Suppression effects last longer than in the midbrain and therefore may lead to subthreshold oscillations that reduce the neuron's membrane potential. Although, subthreshold oscillations in cortical delay-tuned neurons await to be detected, similar oscillations have been detected in the inferior colliculus of bats and frogs (Covey et al., 1996; Feng, 2011). According to our model, relatively strong excitatory inputs are necessary to overcome cortical suppression and pass the spike threshold (Chen and Jen, 1994; Jen and Chen, 1998). This occurs when depolarizations induced by call and echo coincide (blue arrowhead in **Figure 5E**).

The influence of non-monotonicity is also reflected in cortical neurons that shift their delay tuning toward shorter delays with decreasing stimulus intensities (**Figure 6A**). According to the non-monotonicity, the duration of inhibition is prolonged with increasing intensity. Therefore, the inhibitory rebound (excitation II) delays with increasing intensity and thus the best delay is also shifted toward longer delays (**Figures 6B,C**).

Irrespective of the presented echo delay, many cortical neurons show an initial response to the echolocation sequence indicating for building up process of cortical suppression (Bartenstein et al., 2014; Beetz et al., 2016b). Initial responses

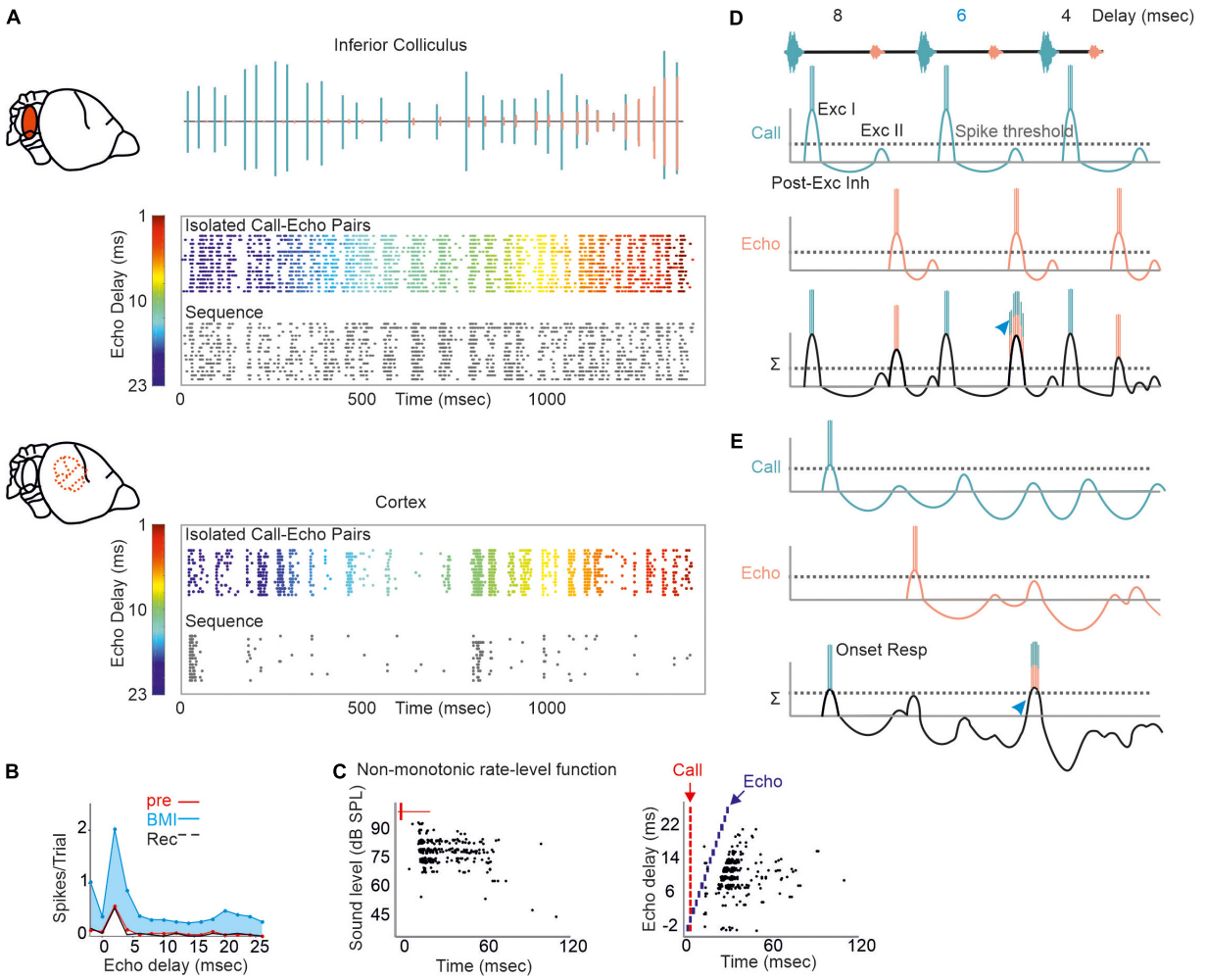

FIGURE 5 | Proposed mechanism of processing naturalistic echolocation sequences. **(A)** Neural response to isolated call-echo pairs (colored raster plot) presented in randomized order and with 500 ms interstimulus time-interval and to a naturalistic echolocation sequence (black raster plot) from the inferior colliculus (*upper*) and auditory cortex (*lower*) of *C. perspicillata*. The naturalistic echolocation sequence is shown as oscillogram where green and orange events indicate calls and echoes, respectively. **(B)** Effect of GABA blocking in a cortical delay-tuned neuron. Blockage with bicuculline methiodide (BMI) reduces the spike rate while the delay-tuning was unaffected. **(C)** Rate-level function (*left*) and delay tuning (*right*) visualized as raster plots of one cortical neuron. Note that the neuron responds non-monotonically with more spikes to faint than to intense sound levels (*left*). Each black dot represents a spike. **(D,E)** Proposed models of processing echolocation sequences in the inferior colliculus **(D)** and auditory cortex **(E)**. For simplicity, the synaptic input to delay-tuned neurons is demonstrated for a sequence containing three call-echo pairs with echo-delays of 8, 6, and 4 ms. Synaptic inputs evoked by calls and echoes are indicated in green and orange. Both inputs are linearly summed (Σ) to explain the post-synaptic potential and spike output of the delay-tuned neurons. Although, responding with spikes to each acoustic event, the collicular neuron shows a facilitatory response [blue arrowhead in **(D)**] to the call-echo pair in which the echo follows the call by 6 ms. The cortical neuron responds more selectively to the 6 ms call-echo pair of the sequence (blue arrowhead). Respectively, data shown in **(A–C)** are adapted from Hechavarría and Kössl (2014) and Beetz et al. (2017).

are not essential for cortical suppression (Edamatsu and Suga, 1993; Beetz et al., 2016b) and in rodents it has been shown that even subthreshold depolarizations are followed by inhibition (Asari and Zador, 2009). Note that our model on processing naturalistic echolocation sequences is purely based on extracellular data obtained in anesthetized, passively listening bats of the species *C. perspicillata*. Our model does not consider the auditory thalamus whose influence on delay tuning is completely unknown in *C. perspicillata*. Future studies should consider performing neural recordings from multiple auditory stages, i.e., midbrain, thalamus, and cortex, at the same time in order to understand the organization of delay-tuning along the ascending auditory pathway. In addition, intracellular recordings monitoring the neuron's membrane potential when the bats are stimulated with naturalistic echolocation sequences are essential.

NEURAL PROCESSING OF COMPLEX NATURALISTIC SCENES

Echolocation calls emitted in highly cluttered environments get reflected off multiple objects. This creates cascades of echoes

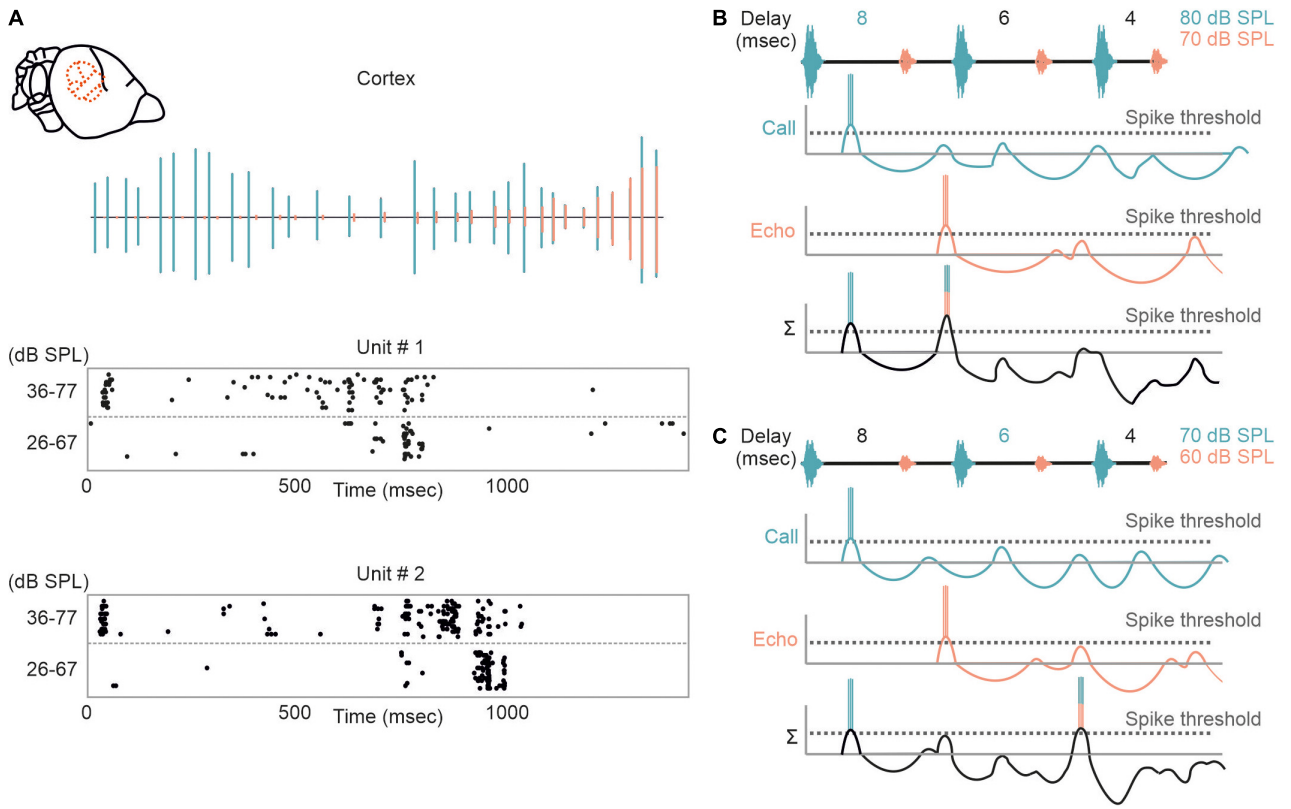

FIGURE 6 | Intensity-dependent shifts in delay tuning in the auditory cortex. **(A)** Neural response of two cortical units to an echolocation sequence is shown as raster plots. (Top) Oscillogram of the sequence with calls and echoes depicted in green and orange, respectively. The sequence was presented at two different intensity ranges (36–77 and 26–67 dB SPL). Note, that the units respond earlier when the bat was stimulated with the high intensity range. **(B,C)** Proposed model explaining the intensity-dependent shift in delay tuning. When stimulated with an intense sequence (80–70 dB SPL), the non-monotonicity of the neuron elongates the inhibitory component and thus the rebound coincides with the initial excitation evoked by the first echo. Delay tuning gets shifted toward shorter delays (6 ms) when the bat gets stimulated with a fainter sequence (70–60 dB SPL). This results from a shortening of inhibition due to the non-monotonicity.

following each call (Moss and Surlykke, 2010). Although bats may reduce the abundance of echo cascades by focusing their sonar beam to single objects (Surlykke et al., 2009a,b; Seibert et al., 2013; Fujioka et al., 2014), echo cascades cannot entirely be avoided (Linnenschmidt and Wiegrebe, 2016). Surprisingly, only a handful of studies tried to shed light onto how the bat's brain processes spatial information from echo cascades in which the echoes were temporally non-overlapping (Beetz et al., 2016a, 2017; Greiter and Firzlaff, 2017; Warnecke et al., 2018, 2021) [for neural results on temporally overlapping echoes that create spectral notches (see Sanderson and Simmons (2000, 2002), Allen et al. (2021))]. While neurons of the auditory midbrain parallelly process spatial information from multiple echoes (Beetz et al., 2017; Warnecke et al., 2018, 2021), the auditory cortex predominantly encodes the most immediate echo and subsequent echoes do not evoke a neural response (Beetz et al., 2016a; Greiter and Firzlaff, 2017). These data indicate that there must be a neural filter from the midbrain to the cortex. In anesthetized, passively listening bats, this filter selects the closest object. This is not a surprise when considering that the closest object represents the highest risk to collide with during flight. However, it is likely that attentional processes of the bat can adapt the filter so that more distant objects could be predominantly processed at cortical level, as it has been shown with behavioral experiments (Fujioka et al., 2016; Amichai and Yovel, 2017). Neural recordings from awake, echolocating bats are necessary to understand how this filter operates and how echo cascades are processed in the brain (Kothari et al., 2018).

Another major challenge accompanied by acoustic orientation is that bats live in a noisy environment enriched with communication and biosonar signals of conspecifics. This situation represents a cocktail party "nightmare" where bats are challenged to extract their own biosonar signals from a soup of noise. Although it has been shown that bats can discriminate their calls from interfering acoustic signals of conspecifics (Schnitzler et al., 1987; Brigham et al., 1989; Jones et al., 1991; Masters et al., 1991, 1995; Obrist, 1995; Amichai et al., 2015), call extraction becomes difficult with increasing noise level. To facilitate signal extraction, bats demonstrate a large repertoire of different behavioral adaptations. Some bats avoid flying in noisy environments (von Frenckell and Barclay, 1987; Beetz et al., 2019). However, due to the massive number of individuals sharing habitats, it is impossible to completely avoid acoustic interference. Additional adaptations are necessary

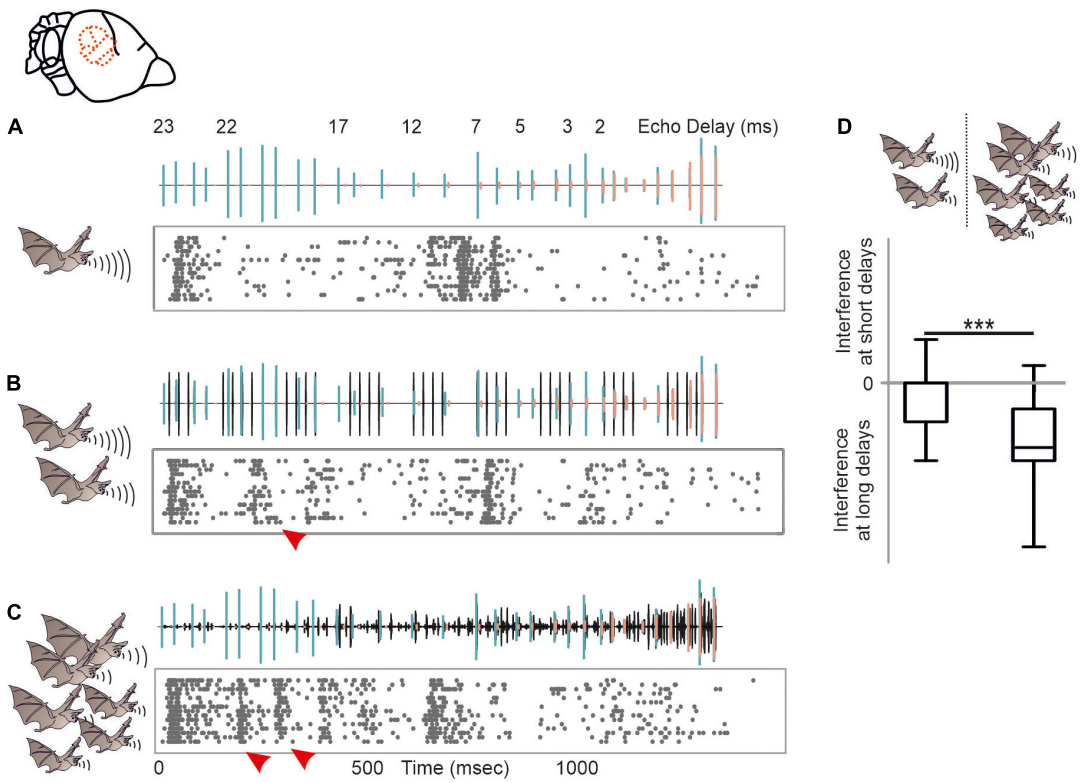

FIGURE 7 | Acoustic interference arising from different naturalistic masker in the auditory cortex of *C. perspicillata*. **(A–C)** Neural activity of a cortical unit in response to the target sequence alone **(A)**, target sequence embedded in a moderate interferer (scenario when two bats echolocate) **(B)**, and target sequence embedded in strong interferer (scenario encountered in a bat colony) **(C)**. Oscillograms of the stimuli are shown above each raster plot. Respectively, call and echoes of the target stimulus are indicated in green and orange, while the interferer is shown in black. **(D)** Acoustic interference, shown as additional spikes in (*red arrowheads* in **B**,**C**) that were absent in **(A)**, preliminary occurs at the beginning of the sequence where long delays of the target sequence were dominant (Kruskal–Wallis test and Dunn's multiple comparison *post hoc* test: $***p < 10^{-5}$). Data from Beetz et al. (2018).

to ensure signal extraction. Bats profit from their highly mobile outer ears. By adjusting the pinna position, they actively control their directional hearing (Gao et al., 2011; Wohlgemuth et al., 2016a). In addition, it has been shown that bats adjust different call parameters, including spectral, temporal, and energy level to ensure discriminability from conspecific signals (Simmons et al., 1975, 1978; Habersetzer, 1981; Miller and Degn, 1981; Suga et al., 1983; Roverud and Grinnell, 1985a; Obrist, 1995; Ibanez et al., 2004; Ratcliffe et al., 2004; Ulanovsky et al., 2004; Gillam et al., 2007; Gillam and McCracken, 2007; Petrites et al., 2009; Tressler and Smotherman, 2009; Hiryu et al., 2010; Hage et al., 2013; Takahashi et al., 2014; Amichai et al., 2015; Cvikel et al., 2015; Luo et al., 2015; Wheeler et al., 2016; Beetz et al., 2019, 2021).

Despite of the large amount of reported behavioral strategies to overcome acoustic interference, we barely know how dramatic signal processing is affected by different naturalistic acoustic interferers at the neuronal level. We therefore tested the potential of acoustic interference of two different maskers on echolocation processing (Beetz et al., 2018). As a control, a target stimulus, represented by a naturalistic echolocation sequence was presented to an anesthetized bat (**Figure 7A**). The target sequence was embedded in two different maskers, a moderate and a strong masker. The moderate masker represented repetitive echolocation calls, a common acoustic scenario when two bats closely echolocate (**Figure 7B**). The strong masker represented an acoustic sequence recorded from a bat colony and contained echolocation and communication signals (**Figure 7C**). While neural processing of the target was mildly affected in the presence of the moderate masker, the strong masker substantially affected target processing (Beetz et al., 2018). Interestingly, acoustic interference, represented by additional spikes due to the presence of the masker were most abundant at the first half of the target sequence that exclusively contained long echo delays (*red arrowheads* in **Figure 7**). This means that call-echo pairs with long delays are more prone to acoustic interference than call-echo pairs with short delays. Our neural data fits very well to behavioral data on signal extraction in the presence of acoustic interferers in bats (Roverud and Grinnell, 1985b). By conditioning bats in a distance discrimination task and challenging them with timely controlled acoustic interferers, Roverud and Grinnell showed that delay tuning may be based on an integration time window. Each emitted echolocation call opens an integration time window in which the bat is highly sensitive to any subsequent acoustic signal (Roverud and Grinnell, 1985b; Neuweiler, 1990). Any acoustic signal following a call emission is automatically interpreted

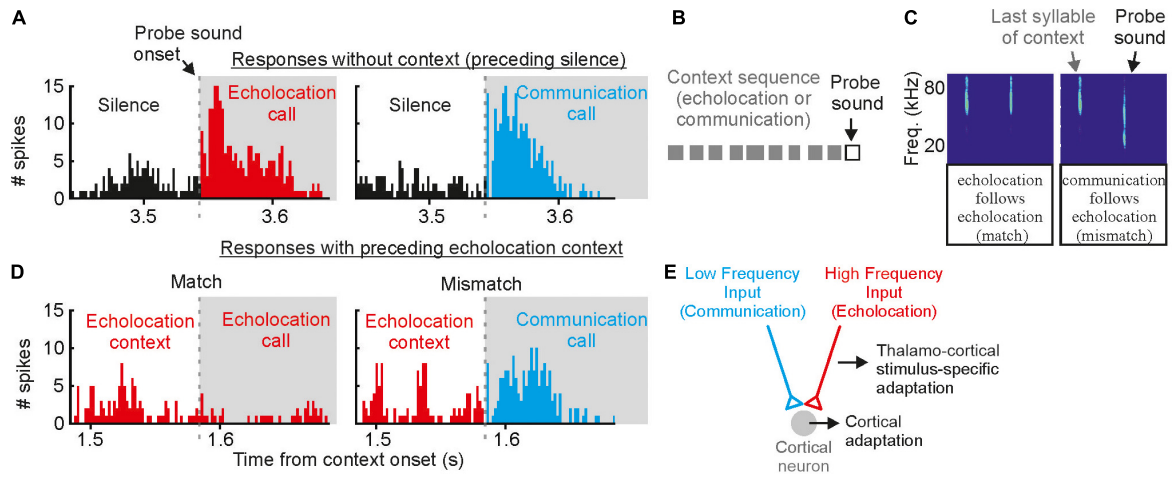

FIGURE 8 | Contextual modulation of auditory responses in the auditory cortex of awake bats. **(A)** Example cortical unit that responds equally well to echolocation and communication sounds preceded by silence. **(B)** Schematic representation of the stimulation paradigm in which context (gray squares) precede a probe sound. **(C)** Spectrograms depicting the last syllable of context and the following probe sound. Two cases are shown: (1) match (echolocation follows echolocation) and (2) mismatch (communication follows echolocation). **(D)** Responses of the same cortical unit as in **(A)** to the echolocation and communication probes preceded by an echolocation sequence. Although the response to the probe was suppressed in both cases, the suppression was less severe in the mismatch. **(E)** Circuit that best explains the results obtained *in vivo* and modeling experiments. Data from Lopez-Jury et al. (2021).

as a corresponding echo and closes the time window. If no acoustic signal follows, the time window gets automatically closed between 27 and 30 ms after call emission, depending on the bat species. The idea of an integration time window gets supported by our data (Beetz et al., 2018). Acoustic interferers only affect delay tuning, when they occur between call emission and echo arrival (Suga et al., 1983; Beetz et al., 2018). After echo arrival, the integration time window gets closed, and the neurons are not sensitive to any interferer. The existence of an integration time window receives support from our findings from the echo cascade processing in the cortex (Beetz et al., 2016a). Because the first echo automatically closes the integration time window, subsequent echoes are not processed, and cortical neurons process the first echo of an echo cascade. The aforementioned neural filter of the auditory cortex goes in line with the idea of an integration time window which seem to be non-existent in subcortical structures like the inferior colliculus (Beetz et al., 2017, 2018).

While the moderate masker only contained high frequency echolocation signals, the strong masker contained both, high frequency echolocation signals and low to high frequency communication signals. We wondered whether the acoustic context, i.e., echolocation and communication may differently affect neural tuning to echolocation or communication signals. This is of special interest when considering that delay-tuned neurons of the cortex have multipeaked frequency tuning curves whose peaks match the peak frequencies of echolocation and communication signals (Hagemann et al., 2010, 2011; Hechavarría et al., 2016a,b, 2020). This raises the question whether echolocation and communication streams are processed in parallel by different subsets of neurons or whether the neurons are, depending on the current behavioral context, more sensitive to echolocation or communication signals? With neural recordings from the auditory cortex of awake *C. perspicillata*, we demonstrated that the neural sensitivity to the context, i.e., echolocation and communication, is strongly affected by the context of preceding sounds (Lopez-Jury et al., 2021). If non-selective neurons, i.e., neurons responding to both echolocation and communication calls, get primed by echolocation signals, they become selective for communication signals with a suppressed response to echolocation calls (**Figure 8**). When the very same neurons get primed with communication signals, then they become more sensitive to lagging echolocation than communication signals. This means that neural suppression is context dependent, and that the cortex is highly sensitive to novel sounds. These results are somehow counterintuitive because they imply that cortical neurons are weakly sensitive to echolocation signals when the bat echolocates, a situation when the neurons should be highly adapted to process echolocation signals. However, although, cortical suppression does reduce neural sensitivity it enhances neural selectivity by sharpening delay tuning (Beetz et al., 2016b). A sensitivity to novel stimuli is also known from stimulus specific adaptations (SSA) according to which neurons are highly sensitive to deviants (novel, unexpected) when they are adapted to standards (repetitive stimuli) (Calford and Semple, 1995; Ulanovsky et al., 2003; Carbajal and Malmierca, 2018). The study on bats evidently shows the behavioral relevance of context dependent neural adaptations (Lopez-Jury et al., 2021).

When comparing results obtained in bats that are often described as "auditory specialists" with data obtained in non-specialized mammals, it becomes evident that "auditory specialists" must cope with the same neurophysiological phenomena including SSA, forward suppression which may push the bat's auditory system to its biological limits. Interestingly, both forward suppression and SSA do not necessarily represent a

shortcoming of processing fast and repetitive stimuli but rather help the bat's auditory system to selectively process behaviorally relevant stimuli.

NEURAL RECORDINGS FROM AWAKE AND ECHOLOCATING BATS

One major goal of neuroscience is to obtain neural activity from animals while the animals show the behavior of interest. Most of the data reviewed here were obtained in lightly anesthetized passively listening bats and thus the validity of the current model of delay-tuning must be tested in actively vocalizing bats. Along the same line of arguments, it is unclear whether a similar cortical suppression in response to naturalistic echolocation sequences occurs in vocalizing animals. Studies on cortical coding of communication sequences have discovered neurons that can keep up with fast repetition rates when the bats were awake but non-vocalizing (syllable trackers, García-Rosales et al., 2018). Such neurons were not reported in anesthetized bats (Hechavarría et al., 2016b). Though communication and echolocation call coding are not necessarily similar, it would be important to assess how the auditory cortex of awake bats processes echolocation sequences. What might be even more important than the awake state might be the vocalizing state. Despite of recent technological advances, neural recordings from actively echolocating bats have rarely been conducted (Sinha and Moss, 2007; Kothari et al., 2018; Weineck et al., 2020; García-Rosales et al., 2022). However, it is indisputable that attentional effects occurring during active vocalization may completely alter neural processing of echolocation signals. Experiments in head-restrained vocalizing bats have shown strong gamma neural rhythms, usually linked to active processes such as attention, coupled to the production of echolocation calls in frontal cortices (**Figure 9**). Such gamma oscillations are less pronounced before the production of communication calls. The same study showed that frontal areas, which are likely involved in vocalization initiation, couple their activity with sensory-motor structures such as the striatum after echolocation (Weineck et al., 2020). In addition, information flows between frontal and auditory cortices reverses directionality after bats echolocate (García-Rosales et al., 2022) indicating that the results could be completely different in vocalizing compared to non-vocalizing bats.

Neural recordings from the auditory cortex and the inferior colliculus, brain regions of great interest when performing experiments in non-vocalizing bats are rare from vocalizing bats (Kawasaki et al., 1988; García-Rosales et al., 2022). Neural recordings in vocalizing bats that are stimulated with a replay of previously emitted echolocation signals are necessary to understand how vocalization and attentional processes affect neural coding. Irrespective of the comparability of data obtained in vocalizing (Kothari et al., 2018) and non-vocalizing bats (Beetz et al., 2016a, 2017; Greiter and Firzlaff, 2017), it is noteworthy that under both recording conditions, neurons predominantly process the closest object when encountering echo information from multiple objects. These results show that conclusions drawn under artificial experimental settings, i.e., in passively listening bats, are worth to compare with experiments done under more naturalistic conditions. With the development of miniature recording devices (Marx, 2021), scientists route the technological requirements that are necessary to unravel neural mechanisms of naturalistic behavior. Not only recording devices, but also naturalistic contexts, like habitat, need to be reconstructed in order to understand neural processing of naturalistic behavior. Hereby, constructing elaborate tunnel mazes with a naturalistic representative size represents another big challenge to unravel the neural mechanisms of bat navigation behavior in future projects (Eliav et al., 2021).

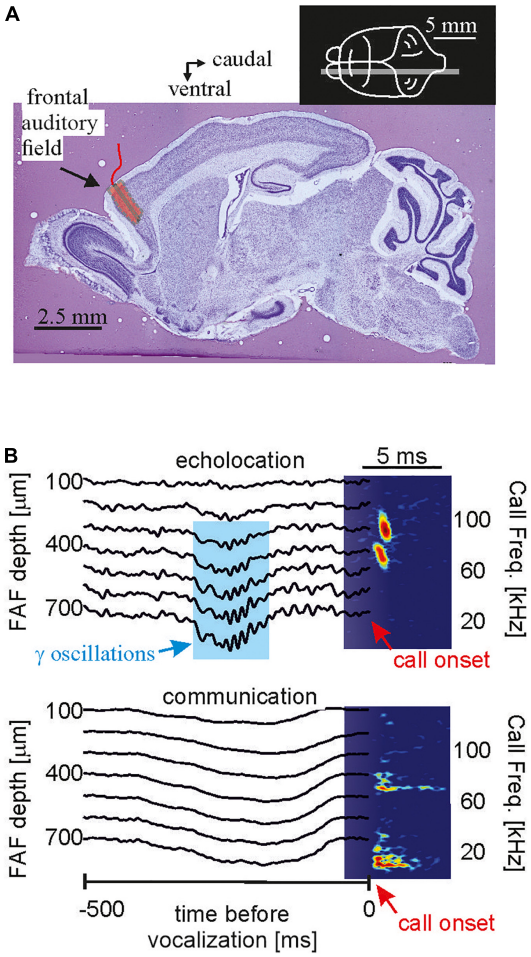

FIGURE 9 | In the bat frontal cortex, gamma oscillations exclusively occur before echolocation but not communication emission. **(A)** Location of the frontal auditory field in a sagittal brain section of the bat *Carollia perspicillata*. **(B)** Neural activity across lamina of the frontal cortex before the production of one echolocation (*upper*) and one communication call (*lower*). Call spectrograms are given as colormaps. Data from Weineck et al. (2020).

CONCLUSION

While enormous progress has been made over the last years in understanding how naturalistic echolocation sequences are

processed in the bat brain, we are still far away of understanding how the brain controls echolocation behavior. To get a deeper understanding on the neural circuits and mechanisms of echolocation behavior, it is fundamental to perform studies under naturalistic stimulus contexts. Intracellular recordings from bats listening to naturalistic echolocation sequences may shed light on the neural mechanisms at the circuit level. At the same time, the development of electrodes that allow researchers to record from hundreds of neurons simultaneously (Hong and Lieber, 2019; Steinmetz et al., 2021; Gardner et al., 2022), gives an opportunity to unravel neural circuits at the neural population level. Of special interest, hereby, are simultaneous recordings from multiple brain regions along the ascending auditory pathway to understand how echolocation signals are processed in parallel. The importance of obtaining neural recordings from a population of neurons, rather than focusing on single neurons, becomes obvious when considering the spatial resolution encoded by delay-tuned neurons. While the bandwidth of delay-tuned neuron lies in the range of milliseconds (Feng et al., 1978; O'Neill and Suga, 1979; Hagemann et al., 2011), bats can discriminate delay differences of a few microseconds (Simmons, 1973, 1979). This discrepancy between neural and behavioral data may be resolved when considering a temporal coding strategy at a population level. According to a temporal code, which is often contrasted by a rate code, the spike time precision conveys information (Macías et al., 2020a). While (Beetz et al., 2016b; Luo et al., 2018) the spike time precision of a neuron varies hundreds of μs, the precision of extracellular field potentials (200–600 Hz), representing a summed response of a population of neurons varies by tens of μs (Luo et al., 2018). Thus, the behavioral data could theoretically be explained when considering data from a neuronal population that fires in synchrony, an effect that could not be characterized at single neuronal level.

Not only the stimulus context, but also the behavioral context must be carefully considered. Neurophysiological studies in vocalizing bats will be one major focus for future projects. However, at the same time, analyzing neural data from vocalizing bats represent another challenge. Each echolocation sequence is unique in its spectro-temporal properties and the animal's attention which cannot necessarily be directly measured make the behavioral context highly variable, a scenario usually avoided by system neuroscientists that investigate neural processing in response to many invariant trials. Instead of trying to control physical properties of acoustic signals, scientists must focus to control the animal's behavior and to average over multiple behavioral rather than stimulus trials. Current neurophysiological studies on freely flying bats mainly focus on performing neural recordings from relatively large fruit-bats while data from small, insectivorous bats are rare. The latter could be related to weight limitations, i.e., the maximum weight that small bats can carry. Therefore, ongoing advancement in developing small tracking and neural recordings devices, opens the possibility to investigate the neurobiology of echolocation behavior under more naturalistic conditions. By combining state-of-the-art recording approaches with naturalistic experimental conditions, scientists have enormous potential to lift the neuroethology of bat navigation to the next level in the upcoming years.

AUTHOR CONTRIBUTIONS

MJB wrote the first draft of the manuscript. JCH made contributions to the draft and funding acquisition. MJB and JCH prepared figures. Both authors contributed to the article and approved the submitted version.

FUNDING

This work was funded by the German Research Foundation (DFG) under grant number 428645493.

REFERENCES

Allen, K. M., Salles, A., Park, S., Elhilali, M., and Moss, C. F. (2021). Effect of background clutter on neural discrimination in the bat auditory midbrain. *J. Neurophysiol.* 126, 1772–1782. doi: 10.1152/jn.00109.2021

Altringham, J. D. (2011). *Bats From Evolution to Conservation*. Oxford: Oxford University Press.

Amichai, E., Blumrosen, G., and Yovel, Y. (2015). Calling louder and longer: how bats use biosonar under severe acoustic interference from other bats. *Proc. R. Soc. B Biol. Sci.* 282:20152064. doi: 10.1098/rspb.2015.2064

Amichai, E., and Yovel, Y. (2017). Bats pre-adapt sensory acquisition according to target distance prior to takeoff even in the presence of closer background objects. *Sci. Rep.* 7:467. doi: 10.1038/s41598-017-00543-8

Asari, H., and Zador, A. M. (2009). Long-lasting context dependence constrains neural encoding models in rodent auditory cortex. *J. Neurophysiol.* 102, 2638–2656. doi: 10.1152/jn.00577.2009

Aytekin, M., Grassi, E., Sahota, M., and Moss, C. F. (2004). The bat head-related transfer function reveals binaural cues for sound localization in azimuth and elevation. *J. Acoust. Soc. Am.* 116, 3594–3605. doi: 10.1121/1.1811412

Barchi, J. R., Knowles, J. M., and Simmons, J. A. (2013). Spatial memory and stereotypy of flight paths by big brown bats in cluttered surroundings. *J. Exp. Biol.* 216, 1053–1063. doi: 10.1242/jeb.073197

Bartenstein, S. K., Gerstenberg, N., Vanderelst, D., Peremans, H., and Firzlaff, U. (2014). Echo-acoustic flow dynamically modifies the cortical map of target range in bats. *Nat. Commun.* 5:4668. doi: 10.1038/ncomms5668

Bates, M. E., Simmons, J. A., and Zorikov, T. V. (2011). Bats use echo harmonic structure to distinguish their targets from background clutter. *Science* 333, 627–630. doi: 10.1126/science.1202065

Beetz, M. J., Garcia-Rosales, F., Kossl, M., and Hechavarria, J. C. (2018). Robustness of cortical and subcortical processing in the presence of natural masking sounds. *Sci. Rep.* 8:6863. doi: 10.1038/s41598-018-25241-x

Beetz, M. J., Hechavarría, J. C., and Kössl, M. (2016b). Temporal tuning in the bat auditory cortex is sharper when studied with natural echolocation sequences. *Sci. Rep.* 6:29102. doi: 10.1038/srep29102

Beetz, M. J., Hechavarría, J. C., and Kössl, M. (2016a). Cortical neurons of bats respond best to echoes from nearest targets when listening to natural biosonar multi-echo streams. *Sci. Rep.* 6:35991. doi: 10.1038/srep35991

Beetz, M. J., Kordes, S., García-Rosales, F., Kössl, M., and Hechavarría, J. C. (2017). Processing of natural echolocation sequences in the inferior colliculus of seba's fruit eating bat, *Carollia perspicillata*. *eNeuro* 4:ENEURO.0314-17.2017. doi: 10.1523/ENEURO.0314-17.2017

Beetz, M. J., Kössl, M., and Hechavarría, J. C. (2019). Adaptations in the call emission pattern of frugivorous bats when orienting under challenging

conditions. *J Comp Physiol A Neuroethol Sens Neural Behav Physiol* 205, 457–467. doi: 10.1007/s00359-019-01337-1

Beetz, M. J., Kössl, M., and Hechavarría, J. C. (2021). The frugivorous bat *Carollia perspicillata* dynamically changes echolocation parameters in response to acoustic playback. *J. Exp. Biol.* 224:jeb234245. doi: 10.1242/jeb.234245

Berkowitz, A., and Suga, N. (1989). Neural mechanisms of ranging are different in 2 species of bats. *Hear. Res.* 41, 255–264. doi: 10.1016/0378-5955(89)90017-8

Boonman, A., Bar-On, Y., Cvikel, N., and Yovel, Y. (2013). It's not black or white-on the range of vision and echolocation in echolocating bats. *Front. Physiol.* 4:248. doi: 10.3389/fphys.2013.00248

Brigham, R. M., Cebek, J. E., and Hickey, M. B. C. (1989). Intraspecific variation in the echolocation calls of 2 species of insectivorous bats. *J. Mammal.* 70, 426–428. doi: 10.2307/1381534

Brinklov, S., Kalko, E. K. V., and Surlykke, A. (2010). Dynamic adjustment of biosonar intensity to habitat clutter in the bat *Macrophyllum macrophyllum* (*Phyllostomidae*). *Behav. Ecol. Sociobiol.* 64, 1867–1874. doi: 10.1007/s00265-010-0998-9

Cahlander, D. A., Mccue, J. J. G., and Webster, F. A. (1964). Determination of distance by echolocating bats. *Nature* 201, 544–546. doi: 10.1038/201544a0

Calford, M. B., and Semple, M. N. (1995). Monaural inhibition in cat auditory-cortex. *J. Neurophysiol.* 73, 1876–1891. doi: 10.1152/jn.1995.73.5.1876

Carbajal, G. V., and Malmierca, M. S. (2018). The neuronal basis of predictive coding along the auditory pathway: from the subcortical roots to cortical deviance detection. *Trends Hear.* 22:2331216518784822. doi: 10.1177/2331216518784822

Casseday, J. H., and Covey, E. (1996). A neuroethological theory of the operation of the inferior colliculus. *Brain Behav. Evol.* 47, 311–336. doi: 10.1159/000113249

Chen, Q. C., and Jen, P. H. S. (1994). Pulse repetition rate increases the minimum threshold and latency of auditory neurons. *Brain Res.* 654, 155–158. doi: 10.1016/0006-8993(94)91582-2

Chiu, C., and Moss, C. F. (2007). The role of the external ear in vertical sound localization in the free flying bat, *Eptesicus fuscus*. *J. Acoust. Soc. Am.* 121, 2227–2235. doi: 10.1121/1.2434760

Covey, E., Kauer, J. A., and Casseday, J. H. (1996). Whole-cell patch-clamp recording reveals subthreshold sound-evoked postsynaptic currents in the inferior colliculus of awake bats. *J. Neurosci.* 16, 3009–3018. doi: 10.1523/JNEUROSCI.16-09-03009.1996

Cvikel, N., Levin, E., Hurme, E., Borissov, I., Boonman, A., Amichai, E., et al. (2015). On-board recordings reveal no jamming avoidance in wild bats. *Proc. R. Soc. B Biol. Sci.* 282:1798. doi: 10.1098/rspb.2014.2274

de la Rocha, J., Marchetti, C., Schiff, M., and Reyes, A. D. (2008). Linking the response properties of cells in auditory cortex with network architecture: cotuning versus lateral inhibition. *J. Neurosci.* 28, 9151–9163. doi: 10.1523/JNEUROSCI.1789-08.2008

Dear, S. P., and Suga, N. (1995). Delay-tuned neurons in the midbrain of the big brown bat. *J. Neurophysiol.* 73, 1084–1100. doi: 10.1152/jn.1995.73.3.1084

Dijkgraaf, S. (1960). Spallanzani's unpublished experiments on the sensory basis of object perception in bats. *Isis* 51, 9–20. doi: 10.1086/348834

Edamatsu, H., and Suga, N. (1993). Differences in response properties of neurons between 2 delay-tuned areas in the auditory-cortex of the moustached bat. *J. Neurophysiol.* 69, 1700–1712. doi: 10.1152/jn.1993.69.5.1700

Eliav, T., Maimon, S. R., Aljadeff, J., Tsodyks, M., Ginosar, G., Las, L., et al. (2021). Multiscale representation of very large environments in the hippocampus of flying bats. *Science* 372:eabg4020. doi: 10.1126/science.abg4020

Falk, B., Jakobsen, L., Surlykke, A., and Moss, C. F. (2014). Bats coordinate sonar and flight behavior as they forage in open and cluttered environments. *J. Exp. Biol.* 217, 4356–4364. doi: 10.1242/jeb.114132

Faure, P. A., and Barclay, R. M. R. (1994). Substrate-gleaning versus aerial-hawking - plasticity in the foraging and echolocation behavior of the long-eared bat, myotis-evotis. *J. Comp. Physiol. A* 174, 651–660. doi: 10.1007/BF00217386

Feng, A. S. (2011). Neural mechanisms of target ranging in FM bats: physiological evidence from bats and frogs. *J. Comp. Physiol. A* 197, 595–603. doi: 10.1007/s00359-010-0533-5

Feng, A. S., Simmons, J. A., and Kick, S. A. (1978). Echo detection and target-ranging neurons in auditory-system of bat *Eptesicus-Fuscus*. *Science* 202, 645–648. doi: 10.1126/science.705350

Firzlaff, U., Schornich, S., Hoffmann, S., Schuller, G., and Wiegrebe, L. (2006). A neural correlate of stochastic echo imaging. *J. Neurosci.* 26, 785–791. doi: 10.1523/JNEUROSCI.3478-05.2006

Firzlaff, U., and Schuller, G. (2003). Spectral directionality of the external ear of the lesser spear-nosed bat, *Phyllostomus discolor*. *Hear. Res.* 181, 27–39. doi: 10.1016/s0378-5955(03)00281-8

Fitzpatrick, D. C., Kanwal, J. S., Butman, J. A., and Suga, N. (1993). Combination-sensitive neurons in the primary auditory-cortex of the moustached bat. *J. Neurosci.* 13, 931–940. doi: 10.1523/jneurosci.13-03-00931.1993

Fitzpatrick, D. C., Suga, N., and Misawa, H. (1991). Are the initial frequency-modulated components of the moustached bats biosonar pulses important for ranging. *J. Neurophysiol.* 66, 1951–1964. doi: 10.1152/jn.1991.66.6.1951

Fujioka, E., Aihara, I., Sumiya, M., Aihara, K., and Hiryu, S. (2016). Echolocating bats use future-target information for optimal foraging. *Proc. Natl. Acad. Sci. U. S. A.* 113, 4848–4852. doi: 10.1073/pnas.1515091113

Fujioka, E., Aihara, I., Watanabe, S., Sumiya, M., Hiryu, S., Simmons, J. A., et al. (2014). Rapid shifts of sonar attention by *Pipistrellus abramus* during natural hunting for multiple prey. *J. Acoust. Soc. Am.* 136, 3389–3400. doi: 10.1121/1.4898428

Fuzessery, Z. M. (1996). Monaural and binaural spectral cues created by the external ears of the pallid bat. *Hear. Res.* 95, 1–17. doi: 10.1016/0378-5955(95)00223-5

Gaioni, S. J., Riquimaroux, H., and Suga, N. (1990). Biosonar behavior of moustached bats swung on a pendulum prior to cortical ablation. *J. Neurophysiol.* 64, 1801–1817. doi: 10.1152/jn.1990.64.6.1801

Galazyuk, A. V., and Feng, A. S. (2001). Oscillation may play a role in time domain central auditory processing. *J. Neurosci.* 21:RC147. doi: 10.1523/JNEUROSCI.21-11-j0001.2001

Galazyuk, A. V., Lin, W. Y., Llano, D., and Feng, A. S. (2005). Leading inhibition to neural oscillation is important for time-domain processing in the auditory midbrain. *J. Neurophysiol.* 94, 314–326. doi: 10.1152/jn.00056.2005

Galazyuk, A. V., Llano, D., and Feng, A. S. (2000). Temporal dynamics of acoustic stimuli enhance amplitude tuning of inferior colliculus neurons. *J. Neurophysiol.* 83, 128–138. doi: 10.1152/jn.2000.83.1.128

Gao, L., Balakrishnan, S., He, W. K., Yan, Z., and Müller, R. (2011). Ear deformations give bats a physical mechanism for fast adaptation of ultrasonic beam patterns. *Phys. Rev. Lett.* 107:214301.

García-Rosales, F., Beetz, M. J., Cabral-Calderin, Y., Kössl, M., and Hechavarría, J. C. (2018). Neuronal coding of multiscale temporal features in communication sequences within the bat auditory cortex. *Commun. Biol.* 1:200

García-Rosales, F., López-Jury, L., Gonzalez-Palomares, E., Wetekam, J., Cabral-Calderín, Y., Kiai, A., et al. (2022). Echolocation reverses information flow in a cortical vocalization network. *bioRxiv [Preprint]* Available online at: https://doi.org/10.1101/2021.03.15.435430 [accessed on January 31, 2022].

Gardner, R. J., Hermansen, E., Pachitariu, M., Burak, Y., Baas, N. A., Dunn, B. A., et al. (2022). Toroidal topology of population activity in grid cells. *Nature* 602, 123–128. doi: 10.1038/s41586-021-04268-7

Gillam, E. H., and McCracken, G. F. (2007). Variability in the echolocation of *Tadarida brasiliensis*: effects of geography and local acoustic environment. *Anim. Behav.* 74, 277–286. doi: 10.1016/j.anbehav.2006.12.006

Gillam, E. H., Ulanovsky, N., and Mccracken, G. F. (2007). Rapid jamming avoidance in biosonar. *Proc. Biol. Sci.* 274, 651–660. doi: 10.1098/rspb.2006.0047

Greiter, W., and Firzlaff, U. (2017). Echo-acoustic flow shapes object representation in spatially complex acoustic scenes. *J. Neurophysiol.* 117, 2113–2124. doi: 10.1152/jn.00860.2016

Griffin, D. R. (1944). Echolocation by blind men, bats and radar. *Science* 100, 589–590. doi: 10.1126/science.100.2609.589

Griffin, D. R. (1953). Bat sounds under natural conditions, with evidence for echolocation of insect prey. *J. Exp. Zool.* 123, 435–465. doi: 10.1002/jez.1401230304

Griffin, D. R. (1958). *Listening in the Dark: The Acoustic Orientation of Bats and Men*. Oxford: Yale University Press.

Griffin, D. R. (2001). Return to the magic well: echolocation behavior of bats and responses of insect prey. *Bioscience* 51, 555–556. doi: 10.1641/0006-3568(2001)051[0555:rttmwe]2.0.co;2

Griffin, D. R., and Novick, A. (1955). Acoustic orientation of neotropical bats. *J. Exp. Zool.* 130, 251–299. doi: 10.1007/s00359-010-0518-4

Grinnell, A. D. (1963). Neurophysiology of audition in bats - temporal parameters. *J. Physiol. Lond.* 167, 67–96. doi: 10.1113/jphysiol.1963.sp007133

Grinnell, A. D., and Griffin, D. R. (1958). The sensitivity of echolocation in bats. *Biol. Bull.* 114, 10–22. doi: 10.2307/1538961

Grinnell, A. D., and Grinnell, V. S. (1965). Neural correlates of vertical localization by echo-locating bats. *J. Physiol. Lond.* 181, 830–851. doi: 10.1113/jphysiol.1965.sp007800

Grothe, B., and Park, T. J. (1998). Sensitivity to interaural time differences in the medial superior olive of a small mammal, the Mexican free-tailed bat. *J. Neurosci.* 18, 6608–6622. doi: 10.1523/JNEUROSCI.18-16-06608.1998

Habersetzer, J. (1981). Adaptive echolocation sounds in the bat *Rhinopoma-Hardwickei* - a field-study. *J. Comp. Physiol.* 144, 559–566. doi: 10.1007/bf01326841

Hage, S. R., Jiang, T. L., Berquist, S. W., Feng, J., and Metzner, W. (2013). Ambient noise induces independent shifts in call frequency and amplitude within the Lombard effect in echolocating bats. *Proc. Natl. Acad. Sci. U. S. A.* 110, 4063–4068. doi: 10.1073/pnas.1211533110

Hagemann, C., Esser, K. H., and Kössl, M. (2010). Chronotopically organized target-distance map in the auditory cortex of the short-tailed fruit bat. *J. Neurophysiol.* 103, 322–333. doi: 10.1152/jn.00595.2009

Hagemann, C., Vater, M., and Kössl, M. (2011). Comparison of properties of cortical echo delay-tuning in the short-tailed fruit bat and the mustached bat. *J. Comp. Physiol. A* 197, 605–613. doi: 10.1007/s00359-010-0530-8

Hahn, W. L. (1908). Some habits and sensory adaptations of cave-inhabiting bats II. *Biol. Bull.* 15, 165–193. doi: 10.2307/1535934

Hartridge, H. (1920). The avoidance of objects by bats in their flight. *J. Physiol. Lond.* 54, 54–57. doi: 10.1113/jphysiol.1920.sp001908

Hartridge, H. (1945). Acoustic control in the flight of bats - reply. *Nature* 156, 692–693. doi: 10.1038/156692b0

Hase, K., Kadoya, Y., Takeuchi, Y., Kobayasi, K. I., and Hiryu, S. (2022). Echo reception in group flight by Japanese horseshoe bats, *Rhinolophus ferrumequinum nippon*. *R. Soc. Open Sci.* 9:211597. doi: 10.1098/rsos.211597

Hechavarría, J., Beetz, M. J., Macías, S., and Kössl, M. (2016a). Distress vocalization sequences broadcasted by bats carry redundant information. *J. Comp. Physiol. A* 202, 503–515. doi: 10.1007/s00359-016-1099-7

Hechavarría, J. C., Beetz, M. J., Macías, S., and Kössl, M. (2016b). Vocal sequences suppress spiking in the bat auditory cortex while evoking concomitant steady-state local field potentials. *Sci. Rep.* 6:39226. doi: 10.1038/srep39226

Hechavarría, J. C., Beetz, M. J., García-Rosales, F., and Kössl, M. (2020). Bats distress vocalizations carry fast amplitude modulations that could represent an acoustic correlate of roughness. *Sci. Rep.* 10:7332. doi: 10.1038/s41598-020-64323-7

Hechavarría, J. C., and Kössl, M. (2014). Footprints of inhibition in the response of cortical delay-tuned neurons of bats. *J. Neurophysiol.* 111, 1703–1716. doi: 10.1152/jn.00777.2013

Hechavarría, J. C., Macías, S., Vater, M., Voss, C., Mora, E. C., and Kössl, M. (2013). Blurry topography for precise target-distance computations in the auditory cortex of echolocating bats. *Nat. Commun.* 4:2587. doi: 10.1038/ncomms3587

Henson, O. W., Pollak, G. D., Kobler, J. B., Henson, M. M., and Goldman, L. J. (1982). Cochlear microphonic potentials elicited by biosonar signals in flying bats, *Pteronotus-P-Parnellii*. *Hear. Res.* 7, 127–147. doi: 10.1016/0378-5955(82)90010-7

Hiryu, S., Bates, M. E., Simmons, J. A., and Riquimaroux, H. (2010). FM echolocating bats shift frequencies to avoid broadcast-echo ambiguity in clutter. *Proc. Natl. Acad. Sci. U. S. A.* 107, 7048–7053. doi: 10.1073/pnas.1000429107

Hoffmann, S., Genzel, D., Prosch, S., Baier, L., Weser, S., Wiegrebe, L., et al. (2015). Biosonar navigation above water I: estimating flight height. *J. Neurophysiol.* 113, 1135–1145. doi: 10.1152/jn.00263.2014

Holland, R. A., Borissov, I., and Siemers, B. M. (2010). A nocturnal mammal, the greater mouse-eared bat, calibrates a magnetic compass by the sun. *Proc. Natl. Acad. Sci. U. S. A.* 107, 6941–6945. doi: 10.1073/pnas.0912477107

Holland, R. A., Thorup, K., Vonhof, M. J., Cochran, W. W., and Wikelski, M. (2006). Navigation - Bat orientation using Earth's magnetic field. *Nature* 444:702. doi: 10.1038/444702a

Hong, G. S., and Lieber, C. M. (2019). Novel electrode technologies for neural recordings. *Nat. Rev. Neurosci.* 20, 330–345. doi: 10.1038/s41583-019-0140-6

Ibanez, C., Juste, J., Lopez-Wilchis, R., and Nunez-Garduno, A. (2004). Habitat variation and jamming avoidance in echolocation calls of the sac-winged bat (*Balantiopteryx plicata*). *J. Mammal.* 85, 38–42. doi: 10.1644/1545-1542(2004)085<0038:hvajai>2.0.co;2

Jen, P. H. S., and Chen, Q. C. (1998). The effect of pulse repetition rate, pulse intensity, and bicuculline on the minimum threshold and latency of bat inferior collicular neurons. *J. Comp. Physiol. A* 182, 455–465. doi: 10.1007/s003590050193

Jen, P. H. S., Wu, C. H., Luan, R. H., and Zhou, X. M. (2002). GABAergic inhibition contributes to pulse repetition rate-dependent frequency selectivity in the inferior colliculus of the big brown bat, *Eptesicus fuscus*. *Brain Res.* 948, 159–164. doi: 10.1016/s0006-8993(02)03056-1

Jensen, M. E., and Miller, L. A. (1999). Echolocation signals of the bat *Eptesicus serotinus* recorded using a vertical microphone array: effect of flight altitude on searching signals. *Behav. Ecol. Sociobiol.* 47, 60–69. doi: 10.1007/s002650050650

Jones, G. (1999). Scaling of echolocation call parameters in bats. *J. Exp. Biol.* 202, 3359–3367. doi: 10.1242/jeb.202.23.3359

Jones, G., Hughes, P. M., and Rayner, J. M. V. (1991). The development of vocalizations in *Pipistrellus-Pipistrellus* (*Chiroptera, Vespertilionidae*) during postnatal-growth and the maintenance of individual vocal signatures. *J. Zool.* 225, 71–84. doi: 10.1111/j.1469-7998.1991.tb03802.x

Jones, G., and Rayner, J. M. V. (1988). Flight performance, foraging tactics and echolocation in free-living daubentons bats *Myotis-Daubentoni* (*Chiroptera, Vespertilionidae*). *J. Zool.* 215, 113–132. doi: 10.1111/j.1469-7998.1988.tb04888.x

Kalko, E. K. V. (1995). Insect pursuit, prey capture and echolocation in pipistrelle bats (microchiroptera). *Anim. Behav.* 50, 861–880. doi: 10.1016/0003-3472(95)80090-5

Kalko, E. K. V., and Schnitzler, H. U. (1989). The echolocation and hunting behavior of daubenton bat, *Myotis-Daubentoni*. *Behav. Ecol. Sociobiol.* 24, 225–238. doi: 10.1007/bf00295202

Kawasaki, M., Margoliash, D., and Suga, N. (1988). Delay-tuned combination-sensitive neurons in the auditory cortex of the vocalizing mustached bat. *J. Neurophysiol.* 59, 623–635. doi: 10.1152/jn.1988.59.2.623

Kick, S. A. (1982). Target-detection by the echolocating bat, *Eptesicus-Fuscus*. *J. Comp. Physiol.* 145, 431–435. doi: 10.1007/bf00612808

Klug, A., Khan, A., Burger, R. M., Bauer, E. E., Hurley, L. M., Yang, L. C., et al. (2000). Latency as a function of intensity in auditory neurons: influences of central processing. *Hear. Res.* 148, 107–123. doi: 10.1016/s0378-5955(00)00146-5

Knowles, J. M., Barchi, J. R., Gaudette, J. E., and Simmons, J. A. (2015). Effective biosonar echo-to-clutter rejection ratio in a complex dynamic scene. *J. Acoust. Soc. Am.* 138, 1090–1101. doi: 10.1121/1.4915001

Kobler, J. B., Wilson, B. S., Henson, O. W., and Bishop, A. L. (1985). Echo intensity compensation by echolocating bats. *Hear. Res.* 20, 99–108. doi: 10.1016/0378-5955(85)90161-3

Kössl, M., Hechavarría, J., Voss, C., Schaefer, M., and Vater, M. (2015). Bat auditory cortex - model for general mammalian auditory computation or special design solution for active time perception? *Eur. J. Neurosci.* 41, 518–532. doi: 10.1111/ejn.12801

Kössl, M., Hechavarría, J. C., Voss, C., Macías, S., Mora, E. C., and Vater, M. (2014). Neural maps for target range in the auditory cortex of echolocating bats. *Curr. Opin. Neurobiol.* 24, 68–75. doi: 10.1016/j.conb.2013.08.016

Kössl, M., Voss, C., Mora, E. C., Macías, S., Foeller, E., and Vater, M. (2012). Auditory cortex of newborn bats is prewired for echolocation. *Nat. Commun.* 3:773. doi: 10.1038/ncomms1782

Kothari, N. B., Wohlgemuth, M. J., Hulgard, K., Surlykke, A., and Moss, C. F. (2014). Timing matters: sonar call groups facilitate target localization in bats. *Front. Physiol.* 5:168. doi: 10.3389/fphys.2014.00168

Kothari, N. B., Wohlgemuth, M. J., and Moss, C. F. (2018). Dynamic representation of 3D auditory space in the midbrain of the free-flying echolocating bat. *Elife* 7:e29053. doi: 10.7554/eLife.29053

Lawrence, B. D., and Simmons, J. A. (1982b). Measurements of atmospheric attenuation at ultrasonic frequencies and the significance for echolocation by bats. *J. Acoust. Soc. Am.* 71, 585–590. doi: 10.1121/1.387529

Lawrence, B. D., and Simmons, J. A. (1982a). Echolocation in bats - the external ear and perception of the vertical positions of targets. *Science* 218, 481–483. doi: 10.1126/science.7123247

Li, N., Gittelman, J. X., and Pollak, G. D. (2010). Intracellular recordings reveal novel features of neurons that code interaural intensity disparities in the inferior colliculus. *J. Neurosci.* 30, 14573–14584. doi: 10.1523/JNEUROSCI.2228-10.2010

Linnenschmidt, M., and Wiegrebe, L. (2016). Sonar beam dynamics in leaf-nosed bats. *Sci. Rep.* 6:29222. doi: 10.1038/srep29222

Lopez-Jury, L., García-Rosales, F., Gonzalez-Palomares, E., Kössl, M., and Hechavarría, J. C. (2021). Acoustic context modulates natural sound discrimination in auditory cortex through frequency-specific adaptation. *J. Neurosci.* 41, 10261–10277. doi: 10.1523/JNEUROSCI.0873-21.2021

Luo, J., Macías, S., Ness, T. V., Einevoll, G. T., Zhang, K., and Moss, C. F. (2018). Neural timing of stimulus events with microsecond precision. *PLoS Biol.* 16:e2006422. doi: 10.1371/journal.pbio.2006422

Luo, J. H., Goerlitz, H. R., Brumm, H., and Wiegrebe, L. (2015). Linking the sender to the receiver: vocal adjustments by bats to maintain signal detection in noise. *Sci. Rep.* 5:18556. doi: 10.1038/srep18556

Ma, X. F., and Suga, N. (2008). Corticofugal modulation of the paradoxical latency shifts of inferior collicular neurons. *J. Neurophysiol.* 100, 1127–1134. doi: 10.1152/jn.90508.2008

Macías, S., Bakshi, K., and Smotherman, M. (2020b). Functional organization of the primary auditory cortex of the free-tailed bat Tadarida brasiliensis. *J. Comp. Physiol. A* 206, 429–440. doi: 10.1007/s00359-020-01406-w

Macías, S., Bakshi, K., Garcia-Rosales, F., Hechavarria, J. C., and Smotherman, M. (2020a). Temporal coding of echo spectral shape in the bat auditory cortex. *PLoS Biol.* 18:e3000831. doi: 10.1371/journal.pbio.3000831

Macías, S., Bakshi, K., and Smotherman, M. (2022). Faster repetition rate sharpens the cortical representation of echo streams in echolocating bats. *eNeuro* 9:ENEURO.0410-21.2021. doi: 10.1523/ENEURO.0410-21.2021

Macías, S., Luo, J., and Moss, C. F. (2018). Natural echolocation sequences evoke echo-delay selectivity in the auditory midbrain of the FM bat, *Eptesicus fuscus*. *J. Neurophysiol.* 120, 1323–1339. doi: 10.1152/jn.00160.2018

Macías, S., Mora, E. C., Hechavarria, J. C., and Kossl, M. (2016b). Echo-level compensation and delay tuning in the auditory cortex of the mustached bat. *Eur. J. Neurosci.* 43, 1647–1660. doi: 10.1111/ejn.13244

Macías, S., Hechavarría, J. C., and Kössl, M. (2016a). Temporal encoding precision of bat auditory neurons tuned to target distance deteriorates on the way to the cortex. *J. Comp. Physiol. A* 202, 195–202. doi: 10.1007/s00359-016-1067-2

Marx, V. (2021). Neuroscientists go wireless. *Nat. Methods* 18, 1150–1154. doi: 10.1038/s41592-021-01281-6

Masters, W. M., Jacobs, S. C., and Simmons, J. A. (1991). The structure of echolocation sounds used by the big brown bat *Eptesicus-Fuscus* - some consequences for echo processing. *J. Acoust. Soc. Am.* 89, 1402–1413. doi: 10.1121/1.400660

Masters, W. M., Raver, K. A. S., and Kazial, K. A. (1995). Sonar signals of big brown bats, *Eptesicus-Fuscus*, contain information about individual identity, age and family affiliation. *Anim. Behav.* 50, 1243–1260. doi: 10.1016/0003-3472(95)80041-7

Measor, K., Yarrow, S., and Razak, K. A. (2018). Topography of sound level representation in the FM sweep selective region of the pallid bat auditory cortex. *Hear. Res.* 367, 137–148. doi: 10.1016/j.heares.2018.05.017

Miller, L. A., and Degn, H. J. (1981). The acoustic behavior of 4 species of vespertilionid bats studied in the field. *J. Comp. Physiol.* 142, 67–74. doi: 10.1007/bf00605477

Mogdans, J., Schnitzler, H. U., and Ostwald, J. (1993). Discrimination of two-wavefront echoes by the big brown bat, *Eptesicus fuscus*: behavioral experiments and receiver simulations. *J. Comp. Physiol. A* 172, 309–323. doi: 10.1007/BF00216613

Moss, C. F., and Surlykke, A. (2010). Probing the natural scene by echolocation in bats. *Front. Behav. Neurosci.* 4:33. doi: 10.3389/fnbeh.2010.00033

Neuweiler, G. (1989). Foraging ecology and audition in echolocating bats. *Trends Ecol. Evol.* 4, 160–166. doi: 10.1016/0169-5347(89)90120-1

Neuweiler, G. (1990). Auditory adaptations for prey capture in echolocating bats. *Physiol. Rev.* 70, 615–641. doi: 10.1152/physrev.1990.70.3.615

Nordmark, J. (1960). Perception of distance in animal echo-location. *Nature* 188, 1009–1010. doi: 10.1038/1881009a0

Obrist, M. K. (1995). Flexible bat echolocation - the influence of individual, habitat and conspecifics on sonar signal-design. *Behav. Ecol. Sociobiol.* 36, 207–219. doi: 10.1007/bf00177798

Obrist, M. K., Fenton, M. B., Eger, J. L., and Schlegel, P. A. (1993). What ears do for bats - a comparative-study of pinna sound pressure transformation in chiroptera. *J. Exp. Biol.* 180, 119–152. doi: 10.1242/jeb.180.1.119

O'Neill, W. E., and Suga, N. (1979). Target range sensitive neurons in auditory-cortex of mustache bat. *Science* 203, 69–73. doi: 10.1126/science.758681

O'Neill, W. E., and Suga, N. (1982). Encoding of target range and its representation in the auditory-cortex of the mustached bat. *J. Neurosci.* 2, 17–31. doi: 10.1523/JNEUROSCI.02-01-00017.1982

Park, T. J., and Pollak, G. D. (1993). Gaba shapes a topographic organization of response latency in the moustache bats inferior colliculus. *J. Neurosci.* 13, 5172–5187. doi: 10.1523/JNEUROSCI.13-12-05172.1993

Park, T. J., and Pollak, G. D. (1994). Azimuthal receptive-fields are shaped by gabaergic inhibition in the inferior colliculus of the moustache bat. *J. Neurophysiol.* 72, 1080–1102. doi: 10.1152/jn.1994.72.3.1080

Peterson, D. C., Voytenko, S., Gans, D., Galazyuk, A., and Wenstrup, J. (2008). Intracellular recordings from combination-sensitive neurons in the inferior colliculus. *J. Neurophysiol.* 100, 629–645. doi: 10.1152/jn.90390.2008

Petrites, A. E., Eng, O. S., Mowlds, D. S., Simmons, J. A., and Delong, C. M. (2009). Interpulse interval modulation by echolocating big brown bats (*Eptesicus fuscus*) in different densities of obstacle clutter. *J. Comp. Physiol. A* 195, 603–617. doi: 10.1007/s00359-009-0435-6

Pierce, G. W., and Griffin, D. R. (1938). Experimental determination of supersonic notes emitted by bats. *J. Mammal.* 19, 454–455. doi: 10.2307/1374231

Portfors, C. V., and Wenstrup, J. J. (1999). Delay-tuned neurons in the inferior colliculus of the mustached bat: implications for analyses of target distance. *J. Neurophysiol.* 82, 1326–1338. doi: 10.1152/jn.1999.82.3.1326

Pye, J. D. (1960). A theory of echolocation by bats. *J. Laryngol. Otol.* 74, 718–729. doi: 10.1017/s0022215100057170

Pye, J. D. (1961a). Echolocation by bats. *Endeavour* 20:101.

Pye, J. D. (1961b). Perception of distance in animal echo-location. *Nature* 190, 361–362. doi: 10.1038/190361a0

Ratcliffe, J. M., Ter Hofstede, H. M., Avila-Flores, R., Fenton, M. B., Mccracken, G. F., Biscardi, S., et al. (2004). Conspecifics influence call design in the Brazilian free-tailed bat, *Tadarida brasiliensis*. *Can. J. Zool.* 82, 966–971.

Roverud, R. C., and Grinnell, A. D. (1985a). Discrimination performance and echolocation signal integration requirements for target detection and distance determination in the cf fm bat, *Noctilio-albiventris*. *J. Comp. Physiol. A* 156, 447–456. doi: 10.1007/bf00613969

Roverud, R. C., and Grinnell, A. D. (1985b). Echolocation sound features processed to provide distance information in the CF/FM bat, *Noctilio-Albiventris* - evidence for a gated time window utilizing both CF and FM components. *J. Comp. Physiol. A* 156, 457–469. doi: 10.1007/bf00613970

Sanderson, M. I., and Simmons, J. A. (2000). Neural responses to overlapping FM sounds in the inferior colliculus of echolocating bats. *J. Neurophysiol.* 83, 1840–1855. doi: 10.1152/jn.2000.83.4.1840

Sanderson, M. I., and Simmons, J. A. (2002). Selectivity for echo spectral interference and delay in the auditory cortex of the big brown bat *Eptesicus fuscus*. *J. Neurophysiol.* 87, 2823–2834. doi: 10.1152/jn.00628.2001

Sanderson, M. I., and Simmons, J. A. (2005). Target representation of naturalistic echolocation sequences in single unit responses from the inferior colliculus of big brown bats. *J. Acoust. Soc. Am.* 118, 3352–3361. doi: 10.1121/1.2041227

Sändig, S., Schnitzler, H. U., and Denzinger, A. (2014). Echolocation behaviour of the big brown bat (*Eptesicus fuscus*) in an obstacle avoidance task of increasing difficulty. *J. Exp. Biol.* 217, 2876–2884. doi: 10.1242/jeb.099614

Schmidt, S., Hanke, S., and Pillat, J. (2000). The role of echolocation in the hunting of terrestrial prey - new evidence for an underestimated strategy in the gleaning bat, *Megaderma lyra*. *J. Comp. Physiol. A* 186, 975–988. doi: 10.1007/s003590000151

Schnitzler, H. U., Kalko, E., Miller, L., and Surlykke, A. (1987). The echolocation and hunting behavior of the bat, *Pipistrellus-Kuhli*. *J. Comp. Physiol. A*. 161, 267–274. doi: 10.1007/BF00615246

Schnitzler, H. U., and Kalko, E. K. V. (2001). Echolocation by insect-eating bats. *Bioscience* 51, 557–569. doi: 10.1641/0006-3568(2001)051[0557:ebieb]2.0.co;2

Seibert, A. M., Koblitz, J. C., Denzinger, A., and Schnitzler, H. U. (2013). Scanning behavior in echolocating common pipistrelle bats (*Pipistrellus pipistrellus*). *PLoS One* 8:e60752. doi: 10.1371/journal.pone.0060752

Siemers, B. M., and Schnitzler, H. U. (2004). Echolocation signals reflect niche differentiation in five sympatric congeneric bat species. *Nature* 429, 657–661. doi: 10.1038/nature02547

Simmons, J. A. (1973). Resolution of target range by echolocating bats. *J. Acoust. Soc. Am.* 54, 157–173. doi: 10.1121/1.1913559

Simmons, J. A. (1979). Perception of echo phase information in bat sonar. *Science* 204, 1336–1338. doi: 10.1126/science.451543

Simmons, J. A. (1989). A view of the world through the bats ear - the formation of acoustic images in echolocation. *Cognition* 33, 155–199. doi: 10.1016/0010-0277(89)90009-7

Simmons, J. A. (2012). Bats use a neuronally implemented computational acoustic model to form sonar images. *Curr. Opin. Neurobiol.* 22, 311–319.

Simmons, J. A. (2014). Temporal binding of neural responses for focused attention in biosonar. *J. Exp. Biol.* 217, 2834–2843.

Simmons, J. A., and Chen, L. (1989). The acoustic basis for target discrimination by fm echolocating bats. *J. Acoust. Soc. Am.* 86, 1333–1350. doi: 10.1121/1.398694

Simmons, J. A., Fenton, M. B., and Ofarrell, M. J. (1979). Echolocation and pursuit of prey by bats. *Science* 203, 16–21. doi: 10.1126/science.758674

Simmons, J. A., Ferragamo, M. J., and Moss, C. F. (1998). Echo-delay resolution in sonar images of the big brown bat, *Eptesicus fuscus*. *Proc. Natl. Acad. Sci. U. S. A.* 95, 12647–12652. doi: 10.1073/pnas.95.21.12647

Simmons, J. A., Howell, D. J., and Suga, N. (1975). Information-content of bat sonar echoes. *Am. Sci.* 63, 204–215.

Simmons, J. A., Kick, S. A., Lawrence, B. D., Hale, C., Bard, C., and Escudie, B. (1983). Acuity of horizontal angle discrimination by the echolocating bat, *Eptesicus-Fuscus*. *J. Comp. Physiol.* 153, 321–330. doi: 10.1007/bf00612586

Simmons, J. A., Lavender, W. A., Lavender, B. A., Childs, J. E., Hulebak, K., Rigden, M. R., et al. (1978). Echolocation by free-tailed bats (Tadarida). *J. Comp. Physiol.* 125, 291–299.

Simmons, J. A., Lavender, W. A., Lavender, B. A., Doroshow, C. A., Kiefer, S. W., Livingston, R., et al. (1974). Target structure and echo spectral discrimination by echolocating bats. *Science* 186, 1130–1132. doi: 10.1126/science.186.4169.1130

Simmons, J. A., Moss, C. F., and Ferragamo, M. (1990). Convergence of temporal and spectral information into acoustic images of complex sonar targets perceived by the echolocating bat, *Eptesicus-Fuscus*. *J. Comp. Physiol. A* 166, 449–470. doi: 10.1007/BF00192016

Simmons, J. A., and Stein, R. A. (1980). Acoustic imaging in bat sonar - echolocation signals and the evolution of echolocation. *J. Comp. Physiol.* 135, 61–84. doi: 10.1007/bf00660182

Simmons, P., and Young, D. (2010). *Nerve Cells and Animal Behaviour*. Cambridge: Cambridge University Press.

Simon, R., Holderied, M. W., and Von Helversen, O. (2006). Size discrimination of hollow hemispheres by echolocation in a nectar feeding bat. *J. Exp. Biol.* 209, 3599–3609. doi: 10.1242/jeb.02398

Sinha, S. R., and Moss, C. F. (2007). Vocal premotor activity in the superior colliculus. *J. Neurosci.* 27, 98–110. doi: 10.1523/JNEUROSCI.2683-06.2007

Smalling, J. M., Galazyuk, A. V., and Feng, A. S. (2001). Stimulation rate influences frequency tuning characteristics of inferior colliculus neurons in the little brown bat, *Myotis lucifugus*. *Neuroreport* 12, 3539–3542. doi: 10.1097/00001756-200111160-00033

Steinmetz, N. A., Aydin, C., Lebedeva, A., Okun, M., Pachitariu, M., Bauza, M., et al. (2021). Neuropixels 2.0: a miniaturized high-density probe for stable, long-term brain recordings. *Science* 372:eabf4588. doi: 10.1126/science.abf4588

Suga, N. (1964). Recovery cycles + responses to frequency modulated tone pulses in auditory neurones of echo-locating bats. *J. Physiol. Lond.* 175, 50–80. doi: 10.1113/jphysiol.1964.sp007503

Suga, N. (2015). Neural processing of auditory signals in the time domain: delay-tuned coincidence detectors in the mustached bat. *Hear. Res.* 324, 19–36. doi: 10.1016/j.heares.2015.02.008

Suga, N., and Manabe, T. (1982). Neural basis of amplitude-spectrum representation in auditory-cortex of the mustached bat. *J. Neurophysiol.* 47, 225–255. doi: 10.1152/jn.1982.47.2.225

Suga, N., O'Neill, W. E., Kujirai, K., and Manabe, T. (1983). Specificity of combination-sensitive neurons for processing of complex biosonar signals in auditory-cortex of the mustached bat. *J. Neurophysiol.* 49, 1573–1626. doi: 10.1152/jn.1983.49.6.1573

Sullivan, W. E. (1982b). Possible neural mechanisms of target distance coding in auditory-system of the echolocating bat *Myotis-Lucifugus*. *J. Neurophysiol.* 48, 1033–1047. doi: 10.1152/jn.1982.48.4.1033

Sullivan, W. E. (1982a). Neural representation of target distance in auditory-cortex of the echolocating bat *Myotis-Lucifugus*. *J. Neurophysiol.* 48, 1011–1032. doi: 10.1152/jn.1982.48.4.1011

Surlykke, A., Ghose, K., and Moss, C. F. (2009a). Acoustic scanning of natural scenes by echolocation in the big brown bat, *Eptesicus fuscus*. *J. Exp. Biol.* 212, 1011–1020. doi: 10.1242/jeb.024620

Surlykke, A., Pedersen, S. B., and Jakobsen, L. (2009b). Echolocating bats emit a highly directional sonar sound beam in the field. *Proc. R. Soc. B Biol. Sci.* 276, 853–860. doi: 10.1098/rspb.2008.1505

Surlykke, A., Miller, L. A., Mohl, B., Andersen, B. B., Christensendalsgaard, J., and Jorgensen, M. B. (1993). Echolocation in 2 very small bats from Thailand - *Craseonycteris-Thonglongya*i and *Myotis-Siligorensis*. *Behav. Ecol. Sociobiol.* 33, 1–12. doi: 10.1007/bf00164341

Surlykke, A., and Moss, C. F. (2000). Echolocation behavior of big brown bats, *Eptesicus fuscus*, in the field and the laboratory. *J. Acoust. Soc. Am.* 108, 2419–2429. doi: 10.1121/1.1315295

Takahashi, E., Hyomoto, K., Riquimaroux, H., Watanabe, Y., Ohta, T., and Hiryu, S. (2014). Adaptive changes in echolocation sounds by *Pipistrellus abramus* in response to artificial jamming sounds. *J. Exp. Biol.* 217, 2885–2891. doi: 10.1242/jeb.101139

Tan, A. Y. Y., Zhang, L. I., Merzenich, M. M., and Schreiner, C. E. (2004). Tone-evoked excitatory and inhibitory synaptic conductances of primary auditory cortex neurons. *J. Neurophysiol.* 92, 630–643. doi: 10.1152/jn.01020.2003

Tressler, J., and Smotherman, M. S. (2009). Context-dependent effects of noise on echolocation pulse characteristics in free-tailed bats. *J. Comp. Physiol. A* 195, 923–934. doi: 10.1007/s00359-009-0468-x

Ulanovsky, N., Fenton, M. B., Tsoar, A., and Korine, C. (2004). Dynamics of jamming avoidance in echolocating bats. *Proc. R. Soc. B Biol. Sci.* 271, 1467–1475. doi: 10.1098/rspb.2004.2750

Ulanovsky, N., Las, L., and Nelken, I. (2003). Processing of low-probability sounds by cortical neurons. *Nat. Neurosci.* 6, 391–398. doi: 10.1038/nn1032

Vater, M., Kossl, M., Foeller, E., Coro, F., Mora, E., and Russell, I. J. (2003). Development of echolocation calls in the mustached bat, *Pteronotus parnellii*. *J. Neurophysiol.* 90, 2274–2290. doi: 10.1152/jn.00101.2003

von Frenckell, B., and Barclay, R. M. R. (1987). Bat activity over calm and turbulent water. *Can. J. Zool.* 65, 219–222. doi: 10.1139/z87-035

von Helversen, D., and von Helversen, O. (2003). Object recognition by echolocation: a nectar-feeding bat exploiting the flowers of a rain forest vine. *J. Comp. Physiol. A* 189, 327–336. doi: 10.1007/s00359-003-0405-3

Voytenko, S. V., and Galazyuk, A. V. (2008). Timing of sound-evoked potentials and spike responses in the inferior colliculus of awake bats. *Neuroscience* 155, 923–936. doi: 10.1016/j.neuroscience.2008.06.031

Wang, Y. N., Pan, Y. X., Parsons, S., Walker, M., and Zhang, S. Y. (2007b). Bats respond to polarity of a magnetic field. *Proc. R. Soc. B Biol. Sci.* 274, 2901–2905. doi: 10.1098/rspb.2007.0904

Wang, X. M., Galazyuk, A. V., and Feng, A. S. (2007a). FM signals produce robust paradoxical latency shifts in the bat's inferior colliculus. *J. Comp. Physiol. A* 193, 13–20. doi: 10.1007/s00359-006-0167-9

Warnecke, M., Macias, S., Falk, B., and Moss, C. F. (2018). Echo interval and not echo intensity drives bat flight behavior in structured corridors. *J. Exp. Biol.* 221:jeb191155. doi: 10.1242/jeb.191155

Warnecke, M., Simmons, J. A., and Simmons, A. M. (2021). Population registration of echo flow in the big brown bat's auditory midbrain. *J. Neurophysiol.* 126, 1314–1325. doi: 10.1152/jn.00013.2021

Wehr, M., and Zador, A. M. (2003). Balanced inhibition underlies tuning and sharpens spike timing in auditory cortex. *Nature* 426, 442–446. doi: 10.1038/nature02116

Weineck, K., García-Rosales, F., and Hechavarría, J. C. (2020). Neural oscillations in the fronto-striatal network predict vocal output in bats. *PLoS Biol.* 18:e3000658. doi: 10.1371/journal.pbio.3000658

Wenstrup, J. J., Nataraj, K., and Sanchez, J. T. (2012). Mechanisms of spectral and temporal integration in the mustached bat inferior colliculus. *Front. Neural Circuits* 6:75. doi: 10.3389/fncir.2012.00075

Wenstrup, J. J., and Portfors, C. V. (2011). Neural processing of target distance by echolocating bats: functional roles of the auditory midbrain. *Neurosci. Biobehav. Rev.* 35, 2073–2083. doi: 10.1016/j.neubiorev.2010.12.015

Wheeler, A. R., Fulton, K. A., Gaudette, J. E., Simmons, R. A., Matsuo, I., and Simmons, J. A. (2016). Echolocating big brown bats, *Eptesicus fuscus*, modulate pulse intervals to overcome range ambiguity in cluttered surroundings. *Front. Behav. Neurosci.* 10:125. doi: 10.3389/fnbeh.2016.00125

Williams, T. C., and Williams, J. M. (1967). Radio tracking of homing bats. *Science* 155, 1435–1436. doi: 10.1126/science.155.3768.1435

Williams, T. C., and Williams, J. M. (1970). Radio tracking of homing and feeding flights of a neotropical bat, *Phyllostomus-Hastatus*. *Anim. Behav.* 18, 302–309. doi: 10.1016/s0003-3472(70)80042-2

Wohlgemuth, M. J., Luo, J., and Moss, C. F. (2016b). Three-dimensional auditory localization in the echolocating bat. *Curr. Opin. Neurobiol.* 41, 78–86. doi: 10.1016/j.conb.2016.08.002

Wohlgemuth, M. J., Kothari, N. B., and Moss, C. F. (2016a). Action enhances acoustic cues for 3-d target localization by echolocating bats. *PLoS Biol.* 14:e1002544. doi: 10.1371/journal.pbio.1002544

Wong, D., Maekawa, M., and Tanaka, H. (1992). The effect of pulse repetition rate on the delay sensitivity of neurons in the auditory-cortex of the FM bat, *Myotis-Lucifugus*. *J. Comp. Physiol. A* 170, 393–402. doi: 10.1007/BF00191456

Wotton, J. M., Haresign, T., Ferragamo, M. J., and Simmons, J. A. (1996). Sound source elevation and external ear cues influence the discrimination of spectral notches by the big brown bat, *Eptesicus fuscus*. *J. Acoust. Soc. Am.* 100, 1764–1776. doi: 10.1121/1.416073

Wotton, J. M., Haresign, T., and Simmons, J. A. (1995). Spatially dependent acoustic cues generated by the external ear of the big brown bat, *Eptesicus-Fuscus*. *J. Acoust. Soc. Am.* 98, 1423–1445. doi: 10.1121/1.413410

Wotton, J. M., and Simmons, J. A. (2000). Spectral cues and perception of the vertical position of targets by the big brown bat, *Eptesicus fuscus*. *J. Acoust. Soc. Am.* 107, 1034–1041. doi: 10.1121/1.428283

Wu, C. H., and Jen, P. H. S. (2006b). The role of GABAergic inhibition in shaping duration selectivity of bat inferior collicular neurons determined with temporally patterned sound trains. *Hear. Res.* 215, 56–66. doi: 10.1016/j.heares.2006.03.001

Wu, C. H., and Jen, P. H. (2006a). GABA-mediated echo duration selectivity of inferior collicular neurons of Eptesicus fuscus, determined with single pulses and pulse-echo pairs. *J. Comp. Physiol. A* 192, 985–1002. doi: 10.1007/s00359-006-0133-6

Wu, G. Y., Li, P. Y., Tao, H. Z. W., and Zhang, L. I. (2006). Nonmonotonic synaptic excitation and imbalanced inhibition underlying cortical intensity tuning. *Neuron* 52, 705–715. doi: 10.1016/j.neuron.2006.10.009

Wu, M. I., and Jen, P. H. S. (1996). Temporally patterned pulse trains affect directional sensitivity of inferior collicular neurons of the big brown bat, *Eptesicus fuscus*. *J. Comp. Physiol. A* 179, 385–393. doi: 10.1007/BF00194992

Xie, R., Gittelman, J. X., and Pollak, G. D. (2007). Rethinking tuning: in vivo whole-cell recordings of the inferior colliculus in awake bats. *J. Neurosci.* 27, 9469–9481. doi: 10.1523/JNEUROSCI.2865-07.2007

Yang, L. C., Pollak, G. D., and Resler, C. (1992). Gabaergic circuits sharpen tuning curves and modify response properties in the moustache bat inferior colliculus. *J. Neurophysiol.* 68, 1760–1774. doi: 10.1152/jn.1992.68.5.1760

Yovel, Y., Falk, B., Moss, C. F., and Ulanovsky, N. (2010). Optimal localization by pointing off axis. *Science* 327, 701–704. doi: 10.1126/science.1183310

Zhou, X. M., and Jen, P. H. S. (2002). The role of GABAergic inhibition in shaping directional selectivity of bat inferior collicular neurons determined with temporally patterned pulse trains. *J. Comp. Physiol. A* 188, 815–826. doi: 10.1007/s00359-002-0367-x

Zhou, X. M., and Jen, P. H. S. (2006). Duration selectivity of bat inferior collicular neurons improves with increasing pulse repetition rate. *Chin. J. Physiol.* 49, 46–55.

Conflict of Interest: The authors declare that the research was conducted in the absence of any commercial or financial relationships that could be construed as a potential conflict of interest.

frontiers | Frontiers in Integrative Neuroscience

BRIEF RESEARCH REPORT
published: 18 May 2022
doi: 10.3389/fnint.2022.892951

An Active Sensing Paradigm for Studying Human Auditory Perception

Dardo N. Ferreiro[1,2], Valentin R. Winhart[1], Benedikt Grothe[1], Bahador Bahrami[2] and Michael Pecka[1]*

[1]*Division of Neurobiology, Faculty of Biology, Ludwig-Maximilians-Universität München, Munich, Germany,* [2]*Department of General Psychology and Education, Ludwig-Maximilians-Universität München, Munich, Germany*

Our perception is based on active sensing, i.e., the relationship between self-motion and resulting changes to sensory inputs. Yet, traditional experimental paradigms are characterized by delayed reactions to a predetermined stimulus sequence. To increase the engagement of subjects and potentially provide richer behavioral responses, we developed Sensory Island Task for humans (SITh), a freely-moving search paradigm to study auditory perception. In SITh, subjects navigate an arena in search of an auditory target, relying solely on changes in the presented stimulus frequency, which is controlled by closed-loop position tracking. A "target frequency" was played when subjects entered a circular sub-area of the arena, the "island", while different frequencies were presented outside the island. Island locations were randomized across trials, making stimulus frequency the only informative cue for task completion. Two versions of SITh were studied: binary discrimination, and gradual change of the stimulus frequency. The latter version allowed determining frequency discrimination thresholds based on the subjects' report of the perceived island location (i.e., target frequency). Surprisingly, subjects exhibited similar thresholds as reported in traditional "stationary" forced-choice experiments after performing only 30 trials, highlighting the intuitive nature of SITh. Notably, subjects spontaneously employed a small variety of stereotypical search patterns, and their usage proportions varied between task versions. Moreover, frequency discrimination performance depended on the search pattern used. Overall, we demonstrate that the use of an ecologically driven paradigm is able to reproduce established findings while simultaneously providing rich behavioral data for the description of sensory ethology.

Keywords: audition, navigation, active sensing, ethology, audiomotor integration, SITh, musicality

OPEN ACCESS

Edited by:
Susanne Hoffmann, Max Planck Institute for Ornithology, Germany

Reviewed by:
Uwe Firzlaff, Technical University of Munich, Germany
Tiziana Vercillo, Radboud University Nijmegen, Netherlands
Kelsey L. Anbuhl, New York University, United States

****Correspondence:***
Dardo N. Ferreiro
ferreiro@bio.lmu.de

Received: *09 March 2022*
Accepted: *19 April 2022*
Published: *18 May 2022*

Citation:
Ferreiro DN, Winhart VR, Grothe B, Bahrami B and Pecka M (2022) An Active Sensing Paradigm for Studying Human Auditory Perception. Front. Integr. Neurosci. 16:892951. doi: 10.3389/fnint.2022.892951

INTRODUCTION

Ethology strives to study behavior that has evolved in natural environments (Tinbergen, 1963; Lorenz, 1981). Nevertheless, behavioral neuroscience research has mainly focused on investigating phenomena by testing—often highly—trained subjects (animals, including humans) in rigid settings using predetermined test regimes. It is becoming increasingly clear that to better understand behavior, perception, and their neural underpinnings, modern neuroethological

research needs to introduce more natural behavior in lab experiments (Krakauer et al., 2017; Datta et al., 2019; Gomez-Marin and Ghazanfar, 2019). Such calls to action are becoming more present in human behavioral research, underscoring how important it is to increase ecological validity (Box-Steffensmeier et al., 2022).

Accordingly, we had developed the Sensory Island Task (SIT; Ferreiro et al., 2020; Amaro et al., 2021) for animals to be tested in a lab environment with the general goal of studying sensory perception while including crucial aspects of natural behavior which would improve the ecological validity of the results. The premise of the SIT paradigm was to reintroduce the natural interdependence of movement and the sensory environment (i.e., active sensing) into laboratory settings. Specifically, we incorporated active sensing and self-motion by coupling changes in the animals' location within a test arena with changes in the presented sensory stimuli.

In previous versions of SIT, we allowed rodents and primates to move unrestricted and thus freely explore an open field arena while their position was tracked for online closed-loop stimulation changes according to their position. Their goal was to find the "target island", a circular area within the arena (∼7% of arena surface), which randomly changes position across trials. Crucially, the only useful cue to solve the task was a change in the sensory stimulation (e.g., sound frequency) elicited when the animal enters the target island, which the animals report by staying within the island for a predefined time period (Ferreiro et al., 2020).

We recently showed that coupling SIT with neural recordings was instrumental in discovering new insights into behavior and neuronal coding in the auditory cortex of gerbils (Amaro et al., 2021; Stecker, 2021). Yet in human research, active sensing is still rarely made use of. An exemplary study by Whitton et al. (2014) tested the ability of mice and humans to use closed-loop audio-motor feedback to locate a hidden spot in a 2D arena. While mice performed this task by actually running around, humans simply moved a cursor on a computer screen *via* a joystick. This more naturalistic design (as compared to traditional forced-choice tasks) already provided valuable insights into the possibility to assess perceptual sensitivity by active sensing and encouraged us to extend our SIT paradigm to humans. Specifically, we investigated auditory frequency discrimination abilities in human subjects using real-time closed-loop feedback based on self-motion in the active sensing framework of SIT.

Most characteristics of the paradigm for humans are the same as described above (i.e., free movement within an arena, stimulation coupled to subject position, no forced choice, etc.). The main differences include a bigger arena (3 × 3 meters) and position tracking *via* handheld wireless controllers, which also serve to start and finish trials (**Figure 1A**).

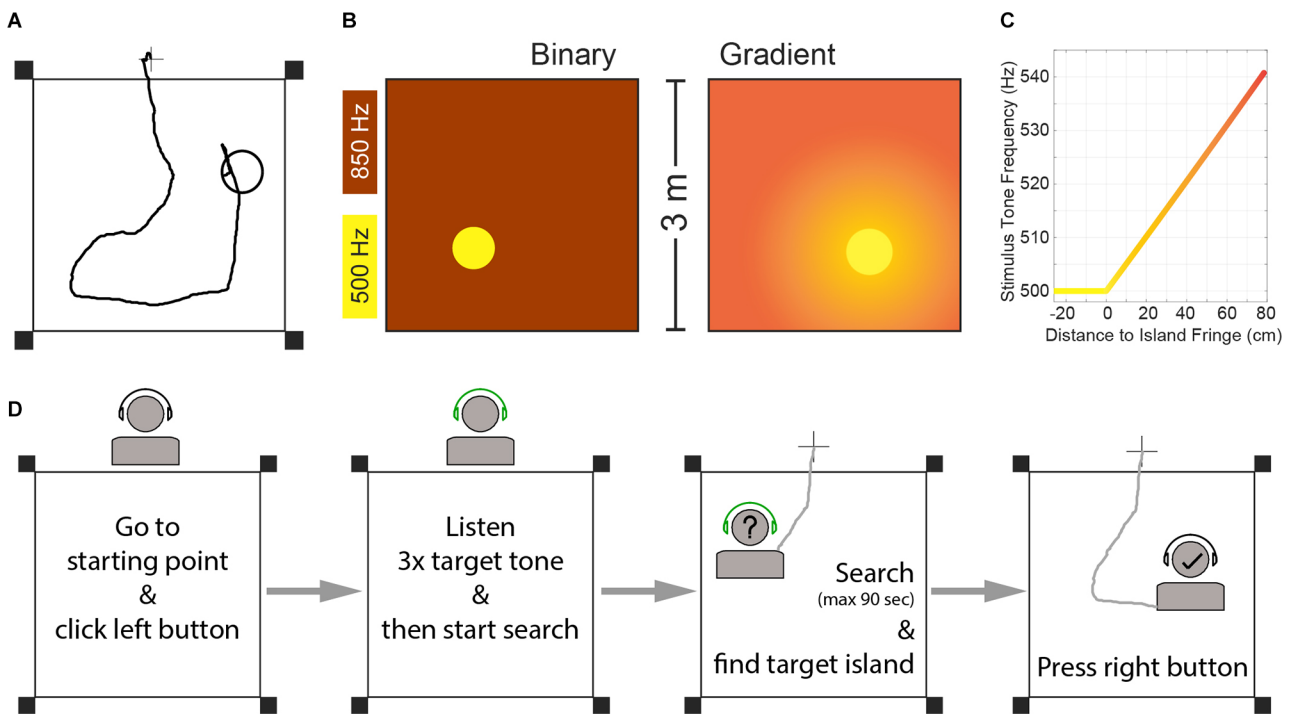

FIGURE 1 | (A) Example trial trajectory and schematic of the experimental arena for human SIT. The circle represents the target island (island radius was 26 cm). The cross outside the arena represents the starting point of each trial. Black squares represent the position of the Oculus Rift sensors. **(B)** Schematic representation of the two task versions. **(C)** Frequency of the stimulation tone pip as a function of the subject's distance to the island fringe for the gradient task. Negative distance values denote positions inside the island. Note: The gradient did not finish at 80 cm distance, but extended over the whole arena. See "Materials and Methods" Section for the full relationship of gradient and distance-to-island. **(D)** Schematic flowchart of trial structure.

Inspired by our previous animal work, we analyzed two task versions, both based on low-frequency sound frequency perception (**Figure 1B**). A "binary" version, where the island and the outside area elicited two distinct frequency stimulations that are easily discriminated; and a gradient version, where the stimulation frequency depended on the distance to the target-island, inspired by the Hidden Object game that children play:

Mary hides a toy somewhere in the room while John waits outside. John comes in and starts looking for the object while Mary indicates how close he is to the hiding place by announcing "hot" or "cold".

We present the implementation of the SIT paradigm in humans (SITh) as a proof-of-concept effort to reinforce the intuition that incorporating more naturalistic environments into experimental procedures in the lab is a worthwhile effort. Nonetheless, we show that with this approach it is possible to reproduce established results from classic literature without requiring extensive training of subjects. Moreover, our approach also allows for nuanced descriptions of human active sensing and the associated locomotive behavior.

MATERIALS AND METHODS

All subjects (18 total, nine males, nine females, mean age = 24.2 ± 2.4 years) who took part in the experiment showed normal audiograms between 125 Hz and 2,000 Hz.

The experimental paradigm used here for humans was inspired by previous research in our lab in animal experiments. For details about non-human versions of the paradigm, as well as for source code to run those experiments, please refer to Ferreiro et al. (2020). All relevant details for the human version are explained below.

Procedure

Subjects moved freely within a square arena (3 × 3 meters) in search of a target island. The circular island (radius = 26 cm) covered 2.36% of the arena's surface and its location was randomized across trials, therefore rendering the auditory stimulation as the only useful cue to find the island. While navigating the arena, subjects carried remote controllers (Oculus Rift, Meta Inc.) in their hands and wore wireless headphones through which sound stimuli were presented. To start a trial they were asked to stand over a marked point on the floor 25 cm outside of the arena (**Figure 1A**), and press a button on the left-hand controller. Upon trial initiation, they heard three repetitions of a 50 ms pulse of the target tone frequency. Their tracked live position (*via* the controllers) was used to determine the auditory stimulation delivered through the headphones. Participants were instructed to search for the place in the arena that would elicit the target frequency heard at the beginning of the trial, by walking naturally without unnecessary arm movements, and to press a right-hand controller button to report having found the island (See "Task Versions" below). Trials finished after participants pressed a button in the right hand controller (thus reporting having found the island) or a time limit of 90 s had been reached. Participants performed first a "binary" version of SITh and a "gradient" version subsequently, with a 5 min pause in between. Before each task version, they were allowed to practice for up to five test trials to get familiarized with the trial structure, after which they performed 30 recorded trials.

Task Versions

Subjects performed first a binary task, in which the stimulus tone frequency was 500 Hz within the island, and 850 Hz in the rest of the arena (**Figure 1B**). After completing 30 trials in that task, they took a 5 min break before continuing with the gradient version. In the gradient task, the target frequency within the island was also 500 Hz, but the frequency outside of the island was proportional to the distance to the island fringe (**Figure 1B**), as follows:

$$Frequency_{Gradient} = Frequency_{Target} * 1.001^{d} \quad (1)$$

Where $Frequency_{Gradient}$ is the frequency in Hz of the stimulus when the subject is outside the target island, $Frequency_{Target}$ is the frequency in Hz of the target island, and d is the distance to the island fringe.

Experimental Setup

The arena was defined as a square of 3-by-3 m, marked on the floor of a classroom with red tape. A black cross indicated the trial starting point (**Figure 1A**).

The experiment was run and controlled using specifically developed code in Python. Auditory stimuli were delivered *via* Bluetooth over-ear headphones (Sennheiser HD450 BT), and consisted of 50 ms pulses of pure tones played at a repetition rate of 4 Hz. The carrier frequency of the stimulus was defined online during the experiment, as it depended on the subject's position within the arena (See "Task Versions").

Stimuli were cosine ramped at the on- and offset (10 ms window), and their amplitude was 60 dB SPL roved ±5 dB. The position of the subjects was determined online by averaging the tracked position of the hand-held controllers in the horizontal plane (i.e., the average position between the two hand-held controllers, which in natural walking conditions lies within the body). The controllers were part of an Oculus Rift VR set, and their position was tracked using four sensors located at the corners of the square arena. Position data were acquired from the Oculus system at 20 Hz sampling rate.

Code Availability

The code used to run and control the experiment, which also managed the data acquisition is freely available at https://gin.g-node.org/dnferreiro/SITh.

Data Analysis

All data were analyzed using Matlab and Python using custom scripts. For the "angle to target" (A2T) calculations, each consecutive pair of position data points in each trial trajectory was used to determine the instantaneous heading vector. Then, the A2T was determined relative to the vector containing the first of the two data points of the heading vector and the center of the target island. Therefore, an A2T of 0 degrees describes a perfectly precise heading (i.e., a step towards

the center of the island). Importantly, head movement was not recorded (participants did not wear the Oculus headset). Therefore no head position dependent stimulation nor analysis were performed.

To calculate musical experience we determined the number of years each subject (based on a post-experimental questionnaire) had spent playing an instrument and/or singing. We did not distinguish by instruments, nor by formal vs. informal training. Values were normalized to the most experienced subject (**Supplementary Figure 1**).

Strategy Classification

A naive human observer was asked to classify trials based on the walked trajectory patterns. Based on our extensive visual analysis of the search patterns, we identified four distinct base strategies. The observer was then instructed to assign each of the trial trajectories into five different categories, either one of the four strategies, or none. Importantly, the observer had no knowledge of the task or the study in general, he was provided only with the walked paths (similar to **Figure 1A**, but without the island position) and the trial presentation for classification was chronologically randomized. The observer was also allowed to flag trials for which unique categorization was perceived to be difficult. Overall, 87% of all trials were classified into one of the four strategies (73% unflagged and 14% flagged) and 13% were classified as no-strategy. The exclusion of flagged trials did not substantially alter the main findings and conclusions (data not shown).

Statistics

Kruskal–Wallis tests were used to test for differences across search strategy distributions. Comparisons of distributions are derived from Mann–Whitney *U* tests with an alpha level = 0.05. These tests were chosen because they are non-parametric and therefore more appropriate for data distributions that deviate from normality (as can be seen from the boxplots). Comparisons of proportions are derived from Chi-square tests with an alpha level = 0.05. When applicable, multiple comparison *p*-value corrections were performed with the Holm-Bonferroni method (Holm, 1979; Aickin and Gensler, 1996).

Data distribution quantification graphs presented as boxplots use the following: black lines depict the median, filled boxes depict the first and the third quartile, error bars (whiskers) depict ± 2.7 standard deviations.

RESULTS

For this study, 18 normal hearing adults participated in SITh. An example trial trajectory and corresponding target island together with schematics of the arena are shown in **Figure 1A**. Once they started a trial, 50 ms pure tone pips were played at a repetition rate of 4 Hz. The frequency of each pip depended on the subject's position within the arena (**Figure 1B**) and the version of the SITh task. Here we report on two task versions:

- "Binary": Stimulus frequency outside the island was always 850 Hz.
- "Gradient": Stimulus frequency outside the island was proportional to the distance to the island (**Figure 1C** and equation 1).

Subjects were asked to start and terminate trials autonomously, with the objective of reporting to hear the target frequency of 500 Hz. A flowchart of the basic trial structure is shown in **Figure 1D** (see "Materials and Methods" Section for details). Importantly, the island position was randomized across trials (see **Supplementary Figure 2A** for island positions across trials), and no instructions were given to the subjects regarding the task structure, island shape and size, nor potential search strategies.

The performance of subjects, measured as a proportion of trials finished within the island, in the binary task was excellent (mean ± SD: 96.13 ± 3.80%, **Figure 2A**). This is not surprising given the large frequency difference between the target and non-target stimuli. By the same metric, the performance in the gradient task decreased for all subjects (44.19 ± 16.75%, **Figure 2A**). However, measuring performance in such a way for the gradient task does not do justice to the actual behavior and sensory perception of the subjects. Because of the stimulus frequency gradient, a hypothetical trial finishing only 10 cm away from the island means that the last frequency heard (LFH) by the subject is 505 Hz (**Figure 1C**). This represents a 1% difference with the target frequency which lies within the range of what traditional experiments have reported (Micheyl et al., 2012).

To better analyze the performance of subjects we computed the histograms of the radial distances to the island's fringe (i.e., perimeter) for the final position of all trials (**Figure 2B**). For binary trials, this confirms the previous performance metric and further shows that the few "incorrect" trials landed very close to the island and could be related to "overshooting" (i.e., pressing the button while still moving). For gradient trials, the distance-to-island histogram is skewed towards within-island final positions. Given that within the island the stimulus frequency was always 500 Hz, we also computed the LFH histogram for the gradient trials (inset, **Figure 2B**). The median value of the LFH distribution was 501.5 Hz, corresponding to a 0.3% difference with the target frequency. Interestingly, this precisely matches the frequency discrimination threshold (frequency difference limen) reported by traditional "stationary" forced-choice experiments (Moore, 1973; Micheyl et al., 2012). The individual subject distributions show a median LFH <1% for 15 out of 18 subjects (**Supplementary Figure 1B**), proving that this metric is robust across subjects. Comparing search time between tasks showed that gradient trials tended to be shorter (**Figure 2C**; Mann-Whitney *U*-test double tail, $P = 0.0253$), which suggests that in fact the gradient cue helped the subjects to reach the island (or at least the general area of the island) faster.

Given the freely moving and non-forced choice nature of SITh, we also analyzed the locomotion patterns of the subjects while searching for the target frequency. While observing task performances, we already had realized that in contrast to rodents in an identical task (Ferreiro et al., 2020), the human subjects were typically not randomly walking through the arena. After

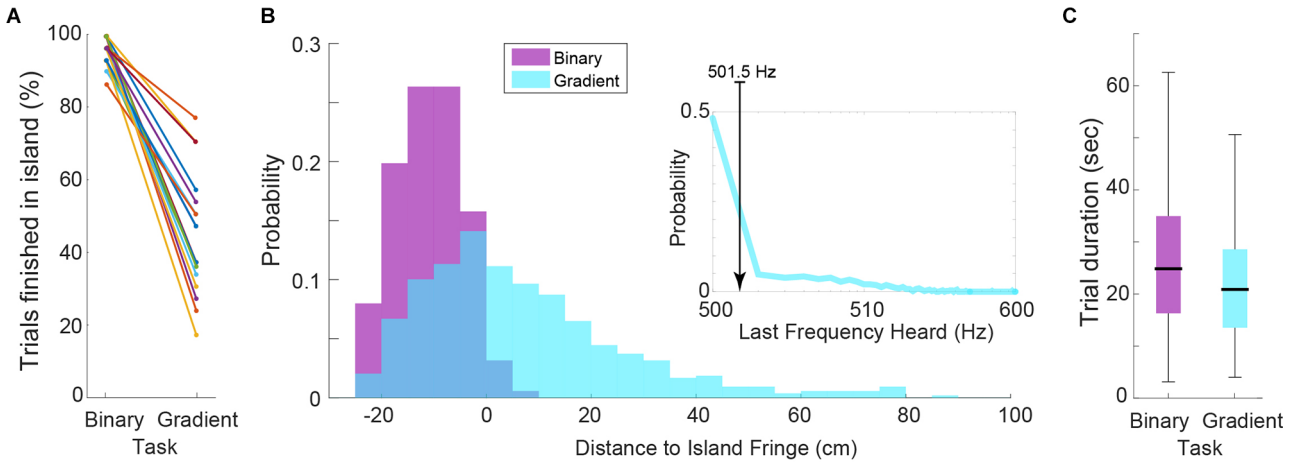

FIGURE 2 | (A) Percentage of trials finished within the target island. Each line represents a subject. Note that while this measure is equal to performance in the binary task, it is not for the gradient task. **(B)** Histograms of the distance to island fringe for all trials across subjects for both task versions. Inset: Histogram of last frequency heard when subjects finished the gradient trials. Median of 501.5 Hz is shown. **(C)** Distributions of trial durations by task ($P = 0.0253$).

a thorough visual inspection of the recorded trial trajectories, we identified four stereotypical navigation patterns (**Figure 3A**). To obtain an objective description of all trials, an independent, naive observer was recruited to classify trials into the four aforementioned search strategies. Importantly, the observer was unaware of the procedure and the objectives of the study and was only provided with images of the trial trajectories without the island position (as depicted in **Figure 3A**). Of the entire 1,080 trials (binary and gradient), 87% were classified into one of the four strategies, while 13% remained unclassified (classified per task version: 91% for binary, 83% for gradient).

We corroborated these trial strategy classifications by an analysis of the heading angle of the walked paths (see "Materials and Methods" Section). Histograms of the angle to target revealed different profiles for each of the four strategies, thus validating the classification into these four different behavioral strategies for island search (**Figure 3B**). Islands were distributed uniformly within the arena across strategies (**Supplementary Figure 2B**), which suggests no effect of island position on strategy choice. Furthermore, we observed differences between strategies already in the initial 2 s of a trial, i.e., before the occurrence of auditory feedback (**Supplementary Figure 3**), suggesting that strategy selection was predetermined.

Next, we asked how strategy usage was represented across subjects (**Figure 3C**). We found that although a few subjects (e.g., subjects 10 and 16) had a dominant strategy and consistently used it regardless of the task version (binary or gradient), most subjects used a mixture of strategies in either task, but with altering proportions between tasks (e.g., subjects 3, 4, 9, 14, and 18). To analyze whether there was a consistent population level change across subjects involving any particular strategy, we performed Mann-Whitney tests comparing the strategy proportions across subjects in binary and gradient trials ($P_{hook} = 0.11$, $P_{grid} = 0.09$, $P_{spiral} = 0.38$, $P_{coordinate} = 0.00011$). This revealed that the coordinate strategy was significantly more adopted when switching to the gradient task.

Given that the hook and coordinate strategies both make use of the online feedback provided by the gradient stimulation (as opposed to the other more rigid, systematic strategies), we wondered why some subjects opted to switch to these adaptive strategies more often than others. Since the changes in frequency near the island fringe are rather small (relative to perceptual levels) during the gradient task, it would be beneficial if subjects were able to reliably identify the target frequency. Such identification could have been favored by a high familiarity with musical training and/or exposure. Therefore, we tested whether the usage of these "adaptive" strategies in the gradient task was associated with the subjects' musical experience (**Figure 3D** and see "Materials and Methods" Section). We did in fact find a correlation between both measures, which suggests that the greater exposure to music subjects had, the more they would be inclined to use an adaptive strategy (Pearson correlation = 0.7; $P = 0.0012$).

Distributions in strategy use on the population level are summarized in **Figure 4A**. After switching to the gradient condition, grid and spiral strategies were used less, and coordinate and hook strategies were more frequent. This change is expected because grid and spiral strategies entail systematic surface coverage, while coordinate and spiral incorporate the sensory feedback during the active search.

Based on these findings, we wondered whether the different search strategies were correlated with different levels of frequency discrimination performance. We, therefore, computed the LFH across strategies (**Figure 4B**, compare **Figure 2B**). Statistical analysis showed that the four strategies differed in their LFH distributions (Kruskal-Wallis test, $P = 2.1463e\text{-}04$; Median values: hook = 503.1 Hz, grid: 502.9 Hz, spiral = 502.9 Hz, coordinate = 500 Hz). This analysis thus demonstrates that the locomotive behavior of subjects

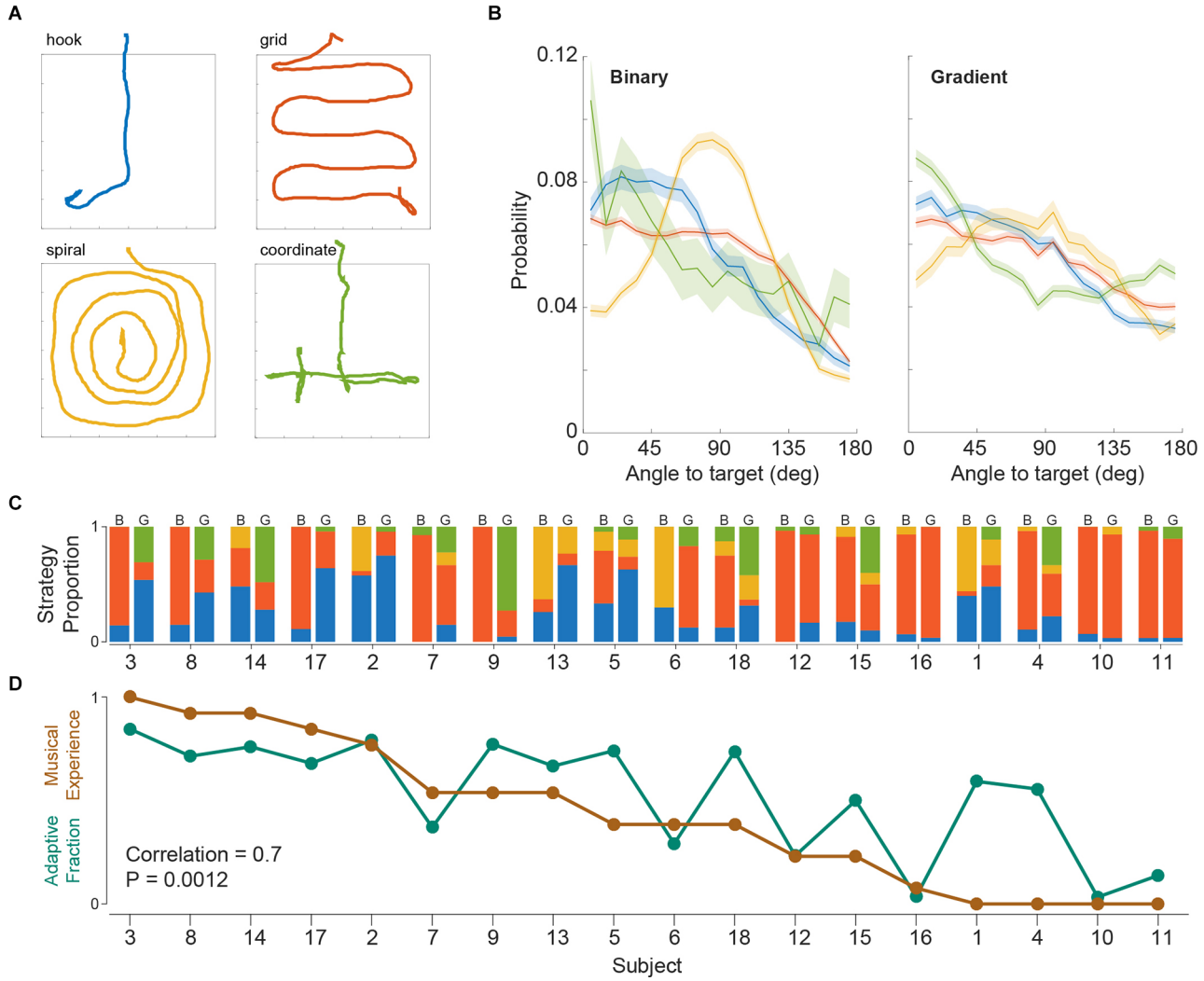

FIGURE 3 | (A) Representative trials of the four stereotypical search strategies. **(B)** Angle to target histograms across strategies (median and 95% confidence interval). **(C)** Change in strategy use as a proportion of trials across subjects. Left and right columns per subject represent binary and gradient task versions respectively. Subject order is the same as panel **(D)**. **(D)** Fraction of trials of hook + coordinate strategies (Adaptive Fraction), and normalized years of musical experience across subjects, for the gradient task.

was correlated with the auditory frequency discrimination performance and suggests that the best performance was achieved when using the coordinate strategy. Performing statistical comparisons of the coordinate vs. each of the other three strategies (Mann-Whitney *U*-tests single tail, Holm-Bonferroni corrected; $P_{\text{coordinate-hook}}$ = 4.8714e-05, $P_{\text{coordinate-grid}}$ = 8.3156e-05, $P_{\text{coordinate-spiral}}$ = 0.0214) confirmed that the coordinate strategy, which was spontaneously adopted by subjects when confronted with the gradient task, is associated with significantly better frequency discrimination performance. We further looked into whether practice influenced the choice of strategy by subjects, but did not find a pattern. Interestingly, while the use of adaptive strategies in the gradient task correlated with the musical experience across subjects (**Figure 3D**), the frequency discrimination performance on average did not (**Supplementary Figures 1A,B**). We did find a mild correlation between LFH and musical experience when including all the trials instead of comparing only with the median LFH (**Supplementary Figure 1C**). However, when removing subjects with zero musical experience (four subjects total), this correlation was lost (**Supplementary Figure 1D**).

We also compared trial duration times across strategies (**Figure 4C**; Kruskal-Wallis test, P = 5.0732e-15; Median values: hook = 16.3 s, grid = 29.1 s, spiral = 33.5 s, coordinate = 25.2 s) and observed that the fastest strategy was the hook, followed by the coordinate (Mann-Whitney *U*-tests single tail, Holm-Bonferroni corrected; $P_{\text{hook-grid}}$ = 1.9402e-13, $P_{\text{hook-spiral}}$ = 4.5475e-07, $P_{\text{hook-coordinate}}$ = 1.3890e-07, $P_{\text{coordinate-spiral}}$ = 0.0253, $P_{\text{coordinate-grid}}$ = 0.0194).

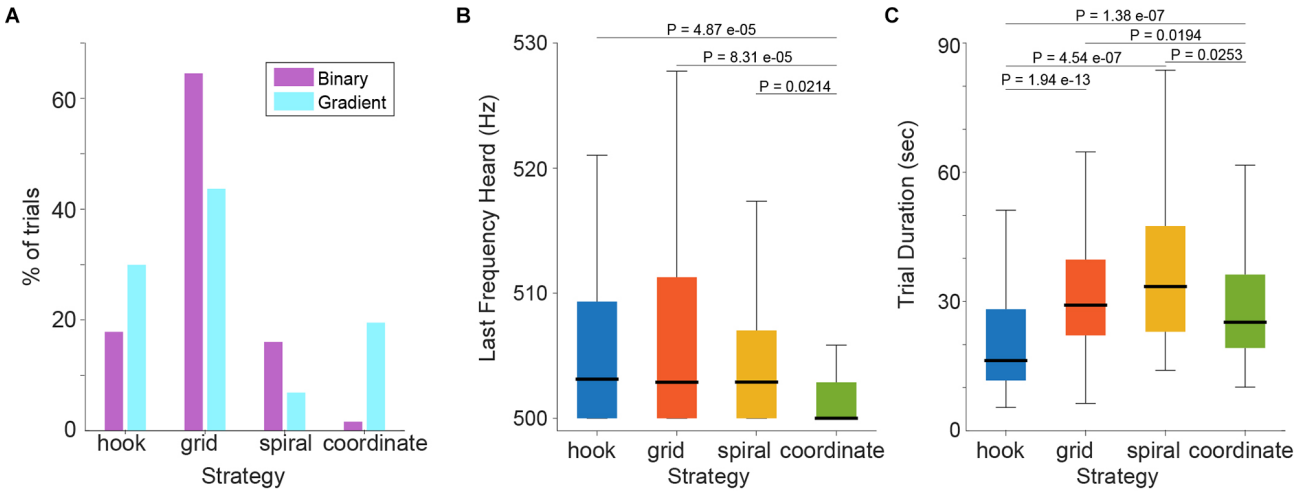

FIGURE 4 | (A) Change in strategy use as a percentage of total trials in the two task versions. **(B)** Last frequency heard by subjects and; **(C)** Trial duration across strategies, in the gradient task.

The data thus indicate that on average trials with adaptive strategies finished faster compared to non-adaptive strategy trials. Interestingly, between the two adaptive strategies, hook trials were even faster than coordinate trials, yet also showed worse frequency performance. These observations together suggest that coordinate strategy users may have invested time "subjectively verifying" the detection of the target frequency. In line with this assumption, we noticed that subjects regularly performed small probing movements (rocking or taking a step back and forth) near or inside the island to determine their perceptual discrimination threshold (i.e., they were not able to detect any further change in frequency) before pressing the button to indicate the end of the trial. Quantification of this fine-tuning behavior (respective trials were flagged by the same naive observer as for strategy classification) confirmed that it was indeed more frequent for coordinate trials during the gradient task (Fraction of trials showing fine-tuning: hook = 0.32, grid: 0.33, spiral = 0.16, coordinate = 0.5000; Chi-square test, Holm-Bonferroni corrected; $P_{\text{coordinate-hook}}$ = 0.02646, $P_{\text{coordinate-grid}}$ = 0.02465, $P_{\text{coordinate-spiral}}$ = 0.00492, $P_{\text{hook-spiral}}$ = 0.16327, $P_{\text{hook-grid}}$ = 0.75306). Thus, it appears that strategy use and resulting discrimination thresholds were also related to the likelihood to optimize trial performance. Interestingly, we also found that subjects that exhibited more trials with fine-tuning behavior also showed a tendency for lower median LFH in the gradient task (**Supplementary Figure 4A**). This tendency was present even when excluding coordinate trials (**Supplementary Figure 4B**). In contrast, no correlation was found between fine-tuning behavior and the standard deviation of the LFH (as a measure of performance variability) nor with musical experience (**Supplementary Figure 4**).

Together, the data show that performance levels in frequency discrimination obtained by using closed-loop feedback during voluntary self-motion in subjects with only a few minutes of training can match those reported using traditional forced-choice paradigms and highly trained participants (Micheyl et al., 2012). Moreover, subjects spontaneously develop various distinct locomotion strategies for task completion, which differ in their average performance outcome.

DISCUSSION

Inspired by contemporary calls to action to bring together laboratory experiments and natural ethological investigations, we investigated the potential of experimental paradigms based on closed-loop audio-motor feedback for application in human psychophysical research.

We tested a new procedure to study sensory perception in humans, which would resemble and encourage natural exploration behavior. Traditional laboratory settings usually predetermine the strategy that can be used to discriminate between stimuli and require *post-hoc* decision-making (i.e., forced-choice after having listened to all alternatives). In contrast, SITh is based on unrestricted self-motion to modulate the test stimuli and thereby allows subjective optimization of performance. Specifically, we incorporated active sensing during self-motion by coupling changes in the subjects' location within a test arena with changes in the presented sensory stimuli and allowed subjects to manipulate the stimulus until they were satisfied with their perceived performance. We focused on sound frequency discrimination, which is a well-established measure of auditory perception. To this end, we implemented a frequency gradient stimulation within an arena, which served as immediate feedback for their navigation.

Due to the attentional burden on cognitive processes imposed by the more naturalistic environment (i.e., locomotion, visual input, feedback evaluation, guided action, etc.), we expected worse discrimination thresholds for our naive subjects compared to those reported from classic experiments

with expert listeners. Surprisingly, we obtained a frequency discrimination threshold of 0.3% on average across all subjects, which matches the results from "stationary" subjects comparing tone pairs in alternative forced-choice tasks (Micheyl et al., 2012). This is surprising given that we allowed subjects only a few minutes to familiarize themselves with the task, while typically highly experienced subjects are used and longer data acquisition periods are needed. This suggests that performing unrestricted experiments might be advantageous for accessing marginal perceptual limits by allowing a range of natural behaviors that may assist the performance under investigation. Real-time sensory feedback and cross-sensory cueing have been shown to be favorable in human psychophysical experiments (Whitton et al., 2017; Clayton et al., 2021). Notably, Whitton et al. (2014) tested subjects on signal-to-noise discrimination by providing closed-loop audio-motor feedback *via* joystick control to move avatars on a screen and reported a similar fine-tuning behavior of subjects when being close to the perceptual threshold, suggesting that this behavior is naturally occurring during active sensing. Participants in our study performed actual translational movements inside an arena. This "real-word" movement may have additional advantages since self-motion and its resulting modulations may aid the interpretation of sensory cues in natural settings (Freeman et al., 2017; Willett et al., 2019).

By analyzing the locomotion behavior of the subjects, we revealed that they spontaneously adopted stereotypical navigation patterns, which we categorized into four search strategies. Interestingly, the analyzed strategies seem to differ in their use of the gradient information. The "spiral" and the "grid" strategies are characterized by systematic surface coverage at the expense of not following gradient cues, while "hook" and "coordinate" describe stimuli adapting behavior, as known to happen for head movement in sound localization (Pollack and Rose, 1967). Consistent with the ability of the strategies to incorporate the gradient cues into the navigation, subjects were more likely to use the coordinate and hook strategies after switching to the gradient condition. These two strategies were characterized before as "gradient descent" and "coordinate descent" in a signal-to-noise ratio gradient task performed by stationary humans *via* a joystick (Whitton et al., 2014). Here we find that the coordinate strategy enabled a smaller frequency discrimination threshold (**Figure 4B**), presumably because it better exploits the gradient cue, while the hook strategy is characterized by rapid (and likely less diligent) honing into the gradient descending frequencies. Accordingly, the hook strategy exhibited the shortest trial durations on average, but larger discrimination thresholds compared to the coordinate strategy. Similarly, the coordinate strategy seems to also save time compared to the systematic (non-adaptive) searches, but without sacrificing accuracy like the hook strategy. These findings can be partially explained by the differences in "fine-tuning behavior", i.e., the fraction of trials in which subjects performed small corrective movements to more exactly determine the location of the target island/last frequency heard before finishing the trial. Such behavior was significantly more frequent in coordinate trials. Accordingly, frequency discrimination thresholds were significantly smaller when using this strategy (when averaging across all subjects and trials). Moreover, a higher proportion of fine-tuning behavior tended to correlate with better discrimination performance across subjects, even when excluding the coordinate trials (**Supplementary Figure 4**). This suggests that performance during active sensing is affected both by the global search strategy and by local adjustments. In the future, it will be interesting to determine whether these advantages of strategy use also pertain to the single-subject level, i.e., do perceptual thresholds of individual subjects change significantly when restricting the search to specific strategies? Conversely, could restricting subjects to the use of a specific strategy minimize performance variability and provide further insight into the capabilities of human perception during active sensing?

Interestingly, while formal musical training has been shown to improve frequency discrimination performance (Micheyl et al., 2006), we did not find a significant gradual relationship between performance and informal musical experience (**Supplementary Figures 1A,B**). Nonetheless, our data suggests that having no musical experience entails a high likelihood of performing worse than subjects with experience (**Supplementary Figures 1C,D**). Musicality of subjects also did correlate with their choice of the search strategy. More musically experienced subjects tended to use "adaptive" strategies (i.e., "coordinate" and "hook"; **Figure 3D**). This suggests that musical experience may influence the subjects' disposition to interact with the available gradient cues, perhaps resembling the natural audiomotor feedback present while singing or playing an instrument. Given that we did not distinguish between formal and informal musical experience, it remains interesting for future studies to determine whether they exert different influences both in the active sensing behavior as well as in the frequency discrimination performance.

In summary, our results provide proof-of-concept for the suitability of SITh for conducting sensory perception studies during naturalistic active sensing behavior. Future studies on the influence of stimulation parameters (such as frequency and tone duration) on auditory perception during active sensing are readily obtainable with the current setup configuration. Furthermore, SITh allows physiological investigations of the neural mechanisms underlying auditory feedback-guided navigation by incorporating mobile EEG recordings (for an example on visual perception see Dowsett et al., 2020). Valuable insights could also be gained by comparing behavioral and physiological results obtained in real-world locomotion with cursor-based and/or virtual reality movement. Since the code to run SITh is freely available and several parameters can be readily adapted (e.g., size of the islands, stimulus parameters, free field speakers instead of headphones, etc.), the experimental paradigm provides superb versatility and should foster further research on the interplay between hearing, self-motion and its neural correlates in the future.

DATA AVAILABILITY STATEMENT

The raw data supporting the conclusions of this article will be made available by the authors, without undue reservation.

ETHICS STATEMENT

The studies involving human participants were reviewed and approved by the ethical board of the Ludwig-Maximilians-Universität medical center and carried out in accordance with the ethical principles of the world medical association for research involving human subjects (Declaration of Helsinki). The patients/participants provided their written informed consent to participate in this study.

AUTHOR CONTRIBUTIONS

DNF and MP conceived the study, designed and conducted the experiments. DNF and VRW analyzed the results. DNF designed and generated the figures. DNF wrote the first draft of the manuscript, and MP, BB, and BG made contributions. All authors contributed to the article and approved the submitted version.

FUNDING

This study was supported by the Deutsche Forschungsgemeinschaft DFG (PE2251/2-1 and DFG Priority Program 1608 to MP, and SFB 870, project B02 to MP and BG), by the European Research Council ERC under the European Union's Horizon 2020 research and innovation program (819040—acronym: rid-O, project to BB), and by the LMU BioMentoring program to DNF.

ACKNOWLEDGMENTS

We thank Tobias Hilbig for developing the software to run SITh experiments, Luca Habelt and Lukas Koller for help with data collection, Sven Schörnich for technical support and Andrey Sobolev and Matthias Kaiser for help with analyses.

SUPPLEMENTARY MATERIAL

The Supplementary Material for this article can be found online at: https://www.frontiersin.org/articles/10.3389/fnint.2022.892951/full#supplementary-material.

Supplementary Figure 1 | (A) Normalized years of musical experience. **(B)** Distribution of last frequency heard across subjects. Both panels: the subjects are ordered by ascending median LFH. Pearson correlation of musical experience and median LFH: rho = -0.38; p = 0.12. **(C)** Pearson correlation of musical experience and LFH across all trials. **(D)** Same as **(C)** but removing four subjects with zero musical experience.

Supplementary Figure 2 | (A) Location of all the islands by task. **(B)** Location of the islands in the gradient task by the strategy used in the corresponding trial.

Supplementary Figure 3 | The first 2 s of the subjects' path for every gradient trial, separated by strategy. The black line depicts the border closest to the starting point. Note that strategy-specific trajectories can be observed even before having sensory feedback (i.e., before crossing the black line).

Supplementary Figure 4 | Fine-tuning behavior tends to correlate with discrimination performance when analyzing all trials **(A)** and when excluding coordinate trials **(B)**. Panels depict the correlation of fine-tuning proportion with normalized musical experience, median last frequency heard or standard deviation of the last frequency heard as a measure of the variability of the performance, respectively. Each dot represents a subject. All panels, y axis: proportion of gradient trials which showed fine tuning behavior. Pearson correlation coefficient and p-values are given in the figure.

REFERENCES

Aickin, M., and Gensler, H. (1996). Adjusting for multiple testing when reporting research results: the Bonferroni vs. Holm methods. *Am. J. Public Health* 86, 726–728. doi: 10.2105/ajph.86.5.726

Amaro, D., Ferreiro, D. N., Grothe, B., and Pecka, M. (2021). Source identity shapes spatial preference in primary auditory cortex during active navigation. *Curr. Biol.* 31, 3875–3883.e5. doi: 10.1016/j.cub.2021.06.025

Box-Steffensmeier, J. M., Burgess, J., Corbetta, M., Crawford, K., Duflo, E., Fogarty, L., et al. (2022). The future of human behaviour research. *Nat. Hum. Behav.* 6, 15–24. doi: 10.1038/s41562-021-01275-6

Clayton, K. K., Asokan, M. M., Watanabe, Y., Hancock, K. E., and Polley, D. B. (2021). Behavioral approaches to study top-down influences on active listening. *Front. Neurosci.* 15:666627. doi: 10.3389/fnins.2021.666627

Datta, S. R., Anderson, D. J., Branson, K., Perona, P., and Leifer, A. (2019). Computational neuroethology: a call to action. *Neuron* 104, 11–24. doi: 10.1016/j.neuron.2019.09.038

Dowsett, J., Dieterich, M., and Taylor, P. C. J. (2020). Mobile steady-state evoked potential recording: dissociable neural effects of real-world navigation and visual stimulation. *J. Neurosci. Methods* 332:108540. doi: 10.1016/j.jneumeth.2019.108540

Ferreiro, D. N., Amaro, D., Schmidtke, D., Sobolev, A., Gundi, P., Belliveau, L., et al. (2020). Sensory island task (SIT): a new behavioral paradigm to study sensory perception and neural processing in freely moving animals. *Front. Behav. Neurosci.* 14:576154. doi: 10.3389/fnbeh.2020.576154

Freeman, T. C. A., Culling, J. F., Akeroyd, M. A., and Brimijoin, W. O. (2017). Auditory compensation for head rotation is incomplete. *J. Exp. Psychol. Hum. Percept. Perform.* 43, 371–380. doi: 10.1037/xhp0000321

Gomez-Marin, A., and Ghazanfar, A. A. (2019). The life of behavior. *Neuron* 104, 25–36. doi: 10.1016/j.neuron.2019.09.017

Holm, S. (1979). A simple sequentially rejective multiple test procedure. *Scand. J. Stat.* 6, 65–70. doi: 10.2307/4615733

Krakauer, J. W., Ghazanfar, A. A., Gomez-Marin, A., MacIver, M. A., and Poeppel, D. (2017). Neuroscience needs behavior: correcting a reductionist bias. *Neuron* 93, 480–490. doi: 10.1016/j.neuron.2016.12.041

Lorenz, K. Z. (1981). "How unitary is "An Instinct"?," in *The Foundations of Ethology*, ed K. Z. Lorenz (Vienna: Springer), 211–220.

Micheyl, C., Delhommeau, K., Perrot, X., and Oxenham, A. J. (2006). Influence of musical and psychoacoustical training on pitch discrimination. *Hear. Res.* 219, 36–47. doi: 10.1016/j.heares.2006.05.004

Micheyl, C., Xiao, L., and Oxenham, A. J. (2012). Characterizing the dependence of pure-tone frequency difference limens on frequency, duration and level. *Hear. Res.* 292, 1–13. doi: 10.1016/j.heares.2012.07.004

Moore, B. C. (1973). Frequency difference limens for short-duration tones. *J. Acoust. Soc. Am.* 54, 610–619. doi: 10.1121/1.1913640

Pollack, I., and Rose, M. (1967). Effect of head movement on the localization of sounds in the equatorial plane. *Percept. Psychophys.* 2, 591–596. doi: 10.3758/BF03210274

Stecker, G. C. (2021). Auditory cortex: representing sound locations during active sensing. *Curr. Biol.* 31, R1042–R1044. doi: 10.1016/j.cub.2021.07.007

Tinbergen, N. (1963). On aims and methods of ethology. *Z. Für Tierpsychol.* 20, 410–433. doi: 10.1111/j.1439-0310.1963.tb01161.x

Whitton, J. P., Hancock, K. E., and Polley, D. B. (2014). Immersive audiomotor game play enhances neural and perceptual salience of weak signals in noise. *Proc. Natl. Acad. Sci. U S A* 111, E2606–E2615. doi: 10.1073/pnas.1322184111

Whitton, J. P., Hancock, K. E., Shannon, J. M., and Polley, D. B. (2017). Audiomotor perceptual training enhances speech intelligibility in background noise. *Curr. Biol.* 27, 3237–3247.e6. doi: 10.1016/j.cub.2017.09.014

Willett, S., Groh, J., and Maddox, R. (2019). "Hearing in a "Moving" visual world: coordinate transformations along the auditory pathway," in *Multisensory Processes, Springer Handbook of Auditory Research*, Vol. 68, eds A. Lee, M. Wallace, A. Coffin, A. Popper and R. Fay (Cham: Springer), 85–104. doi: 10.1007/978-3-030-10461-0_5

Conflict of Interest: The authors declare that the research was conducted in the absence of any commercial or financial relationships that could be construed as a potential conflict of interest.

frontiers | Frontiers in Neural Circuits

ORIGINAL RESEARCH
published: 13 June 2022
doi: 10.3389/fncir.2022.893004

The Role of Central Complex Neurons in Prey Detection and Tracking in the Freely Moving Praying Mantis (*Tenodera sinensis*)

Anne Wosnitza[1], *Joshua P. Martin*[2]*, *Alan J. Pollack*[1], *Gavin J. Svenson*[3] and *Roy E. Ritzmann*[1]

[1] Department of Biology, College of Arts and Sciences, Case Western Reserve University, Cleveland, OH, United States, [2] Department of Biology, Colby College, Waterville, ME, United States, [3] Cleveland Museum of Natural History, Cleveland, OH, United States

Complex tasks like hunting moving prey in an unpredictable environment require high levels of motor and sensory integration. An animal needs to detect and track suitable prey objects, measure their distance and orientation relative to its own position, and finally produce the correct motor output to approach and capture the prey. In the insect brain, the central complex (CX) is one target area where integration is likely to take place. In this study, we performed extracellular multi-unit recordings on the CX of freely hunting praying mantises (*Tenodera sinensis*). Initially, we recorded the neural activity of freely moving mantises as they hunted live prey. The recordings showed activity in cells that either reflected the mantis's own movements or the actions of a prey individual, which the mantises focused on. In the latter case, the activity increased as the prey moved and decreased when it stopped. Interestingly, cells ignored the movement of the other prey than the one to which the mantis attended. To obtain quantitative data, we generated simulated prey targets presented on an LCD screen positioned below the clear floor of the arena. The simulated target oscillated back and forth at various angles and distances. We identified populations of cells whose activity patterns were strongly linked to the appearance, movement, and relative position of the virtual prey. We refer to these as sensory responses. We also found cells whose activity preceded orientation movement toward the prey. We call these motor responses. Some cells showed both sensory and motor properties. Stimulation through tetrodes in some of the preparations could also generate similar movements. These results suggest the crucial importance of the CX to prey-capture behavior in predatory insects like the praying mantis and, hence, further emphasize its role in behaviorally and ecologically relevant contexts.

Keywords: predator, central complex, target detection, movement control, praying mantis, extracellular recording

OPEN ACCESS

Edited by:
M. Jerome Beetz, Julius Maximilian University of Würzburg, Germany

Reviewed by:
Uwe Homberg, University of Marburg, Germany
Stanley Heinze, Lund University, Sweden
Vivek Nityananda, Newcastle University, United Kingdom

***Correspondence:**
Joshua P. Martin
jpmartin@colby.edu

Received: *09 March 2022*
Accepted: *12 May 2022*
Published: *13 June 2022*

Citation:
Wosnitza A, Martin JP, Pollack AJ, Svenson GJ and Ritzmann RE (2022) The Role of Central Complex Neurons in Prey Detection and Tracking in the Freely Moving Praying Mantis (Tenodera sinensis). Front. Neural Circuits 16:893004. doi: 10.3389/fncir.2022.893004

INTRODUCTION

Complex movements, even in supposedly simple animals like insects, are influenced by various brain circuits. This can include sensory-guided movements such as a locust walking on discontinuous substrates (Niven et al., 2010), learned behaviors (Ofstad et al., 2011), navigational behaviors such as path integration (Green et al., 2017; Stone et al., 2017; Turner-Evans et al., 2017),

and foraging movements in an arena (Martin et al., 2015). The central complex (CX) is a brain region that has received attention for its role in controlling complex behaviors (Pfeiffer and Homberg, 2014). This highly conserved set of midline neuropils includes the protocerebral bridge (PB), fan-shaped body (FB) [also called the upper central body (CBU)], ellipsoid body (EB) [also called the lower central body (CBL)], and two paired noduli (**Supplementary Figure S1**). The PB, FB, and EB are unique for being divided into distinct columns or wedge structures that have been found to include spatial information used in navigation. Considerable information is now available about sensory inputs to these neuropils. Much of the data have focused on detection of polarized light (Heinze et al., 2009). Polarized light-sensitive cells in locusts project to the PB in a regular manner that describes a map of polarized sky light (Heinze and Homberg, 2007). Polarized light mapping has also been reported in numerous other insects including dung beetles (el Jundi et al., 2015), monarch butterflies (Heinze and Reppert, 2011), and *Drosophila* (Warren et al., 2019). In addition, non-polarized directional light responses were found in locusts (Rosner and Homberg, 2013; Pegel et al., 2018), cockroaches (Kathman et al., 2014), *Drosophila* (Seelig and Jayaraman, 2013), and monarch butterflies (Heinze and Reppert, 2011). Mechanical inputs from the antennae have been documented in cockroaches (Ritzmann et al., 2008) and flies (Currier et al., 2020; Okubo et al., 2020) as well as from halteres of flies (Kathman and Fox, 2019).

The directional properties in sensory studies have led to consideration of navigational control that has uncovered head direction cells in *Drosophila* (Seelig and Jayaraman, 2015) and cockroach (Varga and Ritzmann, 2016). In addition, the existence of ring attractor pathways between the PB and EB have been demonstrated in *Drosophila* that can integrate angular motion and external visual compass cues into a coherent head direction signal. This signal can be used as one of the inputs to a path integrator (Green et al., 2017; Turner-Evans et al., 2017). Indeed, a path integration model has been developed based on CX recordings and structures in bees (Stone et al., 2017).

Any kind of navigational control requires that the CX affects motor systems, and motor effects have been demonstrated in the CX. Genetic manipulations that resulted in damage to the PB resulted in walking deficits (Strauss, 2002). Extracellular recordings from tethered cockroaches revealed CX neurons that control step frequency (Bender et al., 2010) and turning movements toward a target (Guo and Ritzmann, 2013). In freely walking cockroaches, such recordings revealed several neurons that are active just before turning or forward acceleration (Martin et al., 2015). These data contributed to 2 dimensional maps of forward movement or turning associated with each neuron. The overlap among 2D representations of CX cells suggests a population code that can influence movement in any direction. This control occurs at least in part by altering reflexes to specific joints in the thoracic ganglia (Martin et al., 2015).

Navigational studies suggest that the CX serves to control directional motion. Indeed, a recent study indicates that it plays a role in goal-directed movements (Green et al., 2019). As important as this study was in revealing moment-to-moment neural adjustments, it implied that the fly was moving toward a goal by the fact that it maintained a specific angular bearing as it walked (menotaxis). This is in contrast to recordings in bats that revealed goal-directed cells in the hippocampus that signal the bat's heading toward the location of a specific goal (Sarel et al., 2017).

Predatory insects such as praying mantises (Prete, 1999) and dragonflies (Olberg et al., 2005; Mischiati et al., 2015) provide systems that are similar but different from the above-described navigational behaviors. Rather than foraging movements followed by return to a nest, predators must target a specific easily-identified goal and move toward that goal before making a very precise strike. Failure to precisely guide movements toward the prey means that predators will not eat. Praying mantises employ a unique 3-dimensional visual system to establish distance parameters (Nityananda et al., 2018). Neural correlates for this stereopsis have been identified in the mantis brain (Rosner et al., 2019). For various mantis species, a range of visual stimulus parameters including, among others, size, background contrast, leading edge length, speed, location in the visual field, and relative direction of movement evokes predatory responses (Prete et al., 2011). Regardless of cues, the praying mantis uses this information to stalk and eventually strike the prey. The actual hunting strategy varies among species from active stalking (Prete et al., 2012) to ambush (Inoue and Matsura, 1983). In the so-called "generalist" species, the hunting strategy can switch from stalking to ambush as the praying mantis feeds (Inoue and Matsura, 1983; Bertsch et al., 2019), and the switch can be mimicked by injection of insulin (Bertsch et al., 2019).

Various components of the praying mantis hunting strategy imply considerable high-level control, much of which is reminiscent of navigational control properties seen in other insects. The visual guidance necessary for tracking should rely on neurons that are tuned to specific azimuth angles around the insect's head. Such neurons have been shown to be present in the CX of locusts (Pegel et al., 2018), monarch butterflies (Heinze and Reppert, 2011), and dung beetles (el Jundi et al., 2015). Directed movements are reminiscent of cockroach motor control (Guo and Ritzmann, 2013; Martin et al., 2015) although much more precise. Even the hormonal control of changes in hunting strategy by satiety and insulin suggests modulatory properties such as those seen in the CX of locusts (Nässel and Homberg, 2006) and *Drosophila* (Kahsai et al., 2010). If the sensorimotor control of praying mantis hunting can be shown to be controlled in the CX, it would be possible to directly examine the neural control of both the precise sensory and motor aspects of this behavior in CX neuropils as well as the necessary sensorimotor transformations and context dependent modifications that might occur there.

To examine the role of the CX in predation, we recorded extracellularly from the CX of freely moving praying mantises (*Tenodera sinensis*) as they stalked prey. We began with live prey to establish that CX activity is associated with real predatory behaviors. We then developed a simulated prey system that allowed us to generate reproducible targets around the mantis for quantitative analysis of both sensory and motor aspects of the behavior. In both situations, our recordings revealed units that fired in response to prey or moving targets presented at specific angles and distances around the subject, as well as neurons that

became active just before turning or forward motion. These data suggest that neurons in the CX could control the hunting and targeting movements of the mantis. Some neurons appeared to be involved in both sensory and motor aspects of the targeting behavior. Thus, the CX does appear to play a role in controlling the predatory behaviors in this species of praying mantis.

METHODS

Adult praying mantises (*Tenodera sinensis*) from a laboratory colony were used in all the experiments. The mantises were housed in individual plastic containers and given food and water *ad libitum*. They were kept in a 12/12-h light/dark cycle at 27°C. After the final molt, only 14- to 17-day-old healthy females were chosen for the experiments.

Animal Preparations and Recording

The insects were first anesthetized with ice. After they stopped moving, they were restrained ventral side down against a flat silicone surface with insect pins bent into a hook that surrounded them but did not penetrate any part of them. A plastic collar was positioned around the neck to support the head, and dental wax was placed around the head to stabilize it. The preparation was transferred into a plastic container, and ice was placed around the animals to minimize hemolymph flow and body movements, which could interfere with wire implantation. A small window between the antennae was cut into the cuticle and removed over the brain. Connective tissues and fats were carefully removed to expose the brain. The sheath surrounding the brain was opened mechanically in a small area dorsal to the central complex, and a small amount of saline (Blagburn and Sattelle, 1987) was placed in the head capsule to cover the brain tissue.

One or two wire-bundle tetrodes were used for recording. Each tetrode consisted of four 12-μm nichrome wires (Kanthal RO-800; Sandvik Heating Technology, Hallstahammar, Sweden) twisted together. The tetrode wires were connected to an adaptor and secured in a Delrin and epoxy package. Before each experiment, the tip of each tetrode was cut, polished, and plated with copper such that it had a regular arrow shape and starting impedance of between 0.5 and 1.5 MΩ.

With the brain exposed, the tetrode was inserted into the brain with a micromanipulator, and the adaptor was mounted in the headstage of a Neuralynx Cheetah (Bozeman, MT, United States) digital interface. A separate larger-diameter (56 um) insulated copper wire was inserted into an anterior location in the pronotum to serve as a reference/ground electrode. The tetrode was fixed in the brain at the location that had the best signal:noise ratio and where the units responded to sensory stimuli (i.e., light on or off and/or antennal contact). The head capsule was then covered and sealed with blue-light curable clear glue (Loctite 3,555 transparent Light Cure Adhesive) to anchor the tetrode wires in place, taking care to not obscure the compound eyes and ocelli. A plastic tether was glued to the posterior pronotum and the tetrode (s), and the reference electrode was secured along the pronotum and the tether with the same glue as used on the head as well as with dental wax. Next, constraints were carefully removed, and the animals were transferred into a clear acrylic arena positioned on top of an LCD screen. The animals were given at least 60 min to recover from the cold anesthesia. All the experiments lasted between 2 and 4 h depending on the quality of the neural recordings and preparation.

Videos were either captured at 30 or 120 frames s^{-1} with a Casio Exilim HS camera or at 40 or 100 frames s^{-1} with a Point Gray video camera. The cameras were positioned centrally above the arena so that the entire arena was visible and all movements could be seen. The position of the live or simulated prey and the mantises' head and body position and orientation in the arena were tracked using the DLT tracking software from MATLAB (Hedrick, 2008). From the position and orientation of the mantis' head, the visual field could be defined, and the angular position, size, and velocity of the prey in the field were measured. This allowed us to correlate the stimulus movement to the resulting electro-physiological and locomotor responses.

The data from the Neuralynx system were saved directly to a PC. For each electrode, the collected data included voltage waveforms and time stamps that marked the point in time where an action potential that exceeded a pre-set threshold occurred within a given data file. The data also included synchronization pulses to link the Neuralynx time with coincident high-speed digital video recordings.

Live Prey Experiments

After the tetrodes were placed in the their brain, the subjects were placed in an arena and allowed to recover. Up to 4 cockroach nymphs were then placed in the arena, and both the mantises and the prey were allowed to move freely while their activity was recorded from the tetrodes. Movements were recorded with the camera situated above the arena. Frame-by-frame movements of both the prey and the mantises were quantified offline. After the spikes recorded from the tetrode had been sorted (see below), individual unit time stamps could then be associated with either the mantises' movement or a prey individual that a mantis was targeting.

Simulated Prey System

In order to obtain quantitative data relating brain activity to movement, we developed a simulated prey system that could generate targets at reproducible distances and angles around the mantis' head. Using a computer screen under the transparent arena floor, we could exploit previous observations that praying mantises would target and strike at moving images on a computer screen (Prete et al., 2013). We reasoned that placing a computer screen under the floor of the arena would allow us to repeatedly present the subject with simulated prey at predetermined distances and angles. A custom MATLAB routine generated the simulated prey at various angles around the subject at preset distances. The circle in which the simulated prey appeared could be moved on the screen so that the praying mantis was always kept in the center of the presentations. The simulated prey consisted of a 2 × 1 cm black ellipse that moved back and forth in parts of the circle with the mantis in the center. The target moved at 2 cm/s (**Supplementary Video S1**).

Again, CX activity was recorded from 1 or 2 tetrode bundles that were inserted into the brain targeting the

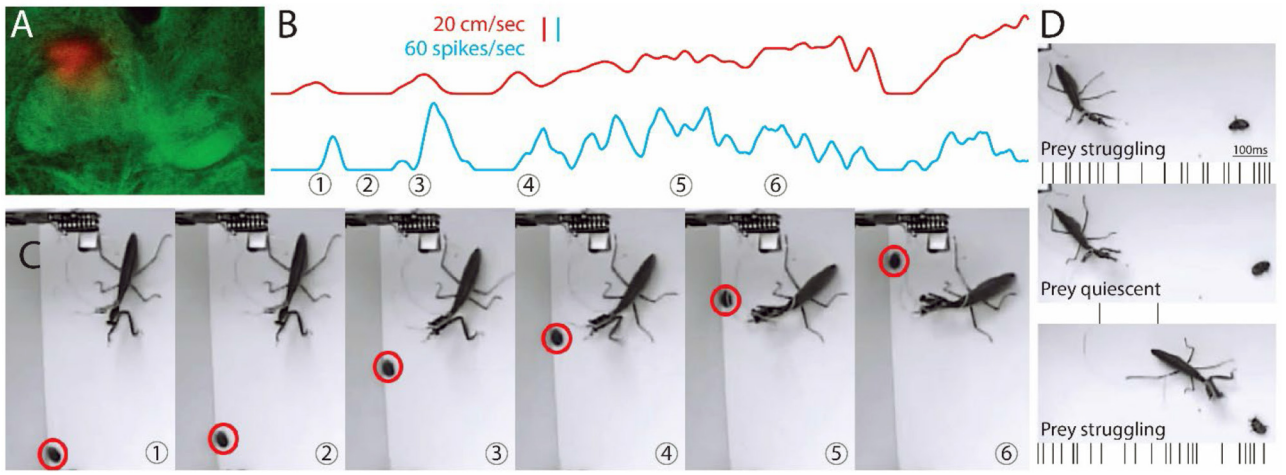

FIGURE 1 | Images from video and recording of a single unit during hunting behavior. **(A)** Location of a tetrode is shown in the dorsal region of the FB on the mantis's right side. **(B)** Shows the activity of the cell (blue) along with the movement of the prey (red). **(C)** Sample frames from **Supplementary Video S1** are shown with time of frame numbers indicated in **(B)**. **(B,C)** Prey starts to move in first frame. Central complex (CX) unit activity increases and then stops when the prey stops (2nd frame). In frame 3, the prey runs as the mantis tracks it, and CX unit activity increases and is maintained through frame 6. Before the mantis tracks the prey, the single CX unit is correlated with mantis movement ($r > 0.7$, sliding Pearson's coefficient). After the mantis orients toward the prey, the same unit is correlated ($r > 0.7$) with prey movement. **(D)** Another prey is on its back and struggles (top) and then stops (middle) and struggles again just before the strike. Activity, shown here as spikes below each frame, is parallel to movement.

CX. In all, we recorded 99 units from 10 preparations where the tetrode location could be determined histologically (**Supplementary Figure S1**). Eight of the preparations used a single tetrode implant. The remaining 2 preparations had 2 tetrodes inserted for a total of 12 tetrode locations. Eight of these tetrodes (68 units) were located in the FB of the CX, while 4 (31 units) were located in the mushroom body (MB). Two of the MB placements were in the peduncle and two in the medial lobe. Because there were few MB recordings, we did not analyze them further but present the data and some contour plots (**Supplementary Figure S3**) for completeness.

The high-speed video camera placed above the arena monitored the praying mantis's movements relative to the simulated prey. When the praying mantis attended to the prey, it turned its head toward the target. This action could include neck movements, rotation of the T1-T2 thoracic joint, or very large turns including leg movements that rotated the body toward the prey. We digitized the movements of the praying mantis and the simulated prey and combined the records with the sorted activity of single CX units. In some preparations, we also injected currents through the tetrodes at the end of the experiment and monitored resulting mantis movements.

The praying mantises readily targeted, stalked, and struck the simulated prey appearing 2.5, 5, 7.5, 10, and 12.5 cm from them. Beyond 12.5 cm, the attention dropped off. We suggest that this was because the flat screen image on the floor was no longer seen by the subject. In support of this, another study using the same arena showed no similar drop off to presentation of a dead cockroach nymph that provided a 3-dimensional image.

Spike-Sorting Analysis

A single unit analysis was performed off-line in Spike2 v7.15 (CED, Cambridge United Kingdom). To sort multi-unit activities into single unit activities, we conducted user-supervised semi-automated tetrode template matching and K-means assisted principal component analysis. Clusters with > 3% of all spike events falling within the 2-ms inter-spike-interval criterion were excluded from analysis, because this suggested that we were not monitoring a single unit. Only single-unit activity with stable amplitude was used for later analyses. Time stamps of all the units were exported and loaded into custom MATLAB scripts for further analysis.

Analysis of Spike Activity Relative to Target and Mantis Movements

Once we obtained the time stamps for each unit, they could then be analyzed relative to target movement or that of the mantis toward the target. In the case of live prey trials (e.g., **Figure 1**), this involved comparing the unit's spike frequency to the prey's movement velocity. In trials involving simulated targets, a much more involved analysis (described below) related spike activity to target movement and/or to the mantis's own movement. In either case, the simulated trial analysis relied on two steps. First, raster plots were constructed relative to the action that was being examined (target or mantis movement). Then, in order to achieve statistical significance in the relationship between spike activity and either target or mantis movement, the data were subjected to spatial temporal receptive field (STRF) analysis of movement.

Analysis of the responses of each identified unit (neuron) proceeded from the aligned time stamp vectors of spikes in each

cell and the per-frame location in Cartesian coordinates of the mantis's head and prothorax, and the prey. The angle between the head and the prothorax ("head angle") was calculated from the angle between a line defined by points on the outer edge of each eye and another line defined by points on the prothorax at the neck joint and the joint of the mesothorax.

To describe the prey stimulus, we first translated and rotated the cartesian coordinates of the head and a point at the center of the prey target to center the head in the new coordinate frame and align the center of the visual field along the positive y-axis. This allowed us to continually represent the location of the prey relative to the visual field of the mantis in every frame of the video, as the mantis moved and turned its head during the trial. In this new coordinate frame, we calculate the Euclidean distance between the prey and the mantis's head ("prey distance") and the angular location of the prey in the visual field ("prey angle").

We produced raster plots and peri-stimulus time histograms (PSTHs) describing the neuron's response to two stimuli: the prey angle and the head angle. For the head angle raster plots, we used a threshold of 2 standard deviations (SDs) above the mean head angle velocity to identify the time when saccades were initiated. For the prey angle plots, we selected a particular visual angle for each cell (see below and in Results for details on how this angle was chosen). The rasters and PSTHs were triggered at the time a head saccade began or when the prey crossed the chosen angle. We calculated the mean of the instantaneous firing rate over all events for each stimulus type using a bootstrapping procedure to calculate a 95% confidence interval (2 SDs). To determine whether a cell responds to the stimulus, we used a threshold procedure. We randomly selected segments of the spike time vector of the same length as the event window (1 s) and the same number of segments as recorded events. We calculated the mean and SD of the firing rate across the segments and defined a threshold of the mean $\pm$ 2 SDs.

To fully characterize the responses of the cells to both the animal's own movement and the visual stimulus of the prey, we used a reverse correlation technique designed for natural stimuli (Theunissen et al., 2001) (see also http://www.strflab.berkeley.edu/), briefly summarized here and in detail below. This method estimates the correlation between a stimulus and the spiking activity of a neuron using a generalized linear model. The model is statistically verified by minimizing the mean squared error between the predicted response to a test portion of the recording and the recorded response. Because we are extending this method to a freely moving animal, the stimulus and response of the animal are necessarily non-random and autocorrelated, increasing the possibility of false-positive correlations. We, therefore, additionally validated the statistical significance of a neuron's response using a shuffle procedure, offsetting the stimulus and response in time, to generate the expected value and standard deviation of correlations attributable to chance.

The reverse correlation method estimates the spatiotemporal receptive field (STRF) for linear-nonlinear models of neurons (**Supplementary Figure S2**). Spike times were binned for each video frame to match the sampling rate of the stimuli. The prey position, in head-centered coordinates, was binned into a 31 $\times$ 31 matrix for each frame. The head velocity was binned into a 21 $\times$ 1 vector covering the range of observed head velocities from right (negative bins) to left (positive bins) saccades. For each frame, the bins for the current prey location (x,y; cm) and head velocity (rad/s) are occupied by a 1 and the remainder by zeros.

The response of each neuron to this combined prey and head movement stimulus matrix was estimated using a generalized linear model. The model incorporates a linear transformation of the stimulus by an STRF, followed by an exponential (Poisson) nonlinearity [modified from Talebi and Baker (2012)]:

$$w(t) = \sum_{i=1}^{M} \sum_{j=1}^{N} \sum_{k=1}^{O} h(i,j,k)\, s(i,j,k-)$$

$$r(t) = e^{w}$$

where s(i,j,k) = the stimulus matrix (size M,N) for the i,jth "pixel" at the kth delay (in frames); h(i,j,k) is the corresponding linear filter (STRF) weight; w(t) = response of the linear filter as a function of time (t); r(t) = estimated model response as a function of time (t). We conducted scaled conjugate gradient optimization, implemented in the strflab interface, to optimize the STRF weights h(i,j,k) and minimize the mean squared error between the estimated model response r(t) and the response measured from the neuron. Delays were chosen to cover time lags from $-$0.5 to 0.5 s.

The STRF was separated into a prey location matrix of 31 $\times$ 31 $\times$ 16 and a head velocity matrix of 31 $\times$ 16. The weight values can be analogized to positive or negative correlation between either the prey location or the head velocity stimulus and a spike at the 0-time delay. To establish a threshold for significant correlation, we used a shuffle procedure. The stimulus and spiking response vectors were each shifted by a random amount, removing the temporal correlation between them but preserving the temporal characteristics of each. STRFs were fitted to the shuffled data. This process was repeated 10 times, and the mean and SD of the STRF weights was calculated. We used a significance threshold of mean weight $\pm$2 SD for each bin of the STRF matrix. These were presented as contour plots surrounding contiguous bins that exceeded the threshold for each time delay.

Because prey movement and head saccades to center the prey in the visual field are naturally correlated, we performed additional analyses to characterize the responses of the cells. We filtered out periods of the recording where head movement and prey movement overlapped by 0.5 s to isolate data where the head or the prey were moving alone. We then produced STRFs for the "head alone" and "prey alone" data subsets. Only cells with STRFs that still exceeded the threshold in one or both of the alone conditions were identified as head-movement selective or prey-movement selective.

Finally, for each cell with STRF weights that exceeded the threshold, we identified the maximum weight across all delays. We plotted the time series of the weights at this maximum prey position or head velocity across all delays. The same thresholding procedure was used to identify periods of significant correlation in the time series. Points to the left of zero represent movement

that occurs preceding spikes, and points to the right represent movement that follows spiking. This means that unlike the raster displays that showed spike activity relative to target or mantis movement at the 0 point, in STRF plots, change in spike activity was taken as the zero point, and movement was plotted before and after that point. Therefore, for example, if target movement was being analyzed, a positive peak to the left of zero would indicate that the unit showed an increase in activity after the target moved. A negative peak would suggest that the unit activity decreased after the target moved. Either of these results would be consistent with a sensory response to the target movement. In contrast, a significant peak to the right of the zero point would suggest that the increase in spike activity in that unit preceded the movement. This occurred when analyzing activity changes relative to the mantis's own movement (such as toward the target) and suggested that the cells could be involved in generating such movements.

We examined the STRF plots relative to presentations at numerous angles and distances around the mantis and then displayed them as contour plots relative to the mantis's head (e.g., **Figures 2C,D**). Positive increases were plotted as brown regions and negative changes as blue regions. Delays in STRF plot peaks relative to the zero point were coded as variations in blue or brown color, as indicated in a legend for the plot.

Histology

Prior to insertion, the tip of the tetrodes was dipped into DiI (DiCarlo et al., 1996), so that its location in the brain could be established histologically after the experiment. Additionally, at the end of each experiment, a 5-mA, 5-ms DC current was applied between the tetrode wires and the reference electrode in order to deposit copper at the recording sites. The brains were then removed and placed in a 20% ammonium sulfide/saline solution for 15 min to precipitate the copper and then rinsed twice in 0.1 M phosphate-buffered saline (PBS). After fixation with 4% paraformaldehyde and 0.25% glutaraldehyde, the brains were again rinsed twice in PBS and dehydrated in an increasing ethanol series (50, 70, 90, 95, and 2 × 100%, 20 min each). The brains were then transferred to a mixture of methyl salicylate and ethanol (1:1), followed by 100% methyl salicylate (45–60 min each). Finally, the brains were mounted in a DPX mounting medium (Electron Microscopy Sciences) between two glass cover slides separated by spacing rings to avoid compression. Whole mounts were scanned with a confocal laser microscope (Leica TCS SP8 gated STED) equipped with a 10× objective (HC PL APO 10×/0.4 dry CS; Leica, Bensheim, Germany) to determine the location of DiI 488 in the brain. Confocal stacks were analyzed offline with the ImageJ software (Schindelin et al., 2012).

In cases where the fluorescent whole mount preparation gave inconclusive results, the copper method was used. The mounting medium was removed using xylene. The brains were then embedded in Paraplast and sectioned at 12 um. The sections were run by Timm's sulfide-silver intensification (Tyrer and Bell, 1974) and then fixed, dehydrated, and covered for imaging. Concentrated brownish deposits occurring in several adjacent serial sections were identified as tetrode locations. Copper deposits coupled with DiI provided strong localization of tetrode locations.

RESULTS

CX Unit Activity With Live Prey

We implanted a set of tetrode wires into the brain of 4 individual praying mantises, targeting the CX and then, after a period of recovery, released the subjects into an arena with 4 cockroach nymphs that provided natural targets. CX activity was sorted into individual units, and their activity was examined relative to prey movement. In the example shown in **Figure 1**, the tetrode was located in the dorsal right FB (**Figure 1A**). Initially, the activity in the unit shown here increased in association with the praying mantis's turns or forward movements (**Supplementary Video S2**). This pattern was consistent with what had been seen previously for cockroach (Martin et al., 2015). The praying mantis eventually began to attend to one of the prey. When this occurred, the same unit's activity increased now in conjunction with prey movement (**Figures 1B,C** and **Supplementary Video S1**). Later, the praying mantis attended to a cockroach nymph that was on its back and struggling to right itself. As long as the prey struggled, the CX neuron was active (**Figure 1D**). However, when the nymph ceased movement, the CX neuron became silent and only returned to activity when the nymph began struggling and continued as the praying mantis stalked and ultimately struck the nymph. Interestingly, as the stalking took place, another nymph walked through the praying mantis's field of view and was ignored by the CX unit that was reporting on the first prey's movements, suggesting a form of selective attention. The recordings for this preparation yielded 8 units, and 3 of these had similar responses to prey movement. The other three preparations yielded 2 out of 5, 1 of 4, and 2 of 6 prey responsive units.

Selective Responses to Simulated Prey Position

In order to obtain quantitative data on CX activity relative to mantis stalking behavior, we switched from live prey to the simulated prey system. As indicated in Methods, these experiments were performed on 10 different praying mantises using a total of 12 tetrode implants. The involvement of CX units in prey stalking requires three properties. First, CX units must be seen to track prey at various distances and angles around the mantis. Second, CX units must show indications that they control movement, as has been demonstrated in cockroach (Martin et al., 2015). Third, at least some CX units should be seen to be associated with actual orientation movements toward a tracked target. We will begin our analysis with activity associated with tracking prey.

Figure 2 shows data from a unit recorded in the left FB (**Figure 2A**) during several simulated prey presentations at various angles around the subject's head. Rasters of recordings from this unit are shown from one simulated prey position (**Figure 2B**). The stimulus moved slowly back and forth at 2 cm/sec. The resulting activity from the unit is lined up according to a zero point as the stimulus passed in front of the mantis's field

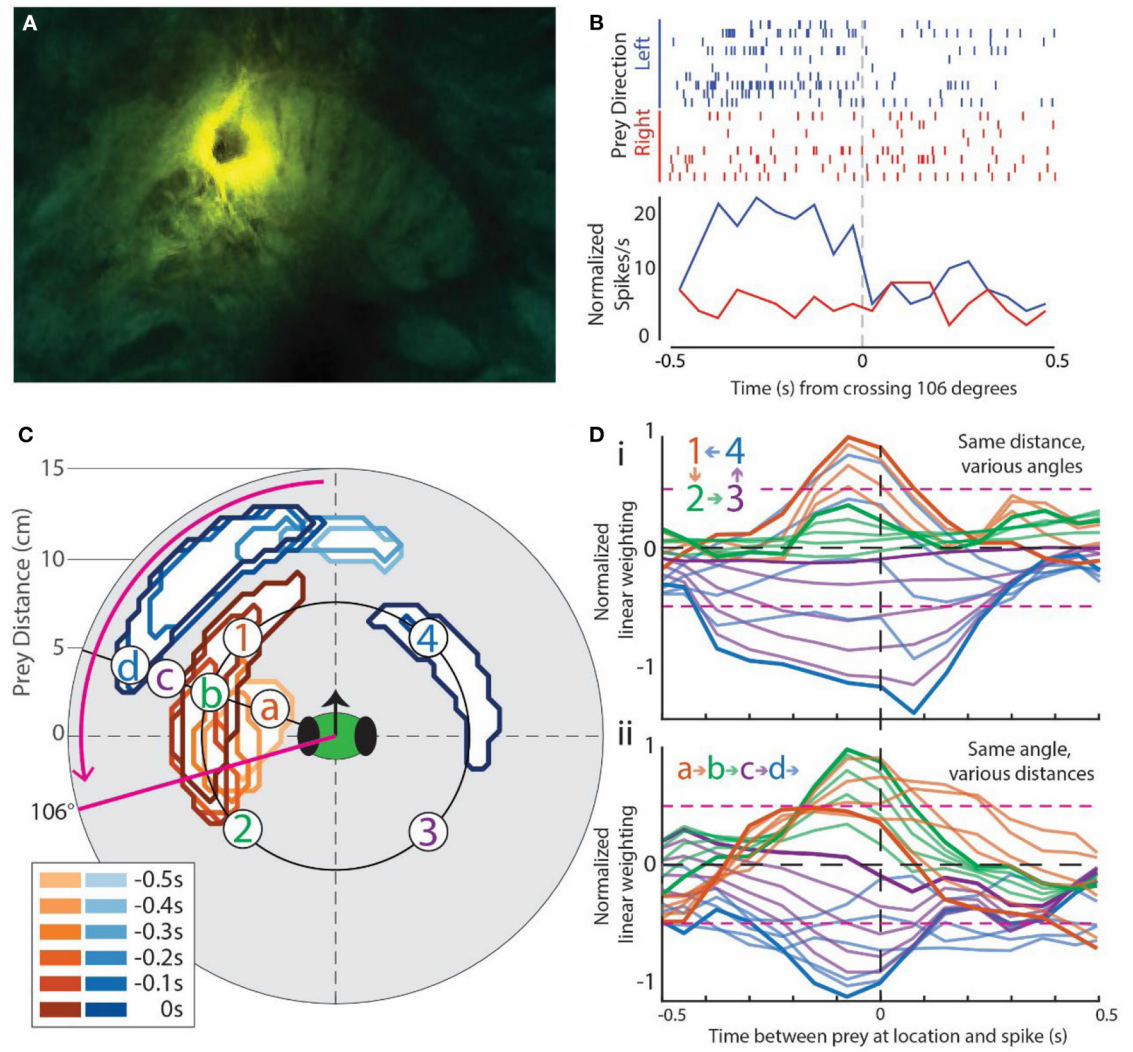

FIGURE 2 | Example of prey-motion-responsive cell. All data in this Figure are from the same cell located in the left fan-shaped body (FB). It was chosen because it exemplified the most common subtype of prey-responsive cells and direction selectivity, and it had clear positive and negative correlation regions in the visual field. **(A)** Image of the central complex showing the lesion dye from the electrode on the mantis's right-side FB. **(B)** Rasters (top) and peri-stimulus time histogram (PSTH, bottom) for the angle at which prey movement elicited the greatest response in this cell, which, in this case, was back and forth around 106° to the left of the mantis's forward-facing visual field [refer to the solid magenta line in **(C)**]. Trials are split into the left- (blue) and right-moving prey (red). The corresponding PSTHs were calculated as the sum * (spikes in bin for all trials)/(number of trials) * (length of the bin). This normalized each PSTH for unequal numbers of left and right trials (see Methods for more detailed explanation). **(C)** Contours outlining the positions of the moving prey with significant weights in the generalized linear model for this cell. Warm colors indicate regions with positive weights (analogous to positive correlation), and cool colors indicate negative weights. The inset box is a legend indicating the delay between prey in the area outlined by the contour (lighter colors for longer delays) and a spike in this cell. In effect, a prey stimulus in the outlined area is associated with a spike at some time delay later. The magenta arrow indicates the direction of prey movement that produced a larger response in the PSTH in **(B)**. **(D)** Spatial temporal receptive field (STRF) plots taken from various locations in the contour plot in **(C)**. A peak to the left of 0 that rises above the 2-SD level (dotted magenta horizontal lines) indicates a strong correlation with movement before an increase in spike activity. A peak that goes below the lower 2 SD line indicates a negative correlation between movement and activity (decrease in spiking). **(Di)** includes samples from 4 numbered regions indicated in **(C)** around the same distance. The color of each curve matches that of the site indicated in **(C)** (labeled a–d). Darker curves are the correlations for prey at the indicated points, and the lighter curves are the correlations at equally spaced points between these points. Light brown lines are at points taken between the points labeled 1 and 2, light green lines from points between 2 and 3, and so on. This progression is indicated in the insert on the plots. **(Dii)** shows lettered responses to sites at the same angle relative to the head of the mantis but at different distances. In this case, sites at which the curves are recorded are indicated as letters on the contour map in **(C)** and colors of the STRF curves match those of the letters in **(C)**.

of view. It should be noted that because the mantis is free to move its head, the angle of the stimulus relative to the mantis's field of view can change. We, therefore, measured the response for all angles and present the raster display for the maximum response angle, in this case 106°. Blue rasters were from trials where the target is moving in a leftward direction, while red rasters were

from trials where the target is moving rightward. The histograms below sum the two sets of responses and show a strong response when the stimulus was moving leftward. In contrast, when the stimulus was moving rightward, there was little or no change in activity.

By repeating the procedure reported in **Figure 2B** at various distances and angles, we were able to produce a contour plot for each unit showing either positive (brown) or negative (blue) correlations associated with movements of the simulated prey (**Figure 2C**). The positive and negative regions were established by generating STRF plots that relate spike activity with, in this case, target movement (**Figure 2D**) at various angles and distances around the mantis's head. A positive correlation typically arises from increased spike rate, whereas a negative correlation comes from decreased spike rate. In the STRF plots, spike activity was located at time 0 on the X axis. The plots then showed the correlation between target movement and spike activity. Plots that rise above 2 SDs to the left of the 0 point indicate positions where simulated prey movement preceded an increase in spike activity. Trials where the curve peaked below negative 2 SDs indicate areas where decrease in spike activity followed the prey movement. Any peak that occurred after the 0 point would normally indicate activity that preceded prey movement. For the most part, peaks to the right of 0 were not seen associated with the simulated prey movement. However, in some rare instances (e.g., blue curves in **Figure 2D**i), a significant peak was carried over to the right of 0. We attribute the carryover in this analysis to the cyclical and continuous nature of the target movement. That is, it may be indicating responses to an earlier target movement with a delay that simply was not captured in the left side peak.

The relationship between the contour plot and the STRF plots is shown by two groups of responses. Activity at various angles around the mantis's head but at the same distance was depicted as 1, 2, 3, or 4 on the contour plot. In **Figure 2D**, these are indicated as color-coded STRF plots. The dark traces were from specific numbered points on the plot, while the lighter colored curves were from angles that lie on a line between them. In the top set of plots (**Figure 2D**i), the excitatory region (1) has large peaks (brown curves) to the left of the 0, indicating a strong correlation with the prey movement. In contrast, the blue region (4) in the contour was associated with curves that have large negative peaks to the left of 0, indicating a significant decrease in activity associated with stimulus presentations at these angles. The regions between those extremes (2 and 3) had varying size peaks. Some angles, which encroached on the brown and blue regions of the contour plot during part of the stimulus movement but were centered outside of the main excitatory or inhibitory

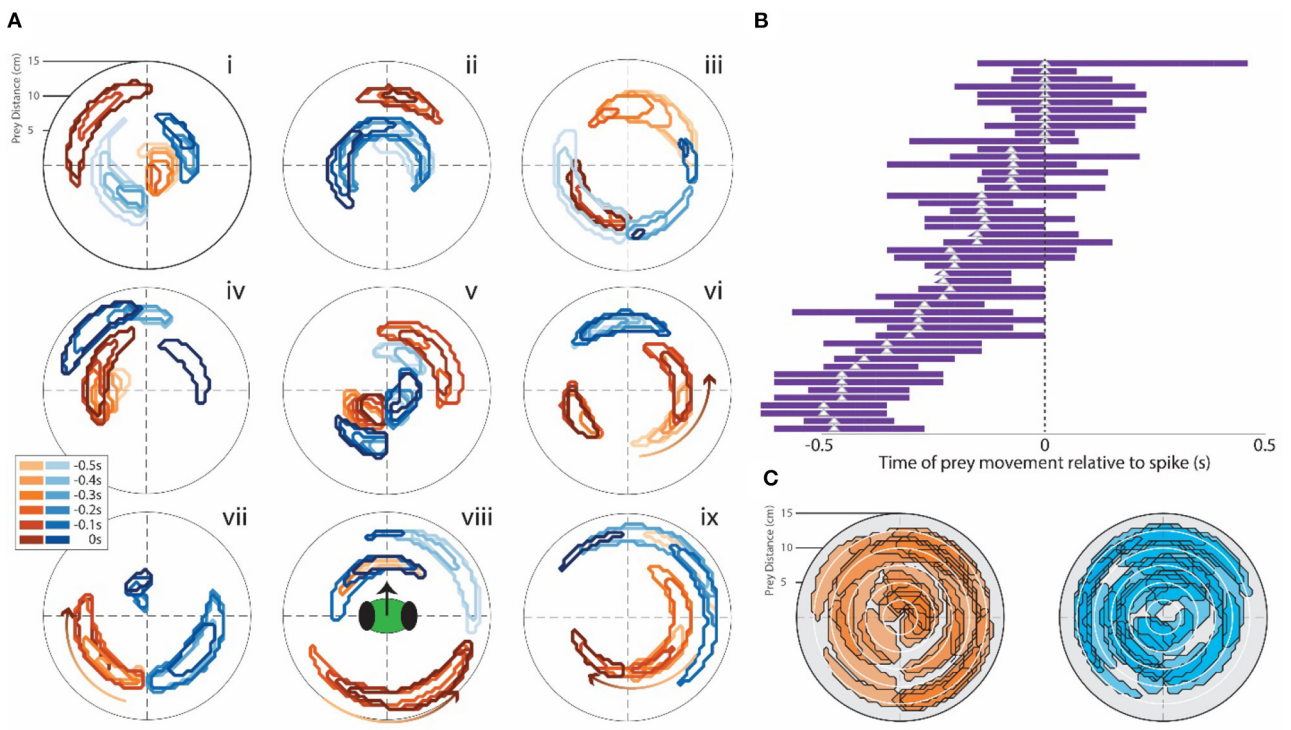

FIGURE 3 | (A) Examples of STRF contour plots (as in **Figure 2C**) for a range of single CX units that responded after the appearance of the target. Note the various different field patterns of positive (brown) and negative (blue) responses to the target. The mantis's head orientation is depicted in contour viii. **(B)** Bars indicate the time period for each neuron where the correlation seen in the STRF curve was above the 2-SD range. The triangle indicates the peak of this curve. All cells that had bars to the left of 0 (point where spike activity changes) responded to target presentation but did not evoke movement of the mantis. These bars represent all cells that showed these response patterns. **(C)** All of the contours we recorded were superimposed on two contour fields: one brown (positive) and one blue (negative). This indicates that the entire area around the head of the mantis is covered by both positive and negative response regions.

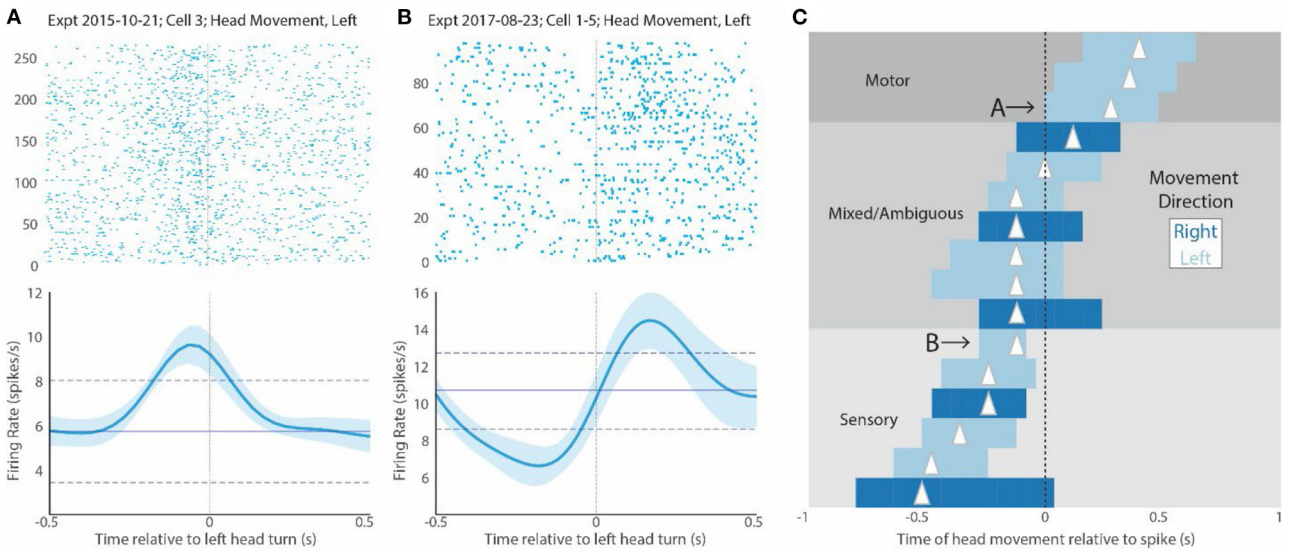

FIGURE 4 | CX activity relative to mantis movement. **(A)** Raster plot of several responses associated with head movement of any kind for a sample cell. The 0 point here indicates the beginning of the head movement. The plot underneath shows the mean and SD firing response of all trials in the raster display. Note that the peak firing precedes the head movement, suggesting that it could contribute to driving the movement. **(B)** Shows a similar display for another cell that responds after the head movement (to the right of 0). This suggests that this cell responds to either proprioceptive or visual inputs associated with the turn or corollary discharge of the motor commands. **(C)** Shows bars indicating the peaks of STRF plots for all cells that were above 2 SDs. As in **Figure 3B**, the length of the bar indicates duration above 2 SDs, and the triangle indicates the peak of the curve. Dark blue bars are associated with rightward head movements, and light bars are associated with leftward head movements. In this display, bars to the left of 0 indicate regions where head movement precedes increase in spiking (0 point). We have labeled bars that are complete in this region as "sensory." In contrast, bars to the right of 0 indicate responses where increases in spike activity (0 point) precede movement. We have labeled bars that are complete in this region as "motor". Bars that span both regions relative to the 0 point are labeled mixed or ambiguous. They could be involved in both motor and sensory effects. Cells whose activity is displayed in **(A,B)** are indicated with letters and arrows. Note that the relationship of the STRF plots relative to the 0 point is the opposite of that seen in the rasters. That is because the 0 point in the STRF plots indicates the point where spike activity increases, whereas the 0 point in the raster display is the point where movement commences.

region, may show weaker responses, while others fail to cross the 2 SD correlation points, indicating no significant response at these angles. The lighter plots showed the transitions between each set of designated points with some reaching significance, while others that were well between the significant regions failed to do so. It should be noted that all of our STRF analysis for this part of the study was conducted on responses that preceded any head movement in order to prevent contamination from proprioceptive or visual responses associated with such actions.

The lower set of plots (**Figure 2D**ii) shows a similar relationship but now examines the distance from the mantis's head rather than angle. Plots were taken from the line depicted on the contour with points a, b, c, and d indicated. Again, the dark plots were from those designated points, and the lighter ones were at distances between them. Here, the strongest correlations were seen in the b region, which was within the excitatory area of the contour plot (**Figure 2C**). The positive peaks fell off at distances a and c, which had weaker correlations or failed to reach significance in the STRF plots (**Figure 2D**ii). At distance d, the STRF plots showed significant negative correlations consistent with the inhibitory region at a greater distance on the contour plot.

Contour plots were generated in this way for all the units recorded in all the 10 experiments. Some had unique properties. Examples are shown in **Figure 3**. Most are similar to the plots shown in **Figure 2B**. Many had excitatory (positive weight) or inhibitory (negative weight) regions located at various distances and angles from the mantis. Some units only showed excitation when the simulated prey moved in a particular direction (as was the case in the cell depicted in **Figure 2**), These were indicated by an arrow on the contours (**Figure 3A**vi–ix). Forty-eight units recorded in the central complex (specifically all in the FB) showed positive weighting with simulated prey movement in some portion of the visual field. The peak weighting in the generalized linear model of spike generation ranged from 0 to −0.5 s before a spike (**Figure 3B**), i.e., prey movement precedes spiking in these cells. Contours for other units, including those recorded in the MB, are shown in **Supplementary Figure S3**. Finally, we considered all CX cells recorded in different animals as a pseudo-population, likely representative of the population in a single animal. When superimposed on one contour plot, the excitatory and inhibitory spatial fields of these cells cover the full range of the visual field tested in these experiments (**Figure 3C**).

Responses Associated With Mantis Movement

We next examined the relationship between neural activity and the mantis's own movement (**Figure 4**). To do this, we digitized the praying mantis's movements in the arena. Most of these were turning movements toward the prey, which occurred in three

stages. Target signals near the front of the praying mantis may require only a small rotation of the head to bring the eyes in line with the stimulus. Larger targeting movements require turning of the thorax. Praying mantises have a joint between the prothoracic and mesothoracic segments that allows them to rotate in the horizontal plane. Even larger turns require leg movements that turn the entire body.

A raster display that is now generated relative to the onset of head movement (time 0), shows that CX activity could be associated with these actions. CX units that respond during targeting can fall into two categories. First, they can respond prior to movement (**Figure 4A**). This effect would be similar to that which was reported in cockroaches, where most of the activity associated with turns or changes in forward stepping preceded movement (Martin et al., 2015). Alternatively, increases in activity could occur after the turn starts (**Figure 4B**). This type of activity would probably represent some form of reafference. It could stem from visual responses as the head rotates relative to its visual world or from proprioceptive cues monitoring head, thoracic, or leg movements and ascending to the brain. These possibilities are not mutually exclusive. Even where activity preceded movement, the continued activity after the turn commences could result from reafference. It is also possible that the same cell only shows motor control activity for a specific set of targeting movements with reafference occurring elsewhere. Finally, since the target moves back and forth, it is possible that some of the activity during the movement period is associated with motor control associated with reversal of target movement.

To further examine the relationship between CX activity and mantis head movement, we performed STRF analyses on all turning movements made by the mantis during each experiment (**Figure 4C**). The peaks of each cell can be divided into 3 groups. For cells with STRF plot peaks totally to the right of 0, all significant changes in spike activity preceded the mantis's movements and could initiate such actions. We label these responses as "motor." For cells with STRF peaks totally to the left of 0, significant activity changes occur during or slightly after movement and probably are associated with reafference or efference copy. Regardless of the source, we refer to these responses as "sensory." Between these cells are cases where significant STRF peaks span 0. That is, the peak begins to the right but extends to the left of 0. These types of neural responses start before movement and continue to show significant increases during the movement. That is, they could initiate the movement but then receive reafference or efference copy during the movement. We label these responses as "mixed."

Finally, in turns associated with the simulated targets, we found several cells that both responded to target appearance and were associated with mantis turning movement (**Figure 5**). These responses fall into 3 categories. Some show responses that attend to the target (magenta bars with peaks to the left of 0) and peaks associated with movement (blue bars) to the left of 0 (reafference or efference copy). We label these responses "sensory," since they only seem to include sensory effects relative to the target, whether that be attention to the target appearance or reafference during the movement. Another category has attention peaks (magenta bars) to the left, but mantis movement peaks (blue bars) totally to the right. These would be cells that respond to the target's appearance and then fire before self-movement starts. We label these "sensorimotor." The remaining cells have peaks associated with target appearance to the left but motor peaks spanning 0 ("mixed" in **Figure 4**). These cells respond to the target appearance and have activity preceding mantis turning but then continue through the actual turn. The cells in the last two categories could be part of a population of cells that controls the entire predatory stalking behavior. The first group could still contribute to the stalking behavior but only in association with cells in the other groups.

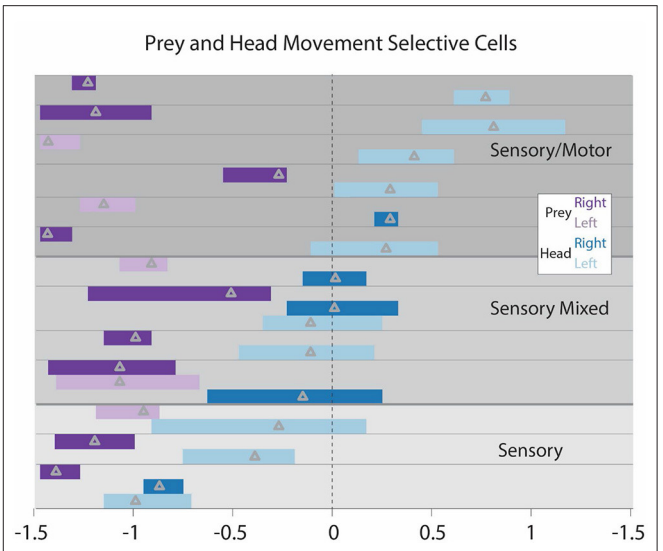

FIGURE 5 | STRF peaks for all cells that both respond to the target movement and respond relative to the praying mantis's movement toward the target. Each cell's peaks are positioned between horizontal lines. Cells are separated into 3 categories. Purely "sensory" cells (bottom 3) have target peaks and mantis head movements to the left. These are cells that respond to the appearance of the target and after the mantis initiates movement. "Sensorimotor" cells (top) have responses associated with target appearance to the left and mantis movement peaks exclusively to the right of 0. These are cells that increase activity with the appearance of the target and have activity significantly increased prior to the movement. "Sensori-mixed" cells (middle) have increased activity associated with target appearance and have increased activity associated with mantis head movement that substantially spans 0. These cells respond to the appearance of the target and have some activity prior to the initiation of mantis head movement that continues throughout the mantis head movement. It should be noted that one sensory and one sensorimotor cells have a slight overlap of the head movement peaks into the opposite region, but we regarded this overlap as minimal. These were subjectively placed in the categories indicated here.

Movement Evoked by Stimulating Through Tetrodes

We routinely passed currents through the tetrodes at the end of the simulated target experiments. We recorded videos in 5 of the analyzed FB preparations (**Figure 6**). All 5 evoked turning movements. The stimulation in 4 of them caused movement toward the side on which the tetrodes were located (3 to the left and 1 to the right). The remaining preparation had two

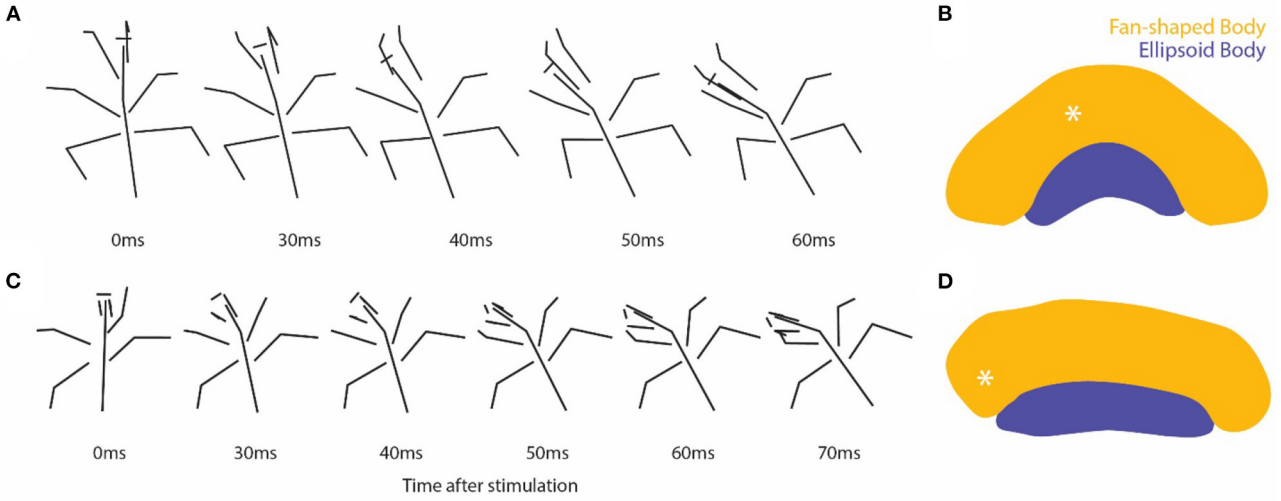

FIGURE 6 | (A,C) Stick figures drawn from individual video frames at the time of stimulation through the tetrodes and 4–6 frames 10 ms apart following that point. **(B,D)** Diagrams of sections in the CX showing the location of tetrode tips (asterisk) for each experiment.

tetrodes implanted, one in the left FB and one in the right MB. The stimulation in this preparation caused movement to the right regardless of which tetrode was stimulated. These stimulus-evoked movements verified that the tetrodes were located in regions at least near where neurons that control movement are located (**Figure 6**). As indicated previously, two-thirds of the tetrodes (8) were shown histologically to be located in the FB. The remaining 4 tetrodes were located in the MB.

DISCUSSION

The results presented here show that neurons in the CX and, more specifically, in the FB both respond to either real or simulated prey and have the capacity to generate turning movements toward that target. Because we used extracellular recording methods, we cannot say exactly which cells we recorded from in any given preparation. Some could be particularly associated with detecting and following the prey, while others generated the appropriate stalking movements to initiate an attack. Still, others may have played a role in both aspects of the behavior. No cases showed changes in spiking associated with the mantis's actual striking behavior. Rather, the activity we recorded in FB neurons seemed to be associated only with the tracking and stalking of the mantis toward the prey. Once near the prey, the strike appears to be ballistic. While the lack of specific neural identification with this technique is a limitation, there are clear benefits. First, we could record for long periods of time, thereby testing a range of angles and distances to which the mantis responded. Second, the recordings were conducted while the mantis was freely moving. This second point is important. A recent study on monarch butterflies (Beetz et al., 2022) that used tetrode recordings showed that properties of CX neurons changed dramatically as the butterflies transitioned from restrained to active flight as well as to freely rotating flight. Thus, in our study, it was critical to ask questions regarding predatory behavior while the mantis was actually engaged in freely moving behavior.

The details of these relationships may well vary from neuron to neuron in the CX. Since our extracellular recordings do not allow us to identify the source of activity at the cellular level, we may be recording CX cells at numerous levels of motor control. Nevertheless, our analysis shows that at least some CX neurons recorded in the FB respond to both natural and simulated prey, as the praying mantis targets and stalks them. While the cells are likely to have branches in the FB, we cannot be certain that they do not also pass through other CX neuropils. Individual cells are biased to particular regions around the head including angle and distance. At least some are activated prior to targeting movements. This result implies that the CX plays a role in sensorimotor control of this predatory behavior. Whether some or all such CX neurons are restricted to predator attention movements will await future studies. Regardless, this function, in at least some CX neurons, appears to be similar to goal-directed target cells recorded in the hippocampus of bats (Sarel et al., 2017). As with the bat study, the mantis neurons we report on here encode both goal distance and goal direction. However, unlike the bat study, we cannot comment on whether the mantis can locate its target if it is temporarily hidden. It will be interesting to examine to what extent the details of the circuits within a predatory insect's CX that result in attention movements toward prey are similar to the navigational mechanisms that have been proposed for *Drosophila* (Green et al., 2017; Turner-Evans et al., 2017; Hulse et al., 2021) and bees (Stone et al., 2017). Do the circuits used in hunting strategies of predators represent the modified navigational circuits used by other insects in foraging or path integration?

We also made 4 recordings in the MB, and 3 of these provided units that showed significant sensory responses (**Supplementary Figure S3**). Because of the relatively small number of MB recordings, we did not analyze these units further. Nevertheless, the fact that they responded to the simulated target in manners similar to the CX units suggests that MB neurons may also play some role in targeting prey. The similarities could arise as a result of similar projections from the visual system to the CX and MB neuropils or by communication between these two large brain regions (Mizunami et al., 1998; Hulse et al., 2021).

The lack of precise identification of each studied neuron could result in ambiguities in our results. Since we recorded from these subjects over hours, it is possible that the electrodes moved at some point in the experiment and were actually recording from different neurons. Thus, the motor and sensory roles of a neuron could result from changes in recording site. While our recordings at all four electrodes of a given tetrode appeared to be constant throughout, we cannot completely eliminate that possibility over the course of a long experiment. Nevertheless, in this case, it probably is not a critical issue. Since the mantis was both detecting and turning toward its prey at essentially the same time, it was using both motor and sensory roles almost simultaneously.

Advantage of Predators for Navigational Studies

Predatory species provide a system in which a clear important target is being sought by a subject. Previous navigational studies focused more broadly on implied navigational systems such as migration of monarch butterflies across North America (Beetz et al., 2022) or moment-to-moment movements of *Drosophila* toward an implied desired direction (Green et al., 2019). However, predators seek a specific target that must be struck in order for them to survive. Not only is the prey target unambiguous, but it can be manipulated by the experimenter either by moving a prey item or, as in our study, mimicking it with a simulated target.

Moreover, that target may be dynamic in itself. The prey will not necessarily remain at a given point but may move through its environment either before being detected or in response to the predator's movements. Problems facing relatively small animals, such as insects as they track moving targets against a background, have been reviewed elsewhere (Gonzalez-Bellido et al., 2016). Two very different strategies have been noted. One is a relatively simple or classical pursuit in which the predator aligns its stalking movements directly toward the prey. This appears to be the strategy that the praying mantises followed in our study. The mantis detects a specific prey item, turns toward it, and closes the distance in order to get near enough the prey for a successful strike. If the prey moves, the mantis simply follows it. In contrast, another well-studied predatory insect, the dragonfly, actually uses an internal model to predict the movements of its prey (Mischiati et al., 2015). In the dragonfly, predictive properties have even been demonstrated at the level of central brain neurons called small target motion detectors (STMDs) recorded intracellularly in restrained insects (Wiederman et al., 2017). Such a system is particularly important for a flying insect making rapid navigational adjustments toward flying prey. It does not appear that such predictions are being made in the slower stalking movements of the praying mantis; however, some predictions could also be made here. Future studies should test this notion.

Our live predator experiments revealed another property that is specific to predator-prey interactions. In order to be successful, the predator cannot constantly switch its attention between targets. Thus, as seen in our **Supplementary Video S2**, once the mantis focuses on one prey item (the one attempting to right itself in the middle of the arena), both the mantis's movements and the CX neuron that we were recording appeared to ignore another cockroach that walked through the mantis's field of view. Since this second cockroach was tracked earlier in the video, it clearly met the criteria for attack.

The selective attention we saw in that video could be explained by "competitive selection," as described in intracellular recordings of STMD neurons of the dragonfly central brain (Wiederman and O'Carroll, 2013). In that study, neural activity was recorded in response to two very different target presentations. Then, both target patterns were presented simultaneously. Rather than producing a response characteristic of the combined patterns for the two targets, the neuron's response locked on to one or the other pattern. In some cases, the pattern would switch from one to the other during the trial, suggesting a competition between patterns that could change during presentation. Indeed, a more recent study used frequency-tagged intracellular trains to identify which target of a pair is selected at any moment (Lancer et al., 2019). It will be interesting to see in both restrained and freely moving preparations what target properties result in both consistency and switching, an issue that is critically important in many animals, particularly in hunting behaviors.

Why Go Through a Region Like the CX?

The latter factors point to issues regarding the role of the CX in the navigational movements that we examined here and those that others have studied elsewhere. One can ask why the insect brain requires something as complex and highly organized as the CX to make directed movements. If an insect was only required to move toward a target, it could accomplish this with a simpler system such as the flip-flop interneurons that were described earlier in dragonflies (Olberg, 1981). However, navigational movements are often affected by many other context-dependent factors. For example, a predator such as the praying mantis may alter its hunting strategy depending on its level of hunger. A recent study demonstrated that higher satiety reduced the distance and angles around the mantis's head to which it would respond (Bertsch et al., 2019). That is, starved mantises stalked much more distant prey. However, as they fed, the distance that they responded to decreased with each meal. Eventually, the mantis switched to an ambush strategy, in which it would strike a prey item that came near but would not actively move toward it.

The effect of satiety on hunting strategy could also be generated in starved mantises by injecting insulin into its abdomen. Insulin is a hormone that increases in response to feeding in a wide range of animals (Mattila and Hietakangas,

2017). Thus, it is likely that neurons in the CX are altered by such hormonal effects. Indeed, a wide range of neuromodulators are known to be present and have effects within the CX (Homberg, 2002; Nässel and Homberg, 2006; Kahsai and Winther, 2011), and are known to alter behavior (Kahsai et al., 2010).

Other factors that can affect directional movement include proprioceptive inputs such as those from the haltere balance organs of flies. The activity from these structures is now known to influence CX neurons (Kathman and Fox, 2019). Moreover, the change in compass properties seen in the monarch butterfly as it transitions from restrained conditions to rigid and then flapping flight appear to stem, at least in part, from efference copy that, again, seems to alter CX activity (Beetz et al., 2022).

The example of context-dependent effects on directional behavior points to possible reasons for movement control to pass through a complex structure like the CX. It also points to the importance of recording techniques that allow one to monitor freely moving behavior over long periods of time even as conditions change. The tetrode recording technique used in this study and the STRF analysis that allowed us to relate CX unit activity with movement of either the prey target or the mantis itself toward that target provide such tools.

In the long run, neuroethological studies seek to explain the neural basis of complex behaviors. As has been pointed out previously, neuroethology in itself brings together two complimentary but often hostile disciplines (Ritzmann and Fox, 2022). Ethologists have traditionally sought to describe behavior while restricting any influence that the observer might impart on the subjects of interest. At the opposite extreme, neurobiologists often try to record in isolated neural structures or highly restrained preparations in order to describe very precise neural properties in identified neurons. Neuroethologists typically attempt to address this conflict by working through stepping stones from descriptions of behavior to ever more restrained preparations. They may arrive at restrained intracellular recordings but only after taking smaller technical steps between the freely moving behavior and a restrained preparation. The tetrode recordings used here and elsewhere provide an important stepping stone between these extremes. In practice, they would serve to link behavioral data to restrained experiments with identified neurons or vice versa.

DATA AVAILABILITY STATEMENT

The raw data supporting the conclusions of this article will be made available by the authors, without undue reservation.

AUTHOR CONTRIBUTIONS

AW, JM, RR, and GS: conception of study. RR, GS, JM, and AW: funding. JM: programs for experimental control and analysis of data. JM and AP: recording live prey experiments. AW: recording simulated prey experiments and processing data. AP: histology. RR and JM: writing manuscript. RR, JM, AW, AP, and GS: editing manuscript. All authors contributed to the article and approved the submitted version.

FUNDING

This material is based on a study supported by the National Science Foundation under (Nos. IOS-1557228 to RR, IOS-1557279 to GS, and IIS-1704366 to JM) and by the German Research Foundation under Fellowship (No. Wo2000/1-1 to AW).

SUPPLEMENTARY MATERIAL

The Supplementary Material for this article can be found online at: https://www.frontiersin.org/articles/10.3389/fncir.2022.893004/full#supplementary-material

Supplementary Video S1 | Sample video of mantis responding to simulated targets. Time stamps of a single unit are depicted at the bottom and as audio.

Supplementary Video S2 | Video taken of a freely moving mantis with tetrode implants hunting cockroach nymphs. Time stamps of one unit are depicted running at the bottom and as audio.

Supplementary Figure S1 | Diagram showing the location of all tetrode recording sites in the fan-shaped body (FB) and mushroom body (MB). White dots are from single tetrode experiments and gray from dual tetrode experiments. Each of the light and dark gray pairs is from the same experiment. The various neuropils are labeled with colors.

Supplementary Figure S2 | (A) Procedure for spiking model estimation. The position of the prey stimulus and head angular velocity (1) are used to generate a spatiotemporal response function for several values of delay before and after a spike in the recorded neuron (2). Linear spatial temporal receptive fields (STRFs) are combined with a nonlinear spike-generating function (3), and the resulting modeled spike train is compared with the actual recorded spike train (4). The STRFs are iteratively modified to reduce the difference between modeled and real spike trains (5). **(B)** Time series is generated for a single spatial bin (white circles) in the (STRF) at various times relative to the spike occurrence at time 0. The normalized value of the weight for the spatial bin at each spike delay is plotted in the graph on the right. The weight is analogous to the correlation between a simulated prey stimulus at that location and the neuron producing a spike at some time before or after the prey is in that location. Larger, positive values for this weight at negative delays (left side of the graph) mean that the prey in this location was associated with the neuron producing increased numbers of spikes after the prey moved. Larger, positive values at positive delays (right side of the graph) mean that the associated event was likely to occur after the neurons produced a spike. This would be seen, i.e., when a motor neuron is involved in generating a movement (refer to **Figure 4** in the main text). Negative peaks at either of these time frames would suggest a decrease in spike activity associated with movement.

Supplementary Figure S3 | Additional cells with significant responses to prey location. **(A)** Contour maps from cells recorded in the central complex (CX) beyond those depicted in **Figure 3A**. **(B)** Contour maps from cells recorded in the mushroom body (MB). In both cases, the borders group the maps from cells recorded from the same tetrode in the same preparation.

REFERENCES

Beetz, M. J., Kraus, C., Franzke, M., Dreyer, D., Strube-Bloss, M. F., Rössler, W., et al. (2022). Flight-induced compass representation in the monarch butterfly heading network. *Curr. Biol.* 32, 338–349. doi: 10.1016/j.cub.2021.11.009

Bender, J. A., Pollack, A. J., and Ritzmann, R. E. (2010). Neural activity in the central complex of the insect brain is linked to locomotor changes. *Curr. Biol.* 20, 921–926. doi: 10.1016/j.cub.2010.03.054

Bertsch, D. J., Martin, J. P., Svenson, G. J., and Ritzmann, R. E. (2019). Predatory behavior changes with satiety or increased insulin levels in the praying mantis (*Tenodera sinensis*). *J. Exp. Biol.* 222, jeb197673. doi: 10.1242/jeb.197673

Blagburn, J. M., and Sattelle, D. B. (1987). Nicotinic acetylcholine receptors on a cholinergic nerve terminal in cockroach. *J. Comp. Physiol.* 161, 215–225. doi: 10.1007/BF00615242

Currier, T. A., Matheson, A. M. M., and Nagel, K. I. (2020). Encoding and control of orientation to airflow by a set of *Drosophila* fan-shaped body neurons. *eLife* 9, e61510. doi: 10.7554/eLife.61510.sa2

DiCarlo, J., Lane, J., Hsiao, S., and Johnson, K. (1996). Marking microelectrode penetrations with fluorescent dyes. *J. Neuorsci. Meth.* 64, 75–81. doi: 10.1016/0165-0270(95)00113-1

el Jundi, B., Warrant, E. J., Byrne, M. J., Khaldy, L., Baird, E., Smolka, J., et al. (2015). Neural coding underlying the cue preference for celestial orientation. *Proc. Natl. Acad. Sci. U.S.A.* 112, 11395–11400. doi: 10.1073/pnas.1501272112

Gonzalez-Bellido, P. T., Fabian, S. T., and Nordström, K. (2016). Target detection in insects: optical, neural and behavioral optimizations. *Curr. Opin. Neurobiol.* 41, 122–128. doi: 10.1016/j.conb.2016.09.001

Green, J., Adachi, A., Shah, K. K., Hirokawa, J. D., Magani, P. S., and Maimon, G. (2017). A neural circuit architecture for angular integration in *Drosophila*. *Nature* 546, 101–106. doi: 10.1038/nature22343

Green, J., Vijayan, V., Mussells Pires, P., Adachi, A., and Maimon, G. (2019). A neural heading estimate is compared with an internal goal to guide oriented navigation. *Nat. Neurosci.* 22, 1460–1468. doi: 10.1038/s41593-019-0444-x

Guo, P., and Ritzmann, R. E. (2013). Neural activity in the central complex of the cockroach brain is linked to turning behaviors. *J. Exp. Biol.* 216, 992–1002. doi: 10.1242/jeb.080473

Hedrick, T. L. (2008). Software techniques for two- and three-dimensional kinematic measurements of biological and biomimetic systems. *Bioinspir. Biomim.* 3, 034001. doi: 10.1088/1748-3182/3/3/034001

Heinze, S., Gotthardt, S., and Homberg, U. (2009). Transformation of polarized light information in the central complex of the locust. *J. Neuorosci.* 29, 11783–11793. doi: 10.1523/JNEUROSCI.1870-09.2009

Heinze, S., and Homberg, U. (2007). Maplike representation of celestial E-vector orientations in the brain of an insect. *Science* 315, 995–997. doi: 10.1126/science.1135531

Heinze, S., and Reppert, S. M. (2011). Sun compass integration of skylight cues in migratory monarch butterflies. *Neuron* 69, 345–358. doi: 10.1016/j.neuron.2010.12.025

Homberg, U. (2002). Neurotransmitters and neuropeptides in the brain of the locust. *Microsci. Res. Tech.* 56, 189–209. doi: 10.1002/jemt.10024

Hulse, B. K., Haberkern, H., Franconville, R., Turner-Evans, D. B., Takemura, S. -Y., Wolff, T., et al. (2021). A connectome of the *Drosophila* central complex reveals network motifs suitable for flexible navigation and context-dependent action selection. *eLife* 10, e66039. doi: 10.7554/eLife.66039

Inoue, T., and Matsura, T. (1983). Foraging strategy of a mantid, *Paratenodera angustipennis S.*: mechanisms of switching tactics between ambush and active search. *Oecolog* 56, 264–271. doi: 10.1007/BF00379700

Kahsai, L., Martin, J. -R., and Winther, A. M. E. (2010). Neuropeptides in the *Drosophila* central complex in modulation of locomotor behavior. *J. Exp. Biol.* 213, 2256–2265. doi: 10.1242/jeb.043190

Kahsai, L., and Winther, A. M. E. (2011). Chemical neuroanatomy of the *Drosophila* central complex: distribution of multiple neuropeptides in relation to neurotransmitters. *J. Comp. Neurol.* 519, 290–315. doi: 10.1002/cne.22520

Kathman, N. D., and Fox, J. L. (2019). Representation of haltere oscillations and integration with visual inputs in the fly central complex. *J. Neuorosci.* 39, 4100–4112. doi: 10.1523/JNEUROSCI.1707-18.2019

Kathman, N. D., Kesavan, M., and Ritzmann, R. E. (2014). Encoding wide-field motion and direction in the central complex of the cockroach *Blaberus discoidalis*. *J. Exp. Biol.* 217, 4079–4090. doi: 10.1242/jeb.112391

Lancer, B. H., Evans, B. J. E., Fabian, J. M., O'Carroll, D. C., and Wiederman, S. D. (2019). A target-detecting visual neuron in the dragonfly locks on to selectively attended targets. *J. Neuorsci.* 39, 8497–8509. doi: 10.1523/JNEUROSCI.1431-19.2019

Martin, J. P., Guo, P., Mu, L., Harley, C. M., and Ritzmann, R. E. (2015). Central-complex control of movement in the freely walking cockroach. *Curr. Biol.* 25, 1–9. doi: 10.1016/j.cub.2015.09.044

Mattila, J., and Hietakangas, V. (2017). Regulation of carbohydrate energy metabolism in *Drosophila melanogaster*. *Genetics* 207, 1231–1253. doi: 10.1534/genetics.117.199885

Mischiati, M., Lin, H. -T., Herold, P., Imler, E., Olberg, R., and Leonardo, A. (2015). Internal models direct dragonfly interception steering. *Nature* 517, 333. doi: 10.1038/nature14045

Mizunami, M., Okada, R., Li, Y., and Strausfeld, N. (1998). Mushroom bodies of the cockroach: activity and identities of neurons recorded in freely moving animals. *J. Comp. Neurol.* 402, 501–519. doi: 10.1002/(SICI)1096-9861(19981228)402:4andlt;501::AID-CNE5andgt;3.0.CO;2-M

Nässel, D. R., and Homberg, U. (2006). Neuropeptides in interneurons of the insect brain. *Cell Tissue Res.* 326, 1–24. doi: 10.1007/s00441-006-0210-8

Nityananda, V., Tarawneh, G., Henriksen, S., Umeton, D., Simmons, A., and Read, J. C. A. (2018). A novel form of stereo vision in the praying mantis. *Curr. Biol.* 28, 588–593. doi: 10.1016/j.cub.2018.01.012

Niven, J. E., Buckingham, C. J., Lumley, S., Cuttle, M. F., and Laughlin, S. B. (2010). Visual targeting of forelimbs in ladder-walking locusts. *Curr. Biol.* 20, 86–91. doi: 10.1016/j.cub.2009.10.079

Ofstad, T. A., Zuker, C. S., and Reiser, M. B. (2011). Visual place learning in *Drosophila melanogaster*. *Nature* 474, 204–207. doi: 10.1038/nature10131

Okubo, T. S., Patella, P., D'Alessandro, I., and Wilson, R. I. (2020). A neural network for wind-guided compass navigation. *Neuron* 107, 924–940. doi: 10.1016/j.neuron.2020.06.022

Olberg, R. M. (1981). Parallel encoding of direction of wind, head, abdomen, and visual pattern movement by single interneurons in the dragonfly. *J. Comp. Physiol.* 142, 27–41. doi: 10.1007/BF00605473

Olberg, R. M., Worthington, A. H., Fox, J. L., Bessette, C. E., and Loosemore, M. P. (2005). Prey size selection and distance estimation in foraging adult dragonflies. *J. Comp. Physiol. A Neuroethol. Sens. Neural Behav. Physiol.* 191, 791–797. doi: 10.1007/s00359-005-0002-8

Pegel, U., Pfeiffer, K., and Homberg, U. (2018). Integration of celestial compass cues in the central complex of the locust brain. *J. Expt. Biol.* 221, jeb171207. doi: 10.1242/jeb.171207

Pfeiffer, K., and Homberg, U. (2014). Organization and functional roles of the central complex in the insect brain. *Annu. Rev. Entomol.* 59, 165–184. doi: 10.1146/annurev-ento-011613-162031

Prete, F. R. (1999). "Prey recognition," in *The Praying Mantids*, eds F. R. Prete H. Wells P. H. Wells and L. E. Hurd (Baltimore, MD: Johns Hopkins University Press), 141–179.

Prete, F. R., Komito, J. L., Dominguez, S., Svenson, G., Lopez, L. Y., Guillen, A., et al. (2011). Visual stimuli that elicit appetitive behaviors in three morphologically distinct species of praying mantis. *J. Comp. Physiol. A* 197, 877–894. doi: 10.1007/s00359-011-0649-2

Prete, F. R., Theis, R., Dominguez, S., and Bogue, W. (2013). Visual stimulus characteristics that elicit tracking and striking in the praying mantises *Parasphendale affinis*, *Popa spurca* and *Sphodromantis lineola*. *J. Exp. Biol.* 216, 4443–4453. doi: 10.1242/jeb.089474

Prete, F. R., Theis, R., Komito, J. L., Dominguez, J., Dominguez, S., Svenson, G., et al. (2012). Visual stimuli that elicit visual tracking, approaching and striking behavior from an unusual praying mantis, *Euchomenella macrops* (Insecta: Mantodea). *J. Insect Physiol.* 58, 648–659. doi: 10.1016/j.jinsphys.2012.01.018

Ritzmann, R. E., and Fox, J. L. (2022). Insect neuroethology: flight constructs a compass for monarch migration. *Curr. Biol.* 32, R72–R74. doi: 10.1016/j.cub.2021.11.051

Ritzmann, R. E., Ridgel, A. L., and Pollack, A. J. (2008). Multi-unit recording of antennal mechanosensitive units in the central complex of

the cockroach, *Blaberus discoidalis*. *J. Comp. Physiol. A* 194, 341–360. doi: 10.1007/s00359-007-0310-2

Rosner, R., and Homberg, U. (2013). Widespread sensitivity to looming stimuli and small moving objects in the central complex of an insect brain. *J. Neurosci.* 33, 8122–8133. doi: 10.1523/JNEUROSCI.5390-12.2013

Rosner, R., von Hadeln, J., Tarawneh, G., and Read, J. C. A. (2019). A neuronal correlate of insect stereopsis. *Nat. Comm.* 10, 2845–2854. doi: 10.1038/s41467-019-10721-z

Sarel, A., Finkelstein, A., Las, L., and Ulanovsky, N. (2017). Vectorial representation of spatial goals in the hippocampus of bats. *Science* 355, 176–180. doi: 10.1126/science.aak9589

Schindelin, J., Arganda-Carreras, I., Frise, E., Kaynig, V., Longair, M., Pietzsch, T., et al. (2012). Fiji: an open-source platform for biological-image analysis. *Nat. Methods* 9, 676–682. doi: 10.1038/nmeth.2019

Seelig, J. D., and Jayaraman, V. (2013). Feature detection and orientation tuning in the Drosophila central complex. *Nature* 503, 262–266. doi: 10.1038/nature12601

Seelig, J. D., and Jayaraman, V. (2015). Neural dynamics for landmark orientation and angular path integration. *Nature* 521, 186–191. doi: 10.1038/nature14446

Stone, T., Webb, B., Adden, A., Weddig, N. B., Honkanen, A., Templin, R., et al. (2017). An anatomically constrained model for path integration in the bee brain. *Curr. Biol.* 27, 3069–3085. doi: 10.1016/j.cub.2017.08.052

Strauss, R. (2002). The central complex and the genetic dissection of locomotor behaviour. *Curr. Opin. Neurobiol.* 12, 633–638. doi: 10.1016/S0959-4388(02)00385-9

Talebi, V., and Baker, C. L. (2012). Natural versus synthetic stimuli for estimating receptive field models: a comparison of predictive robustness. *J. Neuorsci.* 32, 1560–1576. doi: 10.1523/JNEUROSCI.4661-12.2012

Theunissen, F. E., David, S. V., Singh, N. C., Hsu, A., Vinje, W. E., and Gallant, J. L. (2001). Estimating spatio-temporal receptive fields of auditory and visual neurons from their responses to natural stimuli. *Netw. Comp. Neural Syst.* 12, 289. doi: 10.1080/net.12.3.289.316

Turner-Evans, D., Wegener, S., Rouault, H., Franconville, R., Wolff, T., Seelig, J. D., et al. (2017). Angular velocity integration in a fly heading circuit. *eLife* 6, e40577. doi: 10.7554/eLife.23496.031

Tyrer, N. M., and Bell, E. M. (1974). The intensification of cobalt-filled neurone profile using a modication of Timm's sulfide-silver method. *Brain Res.* 73, 151–155. doi: 10.1016/0006-8993(74)91014-2

Varga, A. G., and Ritzmann, R. E. (2016). Cellular basis of head direction and contextual cues in the insect brain. *Curr. Biol.* 26, 1816–1828. doi: 10.1016/j.cub.2016.05.037

Warren, T. L., Giraldo, Y. M., and Dickinson, M. H. (2019). Celestial navigation in *Drosophila*. *J. Exp. Biol.* 222, jeb186148. doi: 10.1242/jeb.186148

Wiederman, S. D., Fabian, J. M., Dunbier, J. R., and O'Carroll, D. C. (2017). A predictive focus of gain modulation encodes target trajectories in insect vision. *eLife* 6, e26478. doi: 10.7554/eLife.26478.018

Wiederman, S. D., and O'Carroll, D. C. (2013). Selective Attention in an Insect Visual Neuron. *Curr. Biol.* 23, 156–161. doi: 10.1016/j.cub.2012.11.048

Conflict of Interest: The authors declare that the research was conducted in the absence of any commercial or financial relationships that could be construed as a potential conflict of interest.

frontiers | Frontiers in Neural Circuits

ORIGINAL RESEARCH
published: 30 June 2022
doi: 10.3389/fncir.2022.862279

Weighting of Celestial and Terrestrial Cues in the Monarch Butterfly Central Complex

Tu Anh Thi Nguyen[1], *M. Jerome Beetz*[1], *Christine Merlin*[2], *Keram Pfeiffer*[1] *and Basil el Jundi*[1,3]*

[1] Biocenter, Zoology II, University of Wuerzburg, Würzburg, Germany, [2] Department of Biology and Center for Biological Clocks Research, Texas A&M University, College Station, TX, United States, [3] Department of Biology, Animal Physiology, Norwegian University of Science and Technology, Trondheim, Norway

Monarch butterflies rely on external cues for orientation during their annual long-distance migration from Northern US and Canada to Central Mexico. These external cues can be celestial cues, such as the sun or polarized light, which are processed in a brain region termed the central complex (CX). Previous research typically focused on how individual simulated celestial cues are encoded in the butterfly's CX. However, in nature, the butterflies perceive several celestial cues at the same time and need to integrate them to effectively use the compound of all cues for orientation. In addition, a recent behavioral study revealed that monarch butterflies can rely on terrestrial cues, such as the panoramic skyline, for orientation and use them in combination with the sun to maintain a directed flight course. How the CX encodes a combination of celestial and terrestrial cues and how they are weighted in the butterfly's CX is still unknown. Here, we examined how input neurons of the CX, termed TL neurons, combine celestial and terrestrial information. While recording intracellularly from the neurons, we presented a sun stimulus and polarized light to the butterflies as well as a simulated sun and a panoramic scene simultaneously. Our results show that celestial cues are integrated linearly in these cells, while the combination of the sun and a panoramic skyline did not always follow a linear integration of action potential rates. Interestingly, while the sun and polarized light were invariantly weighted between individual neurons, the sun stimulus and panoramic skyline were dynamically weighted when both stimuli were simultaneously presented. Taken together, this dynamic weighting between celestial and terrestrial cues may allow the butterflies to flexibly set their cue preference during navigation.

Keywords: insect, central complex, navigation, orientation, landmark, migration, panorama, lepidoptera

OPEN ACCESS

Edited by:
Wolfgang Stein,
Illinois State University, United States

Reviewed by:
Hannah Haberkern,
Janelia Research Campus, United States
Mark A. Frye,
University of California, Los Angeles, United States

***Correspondence:**
Basil el Jundi
basil.el.jundi@ntnu.no

Received: *25 January 2022*
Accepted: *10 June 2022*
Published: *30 June 2022*

Citation:
Nguyen TAT, Beetz MJ, Merlin C, Pfeiffer K and el Jundi B (2022) Weighting of Celestial and Terrestrial Cues in the Monarch Butterfly Central Complex. Front. Neural Circuits 16:862279. doi: 10.3389/fncir.2022.862279

INTRODUCTION

Spatial orientation has been investigated behaviorally in many insects, ranging from desert ants (Wehner, 2003; Wehner and Müller, 2006), honeybees (Brines and Gould, 1979; Edrich et al., 1979; Rossel and Wehner, 1984), dung beetles (el Jundi et al., 2019; Dacke et al., 2021), and locusts (Homberg, 2015), to moths (Dreyer et al., 2018a,b). This also includes the monarch butterfly *(Danaus plexippus)*, which covers a distance of about 4,000 kilometers on its annual migration to its overwintering spots in Central Mexico (Merlin et al., 2012; Merlin and Liedvogel, 2019).

During this long-distance migration, the butterflies use the sun as their main orientation reference (Stalleicken et al., 2005). To successfully maintain their southerly direction over the course of a day, the butterflies integrate time information from the antennae (Merlin et al., 2009; Guerra et al., 2012) and the brain (Sauman et al., 2005) into their sun compass. In addition to the sun, monarch butterflies may also rely on the polarization pattern of the sky for orientation (Reppert et al., 2004). While the pattern of polarized light is perceived by a specialized dorsal region of the monarch butterfly eye, termed the dorsal rim area, the sun is detected by eye regions outside of the dorsal rim area (Sauman et al., 2005; Stalleicken et al., 2006). Celestial information is then transferred *via* the optic lobe and anterior optic tubercle to input neurons of the central complex (CX), termed tangential (TL) neurons (Heinze and Reppert, 2011; Nguyen et al., 2021). These neurons transfer celestial information from the bulb of the lateral complex to the central complex lower division in many insects (Held et al., 2016; el Jundi et al., 2018; Hensgen et al., 2020; Rother et al., 2021), including monarch butterflies (**Figures 1A,B**). As shown for other insects (Stone et al., 2017; Hardcastle et al., 2021), TL cells (in fruit flies termed ring neurons) synapse onto a network of heading-direction cells that flexibly encode the actual flight direction of an animal based on sensory-motor information (Seelig and Jayaraman, 2015; Green et al., 2017; Turner-Evans et al., 2017; Fisher et al., 2019; Kim et al., 2019; Okubo et al., 2020; Hulse et al., 2021). While previous research focused on how the CX processes single celestial stimuli in the monarch butterfly brain (Heinze and Reppert, 2011; Nguyen et al., 2021; Beetz et al., 2022), the controlled single cue conditions in the lab rarely reflect the compound cue conditions found in nature. Thus, to obtain a highly robust compass network, multiple visual cues, such as the sun and polarized light are integrated simultaneously in nature (el Jundi et al., 2014; Lebhardt and Ronacher, 2014). Moreover, experiments on tethered flying monarch butterflies suggest that the butterflies combine a sun stimulus and a panoramic skyline to keep a directed flight heading (Franzke et al., 2020), similar to what has been reported for Australian bull ants (Reid et al., 2011) and honeybees (Towne and Moscrip, 2008; Towne et al., 2017). But how visual sceneries composed of multiple stimuli, such as the sun and polarized light or the sun and a panoramic scene, are combined and how each of the cues is weighted neuronally has not been investigated in the monarch butterfly brain so far. To study this, we recorded intracellularly from TL cells in the monarch butterfly brain and analyzed how they respond to simultaneously presented stimuli, such as a simulated sun and polarized-light stimulus as well as a sun and panoramic-skyline stimulus.

MATERIALS AND METHODS

Animals

Adult monarch butterflies (*Danaus plexippus*) of both sexes were kept in an incubator (I-30VL, Percival Scientific, Perry, IA, USA) with a 12:12 h light-dark cycle at 25°C in Würzburg (Germany). They were provided with 15% sugar solution *ad libitum*. Some animals were caught at College Station, TX, USA during their annual southward migration. These animals were kept in the incubator at an 11:13 h light-dark cycle at 23°C during light and 12°C during dark phases. They were fed with 20% honey solution every second day.

Preparation and Electrophysiology

After clipping off wings and legs, the butterflies were attached to a custom-built holder using dental wax (Omnident, Rodgau Nieder-Roden, Germany). The head capsule was opened frontally and muscle and fat tissue above the brain were removed. At least one of the antennae remained intact to avoid a disruption of circadian inputs to the compass network (Merlin et al., 2009; Guerra et al., 2012). To access the central brain with the electrode, the neural sheath was removed using fine tweezers. Throughout preparation and subsequent neuronal recording, the brain was immersed in monarch ringer (150 mM NaCl, 3 mM KCl, 10 mM TES, 25 mM sucrose, 3 mM $CaCl_2$).

To record intracellularly from individual TL neurons, micropipettes were drawn from borosilicate glass capillaries (inner diameter: 0.75 mm and outer diameter: 1.5 mm, Hilgenberg, Malsfeld, Germany) using a Flaming/Brown horizontal puller (P-97, Sutter Instrument Company, Novato, CA, USA). After loading the micropipette with 4% Neurobiotin (Vector Laboratories, Burlingame, UK, dissolved in 1 M KCl), it was filled with a 1 M KCl solution. The micropipette was connected to an electrode holder with a chloridized silver wire, which was attached to a micromanipulator (Leica Microsystems, Wetzlar, Germany). Another chloridized silver wire served as reference electrode and was inserted into the opened head capsule close the butterfly's mouthparts. Detected signals were amplified 10x using a BA-03X bridge amplifier (npi Elelctronic GmbH, Tamm, Germany). The signal was digitized with sampling rates between 1-20 kHz using a digitizer (Power1401, Cambridge Electronic Design, Cambridge, UK). The neuronal activity was observed on a computer using the software Spike 2 (version 9.00, Cambridge Electronic Design). To obtain recordings from TL neurons, we targeted their output regions in the central complex. All recordings were thus likely obtained from the neurons' axons that enter the central body lower division anteriorly (**Figure 1A**).

Celestial Stimuli

To simulate celestial cues, the same stimulus was used as described in Nguyen et al. (2021). A rotation stage (DT-50, PI miCos GmbH, Karlsruhe, Germany) was dorsally positioned to the animals. For the polarized UV light stimulus, a polarizer was mounted on top of the rotation stage. Because monarch butterflies detect polarized light in the UV range (Sauman et al., 2005; Stalleicken et al., 2005) a UV-LED with an emission peak at 365 nm (LZ1-10UV00-0000, OSRAM Sylvania Inc., Wilmington, MA, US) and a quarter white diffuser (Nr. 251, LEE filters, Hampshire, UK) were placed behind a UV permeable linear polarizer (BVO UV, Bolder Vision Optik Inc., Boulder, CO, USA) in the center of the rotation stage. This allowed us to present equally illuminated polarized UV light to the butterflies. The sun stimulus was presented using an unpolarized green LED with an emission peak at 517 nm (LZ1-10G102-0000, OSRAM, Munich, Germany). This LED was mounted on one of four arms extending from the rotation stage. To control for the influence

of wavelength information, a UV LED was attached to the arm opposite to the green LED. Both light spots were adjusted to an elevation of 30° relative to the animal's head and provided unpolarized light. The angle of the zenithal polarization filter was aligned perpendicular to the two LED arms, which allowed to present the celestial cues in the spatial relationship found in nature. All light stimuli (unpolarized green/UV light, polarized UV light) were adjusted to a photon flux of about 1.4×10^{14} photons/cm^2/s, measured with a spectrometer (Maya2000 Pro, Ocean Optics) at the position where the animal faced the stimuli during recordings. Since the recordings were obtained *via two* setups with identical equipment, the angular positioning of the stimulus varied slightly. The polarization stimulus had an angular extent between 9.6°-10.4° at the butterfly's eye. The angular size of the unpolarized light spots was 1.3°-1.4°. The movements of the rotation stage were controlled *via* a custom-written script for the software MATLAB (Version R2019b, MathWorks, Natick, MA, USA). During the experiments, the rotation stage was turned by 360° in clock- and counterclockwise direction at a constant velocity of 60°/s while testing the response of the TL cells to a single stimulus (sun stimulus *or* polarized light) or a combination of the stimuli (sun stimulus *and* polarized light). As five of the TL neurons were obtained from migratory butterflies, we first tested if they differed in their general tuning characteristics from the recordings obtained in non-migratory butterflies. However, we did not find any differences in the relevant response characteristics tested here between both groups and decided to pool the data. As we often co-labeled several TL neurons from both brain hemispheres, we were unable to define for each recording from which brain hemisphere it was obtained. However, in six out of the ten celestial-cue experiments, TL neurons with synaptic input in the right bulb were either solely stained or showed a stronger staining (**Figure 1B**). In the remaining four experiments, TL neurons with inputs in the left bulb were either stained stronger (two experiments) or showed the same staining strength to TL neurons in the right brain hemisphere (two experiments).

Panoramic Skyline and Sun Stimuli

The panoramic skyline was simulated *via* an LED arena consisting of a circular array of 128x16 RGB-LEDs (M160256CA3SA1, iPixel LED Light Co., Ltd, Baoan Shenzhen, China). The arena covered a visual field of 360° along the horizontal and 43° along the vertical plane around the animal. The LEDs were controlled *via* a Raspberry Pi (Model 3B, Raspberry Pi Foundation, Cambridge, UK). We presented the same panoramic skyline to the butterflies that has been used in recent behavioral experiments on monarch butterflies (Franzke et al., 2020). Each LED above the horizon was adjusted to a photon flux of about 6.68×10^{10} photons/cm^2/s in the blue range (emission peak: 458 nm). LEDs below the horizon were turned off. The panoramic scene was uploaded as an RGB image 8 bits/channel) to the Raspberry Pi and a custom-written program written in Go controlled the rotation movements of the stimulus. To avoid any dark adaption of the animals' eyes or history-dependent effects, a panorama with a flat horizon (*flat panorama*) was presented to the animals while searching for TL neurons. As soon as a TL neuron was successfully targeted, the panoramic scenery with the variable height profile (*panoramic skyline*) was used as a test stimulus. Light intensity differences between the panoramic scenery and the flat panorama were minimized by turning on a similar number of LEDs in both panoramas. To find TL neurons during our experiments, we first stimulated the animal with zenithal polarized light. Once a neuron responded to polarized light, the polarization stimulus was turned off and the panoramic skyline was presented and rotated by 360° around the animal in clock- and counterclockwise direction (at a constant velocity of 60°/s). To combine the panoramic scene with a sun stimulus, one LED above the horizon at an angular elevation of 18.9° was switched to a wavelength emission peak of about 516 nm and an intensity of about 6.14×10^{12} photons/cm^2/s. We combined the sun stimulus either with the flat panorama or with the panoramic skyline. For the former, we moved the sun stimulus around the animal, while the flat panorama stayed stationary. For the latter, we rotated both stimuli around the animal.

Histology and Imaging

To evaluate anatomically the neuron type from which we recorded, Neurobiotin was iontophoretically injected into the cells (1-3.5 nA) for 3-5 min at the end of each experiment. After allowing the Neurobiotin to distribute for 20 min, the brains were dissected out of the head capsule and fixated for 18-24 h at 4°C in a sodium-phosphate buffer containing 4% paraformaldehyde, 0.2% picric acid, and 0.25% glutaraldehyde. They were then rinsed 4 × 15 min in 0.1 M phosphate buffered saline (PBS) and, afterwards, incubated with either Cy3-conjugated to streptavidin (Thermo Fisher Scientific, Waltham, MA USA, 1:1000) or Alexa568-conjugated to streptavidin (Molecular Probes, Eugene, OR, USA, 1:1000) diluted in PBS containing 0.3% Triton-X 100 (PBT) for 3 days at 4°C. The brains were then rinsed with PBT (3 × 20 min) and afterwards with PBS (2 × 20 min), before they were dehydrated through an ascending ethanol series (30, 50, 70, 90, 95, and 100%; 15 min each). Afterwards, the brains were immersed in a 1:1-mixture of ethanol and methyl salicylate (Fisher Scientific GmbH, Schwerte, Germany) for 20 min and then in 100% methyl salicylate for about 1 h at room temperature. The brains were then mounted in Permount (Fisher Scientific) between two cover slips with 10 reinforcement rings (Avery, Toronto, Canada) as spacers. Finally, they were imaged using a confocal microscope (Leica TCS SP8, Wetzlar, Germany) with a 10x air objective (HCX PL-Apo 10x/0.4 CS, Leica).

Data Analysis

To consider a neuron for analysis, the following criteria had to be fulfilled: *i.* stable baseline during stimulus presentation, *ii.* spike amplitudes clearly above noise level and *iii.* distinct immunolabeling of the recorded neuron. If a neuron passed these criteria, the recorded file was imported into MATLAB for further analysis *via* custom-written scripts that included the CircStat toolbox (Berens, 2009). Events during stimulation were detected based on a manually set threshold and were assigned to a particular polarization angle during the polarizer rotation or to a corresponding azimuthal angle during circling of a

light spot. Neuronal spiking rates were estimated by low-pass filtering the instantaneous firing rate of the action potentials and illustrated as sliding window averages (Gaussian filtered, window size: 0.5 s) in the results. The preferred firing directions in response to the stimuli were determined as the mean vector of the bimodal (polarized light) or unimodal (sun stimulus) distribution of stimulus angles at the times of action potentials. The degree, to which the action potentials were clustered at this angular position, was defined as the vector strength. This value ranges from 0 to 1, with higher values indicating more directed responses

In addition to the aforementioned parameters, responses of each trial were binned into 18 bins and spike rate in each bin was calculated. This was used to obtain the modulation strength as described by Labhart (1996) using the following equation:

$$M = \sum_{i=1}^{18} |n_i - \overline{n}|$$

where n is the spiking rate (in spikes/s) and $\overline{n}$ is the average spiking rate over the whole stimulation period. The higher the modulation strength, the stronger is the response of a neuron to a certain stimulus.

To predict the neuronal response to a combination of stimuli and to define the relevance of each cue on the neuronal coding, a weighted linear model was applied. This was based on the responses of the same neuron to the individual stimuli using the following equation:

$$y = r_1 \bullet w + r_2 \bullet (1 - w)$$

where r_1 and r_2 describe the actual response of a neuron to an individual stimulus (e.g., sun stimulus and polarized light for the combined celestial stimuli condition), respectively and w indicates the weighting of them. If $w < 0.5$, the response of r_2 is weighted higher, while $w < 0.5$ indicates that the neuronal response of r_1 dominates the response. To identify the weighting that matches best the actual neuronal response to the combination of both stimuli, we calculated the correlation between the actual neuronal response and the modeled neuronal responses based on different linear weightings. The weighting that exhibited the highest correlation coefficient, was then considered for further analysis.

As we did not have any prediction of whether and how the TL neurons respond to the panoramic skyline, we used the inter-trial difference between single stimulus presentations as reference. Inter-trial differences were determined by treating clock- and counterclockwise responses separately. At first neuronal responses were grouped based on the stimulus rotation. Then, for both rotation directions, we calculated the mean neuronal response and correlated them with the response from each trial. Finally, the correlation coefficients were averaged within and then across rotation groups. The closer the correlation were to unity, the more similar were the neuronal responses across trials. To quantify the neuronal response to the panoramic skyline further, the averaged neuronal response for clock- and counterclockwise rotations was compared with the response to the flat panorama during a 6 s time frame. Both correlation values were averaged across rotation groups again. If the neurons encoded parts of the panoramic skyline, we expected that the neuronal response to the panoramic skyline and the response to the flat panorama correlate less with each other than the neuronal responses across trials.

To further characterize the response of the TL cells to the panoramic skyline, we applied an intensity-based model for different elevations. Circular, excitatory TL neurons' receptive fields were modeled by a Gaussian Kernel (11.5° width ± 2.9° standard deviation, corresponding to 5 pixels width and 2 pixels standard deviation of the arena) in MATLAB. This receptive field size is in a similar range as the excitatory component of measured locust TL neuron receptive fields (Takahashi et al., 2022). When the scene is rotated around the animal, this evokes changes in brightness in the modeled receptive field that are correlated with the silhouette of the panorama. Thus, if a bright sector of the panorama moves through the receptive field, it increases the spiking activity. In turn, if a dark sector of the panorama is moved through the receptive field, it will decrease the spiking activity. However, this change in spiking activity depends on the elevation of the receptive fields (**Figure 3E**), which may vary in monarch butterfly TL neurons, as shown for the homologous neurons in fruit flies (Seelig and Jayaraman, 2013). To reliably test if the TL neurons respond to the panoramic skyline, we defined each row of the LED arena between −16.1° and 16.1° as the center of a possible receptive field and modeled curves of the predicted neuronal modulation at different elevations when the panorama was rotated. To find the best match between the modeled response and the recorded neuronal response at different elevations, we calculated for the modeled responses at each elevation the cross correlation with the measured neuronal response. The modeled curve that exhibited the best match to the recorded neuronal response curve was included for further analysis.

Statistics

To identify whether action potentials in response to the simulated celestial cues are non-uniformly distributed, we applied the Rayleigh-test (significance level <0.05). To test whether the preferred firing directions are significantly clustered around the 0°-180° axis (polarized light) and around 90° (sun stimulus), we used the V-test (significance level <0.05). To test for normal distribution and similar variances of the modulation strengths, the Shapiro-Wilk test and the Levene-test were employed, respectively. If data were normally distributed and exhibited the same variance, parametric hypothesis tests were applied (unpaired *t*-test and paired *t*-test, respectively). Otherwise, non-parametric tests were used (Wilcoxon-rank-sum-test for unpaired and the Wilcoxon signed rank test for paired mean values). For partially paired data, like the observed weighting factors, a mixed linear model was used to test if the mean values differed significantly between the two test groups. Averaged parameters are shown as mean ± standard deviation if not mentioned otherwise.

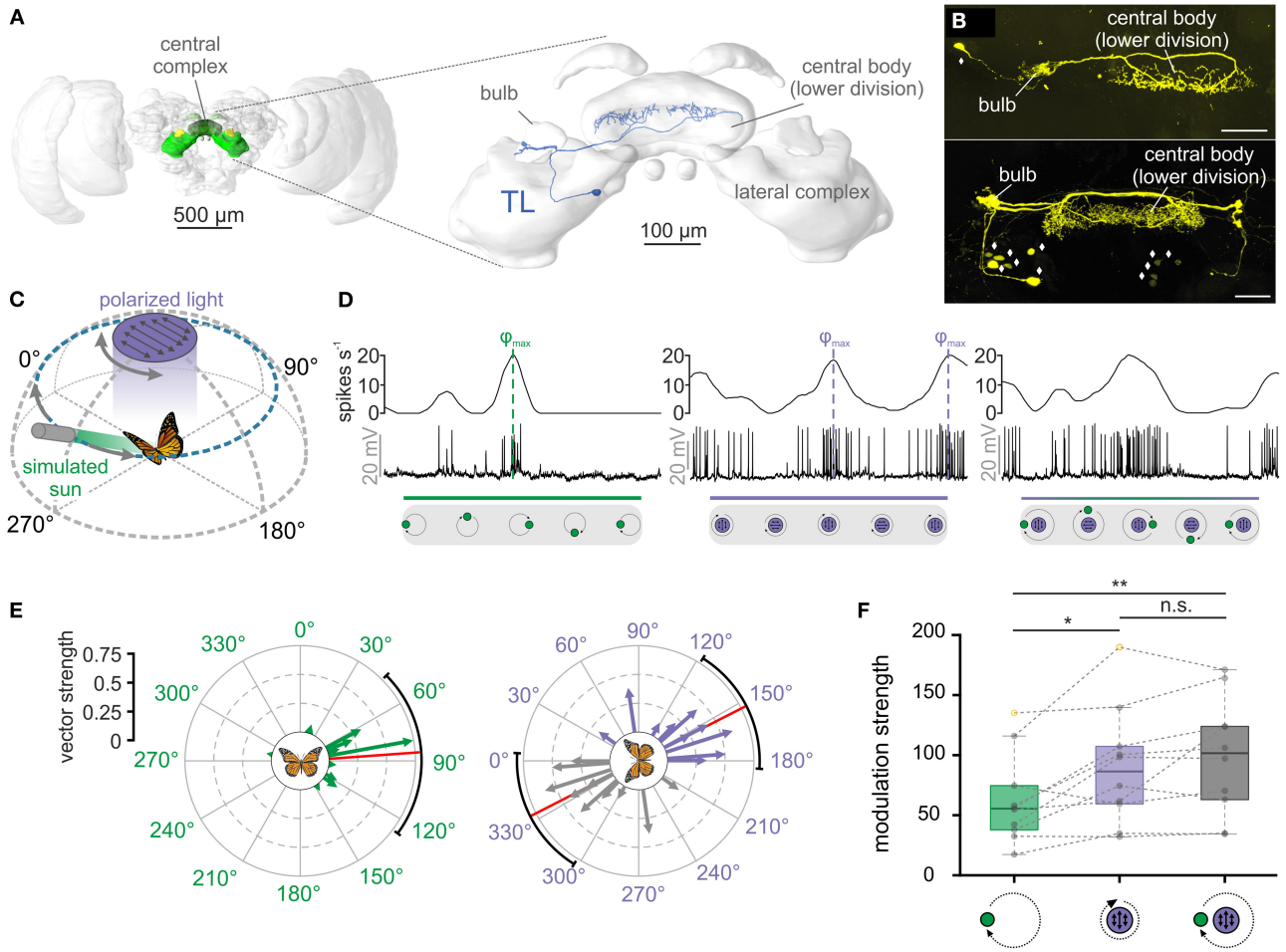

FIGURE 1 | TL neurons of the central complex encode simulated celestial cues. **(A)** Left: Frontal view of the monarch butterfly brain. Highlighted in green are the neuropils of the central complex and lateral complex. Right: The central complex and lateral complex. A reconstructed tangential neuron (TL) is shown in blue. Modified from Heinze et al. (2013). **(B)** Two examples of TL neuron tracings (anterior views) during electrophysiological recordings (maximum intensity projection views). While single cell tracings of one TL cell was possible (top, synaptic input in the right bulb), in most experiments, several TL neurons from both hemispheres were labeled (bottom). Diamonds indicate the position of TL neuron somata. Scale bars: 50 µm. **(C)** Schematic illustration of the presented simulated celestial cues. The polarization stimulus was positioned dorsally to the butterfly and was rotated by 360°. The angle of polarization was aligned with the antero-posterior axis of the animal at the beginning of the rotation. The sun stimulus (elevation: 30°) was moved on a circular path around the animal. The angle of polarized light was oriented perpendicular to the direction of the sun stimulus, simulating their spatial relationship in nature. **(D)** Neural tuning of the same TL neuron to a moving sun stimulus (left), a rotating polarizer (middle) and when both stimuli were presented simultaneously (right). The upper curve of each plot shows the sliding window average of the action potential recordings (middle row). The lower gray boxes illustrate the position of the stimuli during a clockwise 360°-rotation. Preferred firing directions (φ_{max}) to the sun (left) and polarized light (middle) are indicated by dashed vertical lines. **(E)** The preferred firing directions of the tested TL neurons ($n = 10$) in response to the sun stimulus (left) and the polarization stimulus (right). Each arrow represents a single neuron. Arrow length indicates the vector strength (directedness) of the neural tuning. The circular plots are labeled in relation to the animals' body axis (see schematic at the plot's center), with 0° being anterior, 90° being right, and 270° being left to the animal. The mean preferred firing directions (sun stimulus: 85.88° ± 54.94°; polarized light: 152.96° ± 34.16°) are indicated by the red solid lines and the confidence intervals (95%) by the black arcs. **(F)** Modulation strength of neural activity ($n = 10$) in response to the sun stimulus (left), polarized light (middle), and the combination of both celestial cues (right). The neural modulation to the sun stimulus was significantly weaker than to polarized light ($p_{GREENvs.POL} = 0.02$, $t = 2.99$, $n = 10$; paired t-test) and the combination of the stimuli ($p_{GREENvs.COMBO} = 0.002$, $t = -4.38$, $n = 10$; paired t-test), while the modulation strength to polarized light and the combined stimuli did not differ from each other ($p_{POLvs.COMBO} = 0.23$, $t = -1.28$; paired t-test). Gray circles show individual data points. Outliers are indicated in yellow. Dashed gray lines connect individual data points from the same TL neuron. Boxes indicate interquartile range. Whiskers extend to the 2.5th and 97.5th percentiles. Black horizontal lines show the median. n.s.: not significant, $^*p < 0.05$, $^{**}p < 0.01$.

RESULTS

To understand how the monarch butterfly compass integrates multiple visual stimuli, we presented different visual cues in isolation and in combination to the animals while recording intracellularly from TL neurons of the central complex (**Figures 1A,B**). We successfully obtained recordings from 34 TL neurons. 15 TL neurons were tested with a combination of different celestial stimuli and 19 TL neurons with a combination of celestial and terrestrial wide field stimuli. Of the latter group,

all TL cells were tested with the panoramic skyline, 15 of them were exposed long enough to the flat panorama to be included in the inter-trial response analyses and 13 of them were presented the combined sun stimulus and panoramic skyline.

Celestial Cue Integration in TL Neurons

We first tested the neuronal tuning to simulated celestial cues. Similar to previous experiments (Heinze and Reppert, 2011; Nguyen et al., 2021), a moving green light spot served as a sun stimulus while a rotating polarizer illuminated by UV light from the zenith was used to examine polarization sensitivity (**Figure 1C**). To simulate the natural spatial relationship between the sun and polarized light, we oriented the polarization angle perpendicular to the sun-stimulus direction (**Figure 1C**). As expected from previous experiments (Heinze and Reppert, 2011; Nguyen et al., 2021), TL neurons responded to both the sun stimulus and polarized light (**Figure 1D**, left and middle graph). Interestingly, the highest action potential rates (preferred firing directions, φ_{max}) of the TL neuron to the sun stimulus and the polarization stimulus matched the 90°-relationship of the cues in nature. To investigate if this was true for all recorded TL cells, we analyzed the spatial distribution of the preferred firing directions (φ_{max}) in response to the sun stimulus. The preferred firing directions were clustered around 90° in response to the sun stimulus ($p = 0.008$, v = 5.43; V-test; $n = 10$; **Figure 1E**, left) and along the 0° - 180° axis in response to polarized light ($p = 0.03$, v = 4.37; V-test; $n = 10$; V-test; **Figure 1E**, right). Taken together, the spatial relationship between the mean preferred firing directions of the recorded TL neurons when presenting sun and polarization stimulus in isolation matched the natural spatial relationship between both celestial cues.

When we presented both stimuli simultaneously, the neuronal tuning resembled a mixed response (**Figure 1D**, right graph), suggesting that TL neurons integrate both stimuli in a weighted manner. To quantify which of the two stimuli dominated the neuronal response, we compared the modulation strengths in response to the single stimuli (sun stimulus *or* polarized light) with the modulation strengths of the same neurons in response to the combined stimulus (sun stimulus *and* polarized light). The modulation strength in response to the sun stimulus (62.48 ± 37.05, $n = 10$) was significantly weaker than the modulation strength of the same neurons to the polarization stimulus (89.81 ± 48.64, $n = 10$; $p = 0.02$, $t = 2.99$; paired t-test) and to the combination of the stimuli (98.90 ± 48.43, $n = 10$; $p = 0.002$, $t = -4.38$; paired t-test; **Figure 1F**). The modulation strength did not differ between the response to the polarizer and to the combination of the stimuli ($p = 0.23$, $t = -1.28$; paired t-test). This indicates that the polarization input is weighted stronger than the sun-stimulus input and that the response to the combined celestial cues seems to be mainly shaped by the polarization input.

Weighting of Celestial Cues in TL Neurons

To quantify whether polarized light truly dominates the response to the combined celestial cues and how they are weighted in TL neurons, we combined the responses to the isolated stimuli (**Figure 2A**, upper plot) in a weighted linear model and calculated a predicted response to the combined stimuli. By varying the weight between the neuronal response to the polarizer and sun stimulus, we modeled different expected neuronal responses to the combined stimuli and correlated these modeled responses with the actual response to the combined stimuli (**Figure 2A**, blue curve of lower plot). The modeled response with the highest similarity to the actual neuronal response (**Figure 2A**, red curve of lower plot) was selected to determine the neuron-specific cue weighting. A weighting factor of 0 indicated that the combined response was entirely characterized by the sun stimulus while a weighting of 1 represented a tuning that was purely described by the polarization input.

For all neurons, the correlation coefficients obtained through the comparison of the modeled and actual neuronal response were relatively high (**Figure 2B**, inset in upper histogram, 0.86 ± 0.12, $n = 10$), suggesting that the response of TL neurons to the combined celestial stimuli can be well described by the weighted linear model. When presenting sun stimulus and polarized light simultaneously, most TL cells responded stronger to the polarization information (**Figure 2B**, upper histogram), although the light intensity of the stimuli was set to the same photon flux. The bias toward the polarization stimulus may be induced by differences in the absolute sensitivity of the UV and green photoreceptors in the monarch butterfly eye. Thus, we assumed that the UV polarization stimulus may appear brighter to the butterflies than the green sun stimulus due to a higher sensitivity of the photoreceptors to UV light. To test whether this may explain the dominance of the polarization stimulus on the neuronal response to the combined stimuli, we repeated the experiments with a UV sun stimulus that had the same photon flux as the UV polarization stimulus (**Figure 2C**). Again, except for one neuron, the weighted linear model described the actual neuronal response well (**Figure 2B**, inset in lower histogram; 0.77 ± 0.28, $n = 12$), which further confirms that celestial information is linearly integrated in TL neurons. In contrast to the trials with the green sun stimulus and polarized light, the weighting to the combined UV stimuli shifted in favor of the UV sun stimulus (**Figure 2B**, lower histogram). The observed weightings differed significantly between the experiments with the green sun stimulus and polarized light (0.65 ± 0.28, $n = 10$) and the UV sun stimulus and polarized light (0.30 ± 0.23, $n = 12$; $p < 0.001$, $F = 113.31$; ANOVA, **Figure 2B**, boxplots). Taken together, our data show that TL neurons combine celestial cues linearly in monarch butterflies. However, the weighting between the sun and polarization input is highly affected by the spectral content and relative brightness of the presented stimuli.

TL Neurons Are Tuned to a Panoramic Skyline

In addition to celestial cues, recent experiments in *Drosophila melanogaster* suggest that central-complex neurons encode the entire visual scenery around the animal (Seelig and Jayaraman, 2015; Kim et al., 2019). One salient cue in a visual scene that can be used by many insects for orientation is the profile of a panoramic skyline (Graham and Cheng, 2009a,b; Reid et al., 2011; Legge et al., 2014; Franzke et al., 2020). In contrast to the sun and polarized skylight, coding a panoramic skyline

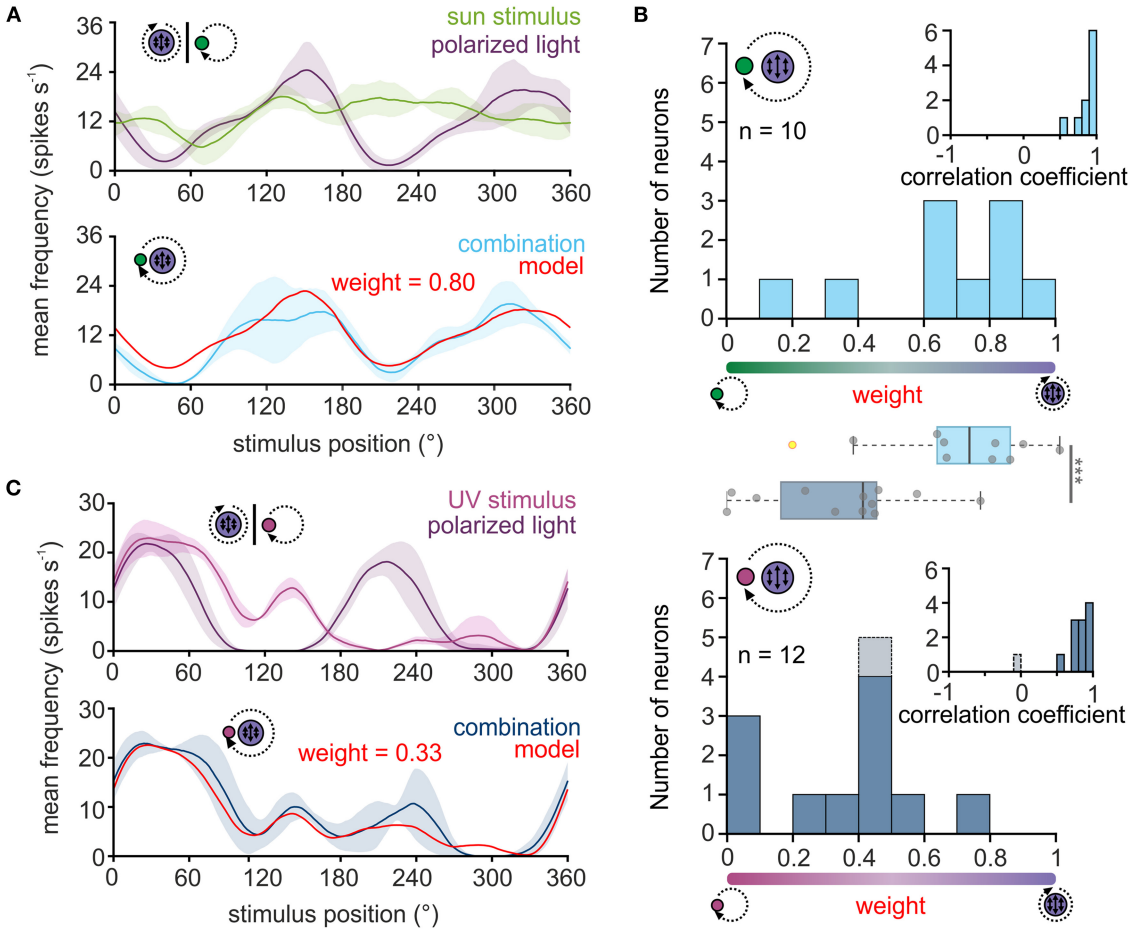

FIGURE 2 | Weighting of celestial cues in TL neurons. **(A,C)** Upper plot: sliding window averages of the action potential rates of two TL neurons to the green sun stimulus [**(A)**, green curve] or UV light spot [**(C)**, magenta] as well as to the polarization stimulus [**(A,C)**, violet curves] are shown. Lower plot: The response of the same neurons as shown in the corresponding upper plots when both stimuli were presented simultaneously [**(A)**, light blue; **(C)** dark blue curve]. Based on the response to the single cues, a weighted linear model was fitted to the data (red curve) and a weighting of the single cues was calculated. A weight between 0 and 0.5 suggests that the sun stimulus **(A)** or the UV light spot **(C)** dominated the combined response while a weight between 0.5 and 1 indicates that the polarization input dominates the combined response. The shaded areas show the standard deviation. **(B)** Histograms of the weighting factors obtained for the experiments with the green sun stimulus and polarized light (top, $n = 10$) and the UV light spot and polarized light (bottom, $n = 12$). Insets show the correlation coefficients which describe how well the weighted linear model explains the measured neural response to the combined stimulus. The weighting factor that was obtained from a low correlation coefficient is shown in gray. Box plots in the middle: While the weighting is shifted to the polarization input when a green sun stimulus was combined with polarized light, the weighting is significantly shifted in favor of the light spot, when a UV light cue was combined with polarized light ($p < 0.001$, $F = 113.31$; linear mixed model ANOVA). Gray circles show individual data points (yellow circles indicate outliers). Boxes indicate interquartile range. Whiskers extend to the 2.5th and 97.5th percentiles. Black horizontal lines show the median. ***$p < 0.001$.

neuronally is more complex as the neurons need to integrate information from different azimuths and elevations to precisely reproduce the silhouette of the panoramic skyline (Dewar et al., 2017). To grasp how the monarch butterfly central complex encodes a panoramic skyline, we placed the butterflies at the center of an LED arena and recorded the neuronal activity of TL neurons while the animals were exposed to a panoramic skyline that was presented at the inner surface of the LED arena. We used the same panoramic skyline that has recently been used to study the monarch butterfly orientation behavior (Franzke et al., 2020; **Figure 3A**). When we rotated the scene around the butterflies, we found that many TL neurons were modulated by the panoramic stimulus (**Figure 3B**). To exclude that these modulations occurred spontaneously, we analyzed the inter-trial variability of the neuronal activity and correlated the neuronal activity in response to each trial (**Figure 3B**, *gray curves*) with the averaged response (**Figure 3B**, *orange curve*). As a control, the neuronal responses of the same TL neurons to a flat panorama (**Figure 3C**) were correlated to the averaged response to the panoramic skyline. Neuronal responses to the panoramic skyline across trials were highly correlated with their averaged response (**Figure 3D**, upper plot) indicating a low inter-trial variability and that the neuronal modulations occurred in response to the rotating panoramic skyline. In contrast, the

neuronal activity in the presence of the flat panorama was poorly correlated with the averaged response to the panoramic skyline (**Figure 3D**, lower plot). The correlation coefficients between inter-trial responses and the averaged response to the panoramic skyline were significantly higher (0.76 ± 0.07) than to the responses to the flat panorama and the averaged responses to the panoramic skyline (-0.02 ± 0.29; $p < 0.001$, sign rank $= 120$, Wilcoxon signed rank test, **Figure 3D**). This demonstrates that monarch butterfly TL neurons encode, in addition to celestial cues, panoramic skylines.

Although it is not trivial to predict the TL response to the presented panoramic skyline, we noticed that the modulation of the spiking activity seemed to correlate negatively with the troughs of the profile (**Figure 3B**), suggesting that they are tuned to changes in brightness during the stimulus rotation. To investigate this hypothesis, we modeled the neuronal responses for fictive TL cells whose neuronal tunings were based on changes in brightness during stimulus rotations. As the receptive fields of the TL neurons can cover patches of different elevations and azimuths (Seelig and Jayaraman, 2013; Takahashi et al., 2022), we varied both the azimuth and elevation (between -16.1° and $+16.1^\circ$) of the center of the modeled neuron's receptive field (**Figure 3E**). For each of the modeled responses (**Figure 3F**, *blue curves*), we calculated its cross correlations with the measured neuronal TL response (**Figure 3F**, *orange curves*). If TL neurons encoded changes in brightness associated with rotations of the panoramic skyline, we expected that one of the modeled neuronal responses will align well with the measured neuronal response. Indeed, most measured neuronal responses correlated well with one of the modeled TL responses (**Figure 3G**). Not surprising, they showed the highest correlation at elevation values between -10.75° and $+10.75^\circ$. In addition, cross correlations allowed us to calculate the azimuthal panorama position that gave the strongest neuronal response. The angular shifts between the measured and modeled TL response leading to the highest correlation coefficient clustered in the anterior field of the animals ($p = 0.045$; $Z = 3.06$, $n = 19$, Rayleigh test; **Figure 3H**).

Weighting of the Sun and Panoramic Scene in TL Neurons

We next wondered how TL neurons encode a visual scene that was composed of a simulated sun and the panoramic skyline. As demonstrated in the example TL neuron, the moving sun stimulus mainly dominated the neuronal response, irrespective of the absence/presence of the panoramic skyline (**Figures 4A,B**), but the modulation of the panoramic profile was additionally encoded in the neuronal response of the TL neuron (arrow in **Figure 4B**). To test whether the TL neurons combine both stimuli in a linear manner, as shown for the celestial cues, we also tested the same neurons' responses to the single stimuli. As expected, the TL neurons responded to the sun stimulus (**Figure 4C**, *green curve*) and the panoramic scene (**Figure 4C**, *orange curve*), when presented individually. Again, we used the neuronal tuning to the single stimuli to model the expected response of the TL neurons to a combined – sun and panorama – stimulus presentation. We then used the modeled neuronal response based on the weighted linear model (**Figure 4C**, *red curve*) and correlated it with the measured neuronal response to both stimuli (**Figure 4C**, *blue curve*). In contrast to the results for the combined celestial cues (**Figure 2**), the weighted linear model did not always result in high correlation values with the measured responses (**Figure 4D**, inset, 0.55 ± 0.29, $n = 13$). For five of the 13 TL neurons (correlation coefficient < 0.5; **Figure 4D**, inset), the neuronal response to the combined celestial and terrestrial cue, i.e., panoramic skyline, could not be explained with a linear model. The predicted weighting factors were highly variable. While responses of some TL neurons were dominated by the sun stimulus (weight < 0.5; **Figure 4D**), responses of other TL neurons were more dominated by the panoramic skyline (weight > 0.5; **Figure 4D**). Taken together, we found a high variance of neuronal coding in cue hierarchy between the sun and the panoramic skyline. This stands in contrast to the results observed with the sun stimulus and the polarized light. Although we were not able to define from which TL subtype we obtained our recordings (see discussion), the results indicate that the cue hierarchy between celestial and terrestrial cues shows a high inter-individual flexibility in monarch butterflies.

DISCUSSION

We show that the monarch butterfly CX integrates multiple visual cues, i.e., celestial and terrestrial panoramic skyline cues for orientation. While the sun stimulus and polarized light were integrated linearly, the coding of the sun stimulus and the panoramic skyline did not always match a linear summation of the neuronal response to the isolated stimuli. Moreover, while polarized light was usually weighted stronger than the green sun stimulus, the weighting of the sun versus the panorama stimulus was set in a variable manner across different TL neurons. This observation is in line with behavioral results on monarch butterflies tested within the same visual setting and might allow the butterflies to set the cue preference in a highly flexible manner between celestial and terrestrial cues (Franzke et al., 2020).

Celestial Coding in the Central Complex

Monarch butterfly TL neurons are sensitive to polarized light (Heinze and Reppert, 2011; Nguyen et al., 2021, this work), similar to what has been reported for TL cells of a wide range of other insects, including desert locusts (Vitzthum et al., 2002; Heinze et al., 2009; Bockhorst and Homberg, 2015; Pegel et al., 2018; Takahashi et al., 2022), field crickets (Sakura et al., 2008), dung beetles (el Jundi et al., 2015), sweat bees (Stone et al., 2017), and fruit flies (Hardcastle et al., 2021). In addition to polarized light, TL neurons in the present study were tuned to a green light spot – likely representing the sun. As we used the responsiveness to the polarization stimulus to physiologically identify the neurons, we might have missed TL neurons that were

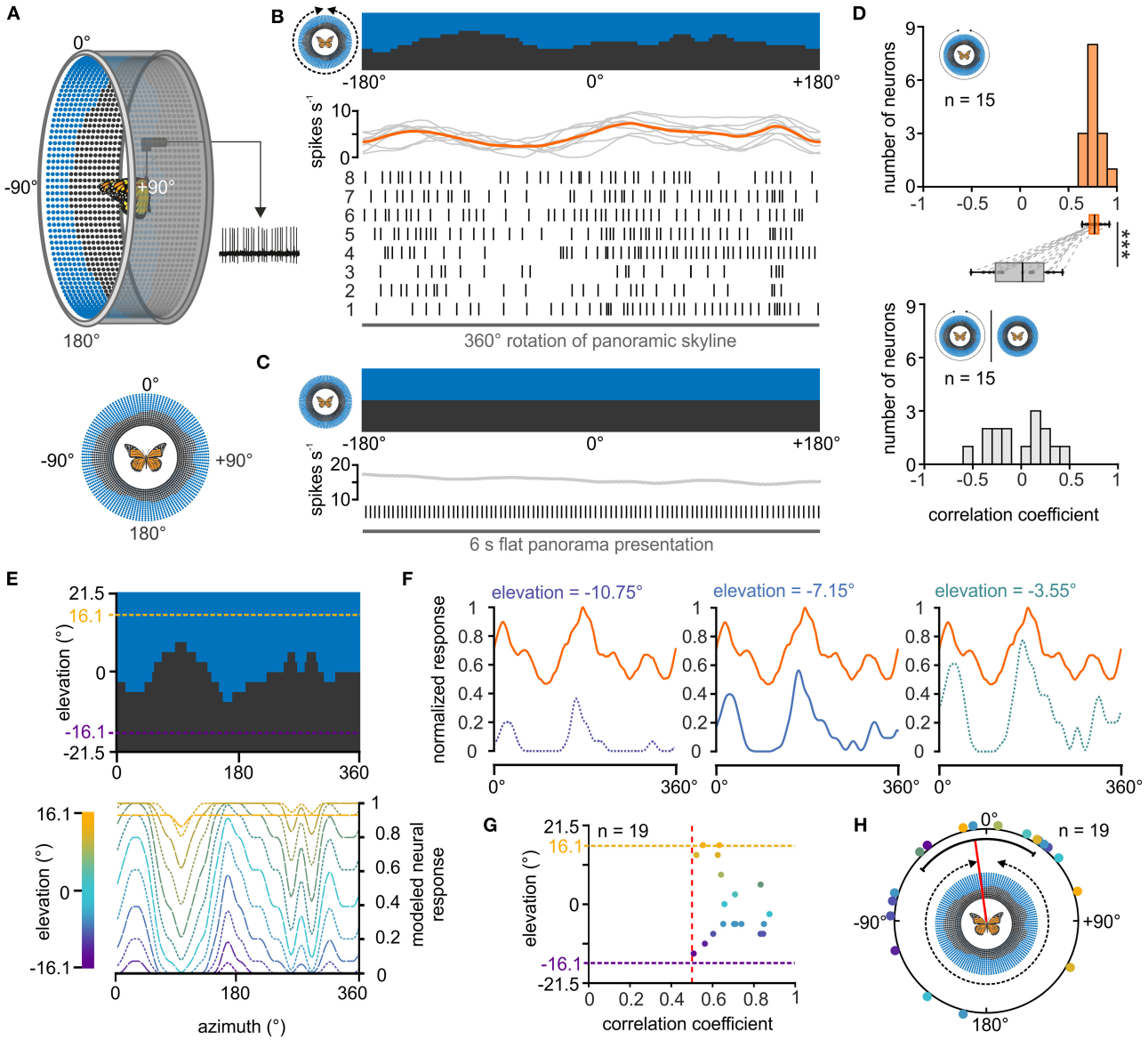

FIGURE 3 | Response of central-complex TL neurons to a panoramic skyline. **(A)** Schematic drawing of the LED arena (top) that was used to test the coding of a panoramic scene in TL neurons. 0° was defined as the direction anterior to the butterfly, before the panoramic scene was rotated by 360° around the animal (bottom). **(B)** The response of a TL neuron to eight 360°-rotations of the panoramic scene is shown as raster plot (middle). Each vertical line represents an action potential. The diagram on top shows the sliding window average of the action potentials for the eight rotations (gray curves) as well as their mean (orange curve). The orientation of the panoramic scene prior to rotation is shown (top). **(C)** The TL neuron does not spontaneously modulate its action potential rate when a flat panorama is presented for 6s. **(D)** Distribution of correlation coefficients when comparing the neural response from each trial with the averaged response (orange, upper panel) and when comparing the neural response to the flat panorama with the averaged response to the panoramic skyline (gray, lower panel). Box plots: The neurons showed a higher inter-trial modulation to the panoramic scene compared to the modulation to the flat panorama ($p < 0.001$; sign rank = 120, Wilcoxon signed rank test). Paired data points across the tested groups are connected by dashed lines. Boxes indicate interquartile range. Whiskers extend to the 2.5th and 97.5th percentiles. Black horizontal lines show the median. ***$p < 0.001$. **(E)** Modeled neuronal response curves to the panoramic skyline of fictive TL neurons that have visual fields centered at different elevations (lower panel). The center of the receptive fields were set for elevations within the panoramic scene (between −16.1° and 16.1°, dashed lines, upper panel). **(F)** The measured neural response of one recorded TL neuron (orange curve) to the panoramic scene plotted against three modeled neural responses whose visual fields were centered at different elevations [see also lower panel in **(E)**]. The measured neural response showed the best match to the modeled modulation at an elevation of −7.15 (middle plot; correlation coefficient = 0.84). **(G)** Elevations of the highest match between the measured TL neuron response and the modeled response plotted against the corresponding correlation coefficients. Each point represents an individual TL neuron ($n = 19$). Vertical, red dashed line indicates a correlation coefficient of 0.5. The vertical dashed lines represent the elevation range for the modeled receptive fields (between −16.1° and 16.1°). **(H)** Azimuthal shifts leading to the maximum correlation between the measured and modeled neural response are plotted for each neuron ($n = 19$). Shifts were clustered in the frontal visual field ($p = 0.045$; $Z = 3.06$, $n = 19$, Rayleigh test). The mean is indicated by a red solid line and the confidence intervals (95%) by a black arc. The color code of the individual TL neurons in G and H corresponds to the color code of the heatmap in **(E)**.

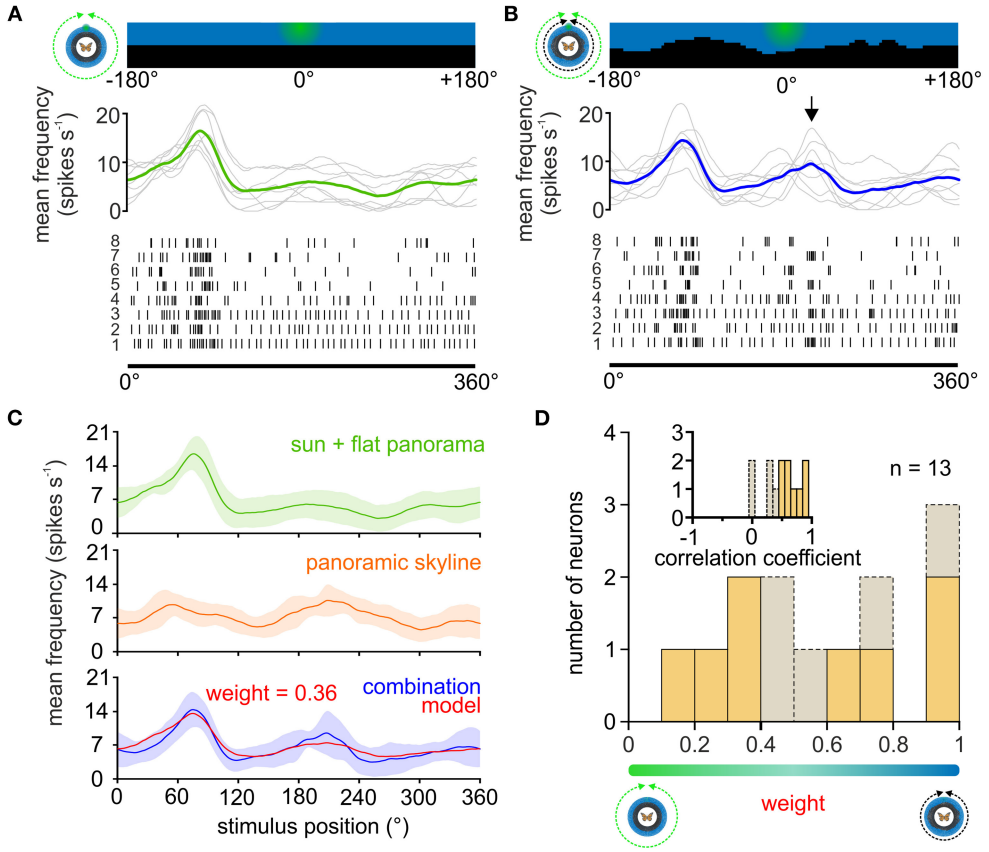

FIGURE 4 | Weighting the sun and panoramic skyline in TL neurons. **(A,B)** The response of a TL neuron to eight 360°-rotations of the sun stimulus **(A)**, and when the sun stimulus and the panoramic scene were rotated simultaneously around the animal **(B)**. The stimulus position prior to rotation is shown (top). The action potentials are shown as raster plots (bottom). Above the raster plots, the sliding window averages of the rotations are shown (middle plot, gray curves). The sliding window averages of the mean spiking frequency are color coded [**(A)**, moving sun stimulus in green; **(B)** moving sun stimulus and panorama in blue]. Arrow indicates an increased spiking activity that was not observed when presenting the sun stimulus alone and thus can be attributed to the panoramic skyline. **(C)** Sliding window averages of the same TL neuron as in **(A,B)** responding to a 360° rotation of different stimuli. From top to bottom: sun stimulus alone (green curve), panoramic skyline alone (orange curve), sun stimulus and panoramic skyline combined (blue curve). A weighted linear model (red curve, lower plot) was fitted to the observed neural activity to the combined stimulus. Shaded areas show the standard deviation. **(D)** The distribution of the weighting factors for experiments with the sun stimulus and panoramic skyline ($n = 13$). Low and high weighting values indicate that the sun stimulus and the panorama dominated the combined response, respectively. The correlation coefficient distribution in the inset indicates how well the weighted linear model described the measured neural response to the combined stimulus. Weighting factors obtained from a low correlation coefficient (<0.5), indicating that the neural response can be explained poorly with a linear model, are shown in gray.

solely tuned to the sun stimulus. However, the here recorded TL neurons are suitable to combine information from the sun and the pattern of polarized light similar to what has been shown in TL neurons in desert locusts (Pegel et al., 2018; Takahashi et al., 2022) and dung beetles (el Jundi et al., 2015), as well as in previous experiments in monarch butterflies (Heinze and Reppert, 2011; Nguyen et al., 2021). Thus, the TL neuron sensitivity to celestial cues is highly conserved and may play a crucial role for the heading coding in a variety of insects. How the TL neurons' gain to visual cues is further affected by an animal's locomotor state, as shown for the corresponding neurons in fruit flies (Seelig and Jayaraman, 2013) and as suggested by a recent study on monarch butterflies (Beetz et al., 2022), awaits to be explored.

We found a fixed spatial relationship between the preferred firing direction to the sun stimulus and the polarization stimulus. The clustering of the preferred sun-stimulus directions to the butterflies' right side is likely a result of a bias in recordings from the right brain hemisphere (at least six out of ten recordings were obtained from right TL neurons). Thus, these cells receive likely visual input from the ipsilateral eye which is well in line with previous recordings from these compass neurons (Heinze and Reppert, 2011). Interestingly, we found that the preferred polarization directions of the same TL neurons were significantly aligned with the animals' longitudinal body axis which is at odds with a previous study (Heinze and Reppert, 2011). This resulted in an orthogonal relationship between the mean preferred sun and polarization directions, which parallels the 90°-relationship between the sun and polarization pattern in nature, an aspect that has also been reported in desert locust TL (Pegel et al., 2018) and optic lobe neurons (el Jundi et al., 2011).

The bias in preferred polarization directions found in our TL neurons could thus be a consequence of a neuronal matched filter for celestial cues, allowing the butterflies to derive the same directional information from different celestial inputs.

Pegel et al. (2019) showed that the preferred firing directions to the sun stimulus differ between the three TL subtypes (TL2a, TL2b, TL3) in desert locusts. The monarch butterfly TL neurons can also be divided anatomically into three subtypes that innervate different layers in the lower division of the central body (Heinze et al., 2013). Unfortunately, we were not able to define from which subtype we performed our recordings as we often co-stained several TL subtypes in one experiment. As shown previously, monarch butterfly compass neurons show the same preferred firing direction, irrespective of the spectral information of the light stimulus (Heinze and Reppert, 2011; Nguyen et al., 2021). However, recordings from compass neurons in the desert locust suggest that the spectral influence on the preferred firing direction is strongly sensitive to the light intensity of the stimuli (Kinoshita et al., 2007; Pfeiffer and Homberg, 2007). It is therefore crucial to study the response characteristics of TL neurons to spectral cues at different light intensities in the future to shed light on how the monarch butterfly compass network may integrate different celestial cues into the central complex and how this represents the celestial cue hierarchy exhibited behaviorally.

Integration of the Panoramic Skyline in the Central Complex

In previous experiments, the sensitivity of TL cells has been studied with respect to vertical stripes (Bockhorst and Homberg, 2017; Omoto et al., 2017; Fisher et al., 2019), grating patterns (Rosner et al., 2019) or small light spots (Seelig and Jayaraman, 2013) in insects. We here found that TL neurons were sensitive to a simulated panoramic skyline by responding to changes in brightness while the panorama was rotated around the animal. As we only tested the response of the monarch TL neurons to one distinct panoramic scene, it has yet to be identified how modifying the frequency and amplitude of the panorama's profile will affect the tuning of the TL neurons. We chose this specific panoramic skyline as a recent behavioral study showed that monarch butterflies are able to use this setting to sustain a directed flight course (Franzke et al., 2020). However, as their orientation performance was indistinguishable from a flight stabilization strategy, it was unclear whether the butterflies can employ compass orientation with respect to a panoramic scene. Although our data do not exclude the possibility that TL neurons transfer motion information to the central complex, our data indicate that the central complex receives visual compass information of the panoramic scene. This suggests that monarch butterflies can use a panoramic skyline as a compass cue to compute a heading with respect to it, which parallels behavioral results from Australian desert ants that can use a panorama to calculate a heading direction (Graham and Cheng, 2009a,b). The structure and relative position of the receptive fields of the TL neurons studied with the panoramic scene are difficult to predict due to the complex nature of the stimulus. Exploring this requires to additionally map their receptive fields with respect to a small visual stimulus (Seelig and Jayaraman 2013), an aspect that was not feasible due to the short recording times of our intracellular recordings. Rather than encoding the current heading, the TL neurons seem to convey visual information into the insect compass, similar to the *Drosophila* ring neurons (Seelig and Jayaraman, 2013; Dewar et al., 2017). In both monarch butterflies and fruit flies, they synapse on a population of neurons termed CL1 neurons (Heinze et al., 2013), called EP-G cells in fruit flies, which likely represent a distinct heading direction within a visual scene based on multimodal information (Seelig and Jayaraman, 2015; Kim et al., 2019; Turner-Evans et al., 2020; Beetz et al., 2022). How monarch butterfly CL1 cells compute a heading based on terrestrial information from TL cells awaits to be answered through neuronal recordings during flight as the coding strongly depends on the animal's locomotory state (Beetz et al., 2022).

Flexible Weighting Between Celestial and Terrestrial Information

When we presented the sun and polarization stimulus simultaneously to the butterflies, the TL neurons combined these cues in a linear manner. These results differ from the dung beetle TL neurons (el Jundi et al., 2015) but are in line with desert locust columnar CX-neurons (Pegel et al., 2019). The polarization UV stimulus was consistently ranked higher than the green sun stimulus in TL neurons in monarch butterflies when presented with a similar relative light intensity. When we presented a UV light spot instead of a green one, the unpolarized light stimulus dominated the neuronal tuning. This switch in cue preference was likely not a result of a change in wavelength but rather a consequence of a change in relative intensity of light, which is in line with the stronger response of TL neurons to UV light than to green light (Nguyen et al., 2021). Thus, as the sun is several magnitudes brighter than the remaining sky in nature, it is likely the dominant cue being encoded in TL neurons under a real sky.

In general, the weighting between the simulated sun and polarized light was very similar across different TL neurons. This low variability in cue preference between TL neurons recorded in different monarch butterflies was similar to what has been found for TL neurons in dung beetles (el Jundi et al., 2015) and suggests that the weighting of celestial cues is determined at an early processing stage in the brain, such as at the level of the photoreceptors. In contrast, the simulated sun and the panoramic skyline were not always linearly integrated in the monarch butterfly central complex. Moreover, the cue preference was highly variable, which is well in line with the high inter-individual difference in the behavioral use of these cues for orientation in a flight simulator (Franzke et al., 2020). This high flexibility indicates that the weighting might not only be set based on the sensitivity of the inputs at the butterfly's eye but might additionally be adjusted at later stages in the brain network. This

would allow a high inter-individual difference in weighting that is based on the animal's internal state, as well as its experience.

DATA AVAILABILITY STATEMENT

The raw data supporting the conclusions of this article will be made available by the authors, without undue reservation.

AUTHOR CONTRIBUTIONS

TN, CM, KP, and BJ: study design. TN: conducting experiments and analysis of data. TN, MB, CM, KP, and BJ: interpretation of data. TN and BJ: drafting of the manuscript. MB, CM, and KP: critical review of the manuscript. BJ: acquired funding. All authors approved of the final version of the manuscript.

FUNDING

This work was supported by the Emmy Noether program of the Deutsche Forschungsgemeinschaft granted to BJ (GZ: EL784/1-1) and a DFG Grant to KP (PF714/5-1).

ACKNOWLEDGMENTS

We thank Dr. James Foster for fruitful comments on our analysis and Kolja Richter and Konrad Öchsner for their help in developing the LED arena. We thank Samantha Iiams, Aldrin Lugena, Guijun Wan and Ying Zhang for their help in capturing monarch butterflies and for checking them for *Ophryocystis elektroscirrha*. In addition, we would like to thank Sergio Siles and Marie Gerlinde Blaese (butterflyfarm.co.cr) for providing us with monarch butterfly pupae.

REFERENCES

Beetz, M. J., Kraus, C., Franzke, M., Dreyer, D., Strube-Bloss, M. F., Roessler, W., et al. (2022). Flight-induced compass representation in the monarch butterfly heading network. *Curr. Biol.* 32, 338–349. doi: 10.1016/j.cub.2021.11.009

Berens, P. (2009). CircStat: A MATLAB toolbox for circular statistics. *J. Stat. Softw.* 31, 1–21. doi: 10.18637/jss.v031.i10

Bockhorst, T., and Homberg, U. (2015). Amplitude and dynamics of polarization-plane signaling in the central complex of the locust brain. *J. Neurophysiol.* 113, 3291–3311. doi: 10.1152/jn.00742.2014

Bockhorst, T., and Homberg, U. (2017). Interaction of compass sensing and object-motion detection in the locust central complex. *J. Neurophysiol.* 118, 496–506. doi: 10.1152/jn.00927.2016

Brines, M. L., and Gould, J. L. (1979). Bees have rules. *Science* 206, 571–573. doi: 10.1126/science.206.4418.571

Dacke, M., Baird, E., el Jundi, B., Warrant, E. J., and Byrne, M. (2021). How dung beetles steer straight. *Ann. Rev. Entomol.* 66, 243–256. doi: 10.1146/annurev-ento-042020-102149

Dewar, A. D. M., Wystrach, A., Phillippides, A., and Graham, P. (2017). Neural coding in the visual system of *Drosophila melanogaster*: how do small neural populations support visually guided behaviours? *PLoS Comput. Biol.* 13, e1005735. doi: 10.1371/journal.pcbi.1005735

Dreyer, D., el Jundi, B., Kishkinev, D., Suchentrunk, C., Campostrini, L., Frost, B. J., et al. (2018a). Evidence for a southward autumn migration of nocturnal noctuid moths in central Europe. *J. Exp. Biol.* 221, jeb179218. doi: 10.1242/jeb.179218

Dreyer, D., Frost, B., Mouritsen, H., Gunther, A., Green, K., Whitehouse, M., et al. (2018b). The Earth's magnetic field and visual landmarks steer migratory flight behavior in the nocturnal Australian bogong moth. *Curr. Biol.* 28, 2160–2166. doi: 10.1016/j.cub.2018.05.030

Edrich, W., Neumeyer, C., and von Heiversen, O. (1979). "Anti-sun orientation" of bees with regard to a field of ultraviolet light. *J. Comp. Physiol.* 134, 151–157. doi: 10.1007/BF00610473

el Jundi, B., Baird, E., Byrne, M. J., and Dacke, M. (2019). The brain behind straight-line orientation in dung beetles. *J. Exp. Biol.* 222, jeb192450. doi: 10.1242/jeb.192450

el Jundi, B., Pfeiffer, K., and Homberg, U. (2011). A distinct layer of the medulla integrates sky compass signals in the brain of an insect. *PLoS One* 6, e27855. doi: 10.1371/journal.pone.0027855

el Jundi, B., Smolka, J., Baird, E., Byrne, M. J., and Dacke, M. (2014). Diurnal dung beetles use the intensity gradient and the polarization pattern of the sky for orientation. *J. Exp. Biol.* 217, 2422–2429. doi: 10.1242/jeb.101154

el Jundi, B., Warrant, E. J., Byrne, M. J., Khaldy, L., Baird, E., Smolka, J., et al. (2015). Neural coding underlying the cue preference for celestial orientation. *Proc. Natl. Acad. Sci. U. S. A.* 112, 11395–11400. doi: 10.1073/pnas.1501272112

el Jundi, B., Warrant, E. J., Pfeiffer, K., and Dacke, M. (2018). Neuroarchitecture of the dung beetle central complex. *J. Comp. Neurol.* 526, 2612–2630. doi: 10.1002/cne.24520

Fisher, Y. E., Lu, J., D'Alessandro, I., and Wilson, R. I. (2019). Sensorimotor experience remaps visual input to a heading-direction network. *Nature* 576, 121–125. doi: 10.1038/s41586-019-1772-4

Franzke, M., Kraus, C., Dreyer, D., Pfeiffer, K., Beetz, M. J., Stöckl, A. L., et al. (2020). Spatial orientation based on multiple visual cues in non-migratory monarch butterflies. *J. Exp. Biol.* 223, 1–12. doi: 10.1242/jeb.223800

Graham, P., and Cheng, K. (2009a). Ants use the panoramic skyline as a visual cue during navigation. *Curr. Biol.* 19, R935–R937. doi: 10.1016/j.cub.2009.08.015

Graham, P., and Cheng, K. (2009b). Which portion of the natural panorama is used for view-based navigation in the Australian desert ant? *J. Comp. Physiol. A* 195, 681–689. doi: 10.1007/s00359-009-0443-6

Green, J., Adachi, A., Shah, K. K., Hirokawa, J. D., Magani, P. S., and Maimon, G. (2017). A neural circuit architecture for angular integration in *Drosophila*. *Nature* 546, 101–106. doi: 10.1038/nature22343

Guerra, P. A., Merlin, C., Gegear, R. J., and Reppert, S. M. (2012). Discordant timing between antennae disrupts sun compass orientation in migratory monarch butterflies. *Nat. Comm.* 3, 958. doi: 10.1038/ncomms1965

Hardcastle, B. J., Omoto, J. J., Kandimalla, P., Nguyen, B. M., Kele,ş, M. F., Boyd, N. K., et al. (2021). A visual pathway for skylight polarization processing in *Drosophila*. *Elife* 10, e63225. doi: 10.7554/eLife.63225

Heinze, S., Florman, J., Asokaraj, S., el Jundi, B., and Reppert, S. M. (2013). Anatomical basis of sun compass navigation II: the neuronal composition of the central complex of the monarch butterfly. *J. Comp. Neurol.* 521, 267–298. doi: 10.1002/cne.23214

Heinze, S., Gotthardt, S., and Homberg, U. (2009). Transformation of polarized light information in the central complex of the locust. *J. Neurosci.* 29, 11783–11793. doi: 10.1523/JNEUROSCI.1870-09.2009

Heinze, S., and Reppert, S. M. (2011). Sun compass integration of skylight cues in migratory monarch butterflies. *Neuron* 69, 345–358. doi: 10.1016/j.neuron.2010.12.025

Held, M., Berz, A., Hensgen, R., Muenz, T. S., Scholl, C., Roessler, W., et al. (2016). Microglomerular synaptic complexes in the sky-compass network of the honeybee connect parallel pathways from the anterior optic tubercle to the central complex. *Front. Behav Neurosci.* 10, 91–105. doi: 10.3389/fnbeh.2016.00186

Hensgen, R., England, L., Homberg, U., and Pfeiffer, K. (2020). Neuroarchitecture of the central complex in the brain of the honeybee: Neuronal cell types. *J. Comp. Neurol.* 20, 1–28. doi: 10.1002/cne.24941

Homberg, U. (2015). Sky compass orientation in desert locusts–Evidence from field and laboratory studies. *Front. Behav. Neurosci.* 9, 346. doi: 10.3389/fnbeh.2015.00346

Hulse, B. K., Haberkern, H., Franconville, R., Turner-Evans, D. B., Takemura, S.-,y., Wolff, T., et al. (2021). A connectome of the Drosophila central complex

reveals network motifs suitable for flexible navigation and context-dependent action selection. *Elife* 10, e66039. doi: 10.7554/eLife.66039

Kim, S. S., Hermundstad, A. M., Romani, S., Abbott, L. F., and Jayaraman, V. (2019). Generation of stable heading representations in diverse visual scenes. *Nature* 576, 126–131. doi: 10.1038/s41586-019-1767-1

Kinoshita, M., Pfeiffer, K., and Homberg, U. (2007). Spectral properties of identified polarized-light sensitive interneurons in the brain of the desert locust *Schistocerca gregaria*. *J. Exp. Biol.* 210, 1350–1361. doi: 10.1242/jeb.02744

Labhart, T. (1996). How polarization-sensitive interneurones of crickets perform at low degrees of polarization. *J. Exp. Biol.* 199, 1467–1475. doi: 10.1242/jeb.199.7.1467

Lebhardt, F., and Ronacher, B. (2014). Interactions of the polarization and the sun compass in path integration of desert ants. *J. Comp. Physiol. A* 200, 711–720. doi: 10.1007/s00359-013-0871-1

Legge, E. L., Wystrach, A., Spetch, M. L., and Cheng, K. (2014). Combining sky and earth: desert ants (*Melophorus bagoti*) show weighted integration of celestial and terrestrial cues. *J. Exp. Biol.* 217, 4159–4166. doi: 10.1242/jeb.107862

Merlin, C., Gegear, R. J., and Reppert, S. M. (2009). Antennal circadian clocks coordinate sun compass orientation in migratory monarch butterflies. *Science* 325, 1700–1704. doi: 10.1126/science.1176221

Merlin, C., and Liedvogel, M. (2019). The genetics and epigenetics of animal migration and orientation: birds, butterflies and beyond. *J. Exp. Biol.* 222, jeb191890. doi: 10.1242/jeb.191890

Merlin, C., Heinze, S., and Reppert, S. M. (2012). Unraveling navigational strategies in migratory insects. *Curr. Opin. Neurobiol.* 22, 353–361. doi: 10.1016/j.conb.2011.11.009

Nguyen, T. A. T., Beetz, M. J., Merlin, C., and el Jundi, B. (2021). Sun compass neurons are tuned to migratory orientation in monarch butterflies. *Proc. Biol. Sci.* 288, 20202988. doi: 10.1098/rspb.2020.2988

Okubo, T. S., Patella, P., D'Alessandro, I., and Wilson, R. I. (2020). A neural network for wind-guided compass navigation. *Neuron* 107, 924–940 e18. doi: 10.1016/j.neuron.2020.06.022

Omoto, J. J., Keleş, M. F., Nguyen, B. M., Bolanos, C., Lovick, J. K., Frye, M. A., (2017). Visual input to the *Drosophila* central complex by developmentally and functionally distinct neuronal populations. *Curr. Biol.* 24, 1098–1110. doi: 10.1016/j.cub.2017.02.063

Pegel, U., Pfeiffer, K., and Homberg, U. (2018). Integration of celestial compass cues in the central complex of the locust brain. *J. Exp. Biol.* 221, jeb171207. doi: 10.1242/jeb.171207

Pegel, U., Pfeiffer, K., Zittrell, F., Scholtyssek, C., and Homberg, U. (2019). Two compasses in the central complex of the locust brain. *J. Neurosci.* 39, 3070–3080. doi: 10.1523/JNEUROSCI.0940-18.2019

Pfeiffer, K., and Homberg, U. (2007). Coding of azimuthal directions *via* time-compensated combination of celestial compass cues. *Curr. Biol.* 17, 960–965. doi: 10.1016/j.cub.2007.04.059

Reid, S. F., Narendra, A., Hemmi, J. M., and Zeil, J. (2011). Polarised skylight and the landmark panorama provide night-active bull ants with compass information during route following. *J. Exp. Biol.* 214, 363–370. doi: 10.1242/jeb.049338

Reppert, S. M., Zhu, H., and White, R. H. (2004). Polarized light helps monarch butterflies navigate. *Curr. Biol.* 14, 155–158. doi: 10.1016/j.cub.2003.12.034

Rosner, R., Pegel, U., and Homberg, U. (2019). Responses of compass neurons in the locust brain to visual motion and leg motor activity. *J. Exp. Biol.* 222, jeb196261. doi: 10.1242/jeb.196261

Rossel, S., and Wehner, R. (1984). Celestial orientation in bees: the use of spectral cues. *J. Comp. Physiol. A* 155, 605–613. doi: 10.1007/BF00610846

Rother, L., Kraft, N., Smith, D. B., el Jundi, B., Gill, R. J., and Pfeiffer, K. (2021). A micro-CT-based standard brain atlas of the bumblebee. *Cell. Tissue Res.* 386, 29–45. doi: 10.1007/s00441-021-03482-z

Sakura, M., Lambrinos, D., and Labhart, T. (2008). Polarized skylight navigation in insects: model and electrophysiology of e-vector coding by neurons in the central complex. *J. Neurophysiol.* 99, 667–682. doi: 10.1152/jn.00784.2007

Sauman, I., Briscoe, A. D., Zhu, H., Shi, D., Froy, O., Stalleicken, J., et al. (2005). Connecting the navigational clock to sun compass input in monarch butterfly brain. *Neuron* 46, 457–467. doi: 10.1016/j.neuron.2005.03.014

Seelig, J. D., and Jayaraman, V. (2013). Feature detection and orientation tuning in the *Drosophila* central complex. *Nature* 503, 262–266. doi: 10.1038/nature12601

Seelig, J. D., and Jayaraman, V. (2015). Neural dynamics for landmark orientation and angular path integration. *Nature* 521, 186–191. doi: 10.1038/nature14446

Stalleicken, J., Labhart, T., and Mouritsen, H. (2006). Physiological characterization of the compound eye in monarch butterflies with focus on the dorsal rim area. *J. Comp. Physiol. A* 192, 321–331. doi: 10.1007/s00359-005-0073-6

Stalleicken, J., Mukhida, M., Labhart, T., Wehner, R., Frost, B., and Mouritsen, H. (2005). Do monarch butterflies use polarized skylight for migratory orientation? *J. Exp. Biol.* 208, 2399–2408. doi: 10.1242/jeb.01613

Stone, T., Webb, B., Adden, A., Weddig, N. B., Honkanen, A., Templin, R., et al. (2017). An anatomically constrained model for path integration in the bee brain. *Curr. Biol.* 27, 3069–3085. doi: 10.1016/j.cub.2017.08.052

Takahashi, N., Zittrell, F., Hensgen, R., and Homberg, U. (2022). Receptive field structure for two celestial compass cues at the input stage of the central complex in the locust brain. *J. Exp. Biol, jeb*.243858. doi: 10.1242/jeb.243858

Towne, W. F., and Moscrip, H. (2008). The connection between landscapes and the solar ephemeris in honeybees. *J. Exp. Biol.* 211, 3729–3736. doi: 10.1242/jeb.022970

Towne, W. F., Ritrovato, A. E., Esposto, A., and Brown, D. F. (2017). Honeybees use the skyline in orientation. *J. Exp. Biol.* 220, 2476–2485. doi: 10.1242/jeb.160002

Turner-Evans, D., Wegener, S., Rouault, H., Franconville, R., Wolff, T., Seelig, J. D., et al. (2017). Angular velocity integration in a fly heading circuit. *Elife* 6, e23496. doi: 10.7554/eLife.23496

Turner-Evans, D. B., Jensen, K. T., Ali, S., Paterson, T., Sheridan, A., Ray, R. P., et al. (2020). The neuroanatomical ultrastructure and function of a biological ring attractor. *Neuron* 108, 145–163. doi: 10.1016/j.neuron.2020.08.006

Vitzthum, H., Müller, M., and Homberg, U. (2002). Neurons of the central complex of the locust *Schistocerca gregaria* are sensitive to polarized light. *J. Neurosci.* 22, 1114. doi: 10.1523/JNEUROSCI.22-03-01114.2002

Wehner, R. (2003). Desert ant navigation: how miniature brains solve complex tasks. *J. Comp. Physiol. A* 189, 579–588. doi: 10.1007/s00359-003-0431-1

Wehner, R., and Müller, M. (2006). The significance of direct sunlight and polarized skylight in the ant's celestial system of navigation. *Proc. Natl. Acad. Sci. U. S. A.* 103, 12575–12579. doi: 10.1073/pnas.0604430103

Conflict of Interest: The authors declare that the research was conducted in the absence of any commercial or financial relationships that could be construed as a potential conflict of interest.

Publisher's Note: All claims expressed in this article are solely those of the authors and do not necessarily represent those of their affiliated organizations, or those of the publisher, the editors and the reviewers. Any product that may be evaluated in this article, or claim that may be made by its manufacturer, is not guaranteed or endorsed by the publisher.

frontiers | Frontiers in Neural Circuits

ORIGINAL RESEARCH
published: 05 July 2022
doi: 10.3389/fncir.2022.895381

Toward Naturalistic Neuroscience of Navigation: Opportunities in Coral Reef Fish

*Shachar Givon[1,2], Renanel Pickholtz[3,4], Eliezer Y. Pickholtz[5], Ohad Ben-Shahar[2,6], Moshe Kiflawi[1,4] and Ronen Segev[1,2,7]**

[1] Department of Life Sciences, Ben-Gurion University of the Negev, Beersheba, Israel, [2] Zlotowski Center for Neuroscience, Ben-Gurion University of the Negev, Beersheba, Israel, [3] School of Zoology, George S. Wise Faculty of Life Sciences, Tel Aviv University, Tel Aviv, Israel, [4] The Interuniversity Institute for Marine Sciences, Eilat, Israel, [5] Independent Researcher, East Brunswick, NJ, United States, [6] Department of Computer Science, Ben-Gurion University of the Negev, Beersheba, Israel, [7] Department of Biomedical Engineering, Ben-Gurion University of the Negev, Beersheba, Israel*

The ability to navigate in the world is crucial to many species. One of the most fundamental unresolved issues in understanding animal navigation is how the brain represents spatial information. Although navigation has been studied extensively in many taxa, the key efforts to determine the neural basis of navigation have focused on mammals, usually in lab experiments, where the allocated space is typically very small; e.g., up to one order of magnitude the size of the animal, is limited by artificial walls, and contains only a few objects. This type of setting is vastly different from the habitat of animals in the wild, which is open in many cases and is virtually limitless in size compared to its inhabitants. Thus, a fundamental open question in animal navigation is whether small-scale, spatially confined, and artificially crafted lab experiments indeed reveal how navigation is enacted in the real world. This question is difficult to study given the technical problems associated with *in vivo* electrophysiology in natural settings. Here, we argue that these difficulties can be overcome by implementing state of the art technology when studying the rivulated rabbitfish, *Siganus rivulatus* as the model animal. As a first step toward this goal, using acoustic tracking of the reef, we demonstrate that individual *S. rivulatus* have a defined home range of about 200 m in length, from which they seldom venture. They repeatedly visit the same areas and return to the same sleeping grounds, thus providing evidence for their ability to navigate in the reef environment. Using a clustering algorithm to analyze segments of daily trajectories, we found evidence of specific repeating patterns in behavior within the home range of individual fish. Thus, *S. rivulatus* appears to have the ability to carry out its daily routines and revisit places of interest by employing sophisticated means of navigation while exploring its surroundings. In the future, using novel technologies for wireless recording from single cells of fish brains, *S. rivulatus* can emerge as an ideal system to study the neural basis of navigation in natural settings and lead to "electrophysiology in the wild."

Keywords: navigation, electrophysiology, rabbitfish, coral reef, *Siganus rivulatus*

OPEN ACCESS

Edited by:
Anna Lisa Stöckl, Julius Maximilian University of Würzburg, Germany

Reviewed by:
Jörg Henninger, Charité Universitätsmedizin Berlin, Germany
Patrick Schultheiss, Julius Maximilian University of Würzburg, Germany

****Correspondence:***
Ronen Segev
ronensgv@bgu.ac.il

Received: *13 March 2022*
Accepted: *30 May 2022*
Published: *05 July 2022*

Citation:
Givon S, Pickholtz R, Pickholtz EY, Ben-Shahar O, Kiflawi M and Segev R (2022) Toward Naturalistic Neuroscience of Navigation: Opportunities in Coral Reef Fish. Front. Neural Circuits 16:895381. doi: 10.3389/fncir.2022.895381

INTRODUCTION

To enable successful navigation, the brain must represent spatial information (Frost and Mouritsen, 2006; Mouritsen et al., 2016). Neural machinery has evolved to deal with the natural habitat and the ways in which different organisms move in and around it. However, almost all studies on navigation have been conducted in the lab where the navigated space is atypical, usually small, artificially enclosed, and sparsely occupied with artificial objects. In contrast, for many species, the natural habitat is open, lacks clear boundaries, is usually virtually limitless (relative to the animal), and is structurally complex (Tsoar et al., 2011; Jacobs and Menzel, 2014). For example, **Figure 1** illustrates the small, restricted environments available in lab studies, as compared to vast complex natural environments. Since different spatial extents and complexities are likely to affect the internal representation of space, to unlock the full capacity of neural representations, the neural representation of the animal's location and other parameters of space must be studied in the wild.

The exploration of neural representations *via* electrophysiology can teach us a great deal about the ways the brain collects and codes information about its surroundings. Research has identified different types of cells involved in the spatial coding of the surroundings. Cells coding different places, termed place cells or grid cells of more than one location coded with specific geometric attributes have been found in rodents (O'Keefe and Dostrovsky, 1971), bats (Yartsev et al., 2011; Yartsev and Ulanovsky, 2013), and primates (O'Mara et al., 1994; Furuya et al., 2014; Courellis et al., 2019). Cells coding for certain attributes of the environment, such as border cells and edge cells, have been documented in rodents (Solstad et al., 2008) and fish (Vinepinsky et al., 2020). Another type of cell activates in response to the animal's behavior, and includes head direction cells in rodents (Taube et al., 1990), bats (Taube et al., 1990; Rubin et al., 2014; Ben-Yishay et al., 2021), and fish (Vinepinsky et al., 2020) as well as movement kinematic cells in rodents (Sargolini et al., 2006) and fish (Vinepinsky et al., 2020).

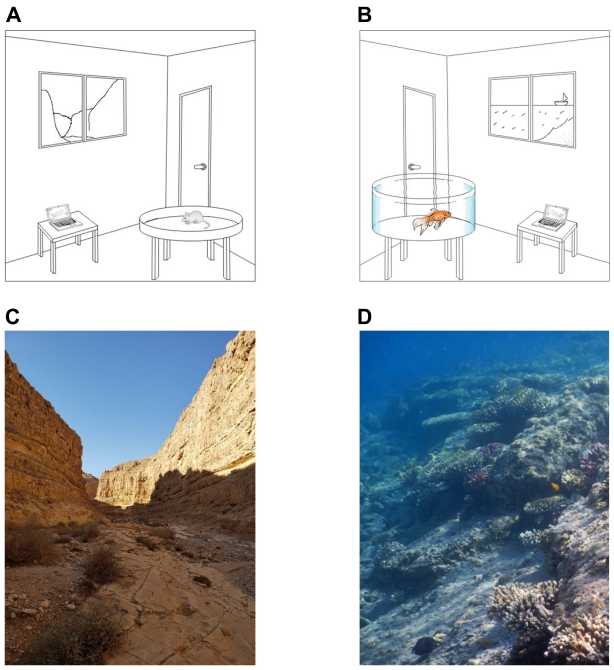

FIGURE 1 | Lab versus natural environments. **(A,B)** Illustration of artificial lab environments for rodents and fish. The lab setting is restricted in terms of size, navigational cues, and complexity. **(C,D)** Two examples of natural environments for terrestrial and aquatic environments. The environments are limitless, rich in cues needed for navigation, and very complex.

While natural environment is different from the small laboratory-based experiments, it is important to specify possible differences that will be obtained by extending the experimental effort outside. For example, animals might not represent the global position with respect to the environment (e.g., place cells), but instead represent the location with respect to a known route in the environment that the animal uses habitually and serves as a geographic anchor. In addition, place cells represent the location of the animal with place fields of about a 10 cm resolution in lab experiment of a 1 m arena. What happens when this space expands by a factor of 1,00,000? It might be that there are not enough cells in the brain to represent this space at the same resolution. The activity patterns of place and grid cells rely on repeating visits to the same locations in space. As the number of visits to every location in space decreases, what happens to the representation of space? Arenas in lab experiments are usually empty or contain only a few objects. A naturalistic environment can be large and populated with many objects. Does this affect the representation of spatial information?

Although electrophysiology in the wild can lead to a better understanding of the ways in which animals navigate in the real world, *in vivo* electrophysiology in the wild presents several difficult technological challenges. The first is the ability to obtain long-term *in vivo* recordings from a freely moving animal. The second is to do so while continuously and accurately monitoring the animal's position and, possibly, its posture/behavior. This leads to a complex set of technological and experimental requirements that are likely to vary depending on the model animal. The recording technology needs to be both durable and equipped with a sufficiently large energy source, while being compatible with the size of the animal to not interfere with its freedom of movement while exploring the habitat. In terms of tracking equipment, none of the devices in the field should restrict the animal's ability to explore the area. In addition to the technical difficulties, there are other challenges due to the natural environment. These include controlling for the numerous confounding variables in the natural environment such as predators, obstacles and other objects.

Clearly, a strategy to study fish requires implementing underwater electrophysiology. Although working underwater presents some difficulties with respect to water- and pressure-proofing the instruments, it does offer the advantage of making these instruments weightless (i.e., neutrally buoyant) and, thus permitting multi-day data acquisition. Even with the unavoidable need to adapt to the natural hydrodynamic form of the fish, prolonged data collection can be achieved with minimal

interference with the animal's behavior, a combination that may be unfeasible in many other model systems.

Recent studies have described a wireless electrophysiological system capable of recording the activity of single neurons in the brain of small free-swimming fish (Vinepinsky et al., 2017, 2020; Cohen et al., 2019). This system is based on a small data logger, which is mounted on the fish while it swims in the habitat. This technology can now support a 16-electrode array to record from the telencephalon, and specifically the pallium, of free-ranging fish and constitutes a critical step toward conducting naturalistic neuroscience.

While the technology described above can be used to monitor various brain-related capacities, its use constrains the selection of a model animal whose size, head shape and the durability of the skull make it possible to attach a neural logger. Ecological constraints exist as well, since if the fish tends to retreat or hunt in small spaces or relies on speed for its survival, the logger would put it at risk. In addition, it must be possible to attach an acoustic tag, which is needed to track the animal's location; which further constrains the size of the study subject.

To study the neurobiology of free-range navigation, the model animal also needs to exhibit clear repetitive navigational patterns. This is of importance as it allows for future electrophysiological data to be collected numerous times from the same locations. In addition, the daily home range should be large enough to challenge the neural machinery to its full capacity, but not too large to enable continuous and accurate tracking of movements. The spatial features of these routines, as well as the habitat itself, should be non-trivial in terms of complexity, thus allowing informative patterns to emerge in the spatial distribution of the animal and the corresponding neural encoding.

Here we describe how these challenges can be met by using the unique advantages of a fish model. We argue that combining recently developed technology together with a careful selection of the fish species can lead to advances in our understanding of navigation. We perform the first step in characterizing the behavior of a possible fish model that can used for this study and show that the rabbitfish, *S. rivulatus*, meets these criteria as well as the constraints imposed by the technology.

For this purpose, we report on the spatial behavior of *S. rivulatus* in its natural reef habitat, as inferred using underwater acoustic telemetry. We describe the results obtained from the analyzes of daily trajectories of four fish, which were monitored for 14–60 days in the northern Gulf of Aqaba (Eilat) at the tip of the Red Sea. Consistent with earlier findings (Pickholtz et al., 2018), we found that the fish maintained a well-defined home range, including fixed sleeping sites. The fish adhered to predictable trajectories within the home range, and engaged in repeatable segments, forming patterns throughout the sections of these trajectories.

MATERIALS AND METHODS

Ethics Statement

All experiments were approved by the Ben-Gurion University of the Negev Institutional Animal Care and Use Committee and were in accordance with government regulations of the State of Israel.

Animals

The model animal chosen for this study was the rivulated rabbitfish (*Siganus rivulatus*) as shown in **Figure 2A**. The study was conducted in its natural coral reef environment in the Gulf of Aqaba (Gulf of Eilat). *S. rivulatus* measuring 24–30 cm in body length and 150–190 g in body weight were used in this study. The fish were collected from the reef while scuba diving at night, to minimize stress to the fish. A small 5 g acoustic tag was surgically implanted in the peritoneal cavity according to the standard procedure (Bridger and Booth, 2003; Gehring et al., 2015; Pickholtz et al., 2018). After surgery, the fish were kept in a large tank of sea water for observation. They were returned to the reef after exhibiting clear signs of recovery, including normal swimming and foraging behavior.

Acoustic Tracking of Fish Position

Underwater acoustic tracking technology (InnovaSea, Boston, MA, United States, and Thelma Biotel, Trondheim, Norway) was used to track the location of the fish over a long period of time. The implanted tags transmit an acoustic signal every 10 s which can be detected up to 70 m away and include the tag's sensed depth and ID. The acoustic signals' frequency range between 69 and 71 kHz, with varying power outputs of 140–150 dB, at these intensities and frequencies the fish are unaffected. The receivers are placed such that they form equilateral triangles for optimal coverage of the area. Once a transmission has been detected, the receivers log the transferred data and the transmission time of arrival. If three or more receivers detect the same transmission, the origin of the signal can be determined by triangulation. **Figure 2B** illustrates the underwater array, tagged fish and receiver layout. Several synchronization tags are positioned in the array to correct for the lag in synchronization between the different receivers. Given that the synchronization tags are located at known static locations, a comparison of their time of arrival with the actual logged ones can be used to adjust the clocks on the receivers. A bird's-eye view of the array along with the locations of the synchronization tags is presented in **Figure 2C**.

To detect the signal's origin location, two localization algorithms were used. The first, solving an optimization problem. For every couple of signal detecting receivers, the difference in time of arrival (DToA) can be calculated. With the DToA, a 3-Dimentional map of the reef detailing the DToA error from every location is created. Such maps, created for every receiver couple combination, are overlapped to find a single location with minimal error.

The second algorithm used machine learning to calculate positions based on the time of arrival of the tag transmissions and ground truth data. Each tag transmits a signal with a distinct identifier (tag ID) detected by geo-referenced underwater receivers distributed in the study area, and tag localization is computed using millisecond-scale differences in signal time-of-arrival to each receiver. In order to estimate localization errors, we ran ground-truth tests with a GPS device (Montana 680t, Garmin, Olathe, KS, United States) within and at the perimeters

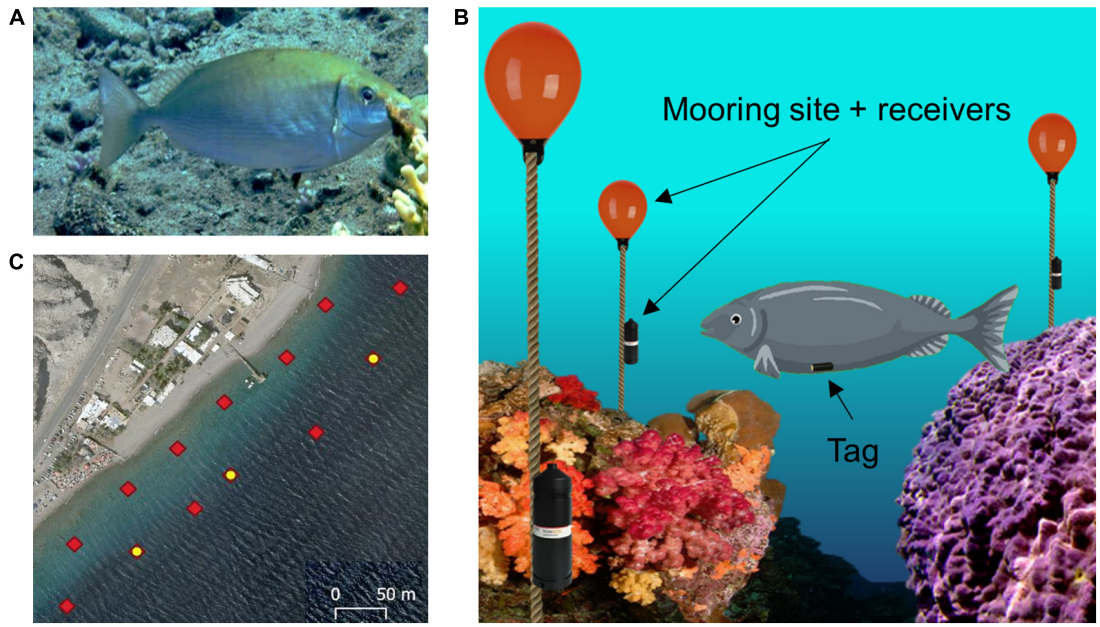

FIGURE 2 | Experimental setup. **(A)** Profile view of a rivulated rabbitfish (*Siganus rivulatus*). **(B)** Illustration of the acoustic tracking system. The fish is fitted with an acoustic tag in the abdominal cavity. An array of acoustic receivers is attached to mooring sites spread throughout the reef environment. **(C)** Array layout deployed in the reef: red diamonds indicate each receiver station; the yellow dots indicate stations with an attached sync tag, which are used for synchronization of the clocks of all the receivers.

of the experimental array, at different times during the study. The median localization error was established as 4 m. Ground-truth data collection was performed by snorkelers or divers moving across the array with several acoustic tags (InnovaSea and Thelma Biotel) at varying depths (0–15 m).

Data Analysis

Definition of the Home Range

To define the home range, we calculated a set of locations by using the alpha shape algorithm with a shrink factor of 0.5 (Matlab boundary function) around the data points of the fish trajectories. The results of the alpha shape algorithm were compared to the kernel-based method (Seaman and Powell, 1996) and found to be similar.

Occupancy Map

The home range was split into 5 m × 5 m bins. For each bin the time spent by each fish was calculated. The map was filtered with Gaussian filter ($\sigma = 2.5$ m). A base-10 logarithm was used for visualization using heatmap.

Detecting Patterns in Fish Daily Trajectories

To detect repeated patterns of swimming, we linearly interpolated the trajectories to obtain a 1-min interval resolution. Interpolation resulted in daily trajectories of equal time resolution.

Data Quality Control

The acoustic tracking cannot follow the fish continuously since occasionally the cluttered acoustic environment blocks transmissions from the acoustic tag or occludes the acoustic signal. This type of disruption is more common during the night since the fish sleep on the sea floor. To ensure data quality for this part of the analysis, we selected contiguous days that had a minimum of 30 data points per hour. We allowed for larger data gaps when analyzing the home range and establishing the sleeping grounds.

Segmentation of Trajectories

To overcome the inherent difficulty in classifying different types of behavior based on long swimming trajectories, we segmented the daily trajectories into 30-min-long segments according to the approach presented in Gehring et al. (2015). In this approach, the segments are used to classify different behaviors based on repetitive attributes of the segments. For this purpose, the daily trajectory was defined as the time between sunrise and sunset in Eilat, with adjustments for seasonal differences between fish. At first, each daily trajectory was segmented into 30-min-long paths with a 50% overlap to avoid phase related phenomena. This was adjusted in later analyzes when no significant phenomena occurred.

Computation of Path Features

Prior to classification, we calculated a set of 13 features that quantified different geometric and temporal properties of the trajectory segments, as listed in **Table 1**. The features were adapted to our data from a set of features defined in previous studies (Gehring et al., 2015; McLean and Skowron Volponi, 2018). Features were divided by the standard deviation of each feature to derive a unit-free measurement.

TABLE 1 | Features characterizing the geometric and temporal aspects of trajectory segments.

Feature	Definition
Distance	$D = \lvert\overrightarrow{x_n} - \overrightarrow{x_i}\rvert$, where $\overrightarrow{x_i}$, $\overrightarrow{x_n}$ are the first and last locations in the segment
Length	$L = \sum_{i=1}^{n-1} \lvert\overrightarrow{x_{i+1}} - \overrightarrow{x_i}\rvert$, where $\overrightarrow{x_i}$ are locations within the segment
Straightness	$S = \frac{D}{L}$
Area	A, Area of convex hull enclosing segment
Median speed	$MS = median\left(\overrightarrow{S}\right)$, $\overrightarrow{S} = \left[\frac{\lvert\overrightarrow{x_2} - \overrightarrow{x_1}\rvert}{1m}, \ldots, \frac{\lvert\overrightarrow{x_n} - \overrightarrow{x_{n-1}}\rvert}{1m}\right]$
Mean distance from center	ρ, distance of segment center of mass from the median of entire data set
Direction auto correlation 5 min	DAC5, correlation coefficient of the swimming directions of 5-min part segments
Direction auto correlation 10 min	DAC10, correlation coefficient of the swimming directions of 10-min part segments
Speed auto correlation 5 min	SAC5, correlation coefficient of the swimming speed of 5-min part segments
Speed auto correlation 10 min	SAC10, correlation coefficient of the swimming speed of 5-min part segments
Day phase	DP, normalized time of segment in the day
Mean angle from center	θ, cosine of the angle between segment center of mass and X axis
Focus	$F = 1 - \frac{4A}{\pi L^2}$

Formal definition of the segment features ranging from fundamental features (e.g., length) to derived features (e.g., focus). All features were normalized to obtain dimensionless features for the clustering algorithm.

Classification of Segments Into Classes

To detect repeated patterns of fish movement, we used a semi-automated clustering algorithm. We first calculated a set of features for each segment that described the geometry, kinematics and temporal characteristics of the segments followed by a standard clustering algorithm as described in detail below.

Dimensionality Reduction

We used principal-component analysis of the 13 features to isolate a limited number of independent dimensions that described the trajectory segments. Based on the eigenvalues, we selected the first four components, which explained 67% of the variance, as the basis of the clustering algorithm.

Semi-Supervised Clustering

To find classes of trajectory segments in each fish, we applied the following clustering algorithm to the first four principal components. We applied agglomerative clustering to obtain an initial set of classes. This was done using the Euclidian distance as a similarity measure (Matlab cluster function). The number of classes was determined by examination of the merger score as clusters merged at each step, and finding the step at which the differences between clusters exceeded 1.5%. Different thresholds were tested with no significant impact on the results. After automatic clustering, the classes were observed and labeled.

RESULTS

We analyzed the patterns of trajectories of the *S. rivulatus* to establish this species as a model animal for the study of the neural basis of spatial cognition. For this purpose, we recorded the trajectories of ten fish in their natural coral reef environment, along the north-eastern shoreline of the gulf of Aqaba (Eilat) in the Red Sea. Fish were tracked for periods of 14–60 days.

Siganus rivulatus Maintain a Home Range in the Reef Environment

Consistent with previous observations (Pickholtz et al., 2018), in the northern Gulf of Aqaba (Eilat), *S. rivulatus* concentrated their daily activity within a home range of approximately 200 m × 50 m, as shown in **Figure 3A**. The home range remained stable over time as shown in **Figure 3B**, where the areas covered by the fish in the first and last days of the study are marked. Within the home range, individual fish visited some areas more frequently than others (**Figure 3C**). These areas corresponded to locations the fish passed through regularly and locations where they spent their time foraging. The fish returned to the same sleeping sites (i.e., sites utilized between sunset and sunrise), with high regularity, as exemplified in **Figure 3C**. An examination of the daily trajectories showed that the fish spent much of the day away from the sleeping site (e.g., in **Figure 3D**).

Siganus rivulatus Exhibits Multiple Strategies of Environment Exploration

Since elementary measures such as the home range size or occupancy cannot capture the full extent of fish behavior, we looked for repeated patterns in the swimming trajectories of the fish. For this purpose, we segmented the daily trajectories into overlapping 30 min segments (see section "Material and Methods", Analysis). Then we extracted spatial and temporal features from each segment (**Table 1** and **Figure 4**), followed by principal component analysis for dimensionality reduction. Finally, we used a semi-automatic clustering to detect classes of trajectory segments (see section "Materials and Methods").

Figure 5 presents the results of the principal component and clustering analyzes for one fish using data obtained through the second of the positioning algorithms. The four principal components varied in score assigned to each feature (**Figure 5A**). Principal component 1 had a higher score to the distance and area features, a negative score to the distance from the center and a near neutral to all others. In contrast, principal component 3 was nearly neutral for all features except the distance from the center to which it had a high score. In a similar manner principal component 4 focused on two specific features, the autocorrelation for direction and speed, to which it had a high score and a negative score, respectively. Principal component 2 accounted for a variety of features both positively and negatively. The four principal components explained 30, 16, 11, and 10% of the variance, respectively.

After scoring all the segments according to the four principal components, the agglomerative clustering algorithm was run and the classes were defined (**Figure 5B** and see section "Materials and Methods"). We found that the *S. rivulatus* exhibited four main trajectory segment patterns. We defined these four trajectory segment classes as follows: (1) scanning: the fish scans a small part of the home range; (2) dwelling: the fish spends time without

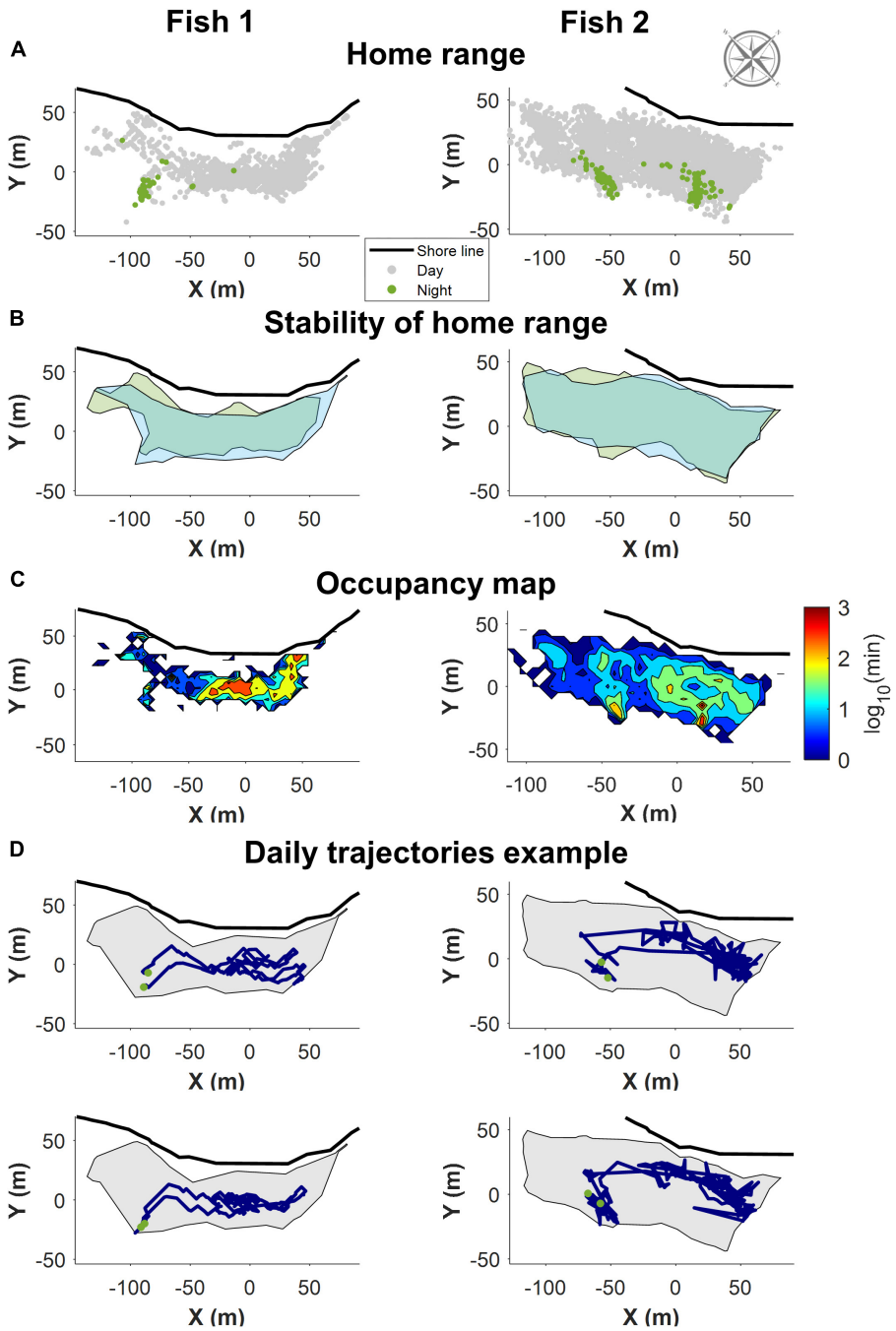

FIGURE 3 | Example of the home range trajectory characteristics of two fish with data obtained through the first of the positioning algorithms. All figures are shown along with the relevant section of shoreline and compass. **(A)** All recorded positions for the fish. In gray are the positions during the day, in green the night-time position. The fish slept in a restricted area in the home range. **(B)** The home range remained stable over time. Boundaries of the area covered the first few days of data in green, and the last few days in blue. **(C)** A heat map visualizing a normalized logarithmic scale of the occupancy map in different areas of the home range. **(D)** Two examples of daily trajectories for each fish. Green dots represent the start and end points for each day. The gray background is the boundary delineating the home range.

moving; (3) long ranging: the fish travels long distances during the segment; and (4) short ranging: the fish travels short distances during the segment. **Figure 6** presents several examples of the trajectory segment analysis for fish 1. Several examples, taken at random times during the tracking period, of 4-h long trajectory segment sequences for one fish are presented in **Figure 6B**. Here, ranging, both slow and fast, were interspersed between periods of scanning and dwelling.

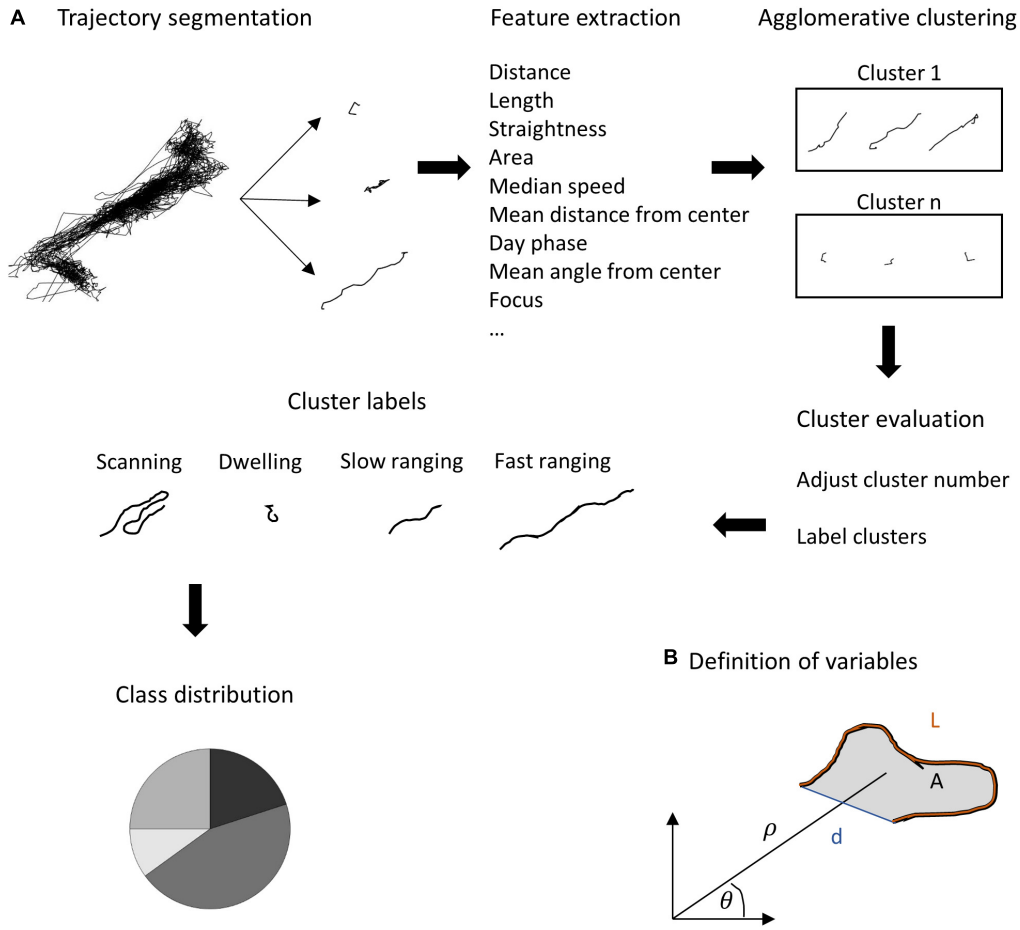

FIGURE 4 | Feature calculations and semi-supervised clustering algorithm. **(A)** The daily trajectory was segmented into overlapping segments. For each segment, a set of features was calculated (see **Table 1** for formal definitions). Agglomerative clustering was applied to the data to obtain a set of classes of trajectory segments. Finally, a manual correction for similar classes was applied to avoid over- splitting of the classes. **(B)** Definition of the fundamental features used for clustering: the path length of the segment (L), the total area of the segment which was defined as the polygon covering the set of points of the segment, the distance from the segment's start and end, (d) The distance and direction of the center of mass of all points defining the segment from the center of the trajectory (ρ and θ, respectively).

Inspection of the behavior across fish, throughout the entire tracking period, revealed that different fish varied in terms of each class (**Figure 6D**). Some fish spent most of the daily trajectory in the scanning class while other fish spent most of the daily trajectory in the dwelling or slow ranging classes. In addition, the fish were consistent in their different trajectory patterns. This can be seen in the occupancy of the trajectory segment classes across days (**Figure 6C**).

DISCUSSION

This study was designed as a preliminary investigation toward establishing the *S. rivulatus* as an animal model for the study of the neural basis of navigation in the wild. For this purpose, we measured the locations of fish in their natural coral reef environment. We characterized the trajectory patterns in the natural environment. We found that the fish maintained a home range, the area in which the animal lives and moves on a regular basis (**Figure 3**). The home range was relatively stable over time. Overall, the *S. rivulatus* behavior was similar with other coral reef fish which maintain home range (Kramer and Chapman, 1999). The fish also returned to roughly the same place to sleep every night. This is an indication that *S. rivulatus* can plan daily routes that start and end in the same place.

We found that the trajectory segments fell into four different classes (**Figure 5B**). This is an indication that the fish used multiple movement patterns in the coral reef environment. Each fish had individual ratios of using the different four strategies of movement (**Figure 6D**) and these different ratios were relatively stable across days for each fish with (**Figure 6C**) higher variability for the lower ratio used strategies. Overall, our results indicate that *S. rivulatus* evidences a complex spatial pattern of movement in the environment.

This work extends the findings of two previous works on the rabbitfish family. The first, a study of *S. rivulatus*, demonstrated the existence of home range behavior in this species in two different environments: The Red Sea and the Mediterranean. The

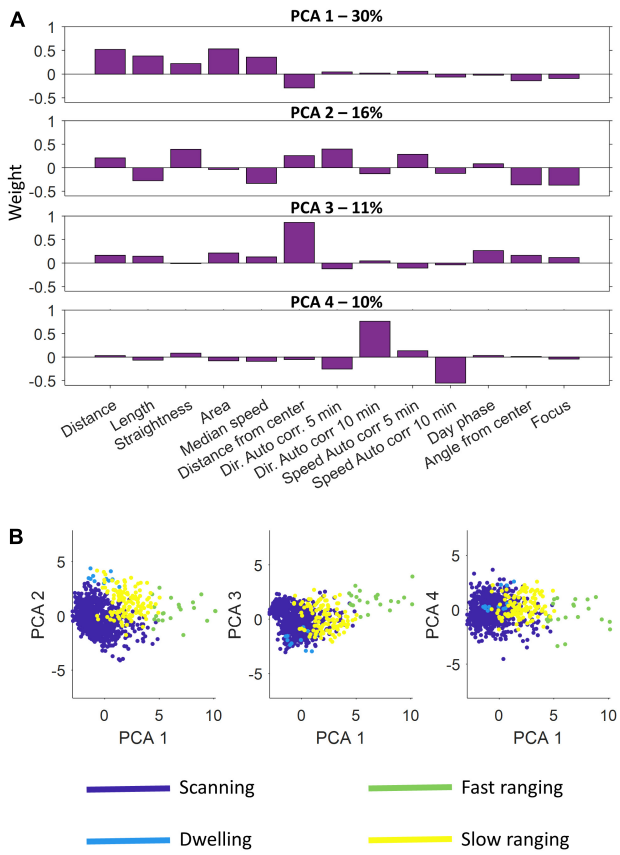

FIGURE 5 | Principal component analysis and semi-automatic agglomerative clustering. **(A)** A principal component analysis was performed on the feature sets of the segments. Shown are the four principal components used. Each component emphasizes a different set of features. **(B)** After dimension reduction using principal component analysis, semi-automatic agglomerative clustering was performed to divide the segments into four classes: scanning, dwelling, fast ranging and slow ranging.

behavior of the fish in the two environments were different in scale, since the fish maintained a much larger home range in the Mediterranean possibly due to substantial differences in the distribution of food in this environment (Pickholtz et al., 2018). The second study found that juvenile rabbitfish (*S. corallinus and S. doliatus*) defined a home range that could be relatively small, and also showed strong homing behavior (Ghanawi et al., 2013; Givon et al., 2022). Our findings thus contribute to a better understanding of the spatial behavior of this species by providing a detailed analysis of the movement strategies employed by the fish in their natural environment.

More broadly in the field of fish navigation there are indications that homing salmons use different strategies which rely on different sensory modalities to return to their spawning grounds (Quinn and Brannon, 1982; Dittman and Quinn, 1996). Here, we showed that *S. rivulatus* use different patterns while exploring the coral reef environment reflected in the trajectory segments classes. In this respect the *S. rivulatus* is similar to the salmon in terms of using different behaviors during exploration. In addition, the fish were shown to use different egocentric (Rodríguez et al., 2002), geometric (Sovrano et al., 2002; Broglio et al., 2011) and visual (Rodríguez et al., 2002; Givon et al., 2022) cues when navigating in different lab settings. In our study, we showed that the trajectory segments could be classified into classes. It remains to be seen which sensory modalities and environmental cues are used by these animals in their daily routes.

In future works it will be possible to add a layer of an electrophysiological aspect to that of the tracking. This raise concerns on the issue of tracking resolution and fish recapturing.

First concern is whether the tracking resolution high enough to allow correlating location and brain activity. This is dependent on resources mainly, with the deploying more receivers in the field the positioning error can be reduced to about a meter. Furthermore, new technologies, including robotics that follow the fish using both acoustic and visual sensors are in development (Zolich et al., 2017). Such robotics can provide more accurate monitoring of fish location and additional dynamics parameters such as head direction and even feeding and social interaction with other conspecific.

The second issue that needs to be addressed is the need to recapture the fish in order to obtain the electrophysiology data. As currently, the technology for real-time positioning exists and relies on acoustic receivers that transmit detection continuously. This allows detection of the fish location at night while the fish sleeps and allows recapturing. All these technologies can provide the needed additional capacity to allow electrophysiology in the wild.

Outlook for Naturalistic Neuroscience

Siganus rivulatus and the coral reef environment both emerged as excellent choices for studying the neural coding of spatial information in the wild. These fish are excellent navigators and can accurately find their way in the coral reef environment. While the size of the natural home range of *S. rivulatus* in the Gulf of Eilat is qualitatively larger than typical lab settings (approx. 200 m × 50 m × 5 m vs. 1 m × 1 m × 1 m), it is still relatively small compared to other species. Thus, with proper equipment it remains tractable in terms of our ability to track the fish (both visually and acoustically), its behavior, and its immediate surroundings. The coral reef habitat of this species represents a non-trivial environment characterized by high complexity and rich content. The elongated topography of the Gulf of Aqaba and its coral reef constrains navigational routes to a pseudo-linear structure, potentially simplifying the neural representation (at the habitat scale) and data analysis. Finally, the capacity to control buoyancy in the aquatic environment makes it possible to fit the fish with a neurological data logger with enough battery power to record brain activity continuously for a week.

The main technological breakthrough that enables the next step of electrophysiology in the wild is the recent development of wireless recording system from behaving fish (Vinepinsky et al., 2017, 2020; Cohen et al., 2019). This technology, which weighs only 2.5 g, enables continuous recording from a fish for several days. This is achieved, in part, by adjusting the

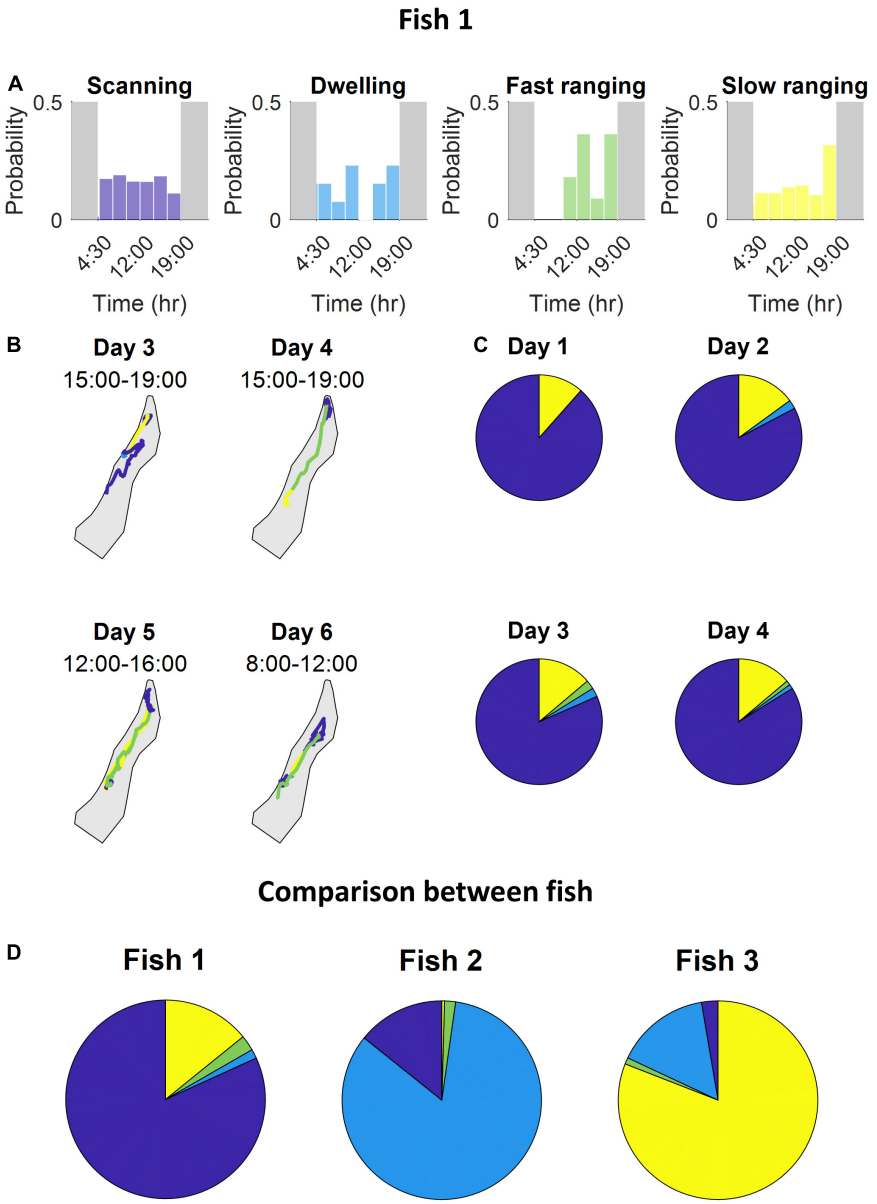

FIGURE 6 | The fish use multiple strategies during the day while exploring the coral reef environment. **(A)** For each class, the probability segments appearing at specific times throughout the day. **(B)** Several examples of 4-h long trajectory segment sequences the fish used to travel between areas where it scans and dwells. **(C)** The time one fish spent engaging in each class of trajectory segments over four consecutive days. The days were similar in their class distribution. **(D)** Time-division of engagement in each class throughout the entire tracking period of each fish. Stability tested among different day groups resulted in a standard error percentage of fish 1 – [0.2,23,36,2.4], fish 2 – [22,4.2,71,0], fish 3 – (28,0.6,24,0.4) for scanning, dwelling, fast ranging and slow ranging, respectively. Variation tested among all fish yielded that all but one class have a substantial variability with a minimal standard error of 75%, fast ranging being the exception with a standard error of 24% (all color maps relate to **Figure 5B**).

floatation of the device so that it is neutrally buoyant such that a 250 g fish can be fitted with a relatively large 35 g battery. This type of experiment means that weeklong data can be collected in a single experiment. With proper design, the neutral buoyancy implant neither interferes with the fish's ability to maintain its balance nor increases drag in a significant way. In experiments with goldfish, the fish were able to swim with this device for up to 2 weeks without any behavioral effects whatsoever (Vinepinsky et al., 2017, 2020; Cohen et al., 2019). This neural logger technology can be modified to record from the brains of fish swimming in the wild and would enable significant insights into the neural basis of navigation in the real world. It is important to note that the home range size of the *S. rivulatus* is also make it possible to retrieve the data logger device since at the end of the experiment using acoustic tag.

From lesion studies in the goldfish (Rodríguez et al., 2002), it is known that the relevant region in the brain is the later pallium at the telencephalon and recording should be targeted in this region. Another option is to record from the central region of the telencephalon that contain cell bodies with connections in other regions of the telencephalon (Northcutt, 2008). In summary, this is an indication that 16 electrodes array is of sufficient resolution to obtain indication about representation of space in the rabbitfish brain.

It should be noted that *S. rivulatus* is not the only choice for the development of electrophysiology in the wild. Other fish species with similar home range sizes can serve a similar purpose, including marine (Kramer and Chapman, 1999) and freshwater species (Baktoft et al., 2017). Beyond fish, the Egyptian bat was developed in recent years into an animal model to assess spatial cognition in large linear arenas (Eliav et al., 2021) and is expected to provide further insights in the future.

Overall, we showed that *S. rivulatus* maintains a home range and can navigate in its natural coral reef environment. The fish can start and end their daily trajectory in roughly the same place. In addition, the fish can use different navigational strategies. The size of the home range is very large compared to regular lab experiments but still small enough to make tracking the fish feasible. The combination of these properties with the technology of recording single cells in the fish brain can lead to the development of electrophysiology in the wild and can provide insights into the neural basis of navigation.

DATA AVAILABILITY STATEMENT

The raw data supporting the conclusions of this article will be made available by the authors upon reasonable request.

ETHICS STATEMENT

The animal study was reviewed and approved by the Ben-Gurion University of the Negev Institutional Animal Care and Use Committee.

AUTHOR CONTRIBUTIONS

SG: formal analysis, investigation, and methodology. RP: investigation. EP: methodology. OB-S, MK, and RS: conceptualization and investigation. All authors contributed to the article and approved the submitted version.

FUNDING

We gratefully acknowledged financial support from the Israel Science Foundation – First Program (Grant No. 281/15), the Israel Science Foundation – First Program (grant no. 555/19), the Israel Science Foundation (grant no. 211/15), the Israel Science Foundation (grant no. 824/21), a Human Frontiers Science Foundation grant RGP0016/2019, the Frankel Center at the Computer Science Department, and the Helmsley Charitable Trust through the Agricultural, Biological and Cognitive Robotics Initiative of Ben-Gurion University of the Negev.

ACKNOWLEDGMENTS

We thank Shai Zilberman, Ynon Hermon, and Shachaf Ben-Ezra for technical assistance.

REFERENCES

Baktoft, H., Gjelland, K. Ø., Økland, F., and Thygesen, U. H. (2017). Positioning of aquatic animals based on time-of-arrival and random walk models using YAPS (Yet Another Positioning Solver). *Sci. Rep.* 7:14294. doi: 10.1038/s41598-017-14278-z

Ben-Yishay, E., Krivoruchko, K., Ron, S., Ulanovsky, N., Derdikman, D., and Gutfreund, Y. (2021). Head-direction coding in the hippocampal formation of birds. *bioRxiv* [preprint]. doi: 10.1101/2020.08.31.274928

Bridger, C. J., and Booth, R. K. (2003). The effects of biotelemetry transmitter presence and attachment procedures on fish physiology and behavior. *Rev. Fish. Sci.* 11, 13–34.

Broglio, C., Gómez, A., Durán, E., Salas, C., and Rodríguez, F. (2011). "Brain and cognition in teleost fish," in *Fish Cognition and Behavior*, eds C. Brown, K. Laland, and J. Krause (Oxford: Wiley), 325–358.

Cohen, L., Vinepinsky, E., and Segev, R. (2019). Wireless electrophysiological recording of neurons by movable tetrodes in freely swimming fish. *JoVE J. Vis. Exp.* 153:e60524. doi: 10.3791/60524

Courellis, H. S., Nummela, S. U., Metke, M., Diehl, G. W., Bussell, R., Cauwenberghs, G., et al. (2019). Spatial encoding in primate hippocampus during free navigation. *PLoS Biol.* 17:e3000546. doi: 10.1371/journal.pbio.3000546

Dittman, A., and Quinn, T. (1996). Homing in Pacific salmon: mechanisms and ecological basis. *J. Exp. Biol.* 199, 83–91. doi: 10.1242/jeb.199.1.83

Eliav, T., Maimon, S. R., Aljadeff, J., Tsodyks, M., Ginosar, G., Las, L., et al. (2021). Multiscale representation of very large environments in the hippocampus of flying bats. *Science* 372:eabg4020. doi: 10.1126/science.abg4020

Frost, B. J., and Mouritsen, H. (2006). The neural mechanisms of long distance animal navigation. *Curr. Opin. Neurobiol.* 16, 481–488. doi: 10.1016/j.conb.2006.06.005

Furuya, Y., Matsumoto, J., Hori, E., Boas, C. V., Tran, A. H., Shimada, Y., et al. (2014). Place-related neuronal activity in the monkey parahippocampal gyrus and hippocampal formation during virtual navigation. *Hippocampus* 24, 113–130. doi: 10.1002/hipo.22209

Gehring, T. V., Luksys, G., Sandi, C., and Vasilaki, E. (2015). Detailed classification of swimming paths in the Morris Water Maze: multiple strategies within one trial. *Sci. Rep.* 5, 1–15. doi: 10.1038/srep14562

Ghanawi, J., Monzer, S., and Saoud, I. P. (2013). Anaesthetic efficacy of clove oil, benzocaine, 2-phenoxyethanol and tricaine methanesulfonate in juvenile marbled spinefoot (*Siganus rivulatus*). *Aquac. Res.* 44, 359–366.

Givon, S., Samina, M., Ben-Shahar, O., and Segev, R. (2022). From fish out of water to new insights on navigation mechanisms in animals. *Behav. Brain Res.* 419:113711. doi: 10.1016/j.bbr.2021.113711

Jacobs, L. F., and Menzel, R. (2014). Navigation outside of the box: what the lab can learn from the field and what the field can learn from the lab. *Mov. Ecol.* 2, 1–22. doi: 10.1186/2051-3933-2-3

Kramer, D. L., and Chapman, M. R. (1999). Implications of fish home range size and relocation for marine reserve function. *Environ. Biol. Fishes* 55, 65–79.

McLean, D. J., and Skowron Volponi, M. A. (2018). trajr: an R package for characterisation of animal trajectories. *Ethology* 124, 440–448.

Mouritsen, H., Heyers, D., and Güntürkün, O. (2016). The neural basis of long-distance navigation in birds. *Annu. Rev. Physiol.* 78, 133–154. doi: 10.1146/annurev-physiol-021115-105054

Northcutt, R. G. (2008). Forebrain evolution in bony fishes. *Brain Res. Bull.* 75, 191–205. doi: 10.1016/j.brainresbull.2007.10.058

O'Keefe, J., and Dostrovsky, J. (1971). The hippocampus as a spatial map: preliminary evidence from unit activity in the freely-moving rat. *Brain Res.* 34, 171–175. doi: 10.1016/0006-8993(71)90358-1

O'Mara, S. M., Rolls, E. T., Berthoz, A., and Kesner, R. P. (1994). Neurons responding to whole-body Motion in the primate hippocampus. *J. Neurosci.* 14, 6511–6523. doi: 10.1523/JNEUROSCI.14-11-06511.1994

Pickholtz, R. S., Kiflawi, M., Friedlander, A. M., and Belmaker, J. (2018). Habitat utilization by an invasive herbivorous fish (*Siganus rivulatus*) in its native and invaded range. *Biol. Invasions* 20, 3499–3512.

Quinn, T. P., and Brannon, E. L. (1982). The use of celestial and magnetic cues by orienting sockeye salmon smolts. *J. Comp. Physiol.* 147, 547–552.

Rodríguez, F., López, J. C., Vargas, J. P., Gómez, Y., Broglio, C., and Salas, C. (2002). Conservation of spatial memory function in the pallial forebrain of reptiles and ray-finned fishes. *J. Neurosci.* 22, 2894–2903. doi: 10.1523/JNEUROSCI.22-07-02894.2002

Rubin, A., Yartsev, M. M., and Ulanovsky, N. (2014). Encoding of head direction by hippocampal place cells in bats. *J. Neurosci.* 34, 1067–1080. doi: 10.1523/JNEUROSCI.5393-12.2014

Sargolini, F., Fyhn, M., Hafting, T., Mcnaughton, B. L., Witter, M. P., Moser, M., et al. (2006). Conjunctive representation of position, direction, and velocity in entorhinal cortex. *Science* 312, 758–762. doi: 10.1126/science.1125572

Seaman, D. E., and Powell, R. A. (1996). An evaluation of the accuracy of kernel density estimators for home range analysis. *Ecology* 77, 2075–2085.

Solstad, T., Boccara, C. N., Kropff, E., Moser, M., and Moser, E. I. (2008). Representation of geometric borders in the entorhinal cortex. *Science* 322, 1865–1868. doi: 10.1126/science.1166466

Sovrano, V. A., Bisazza, A., and Vallortigara, G. (2002). Modularity and spatial reorientation in a simple mind: encoding of geometric and nongeometric properties of a spatial environment by fish. *Cognition* 85, B51–B59. doi: 10.1016/s0010-0277(02)00110-5

Taube, J. S., Muller, R. U., and Ranck, J. B. (1990). Head-direction cells recorded from the postsubiculum in freely moving rats. I. Description and quantitative analysis. *J. Neurosci.* 10, 420–435. doi: 10.1523/JNEUROSCI.10-02-00420.1990

Tsoar, A., Nathan, R., Bartan, Y., Vyssotski, A., Dell'omo, G., and Ulanovsky, N. (2011). Large-scale navigational map in a mammal. *Proc. Natl. Acad. Sci. U.S.A.* 108, E718–E724. doi: 10.1073/pnas.1107365108

Vinepinsky, E., Cohen, L., Perchik, S., Ben-Shahar, O., Donchin, O., and Segev, R. (2020). Representation of edges, head direction, and swimming kinematics in the brain of freely-navigating fish. *Sci. Rep.* 10, 1–16. doi: 10.1038/s41598-020-71217-1

Vinepinsky, E., Donchin, O., and Segev, R. (2017). Wireless electrophysiology of the brain of freely swimming goldfish. *J. Neurosci. Methods* 278, 76–86. doi: 10.1016/j.jneumeth.2017.01.001

Yartsev, M. M., and Ulanovsky, N. (2013). Representation of three-dimensional space in the hippocampus of flying bats. *Science* 340, 367–372. doi: 10.1126/science.1235338

Yartsev, M. M., Witter, M. P., and Ulanovsky, N. (2011). Grid cells without theta oscillations in the entorhinal cortex of bats. *Nature* 479, 103–107. doi: 10.1038/nature10583

Zolich, A., Johansen, T. A., Alfredsen, J. A., Kuttenkeuler, J., and Erstorp, E. (2017). "A formation of unmanned vehicles for tracking of an acoustic fish-tag," in *Proceedings of the OCEANS 2017-Anchorage* 2017, (Piscataway, NJ: IEEE), 1–6.

Conflict of Interest: The authors declare that the research was conducted in the absence of any commercial or financial relationships that could be construed as a potential conflict of interest.

Publisher's Note: All claims expressed in this article are solely those of the authors and do not necessarily represent those of their affiliated organizations, or those of the publisher, the editors and the reviewers. Any product that may be evaluated in this article, or claim that may be made by its manufacturer, is not guaranteed or endorsed by the publisher.

frontiers | Frontiers in Systems Neuroscience

TYPE Original Research
PUBLISHED 01 August 2022
DOI 10.3389/fnsys.2022.920703

OPEN ACCESS

EDITED BY
M. Jerome Beetz,
Julius Maximilian University of Würzburg, Germany

REVIEWED BY
Eran Amichai,
Dartmouth College, United States
Julio C. Hechavarría,
Goethe University Frankfurt, Germany
Shizuko Hiryu,
Doshisha University, Japan

*CORRESPONDENCE
Jinhong Luo
jluo@ccnu.edu.cn

†These authors have contributed equally to this work and share first authorship

RECEIVED 14 April 2022
ACCEPTED 05 July 2022
PUBLISHED 01 August 2022

CITATION
Luo J, Lu M, Wang X, Wang H and Moss CF (2022) Doppler shift compensation performance in *Hipposideros pratti* across experimental paradigms. *Front. Syst. Neurosci.* 16:920703. doi: 10.3389/fnsys.2022.920703

Doppler shift compensation performance in *Hipposideros pratti* across experimental paradigms

Jinhong Luo[1*†], Manman Lu[1†], Xindong Wang[1†], Huimin Wang[1] and Cynthia F. Moss[2]

[1]School of Life Sciences, Institute of Evolution and Ecology, Central China Normal University, Wuhan, China, [2]Department of Psychological and Brain Sciences, Johns Hopkins University, Baltimore, MD, United States

A central aim of neuroethological research is to discover the mechanisms of natural behaviors in controlled laboratory studies. This goal, however, comes with challenges, namely the selection of experimental paradigms that allow full expression of natural behaviors. Here, we explore this problem in echolocating bats that evolved Doppler shift compensation (DSC) of sonar vocalizations to yield close matching between echo frequency and hearing sensitivity. We ask if behavioral tasks influence the precision of DSC in Pratt's roundleaf bat, *Hipposideros pratti*, in three classic laboratory paradigms evoking audio-vocal adjustments: Stationary bats listening to echo playbacks, bats transported on a moving pendulum, and bats flying freely. We found that experimental conditions had a strong influence on the expression of the audiovocal frequency adjustments in bats. *H. pratti* exhibited robust DSC in both free-flying and moving-pendulum experiments but did not exhibit consistent audiovocal adjustments in echo playback experiments. *H. pratti* featured a maximum compensation magnitude of 87% and a compensation precision of 0.27% in the free flight experiment. Interestingly, in the moving pendulum experiment *H. pratti* displayed surprisingly high-precision DSC, with an 84% maximum compensation magnitude and a 0.27% compensation precision. Such DSC performance places *H. pratti* among the bat species exhibiting the most precise audio-vocal control of echo frequency. These data support the emerging view that Hipposiderid bats have a high-precision DSC system and highlight the importance of selecting experimental paradigms that yield the expression of robust natural behaviors.

KEYWORDS

auditory feedback, behavioral plasticity, echolocation, motor control, neuroethology

Introduction

Controlled laboratory studies are employed to discover the mechanisms of natural animal behaviors. Laboratory settings allow researchers to experimentally study selected behaviors, while controlling for environmental variables, offering an opportunity to discover mechanisms that would otherwise prove difficult to reveal in an organism's natural environment. However, studying animals in a laboratory setting comes with other challenges or potential pitfalls. The housing environment alone, for example, can impact many aspects of animal behavior and physiology, including reproduction, circadian rhythm, and immune function, just to list a few (Calisi and Bentley, 2009). Particularly noteworthy, some observations in laboratory experiments may differ from those in the natural environment (Kronfeld-Schor et al., 2013). Hence, understanding the effects of controlled laboratory settings on animals' expression of natural behavior is of great importance.

Echolocating bats are a choice animal model for neuroethological research, partly due to their active sensing behaviors, which can be quantitatively analyzed and linked to neural processes (Griffin, 1958; Moss et al., 2011; Luo and Moss, 2017; Luo et al., 2017, 2018; Kothari et al., 2018). Studying echolocating bats in controlled laboratory environments dates back to Spallanzani's question of how bats avoid obstacles in the dark, as well as to the groundbreaking observations by Donald Griffin and Robert Galambos (Griffin and Galambos, 1941; Griffin, 1958; Grinnell, 2018). Since then, controlled laboratory settings have continued to unravel the mechanisms of echolocation in bats (Popper and Fay, 1995; Thomas et al., 2004; Fenton et al., 2016). In recent years, however, several studies have pointed to distinct differences in the echolocation behavior of bats in the laboratory and in the field. For example, the big brown bat, *Eptesicus fuscus*, does not produce long duration search calls in the laboratory, as it does in the field (Surlykke and Moss, 2000). Daubenton's bat, *Myotis daubentonii*, emits more directional calls of higher intensity in the field than in the laboratory (Surlykke et al., 2009). The minimum frequency of the first search call emitted after the buzz phase in *M. daubentonii* also shows differences between successful and unsuccessful prey captures, but only in the laboratory, and not in the field (Britton and Jones, 1999).

In laboratory settings, experimental paradigms can also affect the expression of bats' natural echolocation behaviors, such as Doppler shift compensation (DSC). DSC is found in bat species that produce echolocation calls consisting of relatively long constant-frequency (CF) components, in combination with frequency modulated (FM) components, and these species are commonly referred to as CF-FM bats (**Figure 1A**). Bats exhibiting DSC are found in the families of Rhinolophidae and Hipposideridae, and two species of Mormoopidae (*Pteronotus parnellii* and *P. personatus*) (Smotherman and Guillén-Servent, 2008; Schnitzler and Denzinger, 2011). Two species of Noctilionidae (*Noctilio albiventris*; *N. leporinus*) that produce quasi-CF signals exhibit partial DSC (Wenstrup and Suthers, 1984). During flight, the echoes received by bats as they approach targets are up-shifted in frequency, due to the Doppler effect, and CF-FM bats show DSC behavior by lowering the emitted call frequency so that the echo frequency is maintained in a narrow frequency range of the bat's most sensitive hearing (Schnitzler, 1968, 1973; Schnitzler and Denzinger, 2011; Hiryu et al., 2016). DSC is one of the most intensely studied audio-vocal behaviors in echolocating bats, and three experimental paradigms have been widely used to investigate the details of their feedback control (**Figures 1B–D**). Although qualitative differences in DSC experimental paradigms have been anecdotally mentioned, most published work has only reported data from a single experimental method (e.g., Schnitzler and Denzinger, 2011; Hiryu et al., 2016). These qualitative comparisons suggested that all flying bats exhibit robust DSC behavior, while bats swung on a pendulum or performing in playback experiments tended to show reduced DSC.

In particular, the expression of DSC behavior in Hipposiderid bats seems to be very sensitive to experimental paradigms. For both *H. speoris* and *H. bicolor*, DSC behavior was not observed in a playback experiment (Schuller, 1980), but partial DSC behavior, with a maximum compensation magnitude of about 55%, was observed in bats moving on a pendulum (Habersetzer et al., 1984). By contrast, two recent studies of *H. armiger* in free-flying experiments reported precision of DSC (0.15∼0.17%) (Schoeppler et al., 2018; Zhang et al., 2019), much higher than previous reports of 0.4∼0.7% (Schnitzler and Denzinger, 2011). Compensation precision is measured as the percentage ratio of the standard variation to the mean of the echo frequencies. The smaller the value, the higher the compensation precision. Furthermore, two studies quantified and compared the DSC performance of *P. parnellii* between two experimental paradigms and confirmed that the accuracy of DSC in *P. parnellii* was indeed higher in free-flying bats than in animals swung on a pendulum (Lancaster et al., 1992; Keating et al., 1994). Nevertheless, one advantage of the playback and moving pendulum paradigms is that the experimental subject remains at the same position during the test, which not only reduces technical challenges of neurophysiological investigations, but also allows for isolating experimental variables that may covary in free-flying experiments. It is noteworthy that both playback and moving pendulum paradigms have also been used to study audiovocal control capability of bat species that do not exhibit DSC behavior, such as the big brown bat (Luo and Moss, 2017) and the Seba's short-tailed bat (Beetz et al., 2021).

Considering the technical advantages of playback and pendulum paradigms for probing mechanisms of DSC behavior

and the long under-appreciated high accuracy of DSC in Hipposiderid bats, we measured and quantitatively compared the DSC behavior in *Hipposideros pratti* across the three experimental paradigms. Our data show that *H. pratti* did not exhibit consistent audiovocal adjustments in the playback experiment, but exhibited robust DSC behavior in both free flight and moving pendulum experiments, with an overall compensation precision in these two paradigms of 0.27%.

Results

We conducted behavioral experiments using the CF-FM bat, *H. pratti*, in the laboratory and compared DSC performance in three experimental paradigms (Figures 1B–D), including bats trained to fly and land on a platform, bats transported in a moving pendulum, and hanging bats listening to frequency-shifted playbacks of their echolocation calls.

Overall vocal behavior of *Hipposideros pratti* in three experimental paradigms

Free flight paradigm

Four individual *H. pratti* (two males and two females) were successfully trained to start from an elevated position, fly toward, and land on a hanging grid (20 cm × 20 cm) over a distance of approximately 4 m in the laboratory (Figure 1B). After each successful landing, the bat received a piece of food reward. For each flight trial, echolocation calls of the bat were recorded by an array of nine broadband ultrasound microphones mounted on the wall facing the approaching animal. All bats learned to perform the landing task after approximately 1 month of training, but data collection only started after bats have been trained for approximately 2 months. *H. pratti* exhibited stereotypical flight behavior, with trajectories typically straight toward the landing platform. Two example flight trials from two individuals are shown in Figure 2A. The

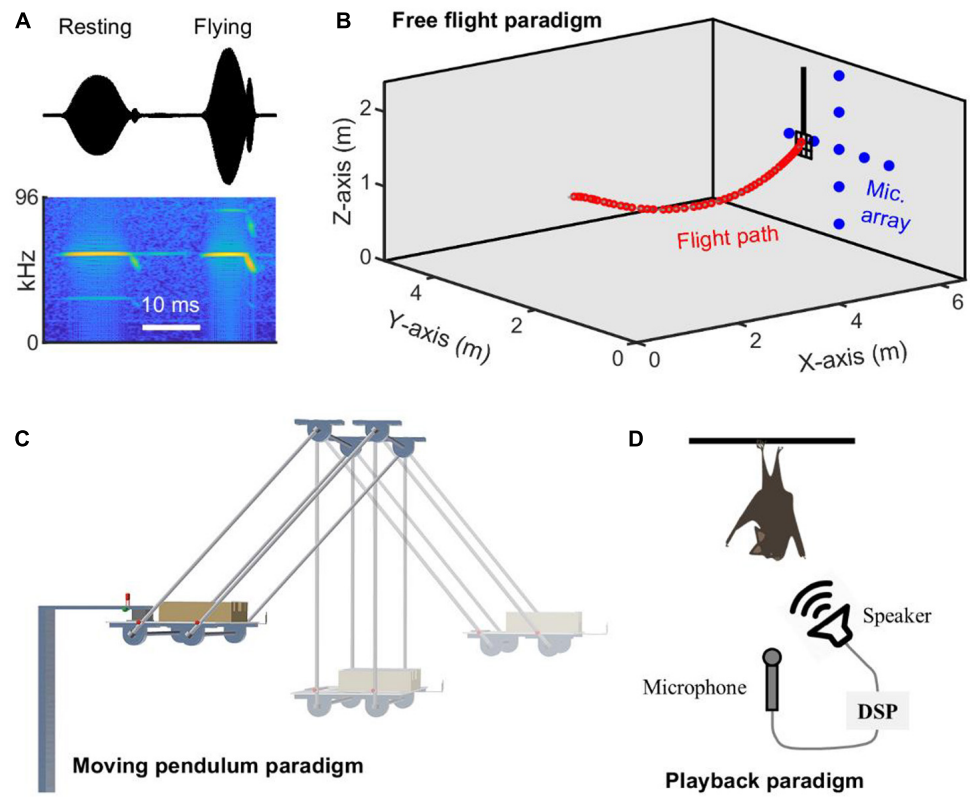

FIGURE 1
Three typical experimental paradigms employed for quantifying Doppler shift compensation behavior in CF-FM echolocating bats. **(A)** Typical examples of echolocation calls produced by the CF-FM bat *Hipposideros pratti* when hanging freely and flying toward a landing platform. Note that the duration, as well as the energy distribution across harmonics, are different, with the call from the flying situation shorter in duration, weaker, and stronger in energy for the first and third harmonics, respectively. **(B)** Free flight paradigm, in which echolocation calls of a trained flying bat were recorded by an array of microphones mounted on the wall, and the flight path was reconstructed based on microphone recordings. **(C)** Moving pendulum paradigm, in which a body-restrained bat was swung back and forth, and the echolocation calls were recorded by an onboard microphone in front of the bat's mouth. **(D)** Playback paradigm, in which a hanging (resting) bat spontaneously produces echolocation calls and receives a frequency-shifted copy of the calls online. In turn, bats may adjust the call frequency in response to frequency-altered auditory feedback. DSP, digital signal processor.

3D spatial positions of *H. pratti* at the time of call emission were reconstructed using the time of arrival differences from the microphone array. From the reconstructed 3D spatial positions between two consecutive calls, we estimated the instantaneous flight speeds of the bats.

Hipposideros pratti exhibited dynamic vocal behavior during an approach to the landing platform (Figure 2B). Specifically, *H. pratti* reached a maximum call rate, a minimum call amplitude, and a minimum call duration around the time of landing. In this study, we used the median of the three time estimates when *H. pratti* reached a maximum call rate, a minimum call amplitude, and a minimum call duration to represent the landing time. This "vocal" landing time may be slightly different from the landing time when they touched the platform, which was not measured. Nevertheless, it is interesting to note that the landing times decoded independently from the three vocal parameters were highly similar and indistinguishable statistically (Paired non-parametric sign-rank test, all three $P > 0.78$). The recorded calls by the static microphones on the wall indicate that *H. pratti* decreased call frequency (peak frequency of the CF component for the dominant 2nd harmonic) during flight, a manifestation of the DSC behavior. Figure 2B (bottom panel) shows the emitted call frequency and the received echo frequency of a typical trial.

Moving pendulum paradigm

We built a moving pendulum setup that consists of a bat holder to restrain the body of *H. pratti* and a miniature microphone (6 mm × 10 mm), mounted in front of the bat nose, to record echolocation calls (Figure 1C). For each trial, the pendulum carrying a bat was released from an elevated position (approximately 45° relative to freely hanging pendulum) with an electromagnetic switch and swung toward a reflective whiteboard (2.2 m × 1.5 m). The trajectory of the moving pendulum was recorded with a high-speed video camera at 100 fps, from which the spatial position and speed of the pendulum were estimated. The distance between the whiteboard and the freely hanging pendulum was 1.5 m, and the minimum and maximum distances between the bat and the whiteboard were 0.2 and 2.56 m. Thus, the bat received high-amplitude

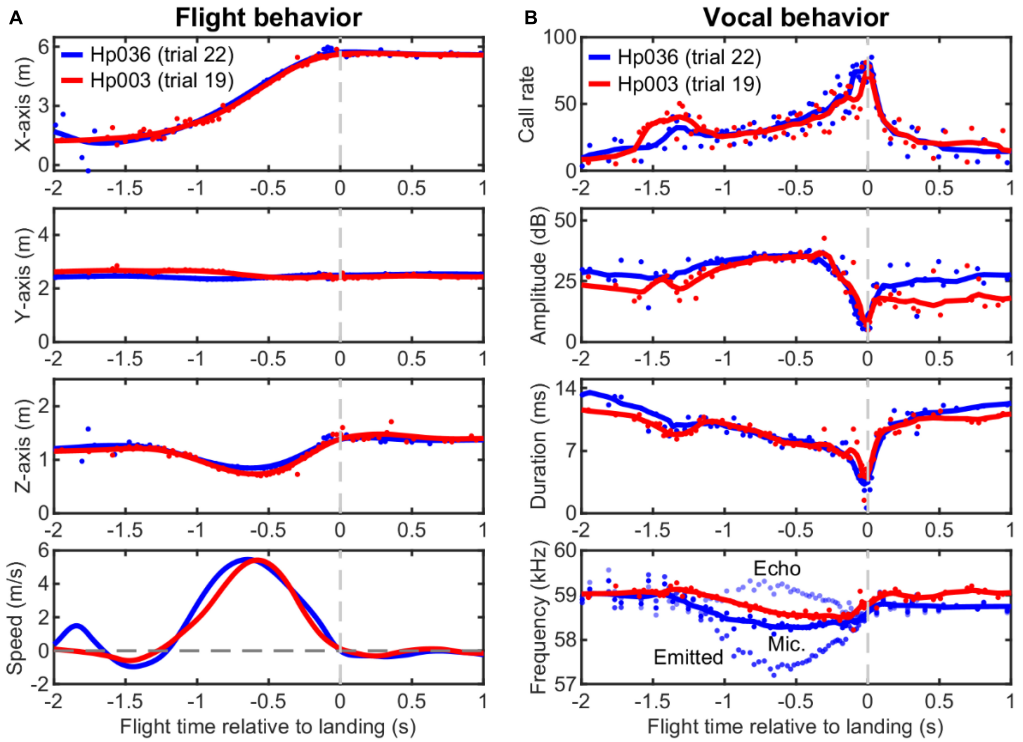

FIGURE 2
Example flight and echolocation behavior of two individuals of *Hipposideros pratti* trained to approach and land on a platform in a flight room. **(A)** Reconstructed three-dimensional (3D) spatial position and the estimated flight speed of the bats using a nine-microphone array mounted on the wall. **(B)** Dynamic adjustments of call parameters of the bats during the approaching flight. Note the highly consistent vocal pattern of the bats for the adjustments of call rate, call amplitude, and call duration that can signify the time of landing events. The call amplitude was measured directly from the central microphone of the array without extra compensation. Based on flight speed (relative to the microphone wall) and call frequency recorded by the static (ground) microphones, the emitted call frequency, and the received echo frequency can be estimated. Thus, we assumed that here that the bat performed DSC using echoes from the microphone wall to its front. For clarity, here we only plotted the emitted call frequency and echo frequency for Hp036. For all panels, original data points are shown as circles and the smoothed traces (nine-point moving average) are shown as solid lines.

echoes at relatively short delays between 1.2 and 15.1 ms. The pendulum reached a maximum speed of 3.34 ± 0.09 m/s and featured a cyclic period of 2.56 ± 0.03 s (Figure 3).

We did not find cyclic vocal adjustments in call rate, amplitude, or duration, but found clear DSC behavior in *H. pratti* (Figure 3). It is noteworthy that *H. pratti* tended to produce calls of reduced amplitude and duration during the second half of the forward swings. Similar to findings observed for other CF-FM bat species in a moving pendulum setup (Habersetzer et al., 1984; Gaioni et al., 1990; Behrend and Schuller, 1999; Boonman et al., 2020), *H. pratti* only compensated for an increase in echo frequency during forward swings by decreasing the emitted call frequency, but not for a decrease in echo frequency during backward swings. Figure 3 (bottom panels) shows two example trials, in which the maximum frequency decreases for two individuals were 1.11 and 0.67 kHz, representing a maximum compensation percentage of 98.6 and 62.8%. The compensation precisions in these two trials, measured as the percentage ratio of the standard variation to the mean of the echo frequencies during the forward swing, were 0.18 and 0.42%. As these two trials were selected to show the maximum variability of the DSC performance of *H. pratti* in the moving pendulum paradigm, it seems that *H. pratti* generally exhibited robust DSC behavior when swinging on a pendulum.

Real-time playback paradigm

We used an auditory feedback perturbation system to broadcast frequency-shifted copies of resting bats' vocalizations at a short time delay. For each trial, one hanging *H. pratti* received 20 consecutive frequency-shifted echolocation calls of a predetermined shift size and delay (Figure 1D). In total, we made preliminary recordings (five trials per bat per condition) from four individual *H. pratti*. Figure 4 showed vocal behaviors of one *H. pratti* from three feedback conditions of 0, 700, and −700 Hz shift sizes. The perturbation window is surrounded by two red dashed vertical lines. We found that during the perturbation window the bat did not adjust either call rate, call amplitude, call duration, or call frequency (peak CF) in response to 0-Hz shifted feedback stimuli (Figures 4A–D). By contrast, in response to both 700 and −700 Hz frequency shifted stimuli, the bat increased call rate (Figures 4E,I), decreased call amplitude (Figures 4F,J) and call duration (Figures 4G,K), at least for the first few calls during the perturbation window. Interestingly, the bat not only decreased the peak frequency for the first a few calls in response to 700 Hz frequency shifted stimuli, but also increased the peak frequency in response to −700 Hz frequency shifted stimuli. That is, the bat exhibited bidirectional compensatory frequency adjustments to auditory feedback stimuli, which is thus not consistent with a DSC behavior in freely flying bats (Figure 2B, bottom panel) or bats

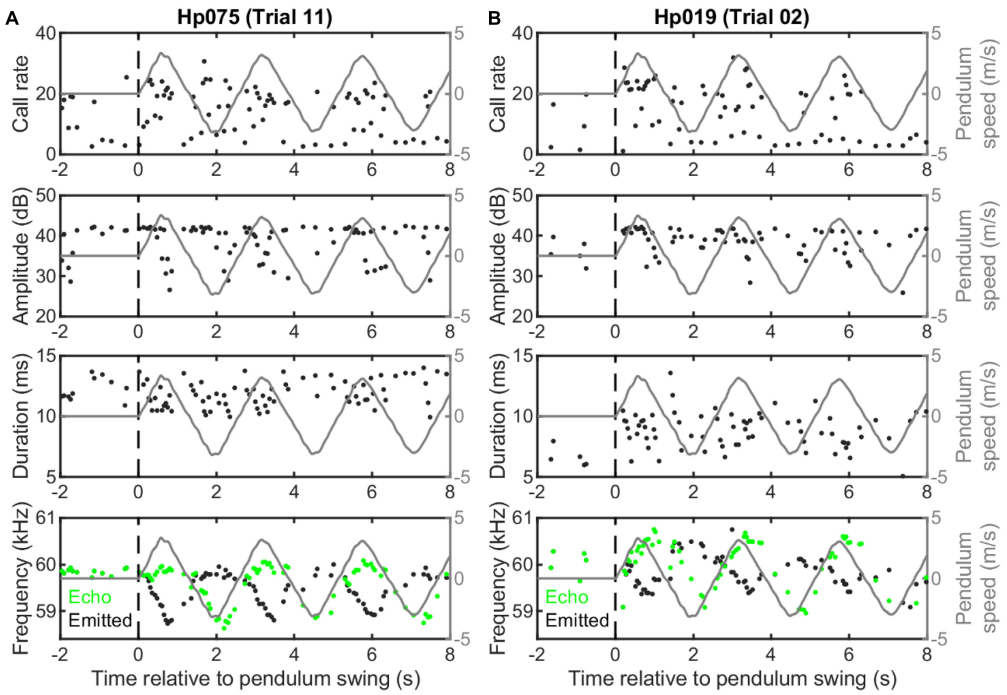

FIGURE 3
Example echolocation behavior of two individuals of *Hipposideros pratti* swung on a pendulum setup. Two trials illustrating higher **(A)** and lower **(B)** quality Doppler shift compensation (DSC) performance of the two bats, as judged by the compensation magnitude and echo-frequency variation. Note, both bats compensated for the Doppler effect by lowering the emitted call frequency only for the forward, but not the backward swings. Also, there were no clear cyclic adjustments of call rate, call amplitude, or call duration during the swings.

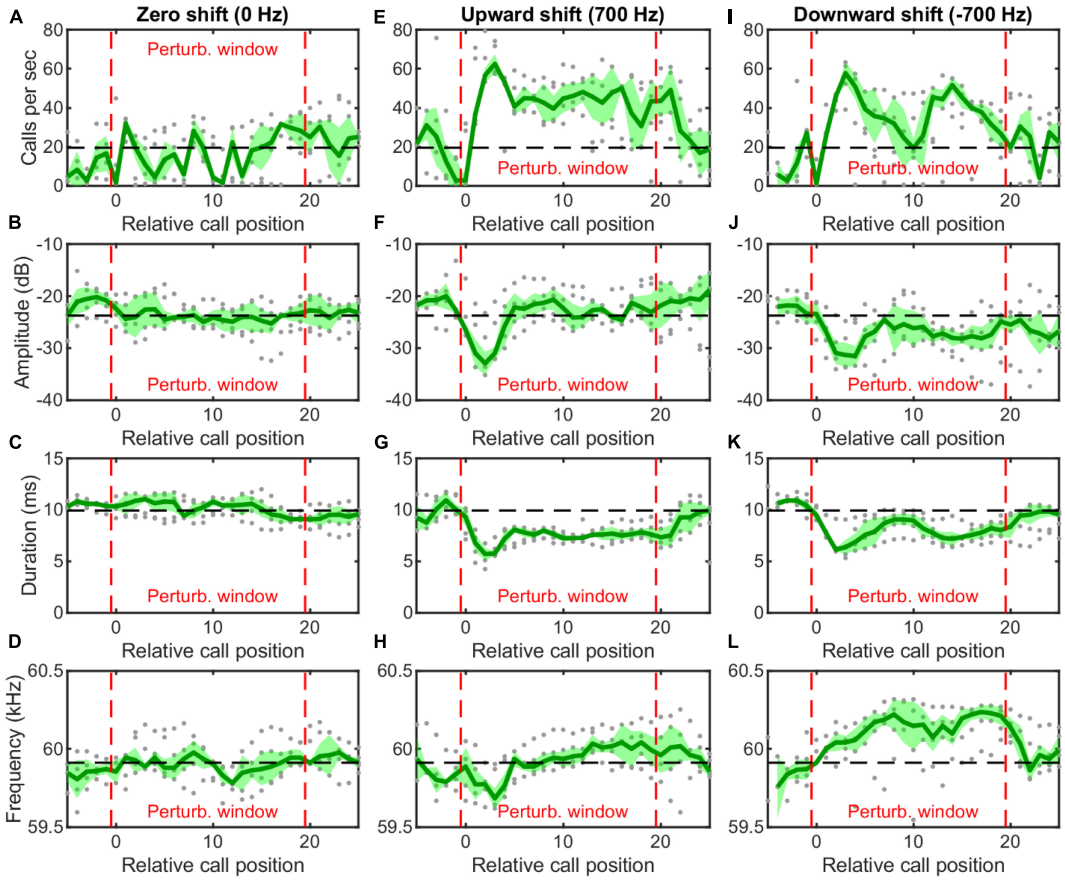

FIGURE 4
Vocal behavior of a hanging *Hipposideros pratti* in response to online frequency-shifted auditory feedback. For each trial, the bat received 20 consecutive frequency-shifted auditory feedback during the perturbation window (between the red dashed lines). The bat did not make any vocal adjustment when received 0-Hz shifted auditory feedback **(A–D)**, but increased call rate **(E,I)**, decreased call amplitude **(F,J)** and call duration **(G,K)**, and decreased **(H)** or increased **(L)** call frequency when received upward shifted and downward shifted auditory feedback for at least a few vocalizations. The gray dots show the individual trial data; the green line and the shaded green area show the average and standard deviation for all the trials (five trials per condition and bat).

transported in a moving pendulum setup (Figure 3, bottom panels). In a detailed study with the same playback setup on another Hipposiderid bat, *H. armiger*, we have shown that online vocal frequency adjustments by *H. armiger* are driven by sensory prediction errors, but not by DSC or by jamming avoidance response (Wang et al., 2022). Thus, below we only made detailed statistical comparisons of the DSC performance of *H. pratti* in the free flight and moving pendulum paradigms.

A comparison of Doppler shift compensation performance between free flight and moving pendulum paradigms

Before we can directly compare the DSC performance of *H. pratti* between the free flight and moving pendulum paradigms, several methodological details should be explained, due to their inherent differences. One principle parameter commonly used to evaluate DSC performance in CF-FM bats is compensation magnitude. Compensation magnitude is typically estimated as the percentage of the maximum frequency reduction by a bat to the speed-induced or Doppler-effect-induced change in resting frequency. Thus, a 100% (full) compensation magnitude means that the CF echo frequency received by the bat during flight, also referred to as reference frequency, equals the CF resting frequency produced by a stationary bat. It is widely reported that the reference frequency of flying CF-FM bats is slightly higher than its resting frequency, with a difference of ∼150–200 Hz in Rhinolophids and *P. parnellii* (Schnitzler and Denzinger, 2011). This means that CF-FM bats under-compensate for the Doppler effect and actively maintain a small frequency offset. Thus, estimating the compensation magnitude requires estimations of the resting frequency and the flight speed. Although most studies quantify

resting frequency as the average call frequency before bats launch into flight (Schnitzler, 1973; Schoeppler et al., 2018), some studies report the average call frequency measured in bats after landing (Hiryu et al., 2008). In this study, we analyzed resting frequency both before the bat took off and after the bat landed on the platform (**Figure 5A**, R1 and R2 phases). Since we did not measure the precise flight onset and offset time with video, and the estimated flight speeds were estimated from microphone array recordings, we took a conservative approach and characterize the following phases: −2.5∼−1.5 s resting before flying (R1), −1.2∼−0.2 s while flying (F), and 0.2∼1.2 s and resting after flying (R2). Time 0 is the vocal landing time. Another reason to exclude the data shortly before the landing is that during this critical period the bat rotates its body and

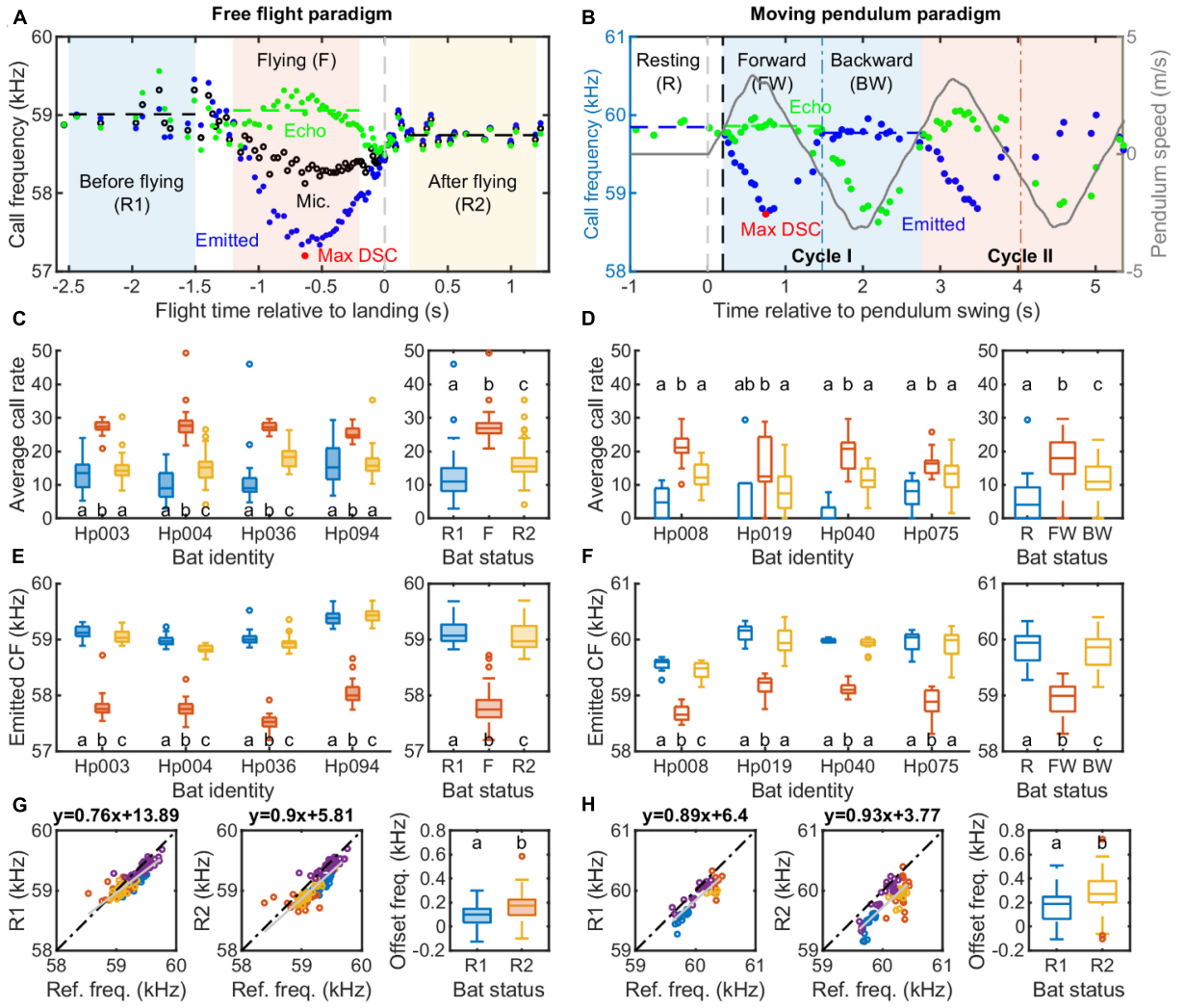

FIGURE 5
Vocal behavior of *Hipposideros pratti* in the free flight and moving pendulum paradigms. **(A)** A detailed illustration of the DSC behavior of a flying bat. For quantitative analyses, a flying trial was divided into three one-second sections: before flying (R1; −2.5∼−1.5 s), during flying (F, −1.2∼−0.2 s), and after flying (R2; 0.2∼1.2 s). Time was referred to as the median of the landing time estimated by the vocal behavior when the bat reached the maximum call rate, minimum call amplitude, and call duration (**Figure 2B**; see section "Materials and methods" for more details). **(B)** A detailed illustration of the DSC behavior of a restrained bat on a moving pendulum. Similar to the flying trials, a pendulum trial was dived into three sections: resting (R, −1∼0 s), Forward (FW) swing, and Backward (BW) swing. For the forward and backward swings, the start and end times were adjusted by the vocal reaction time (delay) of the bat in each trial. Average call rate **(C)** and call frequency **(E)** of *H. pratti* before, during, and after the approach flight at the individual and species levels. Average call rate **(D)** and call frequency **(F)** of *Hipposideros pratti* before (resting), during the forward, and backward swings at the individual and species levels. **(G)** Correlations between the reference frequency and two types of resting frequency (R1, before flying; R2, after flying), and a comparison of the offset frequency between R1 and R2 for the free-flying bats. **(H)** Correlations between the reference frequency and resting frequency (before swing onset) and call frequency during the backward swing, and a comparison of the offset frequency between resting and backward swing for the moving pendulum bats. The sample size for the four individuals, i.e., the number of trials, ranged from 34 to 36 in the free flight experiment, and from 18 to 20 in the moving pendulum experiment.

head from a flight posture to upside-down posture. The bats probably do not rely on the echoes from the microphone wall for DSC during this manuever. Compensation precision was estimated from the flying phase (F). Similar to other bat species transported in a moving pendulum setup (Gaioni et al., 1990; Boonman et al., 2020), there is a reaction time for *H. pratti* in initiating the DSC. In the example trial shown in **Figure 5B**, the reaction time was 0.195 s. We accounted for the reaction time when defining the Resting (R), Forward (FW), and Backward (BW) swing phases. DSC precision was quantified for the forward swing.

The average call rate of freely flying *H. pratti* in the R1, flying (F), and R2 phases are presented in **Figure 5C**; the average call rate of pendulum-transported *H. pratti* in the R, FW, and BW phases are presented in **Figure 5D**. All individuals of *H. pratti* show the highest average call rate during the flying (F) phase and the forward swing phase in the free-flying experiment and the pendulum experiment, respectively (**Figures 5C,D**). Similarly, all individuals of *H. pratti* emitted the lowest call frequency during the flying (F) phase and the forward swing phase of the free flight experiment and the pendulum experiment, respectively (**Figures 5E,F**). **Figures 5G,H** show the relationship between the reference frequency and the resting frequencies. We found that for both experimental paradigms, resting frequency estimated from the "post-flight" phase, i.e., after flying (R2) and during the backward swing (BW), showed a more linear relationship with the reference frequency (Slope: 0.9 vs. 0.76; and 0.93 vs. 0.89). The offset frequency was larger when estimated from the "post-flight" (R2 or BW) phase than from the "pre-flight" (R1 or R) phase (Median: 100 vs. 174 Hz and 188 vs. 272 Hz).

Next, we compared the maximum compensation magnitude and compensation precision between the free flight and moving pendulum paradigms (**Figure 6**). We found that overall *H. pratti* in the free flight experiment had a slightly higher compensation magnitude than in the moving pendulum experiment (**Figure 6A**; Medians, 87.2 vs. 83.9%; Non-parametric Rank-sum test, $P < 0.05$). This difference can also be seen in the offset frequency that was about 100 Hz larger in the moving pendulum experiment (**Figures 5G,H**). However, *H. pratti* exhibited similar compensation precision in both experimental paradigms (**Figures 6B,C**). The overall median compensation precision of *H. pratti* was 0.27 and 0.27% (**Figure 6B**; Non-parametric Rank-sum test, $P > 0.05$), which corresponding to variability (standard variation) in echo frequency of 162 and 165 Hz, respectively (**Figure 6C**; Non-parametric Rank-sum test, $P > 0.05$). As a reference, the median variability of resting frequency before and after flying phases of *H. pratti* in the free flight paradigm was 118 Hz (Quartiles: 65 and 136 Hz) and 116 Hz (Quartiles: 101 and 134 Hz); the median variability of resting frequency before and during the backward swing phases of *H. pratti* in the moving pendulum paradigm was 107 Hz (Quartiles: 67 and 128 Hz) and 149 Hz (Quartiles: 117 and 207 Hz).

Discussion

Compared to the greater horseshoe bats (*R. ferrumequinum*) and mustached bats (*P. parnellii)*, less research effort has been devoted to quantifying DSC performance in Hipposiderid bats. It was long believed that Hipposiderid bats are not able to adjust CF call frequencies to accurately stabilize echo frequencies (Schnitzler and Denzinger, 2011; Hiryu et al., 2016), a view that has been refuted recently with data from *H. armiger* in flight (Schoeppler et al., 2018; Zhang et al., 2019). These two recent studies showed that *H. armiger* in flight shows an overall DSC precision of 0.15∼0.17%, which is comparable to or only slightly poorer than the 0.1∼0.2% compensation precision reported for Horseshoe bats (*R. ferrumequinum, R. euryale, R. rouxii*) and *P. parnellii* (Schnitzler and Denzinger, 2011; Zhang et al., 2019). Our study reveals that *H. pratti* in flight exhibits an overall compensation precision of 0.27%, or a 160 Hz standard variation of the echo frequencies, supporting the emerging view that Hipposiderid bats indeed feature a high-precision DSC system.

Studies of Rhinolophid bats suggest that there are no differences in compensation precision among the species tested in flight, and all featured a compensation precision of 0.1–0.2% (Schnitzler and Denzinger, 2011). However, our data suggest that the precision of the DSC system may be species-specific within the same genus of Hipposiderid bats, with 0.27% compensation precision of *H. pratti*, as reported in the current study, compared with 0.15∼0.17% compensation precision of *H. armiger* (Schoeppler et al., 2018; Zhang et al., 2019). *H. pratti* emits CF echolocation signals that are approximately 12 kHz lower in frequency than *H. armiger* (Lu et al., 2020). Because compensation precision is computed as the percentage ratio of the standard deviation to the mean of the reference frequency, the same value of standard deviation would result in a larger estimate of DSC precision when the reference frequency is lower. Can the 12 kHz difference between *H. pratti* and *H. armiger* account for the observed DSC precision in these two species? Simple math suggests that this is not the case. The ∼12 kHz reference frequency difference can only account for approximately 4% of the compensation precision differences between species. The compensation precision, when measured as a standard deviation around the reference frequency, is still 55 Hz more variable in *H. pratti* than in *H. armiger*. However, a caveat in the precision estimate of *H. pratti* in the current study concerns its flight speed. The study of DSC behavior in flying bats is typically determined from synchronized high-speed video recordings; however, in the current study, we localized the flying bat and derived the instantaneous flight speed using measurements taken with a microphone array. It is known that acoustic localization of sound sources is less

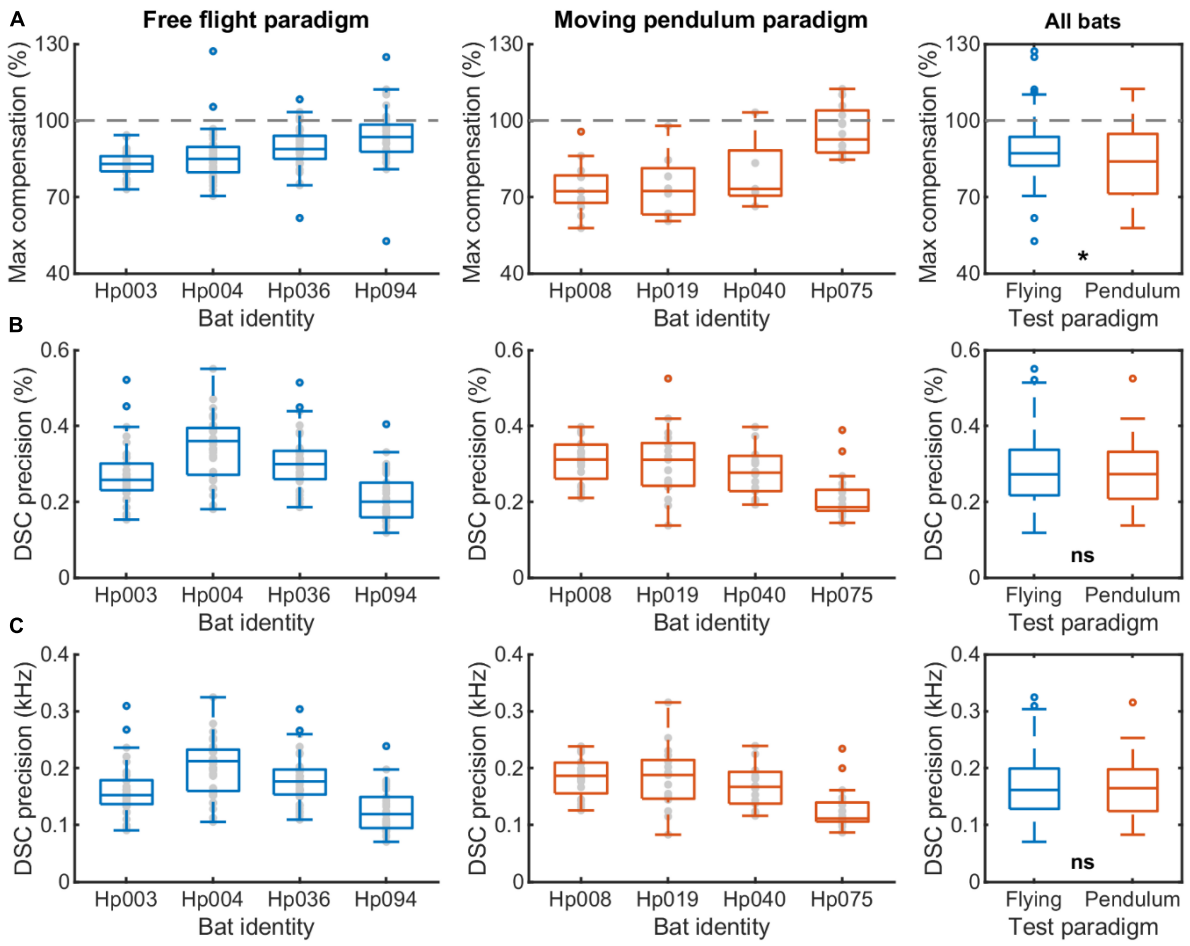

FIGURE 6
A comparison of the DSC performance of *Hipposideros pratti* between the free flight and moving pendulum paradigms. **(A)** Maximum compensation magnitude in percentage. 100% indicates a full compensation for the flight speed induced echo frequency change due to the Doppler effect based on the resting frequency before flying or pendulum swing onset. **(B)** DSC precision in percentage, which was the ratio between the standard variation to the average of the echo frequencies during the forward swing. **(C)** DSC precision in kHz, which was the standard variation of the echo frequencies during the forward swing. The sample size for the four individuals, i.e., the number of trials, ranged from 34 to 36 in the free flight experiment, and from 18 to 20 in the moving pendulum experiment.

accurate than optical methods, with an error up to 5% of the distance to the sound source for some bat species (Surlykke and Kalko, 2008). Thus, our acoustic localization method adds error in the estimation of the bat's instantaneous position and the computed flight speed, which affects the compensation precision. Thus, in future work, it will be critical to measure and compare the compensation precision of *H. pratti* with more accurate localization systems, such as high-speed video, to test whether the compensation precision is species-specific in Hipposideros bats.

One unexpected result from the current study is that *H. pratti* exhibited precise DSC behavior in the moving pendulum experiment. Specifically, the overall compensation precision in four *H. pratti* was 0.27%, ranging from 0.19 to 0.31% across individual animals. The overall maximum compensation magnitude of *H. pratti* was 83.9%, ranging from 72.3 to 92.6% across individual animals. An overall compensation precision of 0.27% is more precise than the overall 0.43% compensation precision reported for *P. parnellii* in a moving pendulum experiment (Lancaster et al., 1992). One reason for a relatively large value of the compensation precision of *P. parnellii* in the study by Lancaster et al. (1992) is that the authors may not have corrected for the bat's reaction time, as pointed out in a study of *P. parnellii* tested with a moving pendulum setup (Gaioni et al., 1990). The study by Gaioni et al. (1990), however, did not report the compensation precision. In our study, we not only corrected for the reaction time of the bat in each trial, but also used an optimization method to search for the reaction time that returned the highest compensation precision. Any other methods, such as the one used by Gaioni et al. (1990), in which reaction time was measured as the time delay between the maximum pendulum speed and the lowest call frequency

of the bat, would result in a lower compensation precision than our method.

We found that *H. pratti* compensated for an overall 84% of full frequency shifts in the moving pendulum experiment, which is among the greatest compensation of bat species tested on swinging pendulums. A previous study reported an overall maximum compensation magnitude of 55 and 56% in two other species of Hipposiderid bat, *H. speoris* and *H. bicolor,* respectively in a moving pendulum experiment (Habersetzer et al., 1984). *P. parnellii* was reported to compensate for on average 80% of the Doppler-shifted echoes (Gaioni et al., 1990). Boonman et al. (2020) found an overall compensation magnitude generally below 80% for three species of Horseshoe bat, *R. ferrumequinum*, *R. blasii*, and *R. hipposideros* (Boonman et al., 2020). It is noteworthy that *R. rouxii* was considered to show a "full compensation" in a pendulum setup as this species' echo frequency fell within a ±300 Hz window around the resting frequency, yet quantitative measurements were not reported (Behrend and Schuller, 1999). Playback experiments on *R. ferrumequinum* suggest that the compensation magnitude of the DSC behavior can be affected by several properties of returning echoes. *R. ferrumequinum,* for example, exhibits a reduced compensation magnitude with decreasing echo amplitude (Smotherman and Metzner, 2003) and with increasing echo delay (Schuller, 1974). Moreover, a higher rate of call emissions also leads to a higher compensation magnitude in *R. ferrumequinum* (Schuller, 1986). In our study, we placed a highly reflective wall at a short distance from the pendulum, which returns high-amplitude echoes at short delays. Bats also significantly increased call rate during the forward swings, compared with both the resting phase and backward swings (**Figure 5D**). Thus, this scenario of echo feedback may have yielded favorable conditions to induce greater DSC magnitude in *H. pratti*. Furthermore, we suggest that the slightly higher average call rate of *H. pratti* in the free flight experiment than in the moving pendulum experiment, as shown in **Figures 5C,D**, may also account for the 3% higher maximum compensation magnitude in the freely flying bats (**Figure 6A**).

To conclude, we have shown that a moving pendulum setup offers a suitable experimental paradigm to investigate the DSC performance of *H. pratti*, and this method offers advantages for concurrent neurophysiological recordings of behaving bats. Our data support the emerging view that Hipposiderid bats have a high-precision DSC system. Methodological inaccuracy in estimating the reaction time that is required to evaluate the DSC performance of bats in pendulum experiments may partially account for an underestimated compensation precision reported in previous studies. It is noteworthy that *H. pratti* in the moving pendulum and free flight experiment exhibited similar DSC performance, but did not show consistent audiovocal adjustments in the playback experiment. Nevertheless, it should be noted that the DSC behavior of bats in the moving pendulum experiment differs from behavior in the free flight experiment in several critical aspects, including (1) there is a clear reaction time of bats in the moving pendulum experiment, but not in the free flight experiment; (2) the average call rate of *H. pratti* is significantly lower in the pendulum experiment than in the free flight experiment, across the resting phases and flying phase; (3) while DSC behavior is accompanied by adjustments of several other signal parameters, such as call amplitude and duration in the free flight experiment, linked vocal adjustments are largely lacking in the moving pendulum experiment. What factors cause these differences will be the subject of future studies.

Materials and methods

Animals

In each of three experiments, four adult *H. pratti* were tested for DSC. The sex of the animals were two males and two females for the free flight experiment, four males for the pendulum experiment, and two males and two females for the playback experiment. Yet, we did not specifically select the sex of the animals in either experiment. All bats were wild-caught with hand nets during the daytime in a cave of Xianning City, Hubei province, China. Bats were housed in social groups of two to five, in custom-made metal cages (40 cm × 40 cm × 40 cm), placed in a room with a regulated air temperature of around 24°C, relative humidity of around 60%, and a reversed light regime of 12 h darkness and 12 h light. Bats had *ad libitum* access to water and food. Capture, housing, and behavioral studies were approved by the Institutional Animal Care and Use Committee of the Central China Normal University.

Experimental setups

All three experiments were conducted in the same test room (6.5 m × 5 m × 2.3 m, length × width × height). The walls and ceiling of the room were covered with acoustic foam of an 8 cm thickness, and the floor was covered with nylon blankets to reduce the echo reflections. In the free flight experiment (**Figure 1B**), a landing grid (20 cm × 20 cm) hung about 0.9 m from the ceiling at approximately 0.8 m distance from a wall equipped with a microphone array. The microphone array contained nine broadband ultrasound microphones (NEUmic, Ultra Sound Advice, United Kingdom) that were configurated into a "+" shape. All microphones were fixed toward the opposite wall in the direction of the approaching bat and the microphone-to-microphone distance was approximately 0.5 m. Note, the exact three-dimensional (3D) position of each microphone was accurately determined with a 1 cm precision at least with a ruler (1 mm precision) for reconstructing the flight path of the vocalizing bat. For each trial, the bat was released from a raised hand of an experimenter from a position

close to the pendulum (see below) and flew approximately 4 m to land on the suspended grid. Although all four *H. pratti* participating in the flying experiment learned to perform the landing task after approximately 1 month of training, data collection for this experiment only started after bats have been trained for approximately 2 months. Training generally took place 5–6 days per week.

For the moving pendulum experiment, a pendulum (**Figure 1C**) was attached to the ceiling close to the wall opposite the microphone array. The pendulum, with an arm length of 1.75 m, was located at 1.6, 2.5, and 2.1 m to the back, left and right wall, and 0.6 m above the floor of the test room, when hanging freely. A reflective wooden board was placed 1.5 m in front of the free-hanging pendulum to return high-intensity echoes to the bat at short delays. The pendulum consisted of a bat holder to restrain the body, but allowed free movement of the head of *H. pratti*. The bat holder was made of metal frames filled with foam in which *H. pratti* maintained a crawling posture. In front of the bat nose, at a distance of 7 cm, a miniature microphone (Custom made, based on SPU0410LR5H, Knowles Corporation, Itasca, IL, United States) was attached to the bat holder frame with an "L" shaped metal bar. Thus, the microphone swung together with the bat in the pendulum and recorded emitted calls without the Doppler effect. Two illuminated colored LEDs separated by 15.3 cm were fixed to one side of the bat holder to facilitate video tracking of the bat's position during the swings by a video camera (1920 × 1080 quality at a100 frame rate; Model FDR-AX700, SONY, Japan). The pendulum was pulled toward the back wall and attached to an electromagnetic switch before the start of each trial. The pendulum movement was started by cutting off the power of the magnetic switch. Video recording and microphone recording were synchronized through a third LED that was lighted by a voltage signal output from an audio interface (see section "Sound recording"). The same voltage signal was recorded by a microphone channel *via* a shortcut cable, while the camera detected the LED signal. The accuracy of the synchronization was ∼10 ms, which was constrained by the much lower sampling rate of the camera (100 Hz), compared to the sampling rate of sound recording (192 kHz).

During the playback experiment, an *H. pratti* hung freely on an elevated (2 m) platform attached to a tripod standing on the floor (**Figure 1D**). The playback setup consisted of a measurement microphone (7016, 1/4-inch Condenser microphone, ACO Pacific, Belmont, CA, United States; with protection grid on) and an ultrasound loudspeaker (Vifa, Avisoft Bioacoustics, Berlin, Germany), which were placed at a 20 and 15 cm distance, respectively, in front of the bat, with the loudspeaker about 15° off the midline. Hanging *H. pratti* produced echolocation calls spontaneously in the setup and received frequency-shifted echo simulating objects at a short delay of ∼4 ms, including 0.6 ms delay for signal processing, 1 ms delay for signal transmissions, and 2 ms digital delay introduced by the experimenter. In this study, we tested bats with three frequency shift sizes of 0, 700, and –700 Hz. A 700 Hz positive frequency shift would be experienced by *H. pratti* flying at a speed of 2 m/s. Similar to other Hipposiderid bats, flying *H. pratti* lower their call frequency to compensate for a positive frequency shift (**Figure 2B**, bottom panel). The amplitude of the echo playbacks was approximately 15 dB weaker than the emitted call, with the maximum peak amplitude of the echo playback at approximately 90 dB SPL. Note, in addition to the echo playbacks, *H. pratti* also received echoes from nearby physical objects, such as the microphone, the loudspeaker, and the floor and walls. A detailed description of the playback setup has been described in a study of *H. armiger* (Under review).

Sound recording

In both the flying and pendulum experiments, echolocation calls of *H. pratti* were recorded, amplified, and digitized before being saved to the hard drive of a desktop computer. In the flying bat experiment, the microphone signal was amplitude by its internal amplifier (i.e., NEUmic); in the pendulum experiment, the microphone signal was amplified by the audio interface amplifier (Fireface 802, RME, Germany). The same audio interface was used to convert analog microphone signals into digital signals at a sampling rate of 192 kHz. Setups were controlled through custom-written programs with SoundMexPro toolbox (Hoertech, Germany) in MATLAB (R2018b, MathWorks, United States). For the playback experiment, echolocation calls were recorded and simulated echoes were played at a sampling rate of 1 MHz with custom-written LabVIEW programs with FPGA chips (PXIe-7858R, National Instruments, Austin, TX, United States).

Data analysis

Sound analysis

Echolocation calls were batch-processed with custom-written scripts in MATLAB. The analysis scripts were created and tested in an earlier study (Lu et al., 2020). Before signal parameter estimation, sound recordings were bandpass filtered ("filtfilt" function) with 4th order Butterworth filter to keep the dominant second harmonic only. The filtered recording was rectified and smoothed ("smooth" function, with 25 points window size), from which background noise floor was estimated. Subsequently, the amplitude threshold for detecting calls was set 2–4 times of this noise floor based on the signal-to-noise (SNR) of the calls. For each identified call, we estimated a set of acoustic parameters, including the peak CF (call frequency of the maximum energy), peak call amplitude, call duration, and inter-pulse-interval (IPI), which are relevant to the current study. Peak CF was measured from an FFT size of 8,192,

resulting in a frequency resolution of 23.4 Hz. Call duration was defined as the time difference between call onset and offset, which were both measured as the time points of –30 dB below the maximum call amplitude. IPI was defined as the time difference between the onset of two consecutive calls. Quality of sound analysis was manually checked for randomly selected recordings as a routine by displaying the waveform, power spectrum, and spectrogram graphically. Particular attention has also been paid to calls of low SNR such as those from the final phase of approaching the landing platform (**Figure 2B**). Manual checking confirmed the high quality of sound analysis. For the free flight experiment where an array of microphones was used, signal parameters were measured from the center microphone (**Figure 1B**) that had the best SNR.

Flight speed

We reconstructed the 3D position of the flying bats at the time of call emission with the microphone array. The 3D location was determined by the triangulation method using the time-of-arrival differences (TOAD) between the microphones. TOADs were computed by cross-correlating the isolated FM component of the dominant 2nd harmonic of the call, as the existence of the CF component seriously affects the accuracy. The FM component was isolated by filtering out the CF component with an elliptic filter ("ellip" function) with the cutoff frequency set to 3 kHz below the peak CF of the call. We only reconstructed the 3D position of the bat when the FM target signal of enough SNR (>12 dB) can be found in at least five recording channels. After reconstructing the 3D position of the bat, we applied a cubic smoothing spline ("csaps" function, with p set to 0.99) for each of the *x*-, *y*-, and *z*-axis data to avoid abrupt position jumping due to limited positioning accuracy. From the smoothed flight trajectory (**Figure 1B**), we estimated the instantaneous flight speed of the bat. As suggested by previous studies, the 3D position from the acoustic localization method may cause up to 10 cm position error in some extreme cases (Surlykke and Kalko, 2008; Surlykke et al., 2009). We found that positioning error particularly affects flight speed estimation when the bat is accelerating and deaccelerating which occurs at the beginning and end of a flight trial. Furthermore, we did not measure the actual landing time when bat touched the landing grid. Hence, we considered the flight speeds at the begging and end of a flight trial inaccurate and did not use them for further analysis.

Pendulum speed

We tracked the two-dimensional (2D) position of the two illuminated LEDs fixed to the side of the pendulum holder during the swings with custom-written scripts in MATLAB. The central positions of the two LEDs were located and their distance in pixel was measured for each frame. Because the physical distance between the two LEDs was fixed (15.3 cm), a change in the pixel distance signifies distortions of the camera lens. We computed the 2D positions of the LED after correcting camera lens distortion. The mid-point of the two LEDs was used to represent the pendulum, from which we estimated the pendulum speed.

Doppler shift compensation performance

We evaluated the DSC performance of *H. pratti* in the free flight and moving pendulum experiments quantitatively, but did not perform a detailed analysis of audiovocal adjustments in the playback experiment. This was because in the playback experiment *H. pratti* exhibited bidirectional adjustments of call frequency and the frequency adjustments were highly variable across the perturbations (**Figures 4H,L**), which were not consistent with DSC of call emissions to stabilize echo frequency. For each trial of the free flight experiment, we first located the "vocal" landing time which was defined as the time when *H. pratti* reached the maximum call rate, minimum call amplitude, or minimum call duration. Using the median of these landing time estimates as a reference, we evaluated DSC performance for the flight period of –1.2∼–0.2 s (**Figure 5A**). For the moving pendulum experiment, DSC performance was evaluated for the forward swing of the first cycle after correcting for the reaction time (**Figure 5B**). DSD performance was evaluated by two parameters, maximum compensation in percentage and DSC precision. Maximum compensation referred to the percentage ratio of the maximum frequency change in flight or in the forward swing (**Figures 5A,B**, red circles) to the expected Doppler effect. Compensation precision referred to the percentage ratio of the standard deviation to the mean of the reference frequency (echo frequency).

To calculate the emitted frequency of the bat during flight, we used the following equation:

$$\overline{F_s = F_m + (c - v_b)/c}.$$

where $\overline{F_m}$ is the signal frequency recorded by the ground microphone, $\overline{v_b}$ is the flight speed of the bat relative to the wall directly to its front (i.e., the microphone wall), c is sound speed in air (343 m/s). Thus, we assumed that the flying bat performed the DSC using echoes from the microphone wall. This assumption was probably not valid during the final landing period when the bat rotates its body and head from a flight posture to a hanging posture, which was one of the reasons we excluded data from the landing maneuver in the DSC analyses (see **Figure 5A**).

From the emitted frequency, we further calculate the echo frequencies received by *H. pratti* during flight and in moving pendulum with the following equation:

$$\overline{F_{echo} = F_s + F_s \times 2 \times v_b/c}$$

Both equations were originally used Schnitzler (1973) and are commonly used for analyzing the call frequency of CF-FM bats (Schnitzler and Denzinger, 2011; Hiryu et al., 2016).

Statistical analysis

Statistical analyses were conducted to compare the DSC performance of *H. pratti* between the free flight and moving pendulum experiments, with the Statistical and Machine Learning toolbox of MATLAB. For all statistical tests, we used the non-parametric Wilcoxon signed-rank test ("ranksum" function) and Wilcoxon rank-sum test ("ranksum" function) test the difference between the medians for paired and non-paired comparisons respectively. A *P*-value of 0.05 was adopted to indicate a statistical significance. Statistical analyses were based on a total of 142 trials from four *H. pratti* in the free flight experiment, ranging from 34 to 36 trials across individual animals, and a total of 75 trials from four *H. pratti* in the moving pendulum experiment, ranging from 18 to 20 trials across individual animals. The total calls involved in the moving pendulum and free flight experiments were 33, 480 and 17, 074.

Data availability statement

The raw data supporting the conclusions of this article will be made available by the authors, without undue reservation.

Ethics statement

The animal study was reviewed and approved by the Institutional Animal Care and Use Committee of the Central China Normal University.

Author contributions

ML, XW, and HW collected the data. JL, ML, and XW analyzed the data. JL and CM wrote the manuscript. All authors contributed to the article and approved the submitted version.

Funding

This study was supported by the National Natural Science Foundation of China (31970426), the Career Development Award from the Human Frontier Science Program (CDA00009/2019-C), the Fundamental Research Funds for the Central Universities (CCNU22QN009; CCNU22LJ003), and the Educational Reformation Research Grant from the Department of Education of Hubei Province (2020147) to JL. National Science Foundation Brain Initiative Grant NCS-FO 1734744 (2017- 2021), Air Force Office for Scientific Research Grant FA9550-14-1-0398NIFTI, and Office of Naval Research Grant N00014-17-1-2736 supported CM's efforts.

Acknowledgments

We thank Ziqi Feng, Yangmin Zhu, and Jie Luo for help in training the flying bats, Huanhuan Li for programming support, and Songlin Huang for engineering support.

Conflict of interest

The authors declare that the research was conducted in the absence of any commercial or financial relationships that could be construed as a potential conflict of interest.

Publisher's note

References

Beetz, M. J., Kössl, M., and Hechavarría, J. C. (2021). The frugivorous bat *Carollia perspicillata* dynamically changes echolocation parameters in response to acoustic playback. *J. Exp. Biol.* 224(Pt 6):jeb234245. doi: 10.1242/jeb.234245

Behrend, O., and Schuller, G. (1999). Binaural infuences on doppler shift compensation of the horseshoe bat *Rhinolophus rouxi*. *J. Comp. Physiol. A* 185, 529–538. doi: 10.1007/s003590050413

Boonman, A., Rieger, I., Amichai, E., Greif, S., Eitan, O., Goldshtein, A., et al. (2020). Echolocating bats can adjust sensory acquisition based on internal cues. *BMC Biol.* 18:166. doi: 10.1186/s12915-020-00904-2

Britton, A. R., and Jones, G. (1999). Echolocation behaviour and prey-capture success in foraging bats: laboratory and field experiments on *Myotis daubentonii*. *J. Exp. Biol.* 202, 1793–1801. doi: 10.1242/jeb.202.13.1793

Calisi, R. M., and Bentley, G. E. (2009). Lab and field experiments: are they the same animal? *Horm. Behav.* 56, 1–10. doi: 10.1016/j.yhbeh.2009.02.010

Fenton, B. M., Grinnell, A. D., Popper, A. N., and Fay, R. R. (2016). *Bat Bioacoustics*. New York, NY: Springer.

Gaioni, S. J., Riquimaroux, H., and Suga, N. (1990). Biosonar behavior of mustached bats swung on a pendulum prior to cortical ablation. *J. Neurophysiol.* 64, 1801–1817. doi: 10.1152/jn.1990.64.6.1801

Griffin, D. (1958). *Listening In The Dark: The Acoustic Orientation Of Bats and Men*. New Haven, CT: Yale University Press.

Griffin, D. R., and Galambos, R. (1941). The sensory basis of obstacle avoidance by flying bats. *J. Exp. Zool.* 86, 481–506. doi: 10.1002/jez.1400860310

Grinnell, A. D. (2018). Early milestones in the understanding of echolocation in bats. *J. Comp. Physiol. A* 204, 519–536. doi: 10.1007/s00359-018-1263-3

Habersetzer, J., Schuller, G., and Neuweiler, G. (1984). Foraging behavior and doppler shift compensation in echolocating hipposiderid bats, *Hipposideros bicolor* and *Hipposideros speoris*. *J. Comp. Physiol. A* 155, 559–567. doi: 10.1007/BF00611919

Hiryu, S., Mora, E. C., and Riquimaroux, H. (2016). "Behavioral and physiological bases for doppler shift compensation by echolocating bats," in *Bat Bioacoustics Springer Handbook of Auditory Research*, eds M. B. Fenton, A. D. Grinnell, A. N. Popper, and R. R. Fay (New York, NY: Springer New York), 239–263. doi: 10.1007/978-1-4939-3527-7_9

Hiryu, S., Shiori, Y., Hosokawa, T., Riquimaroux, H., and Watanabe, Y. (2008). On-board telemetry of emitted sounds from free-flying bats: compensation for velocity and distance stabilizes echo frequency and amplitude. *J. Comp. Physiol. A* 194, 841–851. doi: 10.1007/s00359-008-0355-x

Keating, A. W., Henson, O. W., Henson, M. M., Lancaster, W. C., and Xie, D. H. (1994). Doppler-shift compensation by the mustached bat: quantitative data. *J. Exp. Biol.* 188, 115–129. doi: 10.1242/jeb.188.1.115

Kothari, N. B., Wohlgemuth, M. J., and Moss, C. F. (2018). Dynamic representation of 3d auditory space in the midbrain of the free-flying echolocating bat. *eLife* 7:e29053. doi: 10.7554/eLife.29053

Kronfeld-Schor, N., Bloch, G., and Schwartz, W. J. (2013). Animal clocks: when science meets nature. *Proc. R. Soc. B Biol. Sci.* 280:20131354. doi: 10.1098/rspb.2013.1354

Lancaster, W. C., Keating, A. W., and Henson, O. W. Jr. (1992). Ultrasonic vocalizations of flying bats monitored by radiotelemetry. *J. Exp. Biol.* 173, 43–58. doi: 10.1242/jeb.173.1.43

Lu, M., Zhang, G., and Luo, J. (2020). Echolocating bats exhibit differential amplitude compensation for noise interference at a sub-call level. *J. Exp. Biol.* 223, 225284. doi: 10.1242/jeb.225284

Luo, J., and Moss, C. F. (2017). Echolocating bats rely on audiovocal feedback to adapt sonar signal design. *Proc. Natl. Acad. Sci. U.S.A.* 114, 10978–10983. doi: 10.1073/pnas.1711892114

Luo, J., Kothari, N. B., and Moss, C. F. (2017). Sensorimotor integration on a rapid time scale. *Proc. Natl. Acad. Sci. U.S.A.* 114, 6605–6610. doi: 10.1073/pnas.1702671114

Luo, J., Macias, S., Ness, T. V., Einevoll, G. T., Zhang, K., and Moss, C. F. (2018). Neural timing of stimulus events with microsecond precision. *PLoS Biol.* 16:e2006422. doi: 10.1371/journal.pbio.2006422

Moss, C. F., Chiu, C., and Surlykke, A. (2011). Adaptive vocal behavior drives perception by echolocation in bats. *Curr. Opin. Neurobiol.* 21, 645–652. doi: 10.1016/j.conb.2011.05.028

Popper, A. N., and Fay, R. R. (1995). *Hearing By Bats*. Berlin: Springer Science & Business Media.

Schnitzler, H. U. (1973). Control of doppler shift compensation in the greater horseshoe bat, Rhinolophus ferrumequinum. *J. Comp. Physiol. A* 82, 79–92. doi: 10.1007/BF00714171

Schnitzler, H. U., and Denzinger, A. (2011). Auditory fovea and doppler shift compensation: adaptations for flutter detection in echolocating bats using CF-FM signals. *J. Comp. Physiol. A* 197, 541–559. doi: 10.1007/s00359-010-0569-6

Schnitzler, H.-U. (1968). Die uhraschall-ortungslaute der hufeisen-fledermaeuse (chiroptera-rhinolophidae) in verschiedenen orientierungssituationen. *Z. Vgl. Physiol.* 57, 376–408. doi: 10.1007/bf00303062

Schoeppler, D., Schnitzler, H.-U., and Denzinger, A. (2018). Precise doppler shift compensation in the hipposiderid bat, *Hipposideros armiger*. *Sci. Rep.* 8:4598. doi: 10.1038/s41598-018-22880-y

Schuller, G. (1974). The role of overlap of echo with outgoing echolocation sound in the bat *Rhinolophus ferrumequinum*. *Naturwissenschaften* 61, 171–172. doi: 10.1007/BF00602598

Schuller, G. (1980). Hearing characteristics and doppler shift compensation in South Indian CF-FM bats. *J. Comp. Physiol. A* 139, 349–356. doi: 10.1007/BF00610465

Schuller, G. (1986). Influence of echolocation pulse rate on doppler shift compensation control system in the greater horseshoe bat. *J. Comp. Physiol. A* 158, 239–246. doi: 10.1007/BF01338567

Smotherman, M., and Guillén-Servent, A. (2008). Doppler-shift compensation behavior by Wagner's mustached bat, *Pteronotus personatus*. *J. Acoust. Soc. Am.* 123, 4331–4339. doi: 10.1121/1.2912436

Smotherman, M., and Metzner, W. (2003). Effects of echo intensity on doppler-shift compensation behavior in horseshoe bats. *J. Neurophysiol.* 89, 814–821. doi: 10.1152/jn.00246.2002

Surlykke, A., and Kalko, E. K. V. (2008). Echolocating bats cry out loud to detect their prey. *PLoS One* 3:e2036. doi: 10.1371/journal.pone.0002036

Surlykke, A., and Moss, C. F. (2000). Echolocation behavior of big brown bats, *Eptesicus fuscus*, in the field and the laboratory. *J. Acoust. Soc. Am.* 108:2419.

Surlykke, A., Boel Pedersen, S., and Jakobsen, L. (2009). Echolocating bats emit a highly directional sonar sound beam in the field. *Proc. R. Soc. B Biol. Sci.* 276, 853–860. doi: 10.1098/rspb.2008.1505

Thomas, J. A., Moss, C. F., and Vater, M. (2004). *Echolocation in Bats and Dolphins*. Chicago, IL: University of Chicago Press.

Wang, H., Zhou, Y., Li, H., Moss, C. F., Li, X., and Luo, J. (2022). Sensory error drives fine motor adjustment. *Proc. Natl. Acad. Sci. U.S.A.* 119:e2201275119. doi: 10.1073/pnas.2201275119

Wenstrup, J. J., and Suthers, R. A. (1984). Echolocation of moving targets by the fish-catching bat, *Noctilio leporinus*. *J. Comp. Physiol. A* 155, 75–89. doi: 10.1007/BF00610933

Zhang, Y., Lin, A., Ding, J., Yang, X., Jiang, T., Liu, Y., et al. (2019). Performance of doppler shift compensation in bats varies with species rather than with environmental clutter. *Anim. Behav.* 158, 109–120. doi: 10.1016/j.anbehav.2019.10.008

frontiers | Frontiers in Integrative Neuroscience

TYPE Methods
PUBLISHED 02 September 2022
DOI 10.3389/fnint.2022.965211

OPEN ACCESS

EDITED BY
Andrea Ravignani,
Max Planck Institute for Psycholinguistics, Netherlands

REVIEWED BY
Gary Marsat,
West Virginia University, United States
Jacob Engelmann,
Bielefeld University, Germany
Michael R. Markham,
University of Oklahoma, United States

*CORRESPONDENCE
Till Raab
till.raab@uni-tuebingen.de

RECEIVED 09 June 2022
ACCEPTED 10 August 2022
PUBLISHED 02 September 2022

CITATION
Raab T, Madhav MS, Jayakumar RP, Henninger J, Cowan NJ and Benda J (2022) Advances in non-invasive tracking of wave-type electric fish in natural and laboratory settings. *Front. Integr. Neurosci.* 16:965211. doi: 10.3389/fnint.2022.965211

Advances in non-invasive tracking of wave-type electric fish in natural and laboratory settings

Till Raab[1,2]*, Manu S. Madhav[3], Ravikrishnan P. Jayakumar[4], Jörg Henninger[5], Noah J. Cowan[4] and Jan Benda[1,2,6]

[1]Department for Neuroethology, Institute for Neurobiology, Eberhard Karls Universität, Tübingen, Germany, [2]Centre for Integrative Neuroscience, Eberhard Karls Universität, Tübingen, Germany, [3]Mind/Brain Institute, Johns Hopkins University, Baltimore, MD, United States, [4]Mechanical Engineering Department, Johns Hopkins University, Baltimore, MD, United States, [5]Charité-Universitätsmedizin Berlin, Einstein Center for Neurosciences, NeuroCure Cluster of Excellence, Berlin, Germany, [6]Bernstein Centre for Computational Neuroscience, Eberhard Karls Universität, Tübingen, Germany

Recent technological advances greatly improved the possibility to study freely behaving animals in natural conditions. However, many systems still rely on animal-mounted devices, which can already bias behavioral observations. Alternatively, animal behaviors can be detected and tracked in recordings of stationary sensors, e.g., video cameras. While these approaches circumvent the influence of animal-mounted devices, identification of individuals is much more challenging. We take advantage of the individual-specific electric fields electric fish generate by discharging their electric organ (EOD) to record and track their movement and communication behaviors without interfering with the animals themselves. EODs of complete groups of fish can be recorded with electrode arrays submerged in the water and then be tracked for individual fish. Here, we present an improved algorithm for tracking electric signals of wave-type electric fish. Our algorithm benefits from combining and refining previous approaches of tracking individual specific EOD frequencies and spatial electric field properties. In this process, the similarity of signal pairs in extended data windows determines their tracking order, making the algorithm more robust against detection losses and intersections. We quantify the performance of the algorithm and show its application for a data set recorded with an array of 64 electrodes distributed over a 12 m^2 section of a stream in the Llanos, Colombia, where we managed, for the first time, to track *Apteronotus leptorhynchus* over many days. These technological advances make electric fish a unique model system for a detailed analysis of social and communication behaviors, with strong implications for our research on sensory coding.

KEYWORDS

electric fish, tracking, animal biometric system, behavioral tracking, remote sensing

1. Introduction

Unraveling causal factors driving various animal behaviors in experimental and in particular in observational studies is challenging, since most behaviors result from an integration of a broad range of social and environmental stimuli, internal states, and past experiences (Chapman et al., 1995; Sapolsky, 2005; Boon et al., 2007; Markham et al., 2015). In laboratory studies, environments and contexts are systematically simplified in order to minimize the number of potential factors influencing behaviors (e.g., Bastian et al., 2001; Pantoni et al., 2020). Such studies are tailored to specific behaviors and well-defined contexts. However, behaviors in such constrained settings often deviate from behaviors in natural environments and thus have to be interpreted with care (Cheney et al., 1995; Rendall et al., 1999; Henninger et al., 2018). To discover behavioral traits of interest in the first place, field studies or laboratory experiments with complex, more naturalistic designs are needed. Recent technological advances in remote recording techniques, tags, and data loggers, as well as advances in data analysis, facilitate the collection and evaluation of comprehensive and viable data in naturalistic settings with freely moving and interacting animals (Dell et al., 2014; Hughey et al., 2018; Mathis et al., 2018; Jolles, 2021). These new big-data approaches open up new opportunities in behavioral research in that they potentially allow to quantitatively study animal behaviors in more complex and naturalistic settings (Gomez-Marin et al., 2014; Egnor and Branson, 2016).

A suitable recording technique can be selected from a large variety of available devices and sensors to match the requirements imposed by the model species, environmental conditions, and the scientific question (Hughey et al., 2018). This allows for studying various aspects of animal behaviors across species (e.g., Nagy et al., 2010; Robinson et al., 2012; Strandburg-Peshkin et al., 2015, 2018). A commonly used technique to study animals in their natural habitats is the utilization of animal mounted bio-loggers, e.g., small devices equipped with different sensors like GPS-trackers or microphones (Nagy et al., 2010; Strandburg-Peshkin et al., 2017; Hughey et al., 2018). However, bio-loggers require frequent animal handling and animals are required to carry devices, both inducing a potential bias (Saraux et al., 2011). Furthermore, bio-loggers might miss relevant information, since not all interacting animals might be equipped with a logger (e.g., Strandburg-Peshkin et al., 2019), signal detection range is limited, or data is recorded discontinuously to extend the overall recording period (Strandburg-Peshkin et al., 2017; Hughey et al., 2018).

Alternatively, behaving animals can be tracked by means of remote sensing devices (Kühl and Burghardt, 2013; Theriault et al., 2014; Henninger et al., 2018, 2020; Hughey et al., 2018; Torney et al., 2018; Raab et al., 2019; Aspillaga et al., 2021). In this approach, recorded signals can originate from small micro-transmitters that get affixed to animals (e.g., acoustic telemetry system for fish: Aspillaga et al., 2021) or from the animals themselves (photography, video recordings: Sherley et al., 2010; Lahiri et al., 2011; Theriault et al., 2014; Nourizonoz et al., 2020; ultrasound vocalizations: Surlykke and Kalko, 2008; Seibert et al., 2013; Hügel et al., 2017; electric signals: Henninger et al., 2018; Raab et al., 2019; Fortune et al., 2020). These methods benefit from minimal interference with the animals themselves. On the other hand, covering large observation areas is costly. Also, tracking animal identities can be quite challenging and requires sophisticated and computationally demanding pre-processing of the data (Lahiri et al., 2011; Kühl and Burghardt, 2013; Hughey et al., 2018; Henninger et al., 2020). Here, specific animal biometrics, certain aspects of an animal's appearance or signaling properties, have been shown to allow for individual identification and tracking (Kühl and Burghardt, 2013). However, in order to enable reliable tracking, selected animal biometrics need to be displayed universally throughout the study population whilst showing sufficient variation between single individuals (i.e., biometric profiles that allow for reliable individual identification). If individuals do not have specific invariant characteristics, like, for example, the stripes of a zebra (Lahiri et al., 2011), then tracking algorithms need to handle temporally changing biometric profiles that often overlap in their characteristics (e.g., spatial position and orientation, Madhav et al., 2018).

Electric fish are particularly well-suited for being tracked in the laboratory and in their natural habitats based on remote sensing (Jun et al., 2013; Henninger et al., 2018; Madhav et al., 2018; Raab et al., 2019; Fortune et al., 2020). These fish are capable of producing an electric field through discharges of an electric organ (EOD, Turner et al., 2007) used for electrolocation (Fotowat et al., 2013) and communication (Albert and Crampton, 2005; Smith, 2013; Benda, 2020). The EODs of many electric fish can be recorded by means of an array of submerged electrodes without the need to catch and tag the fish (Henninger et al., 2018). From these recordings, electric signals of individual fish have to be identified and tracked over time. Dependent on electric fish species, EODs are either emitted in short and discrete pulses (pulse-type electric fish; Hagedorn, 1988; Albert and Crampton, 2005; Smith, 2013) or in a sinosoidal fashion (wave-type electric fish; Moortgat et al., 1998). For pulse-type electric fish, tracking individual EODs is rather challenging, since signal features largely overlap between individual fish, i.e., EOD frequencies are highly variable and context dependent (Hagedorn, 1988). In order to, nevertheless, track electric behaviors of pulse-type fish, additional spatio-tempoal tracking using video recordings and elaborate machine-learning approaches are usually required (Jun et al., 2013; Pedraja et al., 2021). In wave-type electric fish, however, the frequency of EODs is individual specific and remarkably stable over minutes to hours (Moortgat et al., 1998), providing a characteristic biometric cue which facilitates individual signal tracking. Previous tracking approaches were either based on

EOD frequency (Henninger et al., 2020) or on spatial electric field properties that can be reconstructed from signal powers across recording electrodes (Madhav et al., 2018). However, both signal features are sensitive to temporal changes. The latter, spatial electric field properties, depends on the fish's spatial position and orientation. The former, EOD frequency, is sensitive to temperature changes (Dunlap et al., 2000) and is actively modulated for electrocommunication (Smith, 2013). Accordingly, both tracking features might fail when fish are close by, either in their EOD frequency or spatially, especially in recordings of electric fish in high densities.

In the following, we describe and evaluate an improved tracking algorithm for wave-type electric fish recorded with electrode arrays. By combining, refining, and extending previous approaches, our algorithm is capable of tracking EODs of individual fish with unprecedented accuracy, i.e., tracking errors occur less often in complex tracking scenarios (e.g., when EOD frequency traces cross each other, Figure 5) which tremendously reduces required post-processing time to manually correct flawed connections. Since both movement behaviors (Madhav et al., 2018; Henninger et al., 2020) and communication (Smith, 2013; Henninger et al., 2018; Fortune et al., 2020) can be analyzed based on EOD recordings, our algorithm is a fundamental advancement for a wide range of behavioral studies on freely moving and interacting electric fish (Raab et al., 2019, 2021). Finally, we demonstrate the performance of our tracking algorithm on recordings of *Apteronotus leptorhynchus* taken with an array of 64 electrodes in a stream in the Llanos in Colombia.

2. Materials and equipment

2.1. Data acquisition

EODs of freely swimming fish were recorded with arrays of monopolar electrodes at low-noise buffer headstages (1×gain, $10 \times 5 \times 5\,\mathrm{mm}^3$, Figure 1B) arranged in grid-like structures (Figures 1A,C,E). Electric signals are amplified (100×gain, 100 Hz high-pass filter, 10 kHz low-pass), digitized at 20 kHz with 16 bit resolution, and stored on external data storage devices for later offline analysis. The custom-built recording systems (npi-electronics GmbH, Tamm, Germany) were powered by car batteries (12 V, 80 Ah). Various configurations of the electrode arrays have been successfully used to record populations of electric fish in the wild (Henninger et al., 2018, 2020, unpublished field-trips: Colombia 2016, 2019, Figures 1A,C,D), as well as in the laboratory (Raab et al., 2019, 2021, Figures 1E,F). The first 64-channel amplifier system required an external computer with two data acquisition boards (PCI-6259, National Instruments, Austin, Texas, USA) for digitizing and storing the data (Henninger et al., 2018, 2020, Colombia 2016). For this first setup, data acquisition was controlled by a C++ software (https://github.com/bendalab/fishgrid). For the 2019 recordings in Colombia we used a modular 16-channel system based on a Raspberry Pi 3B (Raspberry Pi Foundation, UK) that stores the data digitized by an USB data acquisition board (USB-1608GX, Measurement Computing, Norton, MA, USA) on an 256 GB USB stick controlled by python software (https://whale.am28.uni-tuebingen.de/git/raab/Rasp_grid.git) (Figure 1A).

2.2. Spectrograms

EODs of individual fish are identified and extracted from the electric recordings based on their EOD frequency and respective harmonic structure (Figure 2C). For each electrode we compute power spectral densities (PSDs) of overlapping data snippets shifted by $\Delta t \approx 300\,\mathrm{ms}$ (Figure 2A). The size of fast Fourier transform (FFT) windows was set to $n_{\mathrm{fft}} = 2^{15} \approx 1.64\,\mathrm{s}$ (e.g., Raab et al., 2021) or $n_{\mathrm{fft}} = 2^{16} \approx 3.28\,\mathrm{s}$ (e.g., Raab et al., 2019; field recordings displayed in Figure 9) to result in frequency resolutions of 0.6 and 0.3 Hz, respectively, needed to resolve EOD frequencies in high fish densities.

2.3. Extraction of EOD frequencies and feature vector

In order to detect EOD frequencies of all recorded fish, for each time point t_i PSDs from all electrodes were summed up (Figure 2B). The summed PSDs were transformed to decibel levels, $L(f) = 10\log_{10}(P(f)/P_0)$, relative to a power of $P_0 = 1\,\mathrm{mV}^2/\mathrm{Hz}$. In these logarithmic power spectra, peaks were detected (Todd and Andrews, 1999) and groups of harmonics were assigned to their corresponding fundamental frequencies (Figure 2C). See Henninger et al. (2020) and the harmonics.py module in the thunderfish package (https://github.com/bendalab/thunderfish) for details.

Harmonic groups were extracted from the summed power spectra in order to save computing time. Extracting fundamental frequencies from each of n electrodes separately would take n-times longer, but might be more advantageous for separating distant fish that are close by in EOD frequency. We are therefore working on improving the performance of the harmonic-group extraction. The tracking algorithm described in the Section 3 is independent of whether fundamental frequencies were obtained from the individual spectra or the summed one.

For each time point t_i and each signal indexed by k, a feature vector

$$\vec{X}_{k_i} = (f_{k_i},\ L_{k_i}(1),\ \ldots,\ L_{k_i}(n)) \tag{1}$$

is assembled that includes the fundamental EOD frequency, f_{k_i}, and the corresponding logarithmic powers, $L_{k_i}(x)$, in the PSDs

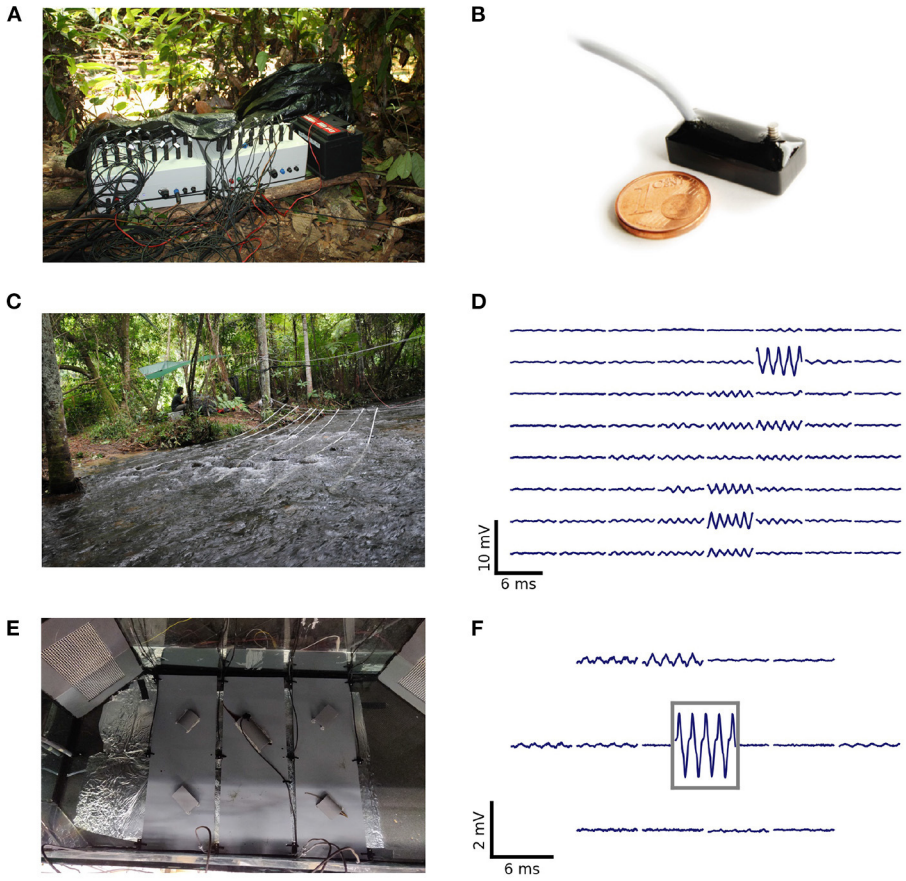

FIGURE 1
Recording systems, electrode arrangements, and corresponding signals of recorded electric fish. **(A)** Two of the Raspbery Pi-based 16-channel amplifiers and recorders used for an array with 32 electrodes. **(B)** Monopolar stainless-steel electrode on headstage used for recordings in the field and laboratory experiments (after Henninger, 2015). **(C)** Recording setup used to record a population of *A. leptorhynchus* in the Rio Rubiano, Colombia, in 2016. Sixty-four electrodes were mounted on PVC-tubes and arranged in an 8 × 8 grid covering an area of 3.5 × 3.5 m^2. **(D)** Snapshot of the electric signals recorded with the setup shown in **(C)**. The top left panel corresponds to the most upstream electrode mounted on the tube closest to the river bank. **(E)** Recording setup used to record electric signals of pairs of *A. leptorhynchus* during competitions in a laboratory experiment (Raab et al., 2021). Fifteen electrodes were uniformly distributed at the bottom of the aquarium and one electrode was placed in the central tube the fish compete for. **(F)** Snapshot of electric signals recorded during the competition experiment shown in **(E)**. The signal framed in gray is from the central electrode located in the optimal tube. The EOD waveform shows the characteristic shoulder that is generic for EODs of *A. leptorhynchus*.

of all n recording electrodes x. Based on this feature vector the individual fish are tracked as described in the following methods.

3. Methods

In the following we present an algorithm for tracking wave-type electric fish in electrode-array recordings. The algorithm merges and extends two complementary approaches that are based on EOD frequency (Henninger et al., 2018, 2020) or on primarily the spatial distribution of signal powers (Madhav et al., 2018). We then test the performance of the tracking algorithm against manually tracked data. Open-source Python scripts for tracking and post-processing of analyzed data can be obtained from https://github.com/bendalab/wavetracker.

3.1. Algorithm for tracking wave-type electric fish

Both EOD frequency and the spatial distribution of EOD power across electrodes change with time and potentially overlap between fish. EOD frequencies can be actively altered in the context of communication (Smith, 2013; Benda, 2020) and the signal powers across electrodes change with the fish's motion (Madhav et al., 2018). This variability and potential overlap in signal features challenges reliable tracking, especially in recordings with many fish.

Furthermore, the existing algorithms track signals in the order of their temporal detection, i.e., signals detected in consecutive time steps are directly assigned to already tracked EOD frequency

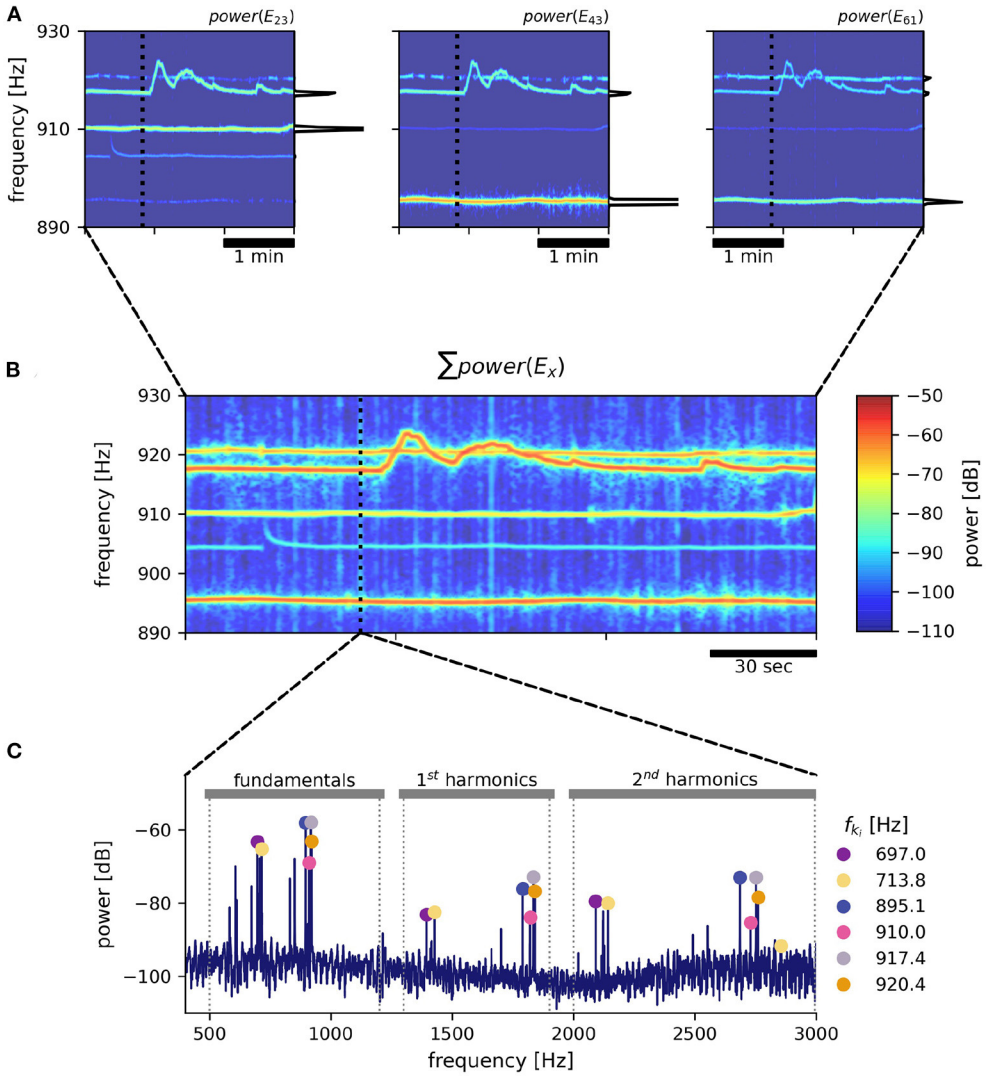

FIGURE 2
EOD frequency extraction from recordings with an electrode array. As an example, a 3 min snippet of a recording with the 8 × 8 array from Rio Rubiano, Colombia, taken during the day of April 10th, 2016 is shown. **(A)** Spectrograms from three different electrodes. Warmer colors represent increased power in respective frequencies. EOD frequencies of individual *A. leptorhynchus* remain rather stable, except during electrocommunication (e.g., EOD frequency trace starting at ∼ 917 Hz). A non-logarithmic PSD extracted at time 50 s indicated by the dotted line is shown at the side of each panel. **(B)** The summed up spectrogram over all electrodes contains distinct traces from many different fish. **(C)** Peaks are detected in the summed up power spectra that are then clustered into frequency groups of a fundamental frequency and at least two of its harmonics, corresponding to a specific fish (Henninger et al., 2020). Fundamental EOD frequencies, their corresponding powers in each electrode and their detection times are stored for subsequent tracking.

traces (Madhav et al., 2018; Henninger et al., 2020). Potentially this leads to tracking errors, because even with the utilization of an electrode array, EODs of freely moving and interacting electric fish are rarely detected continuously, i.e., consecutively in subsequent time steps. Low signal-to-noise ratios, resulting from large distances between fish and recording electrodes or objects like rocks or logs distorting or even blocking electric fields, frequently lead to detection losses. When multiple fish with similar EOD frequencies are recorded simultaneously, EOD frequency traces can potentially cross each other (e.g., in the context of emitted communication signals, Benda, 2020). It is in these occasions in particular, that detection losses frequently result in tracking errors.

In order to improve on these issues, we developed a tracking algorithm which, first, is based on feature vectors that include both EOD frequency and signal power across electrodes (Figure 3) and, second, is less constrained by the temporal sequence of detected signals (Figure 5).

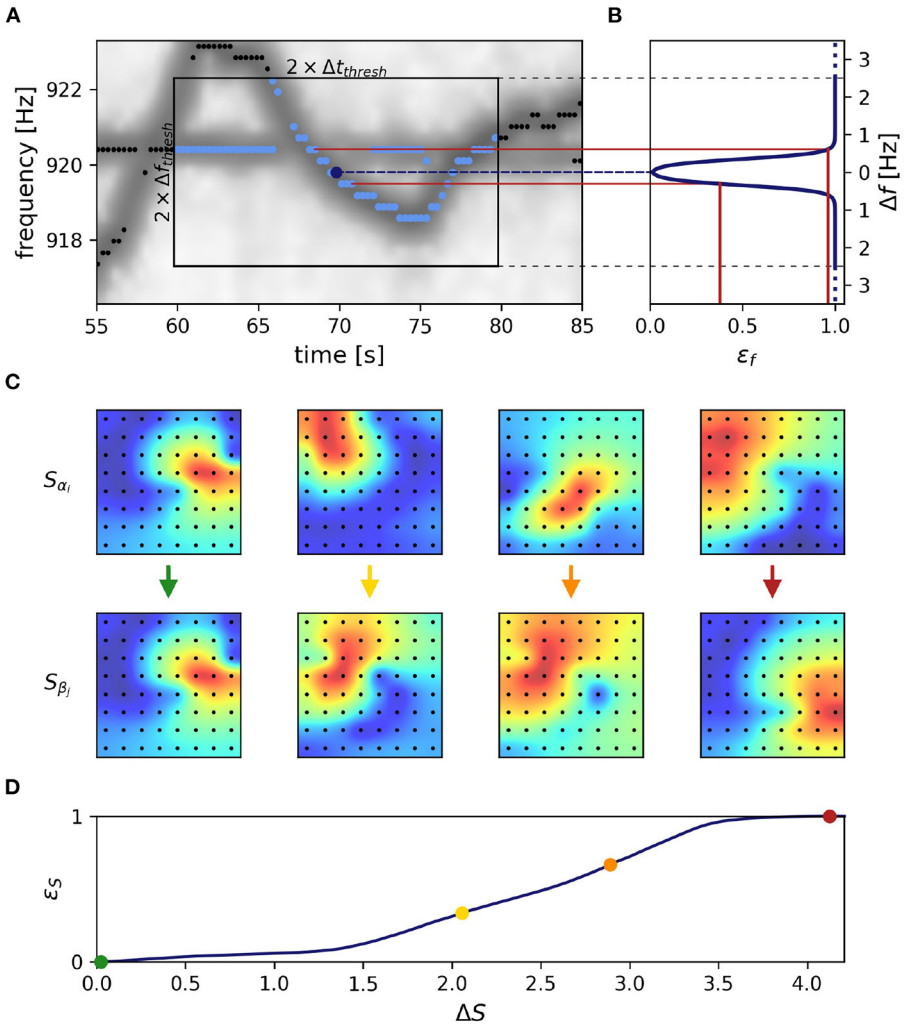

FIGURE 3
Frequency and field errors. **(A)** Summed spectrogram of a 30 s long part of the recording shown in Figure 2B. For each electric fish signal, potential connection partners are limited by a time difference threshold, $\Delta t_{thresh} = 10$ s, and a frequency difference threshold, $\Delta f_{thresh} = 2.5$ Hz. For a given signal α with EOD frequency f_{α_i} at time step i (dark blue dot), potential connection candidates β at different times j (light blue dots) need to be within these thresholds (box), whereas signals beyond these thresholds (black dots) are not considered. **(B)** Absolute frequency differences, Δf Equation (2), are mapped (red lines) to frequency errors, ε_f, using a logistic function, Equation (4) (line), favoring small frequency differences. **(C)** The field error as the second tracking parameter is based on spatial profiles, Equation (5), of signal powers over all electrodes (black dots). The field difference, ΔS, is computed as the Euclidean distance, Equation (6), between the spatial profiles, Equation (5), of potential signal pairs (columns). With decreasing similarity (columns left to right) the field difference increases. Displayed signal pairs (columns) were selected to illustrate the full range of possible field differences and are unrelated to **(A)**. Spatial profiles were interpolated with a gaussian-kernel for illustrative purposes. **(D)** To obtain normalized field errors, ε_S, in a range similar to the one of the frequency errors, ε_f, each field difference is set into perspective to a representative cumulative distribution [Equation (7), black line] of field differences obtained by collecting all potential field differences of a manually selected 30 s window in the recording. The cumulative distribution of potential field differences is computed only once per recording for a 30 s window where fish are active (night time). This way we incorporate a broad distribution of possible field differences when determining field errors. The examples from **(C)** are marked by respectively colored dots.

3.1.1. Distance measure

We start out with extracting feature vectors $\vec{X}_{k_i}$, Equation (1), containing an EOD frequency, f_{k_i}, and its powers, $L_{k_i}(x)$, on all electrodes x, for all signals k and each time step i. In a first step the distance between all pairs of feature vectors, $\vec{X}_{\alpha_i}$ and $\vec{X}_{\beta_j}$, of signals α and β at times $i \neq j$ are quantified. Only pairs within a time difference of $|t_j - t_i| \leq \Delta t_{thresh} = 10$ s and a maximum difference

$$\Delta f_{\alpha_i,\beta_j} = |f_{\alpha_i} - f_{\beta_j}| \tag{2}$$

$\leq \Delta f_{thresh} = 2.5$ Hz between the two EOD frequencies of the feature vectors are considered (Figure 3A).

The distance between the two signals α_i and β_j

$$\varepsilon_{\alpha_i,\beta_j} = \frac{1}{3}\varepsilon_f + \frac{2}{3}\varepsilon_S \tag{3}$$

is computed as a weighted sum of the frequency error, ε_f, and the field error, ε_S. Both errors range from 0 to 1 and are explained in the following sections. The field error gets twice the weight of the frequency error, because tracking issues usually arise in spite of low frequency errors. Nevertheless, the frequency error remains a relevant tracking feature, especially when fish are in close proximity resulting in low field errors.

3.1.2. Frequency error

The frequency error is based on the difference in EOD frequencies, Equation (2) and has been used previously to track signals of electric fish (Henninger et al., 2018, 2020). We transform the EOD frequency difference, Equation (2), into the frequency error

$$\varepsilon_f(\Delta f) = \frac{1}{1 + e^{-\frac{\Delta f - f_0}{df}}} \tag{4}$$

via a logistic function, that maps the EOD frequency difference, Δf, onto the interval from zero to one. The turning point of the logistic function at $f_0 = 0.35$ Hz and the corresponding inverse slope, $df = 0.08$ Hz ensure a maximum frequency error already at small EOD frequency differences of about 0.8 Hz (Figure 3B). This transformation mitigates very small frequency differences and equalizes larger frequency differences in the assessment of whether two signals α and β originate from the same or different fish.

3.1.3. Field error

EOD frequency traces of electric fish occasionally cross each other, e.g., when individuals actively alter their EOD frequency in the context of communication (e.g., Zupanc, 2002; Triefenbach and Zakon, 2008; Raab et al., 2021, Figure 3A). In these situations, frequency as a tracking feature fails. This is where the spatial properties of a signal, i.e., signal powers across recording electrodes that reflect the position and orientation of a fish, come into play (Madhav et al., 2018, Figure 3C). The signal powers, $L_{k_i}(x)$, are rescaled to the spatial profile

$$S_{k_i}(x) = \frac{L_{k_i}(x) - \min\limits_x L_{k_i}(x)}{\max\limits_x L_{k_i}(x) - \min\limits_x L_{k_i}(x)}\,, \tag{5}$$

ranging between 0 and 1, for the smallest and largest power of that signal, respectively.

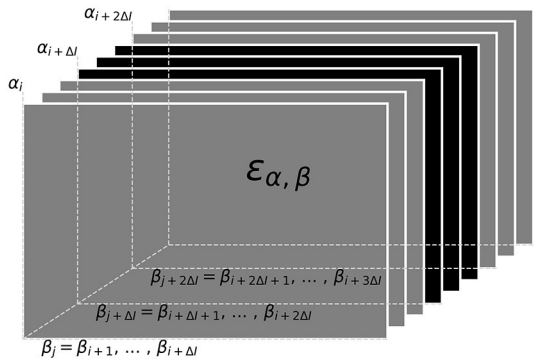

FIGURE 4
Distance cube containing all distances, $\varepsilon_{\alpha,\beta}$ Equation (3), for possible signal pairs α and β within the current tracking window. Each layer, referring to a time step i, contains the distances between all signals α_i detected at this time and their potential signal partners β_j detected maximally 10 s after signal α_i (ΔI time-steps after i). Distances in gray layers correspond to signal pairs where one signal partner could potentially have a smaller distance to a signal outside the error cube. Only connections based on the distances in the central black layers can be assumed to be valid, since all potential connections of both signal partners are within the error cube. Connections established for the black layers are assigned to signal traces obtained in previous tracking steps in a second step.

The field difference ΔS, i.e., the difference between the spatial profiles of two signals α and β at times i and j, is computed as their Euclidean distance according to

$$\Delta S_{\alpha_i,\beta_j} = \sqrt{\sum_{x=1}^{n} (S_{\alpha_i}(x) - S_{\beta_j}(x))^2} \tag{6}$$

However, the magnitude of this difference depends on the configuration of the electrode array, especially on the number of recording electrodes. To obtain field errors, ε_S, that are independent of electrode configuration, we map the field differences through a cumulative distribution of field differences extracted from a manually selected and representative 30 s window:

$$\varepsilon_S(\Delta S_{\alpha_i,\beta_j}) = \int_0^{\Delta S_{\alpha_i,\beta_j}} p(\Delta S)\, d\Delta S \tag{7}$$

The distribution of field differences, $p(\Delta S)$, is estimated from the field differences between potential signal pair ($\Delta t_{i,j} \leq \pm 10$ s, any frequency difference) within a 30 s data snippet where fish can be assumed to be active, i.e., during night time (Figure 3D). This way we incorporate a broad distribution of possible field differences when determining field errors.

3.1.4. Tracking within a data window

Now that we have a quantification for the distance ε, Equation (3), between to signals we can proceed with the

actual tracking algorithm. Based on the distances, the algorithm decides which signal pairs belong together in order to track individual fish throughout a recording. Computing the distances between all pairs of signals of a recording at once, however, is not feasible. Instead we break down the tracking into tracking windows of 30 s at a time (Figure 5). Within these tracking windows, we first compute the distances, ε, between each potential signal pair α_i and β_j and store them in a three-dimensional distance cube, where the first two dimensions refer to signals α_i and β_j and the third dimension to the time steps i where signals α_i have been detected (Figure 4). Accordingly, we have different numbers of signals α_i for each time step i and, consequently, the number of elements in the second dimension, referring to signals β_j from all time steps $j > i$ is also variable. Note that, each signal considered in the distance cube is only referred to as α once, but potentially multiple times as β. For example, a signal that is referred to as $\beta_j = \beta_{i+1}$ in the first layer of the distance cube (see Figure 4) is referred to as α_{i+1} in the next layer of the distance cube.

For the actual tracking step, signal pairs are connected and assigned to potential fish identities based on the values in the distance cube. The algorithm described in the following (Figure 5) is a kind of clustering algorithm that has a notion of temporal sequence. The resulting clusters are traces of different fish identities ("labels") tracked over time.

The signal pairs are traversed in order of ascending distances. If one of α_i or β_j have already been assigned to a fish identity, then this pair is added to this fish identity. If α_i coincides with one fish identity and β_j with another one, then the two fish identities are merged. If neither α_i nor β_j match an existing fish identity, the pair is assigned to a new fish identity. Assignment to or merging of fish identities are only possible in the absence of temporal conflicts, i.e., a fish identity cannot have more than one signal at the same time. In case of temporal conflicts, the signal pair is ignored and the algorithm proceeds with the next one. As a result, we obtain signal traces built upon minimal signal errors within a 30 s tracking window (Figure 5).

Since signals within the first and last 10 s of a tracking window could have lower distances to signals outside the current tracking window, these connections are potentially flawed (gray layers in Figure 4; gray bars in Figure 5). Only connections established within the central 10 s take all other potential signal partners into account. Accordingly, only the section of assembled signal traces corresponding to these central 10 s of the current tracking window is considered for further processing, where the signal traces are appended to already validated, previously detected ones (Figure 6).

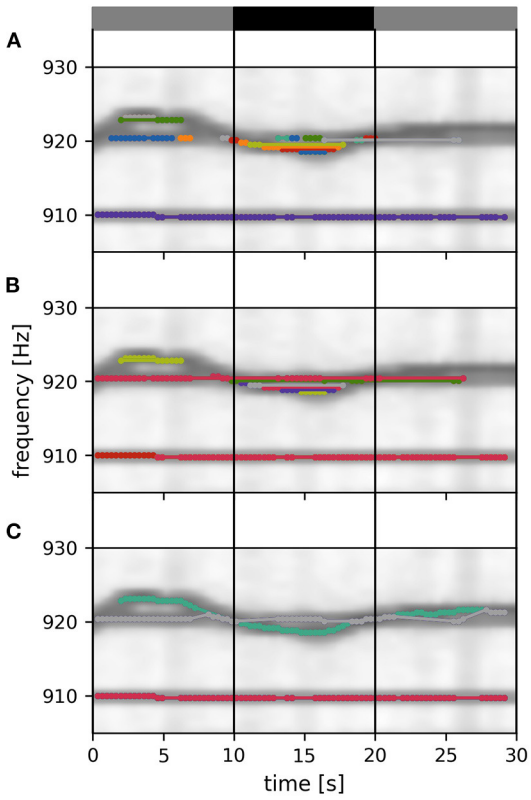

FIGURE 5
Tracking within a data window. Signals detected in a 30 s data window are connected to each other and assigned to fish identities according to their distance ε, Equation (3). Signal pairs with smaller distances are connected first. With increasing distance values, more connections and identities are formed, complemented, or merged, ensuring no temporal overlap. Different stages of this tracking step are displayed in **(A–C)**. **(A)** Twenty percent of all possible connections of the displayed tracking window are formed. At this tracking stage a multitude of separate signal traces (different colors) are still present. **(B)** Forty percent of all possible connections of the displayed tracking window are formed. **(C)** Final output of the tracking step. All possible connections of the displayed tacking window are formed. The remaining three EOD frequency traces (in the displayed time and frequency segment) correspond to three different fish identities. Only signal pairs within the central 10 s of an 30 s tracking window (vertical lines) are assigned to already established fish identities from previous tracking windows. The summed spectrogram of a 30 s long part of the recording shown in Figure 2B is shown in the background.

3.1.5. Assembly of tracking results over data windows

The assignment of the 10 s long signal traces obtained by the tracking algorithm from 30 s long data windows (Figure 6A) to preceding tracking steps (Figure 6B) proceeds, similar to the algorithm described above, based on the smallest distances between them.

First, the distance between those signals α within the first 10 s of the current tracking window of already established fish identities and new signals β from the central 10 s of the current tracking window are computed. Then, starting with the pair with the smallest distance, the new signal trace containing signal β (for example the green dot in Figure 6C), is connected

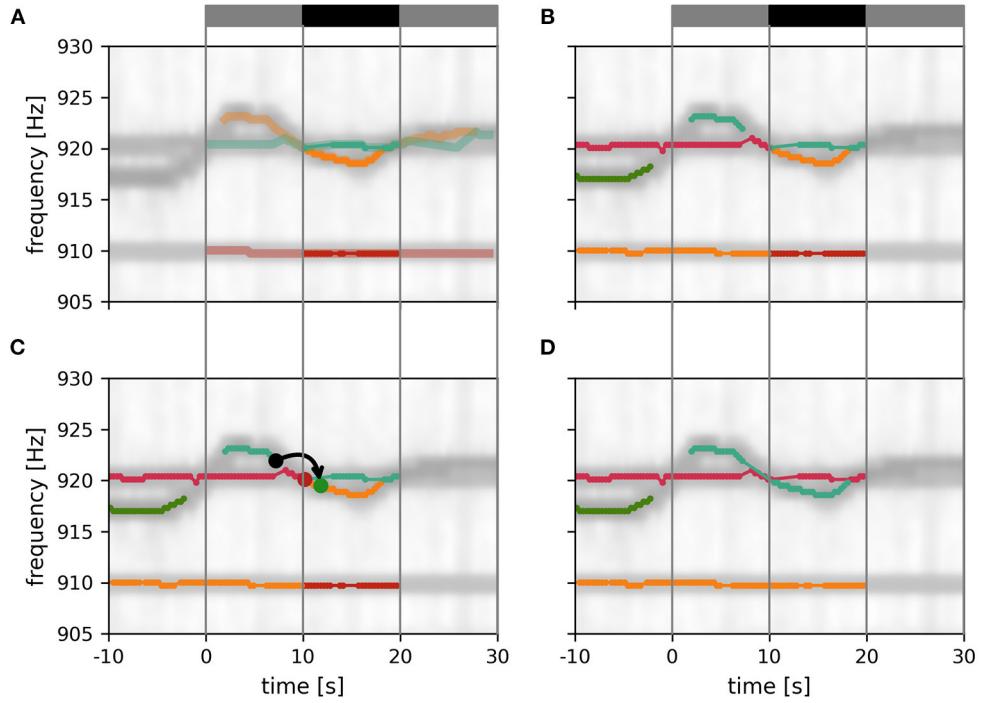

FIGURE 6
Assembly of tracking results over data windows. **(A)** New fish identities established within the current tracking window (gray and black bar on top). Only the central 10 s of these EOD frequency traces (solid traces; black bar) can be assumed to be valid since signals before and after (transparent traces; gray bars) have potential signal partners outside the tracking window. **(B)** Additional display of EOD frequency traces established in previous iterations of the tracking algorithm. **(C)** Signal traces are connected according to the smallest possible distance measure between any signal between the last 10 s of the established fish identities ($10\,\text{s} < t < 10\,\text{s}$) and the central 10 s of the new fish identities ($10\,\text{s} < t < 20\,\text{s}$). In the example shown, the distance between the origin signal (black dot) and the target signal (green dot) is the smallest between these two signal traces, accordingly the two signal traces are merged (green and orange lines). An alternative signal (red dot) has a larger distance to the origin signal. **(D)** Final result of the tracking algorithm that will be used for the next iteration.

to the established signal trace (from previous tracking steps) containing signal α (for example, the black dot in Figure 6C). This step is repeated with signal pairs of increasing distance until all possible connections are established (Figure 6D).

The described tracking within a data window and the subsequent assignment to previously established fish identities is repeated with data windows shifted by 10 s until the end of the recording is reached. In each iteration, the distance cube is updated. The first layers corresponding to the first 10 s of the previous tracking window are removed (frontal gray layers in Figure 4) and new layers for the next 10 s beyond the last tracking window are extended to the error cube in preparation for the next iteration of tracking.

3.2. GUI for checking and correcting tracking results

Even though the introduced algorithm is capable of resolving most tracking conflicts correctly when tracking EODs of wave-type electric fish, occasional tracking errors still remain. We developed a GUI that allows to visually inspect and validate tracked EOD frequency traces and to fix flawed connections (Figure 7). Flawed connections can easily be identified by their clear deviation from the spectrogram displayed in the background. Furthermore, signal traces with a detection gap beyond the temporal threshold of $\Delta t_{thresh} = 10\,\text{s}$ of the tracking algorithm can be manually connected based on visual cues from the spectrogram. The resulting validated signal traces are then stored and further analyzed (e.g., Raab et al., 2019, 2021).

4. Results

The complexity of the data set we recorded in Colombia in 2016 led us to the development of the presented tracking algorithm. The high density of fish in this data set (about 25 fish within $3.5 \times 3.5\,\text{m}^2$) results in many individual EOD frequency traces, where EOD frequencies were often very similar and frequently cross each other, in particular in the context of communication (Figure 9). This severely challenged previous tracking approaches (Madhav et al., 2018;

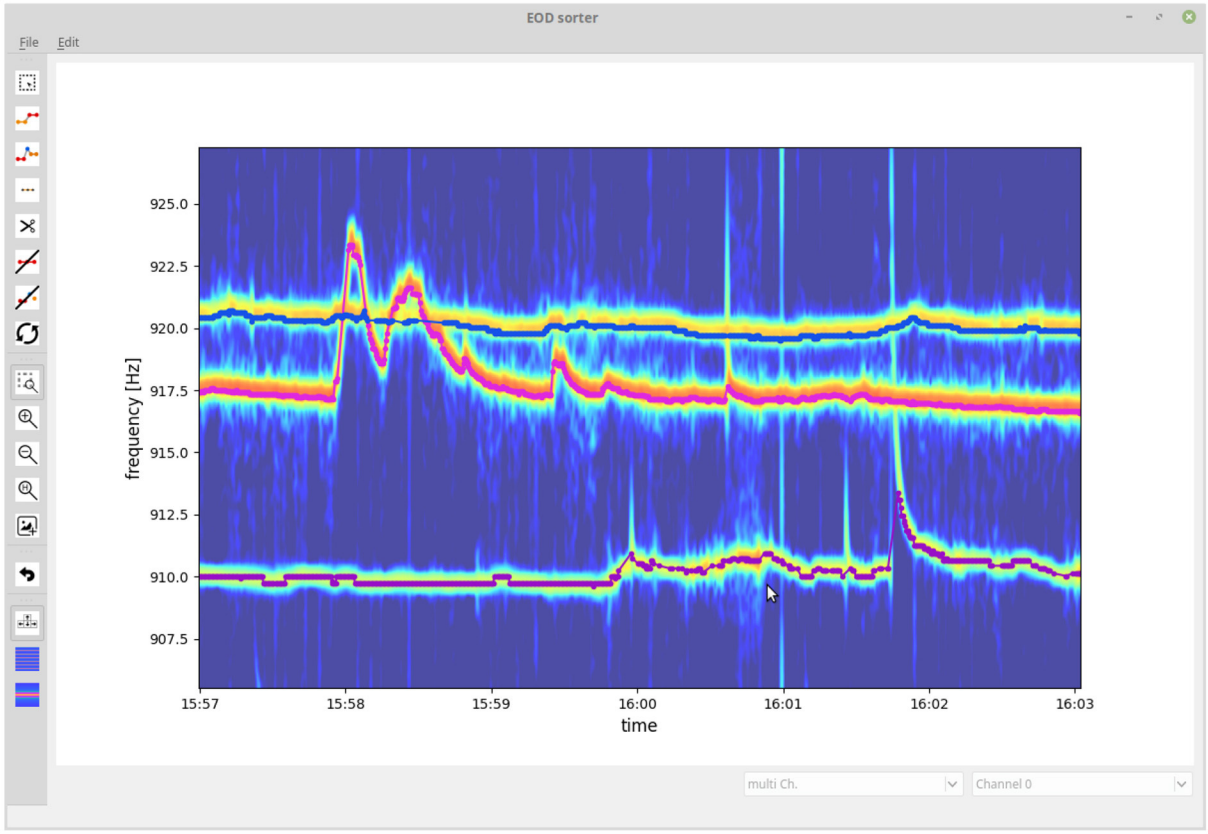

FIGURE 7
Graphical user interface for validating and fixing tracking results. The user is presented with the tracked signal traces (EOD frequency traces) displayed on top of a spectrogram summed up across recording electrodes. The user can delete, cut, and connect signal traces or delete signals not originating from electric fish.

Henninger et al., 2020), thus a better tracking algorithm was required. The improved algorithm resolves many tracking issues resulting from crossing EOD frequency traces and facilitates the evaluation of wave-type electric fish recordings even in abundant populations. In the following we evaluate the performance of the developed algorithm and highlight how it can be used to advance our knowledge about the behavior of freely moving and interacting electric fish by facilitating laboratory studies as well as natural field observations.

4.1. Performance of the tracking algorithm

In order to quantify the performance of the presented tracking algorithm, we evaluate potential tracking conflicts that occur during the analysis of a datasets we recorded with an 8×8 electrode array in Colombia during the day of April 10^{th}, 2016 for 10 h:50 m. First, we tracked the fish with the presented algorithm and then visually inspected, corrected, and validated the tracking results using the GUI (Figure 7). Second, we run the tracking algorithm again and compared the connections made by the algorithm with the manually improved ones. That is, for each signal α_i we inspected all possible connections with a signal β_j (one row in the distance cube) within the central 10 s of the current tracking window. If all the β_j for a given α_i were assigned to the same fish identity in the visually corrected tracking results, we have no potential conflict and these connections were not further considered for quantifying the performance of the algorithm, because these are the simple cases with a single fish within the maximum EOD frequency difference, Δf_{thresh}, of 2.5 Hz. If, however, the possible connections involved two or more fish identities, a tracking conflict was possible. For each such potential tracking conflict, we extracted the EOD frequency difference Δf, Equation (2), field difference ΔS, Equation (6), frequency error ε_f, Equation (4), field error ε_S, Equation (7), and resulting distance measure ε, Equation (3), between the signal α_i and the best signal partner β_j, the one with the smallest distance ε, associated with the same fish identity as in the visually corrected signal traces (true connection), as well as between the signal α_i and the best

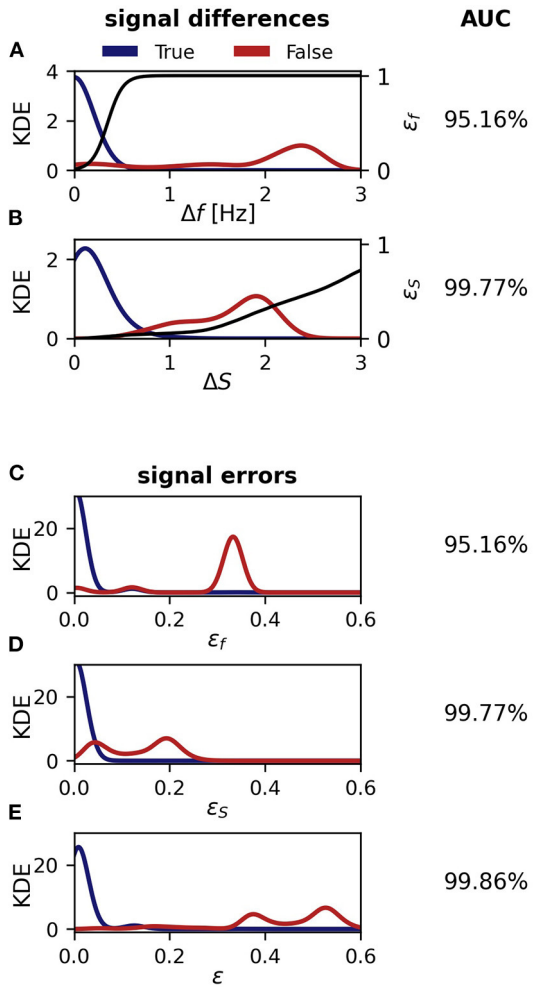

FIGURE 8
Performance of the tracking algorithm. Conflicts appear if signals could be connected to multiple different fish identities, that have been manually corrected and checked *post-hoc* (Figure 7). In most but not all cases, correct connections have smaller signal differences or errors (blue) than wrong connections (red). Shown are kernel density estimates (KDE) for the various signal differences, errors, and distances. The overlap of the distributions was quantified by the AUC of an ROC-analysis as indicated in the right column. **(A)** EOD frequency differences, Δf Equation (2). A logistic function, Equation (4) (black line), translates EOD frequency differences to frequency errors, ε_f. **(B)** Field differences, ΔS, Equation (6). The cumulative distribution (black line) of field differences of all pairings, not only from conflicts, translates field differences to field errors, ε_S, Equation (7). **(C)** Frequency error, ε_f, Equation (4). **(D)** field error, ε_S, Equation (7). **(E)** Combined distance measure, ε, Equation (3). Note, that frequency and field errors **(C,D)** are mapped *via* monotonically increasing functions from signal differences **(A,B)** and thus result in the same fraction of correct connections and AUC values. However, the distance measure combining both field and frequency error performs best.

signal partner β_j belonging to a different fish identity (false connection). Further fish identities of the β_j with larger distances were ignored.

In order to assess the performance of each signal feature difference (Δf & ΔS) and distance measure (ε_f, ε_S, ε) in separating true from false connections, we computed the fraction of signal differences or errors of true connections being smaller than those of the corresponding false connections. If this fraction would be 100% then the tracking algorithm would always have connected the right signals. In addition we quantified the overlap of the two distributions by the area under the curve (AUC) of a receiver-operating characteristic (ROC). Despite an overlap (low AUC values) in principle 100% correct connections would be possible, but an overlap demonstrates that fixed decision thresholds are not feasible.

We start with evaluating the 464 tracking conflicts from a 5 min snippet being especially challenging to track, because of several crossings of EOD frequency traces (Figure 8). A small frequency range of this 5 min data snippet is displayed in Figure 7. The least reliable tracking feature appears to be the difference in EOD frequency (Δf and ε_f). Frequency differences of true connections were smaller than the ones of false connections in only 94.83% (440/464) of the cases (Figures 8A,C). Better results can be achieved based on the field error (ΔS and ε_S) as a tracking feature. The field differences of true connections were smaller in 99.57% (462/464) of the cases (Figures 8B,D). However, this performance can even be improved when using the distance measure, ε, that combines both the frequency error, ε_f, and field error, ε_S. In 99.87% (462/464) of the tracking conflicts, true connections had smaller distances than false connections (Figure 8E). The AUC values for all measures were similar to the fractions of correct connections (Δf and ε_f: AUC = 95.16%, ΔS and ε_S: AUC = 99.77%, ε: AUC = 99.86%), indicating a small but existing overlap between the two distributions.

The 261 344 tracking conflicts of the whole recording yield similar results. However, the higher proportion of "easy" tracking conflicts increased the performance of the various features in general and differences between them were less pronounced. Nevertheless, EOD frequency still performed worse (99.73% correct connections) than field difference (99.81% correct connections). Again, combining both into the distance measure, Equation (3), resulted in the best performance (99.95% correct connections). Correspondingly, the overlap between the two distributions was reduced (Δf and ε_f: AUC = 99.79%, ΔS and ε_S: AUC = 99.85%, ε: AUC = 99.98%).

In order to put these high numbers in perspective, we estimate the time required to post-process signal traces obtained for the whole dataset recorded during the day of April 10^{th}, 2016, in Colombia (including 261, 344 potential tracking conflicts) when using (i) only frequency difference, (ii) only electric field difference, or (iii) the combined signal error ε_S as tracking parameter. Finding and correcting single tracking errors using our GUI (Figure 7) requires about 15 s each (personal experience). Accordingly, post-processing signal traces of the whole recording would require about 3 h when

solely frequency is used as tracking feature, 2 h when the field difference alone is used for tracking, and only about 30 min when our combined signal error ε_S is used. However, note that the dataset used here to illustrate the performance of the algorithm is the most complex ever recorded to our knowledge. With decreasing complexity, i.e., less fish in a recording, the amount of potential tracking conflicts, and thereby the required post-processing time, rapidly decreases.

Furthermore, a major advancement of the presented algorithm is represented by the tracking process itself, i.e., tracking signals in discrete tracking windows according to the similarity of signal pairs (Figure 5). However, this advancement is only validated by human observers, since the recreation of previous tracking approaches is too demanding for the sole purpose of accuracy comparison.

4.2. Applications of the developed algorithm

By means of the developed algorithm we were able, for the first time, to track electric signals of individual fish for multiple consecutive days in a natural, high density population of *A. leptorhynchus* recorded in a stream in Colombia (Figure 9). This allowed for novel insights into the natural behavior of these fish in the wild, including their communication and movement behaviors. A preliminary analysis of the tracked fish indicates that many fish stay pretty stationary within distinct areas for multiple days (Figure 10). Other fish, especially during the night, can only be tracked for short time periods, suggesting these fish only transit through the area covered by the electrode array (Figure 9A). Furthermore, fish seem to interact with each other by modulating their EOD frequency in various ways and on many different time scales ranging from seconds to many minutes, if not even hours. This includes not only distinct communication signals like rises (Raab et al., 2021, Figure 9B), but also other not yet classified EOD frequency modulations, for example multiple EOD frequency traces entwining each other (Figure 9C).

Such natural observations are invaluable since only in the wild, the whole scope of an animal's behavior can be observed in the context of all relevant stimuli and conditions that shaped these behaviors through evolutionary adaptations. Accordingly, such natural observations yield the unique opportunity to discover novel and unexpected behavioral traits and associated causalities. For example, Fortune et al. (2020) described behavioral and physiological adaptations of *Eigenmannia vicentespelea*, another gymnotiform wave-type electric fish, in response to living in a constantly dark cave. *E. vicentespelea* developed increased territoriality and enhanced EOD amplitudes in comparison to *Eigenmannia trilineata*, not living in caves, to face the challenges of their specific habitat. If not for the corresponding field study, these behavioral and physiological adaptations probably never would have been discovered.

Furthermore, field studies are also essential to validate conclusions drawn form laboratory experiments, which is especially important since behaviors observed in the laboratory often deviate from those observed in the wild (Cheney et al., 1995; Rendall et al., 1999; Henninger et al., 2018). In our case, the preliminary behavioral observations we made in Colombia and described above fit to and support the conclusions of our recent laboratory experiments (Raab et al., 2019, 2021). In these experiments we used the algorithm presented here to track individual electric signals of *A. leptorhynchus* in different behavioral contexts. This includes the evaluation of individual spatio-temporal movement behaviors in a freely moving and interacting group of 14 *A. leptorhynchus* (Raab et al., 2019) as well as the communication behavior of pairs of *A. leptorhynchus* competing over a shelter during staged competitions (Raab et al., 2021). In both laboratory and field observations, fish produce the majority of rises as electrocommunication signals during the night (Raab et al., 2021, Figure 9A), are more stationary during the day compared to the night (Raab et al., 2019, Figure 10), and seem to not remain completely stationary for the whole inactive day-phase but rather show short periods of activity (Raab et al., 2019, Figure 10). The observed stationarity of fish observed in our field recordings also fit to our suggestion of *A. leptorhynchus* establishing a dominance hierarchy to regulate an individual's access to resources (Raab et al., 2021). Due to the fish's stationarity, repetitive conflicts with the same individuals are presumably inevitable and the establishment of a dominance hierarchy can be assumed to be the most economic way to resolve these conflicts (Sapolsky, 2005).

Finally, the evaluation of natural recordings very accurately illustrate the advantages and limitations of the presented algorithm. While crossing EOD frequency traces can usually be resolved accurately (Figure 9B), reliable tracking usually fails when too many signals traces are of similar EOD frequency and entwine in diffuse EOD frequency alterations (Figure 9C). In these occasions the signals of multiple fish superimpose in the spectrogram analysis (Figure 9C) for longer time periods. As a consequence, the corresponding detected signals comprise signal powers of multiple fish. Accordingly, their clear assignment to one of the involved identities is usually impossible after the EOD frequency traces disentangle.

5. Discussion

Previous approaches on tracking wave-type EODs of individual wave-type electric fish either utilized their EOD frequency (Henninger et al., 2020) or the spatial profile of their electric fields (Madhav et al., 2018) as tracking features. We assessed the performance of both

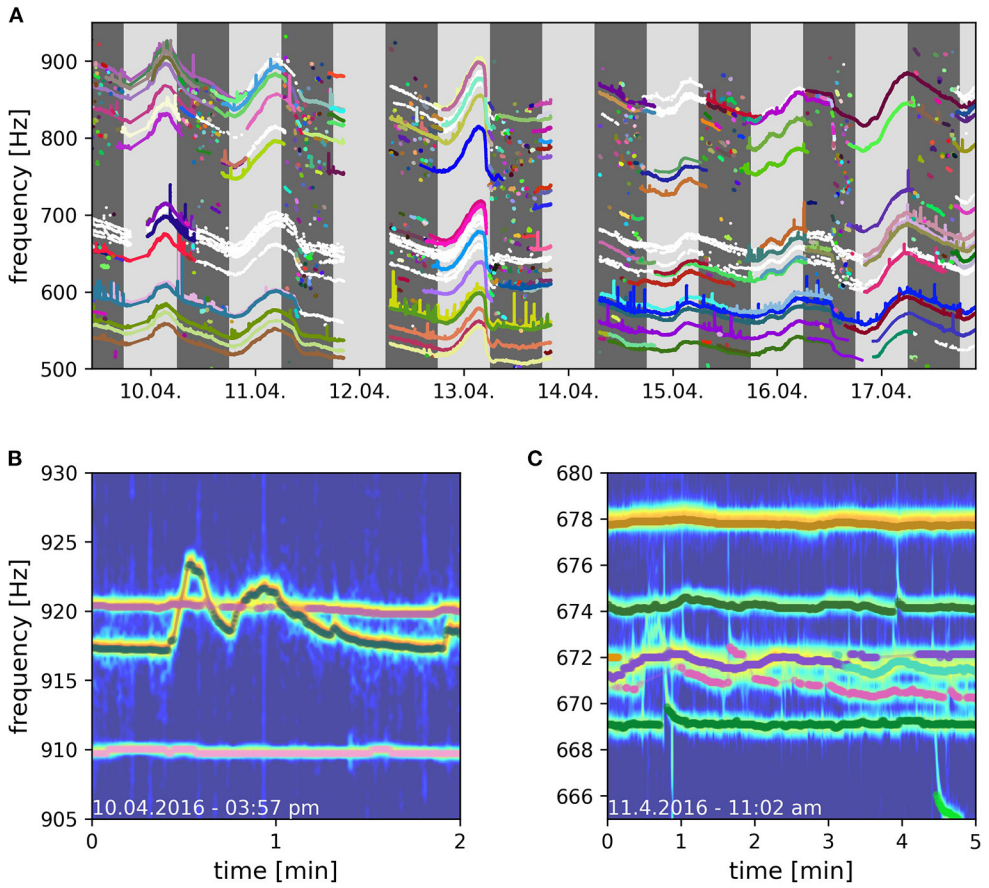

FIGURE 9
Long-term field recording of *A. macrostomus*, a member of the *A. leptorhynchus* species group, in Colombia, 2016. EODs were recorded with a 64 channel electrode array covering 3.5 × 3.5 m^3. **(A)** Eight days of detected and tracked EOD frequencies. Successfully tracked and validated signal traces of different fish are indicated in different colors. Signal traces that could not be clearly validated are indicated in white. Dark gray areas indicate night time, light gray areas day time. **(B)** Signal traces of three fish where the crossing EOD frequency traces of the upper two fish could reliably be resolved by the tracking algorithm. **(C)** Too many signal traces with similar frequencies compromise the tracking algorithm (670 – 672 Hz). Frequency peaks in PSDs belonging to multiple fish temporally overlay and prevent successful tracking.

signal features alone as well as a combination of both, based on tracking conflicts occurring while processing a recording of a natural, high density population of *A. leptorhynchus* in a stream in Colombia. The comparison of spatial field properties clearly performs better than a comparison of EOD frequencies. Certainly, the EOD frequency of *A. leptorhynchus* can be remarkably stable over minutes to hours (Moortgat et al., 1998). However, EOD frequency changes with various magnitudes on various time scales can regularly be observed, because of its strong temperature dependence (Dunlap et al., 2000), actively produced electrocommunication signals (e.g., Zupanc, 2002; Triefenbach and Zakon, 2008; Smith, 2013; Benda, 2020; Raab et al., 2021), and also as an artifact of the EOD frequency extraction from the PSDs (Figure 2). Accordingly, the suitability of EOD frequency as tracking feature decreases the more fish are recorded and analyzed simultaneously, since EOD frequency differences between fish are potentially smaller and interactions between fish involving active EOD frequency modulations can be assumed to be more frequent. Therefore, spatial field properties reflecting a fish's spatial position and orientation represent a more robust tracking feature, especially when only those signal pairs with small EOD frequency differences are considered for comparison and tracking.

The best tracking performance is achieved by using both EOD frequency differences and field differences. This combined signal distance implements a tracking bias that helps to resolve tracking conflicts in at least two scenarios, where tracking solely based on field differences fail. First, if two fish swim close to each other with similar orientations, then their spatial profiles are similar but they can be still differentiated based on their EOD frequencies. Second, in the event of crossing EOD frequency

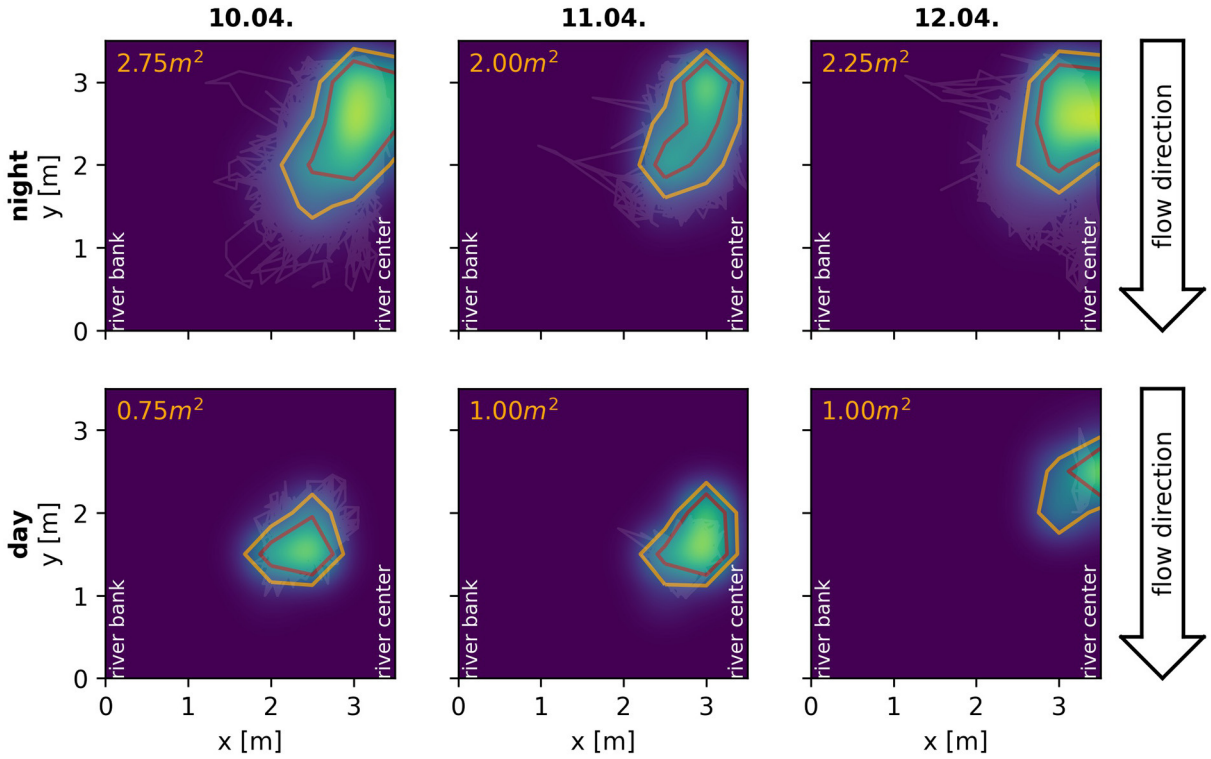

FIGURE 10
Spatial behavior of a single *A. macrostomus* detected and tracked consecutively for 4 days. Heat-maps and contour lines show the fish's probability of presence across the monitored 3.5×3.5 m^2 area of the river during the night **(top)** and day **(bottom)**. The observation area ranged from the river bank ($x = 0$) to the center of the river ($x = 3.5$) with similar extend in the flow direction of the river (see Figure 1C). Heat-maps of signal powers over electrodes are interpolated using a gaussian-kernel for illustrative purposes. Orange contour lines include the area in which the fish spends more than 50% of the time, the red lines more than 75% of the time respectively. Even though the fish certainly shows movement behaviors, especially during the night, it remains remarkably stationary in a specific location of the obervation area for four consecutive days.

traces, temporarily only one signal can be extracted by detecting peaks in the PSD (Figure 3A). So neither the EOD frequency difference nor the difference in spatial profiles provide a meaningful hint for tracking in the moment of the intersection. Adding EOD frequency difference to the distance measure then slightly favors connections of signal pairs with more similar EOD frequencies, resulting in a bias for superimposed signals detected at the intersection to be connected to the EOD frequency trace of the fish with a more constant EOD frequency (Figure 5, grey trace in bottom panel). The other signal traces, accordingly, remain to be connected across the intersection afterwards.

More important for the improved performance of the presented tracking algorithm is the algorithm itself, in addition to the combined distance measure. The tracking algorithm establishes connections within an extended tracking window based on smallest distances (Figure 5). This is in contrast to existing tracking algorithms (Henninger et al., 2018, 2020; Madhav et al., 2018), that immediately connect the signals detected in a given time step to known fish identities.

When studying animals and their behaviors by means of evaluating external recordings, we rely on the detection of sensory cues emitted actively or passively by the animals themselves (Dell et al., 2014; Hughey et al., 2018). In cluttered environments or when signals are weak (low signal-to-noise-ratio), reliable signal detection is often impaired and detection losses frequently occur. These detection gaps complicate reliable tracking, especially when signals are tracked according to their temporal occurrence. In recordings of electric fish, detection losses frequently result from fish being too far away from recording electrodes, from the electric fields being blocked by any objects between a fish and recording electrodes, or by intersections of EOD frequencies. The resulting tracking failures can be avoided with the presented algorithm, since it relies less on the temporal sequence of detected signals. Rather, connections are established according to the smallest distances within extended tracking windows.

Despite the high fractions of correct connections (Figure 8), the resulting EOD frequency traces need to be corrected manually. This is in particular necessary in sections with close by EOD frequencies or when EOD frequency traces cross each other due to active modulations. Recordings of only a few fish with well-separated EOD frequencies require much less or even no manual interventions. With the current state of the presented algorithm we push the limits to more complicated signal interactions, but the performance still is not perfect for interesting scenes with a lot of interactions (Figure 9). Deep neural networks that are successfully used to track animal pose (e.g., Mathis et al., 2018), or to annotate acoustic signals from various animals (e.g., Steinfath et al., 2021), might be an interesting option to further improve tracking performance. Such approaches, however, require extensive training data sets. Our tracking algorithm and evaluated data sets might set the basis for developing and training of deep neural networks in the future.

6. Conclusion

The self-generated electric fields of electric fish offer an unique opportunity for studying natural movement and communication behaviors of nocturnal fish in freely interacting populations. The EODs of whole groups can be recorded simultaneously by means of electrode arrays submerged in the water—without the need to catch and tag the fish. The presented algorithm for tracking wave-type electric fish combines previous approaches based on either their individual-specific EOD frequencies (Henninger et al., 2020) or the spatial profiles of electric fields resulting from a fish's location and orientation (Madhav et al., 2018). The algorithm uses a compound signal distance, that incorporates both EOD frequencies and spatial profiles. We developed a new temporal clustering method that assembles fish identities from all signals within a large tracking window according to ascending signal distances. With this approach, our algorithm improves in resolving tracking issues mainly resulting from crossing EOD frequency traces or detection losses, which tremendously reduces required post-processing time and makes this technique more feasible even in long-term observational studies on freely moving electric fish. Since tracked EOD traces allow insights into both movement and communication behaviors, a reliable tracking algorithm is key to many behavioral studies, both in the laboratory and in the field, that have not been possible before. From such big-data behavioral studies we expect many novel insights into the sensory ecology and into social and communication behaviors of these fascinating fishes (Henninger et al., 2018; Raab et al., 2019, 2021; Fortune et al., 2020), that also impact the way we study sensory processing.

Data availability statement

The original contributions presented in the study are included in the article/supplementary materials, further inquiries can be directed to the corresponding author/s.

Ethics statement

Ethical review and approval was not required for the animal study because the illustrated data includes observational recordings of electric fish in the wild (no ethics approval required since recordings were purely observational). Laboratory recordings illustrated in Figure 1E were approved by the Regierungspräsidium Tübingen (permit no. ZP 04/20 G).

Author contributions

The algorithm described and presented in this manuscript was developed by TR but builds upon collective or individual ideas shared between all other authors. MM, RJ, and NC developed the idea to utilize spatial electric field properties of individual electric fish as a feature to track their EODs (Madhav et al., 2018). JH and JB provided the tools required for detecting and extracting electric signals of wave-type electric fish in multi-electrode grid recordings and developed the first algorithmic approaches to track EODs of electric fish by means of their individual specific EOD frequency (Henninger et al., 2020). TR developed the here presented tracking algorithm which combines and refines previous approaches, including the implementation of the combined signal distance, which considers both electric field difference and EOD frequency, to determine signal similarities, as well as the idea to tack signals according to their similarity (combined signal distance) in discrete tracking windows, developed software tools to inspect and post-process tracked EOD traces, illustrated and evaluated the algorithm, and wrote the manuscript. Many of the ideas realized in the presented algorithm originated from collaborations and numerous discussion of TR with other authors. All authors contributed to the article and approved the submitted version.

Funding

This work was supported by Deutsche Forschungsgemeinschaft, Open Access Publishing Fund of University of Tübingen, the Center of Integrative Neuroscience at the University of Tübingen through the mini RTG Sensory Flow Processing across Modalities and Species, and the National

Science Foundation under grand no. 1557858 to NC a Kavli NDI Distiguished Postdoctoral Fellowship to MM.

Acknowledgments

We thank Eric Fortune for important discussions and improvements to the tracking system.

Conflict of interest

The authors declare that the research was conducted in the absence of any commercial or financial relationships that could be construed as a potential conflict of interest.

Publisher's note

All claims expressed in this article are solely those of the authors and do not necessarily represent those of their affiliated organizations, or those of the publisher, the editors and the reviewers. Any product that may be evaluated in this article, or claim that may be made by its manufacturer, is not guaranteed or endorsed by the publisher.

References

Albert, J. S., and Crampton, W. G. R. (2005). "Diversity and phylogeny of neotropical electric fishes (gymnotiformes)," in *Electroreception*, eds T. H. Bullock, C. D. Hopkins, A. N. Popper, and R. R. Fay (New York, NY: Springer), 360–409. doi: 10.1007/0-387-28275-0_13

Aspillaga, E., Arlinghaus, R., Martorell-Barceló, M., Follana-Berná, G., Lana, A., Campos-Candela, A., et al. (2021). Performance of a novel system for high-resolution tracking of marine fish societies. *Anim. Biotelemetry* 9, 1–14. doi: 10.1186/s40317-020-00224-w

Bastian, J., Schniederjan, S., and Nguyenkim, J. (2001). Arginine vasotocin modulates a sexually dimorphic communication behavior in the weakly electric fish *Apteronotus leptorhynchus*. *J. Exp. Biol.* 204, 1909–1923. doi: 10.1242/jeb.204.11.1909

Benda, J. (2020). "The physics of electrosensory worlds," in *The Senses: A Comprehensive Reference*, Vol. 7, eds B. Fritzsch and H. Bleckmann (Cambridge: Elsevier; Academic Press), 228–254. doi: 10.1016/B978-0-12-805408-6.00016-6

Boon, A. K., Réale, D., and Boutin, S. (2007). The interaction between personality, offspring fitness and food abundance in north American red squirrels. *Ecol. Lett.* 10, 1094–1104. doi: 10.1111/j.1461-0248.2007.01106.x

Chapman, C., Chapman, L., and Wrangham, R. (1995). Ecological constraints on group size: an analysis of spider monkey and chimpanzee subgroups. *Behav. Ecol. Sociobiol.* 36, 59–70. doi: 10.1007/BF00175729

Cheney, D. L., Seyfarth, R. M., and Silk, J. B. (1995). The role of grunts in reconciling opponents and facilitating interactions among adult female baboons. *Anim. Behav.* 50, 249–257. doi: 10.1006/anbe.1995.0237

Dell, A. I., Bender, J. A., Branson, K., Couzin, I. D., de Polavieja, G. G., Noldus, L. P., et al. (2014). Automated image-based tracking and its application in ecology. *Trends Ecol. Evol.* 29, 417–428. doi: 10.1016/j.tree.2014.05.004

Dunlap, K., Smith, G., and Yekta, A. (2000). Temperature dependence of electrocommunication signals and their underlying neural rhythms in the weakly electric fish, *Apteronotus leptorhynchus*. *Brain Behav. Evol.* 55, 152–162. doi: 10.1159/000006649

Egnor, S. E. R., and Branson, K. (2016). Computational analysis of behavior. *Annu. Rev. Neurosci.* 39, 217–236. doi: 10.1146/annurev-neuro-070815-013845

Fortune, E. S., Andanar, N., Madhav, M., Jayakumar, R. P., Cowan, N. J., Bichuette, M. E., et al. (2020). Spooky interaction at a distance in cave and surface dwelling electric fishes. *Front. Integr. Neurosci.* 14, 561524. doi: 10.3389/fnint.2020.561524

Fotowat, H., Harrison, R. R., and Krahe, R. (2013). Statistics of the electrosensory input in the freely swimming weakly electric fish *Apteronotus leptorhynchus*. *J. Neurosci.* 33, 13758–13772. doi: 10.1523/JNEUROSCI.0998-13.2013

Gomez-Marin, A., Paton, J. J., Kampff, A. R., Costa, R. M., and Mainen, Z. F. (2014). Big behavioral data: psychology, ethology and the foundations of neuroscience. *Nat. Neurosci.* 17, 1455–1462. doi: 10.1038/nn.3812

Hagedorn, M. (1988). Ecology and behavior of a pulse-type electric fish, hypopomus occidentalis (gymnotiformes, hypopomidae), in a fresh-water stream in panama. *Copeia* 1988, 324–335. doi: 10.2307/1445872

Henninger, J. (2015). *Social interactions in natural populations of weakly electric fish* (Ph.D. thesis). Eberhard Karls Universität, Tübingen, Germany.

Henninger, J., Krahe, R., Kirschbaum, F., Grewe, J., and Benda, J. (2018). Statistics of natural communication signals observed in the wild identify important yet neglected stimulus regimes in weakly electric fish. *J. Neurosci.* 38, 5456–5465. doi: 10.1523/JNEUROSCI.0350-18.2018

Henninger, J., Krahe, R., Sinz, F., and Benda, J. (2020). Tracking activity patterns of a multispecies community of gymnotiform weakly electric fish in their neotropical habitat without tagging. *J. Exp. Biol.* 223, jeb206342. doi: 10.1242/jeb.206342

Hügel, T., van Meir, V., Munoz-Meneses, A., Clarin, B.-M., Siemers, B. M., and Goerlitz, H. R. (2017). Does similarity in call structure or foraging ecology explain interspecific information transfer in wild *Myotis bats? Behav. Ecol. Sociobiol.* 71, 168. doi: 10.1007/s00265-017-2398-x

Hughey, L. F., Hein, A. M., Strandburg-Peshkin, A., and Jensen, F. H. (2018). Challenges and solutions for studying collective animal behaviour in the wild. *Philos. Trans. R. Soc. Lond. B Biol. Sci.* 373, 20170005. doi: 10.1098/rstb.2017.0005

Jolles, J. W. (2021). Broad-scale applications of the Raspberry Pi: a review and guide for biologists. *Methods Ecol. Evol.* 12, 1562–1579. doi: 10.1111/2041-210X.13652

Jun, J. J., Longtin, A., and Maler, L. (2013). Real-time localization of moving dipole sources for tracking multiple free-swimming weakly electric fish. *PLoS ONE* 8, e66596. doi: 10.1371/journal.pone.0066596

Kühl, H. S., and Burghardt, T. (2013). Animal biometrics: quantifying and detecting phenotypic appearance. *Trends Ecol. Evol.* 28, 432–441. doi: 10.1016/j.tree.2013.02.013

Lahiri, M., Tantipathananandh, C., Warungu, R., Rubenstein, D. I., and Berger-Wolf, T. Y. (2011). "Biometric animal databases from field photographs: identification of individual zebra in the wild," in *Proceedings of the 1st ACM International Conference on Multimedia Retrieval*, New York, 1–8. doi: 10.1145/1991996.1992002

Madhav, M. S., Jayakumar, R. P., Demir, A., Stamper, S. A., Fortune, E. S., and Cowan, N. J. (2018). High-resolution behavioral mapping of electric fishes in Amazonian habitats. *Sci. Rep.* 8, 5830. doi: 10.1038/s41598-018-24035-5

Markham, A. C., Gesquiere, L. R., Alberts, S. C., and Altmann, J. (2015). Optimal group size in a highly social mammal. *Proc. Natl. Acad. Sci. U.S.A.* 112, 14882–14887. doi: 10.1073/pnas.1517794112

Mathis, A., Mamidanna, P., Cury, K. M., Abe, T., Murthy, V. N., Mathis, M. W., et al. (2018). DeepLabCut: markerless pose estimation of user-defined body parts with deep learning. *Nat. Neurosci.* 21, 1281–1289. doi: 10.1038/s41593-018-0209-y

Moortgat, K., Keller, C., Bullock, T., and Sejnowski, T. (1998). Submicrosecond pacemaker precision is behaviorally modulated: the gymnotiform electromotor pathway. *Proc. Natl. Acad. Sci. U.S.A.* 95, 4684–4689. doi: 10.1073/pnas.95.8.4684

Nagy, M., Ákos, Z., Biro, D., and Vicsek, T. (2010). Hierarchical group dynamics in pigeon flocks. *Nature* 464, 890–893. doi: 10.1038/nature08891

Nourizonoz, A., Zimmermann, R., Ho, C. L. A., Pellat, S., Ormen, Y., Prevost-Solie, C., et al. (2020). EthoLoop: automated closed-loop neuroethology in naturalistic environments. *Nat. Methods* 17, 1052–1059. doi: 10.1038/s41592-020-0961-2

Pantoni, M. M., Herrera, G. M., Van Alstyne, K. R., and Anagnostaras, S. G. (2020). Quantifying the acoustic startle response in mice using standard digital video. *Front. Behav. Neurosci.* 14, 83. doi: 10.3389/fnbeh.2020.00083

Pedraja, F., Herzog, H., Engelmann, J., and Jung, S. N. (2021). The use of supervised learning models in studying agonistic behavior and communication in weakly electric fish. *Front. Behav. Neurosci.* 15, 718491. doi: 10.3389/fnbeh.2021.718491

Raab, T., Bayezit, S., Erdle, S., and Benda, J. (2021). Electrocommunication signals indicate motivation to compete during dyadic interactions of an electric fish. *J. Exp. Biol.* 224, jeb242905. doi: 10.1242/jeb.242905

Raab, T., Linhart, L., Wurm, A., and Benda, J. (2019). Dominance in habitat preference and diurnal explorative behavior of the weakly electric fish *Apteronotus leptorhynchus*. *Front. Integr. Neurosci.* 13, 21. doi: 10.3389/fnint.2019.00021

Rendall, D., Seyfarth, R. M., Cheney, D. L., and Owren, M. J. (1999). The meaning and function of grunt variants in baboons. *Anim. Behav.* 57, 583–592. doi: 10.1006/anbe.1998.1031

Robinson, P. W., Costa, D. P., Crocker, D. E., Gallo-Reynoso, J. P., Champagne, C. D., Fowler, M. A., et al. (2012). Foraging behavior and success of a mesopelagic predator in the northeast pacific ocean: insights from a data-rich species, the northern elephant seal. *PLoS ONE* 7, e36728. doi: 10.1371/journal.pone.0036728

Sapolsky, R. M. (2005). The influence of social hierarchy on primate health. *Science* 308, 648–652. doi: 10.1126/science.1106477

Saraux, C., Le Bohec, C., Durant, J. M., Viblanc, V. A., Gauthier-Clerc, M., Beaune, D., et al. (2011). Reliability of flipper-banded penguins as indicators of climate change. *Nature* 469, 203–206. doi: 10.1038/nature09630

Seibert, A.-M., Koblitz, J. C., Denzinger, A., and Schnitzler, H.-U. (2013). Scanning behavior in echolocating common pipistrelle bats (*Pipistrellus pipistrellus*). *PLoS ONE* 8, e60752. doi: 10.1371/journal.pone.0060752

Sherley, R. B., Burghardt, T., Barham, P. J., Campbell, N., and Cuthill, I. C. (2010). Spotting the difference: towards fully-automated population monitoring of African penguins *Spheniscus demersus*. *Endangered Species Res.* 11, 101–111. doi: 10.3354/esr00267

Smith, G. T. (2013). Evolution and hormonal regulation of sex differences in the electrocommunication behavior of ghost knifefishes (apteronotidae). *J. Exp. Biol.* 216, 2421–2433. doi: 10.1242/jeb.082933

Steinfath, E., Palacios-Munoz, A., Rottschofer, J. R., Yuezak, D., and Clemens, J. (2021). Fast and accurate annotation of acoustic signals with deep neural networks. *eLife* 10, e68837. doi: 10.7554/eLife.68837

Strandburg-Peshkin, A., Clutton-Brock, T., and Manser, M. B. (2019). Burrow usage patterns and decision-making in meerkat groups. *Behav. Ecol.* 31, 292–302. doi: 10.1093/beheco/arz190

Strandburg-Peshkin, A., Farine, D. R., Couzin, I. D., and Crofoot, M. C. (2015). Shared decision-making drives collective movement in wild baboons. *Science* 348, 1358–1361. doi: 10.1126/science.aaa5099

Strandburg-Peshkin, A., Farine, D. R., Crofoot, M. C., and Couzin, I. D. (2017). Habitat and social factors shape individual decisions and emergent group structure during baboon collective movement. *eLife* 6, e19505. doi: 10.7554/eLife.19505

Strandburg-Peshkin, A., Papageorgiou, D., Crofoot, M. C., and Farine, D. R. (2018). Inferring influence and leadership in moving animal groups. *Philos. Trans. R. Soc. B Biol. Sci.* 373, 20170006. doi: 10.1098/rstb.2017.0006

Surlykke, A., and Kalko, E. K. V. (2008). Echolocating bats cry out loud to detect their prey. *PLoSONE* 3, e2036. doi: 10.1371/journal.pone.0002036

Theriault, D. H., Fuller, N. W., Jackson, B. E., Bluhm, E., Evangelista, D., Wu, Z., et al. (2014). A protocol and calibration method for accurate multi-camera field videography. *J. Exp. Biol.* 217, 1843–1848. doi: 10.1242/jeb.100529

Todd, B. S., and Andrews, D. C. (1999). The identification of peaks in physiological signals. *Comput. Biomed. Res.* 32, 322–335. doi: 10.1006/cbmr.1999.1518

Torney, C. J., Lamont, M., Debell, L., Angohiatok, R. J., Leclerc, L.-M., and Berdahl, A. M. (2018). Inferring the rules of social interaction in migrating caribou. *Philos. Trans. R. Soc. B Biol. Sci.* 373, 20170385. doi: 10.1098/rstb.2017.0385

Triefenbach, F., and Zakon, H. (2008). Changes in signalling during agonistic interactions between male weakly electric knifefish, *Apteronotus leptorhynchus*. *Anim. Behav.* 75, 1263–1272. doi: 10.1016/j.anbehav.2007.09.027

Turner, C. R., Derylo, M., de Santana, C. D., Alves-Gomes, J. A., and Smith, G. T. (2007). Phylogenetic comparative analysis of electric communication signals in ghost knifefishes (gymnotiformes: Apteronotidae). *J. Exp. Biol.* 210, 4104–4122. doi: 10.1242/jeb.007930

Zupanc, G. K. (2002). From oscillators to modulators: behavioral and neural control of modulations of the electric organ discharge in the gymnotiform fish, apteronotus leptorhynchus. *J. Physiol.* 96, 459–472. doi: 10.1016/S0928-4257(03)00002-0

frontiers | Frontiers in Integrative Neuroscience

TYPE Original Research
PUBLISHED 16 September 2022
DOI 10.3389/fnint.2022.914246

OPEN ACCESS

EDITED BY
Manu Madhav,
University of British Columbia, Canada

REVIEWED BY
Paul Graham,
University of Sussex, United Kingdom
Patrick Schultheiss,
Julius Maximilian University
of Würzburg, Germany

*CORRESPONDENCE
Ayse Yilmaz
ayse.yilmaz-heusinger@biol.lu.se

RECEIVED 06 April 2022
ACCEPTED 14 July 2022
PUBLISHED 16 September 2022

CITATION
Yilmaz A, Gagnon Y, Byrne MJ, Foster JJ, Baird E and Dacke M (2022) The balbyter ant *Camponotus fulvopilosus* combines several navigational strategies to support homing when foraging in the close vicinity of its nest.
Front. Integr. Neurosci. 16:914246.
doi: 10.3389/fnint.2022.914246

The balbyter ant *Camponotus fulvopilosus* combines several navigational strategies to support homing when foraging in the close vicinity of its nest

Ayse Yilmaz[1]*, Yakir Gagnon[1], Marcus J. Byrne[2], James J. Foster[1,3,4], Emily Baird[5] and Marie Dacke[1,2]

[1]Lund Vision Group, Department of Biology, Lund University, Lund, Sweden, [2]School of Animal, Plant and Environmental Sciences, University of the Witwatersrand, Johannesburg, South Africa, [3]Biocenter, University of Wuerzburg, Wuerzburg, Germany, [4]Neurobiology, University of Konstanz, Konstanz, Germany, [5]Department of Zoology, Stockholm University, Stockholm, Sweden

Many insects rely on path integration to define direct routes back to their nests. When shuttling hundreds of meters back and forth between a profitable foraging site and a nest, navigational errors accumulate unavoidably in this compass- and odometer-based system. In familiar terrain, terrestrial landmarks can be used to compensate for these errors and safely guide the insect back to its nest with pin-point precision. In this study, we investigated the homing strategies employed by *Camponotus fulvopilosus* ants when repeatedly foraging no more than 1.25 m away from their nest. Our results reveal that the return journeys of the ants, even when setting out from a feeder from which the ants could easily get home using landmark information alone, are initially guided by path integration. After a short run in the direction given by the home vector, the ants then switched strategies and started to steer according to the landmarks surrounding their nest. We conclude that even when foraging in the close vicinity of its nest, an ant still benefits from its path-integrated vector to direct the start of its return journey.

KEYWORDS

ants, *Camponotus fulvopilosus*, path integration, terrestrial landmarks, short-range navigation, cue weighting

Introduction

Path integration is a widespread strategy, employed by many arthropods - including ants, fiddler crabs, beetles, and spiders - to successfully navigate between their home and a feeding place (ants; Müller and Wehner, 1988; fiddler crabs; Zeil, 1998; homing dung beetles Dacke et al., 2020; Yilmaz et al., 2021; spiders; Mittelstaedt, 1983). By keeping track of the directions and distances traveled, and continually integrating these into a single vector, these animals can safely return home even after exploring unfamiliar terrain. Many ants use path integration as their primary system for long-range

navigation but can also combine it with learned visual information for improved precision and overall navigational success (Collett et al., 1998; Wehner et al., 2016; Buehlmann et al., 2020a). If these two systems are set into conflict experimentally by, for example, artificially rotating the visual surroundings, most species take a compromise direction when aiming to return to their nests (reviewed in Wehner et al., 2016), resulting in a vector that lies between the two stimuli (Collett, 2012; Wystrach et al., 2015).

The relative weightings of directional guidance from path integration and visual terrestrial landmarks during navigation seems to vary across species, individual experience and specific habitat characteristics (Buehlmann et al., 2020a). For instance, path integration is especially important when naïve ants explore unfamiliar habitats, enabling the inexperienced forager to gradually learn terrestrial landmarks along the new route (Wehner et al., 2004; Müller and Wehner, 2010; Fleischmann et al., 2016). Experienced foragers can then make use of panoramic cues and visual sequences of landmarks along their homeward routes to guide themselves toward the vicinity of their nest, and to finally pin-point the exact location of its entrance (Wehner and Räber, 1979). Ants living in cluttered, landmark-rich environments readily combine directional information from path integration with visual landmarks as soon as they recognize a familiar visual landscape when seen from a new location (Narendra, 2007a), while ants from visually poor habitats rely exclusively on path integration for homing when transferred to an unfamiliar place (Buehlmann et al., 2011).

In contrast to most ants and other homing arthropods, the dung beetle *Scarabaeus galenus* relies primarily (if not exclusively) on path integration to locate its burrow (Dacke et al., 2020; Yilmaz et al., 2021). It is important to note that these short-range navigators (often < 2 m) (Dacke et al., 2020) forage in the landmark-rich African savanna. Whether the apparent inability of the beetle to extract directional information from terrestrial landmarks is related to an incapacity to learn and memorize landmarks, or the possession of a very precise path integrating system, or the short foraging distances involved is currently not known.

In this study, we aimed to define the relative use of landmarks and path integration for short distance navigation in the tawny balbyter ant, *Camponotus fulvopilosus*. This golden-haired species of ants builds its nests under fallen trees, rock slabs or at the base of small bushes in the landmark rich savanna habitats in northern South Africa (Robertson and Zachariades, 1997; see **Supplementary Figure 1** for photographic representation of its habitat) and forage individually on the ground for insects or in trees for honeydew (Marsh, 1986; Robertson and Zachariades, 1997, personal observation). In this study, foraging *C. fulvopilosus ants* were trained to feeders placed only 1.25 m away from their nests and then passively displaced around or away from their nest as they attempted to return home. We conclude that even when foraging in the close vicinity of their nest, *C. fulvopilosus* ants benefit from their path-integrated vectors to accurately set out in a homeward direction.

Materials and methods

Animals

Experiments were performed with *C. fulvopilosus* (**Figure 1**) in February 2019 on the game farm Stonehenge, near Vryburg, South Africa (26°23′56″S, 24°19′36″E), using three nests located approx. 15 m apart from each other. *C. fulvopilosus* are easily distinguished from other members of the genus by thick yellow hairs on their gaster (Robertson and Zachariades, 1997; **Figure 1**). Our experiments were limited to minor and medium-sized workers as these are the active foragers within the genus (Josens et al., 2009; Yilmaz et al., 2014, 2016, 2017).

Activity rhythm measurements

Before the experiments, we monitored the daily activity rhythm of two *C. fulvopilosus* nests for 6 days. A GoPro camera (Hero 6, GoPro, Inc., United States) was placed above each nest and set to capture an image every 10 min from 05.00 to 07.00 and from 19.00 to 20.00, and every 30 min for the remainder of the day. The captured images allowed us to manually identify the number of *C. fulvopilosus* ants present within a 30 cm radius of the nest with increased temporal resolution around sunrise and sunset. Temperature was measured every 30 min (Termometerfabriken Viking AB, Art No: 02038).

Foraging distance measurements

For an estimate of natural foraging distances for *C. fulvopilosus,* 14 individuals encountered at random were located away from their nest while they were searching for food, provided with sucrose solution and followed back until they reached their nest. The direct distance between their nest and the point where they had been located while foraging measured.

Behavioral experiments

General experimental procedure

A petri dish (3 cm diameter) feeder, filled with meal worms and sucrose solution, was placed on top of a sand covered wooden plate (5 cm × 5 cm) 125 cm away from the nest entrance (**Figure 1**). Training started at 06:30 and continued until the last ant entered the nest (ca. 19:00). Ants reaching the feeder

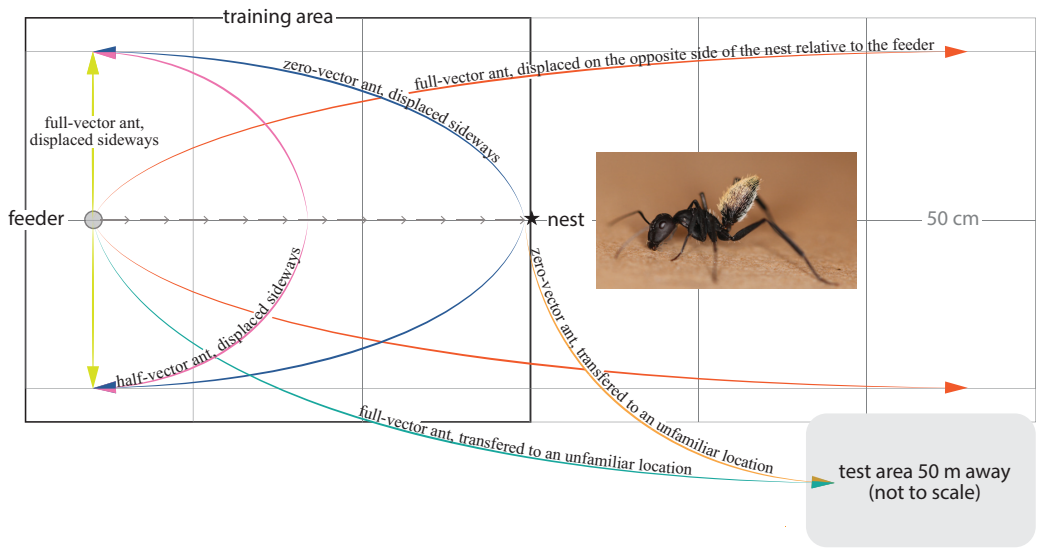

FIGURE 1
The balbyter ant *Camponotus fulvopilosus* and experimental treatments. The ants were trained to forage on a sucrose solution at a feeder (gray circle), 125 cm away from the nest (star) (Gray arrows, direct path home). Once trained, the ants located the feeder and started to drink from it, were either caught there (full-vector ants, green and yellow), or allowed to fill their gaster and return toward their nest. These ants were then either caught 0.62 m along their path (half-vector ants, pink) or just before they entered their nest (zero-vector ants, blue or orange). Captured ants were then transferred to an unfamiliar test area 50 m away (green), or displaced to a position 50 cm to either side of the feeder (yellow) or to the corresponding position 125 cm on the opposite side of the nest relative to the feeder (orange).

for the first time were marked with a unique multi-color code (Motip Lackstift Acryl, MOTIP DUPLI GmbH, Haßmersheim, Germany) on the thorax and/or gaster for identification. This allowed us to record the foraging behavior of each individual. Ants that had foraged at least 6 times over a maximum of 2 days, and that ran directly to the feeder and back to the nest without any hesitation, were assigned to one of the 5 experimental conditions. The homebound paths of the ants were recorded from above using a camera (Sony HDR-HC5E Handycam fitted with a 0.66× wide angle lens, Rynox, Japan) mounted on a tripod. The camera set up was present throughout the study. Depending on the experimental condition, the homebound path taken by the ant was either filmed for 4 min or until the ant reached its covered nest entrance.

Transfer to an unfamiliar test area

One group of ants was caught individually at the feeder (full-vector ants, Figure 1) by placing an opaque tube over the feeder. The ant and the feeder were then directly transferred to a test area 50 m away, surrounded by an array of different natural landmarks. Here, the feeder was carefully placed on the ground and the opaque tube was removed to release the ant. This whole procedure took approximately 1 min. A second group of ants was instead caught in the opaque tube just before they entered their nest (zero-vector ants, Figure 1) and released in the same test area. As these ants had almost reached their nest when they were caught, their path integrator had nearly been reset to zero.

Displacement in the vicinity of the nest

A third group of ants was again caught at the feeder as above (full-vector ants) and displaced 50 cm to the right or to the left from this position (Figure 1). A fourth experimental group of full-vector ants was instead moved 125 cm to the opposite side of the nest relative to the feeder and released 50 cm to the right or to the left of this position (Figure 1). Upon their release, ants from these third and fourth groups set out from a position in space where the nest directions, as dictated by the terrestrial landmarks and those dictated by the path integration, were set in conflict indicating different nest directions. Yet another two groups of ants, the fifth and the sixth group, were caught at 62 cm along their path (half-vector ants) and just before they entered their nest (zero-vector ants) and subsequently released 50 cm to the right or to the left of the feeder (Figure 1). Before each ant was released, the nest was covered with a sandblasted petri dish and the training area was carefully brushed to remove olfactory cues.

Data analysis

The filmed trajectories of ants were tracked using a custom-made software integrated in Matlab (Mathworks Inc.). The tracks were visualized and analyzed in Julia (Bezanson et al., 2017). Pixel coordinates representing the ant's position were converted to real world coordinates with the Camera Calibration tool in Matlab. This also accounted for possible

distortions in the camera optics. A parametric spline with a factor of 500 and an order of two were used to smooth the coordinates of the ants' trajectories (Schoenberg, 1971). The vector length for each ant was calculated as the radial (shortest) distance from the release point to the turning point i.e., where the ants changed their direction by a minimum of 60° and then walked along a curved path (see also Dacke et al., 2020). To identify this point in space, the segment of the path containing the turning point was first defined from the derivative of the spline at the spline's knots (where the sequential smoothing polynomials connected). The exact location of the turning point was then defined as the first point along the identified segment at which the ant's direction (calculated from the derivative) deviated from the direction at the first of two consecutive knots by more than 60°. The center of search was determined as the mean coordinate of the track, i.e., from the defined turning point until the end of the track or until 4 min had passed from the turning point. The full width at half maximum (FWHM) in Figures 3, 5 refers to the region with the highest search density, calculated as the width of a fitted 2D Gaussian distribution at half of its maximum amplitude.

Vector lengths and the angular distributions of turning points in relation to the ants' homeward direction were analyzed using Sigmaplot (Systat Software, Inc., San Jose, CA, United States) and Oriana 4.0 (Kovach Computing Services, Anglesey, United Kingdom), respectively. A Rayleigh test was used to test for uniformity of the circular distribution of turning points and a *V*-test was performed to test whether angular positions of the turning points – if significantly different from random – were clustered around the (fictive) nest direction.

Results

General description of foraging behavior

The mean natural foraging distance of *C. fulvopilosus* workers in the woodland-savanna area examined was 20 m ± 6.3 m (mean ± sd, $n = 14$), with minimum and maximum distances of 8 and 31.3 m, respectively. Even though recruitment behavior with up to 5 individuals was occasionally observed, workers mainly foraged alone. From observation, the inbound and outbound paths of the foraging ants differed between individuals, indicating that the foragers do not follow trail pheromones. This also held true for the first foraging trips of the trained ants.

Camponotus fulvopilosus started their activity early in the morning between 06.00 and 06.30 with an increase in numbers foraging between 14:30 and 15:00, followed by a gradual decrease from 17:00 to 19:00, after which foragers could no longer be observed (Figure 2).

Ants transferred to an unfamiliar test area navigate by path integration

When caught at the feeder and transported to an unfamiliar test area 50 m away (Figure 1), the full-vector ants were still drinking, and showed no sign of disturbance by being covered and moved. When full, as indicated by a swollen gaster, the ants quickly ran in the direction of their fictive nest (i.e., the position of their nest had it been moved with them) for 41.5 ± 25.8 cm (Figure 3Ai) before they made a turn (defined as their turning points) and initiated a systematic search. An analysis of the positions of the ants at a radial distance of 10 cm from the release point clearly revealed that the initial directions traveled were clustered in the direction of the fictive nest ($P < 0.0001$, $r = 0.94$, Rayleigh test, $P < 0.0001$, *V*-test, μ: 335.9° ± 6.0°, $V = 0.85$, $n = 14$) (Figure 3Bi). This also held true for the spatial distribution of their turning points ($P < 0.0001$, $r = 0.94$, Rayleigh test, $P < 0.0001$, *V*-test, μ: 344.9° ± 5.7°, $V = 0.91$, $n = 14$). The subsequent searches centered 25 cm away from the release point (*x*-axis: −9.9 ± 18.7 cm, *y*-axis: −100.9 ± 22.1 cm, Figure 3Ci).

In contrast, the zero-vector ants released in the same test area were no longer oriented to a specific (fictive nest) direction (Figure 3Aii). The center of search in this group was rather located around their point of release (0, −125 cm), that is, around the fictive nest position as indicated by their nearly zeroed path-integrator (*x*-axis: −3.5 ± 26.9 cm, *y*-axis: −121.7 ± 23.2 cm) (Figure 3Cii). Analysis of the angular distribution of these zero-vector ants when at a radius of 10 cm away from their point of release further confirmed that this group of ants were indeed randomly oriented ($P = 0.1$, $r = 0.3$, Rayleigh test, $n = 14$) (Figure 3Bii). Overall, the results indicate that *C. fulvopilosus* workers relied on path integration for homing when released in an unfamiliar area. The non-directed behavior of the zero-vector ants also confirms that landmarks (distant or local) did not provide any guidance from this presumed unfamiliar point of release.

Path integration guides initial homing even when foraging only 125 cm away from the nest

Ants caught at the feeder and displaced 50 cm sideways to the right or to the left of it, first set off in the direction of their fictive nest (straight ahead) and ran in this direction for $48.05 \pm 20.8_{left}$ and $64.7 \pm 32.1_{right}$ cm before adjusting their bearings toward the actual position of the real nest (Figure 4Ai and Supplementary Figure 2). As expected, an analysis of the positions of the ants at a radial distance of 10 cm from the release point revealed that the initial directions traveled by the ants were clustered in the direction of the fictive (rather than the real) nest ($P_{left} < 0.0001$, $r = 0.98$, Rayleigh test, $P_{left} < 0.0001$,

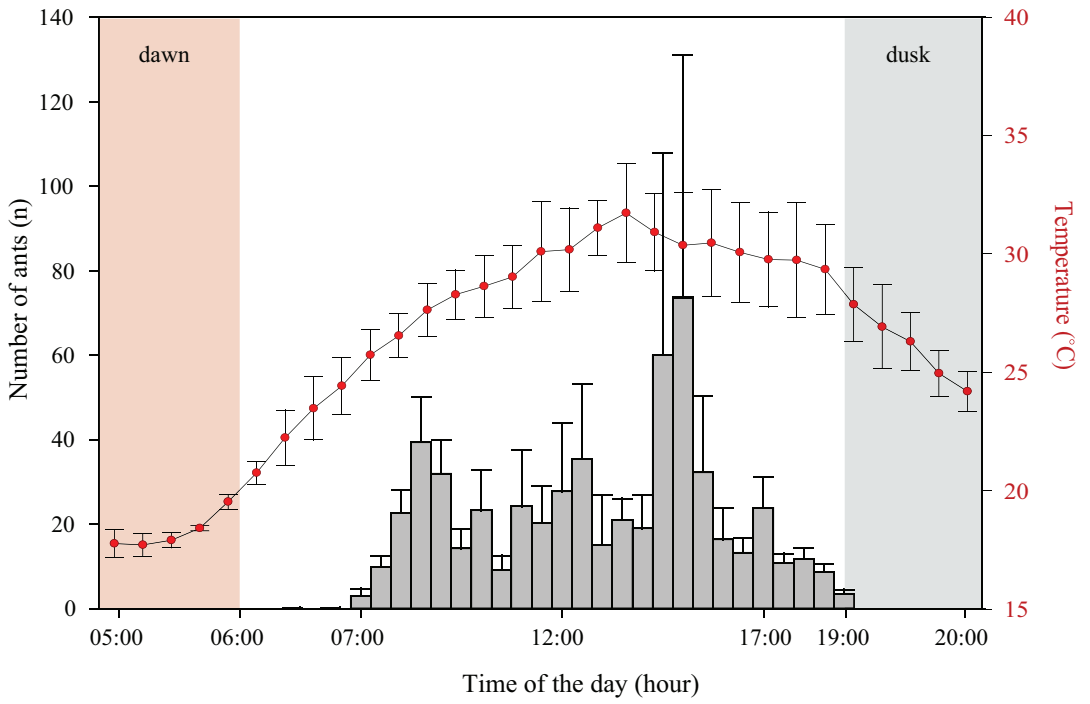

FIGURE 2
Activity rhythm. The activity period of *Camponotus fulvopilosus* foragers (bars) and air temperature measurements (red dots). Error bars represent standard deviation.

V-test, μ: 359.6° ± 3.9°, $V = 0.98$, $n = 10$; $P_{right} < 0.0001$, $r = 0.87$, Rayleigh test, $p_{right} < 0.0001$, *V*-test, μ: 7.2 ± 8.7°, $V = 0.87$, $n = 14$) (Figure 4Bi). A similar pattern was recorded for the relative spatial distribution of the ants' turning points ($P_{left} < 0.0001$, $r = 0.99$, Rayleigh test, $P_{left} < 0.0001$, *V*-test, μ: 5.9 ± 2.47°, $V = 0.98$, $n = 10$; $P_{right} < 0.0001$, $r = 0.97$, Rayleigh test, $p_{right} < 0.0001$, *V*-test, μ: 359. ± 4.47°, $V = 0.96$, $n = 14$). From the turning point onward, the paths of the ants curved toward their real nest (Figure 4Ai and Supplementary Figure 2). This suggests that the homing ants first set out in the direction indicated by their path integrator, but then changed their bearings to agree with the directional information provided by its well-known surroundings.

When instead moved from the feeder to a corresponding position, displaced 50 cm to the right or to the left of the feeder, on the opposite side of the nest (Figure 1) the ants showed an even greater conflict between the directional information provided by their path-integrator and local landmarks. The full-vector ants nonetheless initially set off in the direction of the fictive nest, i.e., away from their real nest, and ran in this direction for 23.9_{left} ± 9.9 cm and 30.9_{right} ± 14.1 cm (Figure 5A). Consequently, an analysis of the positions of the ants at a radial distance of 10 cm from the release point clearly revealed that the initial directions traveled by the ants were clustered in the direction of the fictive nest, i.e., directly away from the real nest (Figure 5B) ($P_{left} < 0.0001$, $r = 0.98$, Rayleigh test, $P_{left} < 0.0001$, *V*-test, μ: 7.4 ± 6.2°, $V = 0.97$, $n = 6$); ($P_{right} < 0.0001$, $r = 0.96$, Rayleigh test, $P_{right} < 0.0001$, μ: 351.0 ± 6.3°, $V = 0.95$, $n = 9$). This also held true for the relative spatial distribution of their turning points ($P_{left} < 0.0001$, $r = 0.90$, Rayleigh test, $P_{left} < 0.0001$, *V*-test, μ: 11.2 ± 14.0°, $V = 0.88$, $n = 6$); ($P_{right} < 0.0001$, $r = 0.88$, Rayleigh test, $P_{right} < 0.0001$, μ: 350.3 ± 11.5°, $V = 0.86$, $n = 9$). The ants then adjusted their bearings toward the true position of their real nest.

Unlike the full-vector ants, the trajectories of half-vector ants (caught after running half of their home vector then displaced 50 cm sideways to the left or right of the feeder) were instead biased toward the position of the real nest (Figure 4Aii). An analysis of the angular distribution of the half-vector ants at a radius of 10 cm away from their point of release further confirmed that this group of ants were indeed oriented toward the real nest ($P_{left} = 0.003$, $r = 0.76$, Rayleigh test, $P_{left} < 0.01$, *V*-test, μ: 334.3° ± 16.6°, $V = 0.74$, $n = 9$; $P_{rightt} = 0.004$, $r = 0.71$, Rayleigh test, $P_{right} < 0.001$, *V*-test, μ: 13.3° ± 17.4°, $V = 0.64$, $n = 10$) (Figure 4Bii). As for half-vector ants, the trajectories resulting from displaced zero-vector ants (caught just before entering their nest and again displaced 50 cm sideways to the left and right of the feeder), were biased toward the real nest direction ($P_{left} = 0.05$, $r = 0.65$, Rayleigh test, $P_{left} = 0.01$, *V*-test, μ: 13.6° ± 20.3°, $V = 0.57$, $n = 6$; $P_{right} = 0.01$, $r = 0.8$, Rayleigh test, $P_{right} < 0.01$, *V*-test, μ: 334.3° ± 21.9°, $V = 0.78$, $n = 7$) (Figures 4Aiii,Biii).

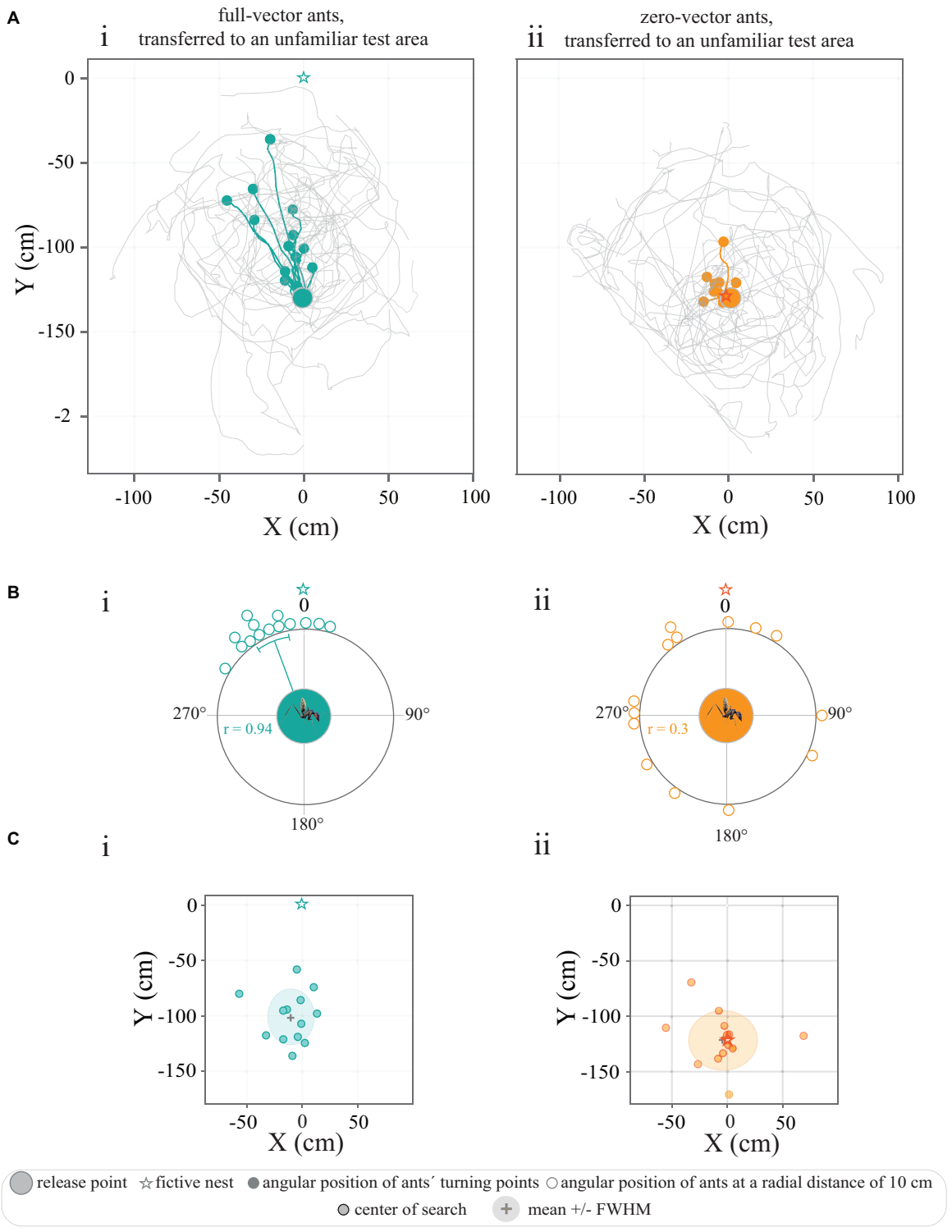

FIGURE 3
Tracks of full-vector and zero-vector ants transferred to an unfamiliar test area. **(A)** Trajectories represent the paths of ants caught **(i)** at the feeder (full-vector ants, green) or **(ii)** just before they entered their nest (zero-vector ants, orange). Colored trajectories illustrate the paths of individual ants until their turning point (filled circles). Gray paths illustrate their search after the turning point. **(Bi–iii)** Circular graphs represent the angular positions of ants at a radial distance of 10 cm away from the release point in relation to the normalized fictive nest direction (0°). And colored line within the circular graphs indicate mean angles, and the associated sectors represent the 95% confidence interval of the mean. r represents mean vector length. **(C)** The center of the search paths described with respect to the location of the fictive nest (star). Gray crosses and shaded colored areas mark the mean and the full width at half maximum (FWHM) of the data.

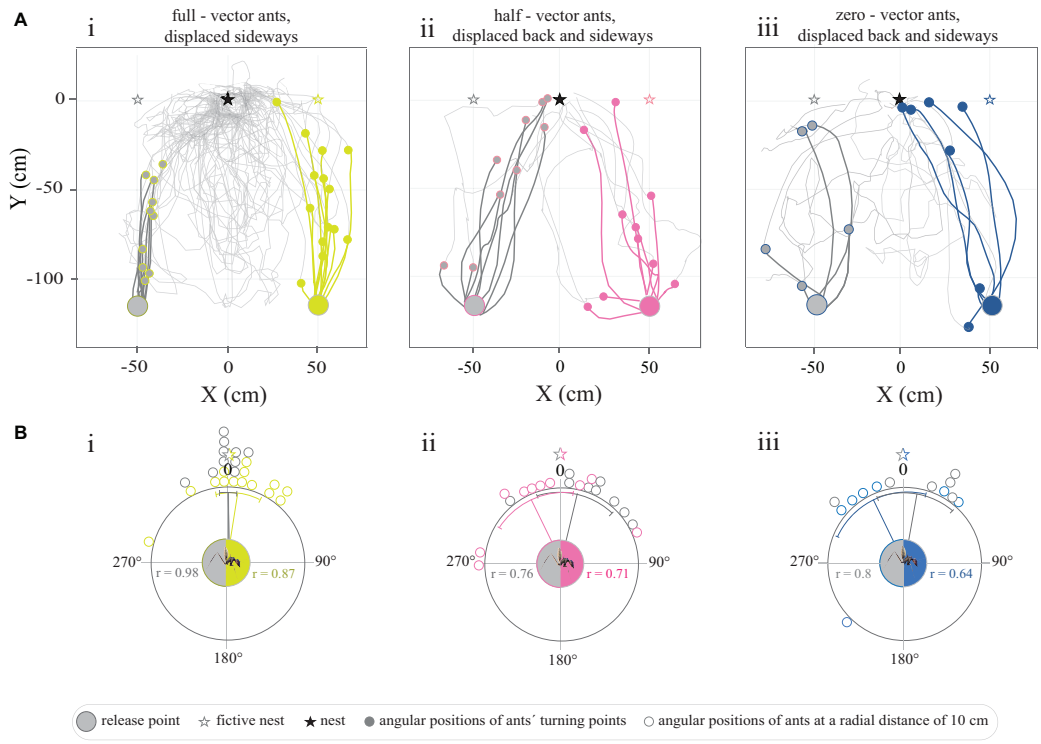

FIGURE 4
Tracks of full-vector, half-vector, and zero-vector ants displaced within the vicinity of the nest. **(A)** Trajectories represent the paths traveled upon the release of ants captured **(i)** at the feeder (full-vector ants, dark gray-yellow), **(ii)** midway on their route home (half-vector ants, dark gray-pink), or **(iii)** just before they entered their nest (zero-vector ants, dark gray-blue). Light gray paths illustrate their search. **(Bi–iii)** Circular graphs represent the angular positions of ants at a radial distance of 10 cm from the release point in relation to the normalized fictive nest direction (0°). Gray and colored lines within the circular graphs indicate mean angles, associated sectors represent the 95% confidence interval of the mean. r represents mean vector length.

Discussion

After having repeatedly foraged only 125 cm away from its nest, *C. fulvopilosus* ants displaced at a feeder first set out in the direction given by their path integrator (**Figure 4**). Then, approximately 50 cm down the path, they instead adjusted their course according to surrounding landmarks and reliably pinpointed the position of their nest entrance. These results clearly demonstrate that both navigational systems are actively engaged in the balbyter ants even when foraging only slightly more than 1 m away from their nest.

Camponotus fulvopilosus relies on path integration to initiate its return journey when on an unfamiliar territory

After transferring *C. fulvopilosus* foragers, with an expected home-vector of approximately 1.25 m, to a distant test area with a new array of landmarks, the ants ran 41.5 cm on average in the direction of their fictive nest before they started to run along a curved track, resembling the well documented search patterns of other ant species (see for example Wehner and Srinivasan, 1981; Schultheiss and Cheng, 2011; **Figure 3Ai**). This clearly demonstrated that *C. fulvopilosus* ants develop and rely on their home-vectors for homing even after repeatedly foraging over the relatively short distance of 125 cm.

The finding that the full-vector *C. fulvopilosus* ants did not run off their entire home vector before they engaged in a systematic search is similar to earlier observations in other ant species inhabiting landmark rich habitats (*Gigantiops destructor*, Beugnon et al., 2005; *Formica japonica*, Fukushi, 2001; *Melophorus bagoti*, Narendra, 2007a,b; Buehlmann et al., 2011; Cheng et al., 2012; Schultheiss et al., 2016), but contrasts to the strong adherence to the path-integrated vector in ants living in landmark-poor environments (*Cataglyphis* fortis, Buehlmann et al., 2011; see also *Melophorus sp.* in Schultheiss et al., 2016). The early break-off from the home-vector in *C. fulvopilosus* ants thus further supports the hypothesis that the adherence to the home vector is inversely correlated with the density of vegetation in the habitat of the species (Buehlmann et al., 2020a) and likely reflects a functional adaptation of the navigational system to maximize the probability of finding

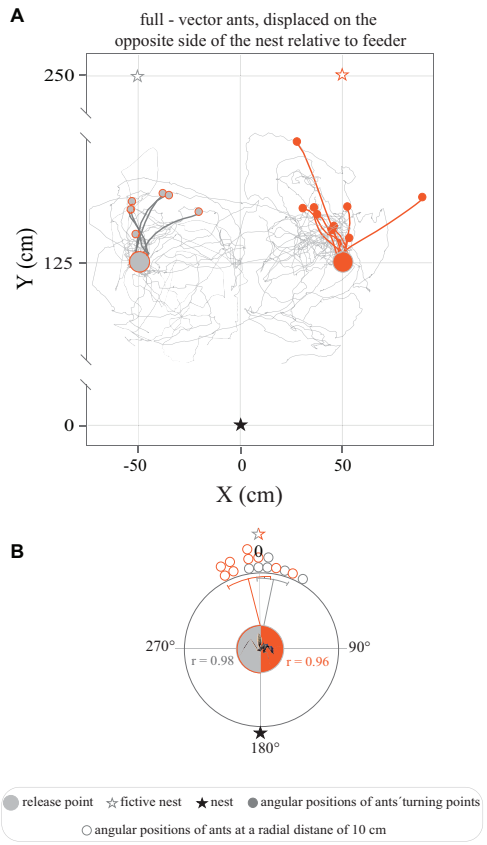

FIGURE 5
Tracks of full-vector ants displaced from the feeder to the opposite side of the nest. **(A)** Trajectories represent the paths traveled upon the release of ants captured at the feeder and moved to the opposite side of the nest, with a 50 cm displacement right or left relative to the feeder. **(B)** Circular graphs represent the angular positions of ants at a radial distance of 10 cm from the release point in relation to the normalized fictive nest direction (0°). Gray and orange lines indicate mean angles, associated sectors represent the 95% confidence interval of the mean. r represents mean vector length.

the nest (Narendra, 2007b). Interestingly, the homing dung beetle *Scarabaeus galenus*, active in the same landmark-rich habitat as *C. fulvopilosus* ants, runs off as much as 95% of their 1.25 m home-vector, before initiating a winding search for their burrows under identical experimental conditions (Dacke et al., 2020). This strong adherence to the path-integrated vector is likely explained by the apparent inability of the beetles to navigate by the use of landmarks (Dacke et al., 2020).

The transfer of zero-vector ants to the same distant test-area gained an entirely different result; these ants ran in random directions from their point of release and initiated their systematic searches around the same point in space, i.e., close to the fictive position of their nest (**Figures 3Aii,Cii**). Given the unfamiliarity of these ants with the surrounding visual scene at the test area, this outcome is not surprising but nicely demonstrates that the testing area – chosen to lie outside the foraging range of the workers – did not provide the transferred ants with any navigationally relevant visual information to point them in a nest-ward direction.

Camponotus fulvopilosus relies on path integration to initiate its return journey when foraging in the close vicinity of the nest

When displaced 50 cm sideways in the familiar surroundings around their nest, full-vector *C. fulvopilosus* foragers still followed their home vectors (i.e., they ran directly toward their fictive nests) for the first 64 ± 32 cm (right displacement) and 38 ± 16 cm (left displacement) of their return journeys (**Figure 4Ai**). After this point, they headed toward the real nest (**Figure 4Ai**), presumably guided by the landmarks around them. That is, the full-vector ants initially set out in the direction given by their home-vectors, and then switched to following the terrestrial landmark information further down the homeward route. When released at the same locations (50 cm left or right of the feeder, see **Figure 1**), displaced zero-vector ants, that had no vector or a very short vector to help point them in the correct direction, at first were more spread in their initial bearings, but were still all able to return home (**Figure 4Aiii**), most likely by using landmarks. This suggests that full-vector *C. fulvopilosus* ants, when displaced to the exact same two locations (50 cm sideway from the feeder) could also have returned home by relying solely on landmarks, but instead used their path-integrated vector to guide the initial segments of their return paths. This also held true for full-vector ants displaced from the feeder to the opposite side of the nest, that were observed to initially run directly away from their nest (**Figures 1**, **5**).

The weight given to path-integration and landmarks shifts with the relative length of the home vector

When captured midway on their route home (half-vector ants) and displaced to either of two locations (50 cm sideways from the feeder, see **Figure 1**) ants were – unlike the full-vector ants – already initially biased toward their real nest (**Figures 4Aii,Bii**). This suggests that after running off half of their home vector, the relative weight given to the directional information provided by local landmarks had increased. This corresponds with previous findings with *Cataglyphis fortis* ants that had run off 60% of their home vector and consequently responded more strongly to learnt visual landmarks than those ants that had run off only 10% of their home vector (Buehlmann et al., 2018). It has further been shown in *Melophorus bagoti* and

C. nodus ants that the weighting given to landmarks increases with accumulated visual experience (Freas and Cheng, 2017; Fleischmann et al., 2018). In general, it is believed that for most ants the relative weight given to directional information is biased toward the more reliable source of information (Reid et al., 2011; Collett, 2012; Legge et al., 2014; Wystrach et al., 2015; Wehner et al., 2016). This suggests that at the start of the short return journey (1.25 m), *C. fulvopilosus* ants weight directional information provided by the home vector more strongly than information provided by landmarks. Whether this is also the case in other ant species when foraging in the close vicinity of their nests remains to be shown.

Several navigational strategies support homing when foraging in close vicinity to the nest

Our study suggests that *C. fulvopilosus*, like many other ant species, optimizes its homing strategy by weighting the relationship between directional information provided by path integration and visual landmarks, even when foraging over the relatively short foraging distances evaluated in this study. The weighting relationship of these two navigational strategies is shaped by species specific-visual habitat characteristics (see also Cheng et al., 2012), with ants living in landmark-rich habitats relying less strongly on path integration when transferred to an unfamiliar test area or when familiar landmarks were removed (Fukushi, 2001; Beugnon et al., 2005; Narendra, 2007b; Schultheiss et al., 2016). The inclusion of landmark information into a navigational toolkit increases the precision of the navigational system as a whole (Buehlmann et al., 2020a) but comes at the cost of energy and requires an improved cognitive capacity with more complex neuronal implementation (Rössler, 2019; Buehlmann et al., 2020b; Kamhi et al., 2020). Many ant species perform learning walks, including frequent rotations around their own body axis, for several days to establish a *de novo* long-term memory of stable nest related visual cues (Fleischmann et al., 2016, 2017; Jayatilaka et al., 2018; Zeil and Fleishmann, 2019). Whether *C. fulvopilosus* ants also perform learning walks or acquire their landmark information by some other way is yet unknown, but the ants convincingly demonstrate the cognitive capacity to learn and process this type of navigation-relevant visual information. Starting their short return journeys in the direction dictated by their home-vector probably places them in the best possible position to utilize the stored memory of landmarks in the most efficient way.

Interestingly, homing beetles – which inhabit the same environment as the *C. fulvopilosus* ants – show no indication of rotations (to look back at their burrow), learning walks of increasing distance or any other signs of the inclusion of landmarks for navigational purposes (Dacke et al., 2020). In addition, the beetles engage in an extended, circling search to locate their semi-permanent burrows in response to 50 cm sideway displacements at the feeder (Dacke et al., 2020). Equipped with the ability to correct for these types of passive displacements by using landmarks, an ant will locate its nest much more efficiently (see **Figure 4** in this study and Figure 5 in Dacke et al., 2020). These differences in navigation strategies likely reflect the ecological needs of these two groups of navigators; an ant without a nest and a colony perishes rapidly, while a solitary beetle can dig a new burrow within the next hour with little fitness cost.

In summary, the combination of path-integration and landmarks for navigation effectively guides *C. fulvopilosus* – and other ants – to quickly orient themselves in a nest-ward direction. Further down the path, known landmark memories allow them to locate their nests more accurately even if displaced from their intended route (experimentally or by a strong gust of wind). Our results thus emphasize the benefit of several navigational strategies to support homing even when foraging only a couple of meters away from home.

Data availability statement

The raw data supporting the conclusions of this article will be made available by the authors, without undue reservation.

Author contributions

AY, EB, and MD designed the experiments. AY, EB, MD, MB, and JF performed the experiments. YG designed the software for data analysis. AY analyzed the data. AY and MD wrote and revised the manuscript. All authors have read, revised, and agreed to the published version of the manuscript.

Funding

This work was supported by the Human Frontiers Science Program (RGP0002/2017, EB), Swedish Research Council (2020-04046, MD), and the European Research Council (817535-Ultimate-COMPASS, MD).

Acknowledgments

We are grateful to Matthew Collett for helpful discussions when interpreting the data and Valentin Gillet for counting ants for the activity rhythm measurements. We also thank Sharon and Alwyn Smit at Stonehenge game farm for hosting us during this project.

Conflict of interest

The authors declare that the research was conducted in the absence of any commercial or financial relationships that could be construed as a potential conflict of interest.

Publisher's note

All claims expressed in this article are solely those of the authors and do not necessarily represent those of their affiliated organizations, or those of the publisher, the editors and the reviewers. Any product that may be evaluated in this article, or claim that may be made by its manufacturer, is not guaranteed or endorsed by the publisher.

Supplementary material

The Supplementary Material for this article can be found online at: https://www.frontiersin.org/articles/10.3389/fnint.2022.914246/full#supplementary-material

References

Beugnon, G., Lachaud, J., and Chagne, P. (2005). Use of long-term stored vector information in the neotropical ant *Gigantiops destructor*. *J. Insect Behav.* 18, 415–432. doi: 10.1007/s10905-005-3700-8

Bezanson, J., Edelman, A., Karpinski, S., and Shah, V. B. (2017). Julia: a fresh approach to numerical computing. *SIAM Rev.* 59, 65–98. doi: 10.1137/141000671

Buehlmann, C., Cheng, K., and Wehner, R. (2011). Vector-based and landmark-guided navigation in desert ants inhabiting landmark-free and landmark-rich environments. *J. Exp. Biol.* 214, 2845–2853. doi: 10.1242/jeb.054601

Buehlmann, C., Fernandes, A. S. D., and Graham, P. (2018). The interaction of path integration and terrestrial visual cues in navigating desert ants: what can we learn from path characteristics? *J. Exp. Biol.* 221:jeb167304. doi: 10.1242/jeb.167304

Buehlmann, C., Mangan, M., and Graham, P. (2020a). Multimodal interactions in insect navigation. *Anim. Cogn.* 23, 1129–1141. doi: 10.1007/s10071-020-01383-2

Buehlmann, C., Wozniak, B., Goulard, R., Webb, B., Graham, P., and Niven, J. E. (2020b). Mushroom bodies are required for learned visual navigation, but not for innate visual behavior, in ants. *Curr. Biol.* 30, 3438–3443.e2. doi: 10.1016/j.cub.2020.07.013

Cheng, K., Middleton, E. J. T., and Wehner, R. (2012). Vector-based and landmark-guided navigation in desert ants of the same species inhabiting landmark-free and landmark-rich environments. *J. Exp. Biol.* 215, 3169–3174. doi: 10.1242/jeb.070417

Collett, M. (2012). How navigational guidance systems are combined in a desert ant. *Curr. Biol.* 22, 927–932. doi: 10.1016/j.cub.2012.03.049

Collett, M., Collett, T. S., Bisch, S., and Wehner, R. (1998). Local and global vectors in desert ant navigation. *Nature* 394, 269–272. doi: 10.1038/28378

Dacke, M., El Jundi, B., Gagnon, Y., Yilmaz, A., Byrne, M., and Baird, E. (2020). A dung beetle that path integrates without the use of landmarks. *Anim. Cogn.* 23, 1161–1175. doi: 10.1007/s10071-020-01426-8

Fleischmann, P. N., Christian, M., Mueller, V. L., Roessler, W., and Wehner, R. (2016). Ontogeny of learning walks and the acquisition of landmark information in desert ants, *Cataglyphis fortis*. *J. Exp. Biol.* 219, 3137–3145. doi: 10.1242/jeb.140459

Fleischmann, P. N., Grob, R., Wehner, R., and Rössler, W. (2017). Species-specific differences in the fine structure of learning walk elements in *Cataglyphis* ants. *J. Exp. Biol.* 220, 2426–2435. doi: 10.1242/jeb.158147

Fleischmann, P. N., Rössler, W., and Wehner, R. (2018). Early foraging life: spatial and temporal aspects of landmark learning in the ant *Cataglyphis noda*. *J. Comp. Physiol. A* 204, 579–592. doi: 10.1007/s00359-018-1260-6

Freas, C. A., and Cheng, K. (2017). Learning and time-dependent cue choice in the desert ant, *Melophorus bagoti*. *Ethology* 123, 1–13. doi: 10.1111/eth.12626

Fukushi, T. (2001). Homing in wood ants, *Formica japonica*: use of the skyline panorama. *J. Exp. Biol.* 204, 2063–2072. doi: 10.1242/jeb.204.12.2063

Jayatilaka, P., Murray, T., Narendra, A., and Zeil, J. (2018). The choreography of learning walks in the Australian jack jumper ant *Myrmecia croslandi*. *J. Exp. Biol.* 221:art.jeb185306. doi: 10.1242/jeb.185306

Josens, R., Eschbach, C., and Giurfa, M. (2009). Differential conditioning and long- term olfactory memory in individual *Camponotus fellah* ants. *J. Exp. Biol.* 212, 1904–1911. doi: 10.1242/jeb.030080

Kamhi, J. F., Barron, A. B., and Narendra, A. (2020). Vertical lobes of the mushroom bodies are essential for view-based navigation in Australian *Myrmecia* ants. *Curr. Biol.* 30, 3432–3437. doi: 10.1016/j.cub.2020.06.030

Legge, E. L. G., Wystrach, A., Spetch, M. L., and Cheng, K. (2014). Combining sky and earth: desert ants (*Melophorus bagoti*) show weighted integration of celestial and terrestrial cues. *J. Exp. Biol.* 217, 4159–4166. doi: 10.1242/jeb.107862

Marsh, A. C. (1986). Checklist, biological notes and distribution of ants in the central Namib Desert. *Madoqua* 14, 333–344.

Mittelstaedt, H. (1983). The role of multimodal convergence in homing by path integration. *Fortschr. Zool.* 28, 197–212.

Müller, M., and Wehner, R. (1988). Path integration in desert ants, *Cataglyphis fortis*. *Proc. Natl. Acad. Sci. U.S.A.* 85, 5287–5290. doi: 10.1073/pnas.85.14.5287

Müller, M., and Wehner, R. (2010). Path integration provides a Scaffold for landmark learning in desert ants. *Curr. Biol.* 20, 1368–1371. doi: 10.1016/j.cub.2010.06.035

Narendra, A. (2007a). Homing strategies of the Australian desert ant *Melophorus bagoti* II. Interaction of the path integrator with visual cue information. *J. Exp. Biol.* 210, 1804–1812. doi: 10.1242/jeb.02769

Narendra, A. (2007b). Homing strategies of the Australian desert ant *Melophorus bagoti* I. Proportional path-integration takes the ant half-way home. *J. Exp. Biol.* 210, 1798–1803. doi: 10.1242/jeb.02768

Reid, S. F., Narendra, A., Hemmi, J. M., and Zeil, J. (2011). Polarised skylight and the landmark panorama provide night-active bull ants with com- pass information during route following. *J. Exp. Biol.* 214, 363–370. doi: 10.1242/jeb.049338

Robertson, H. G., and Zachariades, C. (1997). Revision of the *Camponotus fulvopilosus* (De Geer) species-group (Hymenoptera: Formicidae). *Afr. Entomol.* 5, 1–18.

Rössler, W. (2019). Neuroplasticity in desert ants (Hymenoptera: Formicidae) – importance for the ontogeny of navigation. *Myrmeco. News* 29, 1–20.

Schoenberg, I. J. (1971). On equidistance cubic spline interpolation. *Bull. Am. Math. Soc.* 77, 1039–1044. doi: 10.1090/S0002-9904-1971-12853-7

Schultheiss, P., and Cheng, K. (2011). Finding the nest: inbound searching behaviour in the Australian desert ant, *Melophorus bagoti*. *Anim. Behav.* 81, 1031–1038. doi: 10.1016/j.anbehav.2011.02.008

Schultheiss, P., Stannard, T., Pereira, S., Reynolds, A. M., Wehner, R., and Cheng, K. (2016). Similarities and differences in path integration and search in two species of desert ants inhabiting a visually rich and a visually barren habitat. *Behav. Ecol. Sociobiol.* 70, 1319–1329. doi: 10.1007/s00265-016-2140-0

Wehner, R., and Räber, F. (1979). Visual spatial memory in desert ants, *Cataglyphis bicolor* (Hymenoptera: Formicidae). *Experientia* 35, 1569–1571. doi: 10.1007/BF01953197

Wehner, R., and Srinivasan, M. V. (1981). Searching behavior of desert ants, genus *Cataglyphis* (Formicidae, Hymenoptera). *J. Comp. Physiol.* 142, 315–338. doi: 10.1007/BF00605445

Wehner, R., Hoinville, T., Cruse, H., and Cheng, K. (2016). Steering intermediate courses: desert ants combine information from various navigational routines. *J. Comp. Physiol. A* 202, 459–472. doi: 10.1007/s00359-016-1094-z

Wehner, R., Meier, C., and Zollikhofer, C. (2004). The ontogeny of foraging behaviour in desert ants, *Cataglyphis bicolor*. *Ecol. Entomol.* 29, 240–250.

Wystrach, A., Mangan, M., and Webb, B. (2015). Optimal cue integration in ants. *Proc. Biol. Sci.* 282:20151484. doi: 10.1098/rspb.2015.1484

Yilmaz, A., Aksoy, V., Camlitepe, Y., and Giurfa, M. (2014). Eye structure, activity rhythms, and visually driven behaviour are tuned to visual niche in ants. *Front. Behav. Neurosci.* 8:205. doi: 10.3389/fnbeh.2014.00205

Yilmaz, A., Dyer, A. G., Rössler, W., and Spaethe, J. (2017). Innate colour preference, individual learning and memory retention in the ant *Camponotus blandus*. *J. Exp. Biol.* 220, 3315–3326. doi: 10.1242/jeb.158501

Yilmaz, A., Gagnon, Y., Byrne, M., Baird, E., and Dacke, M. (2021). Cold-induced anesthesia impairs path integration memory in dung beetles. *Curr. Biol.* 32:2. doi: 10.1016/j.cub.2021.10.067

Yilmaz, A., Lindenberg, A., Albert, S., Grübel, K., Spaethe, J., Rössler, W., et al. (2016). Age-related and light-induced plasticity in opsin gene expression and in primary and secondary visual centers of the nectar-feeding ant *Camponotus rufipes*. *Devel. Neurobio.* 76, 1041–1057. doi: 10.1002/dneu.22374

Zeil, J. (1998). Homing in fiddler crabs (*Uca lactea* annulipes and *Uca vomeris*: Ocypodidae). *J. Comp. Physiol. A* 183, 367–377. doi: 10.1007/s003590050263

Zeil, J., and Fleishmann, P. N. (2019). The learning walks of ants (Hymenoptera: Formicidae). *Myrmecol. News* 29, 93–110.

frontiers | Frontiers in Neural Circuits

TYPE Original Research
PUBLISHED 23 September 2022
DOI 10.3389/fncir.2022.940989

OPEN ACCESS

EDITED BY
Susanne Hoffmann,
Max Planck Institute for Ornithology, Germany

REVIEWED BY
Mélanie Guigueno,
McGill University, Canada
Gianina Ungurean,
Max Planck Institute for Biological Intelligence, Germany

*CORRESPONDENCE
Matt Gaidica
mgaidica@umich.edu

RECEIVED 10 May 2022
ACCEPTED 05 September 2022
PUBLISHED 23 September 2022

CITATION
Gaidica M and Dantzer B (2022) An implantable neurophysiology platform: Broadening research capabilities in free-living and non-traditional animals.
Front. Neural Circuits 16:940989.
doi: 10.3389/fncir.2022.940989

An implantable neurophysiology platform: Broadening research capabilities in free-living and non-traditional animals

Matt Gaidica[1]* and Ben Dantzer[1,2]

[1]Department of Psychology, University of Michigan, Ann Arbor, MI, United States, [2]Department of Ecology and Evolutionary Biology, University of Michigan, Ann Arbor, MI, United States

Animal-borne sensors that can record and transmit data ("biologgers") are becoming smaller and more capable at a rapid pace. Biologgers have provided enormous insight into the covert lives of many free-ranging animals by characterizing behavioral motifs, estimating energy expenditure, and tracking movement over vast distances, thereby serving both scientific and conservational endpoints. However, given that biologgers are usually attached externally, access to the brain and neurophysiological data has been largely unexplored outside of the laboratory, limiting our understanding of how the brain adapts to, interacts with, or addresses challenges of the natural world. For example, there are only a handful of studies in free-living animals examining the role of sleep, resulting in a wake-centric view of behavior despite the fact that sleep often encompasses a large portion of an animal's day and plays a vital role in maintaining homeostasis. The growing need to understand sleep from a mechanistic viewpoint and probe its function led us to design an implantable neurophysiology platform that can record brain activity and inertial data, while utilizing a wireless link to enable a suite of forward-looking capabilities. Here, we describe our design approach and demonstrate our device's capability in a standard laboratory rat as well as a captive fox squirrel. We also discuss the methodological and ethical implications of deploying this new class of device "into the wild" to fill outstanding knowledge gaps.

KEYWORDS

physiology, sleep, accelerometer, closed-loop, wireless, implantable

Introduction

Over the past 100 years, behavioral and physiological research has undergone a striking technological progression. Increasingly, microscopes, binoculars, and restrictive manipulandum are being replaced by small electronics that promote freedom of movement while describing internal and external animal states with unprecedented

accuracy (Wilson et al., 2008; Wilmers et al., 2015; Williams et al., 2020). Major advances were pioneered in aquatic birds, demonstrating the utility of hermetically sealed "biologgers" to characterize subsurface porpoising and diving behavior (Butler and Woakes, 1979; Yoda et al., 1999). Breakthroughs in component miniaturization, computational capacity, and low-power optimization have all contributed to the modern form factor and capability of biologgers and similar animal-borne telemetry systems (Wilmers et al., 2015; Harcourt et al., 2019; Whitford and Klimley, 2019). For example, spatially resolute wireless tracking systems have been used to investigate social complexity in bats (Ripperger et al., 2016, 2019), understand nesting in starlings (Kirkpatrick et al., 2021), and pave the way for characterizing complex pair-bonding relationships. Small GPS loggers have utilized novel satellite networks to research migratory patterns of birds (Jetz et al., 2022) and were key to identifying the single longest migration on record in a gray whale (Mate et al., 2015). Increasingly, technology is enabling a better understanding of how animals interact with their natural environment to serve fundamental scientific and conservational endpoints (Chmura et al., 2018; Jetz et al., 2022).

Despite major innovations, a species-wide gap remains in using biologgers to understand neural physiology outside of the laboratory (Rattenborg et al., 2017). Behavior restricted by neural recording techniques that require a tether or enclosed recording chamber (Aulehner et al., 2022), and the removal of natural cues regulating sleep-wave cycles (called, *Zeitgebers*) such as light, temperature, social interaction, and resource availability may drastically affect, or even nullify, physiological interpretations of such data. In particular, understanding the natural transitions between rest and activity (or vice versa), and the complex architecture of neural states within sleep itself, represents a major barrier in describing the function and evolutionary process of sleep (Roth et al., 2010; Aulsebrook et al., 2016; Eban-Rothschild et al., 2017; Anafi et al., 2019). For example, discovering that birds sleep mid-flight (Rattenborg et al., 2016) or that some animals sleep one hemisphere at a time (Mascetti, 2016) is contrary to our conventional understanding of how sleep and movement are related. Sleep remains an enigmatic quiescent state that plays a number of vital roles, both for individuals and groups (Mistlberger and Skene, 2004). Although accelerometers have been widely deployed and repurposed to meet challenges in quantifying sleep, they are fraught with validation issues in animals that are not easily observed (Gaidica et al., 2021). For example, Loftus et al. (2022) used collar-mounted accelerometers to determine sleep but ultimately failed to find evidence for a change in sleep intensity after sleep deprivation in wild non-human primates. This finding is inconsistent with decades of research suggesting that electrophysiological "deep" sleep has a rebounding effect to support homeostasis (Rechtschaffen, 1998), calling to question the utility of collar (or wrist) mounted inertial sensors.

Progress toward recording or transmitting neural activity in free-ranging animals has been made using small, externally fitted biologgers (Vyssotski et al., 2006; Rattenborg et al., 2008; Hoffmann et al., 2019; Massot et al., 2019). However, these devices are limited to species and environments where attaching the device directly to the head does not threaten naturalistic behaviors, such as entering and exiting burrows or nests. Therefore, until similar devices can be embedded within the organism and subsequently removed without consequence, the repertoire of species for which neural data (which provides crucial information about sleep) can be collected will be inherently limited (Forin-Wiart et al., 2019). To that end, implantable telemetry systems that require nearby antennas offer a glimpse into how such a feat can be accomplished (Chang et al., 2011), but at present, fully "autonomous" solutions are lacking.

In this study, we demonstrate progress toward a bridge between laboratory and field science that can be applied across species. Specifically, we developed an implantable biologging platform capable of broadening the understanding of neurophysiology and behavior in freely moving animals (**Figure 1**). Our biologger is based around a low-cost, highly capable Bluetooth Low Energy (BLE; see **Table 1**) microprocessor that schedules onboard recording of biopotential data. We first explored the general constraints and possibilities of embedded BLE technology by using our biologger to perform closed-loop audio stimulation in a freely behaving rat, a technique that could be used to enhance slow-wave (SW) neural rhythms that occur in NREM sleep (Bellesi et al., 2014) or tied together with other behavioral paradigms. Next, we demonstrated the utility of an implantable device by recording sleep in a captive squirrel from the comfort of their nest box. We showcase several important advancements in biologging, including sterile best practices, the ability for "wild" animals to survive the biologger implant and explant processes, and the increased capability of a platform that can be reconfigured in real-time and repurposed for multiple deployments. Although we focused on neurophysiology, the onboard accelerometer make more conventional insights into animal movement and behavioral motifs possible (Chimienti et al., 2016; Hammond et al., 2016). Finally, our biologger's native wireless capability enables emerging use cases (e.g., proximity logging and spatial trilateration) to address further gaps in neurophysiological and behavioral research.

Materials and methods

In this section, we outline the biologger hardware and software architecture (see section "Hardware and software architecture"), biological interface (section "Biological interface"), surgical procedures (section "Surgical procedures"),

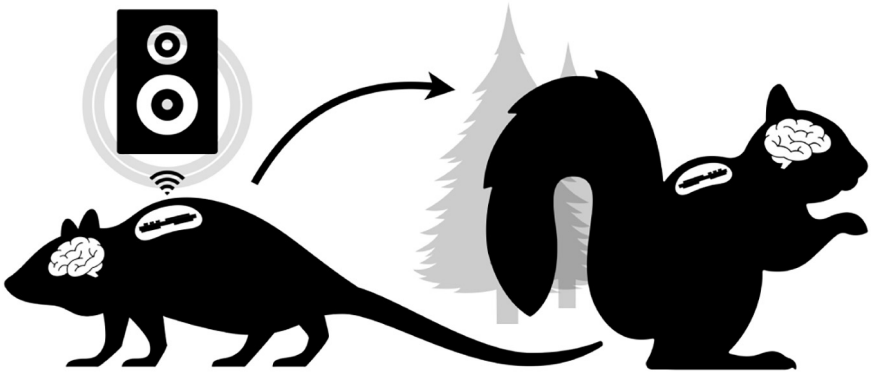

FIGURE 1
Conceptual Overview. The laboratory setting (left) does not have tools to enable freely behaving neurophysiology in novel experimental paradigms (e.g., low-latency wireless cuing of an external speaker to modulate neural rhythms in real-time). Ideally, the same "biologger" platform can translate to ethical free-ranging experiments (right) utilizing alternative device modes that support autonomous deployment.

and metrics and statistics (section "Metrics and statistics") presented in our results.

Hardware and software architecture

Biologger hardware

Power is provided by a 20 mm, 3 V coin-cell battery (2032, Energizer) that is fed into a series of voltage regulators (Figure 2A). The 1.8 V regulation (TPS62243, Texas Instruments) provides the main power rail for all components and is then inverted (MAX1720, Analog Devices) and regulated to −1.5 V (TPS72301, Texas Instruments) and 1.5 V (TPS7A2015, Texas Instruments) to provide a bipolar source. Digital components consist of the Bluetooth Low-energy (BLE, Version 5.2) Microprocessor (MCU; CC2652R, Texas Instruments) that performs logic, computation, and wireless communication through a single chip RF Balun (2450BM14G0011, Johanson Technology) and 2.4 GHz chip antenna (2450AT42B100, Johanson Technology). The BLE-MCU passively senses battery voltage and an optional external thermistor (GA100K6A1IA, TE Connectivity; single-dotted lines), as well as communicates across two, 3-wire SPI buses (double-dashed lines). The first SPI bus accesses a 6-axis accelerometer and gyroscope inertial sensor (LSM6DSOXTR, STMicroelectronics) and 2 Gb of NAND memory storage (MT29F2G01, Micron). The second SPI bus accesses the Analog section consisting of a 4-channel, 24-bit analog front-end biopotential amplifier (ADS1294, Texas Instruments) which collects bipolar biopotentials through an onboard passive filter network (0.25 Hz high-pass and antialiasing) and is available through a 1.27 mm-spaced pad array outfitted with a gold pin solder connector (851-43-008-10-001000, Mill-Max). Digital grounds are planar and tied to the analog circuits through a ground star. The printed circuit board (PCB; manufactured by PCBONLINE) has four layers (1 oz copper, 0.062" total thickness; Figure 2B) and was designed using KiCAD. We attempted to separate digital and analog components between the middle layers, and ground planes were structured according to manufacturer recommendations. All components (Figure 2C) were encased in 3D-printed biocompatible acrylic (Stratasys J750 with M3 crystal resin, designed with Autodesk Fusion 360). Electrode fabrication and silicone encapsulation are covered in detail below. The gross weight of the biologger was approximately 8.5 g (34% battery, 24% PCB, 22% 3D-printed case, and 20% epoxy and silicone).

A robust battery connection was required for this application. Metallic batteries can be heat damaged by soldering directly to their surface, and thus, we welded our own tabs to each side using a miniature spot welder (*ι*SW-001, Montex). Once welded, the cathode (positive) tab was directly soldered (X-TRONIC 5000 rework station, AIM 0.015" solder) to the biologger using a specially designed PCB pad, and the anode (negative) tab was connected to an underlying PCB pad using a short length of wire (26 gauge, Adafruit Industries). All soldering was performed with a filtered fume extractor (FES150, KNOKOO) and washed using flux remover (4140A, MG Chemicals).

Biologger software

Biologger software was developed in the C programming language using the Texas Instruments SDK (Version 5.2) within Code Composer Studio. Programming was made possible using a Texas Instruments development board (LP-CC2652RB) and a custom circuit board interface to supply power and communication to an 8-pin programming port on the biologger. The native Texas Instruments power policy was used to achieve low-power idle modes which automatically engage between application tasks.

TABLE 1 Glossary.

Term	Definition
Bluetooth low energy (BLE)	A wireless network technology operating in the 2.4 GHz band standardized by the Bluetooth Special Interest Group.
BLE: central device	A device that connects to many peripheral devices often in charge of reading, writing, or receiving notifications/indications of BLE characteristics.
BLE: peripheral device	A device that advertises a service with many individual characteristics (i.e., pieces of data).
BLE: advertising	Advertisements contain limited information and are required to initiate a BLE connection.
BLE: service	Services can have many characteristics (e.g., a car dashboard service may contain characteristics for speed and fuel).
BLE: characteristic	Characteristics describe and house a single piece of variable-length data. These can be read from, written to, notify (without read-receipt), or indicate (with read-receipt).
BLE: latency	Latency is the time it takes for data to wirelessly transfer. This can be modified by the central-peripheral connection settings and is inherently limited by random delays (<10 ms) in the BLE protocol to avoid data collisions.
Printed circuit board (PCB)	A multilayer, precisely machined epoxy resin laminate board that is computer-designed and connects soldered components.
Biopotential	Any biological signal detectable by means of recording a difference in voltage between two leads.
Electroencephalography (EEG)	Biopotentials detected from outside the brain, typically representing cortical neural activity.
Light emitting diode (LED)	Small lights that can be soldered to a PCB.
Slow-wave activity (SWA)	A neural biopotential typically observed during non-rapid eye movement sleep characterized by slow (0.5–4 Hz), large amplitude oscillations over the prefrontal cortex.

Onboard biopotential filtering was achieved using the ARM-based CMSIS digital signal processing library and biquad cascade IIR filters. Bandpass filters coefficients were designed using ASN Filter Designer (Advanced Solutions Nederland B.V.).

The biologger runs some utilities regardless of the experiment, including a 1-s timer that maintains time and records biologger voltage, thermistor temperature, and the current time every 60 s for *post hoc* retrieval. Time is also logged during specific user actions, such as when settings or operating modes are changed. If battery voltage is less than 2.4 V the biologger settings are reset to defaults and writing to memory is halted to avoid undefined behavior that occurs outside of normal operating specifications. If the onboard memory is full, further writes will be rejected. Given these constraints, the bio-logger will eventually drain itself and cease to operate in a graceful manner. Specific functions initiated by the user include a recording scheduler that subsamples accelerometer (1 and 10 Hz options) and biopotential (125 Hz) data at regular intervals (e.g., record for 5 min every 60 min) and a closed-loop system which is described in detail below.

All data is stored in non-volatile (i.e., to persist without power) NAND memory in a serial fashion as self-contained, 32-bit packets. The first 8 bits encode a data type, and the remaining 24 bits encode data. This method makes data retrieval standard and robust, removing the overhead of implementing a filesystem that can be easily corrupted. Furthermore, although a filesystem has compression capabilities, should the biologger ever be damaged or undergo a catastrophic failure it is likely that partial data can be recovered if the memory module is intact.

Biologger configuration utility

In general, custom BLE service characteristics enable the transfer of data, define the biologger state, and scheduled routines. The primary interface to control settings and view streaming data were built using Xcode (Version 13) using the Swift programming language. The app (called, "ESLO") was deployed to an iPhone 12 Pro Max (**Figure 3A**). Biologgers were detected and connected based on a static address pattern. The app syncs date-time information to the biologger's internal clock and indicates vital information (**Figure 3A**, upper-right): signal strength, battery voltage, thermistor temperature, motion activity, and current memory storage address. A built-in terminal area (**Figure 3A**, upper-left) allows for debugging messages to be printed and exported following a connection. Recording schedules, biopotential channels (labeled "EEG"), closed-loop controls (labeled "SWA"), and accelerometer modes and advertising modes ("Adv+") are modified by the middle control set. Settings are synced from the biologger upon connecting and then manually "pushed" to the biologger after being modified. A reset button sets the biologger memory address to zero and also initiates "shelf mode" (see operating modes in **Table 2**). The dark panel (bottom) streams real-time data from the biologger: shown are 3-axes of accelerometer data and 2 EEG/biopotential channels. Centering data around zero ("Rm Offset") and use of scientific units ("Sci Units") can be toggled. A biologger can only be connected to one central device to avoid conflicts. Once the iOS app disconnects, the biologger will behave according to user settings. Subsequent connections to the biologger can be made based on the advertising interval, which defaults to 500 ms, but can be extended to a random interval of 30–60 s ("Adv+") to decrease advertising power and provide a non-overlapping beacon if multiple biologgers are deployed in the same area.

Biologger data retrieval

The biologger has an 8-pin programming and communication port where a "data dump" can occur using a standard two-wire serial protocol. A dedicated module was built for this function using an Arduino microcontroller with

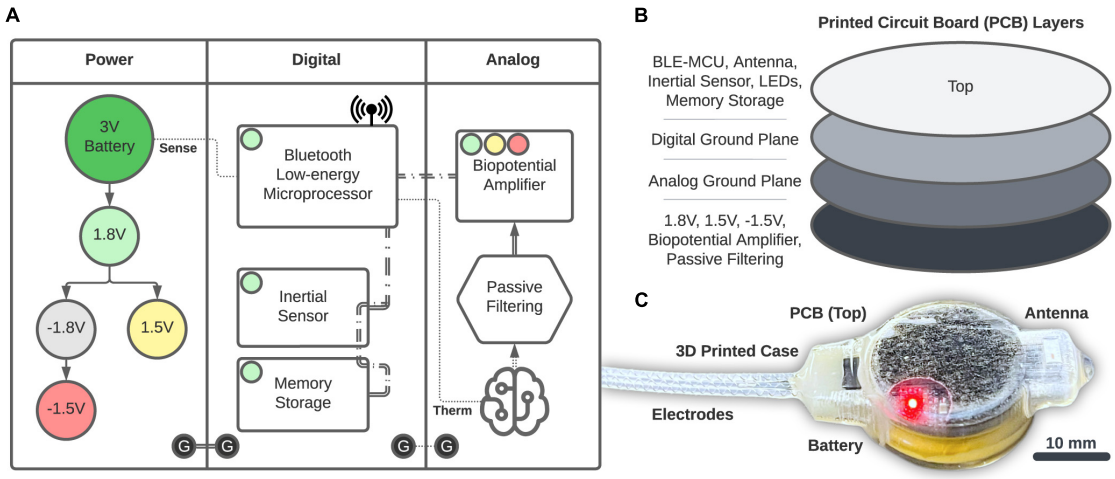

FIGURE 2
Biologger hardware. **(A)** High-level overview of the power, digital, and analog systems. **(B)** Component placement relative to the four-layer PCB. **(C)** The 3D-printed case with the PCB and electrodes encapsulated in silicone.

an onboard micro-SD card (Figure 3B; Feather M0 Adalogger, Adafruit). In brief, after biologgers were explanted, extracted from their case, and cleaned, a custom 3D-printed clamp with an 8-pin pogo connector was used to break out the biologger programming pins. The biologger was then inserted into the data dump module and data was transferred from the biologger memory module to the micro-SD card. Although we also created a wireless data retrieval utility, having a dedicated system to offload data was simpler. Once the data is retrieved, the biologger is ready to be reused, sparring only the soldered electrode connector which is met with epoxy during encasing.

Closed-loop control

The biologger is capable of performing low-latency detection of neural rhythms when specific criteria are met. The closed-loop mode begins with a base station (LP-CC2652R1, Texas Instruments) connecting to the biologger, which is uniquely identified through a static address. After connecting, the biologger fills a fixed-size rolling buffer with incoming single-channel EEG data. After initially filling the buffer with 2 s of data, a detection algorithm is performed every 100 ms. We focused on the SW frequency band (0.5–4 Hz) characteristic of NREM sleep. The detection algorithm begins by decomposing a Fourier transform and finding the center frequency (F_c) and phase of the ongoing neural rhythm. If F_c falls within the SW band, the ratio between the SW band power and power in the 6–12 Hz (empirically derived) range meets the user-set threshold, and the max amplitude of the bandpass filtered SW data (0.5–4 Hz Butterworth) meets a user-set threshold, the algorithm continues. If F_c is detected as being greater than 2 Hz, the algorithm is rerun on only the tail-end (1-s worth) of data to increase temporal sensitivity. The biologger packages relevant metadata including time, trial number, F_c, and the phase at F_c for wireless transmission (16 bytes total) to the base station.

When the base station receives the detection packet, it calculates a delay to play a 50 ms audio tone centered on a specific phase of F_c. Thus, phase precise closed-loop audio stimulation is achieved. The audio tone (calibrated to 50 dB) is generated by a standalone pink noise generator (NOISE2, Electric Druid) and amplification circuit with a manual volume knob. A bicolor LED was placed in the video frame of an overhanging camera to coordinate *post hoc* analysis of trials. Sham trials that excluded audio occurred with a 10% probability and were indicated by the LED as red versus green to easily differentiate trial conditions in video.

Once the biologger sends the stimulation packet, it continues to collect peri-detection biopotential data for another 2 s. After the entire trial buffer (4 s) is full, the biologger sends the entire data stream to the base station and saves it with the trial metadata to a micro-SD card. Trial metadata and biopotential data were combined with video data using custom scripts in MATLAB to generate peri-stimulus plots, as well as videos to ensure device function and animal behavioral state.

Biological interface

Electrodes

Electrodes are typically made of a single piece of solid wire using a variety of different anticorrosive, biocompatible metals and alloys (Geddes and Roeder, 2003). Solid wire has the advantage of low resistivity but can easily shear when bent only a few times. A multi-strand cable is worse yet, as air gaps between wires can wick, collect, and hold moisture which

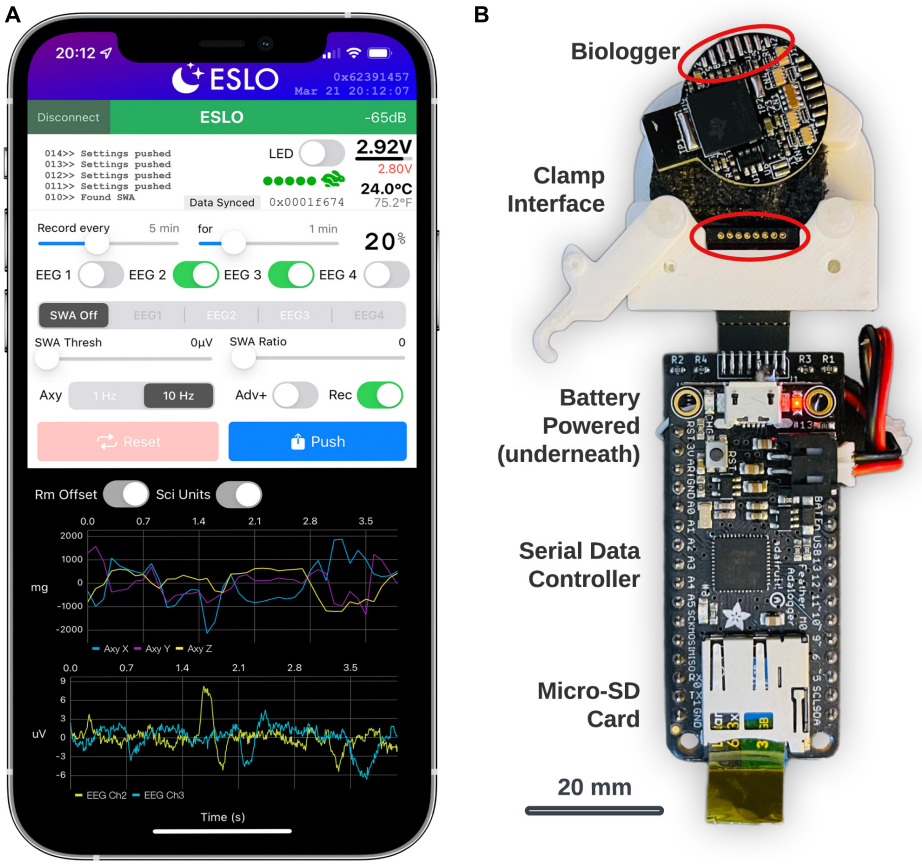

FIGURE 3
Biologger iOS app configuration utility and data dump module. **(A)** The app is shown in a connected state with a biologger. These settings represent a recording schedule mode where two channels of biopotentials (EEG2 and EEG3) will record with a 20% duty cycle and accelerometer (Axy) data will record at 10 Hz. **(B)** The data dump module is shown below the biologger interface. The bottom of the biologger is displayed here to appreciate how the programming port pins interface with the pogo connector (circled in red) in the custom clamp module. Data from the biologger memory is transferred serially through the main data controller board on the micro-SD card.

TABLE 2 Operating modes and power estimates.

Mode	Description	Current	Power	Biologger lifetime
Shelf	BLE radio is off until the biologger detects significant motion ("shake to wake")	44 µA	79.2 µW	6.8 years
Beacon	Biologger advertises its BLE service and becomes connectable every 30–60 s	0.5 mA	0.9 mW	40 days
Connected	Biologger is actively connected to a central device (e.g., iOS app)	2.3 mA	4.14 mW	4.3 days
Biopotentials	All 4 biopotential channels are on with 1 Hz accelerometer	2.8 mA	5.04 mW	3.5 days
Recording Ex. 1	2 biopotentials, 1 Hz accelerometer record 1 min every 5 min (20% duty cycle)	0.48 mA	0.86 mW	20 days
Recording Ex. 2	10 Hz accelerometer is always recording	130 µA	234 µW	76 days

All estimates are based on a 2032 battery (3 V, 240 mAh) operating at 85°F.

degrades performance. Therefore, we developed a method to create single-conductor, helical (i.e., wound) electrodes not entirely unlike those used in human pacemaker applications (see also, Open Source Instruments online methods). We used 36 gauge (0.127 mm) 80 nichrome wire (Master Wire Supply) as the electrode and a piece of 0.38 mm steel music wire to wrap the electrodes. The nichrome and music wire were autoclaved before constructing the electrodes. First, the nichrome wire was attached to the top of the music wire with hot glue. Once secured, the nichrome wire was wrapped around the music wire

to create the helix at a rate of roughly 10 turns per cm, and for a length of 30 cm. The nichrome wire was then clipped at both ends of the music wire and slid off. A sterile syringe (3 ml) was then filled with medical-grade silicone (A-100, Factor II). In preparation, translucent heat shrink tubing (Flexible 1.17 mm, Alpha Wire) was cold sterilized in a glutaraldehyde solution (Wavicide 01, Medical Chemical Corporation) for 12 h and then air-dried. The helical nichrome was then inserted into the heat shrink tubing and cinched at one end using a blunt needle to which the syringe was attached (using a Luer-style twist lock) and then local heat was applied to this junction to create a temporary seal. The syringe was then depressed to force the silicone into the tube cavity covering about 50% of the electrode. The heat shrink was then pinched at the syringe junction so it could not slide off and heated toward the open end of the heat shrink with moderate force to elongate the tubing as it was heated, ultimately enclosing the electrode and forcing the silicone into the remaining end of the heat shrink tubing. After the silicone encapsulated the wire, the electrode unit was pulled off of the blunt needle (and syringe) and the heat shrink tube was sheared at its furthest end where silicone had not entered. The internal silicone was left to set for >24 h and each electrode unit was eventually cut in half to create two, 15 cm pieces that were soldered to the biologger electrode port.

Encasing and encapsulation

Electrodes were interfaced with the biologger using a soldered connection. A small piece of custom cut, 1 mm foam was placed on the bottom of the 3D-printed case to eliminate hard surface-to-surface interfaces and reduce internal movement. Once the biologger was situated in the main part of the case, it was enclosed from its bottom side using a 3D-printed disc and medical device epoxy (EA M-31CL, Loctite) around the disc's circumference which was held tight during the drying period using Kapton tape. The electrodes were fed through a 3D-printed conduit which interfaced to the case's main body. The conduit was epoxied to the main case and then epoxy was injected into the conduit area around the electrode connector and base of the electrodes to create a structural interface to resist moisture from wicking into the biologger case. Once the epoxy was set (24 h), 6 g of a two-part silicone elastomer (RTV-4020, Factor II) were mixed and then degassed at 30 in Hg for 2 min in a vacuum chamber (1.5-gallon chamber, Ablaze Custom). The silicone was then poured into a 3 ml syringe which was centrifuged (custom made) to consolidate the silicone toward the ejection side. With the biologger suspended from the tail-end of its electrodes, silicone was applied through the syringe and an 18-gauge needle from 1 cm above the electrode interface all the way down onto the whole of the biologger. Excess silicone was allowed to drip into a small, disposable cup below. The biologger was then covered with a bell jar and allowed to sit for >24 h.

At all times, sterile best practices were followed during device preparation and handling. Once the biologger silicone was set, and 12 h prior to surgery, the biologger and electrodes were cold sterilized in a glutaraldehyde solution, after which it was placed into a large, empty sterile syringe (60 ml) for transport to the operating room.

Surgical procedures

All procedures were approved by the University of Michigan Institutional Animal Care and Use Committee (IACUC) and Unit for Laboratory Animal Medicine (ULAM) under protocol PRO00009223. Red squirrels (*Tamiasciurus hudsonicus*) and fox squirrels (*Sciurus niger*) were trapped at Saginaw Forest in Ann Arbor, MI, under the Department of Natural Resources (DNR) Scientific Collectors Permit SC-1650. We used both species of squirrel to assess acclimation to captivity and tolerance of surgical procedures, such that we use squirrels in plural to describe the procedures. However, we use a single case study of a fox squirrel (∼430 g) in our results. We obtained rats (∼250 g) from our institutional reuse program.

Animals were anesthetized using 5% isoflurane (item 402017, MWI Animal Health) mixed with pure oxygen (Cryogenic Gases) in a custom plexiglass induction chamber. We found that squirrels required an immediate dose of the sedative dexmedetomidine (item 502019, MWI Animal Health) at 100 μg/kg to tolerate the surgery. Thus, after moving animals to the stereotactic frame, rats were maintained at slightly higher levels of isoflurane (∼2%) than squirrels (∼1.25%) because of the sparing effects of dexmedetomidine.

Animals were given a pre-surgical analgesic of carprofen at 5 mg/kg (University of Michigan ULAM Pharmacy) and antibiotic cefazolin at 50 mg/ml (item 501099, MWI Animal Health). Internal body temperature was constantly monitored using a handheld small animal thermometer and regulated using an adjustable infrared warming pad (RT-0520, Kent Scientific). Eye ointment was applied, then the animals were shaved using handheld clippers. Animals were then secured using rat-sized ear bars in the stereotactic frame (model 963, Kopf Instruments) and repositioned in the gas mask (item 751859, Harvard Apparatus). Three alternating applications of rubbing alcohol and betadine were applied to the surgical area and then the surgical area was draped using plastic (Press'n Seal, GLAD).

A one-inch medial-lateral incision was made behind the neck and then a small posterior subcutaneous pocket was exposed and irrigated with sterile saline (item 5102245, MWI Animal Health) and kept hydrated with gauze. A half-inch anterior-posterior midline incision was made over the skull and then retracted to identify the bregma and lambda skull sutures. Although a squirrel brain atlas was not available, squirrels have roughly the same anatomical proportions as rats (see Paxinos and Watson, 2007). Four, 1 mm screw holes were placed in

the skull over the left and right frontal cortex (AP: 1.5 mm, ML: ±1.5 mm, relative to bregma) for signal leads and the left and right cerebellum (AP: −1.5 mm, ML: ±1.5 mm, relative to lambda) for reference leads.

A subcutaneous route was established from the skull to the neck incision for the electrodes. All open sites were irrigated at least three times with sterile saline. Electrodes were first routed to the skull area and then the biologger was placed into the subcutaneous pocket. The posterior reference electrodes were clipped, stripped to expose 2 mm of wire, secured in the skull holes using a stainless-steel screw, and covered with a two-part cold-curing dental cement (Teets Cold Cure, item 525000, A-M Systems). Next, the frontal leads were secured using a similar method, and a smooth head cap was formed with the dental cement.

Incisions were closed using a 5-0 nylon suture (item M-N518R19, AD Surgical). Animals were tapered from isoflurane and placed on a recovery heating pad. Rats recovered in a standard, acrylic home cage until ambulatory, whereas squirrels were administered a 1 mg/kg dose of atipamezole (item 032800, MWI Animal Health) to reverse the dexmedetomidine, and allowed to recover in their home cage. For at least 1 day following surgery, rats received an injection of carprofen at 5 mg/kg and a similar dose was mixed in nut butter and offered to squirrels.

Housing

Rats were housed in standard rodent cages, received *ad libitum* water and chow (5L0B, LabDiet), and were provided enrichment items. Squirrels were housed in a larger cage made for small primates that included naturalistic elements (e.g., sticks and grass) as well as a custom-made nest box (9 cu. in.). Squirrels were also given *ad libitum* water and chow, but they were fed a mixture of nuts, seeds, and fresh berries to replicate their natural diet. Cages were recorded using two video cameras (Wyze Cam v3). All animals were kept on a standard 12-h light-dark cycle (coordinated with ambient conditions) and for squirrels, the temperature was reduced to 60°F.

Metrics and statistics

Biologger latencies

To determine algorithmic latency, we extracted the relevant code and placed two C-code statements (*Clock_getTicks*, accurate to 10 μs) around the algorithm block and ran it 1,000 times, storing each calculated latency to a 32-bit unsigned integer array. The latency array was then exported to a binary file and imported into MATLAB to generate the latency metrics.

To determine BLE wireless latency, we physically connected a biologger to a base station with a synchronization cable. The biologger sent a pulse following the statement that initiated a wireless indication (16-bytes) to the base station. The base station detected the pulse through a hardware interrupt that reset a clock variable (using *Clock_getTicks*). When the base station registered the wireless indication, the clock was re-referenced, and the time difference was calculated and analyzed in a similar manner to algorithm latency using 1,000 trials.

Sleep cycle

The ebb and flow of SW sleep characterized by 0.5–4 Hz oscillations—sometimes called NREM, or stage N3 sleep—can be used to determine a sleep cycle (Patel et al., 2022). To obtain a single SW power vector, we quantified SW power magnitude over time using a spectrogram (MATLAB, *pspectrum*) and averaged it across the frequency dimension. We tested for a cyclical component of these data using a standard power spectrum. To determine if the resulting power spectrum data was not due to chance alone, we randomly permuted the SW power magnitude time series (n = 10,000 surrogates), recalculated the power spectrum for each, and then tested how often each frequency bin for the actual power spectrum was larger than the surrogate distribution.

Results

Closed-loop auditory stimulation

We implanted our biologger in rats (*Rattus norvegicus*) for up to 7 days to assess the biological compatibility of small rodents and demonstrate utility in closed-loop experiments. We collected biopotential data at 125 Hz and performed real-time detection of SWs including information about the dominant (or, center) frequency and instantaneous phase (the "algorithm," see section "Materials and methods" and **Supplementary Figure 1**). Although parameters will vary depending on the type of experiment, we suggest that algorithm runtime and wireless latency are relatively ubiquitous "fixed costs," and important to characterize so that they can be included as line delays in the closed-loop control system. Algorithm runtime on our entire input signal (2 s of data) was 20.06 ± 0.01 ms (n = 1,000 trials). When SWs occurred at higher frequencies (>2 Hz), our algorithm reanalyzed only the tail portion of the data stream to increase detection specificity, resulting in an aggregate runtime of 25.55 ± 0.01 ms (n = 1,000 trials; an additional cost of 5.49 ms). Note that both devices—the peripheral (biologger) and central—handshake on a 10 ms connection interval prior to engaging in any further communication, but that the BLE protocol contains immutable random jitter to avoid packet collisions from multiple devices. We found our wireless latency to be 10.17 ± 1.74 ms (n = 1,000 trials), congruent with the intended connection interval. Only 0.3% of our wireless transmissions were outside three SDs of the mean with the largest difference being a single trial with a latency of 24.54 ms.

These results may vary based on signal strength and 2.4 GHz band congestion.

Taken together, we were able to estimate the future signal of ongoing biopotentials with high accuracy by quantifying and anticipating system delays (**Figure 4**). Practically, from detection on the biologger to an audio stimulus from the wireless base station, we incur a 30° lag given a 2.5 Hz SW, and when that is accounted for, we obtain precision to within 1.5°. However, it should be appreciated that many biopotentials, and specifically neural EEG, rarely oscillate for many cycles at the same frequency, such that signal estimation is prone to error based on the location of recording, behavior being engaged, and organism itself.

Approximating a free-ranging deployment

We implanted a fox squirrel (*S. niger*) with our biologger to demonstrate the ability to obtain freely behaving behavior and physiology in a diurnal rodent (**Figure 5**). Our biologging recording utility includes the ability to modify the duty cycle of recordings, which are saved on-board. Here, we used a 100% duty cycle to record a full night's worth of biopotential (sampled at 125 Hz) and accelerometer data (sampled at 1 Hz). We demonstrated the ability to retrieve these data for *post hoc* analysis through a biologger explant and humanely return the squirrel to its home territory in the forest.

We verified squirrel behavior using an overhead nest camera (**Supplementary Figure 2**). It was evident that SW activity dominates the neural EEG when movement ceases, consistent with NREM sleep (**Figures 5B,C**). Overall, SW activity presented regularly throughout the night in our squirrel. We further demonstrated the utility of high-fidelity physiology by assessing the SW cycle length (i.e., sleep cycle) from these data (**Figure 6**). Our squirrel had a sleep cycle of 2.95 cycles per hour ($P < 0.001$), or roughly 20 min.

Discussion

We developed and then deployed a wireless biologger in two experimental paradigms. Firstly, we showed that a closed-loop control system can be built around on-board algorithmic capabilities and low-latency wireless communication. Secondly, we demonstrated multi-day biologger durability in a freely behaving squirrel. Beyond technical or experimental capability, our biologgers were reused without incident, sparing only a few parts. We estimated that our devices had a one-time use cost of $120 (at quantity 25), a price point that enables large-scale deployments where neurophysiology is typically cost prohibitive. Taken together, our biologger device represents a single platform to support free-living neurophysiology that can be interacted with in real time in a laboratory setting or deployed autonomously in the field.

We propose that low-cost, implantable biologgers are one solution to approaching outstanding questions relating to the evolution of sleep. Squirrels are one such animal where rich data exist regarding social structure, waking behavior, and energetics (Boon et al., 2008; Fletcher et al., 2014; Studd et al., 2019, 2020; Dantzer et al., 2020), yet how squirrels sleep in the wild remains largely uncharted (but see Walker et al., 1977; Krilowicz et al., 1988). Although we (and others) have identified that squirrels sacrifice rest during autumn when storing food is critical to survival (Williams et al., 2016; Gaidica et al., 2021), it is unclear if sleep adapts to cope with, or enable such extreme fluctuations in waking behavior. We showed here that SW activity cycles roughly every 20 min in captivity which may be a useful parameter to evaluate in natural conditions given the strong relationship (found mostly in laboratory settings) between SWs, memory, and fitness (O'Hearn, 2021). Squirrels also highlight issues related to quiescent behavioral states indistinguishable from sleep as measured by movement alone (Halsey et al., 2009; Brown et al., 2013). We clearly observed extended bouts of active rest (e.g., motionless but eyes-open) in our captive squirrel. This is an effect known as "masking," where animals like squirrels will use the confines of their nest not only for sleep but to mitigate exposure to weather and predators (Rietveld et al., 1993). Masking events are, therefore, challenging to discern through inertial sensors alone because they depend on stochastic environmental conditions often covert to the observer (Brown et al., 2013). Since many of the questions regarding the function of sleep depend on the prevalence and precise timing of sleep states, it is hard to imagine how those would be sufficiently addressed without neurophysiology.

The ability to implant a neural recording device opens several avenues to behavioral neuroscientists interested in fieldwork. For example, contact tracing has become a popular method by which individual interactions can be quantified (Berkvens et al., 2019) but there are few instances that describe changes in brain activity during socializing (but see Zhang and Yartsev, 2019) or conflicts in the wild. Unencumbered movement made possible by an implantable may also usher naturalistic problem-solving tasks that can probe intra- and inter-species cognition. Leaver et al. (2020) demonstrated an interaction between paw preference and learning in a novel paw preference test with wild gray squirrels which could be supplemented by understanding the neural correlates of paw preference and reaching dynamics (Bova et al., 2020).

The species candidate pool for neuro-biologging is going to be fundamentally limited by battery power into the future (Laske et al., 2021). While semiconductor size will continue to decrease exponentially (halving every 18 months), battery technology has failed to keep pace, ultimately playing into ethical concerns regarding the "5% rule": a device should never

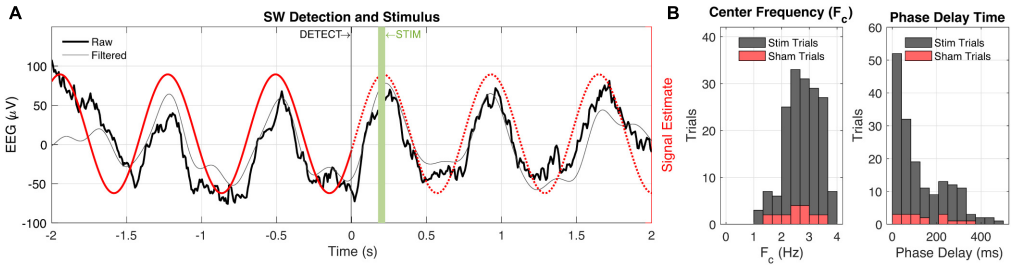

FIGURE 4
Closed-loop slow-wave activity detection and audio stimulation. **(A)** Peri-detection EEG data are shown (black) with a 0.5–4 Hz bandpass filter applied to better visualize slow-wave (SW) activity. The signal estimate (red) is based on the center frequency and phase estimation of the biologger which is relayed to the base station at $t = 0$. The base station subsequently estimates a phase delay time to play 50 ms audio stimulus at the up-going phase of the ongoing SW activity. **(B)** Session-wide ($n = 202$ trials) values for center frequency (Fc, left) and phase delay time (right). Sham trial distributions (10% probability) are shown in red.

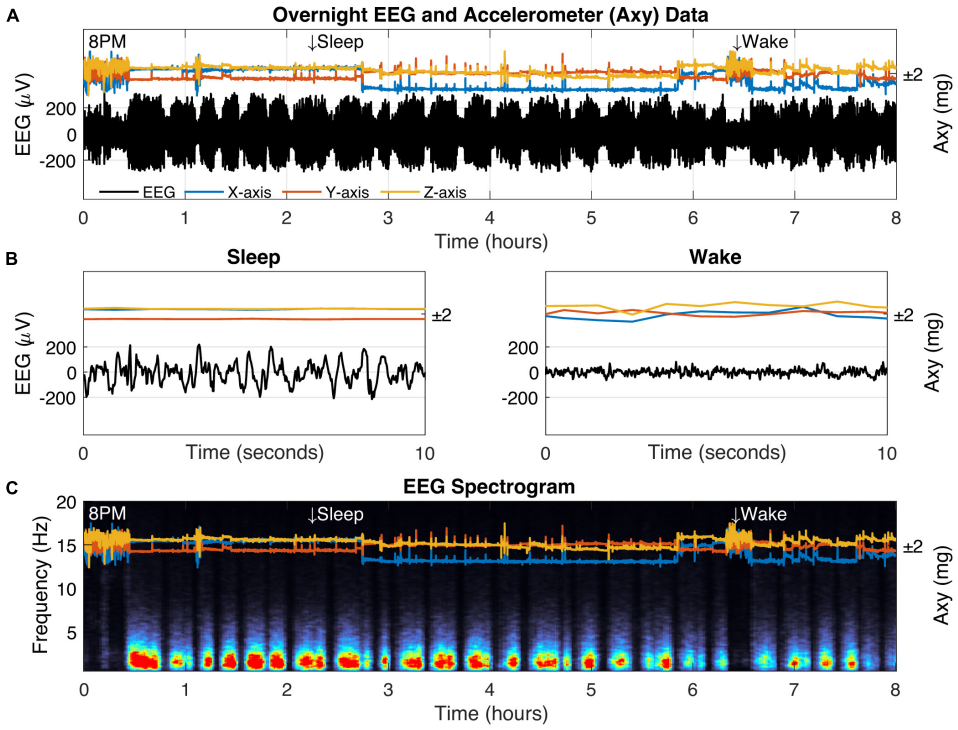

FIGURE 5
Biologging overnight in a freely behaving captive fox squirrel. **(A)** Eight hours of biologger data beginning at 8 p.m. showing EEG data (black) and 3D accelerometer data from the *x*-axis (blue), *y*-axis (orange), and *z*-axis (yellow). Representative sleep and wake epochs are marked along the top and the same data is shown in where **(B)** time has been restricted to a 10-s window. **(C)** The EEG spectrogram showing the relative power for each frequency (1–20 Hz) across time (red colors indicate high power).

exceed 5% of an animal's mass (Portugal and White, 2018; Kay et al., 2019). Smaller batteries not only decrease in capacity, but our tests show that they are incapable of providing stable power (e.g., 2016 style battery), likely due to the high transient demands of a wireless radio and bio-amplifier. Although power efficiency is increasing in this device class, it will remain a challenge over the next several years to record continuously from neural biologgers for more than a few days in small animals (<50 grams). One potential solution that we explored with our biologger configuration utility is to subsample physiological data through duty-cycled (i.e., scheduled) recording routines, which can still provide a wealth of data tailored to a set experimental duration (van Hasselt et al., 2021). However, the growing use cases of the coin-cell form factor, including the ability to use rechargeable batteries (see Musk, 2019 and Neuralink), and the implementation of integrated regenerative

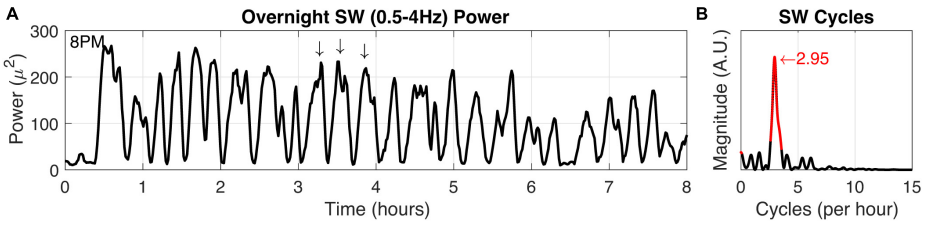

FIGURE 6
Squirrel SW cycle duration. **(A)** Power in the SW band (0.5–4 Hz) was calculated from overnight recording data (8 h). Arrows indicate high SW power and also demonstrate characteristic SW cycle frequency in a 1-h window. **(B)** The SW time-frequency relationship was calculated to determine fundamental frequencies that may occur in the SW activity. Highly significant ($P < 0.001$) values and the peak magnitude were calculated (both in red).

sources (Iyer et al., 2022), is promising, but also depends on the experimental paradigm and access to the animal (Kim et al., 2021; Wright et al., 2022).

More research is needed to address the efficacy of releasing an animal into their natural habitat with a neural biologger, especially if it requires multiple procedures and a survival endpoint (Rattenborg et al., 2008). Some meta-analyses (mostly in birds and marine mammals) do show that biologgers can have slight but statistically significant negative impacts on animals (Barron et al., 2010; Bodey et al., 2018) whereas others do not (Bridge et al., 2013). Current evidence suggests that implantation of biologgers may be the better option compared to the external attachment as implanted devices do not seem to have long-lasting impacts on natural behavior, markers of inflammation, or detrimental effects on survival and reproduction in free-living animals (White et al., 2012; Shuert et al., 2015; Horning et al., 2017; Lameris and Kleyheeg, 2017; Forin-Wiart et al., 2019; Won et al., 2020). Meta-analyses have consistently shown that the method of attachment of a biologger influences the costs with external tags having the most detrimental effects and implanted devices having few significant impacts (White et al., 2012; Bodey et al., 2018). External attachment of biologgers may carry such costs because they increase the risk of entanglement, visual conspicuousness to predators, or increase costs of movement due to drag produced by the devices, whereas implantables promote freedom of movement and natural kinematics while maintaining the integrity of animal skin or fur allowing for natural interactions and grooming (Forin-Wiart et al., 2019). However, extended post-surgical observation that typically benefits an animal may lead to territories being overtaken or resources being poached in some species (Hendrix et al., 2020) and temporary removal of an animal may also have direct and indirect consequences on parental care or social dynamics in an ecosystem (Bulla et al., 2019). Detailed studies in the laboratory also show that any costs of implanted bio-loggers are short-lived as long as the total mass of the device does not exceed 3–5% of the total body mass of an individual (Casper, 2009). For example, a bio-telemetry device that was implanted in rats that were ∼1% of their average body mass had no impact on post-implantation body mass and the impacts on their behavior only lasted 2 days after surgery (Leon et al., 2004). However, Bakker et al. (2014) found that recovery of more complex motor behaviors following a neural implant in a non-human primate took 8–31 days.

There were clear advantages of performing this work on campus with veterinarian oversight. For example, we noticed mild seroma (i.e., fluid) development at the bio-logger implant site in in our early rat surgeries that was determined to be bacterial. To offer additional antibiotic coverage, we were able to quickly adjust our protocol—from using enrofloxacin to cefazolin—after which, we experienced no seromas and completely healthy surgical recovery in rats and squirrels (see also McCauley and Wehrens, 2010; Wedel et al., 2014). These refinements work toward the capability of performing bio-logger implants at a field station; the main considerations being the maintenance of a sterile surgical field, portable equipment and consumables, and suitable recovery and animal housing areas. Researchers should be prepared to work closely with their veterinarians and IACUC to establish suitable offsite procedures suited for the species of interest.

Conclusion

In conclusion, the ability to record neural electrophysiology in a freely behaving animal, compute and communicate wirelessly with low-latency, and reduce deployment costs to enable large cohort studies are major hurdles we sought to address with our biologger. Despite some outstanding challenges, these capabilities have the potential to reveal novel insights while expanding the repertoire of species from which our scientific assumptions are built upon.

Data availability statement

The datasets presented in this study can be found in online repositories. The names of the repository/repositories

and accession number(s) can be found in the article/**Supplementary material**.

Ethics statement

The animal study was reviewed and approved by the University of Michigan Institutional Animal Care and Use Committee (IACUC) and Unit for Laboratory Animal Medicine (ULAM).

Author contributions

MG was the primary scientist and engineer. BD provided mentorship and expert feedback on approach and implementation. MG and BD wrote the manuscript. Both authors contributed to the article and approved the submitted version.

Funding

This work was funded by the University of Michigan and directly supported by the Translational Research Institute through NASA Cooperative Agreement NNX16AO69A.

Acknowledgments

We would like to thank the ULAM staff at the University of Michigan—namely, Lucy Kennedy and Stephanie Yang—for their ongoing, hands-on support in working with novel species and techniques. We acknowledge our privileged land use of the Saginaw Forest area in Michigan and the flora and fauna it encompasses. We would like to recognize the fruitful feedback and collaborative support from the laboratories of Dan Leventhal and Ada Eban-Rothschild.

Conflict of interest

The authors declare that the research was conducted in the absence of any commercial or financial relationships that could be construed as a potential conflict of interest.

Publisher's note

All claims expressed in this article are solely those of the authors and do not necessarily represent those of their affiliated organizations, or those of the publisher, the editors and the reviewers. Any product that may be evaluated in this article, or claim that may be made by its manufacturer, is not guaranteed or endorsed by the publisher.

Supplementary material

The Supplementary Material for this article can be found online at: https://www.frontiersin.org/articles/10.3389/fncir.2022.940989/full#supplementary-material

References

Anafi, R. C., Kayser, M. S., and Raizen, D. M. (2019). Exploring phylogeny to find the function of sleep. *Nat. Rev. Neurosci.* 20, 109–116. doi: 10.1038/s41583-018-0098-9

Aulehner, K., Bray, J., Koska, I., Pace, C., Palme, R., Kreuzer, M., et al. (2022). The impact of tethered recording techniques on activity and sleep patterns in rats. *Sci. Rep.* 12:3179. doi: 10.1038/s41598-022-06307-3

Aulsebrook, A. E., Jones, T. M., Rattenborg, N. C., Roth, T. C., and Lesku, J. A. (2016). Sleep ecophysiology: integrating neuroscience and ecology. *Trends Ecol. Evol.* 31, 590–599. doi: 10.1016/j.tree.2016.05.004

Bakker, J., Klomp, R., Rijnbeek, M. W., Arndt, S. S., Philippens, I. H., and Langermans, J. A. (2014). Recovery time after intra-abdominal transmitter placement for telemetric (neuro) physiological measurement in freely moving common marmosets (*Callitrix jacchus*). *Anim. Biotelem.* 2:10. doi: 10.1186/2050-3385-2-10

Barron, D. G., Brawn, J. D., and Weatherhead, P. J. (2010). Meta-analysis of transmitter effects on avian behaviour and ecology. *Methods Ecol. Evol.* 1, 180–187. doi: 10.1111/j.2041-210X.2010.00013.x

Bellesi, M., Riedner, B. A., Garcia-Molina, G. N., Cirelli, C., and Tononi, G. (2014). Enhancement of sleep slow waves: underlying mechanisms and practical consequences. *Front. Syst. Neurosci.* 8:208. doi: 10.3389/fnsys.2014.00208

Berkvens, R., Olivares, I. H., Mercelis, S., Kirkpatrick, L., and Weyn, M. (2019). "Contact Detection for Social Networking of Small Animals," in *Advances on P2P, Parallel, Grid, Cloud and Internet Computing Lecture Notes on Data Engineering and Communications Technologies*, eds F. Xhafa, F.-Y. Leu, M. Ficco, and C.-T. Yang (Cham: Springer International Publishing), 405–414. doi: 10.1007/978-3-030-02607-3_37

Bodey, T. W., Cleasby, I. R., Bell, F., Parr, N., Schultz, A., Votier, S. C., et al. (2018). A phylogenetically controlled meta-analysis of biologging device effects on birds: deleterious effects and a call for more standardized reporting of study data. *Methods Ecol. Evol.* 9, 946–955. doi: 10.1111/2041-210X.12934

Boon, A. K., Réale, D., and Boutin, S. (2008). Personality, habitat use, and their consequences for survival in North American red squirrels *Tamiasciurus hudsonicus*. *Oikos* 117, 1321–1328. doi: 10.1111/j.0030-1299.2008.16567.x

Bova, A., Gaidica, M., Hurst, A., Iwai, Y., Hunter, J., and Leventhal, D. K. (2020). Precisely timed dopamine signals establish distinct kinematic representations of skilled movements. *eLife* 9:e61591. doi: 10.7554/eLife.61591

Bridge, E. S., Kelly, J. F., Contina, A., Gabrielson, R. M., MacCurdy, R. B., and Winkler, D. W. (2013). Advances in tracking small migratory birds: a technical review of light-level geolocation: light-level geolocation dataloggers. *J. Field Ornithol.* 84, 121–137. doi: 10.1111/jofo.12011

Brown, D. D., Kays, R., Wikelski, M., Wilson, R., and Klimley, A. (2013). Observing the unwatchable through acceleration logging of animal behavior. *Anim. Biotelem.* 1:20. doi: 10.1186/2050-3385-1-20

Bulla, M., Valcu, M., Rutten, A. L., and Kempenaers, B. (2019). Temporary mate removal during incubation leads to variable compensation in a biparental shorebird. *Front. Ecol. Evol.* 7:93. doi: 10.3389/fevo.2019.00093

Butler, P. J., and Woakes, A. J. (1979). Changes in heart rate and respiratory frequency during natural behaviour of ducks, with particular reference to diving. *J. Exp. Biol.* 79, 283–300. doi: 10.1242/jeb.79.1.283

Casper, R. M. (2009). Guidelines for the instrumentation of wild birds and mammals. *Anim. Behavi.* 78, 1477–1483.

Chang, P., Hashemi, K. S., and Walker, M. C. (2011). A novel telemetry system for recording EEG in small animals. *J. Neurosci. Methods* 201, 106–115. doi: 10.1016/j.jneumeth.2011.07.018

Chimienti, M., Cornulier, T., Owen, E., Bolton, M., Davies, I. M., Travis, J. M. J., et al. (2016). The use of an unsupervised learning approach for characterizing latent behaviors in accelerometer data. *Ecol. Evol.* 6, 727–741. doi: 10.1002/ece3.1914

Chmura, H. E., Glass, T. W., and Williams, C. T. (2018). Biologging physiological and ecological responses to climatic variation: new tools for the climate change era. *Front. Ecol. Evol.* 6:92. doi: 10.3389/fevo.2018.00092

Dantzer, B., McAdam, A. G., Humphries, M. M., Lane, J. E., and Boutin, S. (2020). Decoupling the effects of food and density on life-history plasticity of wild animals using field experiments: insights from the steward who sits in the shadow of its tail, the North American red squirrel. *J. Anim. Ecol.* 89, 2397–2414. doi: 10.1111/1365-2656.13341

Eban-Rothschild, A., Giardino, W. J., and de Lecea, L. (2017). To sleep or not to sleep: neuronal and ecological insights. *Curr. Opin. Neurobiol.* 44, 132–138. doi: 10.1016/j.conb.2017.04.010

Fletcher, Q. E., Speakman, J. R., Boutin, S., Lane, J. E., McAdam, A. G., Gorrell, J. C., et al. (2014). Daily energy expenditure during lactation is strongly selected in a free-living mammal. *Funct. Ecol.* 29, 195–208. doi: 10.1111/1365-2435.12313

Forin-Wiart, M.-A., Enstipp, M. R., Le Maho, Y., and Handrich, Y. (2019). Why implantation of bio-loggers may improve our understanding of how animals cope within their natural environment. *Integr. Zool.* 14, 48–64. doi: 10.1111/1749-4877.12364

Gaidica, M., Studd, E., Wishart, A. E., Gonzalez, W., Lane, J., McAdam, A. G., et al. (2021). Using a homeogram to detect sleep in free-living animals. *bioRxiv* [Preprint]. doi: 10.1101/2021.10.14.464397

Geddes, L. A., and Roeder, R. (2003). Criteria for the selection of materials for implanted electrodes. *Ann. Biomed. Eng.* 31, 879–890. doi: 10.1114/1.1581292

Halsey, L. G., Green, J. A., Wilson, R. P., and Frappell, P. B. (2009). Accelerometry to estimate energy expenditure during activity: best practice with data loggers. *Physiol. Biochem. Zool.* 82, 396–404. doi: 10.1086/589815

Hammond, T. T., Springthorpe, D., Walsh, R. E., and Berg-Kirkpatrick, T. (2016). Using accelerometers to remotely and automatically characterize behavior in small animals. *J. Exp. Biol.* 219, 1618–1624. doi: 10.1242/jeb.136135

Harcourt, R., Sequeira, A. M. M., Zhang, X., Roquet, F., Komatsu, K., Heupel, M., et al. (2019). Animal-borne telemetry: an integral component of the ocean observing toolkit. *Front. Mar. Sci.* 6:326. doi: 10.3389/fmars.2019.00326

Hendrix, J. G., Fisher, D. N., Martinig, A. R., Boutin, S., Dantzer, B., Lane, J. E., et al. (2020). Territory acquisition mediates the influence of predators and climate on juvenile red squirrel survival. *J. Anim. Ecol.* 89, 1408–1418. doi: 10.1111/1365-2656.13209

Hoffmann, S., Trost, L., Voigt, C., Leitner, S., Lemazina, A., Sagunsky, H., et al. (2019). Duets recorded in the wild reveal that interindividually coordinated motor control enables cooperative behavior. *Nat. Commun.* 10:2577. doi: 10.1038/s41467-019-10593-3

Horning, M., Haulena, M., Tuomi, P. A., Mellish, J.-A. E., Goertz, C. E., Woodie, K., et al. (2017). Best practice recommendations for the use of fully implanted telemetry devices in pinnipeds. *Anim. Biotelemetry* 5:13. doi: 10.1186/s40317-017-0128-9

Iyer, V., Gaensbauer, H., Daniel, T. L., and Gollakota, S. (2022). Wind dispersal of battery-free wireless devices. *Nature* 603, 427–433. doi: 10.1038/s41586-021-04363-9

Jetz, W., Tertitski, G., Kays, R., Mueller, U., Wikelski, M., Åkesson, S., et al. (2022). Biological Earth observation with animal sensors. *Trends Ecol. Evol.* 37, 293–298. doi: 10.1016/j.tree.2021.11.011

Kay, W. P., Naumann, D. S., Bowen, H. J., Withers, S. J., Evans, B. J., Wilson, R. P., et al. (2019). Minimizing the impact of biologging devices: using computational fluid dynamics for optimizing tag design and positioning. *Methods Ecol. Evol.* 10, 1222–1233. doi: 10.1111/2041-210X.13216

Kim, C. Y., Ku, M. J., Qazi, R., Nam, H. J., Park, J. W., Nam, K. S., et al. (2021). Soft subdermal implant capable of wireless battery charging and programmable controls for applications in optogenetics. *Nat. Commun.* 12:535. doi: 10.1038/s41467-020-20803-y

Kirkpatrick, L., Hererra Olivares, I., Massawe, A., Sabuni, C., Leirs, H., Berkvens, R., et al. (2021). ProxLogs: miniaturised proximity loggers for monitoring association behaviour in small mammals. *bioRxiv* [Preprint]. doi: 10.1101/2021.02.28.432842

Krilowicz, B. L., Glotzbach, S. F., and Heller, H. C. (1988). Neuronal activity during sleep and complete bouts of hibernation. *Am. J. Physiol. Regul. Integr. Comp. Physiol.* 255, R1008–R1019. doi: 10.1152/ajpregu.1988.255.6.R1008

Lameris, T. K., and Kleyheeg, E. (2017). Reduction in adverse effects of tracking devices on waterfowl requires better measuring and reporting. *Anim. Biotelemetry* 5:24. doi: 10.1186/s40317-017-0139-6

Laske, T. G., Garshelis, D. L., Iles, T. L., and Iaizzo, P. A. (2021). An engineering perspective on the development and evolution of implantable cardiac monitors in free-living animals. *Philos. Trans. R Soc. Lond. B Biol. Sci.* 376:20200217. doi: 10.1098/rstb.2020.0217

Leaver, L. A., Ford, S., Miller, C. W., Yeo, M. K., and Fawcett, T. W. (2020). Learning is negatively associated with strength of left/right paw preference in wild grey squirrels (Sciurus carolinensis). *Learn. Behav.* 48, 96–103. doi: 10.3758/s13420-019-00408-2

Leon, L. R., Walker, L. D., DuBose, D. A., and Stephenson, L. A. (2004). Biotelemetry transmitter implantation in rodents: impact on growth and circadian rhythms. *Am. J. Physiol. Regul. Integr. Comp. Physiol.* 286, R967–R974. doi: 10.1152/ajpregu.00380.2003

Loftus, J. C., Harel, R., Núñez, C. L., and Crofoot, M. C. (2022). Ecological and social pressures interfere with homeostatic sleep regulation in the wild. *eLife* 11:e73695. doi: 10.7554/eLife.73695

Mascetti, G. G. (2016). Unihemispheric sleep and asymmetrical sleep: behavioral, neurophysiological, and functional perspectives. *NSS* 8, 221–238. doi: 10.2147/NSS.S71970

Massot, B., Arthaud, S., Barrillot, B., Roux, J., Ungurean, G., Luppi, P.-H., et al. (2019). ONEIROS, a new miniature standalone device for recording sleep electrophysiology, physiology, temperatures and behavior in the lab and field. *J. Neurosci. Methods* 316, 103–116. doi: 10.1016/j.jneumeth.2018.08.030

Mate, B. R., Ilyashenko, V. Y., Bradford, A. L., Vertyankin, V. V., Tsidulko, G. A., Rozhnov, V. V., et al. (2015). Critically endangered western gray whales migrate to the eastern North Pacific. *Biol. Lett.* 11:20150071. doi: 10.1098/rsbl.2015.0071

McCauley, M. D., and Wehrens, X. H. T. (2010). Ambulatory ECG recording in mice. *J. Vis. Exp.* 39:1739. doi: 10.3791/1739

Mistlberger, R. E., and Skene, D. J. (2004). Social influences on mammalian circadian rhythms: animal and human studies. *Biol. Rev.* 79, 533–556. doi: 10.1017/S1464793103006353

Musk, E. (2019). *An integrated brain-machine interface platform with thousands of channels*. San Francisco, CA: Neuralink, 12.

O'Hearn, L. A. (2021). The therapeutic properties of ketogenic diets, slow-wave sleep, and circadian synchrony. *Curr. Opin. Endocrinol. Diabetes Obes.* 28, 503–508. doi: 10.1097/MED.0000000000000660

Patel, A. K., Reddy, V., and Araujo, J. F. (2022). *"Physiology, Sleep Stages," StatPearls*: (Treasure Island, FL: StatPearls Publishing).

Paxinos, G., and Watson, C. (2007). *The rat brain in stereotaxic coordinates*. Amsterdam: Academic Press.

Portugal, S. J., and White, C. R. (2018). Miniaturization of biologgers is not alleviating the 5% rule. *Methods Ecol. Evol.* 9, 1662–1666. doi: 10.1111/2041-210X.13013

Rattenborg, N. C., de la Iglesia, H. O., Kempenaers, B., Lesku, J. A., Meerlo, P., and Scriba, M. F. (2017). Sleep research goes wild: new methods and approaches to investigate the ecology, evolution and functions of sleep. *Philos. Trans. R Soc. Lond. B Biol. Sci.* 372:20160251. doi: 10.1098/rstb.2016.0251

Rattenborg, N. C., Voirin, B., Cruz, S. M., Tisdale, R., Dell'Omo, G., Lipp, H.-P., et al. (2016). Evidence that birds sleep in mid-flight. *Nat. Commun* 7:12468. doi: 10.1038/ncomms12468

Rattenborg, N. C., Voirin, B., Vyssotski, A. L., Kays, R. W., Spoelstra, K., Kuemmeth, F., et al. (2008). Sleeping outside the box: electroencephalographic measures of sleep in sloths inhabiting a rainforest. *Biol. Lett.* 4, 402–405. doi: 10.1098/rsbl.2008.0203

Rechtschaffen, A. (1998). Current perspectives on the function of sleep. *Perspect. Biol. Med.* 41, 359–390. doi: 10.1353/pbm.1998.0051

Rietveld, W. J., Minors, D. S., and Waterhouse, J. M. (1993). Circadian rhythms and masking: an overview. *Chronobiol. Int.* 10, 306–312. doi: 10.1080/07420529309059713

Ripperger, S., Josic, D., Hierold, M., Koelpin, A., Weigel, R., Hartmann, M., et al. (2016). Automated proximity sensing in small vertebrates: design of miniaturized sensor nodes and first field tests in bats. *Ecol. Evol.* 6, 2179–2189. doi: 10.1002/ece3.2040

Ripperger, S. P., Carter, G. G., Page, R. A., Duda, N., Koelpin, A., Weigel, R., et al. (2019). Thinking small: next-generation sensor networks close the size gap in vertebrate biologging. *bioRxiv* [Preprint]. doi: 10.1101/767749

Roth, T. C., Rattenborg, N. C., and Pravosudov, V. V. (2010). The ecological relevance of sleep: the trade-off between sleep, memory and energy conservation. *Philos. Trans. R Soc. Lond. B Biol. Sci.* 365, 945–959. doi: 10.1098/rstb.2009.0209

Shuert, C., Horning, M., and Mellish, J.-A. (2015). The effect of novel research activities on long-term survival of temporarily captive steller sea lions (*Eumetopias jubatus*). *PLoS One* 10:e0141948. doi: 10.1371/journal.pone.0141948

Studd, E. K., Landry-Cuerrier, M., Menzies, A. K., Boutin, S., McAdam, A. G., Lane, J. E., et al. (2019). Behavioral classification of low-frequency acceleration and temperature data from a free-ranging small mammal. *Ecol. Evol.* 9, 619–630. doi: 10.1002/ece3.4786

Studd, E. K., Menzies, A. K., Siracusa, E. R., Dantzer, B., Lane, J. E., McAdam, A. G., et al. (2020). Optimisation of energetic and reproductive gains explains behavioural responses to environmental variation across seasons and years. *Ecol. Lett.* 23, 841–850. doi: 10.1111/ele.13494

van Hasselt, S. J., Verhulst, S., Piersma, T., Rattenborg, N. C., and Meerlo, P. (2021). A comparison of continuous and intermittent EEG recordings in geese: How much data are needed to reliably estimate sleep–wake patterns? *J. Sleep Res.* 31:e13525. doi: 10.1111/jsr.13525

Vyssotski, A. L., Serkov, A. N., Itskov, P. M., Dell'Omo, G., Latanov, A. V., Wolfer, D. P., et al. (2006). Miniature neurologgers for flying pigeons: multichannel EEG and action and field potentials in combination with GPS recording. *J. Neurophysiol.* 95, 1263–1273. doi: 10.1152/jn.00879.2005

Walker, J. M., Glotzbach, S. F., Berger, R. J., and Heller, H. C. (1977). Sleep and hibernation in ground squirrels (Citellus spp): electrophysiological observations. *Am. J. Physiol. Regul. Integr. Comp. Physiol.* 233, R213–R221. doi: 10.1152/ajpregu.1977.233.5.R213

Wedel, J., Weij, M., Oosten, A. S., and Hillebrands, J.-L. (2014). Simultaneous subcutaneous implantation of two osmotic minipumps connected to a jugular vein catheter in the rat. *Lab. Anim.* 48, 338–341. doi: 10.1177/0023677214543089

White, C. R., Cassey, P., Schimpf, N. G., Halsey, L. G., Green, J. A., and Portugal, S. J. (2012). Implantation reduces the negative effects of bio-logging devices on birds. *J. Exp. Biol.* 216:jeb.076554. doi: 10.1242/jeb.076554

Whitford, M., and Klimley, A. P. (2019). An overview of behavioral, physiological, and environmental sensors used in animal biotelemetry and biologging studies. *Anim. Biotelemetry* 7:26. doi: 10.1186/s40317-019-0189-z

Williams, C. T., Wilsterman, K., Zhang, V., Moore, J., Barnes, B. M., and Buck, C. L. (2016). The secret life of ground squirrels: accelerometry reveals sex-dependent plasticity in above-ground activity. *R. Soc. Open Sci.* 3:160404. doi: 10.1098/rsos.160404

Williams, H. J., Taylor, L. A., Benhamou, S., Bijleveld, A. I., Clay, T. A., Grissac, S., et al. (2020). Optimizing the use of biologgers for movement ecology research. *J. Anim. Ecol.* 89, 186–206. doi: 10.1111/1365-2656.13094

Wilmers, C. C., Nickel, B., Bryce, C. M., Smith, J. A., Wheat, R. E., and Yovovich, V. (2015). The golden age of bio-logging: how animal-borne sensors are advancing the frontiers of ecology. *Ecology* 96, 1741–1753. doi: 10.1890/14-1401.1

Wilson, R., Shepard, E., and Liebsch, N. (2008). Prying into the intimate details of animal lives: use of a daily diary on animals. *Endang. Spec. Res.* 4, 123–137. doi: 10.3354/esr00064

Won, S. M., Song, E., Reeder, J. T., and Rogers, J. A. (2020). Emerging modalities and implantable technologies for neuromodulation. *Cell* 181, 115–135. doi: 10.1016/j.cell.2020.02.054

Wright, J. P., Mughrabi, I. T., Wong, J., Mathew, J., Jayaprakash, N., Crosfield, C., et al. (2022). A fully implantable wireless bidirectional neuromodulation system for mice. *Biosens. Bioelectron.* 200:113886. doi: 10.1016/j.bios.2021.113886

Yoda, K., Sato, K., Niizuma, Y., Kurita, M., Bost, C., Le Maho, Y., et al. (1999). Precise monitoring of porpoising behaviour of Adelie penguins determined using acceleration data loggers. *J. Exp. Biol.* 202, 3121–3126. doi: 10.1242/jeb.202.22.3121

Zhang, W., and Yartsev, M. M. (2019). Correlated neural activity across the brains of socially interacting bats. *Cell* 178, 413–428.e22. doi: 10.1016/j.cell.2019.05.023

frontiers | Frontiers in Neural Circuits

TYPE Review
PUBLISHED 23 September 2022
DOI 10.3389/fncir.2022.970434

OPEN ACCESS

EDITED BY
Karen A. Mesce,
University of Minnesota Twin Cities, United States

REVIEWED BY
Lara S. Burchardt,
Radboud University, Netherlands
Ronen Segev,
Ben-Gurion University of the Negev, Israel

*CORRESPONDENCE
Melissa J. Coleman
mcoleman@keckscl.claremont.edu

RECEIVED 15 June 2022
ACCEPTED 31 August 2022
PUBLISHED 23 September 2022

CITATION
Coleman MJ, Day NF and Fortune ES (2022) Neural mechanisms for turn-taking in duetting plain-tailed wrens.
Front. Neural Circuits 16:970434.
doi: 10.3389/fncir.2022.970434

Neural mechanisms for turn-taking in duetting plain-tailed wrens

Melissa J. Coleman[1]*, Nancy F. Day[2] and Eric S. Fortune[3]

[1]W.M. Keck Science Department, Claremont McKenna, Scripps and Pitzer Colleges, Claremont, CA, United States, [2]Department of Psychology, Whitman College, Walla Walla, WA, United States, [3]Department Biological Sciences, New Jersey Institute of Technology, Newark, NJ, United States

Recent studies conducted in the natural habitats of songbirds have provided new insights into the neural mechanisms of turn–taking. For example, female and male plain–tailed wrens (*Pheugopedius euophrys*) sing a duet that is so precisely timed it sounds as if a single bird is singing. In this review, we discuss our studies examining the sensory and motor cues that pairs of wrens use to coordinate the rapid alternation of syllable production. Our studies included behavioral measurements of freely–behaving wrens in their natural habitat and neurophysiological experiments conducted in awake and anesthetized individuals at field sites in Ecuador. These studies show that each partner has a pattern-generating circuit in their brain that is linked *via* acoustic feedback between individuals. A similar control strategy has been described in another species of duetting songbird, white–browed sparrow–weavers (*Plocepasser mahali*). Interestingly, the combination of neurophysiological results from urethane-anesthetized and awake wrens suggest a role for inhibition in coordinating the timing of turn–taking. Finally, we highlight some of the unique challenges of conducting these experiments at remote field sites.

KEYWORDS

antiphonal, birdsong, duets, central pattern generator, auditory feedback, neuroethology

Introduction

Social behaviors rely on sensory signals sent between a "sender" and a "receiver". Signals produced by the sender often modulate the behavior of the receiver. For example, in most songbird species, males broadcast a song that may be heard by conspecifics (Figure 1A). These males produce their songs with at least two social goals – to attract females for reproduction and to repel competing males (Catchpole and Slater, 2018). When conspecifics respond to these songs, the sender/receiver relationship often reverses. If a male is the sender when producing its song to attract a female, it becomes the receiver when the female approaches it and produces a copulation solicitation display (Elie et al., 2019; Perkes et al., 2019). Indeed, in many social behaviors, individuals are constantly switching between roles as sender and receiver (Baker et al., 2019).

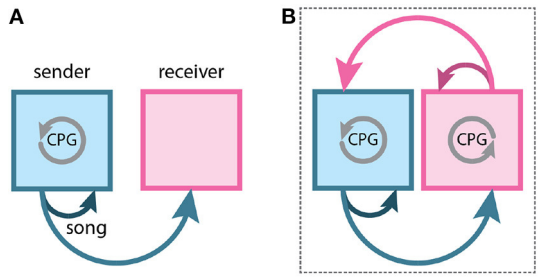

FIGURE 1
Social behaviors require communication between two animals. **(A)** Most neural studies of song control in songbirds focus on species in which only the male sings. In these birds, the pattern for the song is generated by a central pattern generator (CPG) in the male's brain (gray circular arrow). The song is then heard by the female (lighter-blue arrow), the receiver. The song is also heard by the male (dark blue arrow), which is required for song maintenance. **(B)** Turn-taking in wrens requires the exchange of information between a female and male. In duetting birds, singing is controlled by a CPG in the brain of each individual. The song of one individual is heard by the other and modulates the ongoing behavior of the partner. Thus, the two animals form a single circuit for the control of turn–taking (dotted box).

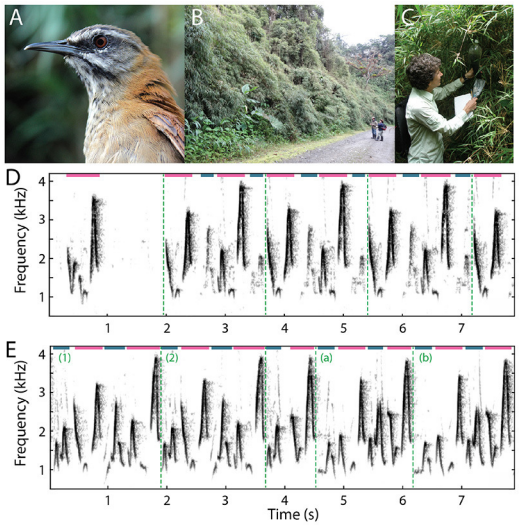

FIGURE 2
Field recordings of plain-tailed wren songs. **(A)** Photo of a plain-tailed wren. **(B)** Plain-tailed wrens live in dense bamboo on the slopes of the Andes. Photo taken near the Yanayacu Biological Field Station and Center for Creative Studies near Cosanga, Ecuador. **(C)** Setting up microphones in the bamboo to record wren duets. The microphones were covered with 2L soda bottles to protect them from rain. **(D)** Spectrogram of the beginning of a plain-tailed wren duet captured in the field. The female first sang a syllable as part of her solo song, then the male joined the duet. In this example, the male was further away from the microphone, so his syllables are of lower amplitude and can therefore be more readily distinguished from the female syllables. Female syllables are denoted with light magenta lines, and male with dark blue lines at the top of the spectrogram. Motifs (repeated sequences of syllables) are distinguished by vertical dashed green lines. **(E)** Segment of a song recorded in the field in which the structure of the duet changed. The first two motifs (1,2) are the same, then the birds produced a shortened motif around 4 sec of this recording. After the shortened motif, the pair sung a different motif (a,b). Syllables and motifs are labeled as in **(D)**. Spectrograms were rendered in Matlab (MathWorks) using the spectrogram function (95% overlap, either 512- or 1,024-point window, sample rates of 10 or 25 kHz).

In turn–taking, a social behavior in which participants alternate behaviors, there is a rapid switching of sender and receiver roles in each participant (Pika et al., 2018; Elie et al., 2019; Banerjee and Vallentin, 2022). This alternation highlights a commonly overlooked feature of social behavior; when both participants act as both sender and receiver, an emergent feedback loop can form (Fortune et al., 2011; Coen and Murthy, 2016; Coleman and Fortune, 2018; Coleman et al., 2021) (Figure 1B). This feedback loop is mediated by the sensory signals that link activity in the brains of each participant. There has been a growing appreciation of the back-and-forth exchange of acoustic information between females and males across songbird species: both sexes are believed to have sung in the common ancestor of songbirds (Odom et al., 2014). Therefore, this form of emergent feedback loop for turn–taking is likely present in the common ancestor of songbirds.

How does neurophysiological activity in each participant generate tightly coordinated turn-taking? Tightly-coordinated duet singing in songbirds, such as plain-tailed wrens (*Pheugopedius euophrys*) and white–browed sparrow–weavers (*Plocepasser mahali*), are particularly well–suited for the study of the neural mechanisms of turn-taking (Brenowitz, 2021). Remarkably, we are aware of only three studies that examine the neural mechanisms for the control of duetting in songbirds (Fortune et al., 2011; Hoffmann et al., 2019; Coleman et al., 2021).

In this review, we focus on our work with plain-tailed wrens (Figure 2A; Fortune et al., 2011; Coleman et al., 2021). These birds live in thick bamboo on the slopes of the Andes in Ecuador (Figure 2B), between 2200–2400 meters above sea level. Female and male pairs of birds sing a learned duet in which they rapidly (up to 6 Hz) alternate the production of their vocalizations so quickly and precisely (Figures 2D,E) it sounds as if a single bird is singing. Our behavioral and neurophysiological experiments were conducted at remote field stations in Ecuador, within the natural habitats of the animals. These field studies presented numerous challenges, both practical and scientific.

One interesting practical challenge that led to unexpected scientific insights was the choice of neurophysiological techniques. Initially we relied on recordings conducted in anesthetized wrens as these experiments seemed more feasible

at our field sites (Fortune et al., 2011). Unexpectedly, these recordings in anesthetized birds were critical for the discovery of a likely role of inhibition for the coordination of duet singing in awake birds (Coleman et al., 2021).

Background

Birdsong is a learned behavior that requires interactions between sensory and motor information in the brain (Mooney, 2014). In songbirds, juveniles match their own vocal output to a memory of a tutor song (Konishi, 1965; Ikeda et al., 2020). Once birds learn their song, ongoing auditory feedback is necessary to maintain their vocalizations, as song degrades when birds are deafened (Nordeen and Nordeen, 1992; Doupe and Kuhl, 1999; Leonardo and Konishi, 1999; Brainard and Doupe, 2001; Horita et al., 2008). This auditory feedback modulates motor circuits in the brain that control singing (Roberts et al., 2017). The neural basis of these sensorimotor interactions has been primarily studied in species in which only the male sings, such as zebra finches (*Taeniopygia guttata*), white-crowned sparrows (*Zonotrichia leucophrys*), bengalese finches (*Lonchura striata*), and canaries (*Serinus canaria*). The key difference between songbirds in which only males sing and duetting species in which both females and males sing together is the rapid exchange of acoustic information between birds. This information exchange is used, at a minimum, for the coordination of the duet performance.

There are dedicated circuits in songbird brains, known as the "song system", that have been shown to control song learning, production, and maintenance (Brainard and Doupe, 2002; Mooney, 2014). Specifically, a nidopallial area known as HVC (proper name) is a site of sensorimotor integration for song (Mooney and Prather, 2005; Roberts et al., 2017). HVC is necessary for song production (Nottebohm et al., 1976) and contains neurons that form the pattern-generating circuit for song. Stimulation of HVC can 'reset' the temporal patterning of song (Vu et al., 1994) and cooling HVC can slow song production (Long and Fee, 2008). HVC neurons are not only active when the bird is singing but also when the bird hears playbacks of its own song (Margoliash, 1983; Margoliash and Konishi, 1985; Prather et al., 2008). Interestingly, in species in which only males sing, the temporal pattern of HVC neuron activity is nearly identical when the birds are singing and to playback to their song (Prather et al., 2008; Mooney, 2014). The similarity in sensory- and motor-related HVC activity makes it challenging to differentiate these two signals.

Duetting birds, in contrast, receive two categories of feedback. From the perspective of an individual bird, the duet is composed of two types of syllables, those that it produced (autogenous) and those produced by the partner (heterogenous). Any syllable produced by the bird must involve the generation of motor patterns in the brain for singing, and hearing its own vocal output (Figure 1B). In contrast, when the other bird sings, there is no motor output. This is where duetting birds offer an advantage–when one of the birds is singing, its HVC has a sensorimotor interaction that is presumably similar to that which occurs in non-duetting species of songbirds. But when the partner bird is singing, it only receives sensory feedback. Therefore, we can use these different forms of sensory feedback to help us understand how behaviors are coordinated between two individuals.

Turn-taking and other behaviors in plain-tailed wrens

To understand behavioral rules used by duetting wrens, we placed microphones in the thick bamboo stands in which they live (Figures 2B,C; Fortune et al., 2011). The birds sing extremely loud duets – we measured over 80 dB SPL standing within a few meters of the birds. The duet durations ranged from a few seconds to over 2 minutes of continuous singing (as reported in Mann et al., 2006). Birds repeated short-duration motifs, typically less than 2 seconds, composed of four to six unique syllables (Figures 2D,E). Females and males alternated syllable production within each motif, although individuals occasionally dropped a syllable (see Figure 1C in Fortune et al., 2011). The patterns of syllables in duets often sound quite consistent. Visual inspection of spectrograms, however, show that individuals make small changes in acoustic features, particularly in the time-varying frequency within syllables, over the duration of duets (Figure 2E). These variations appear to add additional complexity to duet performances. Future experiments may examine the potential relevance of these variations to the animals, and test whether each bird is responding to changing acoustic dynamics in its partner's syllables.

These recordings also showed that wrens produce "solo" songs in which either the female or male sings by itself (Figure 2D; see Figure 1 in Fortune et al., 2011). When males sing alone, their syllables are generally produced at much lower amplitudes than when they sing in duets. We also found that the solo songs of both individual female and individual male wrens are composed of similar syllables and sequences of syllables as seen in duets (see Figure 1 in Fortune et al., 2011).

Plain-tailed wrens are not prolific singers, singing perhaps dozens of duets in a day. We observed differences in singing from day-to-day: on some days they produced very few or no songs, whereas on other days all pairs of birds in the area sang throughout the day. We do not know the causes of these variations in singing (weather, food availability, etc.), but the song-producing circuits in the brain are likely modulated by environmental cues.

We also observed that the patterns of duet singing sometimes shift during longer-duration duets, resulting in an overt change in the cadence of the song (Figure 2E). How

and why birds make these changes is unknown. On one hand, these changes in cadence may be a form of error correction following a poorly produced syllable. Alternatively, these changes may be cues used in territorial defense, to reinforce pair bonds, or as a mechanism for sexual selection. We also observed differences in duetting between birds in their natural habitat and when in captivity. Pairs of wrens in captivity typically sang shorter duration duets, on the order of seconds, and rarely produced longer duets. As a result, our neurophysiological experiments focused on shorter duration duets, and have not addressed mechanisms that underlie changes in cadence found in some longer duets.

Exchange of sensory information in solo and duet singing

In plain-tailed wrens, acoustic cues alone are sufficient for the coordination of duetting, as birds that are visually isolated from each other produce normal duets. Remarkably, on a few occasions captured birds that were held temporarily in cloth bags duetted with their uncaptured partners. Additionally, wrens can initiate duets with more than ten meters between the individuals. In the field, we have heard duets in which one of the birds is adjacent to our location but the other bird is deep in the bamboo (Figure 2D). Delays due to the speed of sound – 10 meters is traversed in about 30 ms – are obvious to human listeners and affect the timing of turn–taking during duets.

Acoustic cues from the partner can modulate the timing of the duet. We observed a difference between solo and duet songs in the timing of syllables (Fortune et al., 2011). In both females and males, solo songs showed greater variability in the intersyllable intervals when compared to duets (Fortune et al., 2011). This change likely results from hearing partner syllables during duet singing. These data suggest that each bird has a pattern-generating circuit in its brain that produces its song, as is typical in oscine passeriform birds, and that sensory cues from the partner modulate the temporal dynamics of this pattern-generating circuit (Figure 1B).

These behavioral observations provided the framework for our neurophysiological recordings. In short, duet singing is produced by central pattern-generators (CPGs) in each bird, and acoustic cues from the partner modulate the timing of these CPGs. From previous studies, we knew that HVC acts as a CPG for song production (Long and Fee, 2008) and that HVC neurons receive auditory input (Margoliash, 1983; Mooney et al., 2001; Coleman et al., 2007). We therefore focused on HVC for neurophysiological recordings.

Neurophysiological mechanisms for the coordination of duet performances

To understand the neural mechanisms for duet singing, we used two categories of neurophysiological recordings: recordings in urethane-anesthetized birds (Fortune et al., 2011), and recordings in awake, singing wrens (Coleman et al., 2021). Based on extensive previous work in other songbird species, we expected substantial differences in the patterns of neurophysiological activity in these two conditions. Previous studies in which HVC recordings were made in urethane-anesthetized birds showed that HVC neurons are highly selective for the bird's own learned song and typically do not respond to conspecific vocalizations (Margoliash, 1986; Mooney, 2000; Mooney et al., 2001). In these experiments, the bird is anesthetized, an electrode is placed in HVC, and pre-recorded songs and other sound stimuli are repeatedly played to the bird. We therefore expected that in plain-tailed wrens, neurons in HVC would respond to the bird's own vocalizations; that is, HVC neurons in males would respond to male syllables and neurons in females would respond to female syllables.

We captured wrens and made electrophysiological recordings from HVC neurons in urethane-anesthetized animals (Figures 3A–C; Fortune et al., 2011). In these experiments, we presented short duration duet songs, songs that contained only the female or male syllables, and songs in which the inter-syllable intervals were digitally altered. Surprisingly, we found that neurons in both female and male HVC not only responded to their own syllables, as expected, but also to the other bird's syllables. Further, we found that neurons in HVC responded most strongly to the combined duet performance. That is, HVC neurons responded more to playback of intact duets than to the sum of the responses to the female and male components played separately (Fortune et al., 2011). This result suggested that, even though each bird only sings its part, the neural circuits controlling their singing integrate the combined output of the two birds. This was the first clue we had that the neural system for turn-taking spans both birds (see Figure 1B), as neurons responded best to the combined signal.

We also observed an interesting sex difference in HVC activity. HVC neurons in males responded more strongly to female syllables than to their own syllables (see Figure 3B in Fortune et al., 2011). In other words, HVC neurons in males responded more strongly to heterogenous cues than autogenous cues. In females, neurons responded more to autogenous cues (the female syllables) than heterogenous. In sum, neurons in both females and males responded more strongly to female syllables. This suggested that female syllables have more salience in the coordination of duet performances than male syllables. We interpreted this result that females provide the leading cues

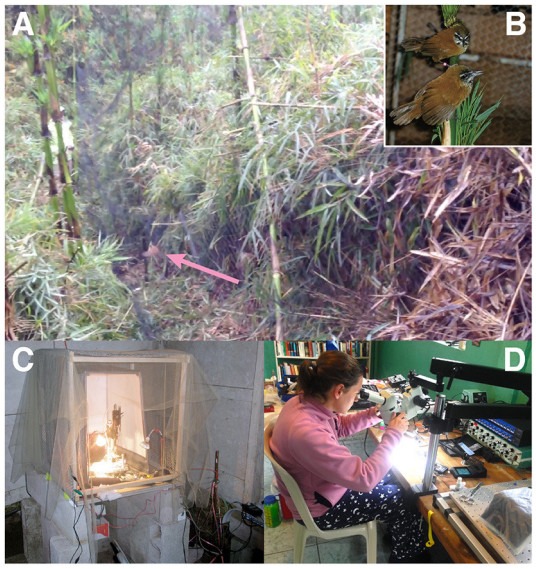

FIGURE 3
Capture and electrophysiological recording preparation. **(A)** A photograph of a plain-tailed wren (pink arrow) that was caught by a mist net. **(B)** A female (top) and male (bottom) plain-tailed wren in captivity. **(C)** The first electrophysiological rig that we used for recordings in urethane-anesthetized wrens. The vibration isolation table was a large tile plate that rested on tennis balls atop cinder blocks. A mesh was placed over the rig to prevent flying insects from interfering with the recordings. Note the copper rod used for grounding to the right of the rig. **(D)** Electrode arrays for chronic recordings were constructed at the field station in an improvised experimental rig–visible are the temperature controller (bottom right), amplifier and recording system (center right), and microscope mounted to a door used as the table. Both **(C,D)** are at the Yanayacu Biological Field Station and Center for Creative Studies.

for coordinating duet performances. A similar conclusion was made in duetting bay wrens, based on behavioral results (Levin, 1996a,b).

What neural mechanisms give rise to the facilitated responses to duets in HVC? To understand the mechanisms by which HVC neurons integrate signals, we digitally manipulated either the female or male solo song by altering the gaps in between syllables (see Figure 4 in Fortune et al., 2011). For example, we modified or eliminated the gaps between syllables and discovered that stimuli with proper timing of syllables elicited significantly greater responses than stimuli that did not have proper timing. These data suggested the pattern generating circuit in each bird is tuned to the temporal structure of duet singing. Stimuli with normal gaps elicit stronger responses because the timing of sensory cues matches the temporal structure of the CPG. In contrast, stimuli with abnormal or missing gaps do not match the temporal structure of the CPG, resulting in weaker activation.

This finding may be a potential neural mechanism for a behavioral observation seen in duets recorded in the field. When females and males produce sequences of solo syllables, the temporal order of the syllables is similar to that when they sing duets, reflecting the role of a CPG in song production. Critically, when a bird (usually a male) drops a syllable, the partner often continues to sing its normal pattern of syllables. Interestingly, the inter-syllable interval is altered without the male, suggesting heterogenous input modulates the timing of the ongoing CPG (see Figure 1 in Fortune et al., 2011).

Neurophysiological recordings from duetting wrens

Our initial experiments suggested that circuits in HVC integrate information from both birds (Fortune et al., 2011). However, these experiments were conducted in urethane-anesthetized birds, and it was unclear how auditory feedback from the partner influenced vocal production and turn-taking in awake, behaving birds. To understand the neural mechanisms of sensory-motor interactions underlying turn-taking we needed to record from birds when they were duetting. Knowing these experiments would be technically challenging in remote field sites, we decided to use multi-unit recordings (record from multiple neurons at one time). We also had to consider what type of equipment would be best to capture the neural activity in duetting birds. We decided to use a commercially available wireless recording system (Multi-Channel Systems MCS GmbH, Germany) for two reasons. First, wrens require bamboo in their cages which is incompatible with wired tethers. Second, wireless recording systems require less hardware that is also easier to implement at field sites.

We captured pairs of wrens on their territories (Figure 3A) at the Yanayacu Biological Field Station and maintained them for a short time (1–2 days) (Figure 3B) to allow them to adjust to captivity prior to surgery. Chronic electrodes were constructed in the field (Figure 3D) and were composed of four 50 micron wires with an additional reference and silver ground. The electrodes were implanted into either the left or right HVC. Once each bird recovered from surgery, we then captured the neural activity with a combined amplifier/digitizer that we attached to the electrode connector on the head of the bird. This amplifier/digitizer was powered by a battery that we placed on the back of a bird. One of the challenges we did not anticipate was designing a jacket for the battery. Our first attempts were using jackets created for zebra finches. However, we quickly realized these jackets did not work for the wrens who live in thick bamboo and were much more adept at using their legs and talons to remove the battery. We eventually designed a harness that secured the battery to the back of the wrens and did not impede their behavior.

Based on work in other songbirds and our previous finding in anesthetized wrens (Margoliash, 1986; Mooney, 2000;

Mooney et al., 2001; Fortune et al., 2011), we expected an increase in HVC activity when each bird was singing (premotor activity) and an increase in HVC activity when each bird heard its partner (auditory-evoked activity). When we recorded from HVC of duetting wrens, we found that HVC activity in both the female and the male increased when they produced their own syllables, as expected (Figure 4, solid blue and magenta traces). However, we did not see an increase in HVC activity when either bird heard its partner's syllables. That is, there was an alternation of HVC activity that matched the alternation of syllable production in the pair (see also Figure 1A in Coleman et al., 2021).

Interestingly, this alternation of HVC activity was also found in duetting white–browed sparrow–weaver (Hoffmann et al., 2019). The alternation in HVC premotor activity does not explain how birds synchronize their vocalizations. How does heterogenous auditory feedback modulate the timing of vocalizations in partner birds? Surprisingly, a clue came from a comparison of results from experiments in awake and anesthetized wrens.

We used urethane as an anesthetic – urethane blocks GABAergic transmission (Accorsi-Mendonça et al., 2007). When the wrens were awake, HVC neurons were only active when the bird was singing its own syllables (premotor activity). However, under urethane anesthesia, HVC neurons, particularly in males, responded to playback of syllables from both birds (Figure 4, gray traces with blue and magenta outlines). This finding supported the idea that heterogenous activity in awake animals activates GABAergic circuits that inhibit premotor activity in HVC. Urethane blocks this inhibition so that when the birds are anesthetized, heterogenous auditory input is 'unmasked' and now excites HVC neurons. Future experiments will more directly test the role of GABAergic inhibition in timing of turn-taking in wrens.

GABAergic inhibition has also been shown to coordinate another form of turn–taking in songbirds. In an elegant study, Benichov and Vallentin (2020) studied the neural basis for the coordination of calls between male zebra finches. Microinfusion of muscimol, a GABA agonist, resulted in a degradation of the timing of responses to calls. However, microinfusion of gabazine, a GABA antagonist, decreased the latency of responses to calls. This result contributes to the idea that turn–taking is an ancestral feature in songbirds and that inhibition may be a phylogenetically wide-spread neural mechanism for turn–taking. Odom et al. (2014) found that female singing is found in 71 percent of the species they surveyed across 32 families. A phylogenetic analysis of these data suggest that female song may be ancestral to oscine passeriform birds (Odom et al., 2014), a potential basis for turn-taking in these ancestral species.

The idea of inhibitory feedback between individuals is intriguing as it can help prevent overlapping vocalizations, a hallmark of turn-taking. Inhibitory feedback could also help explain the fast alternation of syllables. Once a neuron is inhibited, it can rebound from the inhibition (post-inhibitory rebound; PIR) and fire action potentials more quickly and at a higher firing rate. In addition, PIR may help explain the supralinear response to playback of duet song–HVC responded most strongly to the combined duet performance. Perhaps this supralinear response is due to post-inhibitory rebound. Inhibition also supports the model that the two individuals act as a single circuit (Figure 1B). In this model, each bird produces song through a pattern-generating circuit and the timing of the pattern is modulated by inhibitory feedback from the partner–much like a half-center oscillator (Marder and Calabrese, 1996; Calabrese, 1999).

Inhibition may be a neural mechanism used for the precise coordination of turn-taking in other species of duetting songbirds. For example, we hypothesize that duetting birds which have precise alternation of their vocalizations, like white–browed sparrow–weavers (Hoffmann et al., 2019) and canebrake wrens, (Rivera-Cáceres et al., 2016), may rely on inhibition. However, other duetting species whose duets are less tightly coordinated, like the black-bellied wren (Logue, 2007), may not use feedback inhibition and might rely on other neural mechanisms for coordination. This hypothesis, that inhibition emerges as a mechanism to improve the precision of timing of turn–taking, can be examined in additional comparative studies.

Practical challenges to field work with plain-tailed wrens

Neuroethological studies conducted in an animal's native habitat allow the organisms to express a wider spectrum of its behavioral repertoire. The wider and more naturalistic expression of behavior allows scientists to address new questions concerning the control of behavior with greater confidence in the relevance of the findings. However, work at field sites introduce numerous experimental, practical, and scientific challenges that are reduced in laboratory settings. Lack of control, repeatability, implementation of technologies, access to technical support, and the enormous array of practical issues of working in remote uncontrolled habitats are serious barriers to scientific progress.

As expected, we faced biological and practical obstacles in establishing our research program using plain-tailed wrens. For example, a major hurdle in studying these birds is that they live in dense chusquea bamboo (Figure 2B). To capture the wrens, we discovered that we had to cut thin paths in the bamboo within their territories for our nets (Figure 3A). The nets themselves were constantly becoming tangled in the bamboo, and the birds, which navigate dense foliage every day, were well prepared to evade becoming tangled in the nets. The most successful approach for catching the wrens was to present a few playbacks of conspecific duets just after erecting the nets.

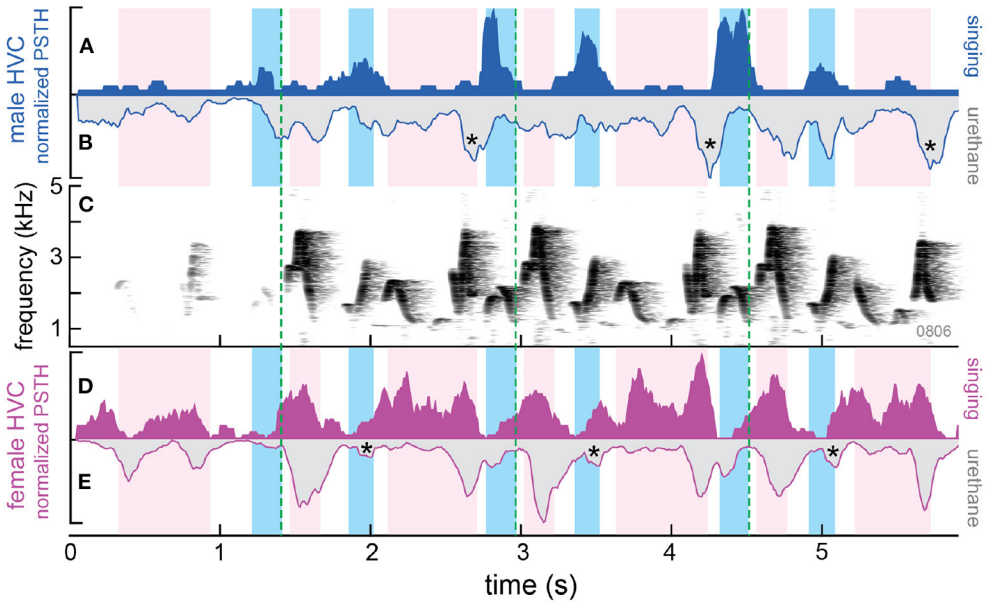

FIGURE 4
Differences in patterns of HVC activity in awake vs. anesthetized wrens. Background shading indicates the time each bird sang a syllable: darker blue for male and lighter magenta for the female. **(A)** Normalized PSTH shows HVC activity recorded from the male while duetting (singing; solid blue). **(B)** Inverted PSTH showing activity in response to playback (20 repetitions) of the same duet while the male was anesthetized with urethane. The histogram for activity during urethane anesthesia has been inverted to highlight the temporal relations in HVC activity when the bird is awake and singing and when the bird is anesthetized. Stars highlight increases in HVC activity near the end of partner (female) syllables. These increases in HVC activity may be inhibitory auditory responses in awake birds that are revealed by the action of urethane anesthesia. **(C)** Spectrogram of the duet produced by the pair of wrens. Dotted green lines highlight repetitions of duet motifs. **(D,E)** HVC neural activity in the female during singing and urethane as in **(A,B)**. Stars same as in **(B)**, but for recordings in the female.

Perhaps not surprisingly, the wrens were able to rapidly pin–point the locations of playback speakers, which we placed near the center of the net often about 0.5 m above the ground.

Another major hurdle is that our experiments rely on capturing both individuals of a female–male pair. The birds are monomorphic, making it difficult to distinguish during capture. We discovered that if the female was captured in the net first, the male would often simply depart. In contrast, if the male was captured first, the female would remain and was particularly aggressive in countersinging and exploring near the site of playback, facilitating her capture. Once in captivity, males tended to be more gregarious whereas the females tended to be more shy. For example, after capture, males readily accept worms and other food from experimenters hands, whereas females remained wary of humans.

Feeding the wrens was its own challenge. Wrens eat live insects, and we provided them with live crickets every hour. We were able to capture relatively small quantities of wild crickets by hand at our field site. Fortunately, there is a foundation near Quito, Wikiri, dedicated to frog conservation (www.wikiri.com.ec). Their efforts in frog conservation required that they farm crickets–which became the commercial source of the large numbers of crickets needed for our project.

Finally, wrens rely on nests in the bamboo to survive the cold nights (less than 12 degrees C) of their high–altitude habitats. To keep birds warm at our field sites that did not have heating, we placed our hot bead sterilizer (used for sterilizing surgical instruments) under a blanket that covered the cages at night.

As to more practical issues, electrophysiological studies require a truck-load of equipment that we had to transport to our field sites (Figures 3C,D). Of course, this equipment also requires electricity and, for our initial experiments, the electricity at our field station, the Yanayacu Biological Field Station and Center for Creative Studies, was generated from local hydro-power. The power depended on rain: the power would sometimes run out and so we had to implement a 12 V backup system using car batteries that were charged *via* solar panels.

Unexpectedly, the electrical grounding at our field sites was terrible to non-existent. For grounding, we purchased a 2 m copper rod (1.5 cm diameter) that we placed into the soil near our recording systems (see Figure 3C). Many of our initial experiments in anesthetized wrens were done in a shack that was open to the surrounding cloud forest. We had to protect the recording electrode from the many, many insects that were attracted to our lights, so we used a gauze-like material (chiffon) that we draped over the rig (Figure 3C).

Technical problems that are simple to solve in the laboratory are often more difficult to solve in the field. For example, to solve a saturation problem with our amplifier, the company advised us to send the amplifier back to them to change an internal setting. The solution we eventually used turned out to be simple. We had inadvertently created a small battery between our recording electrode and our reference electrode by using two different materials – our recording electrode was made from carbon and the reference electrode was silver. To solve this problem, we purchased a carbon art pencil, cut off the tip, and used Silverprint (GC Electronics, Rockford IL USA) to make it into a reference electrode. It worked like a charm.

Despite these challenges, we find field work personally and scientifically rewarding. Personally, solving problems in the field is enjoyable as it often requires a deeper understanding of the fundamentals of the tools and approaches that we use. For example, in the lab you might simply replace a part or send it for repair whereas in the field you often must devise alternative solutions. Scientifically, each species has evolved in its own environment and therefore has its own idiosyncrasies. These idiosyncrasies provide insights into, for example, how variability in nervous system control strategies is used to produce variability in behaviors. Further, biology requires a comparative approach to differentiate universal mechanisms from idiosyncratic features. Field studies are often the only avenue to study non-traditional species.

Discussion

We believe the conceptualization of interacting animals acting as a unit is useful for the study of social behaviors in other species including duetting in Drosophila (LaRue et al., 2015; Coen and Murthy, 2016), singing mice (Okobi et al., 2019), antiphonal communcation in primates (Miller et al., 2009; Takahashi et al., 2013; Pika et al., 2018), and humans (Levinson, 2016). We found that the nervous system of plain-tailed wrens is 'tuned' to the combined performance, therefore, thinking of cooperating individuals as a single unit may reveal neural mechanisms that are not obvious or present when thinking of animals as simple senders or receivers.

Future studies using plain-tailed wrens could focus on three major questions. First, How do males and females learn their respective parts? In other words, how do wrens of each sex learn the timing and identity of their own syllables? One possibility is that both female and male wrens learn both parts of the duet and then participate in duets as adults, in sex-specific manner. Alternatively, females only learn and sing female syllables. Gaining insights to song learning requires longitudinal recordings while young wrens hear adult models and then later develop their songs. One potential role of chorusing, in which several plain-tailed wrens simultaneously perform the same syllables (Mann et al., 2006), is in learning sex-appropriate roles in duet singing (Rivera-Cáceres et al., 2018).

Second, how do plain-tailed wrens learn to coordinate duet performances with their partners as adults? Anecdotally, when we caught female and male wrens from different territories, they sang together. Initially, the duet is not well-coordinated and very short (2–5 motifs), but after time the synchronization and the length of the song improves. One experiment to test this is to form new male/female pairings of wrens from distant territories or even from groups that sing different dialects. We could then quantify the changes in duet performances that emerge over time. Further, we predict an emergence of clear inhibitory responses in the brains of each wren as duet performances improves. Finally, what are the rules for duetting in plain-tailed wrens? Several studies in other species have described the behavioral rules and signals embodied in duet performances (Logue, 2006, 2007; Rivera-Cáceres et al., 2016; Rivera-Cáceres et al., 2018). Understanding these rules in plain-tailed wrens may facilitate future experiments that may reveal the roles of neural activity in HVC and other song nuclei in turn-taking.

Author contributions

All authors listed have made a substantial, direct, and intellectual contribution to the work and approved it for publication.

Funding

This study was supported by NSF IOS-1146792 (MC), NSF IOS-1146855 (EF).

Acknowledgments

We thank Harold Greeney and José Simbaña for support of our efforts at the Yanayacu Biological Field Station and Center for Creative Studies. We thank Santiago Burneo, and Alejandra Camacho for logistical support in Ecuador, and Ignacio Moore for the use of his truck. We also thank Stephanie White for her generous support.

Conflict of interest

The authors declare that the research was conducted in the absence of any commercial or financial relationships that could be construed as a potential conflict of interest.

Publisher's note

All claims expressed in this article are solely those of the authors and do not necessarily represent those of their affiliated

References

Accorsi-Mendonça, D., Leão, R. M., Aguiar, J. F., Varanda, W. A., and Machado, B. H. (2007). Urethane inhibits the GABAergic neurotransmission in the nucleus of the solitary tract of rat brain stem slices. *Am. J. Physiol. Regulat. Integrat. Compar. Physiol.* 292, R396-R402. doi: 10.1152/ajpregu.00776.2005

Baker, C. A., Clemens, J., and Murthy, M. (2019). Acoustic pattern recognition and courtship songs: Insights from insects. *Annu. Rev. Neurosci.* 42, 129–147. doi: 10.1146/annurev-neuro-080317-061839

Banerjee, A., and Vallentin, D. (2022). Convergent behavioral strategies and neural computations during vocal turn-taking across diverse species. *Curr. Opin. Neurobiol.* 73, 102529. doi: 10.1016/j.conb.2022.102529

Benichov, J. I., and Vallentin, D. (2020). Inhibition within a premotor circuit controls the timing of vocal turn-taking in zebra finches. *Nat. Commun.* 11, 221. doi: 10.1038/s41467-019-13938-0

Brainard, M. S., and Doupe, A. J. (2001). Postlearning consolidation of birdsong: stabilizing effects of age and anterior forebrain lesions. *J. Neurosci.* 21, 2501–2517. doi: 10.1523/JNEUROSCI.21-07-02501.2001

Brainard, M. S., and Doupe, A. J. (2002). What songbirds teach us about learning. *Nature* 417, 351–358. doi: 10.1038/417351a

Brenowitz, E. A. (2021). Taking turns: the neural control of birdsong duets. *Proc. Natl. Acad. Sci. U.S.A.* 118, 2108043118. doi: 10.1073/pnas.2108043118

Calabrese, R. L. (1999). Neural coordination: taking the lead from a model. *Curr. Biol.* 9, R680-R683. doi: 10.1016/S0960-9822(99)80438-2

Catchpole, C. K., and Slater, P. J. B. (2018). *Bird Song, 2nd Edn.* Cambridge: Cambridge University Press.

Coen, P., and Murthy, M. (2016). Singing on the fly: sensorimotor integration and acoustic communication in *Drosophila. Curr. Opin. Neurobiol.* 38, 38–45. doi: 10.1016/j.conb.2016.01.013

Coleman, M. J., Day, N. F., Rivera-Parra, P., and Fortune, E. S. (2021). Neurophysiological coordination of duet singing. *Proc. Natl. Acad. Sci. U.S.A.* 118, e2018188118. doi: 10.1073/pnas.2018188118

Coleman, M. J., and Fortune, E. S. (2018). Duet singing in plain-tailed wrens. *Curr. Biol.* 28, 643–645. doi: 10.1016/j.cub.2018.02.066

Coleman, M. J., Roy, A., Wild, J. M., and Mooney, R. (2007). Thalamic gating of auditory responses in telencephalic song control nuclei. *J. Neurosci.* 27, 10024–10036. doi: 10.1523/JNEUROSCI.2215-07.2007

Doupe, A. J., and Kuhl, P. K. (1999). Birdsong and human speech: common themes and mechanisms. *Annu. Rev. Neurosci.* 22, 567–631. doi: 10.1146/annurev.neuro.22.1.567

Elie, J. E., Hoffmann, S., Dunning, J. L., Coleman, M. J., Fortune, E. S., and Prather, J. F. (2019). From perception to action: the role of auditory input in shaping vocal communication and social behaviors in birds. *Brain Behav. Evol.* 94, 51–60. doi: 10.1159/000504380

Fortune, E. S., Rodriguez, C., Li, D., Ball, G. F., and Coleman, M. J. (2011). Neural mechanisms for the coordination of duet singing in wrens. *Science* 334, 666–670. doi: 10.1126/science.1209867

Hoffmann, S., Trost, L., Voigt, C., Leitner, S., Lemazina, A., Sagunsky, H., et al. (2019). Duets recorded in the wild reveal that interindividually coordinated motor control enables cooperative behavior. *Nat. Commun.* 10, 2577. doi: 10.1038/s41467-019-10593-3

Horita, H., Wada, K., and Jarvis, E. D. (2008). Early onset of deafening-induced song deterioration and differential requirements of the pallial-basal ganglia vocal pathway. *Eur. J. Neurosci.* 28, 2519–2532. doi: 10.1111/j.1460-9568.2008.06535.x

Ikeda, M. Z., Trusel, M., and Roberts, T. F. (2020). Memory circuits for vocal imitation. *Curr. Opin. Neurobiol.* 60, 37–46. doi: 10.1016/j.conb.2019.11.002

Konishi, M. (1965). The role of auditory feedback in the control of vocalization in the white-crowned sparrow. *Zeitschrift f¨ur* Tierpsychol. 22, 770–783. doi: 10.1111/j.1439-0310.1965.tb01688.x

LaRue, K. M., Clemens, J., Berman, G. J., and Murthy, M. (2015). Acoustic duetting in drosophila virilis relies on the integration of auditory and tactile signals. *eLife* 4, e27. doi: 10.7554/eLife.07277.027

Leonardo, A., and Konishi, M. (1999). Decrystallization of adult birdsong by perturbation of auditory feedback. *Nature* 399, 466–470. doi: 10.1038/20933

Levin, R. N. (1996a). Song behaviour and reproductive strategies in a duetting wren, *Thryothorus nigricapillus*: I. removal experiments. *Animal Behav.* 52, 1093–1106. doi: 10.1006/anbe.1996.0257

Levin, R. N. (1996b). Song behaviour and reproductive strategies in a duetting wren, *Thryothorus nigricapillus*: II. playback experiments. *Animal Behav.* 52, 1107–1117. doi: 10.1006/anbe.1996.0258

Levinson, S. C. (2016). Turn-taking in human communication–origins and implications for language processing. *Trends Cogn. Sci.* 20, 6–14. doi: 10.1016/j.tics.2015.10.010

Logue, D. M. (2006). The duet code of the female black-bellied wren. *Condor.* 108, 326–335. doi: 10.1093/condor/108.2.326

Logue, D. M. (2007). How do they duet? sexually dimorphic behavioural mechanisms structure duet songs in the black-bellied wren. *Animal Behav.* 73, 105–113. doi: 10.1016/j.anbehav.2006.05.011

Long, M. A., and Fee, M. S. (2008). Using temperature to analyse temporal dynamics in the songbird motor pathway. *Nature* 456, 189–194. doi: 10.1038/nature07448

Mann, N. I., Dingess, K. A., and Slater, P. J. B. (2006). Antiphonal four-part synchronized chorusing in a Neotropical wren. *Biol. Lett.* 2, 1–4. doi: 10.1098/rsbl.2005.0373

Marder, E., and Calabrese, R. L. (1996). Principles of rhythmic motor pattern generation. *Physiol. Rev.* 76, 687–717. doi: 10.1152/physrev.1996.76.3.687

Margoliash, D. (1983). Acoustic parameters underlying the responses of song-specific neurons in the white-crowned sparrow. *J. Neurosci.* 3, 1039–1057. doi: 10.1523/JNEUROSCI.03-05-01039.1983

Margoliash, D. (1986). Preference for autogenous song by auditory neurons in a song system nucleus of the white-crowned sparrow. *J. Neurosci.* 6, 1643–1661. doi: 10.1523/JNEUROSCI.06-06-01643.1986

Margoliash, D., and Konishi, M. (1985). Auditory representation of autogenous song in the song system of white-crowned sparrows. *Proc. Natl. Acad. Sci. U.S.A.* 82, 5997–6000. doi: 10.1073/pnas.82.17.5997

Miller, C. T., Beck, K., Meade, B., and Wang, X. (2009). Antiphonal call timing in marmosets is behaviorally significant: interactive playback experiments. *J. Compar. Physiol. A* 195, 783–789. doi: 10.1007/s00359-009-0456-1

Mooney, R. (2000). Different subthreshold mechanisms underlie song selectivity in identified HVc neurons of the zebra finch. *J. Neurosci.* 20, 5420–5436. doi: 10.1523/JNEUROSCI.20-14-05420.2000

Mooney, R. (2014). Auditory–vocal mirroring in songbirds. *Philos. Trans. R. Soc. B Biol. Sci.* 369, 20130179. doi: 10.1098/rstb.2013.0179

Mooney, R., Hoese, W., and Nowicki, S. (2001). Auditory representation of the vocal repertoire in a songbird with multiple song types. *Proc. Natl. Acad. Sci. U.S.A.* 98, 12778–12783. doi: 10.1073/pnas.221453298

Mooney, R., and Prather, J. F. (2005). The HVC microcircuit: the synaptic basis for interactions between song motor and vocal plasticity pathways. *J. Neurosci.* 25, 1952–1964. doi: 10.1523/JNEUROSCI.3726-04.2005

Nordeen, K. W., and Nordeen, E. J. (1992). Auditory feedback is necessary for the maintenance of stereotyped song in adult zebra finches. *Behav. Neural Biol.* 57, 58–66. doi: 10.1016/0163-1047(92)90757-U

Nottebohm, F., Stokes, T. M., and Leonard, C. M. (1976). Central control of song in the canary, serinus canarius. *J. Comp. Neurol.* 165, 457–486. doi: 10.1002/cne.901650405

Odom, K. J., Hall, M. L., Riebel, K., Omland, K. E., and Langmore, N. E. (2014). Female song is widespread and ancestral in songbirds. *Nat. Commun.* 5, 3379. doi: 10.1038/ncomms4379

Okobi, D. E., Banerjee, A., Matheson, A. M. M., Phelps, S. M., and Long, M. A. (2019). Motor cortical control of vocal interaction in neotropical singing mice. *Science* 363, 983–988. doi: 10.1126/science.aau9480

Perkes, A., White, D., Wild, J. M., and Schmidt, M. (2019). Female songbirds: the unsung drivers of courtship behavior and its neural substrates. *Behav. Processes*. 163, 60–70. doi: 10.1016/j.beproc.2017.12.004

Pika, S., Wilkinson, R., Kendrick, K. H., and Vernes, S. C. (2018). Taking turns: bridging the gap between human and animal communication. *Proc. R. Soc. B Biol. Sci*. 285, 20180598. doi: 10.1098/rspb.2018.0598

Prather, J. F., Peters, S., Nowicki, S., and Mooney, R. (2008). Precise auditory-vocal mirroring in neurons for learned vocal communication. *Nature* 451, 305–310. doi: 10.1038/nature06492

Rivera-Cáceres, K. D., Quirós-Guerrero, E., Araya-Salas, M., and Searcy, W. A. (2016). Neotropical wrens learn new duet rules as adults. *Proc. R. Soc. B Biol. Sci*. 283, 20161819. doi: 10.1098/rspb.2016.1819

Rivera-Cáceres, K. D., Quirós-Guerrero, E., Araya-Salas, M., Templeton, C. N., and Searcy, W. A. (2018). Early development of vocal interaction rules in a duetting songbird. *R. Soc. Open Sci*. 5, 171791. doi: 10.1098/rsos.171791

Roberts, T. F., Hisey, E., Tanaka, M., Kearney, M. G., Chattree, G., Yang, C. F., et al. (2017). Identification of a motor-to-auditory pathway important for vocal learning. *Nat. Neurosci*. 20, 978–986. doi: 10.1038/nn.4563

Takahashi, D. Y., Narayanan, D. Z., and Ghazanfar, A. A. (2013). Coupled oscillator dynamics of vocal turn-taking in monkeys. *Curr. Biol*. 23, 2162–2168. doi: 10.1016/j.cub.2013.09.005

Vu, E. T., Mazurek, M. E., and Kuo, Y. C. (1994). Identification of a forebrain motor programming network for the learned song of zebra finches. *J. Neurosci*. 14, 6924–6934. doi: 10.1523/JNEUROSCI.14-11-06924.1994

frontiers | Frontiers in Neural Circuits

TYPE Correction
PUBLISHED 08 December 2022
DOI 10.3389/fncir.2022.1068385

OPEN ACCESS

APPROVED BY
Frontiers Editorial Office,
Frontiers Media SA, Switzerland

*CORRESPONDENCE
Melissa J. Coleman
mcoleman@keckscl.claremont.edu

RECEIVED 12 October 2022
ACCEPTED 28 November 2022
PUBLISHED 08 December 2022

CITATION
Coleman MJ, Day NF and Fortune ES (2022) Corrigendum: Neural mechanisms for turn-taking in duetting plain-tailed wrens. *Front. Neural Circuits* 16:1068385. doi: 10.3389/fncir.2022.1068385

Corrigendum: Neural mechanisms for turn-taking in duetting plain-tailed wrens

Melissa J. Coleman[1]*, Nancy F. Day[2] and Eric S. Fortune[3]

[1]W.M. Keck Science Department, Claremont McKenna, Scripps and Pitzer Colleges, Claremont, CA, United States, [2]Department of Psychology, Whitman College, Walla Walla, WA, United States, [3]Department Biological Sciences, New Jersey Institute of Technology, Newark, NJ, United States

KEYWORDS

antiphonal, birdsong, duets, central pattern generator, auditory feedback, neuroethology

A corrigendum on
Neural mechanisms for turn-taking in duetting plain-tailed wrens

by Coleman, M. J., Day, N. F., and Fortune, E. S. (2022). *Front. Neural Circuits* 16:970434. doi: 10.3389/fncir.2022.970434

In the published article, there was an error in affiliation 1. Instead of "W.M. Keck Science Department, Scripps and Pitzer Colleges, Claremont, CA, United States," it should be "W.M. Keck Science Department, Claremont McKenna, Scripps and Pitzer Colleges, Claremont, CA, United States".

The authors apologize for this error and state that this does not change the scientific conclusions of the article in any way. The original article has been updated.

Publisher's note

All claims expressed in this article are solely those of the authors and do not necessarily represent those of their affiliated organizations, or those of the publisher, the editors and the reviewers. Any product that may be evaluated in this article, or claim that may be made by its manufacturer, is not guaranteed or endorsed by the publisher.

frontiers | Frontiers in Neural Circuits

TYPE Original Research
PUBLISHED 03 October 2022
DOI 10.3389/fncir.2022.994548

OPEN ACCESS

EDITED BY
Anna Lisa Stöckl,
University of Konstanz, Germany

REVIEWED BY
Nicolas Giret,
UMR9197 Institut des Neurosciences Paris Saclay (Neuro-PSI), France
Fabian Heim,
Max Planck Institute for Biological Intelligence, Germany

*CORRESPONDENCE
Jonathan F. Prather
Jonathan.Prather@uwyo.edu

RECEIVED 15 July 2022
ACCEPTED 02 September 2022
PUBLISHED 03 October 2022

CITATION
Lawley KS, Fenn T, Person E, Huber H, Zaharas K, Smith P, Coulter A and Prather JF (2022) Auditory processing neurons influence song evaluation and strength of mate preference in female songbirds.
Front. Neural Circuits 16:994548.
doi: 10.3389/fncir.2022.994548

Auditory processing neurons influence song evaluation and strength of mate preference in female songbirds

Koedi S. Lawley[1], Thomas Fenn[2], Emily Person[2], Holly Huber[2], Kristina Zaharas[2], Perry Smith[2], Austin Coulter[2] and Jonathan F. Prather[2]*

[1]Department of Veterinary Integrative Biosciences, School of Veterinary Medicine and Biomedical Sciences, Texas A&M University, College Station, TX, United States, [2]Neuroscience Program, Department of Zoology & Physiology, University of Wyoming, Laramie, WY, United States

Animals use a variety of complex signaling mechanisms to convey an array of information that can be detected by conspecifics and heterospecifics. Receivers of those signals perceive that information and use it to direct their subsequent actions. Thus, communication such as that which occurs between senders and receivers of vocal communication signals can be a powerful model in which to investigate the neural basis of sensory perception and action initiation that underlie decision-making. In this study, we investigated how female songbirds perceive the quality of acoustic signals (songs) performed by males and use that information to express preference for one song among many possible alternatives. We use behavioral measurement of song preference before and after lesion-induced alteration of activity in an auditory processing area (caudal nidopallium, NC) for which we have previously described its interconnections with other auditory areas and downstream reward pathways. Our findings reveal that inactivating NC does not change a female's ability or willingness to perform behavioral indicators of mate choice, nor does it change their ability to identify the songs of individual males. However, lesioning NC does induce a decrease in the strength of song preference for specific males more than others. That decrease does not result in a complete elimination of preference, as female preferences for specific males are still evident but not as strongly expressed after lesioning of NC. Taken together, these data indicate that NC plays a role in a female's strength of preference in song evaluation and mate choice, and activity in NC is an important facet of mate choice.

KEYWORDS

communication, perception - action, decision-making, neurobiology, hearing

Introduction

Organisms continuously perceive and process sensory information, determine the value of that information, and use it to select one action from many possible alternatives (Kable and Glimcher, 2009). These assessments and the associated actions result in decisions that have many biological and social impacts on the life of an organism. Such decisions can include where to forage, whether to flee, and perhaps the most evolutionarily significant decision of the partner with whom they will mate. In humans and other mammals, neural networks involving complex interactions between associational cortices and reward centers have been implicated in assessing stimulus value, and additional networks associated with motor initiation have also been well characterized (Gold and Shadlen, 2007). However, the neural mechanisms behind this complex processing of sensory information and the link between sensory information and motor activation remains poorly understood. Here we turn to an animal model to investigate those neural mechanisms and their associated roles.

Mate choice can be a useful model to explore the neural mechanisms of decision-making. Females of many species must perceive and evaluate sensory information such as plumage, ornamentation, behavioral displays, and vocalizations from members of the opposite sex to evaluate a male's quality (reviewed in Catchpole and Slater, 2008). The female can then use that information to selectively engage in courtship and copulatory behaviors with the suitor that she prefers most strongly. In the present study, we investigated female songbirds to identify the neural structures through which females recognize and evaluate the quality of male songs and use that information to choose their mates.

The behaviors expressed in songbird courtship and the circuits of the songbird brain provide an experimentally approachable context to characterize the links between neural activation and behavior (reviewed in Murphy et al., 2020; Fujii et al., 2022). In many songbird species, including the Bengalese finches (BF; *Lonchura striata domestica*) studied here, adult males can sing but females cannot (Catchpole and Slater, 2008; Mooney et al., 2008), but recent studies have highlighted that female song is more common than was previously appreciated (Odom et al., 2014; Langmore, 2020). Females recognize individual males by their songs and evaluate the quality of those songs to choose one mate from many suitors (Catchpole, 1987; Searcy and Yasukawa, 1996; Nowicki and Searcy, 2004; Catchpole and Slater, 2008). Adult female songbirds can perceive and evaluate even very subtle differences between songs (Clayton, 1988; Searcy and Brenowitz, 1988; Cynx et al., 1990; Searcy, 1990; Vernaleo and Dooling, 2011), and they use the suite of information obtained from those song performances to select their mate (Catchpole and Slater, 2008).

Studies of songbirds provide a key experimental advantage in that song is a unimodal stimulus. Even though mate choice involves information obtained through a variety of modalities, song is so influential that females will solicit copulation by performing a copulation solicitation display (CSD) in response to song even if no male is physically present (Searcy and Marler, 1981; Searcy et al., 1981; Searcy and Andersson, 1986; Candolin, 2003; Riebel, 2009; Byers et al., 2010; Dunning et al., 2014). Female perception and mate choice are best measured through CSD production, but other behaviors may also serve as proxies of female mate preference. Prior work from our group revealed that a female BF's song preference is reflected in not only the number of CSDs she performs but also the number of calls that she produces during song presentation (Dunning et al., 2014). Therefore, calls provide an easily detected and quantified measure of female mate preference (Dunning et al., 2014, 2020). In the present study, we use that well-established method to investigate the role of a specific set of auditory processing neurons in a female's behavioral expression of mate choice.

Many previous studies have revealed specific auditory brain regions that are active in response to the playback of song (Woolley and Doupe, 2008; Prather, 2013; Monbureau et al., 2015; Van Ruijssevelt et al., 2018). The activity of those cells can be dependent on not only the acoustic properties of the stimulus but also more complex social contexts, such as whether the song was performed by a conspecific or a heterospecific, or whether the song was familiar, such as the song or call of a mate, vs. a novel song stimulus (Gentner et al., 2004; Terpstra et al., 2004). One brain region that exhibits such selective responses is the caudal nidopallium (NC). Previous studies of NC in male songbirds have shown that following lesions to the medial portion of this area (NCM), there is a reduction in song recognition and preference for familiar (tutor) song (Gobes and Bolhuis, 2007). Other studies have shown that when NCM or the central portion of NC (NCC) are temporarily inactivated, females show a decrease in affiliative behavior with conspecific males (Tomaszycki and Blaine, 2014; Van Ruijssevelt et al., 2018). Together these results point to NC as a site associated with complex perceptions, and they suggest that in female songbirds, NC plays a role in preference for songs performed by conspecifics. We extended that study to investigate the degree to which NC activity also shapes individual recognition of multiple conspecifics and selective preference for one individual among many suitors.

Here, we used a well-established means of measuring the preference of female Bengalese finches for one song among many conspecific stimuli (Dunning et al., 2014, 2020), and we combined that with an excitotoxic means of lesioning only somas within NC while leaving fibers of passage intact (Jarrard, 1989). We explored the role of NC in shaping female expression of behavioral indicators of mate preference by performing behavioral tests of mate preference before and after placement of bilateral lesions in NC of each subject. Our results reveal that chemically lesioning NC while leaving fibers of passage intact does not change a female's ability or willingness to engage in

behavioral indicators of mate preference, nor does it alter a female's ability to identify the songs of individual males. Instead, lesion-induced changes in NC activity resulted in a change in the strength of preference for individual males. NC lesions result in a reduction of selectivity such that songs that were previously strongly preferred become less attractive, and songs that were previously least preferred become more attractive. Importantly, these reductions of selectivity do not result in a complete elimination of preference, indicating that activity in NC plays a key role in a female's strength of preference for specific songs from among the array of song stimuli that she hears.

Materials and methods

Care and handling of experimental subjects

We performed all experiments using adult (age >120 days post-hatch) BFs obtained from a commercial breeder (The Finch Farm, WA). All procedures were approved by the University of Wyoming Animal Care and Use Committee, and procedures were in compliance with recommendations from that group and state and federal regulations governing the housing and use of songbirds. A total of 28 (12 experimental, 10 controls, six shams) female subjects were used. At the end of behavioral recordings, birds were euthanized by an overdose of isoflurane and tissue was collected. Throughout all aspects of the study, care was taken to ensure health and comfort of all experimental subjects.

Animal housing and preparation for recording

We maintained a 15:9 light:dark photoperiod, and seed, water and grit were available *ad libitum*. We housed females in groups of no more than six birds in a wire cage (41 cm × 33 cm × 24 cm) within a sound-attenuating chamber. Prior to experimentation, we identified males by song performance. Females were identified by the presence of calls but the absence of songs over the course of three or more days of continuous recording in a sound attenuating chamber (Dunning et al., 2014). Sex was confirmed histologically at the end of each experiment. Following well established protocols (Dunning et al., 2014, 2020), females were housed in all-female groups to prevent physical interaction with male birds, but females could still hear conspecific male songs from neighboring chambers. Females were housed in this all-female arrangement for 3–5 days prior to beginning behavioral tests. During that time, they did not interact with males of their species, but females could have heard faint vocalizations from conspecific males residing in other chambers in the lab (Vyas et al., 2009; Dunning et al., 2014). None of the females studied here had ever interacted with the males from whom the song stimuli were recorded. During behavioral tests, females were housed individually in sound-attenuating chambers where songs were played (see below) and the female's behavioral responses (e.g., calls) were recorded by audio and video monitoring. At the time of each behavioral test, we moved the female to the chamber where we performed the behavioral tests (41 cm × 33 cm × 24 cm), and the bird was allowed to acclimate for at least 30 min after moving from the holding chamber and the beginning of testing (Banerjee and Adkins-Regan, 2011; Dunning et al., 2014, 2020).

Song stimulus preparation and presentation

Similar to methods we have used previously to measure mate preference in female BF's (Dunning et al., 2014), the undirected songs of six individual Bengalese finch males and one zebra finch male were recorded for at least 24 h (range 24–36 h) in a sound attenuated chamber in which we provided seed and water *ad libitum*. Because the males resided in the chamber alone, these were undirected song performances. We monitored vocal behavior using a microphone (Shure model SM57) positioned immediately adjacent to the bird's cage (41 cm × 33 cm × 24 cm), and we used custom software to continually record sounds and save them onto a computer hard drive (Sound Analysis Pro; songs were bandpass filtered 300–10,000 Hz; Matlab software; Tchernichovski et al., 2000). For each male, we composed an aggregate song file from several individual song performances (average of five songs; range three to nine songs; individual songs were separated by 1 s of silence) which together were approximately 47 s (range 42–52 s) to control for song duration. Thus, each male was represented by a concatenated song stimulus containing several songs collected for a total duration of about 47 s of audio and silence (see Dunning et al., 2014 for more details). Importantly for the behavioral experimental design used here, there were individual-specific differences in the properties of these songs (e.g., different song properties for each male) but the same stimuli were used in behavioral testing of mate preference before and after placement of bilateral lesions in NC of each subject.

Behavioral test of mate preference

Behavioral testing began immediately after the 30 min waiting period following transfer from the group housing cage to the individual testing cage (Dunning et al., 2014). Consistent with the female becoming acclimated during that time, females engaged in behaviors indicating their comfort (e.g., feeding,

drinking, grooming), and in each test we ensured that we had observed these behaviors prior to beginning.

Song stimuli were presented at 70 dB through a speaker (Sound Acoustics) residing in the sound attenuated chamber (70 dB measured 13 cm from speaker, distance between the bird and the speaker varied from 5 to 22 cm based on the bird's location as it moved within the cage). The sequence of song presentation was randomized for each test using a computer, with an interval of 20 s of silence between the aggregate song files of different males. We presented each aggregate song stimulus from each male once per test, and we tested birds no more than two times per day to prevent overexposure and habituation to the stimuli. We viewed the birds and recorded audio through a camera (General Electric model 45231) inside the sound attenuating chamber and measured each female's behavioral responses in real time. Because the audio and video recording camera was so close to the female, we could detect even very low amplitude calls, and we could visually confirm the occurrence of a call. Females displayed many behaviors such as calling, perch hopping, beak swiping, and wing flapping when presented with the song stimuli. These behaviors have been noted previously, and calls have been shown to be closely related to the expression of CSDs and mate preference (Dunning et al., 2014). Therefore, we quantified mate preference by counting the number of calls that each female produced during playback of each song stimulus.

To ensure that we had sufficient resolution to define each female's song preferences, we used well-established criteria to define a valid behavioral test of preference (Dunning et al., 2014). Each test involved playing all seven male song stimuli to each female. We required that female subjects called a minimum of 10 times in response to the song of at least one individual male or at least four times to the songs of at least two different males in order for a behavioral test to be considered valid (Dunning et al., 2014). If a bird did not complete four valid tests by the time that it had been tested eight times in Phase 1, then we ceased testing for that bird and excluded it from the Results (this was the case for only one of the females that we tested). We quantified the number of calls to six male BF conspecific song stimuli and one male zebra finch heterospecific song stimulus to determine each female bird's rank ordering and strength of preference among song stimuli. All calls performed during song presentations were included in those computations. We performed behavioral tests of song preference before (Phase 1) and after surgical manipulation (Phase 2) to quantify any changes in preference that emerged as a result of lesioning NC (**Figure 1**).

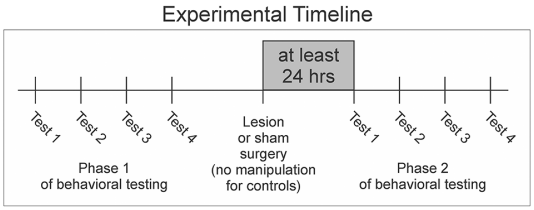

FIGURE 1
Females underwent two phases of behavioral testing. In each phase, females completed four valid tests of preference for songs performed by each of seven males. After the completion of Phase 1, experimental and sham birds received either lesion or sham surgeries before moving onto Phase 2. No manipulation was performed on control birds (detailed in "Methods" Section).

Surgery for placement of focal lesions

After recording the female's pre-manipulation song preferences, we made bilateral chemical lesions to NC (N = 12 birds) using ibotenic acid (500 nl, 1 mg/ml in deionized water; Cayman Chemical, MN). During that procedure, birds were anesthetized with isoflurane (inhalation of 1%–3% in 100% oxygen) and placed in a customized stereotaxic device to immobilize the head and beak. We made a small incision in the scalp and created a small opening in the skull (head angle: 45°, 0.4 mm anterior, 2.5 mm lateral from mid sagittal sinus), and lowered a microsyringe (Neurosyringe, Hamilton company, MO) to a depth of 2.0 mm beyond contact with the surface of the brain. Following the injections, the exposed brain was covered with an inert polymer (Kwik-Sil, World Precision Instruments, FL), the skin was closed with a tissue adhesive (Vetbond, 3M, MN), and topical anesthetic was applied to the skin (4% lidocaine, HI-Tech, NY). Following surgery, all birds resumed their normal behavior within several hours.

Following complete recovery, each bird was returned to an individual-housing chamber and allowed to recover for at least 24 h before we retested song preferences in Phase 2. In our sham birds (N = 3 birds), the incision and opening in the skull were made, the injection syringe was inserted into the brain, but no drug was injected. In other sham birds (N = 3 birds), the incision and opening were made, we waited an amount of time comparable to that of the injection, and the opening and skin were resealed. In all measures reported in the Results, there were no significant differences between those groups. For example, three of the birds produced more calls after lesioning than before, and three produced fewer calls than before. Each of those trios contained members of each sham surgical treatment group, and on average there was no difference between the two sham surgical treatment groups. Therefore, both sham treatments are reported in the Results as sham birds (N = 6 birds). In our control birds (N = 10 birds), we made no surgical manipulation of any kind between phases one and two of behavioral testing. In all behavioral tests, we followed the same paradigm in Phase 2 (after lesioning CM or after performing sham surgery or in the second half of control testing) as we did in Phase 1 (prior to lesioning NC or prior to performing sham surgery or in the first half of control testing).

Tissue collection and histological processing

After the end of post-manipulation behavioral testing, each female was deeply anesthetized using isoflurane and perfused transcardially with ice-cold 0.9% phosphate buffered saline followed by ice-cold 4% paraformaldehyde. We carefully removed the brain and placed it in 4% PFA for 24 h before being transferred to a 30% sucrose paraformaldehyde cryoprotecting solution for 72 h. We cut parasagittal sections

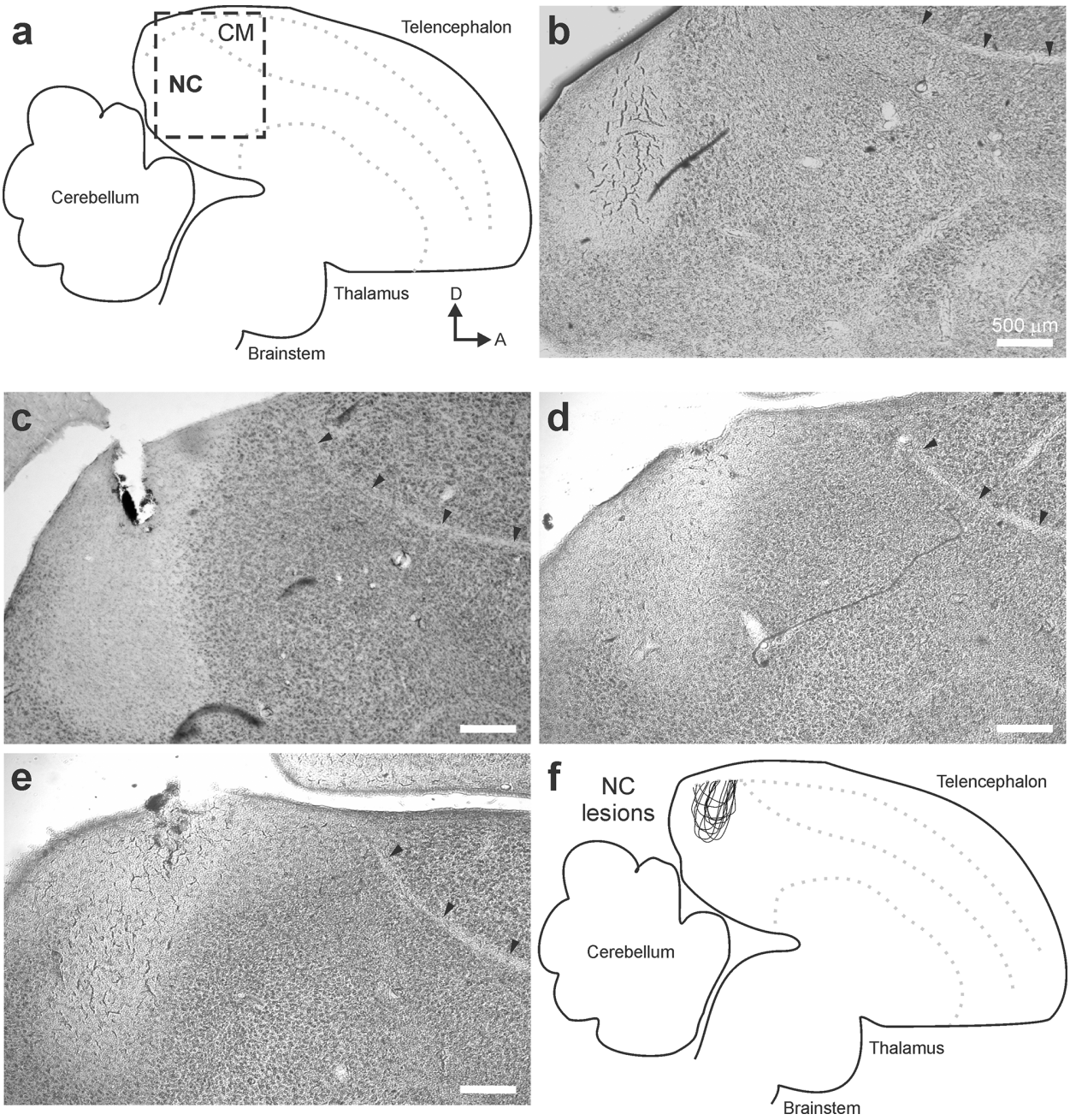

FIGURE 2
Lesions were restricted to NC. **(A)** The location of NC was recognized by its relative position in the brain as well as lamina that serve as anatomical landmarks. **(B–E)** At the end of each experiment, brain tissue was collected and used to verify the location of each lesion in each hemisphere. In no case did lesions affect tissue anterior of the lamina mesopallialis (small arrows; an easily recognizable interface between NC and CM) or inferior of the dorsal arcopallium lamina (not shown; another easily recognizable interface between the nidopallium and the arcopallium). **(F)** An overlay of traces of individual lesion sites confirmed that all lesions were restricted to NC.

(50 microns thickness) on a freezing microtome and placed them individually in wells containing phosphate buffer. Tissue sections were then mounted onto gelatin coated slides and allowed to dry overnight. The following day, tissue was stained with cresyl violet and viewed under a microscope (Olympus BX51 Brightfield Microscope; Olympus, PA) equipped with an RT-SE camera (SPOT 9.4 Slider-6, MA) and analyzed with SPOT software (version 5.1, MA). We compared our data to a stereotaxic atlas (Oregon Health and Science University, Portland, OR 97239[1]) to confirm accuracy of lesion placement. As elaborated in the Results, the extent of all lesions in birds described here was entirely within NC. Experimenters were blind to the results of the behavioral tests during the analysis of lesion placement.

Statistical analysis

We quantified each female's response to each song stimulus by counting the number of calls that the female performed in response to each stimulus (Dunning et al., 2014). We used those data to identify each female's most-preferred through least-preferred stimulus. To compare the pre-manipulation vs. post-manipulation conditions, we used nonparametric tests to compare the number of calls produced, and we used two sample Kolmogorov-Smirnov tests to compare the distributions of responses across the seven males from which song stimuli were recorded (Sokal and Rohlf, 2011). We used linear regression to compute the slope and intercept of data used to quantify strength of preference, and those same tests enabled us to perform statistical comparisons of those slope and intercept values against expected models (e.g., is slope different than zero; Sokal and Rohlf, 2011). In all tests, significance was assessed at alpha = 0.05. Values are reported as either individual values (e.g., range of numbers of calls) or means ± SE.

Results

NC lesioned females were unchanged in their ability to indicate mate preference

All lesions were restricted to NC (**Figure 2**, N = 12 birds). Lesions commonly extended along the axis on which the injection was made (**Figures 2B–E**). Similar to results from previous injections in NC, affected volumes typically extended 250–350 microns in the medial-lateral direction (Bloomston et al., 2022). As in previous reports, song playback resulted in call responses during the song presentation (Dunning et al., 2014, 2020). Calls produced by the females in this study were trills of the type described previously as amplitude modulated calls in adult female Bengalese finches (Yoneda and Okanoya, 1991). On average, female birds called 302 ± 29 times in response to all song stimuli in Phase 1 or Phase 2 (range 16–1,127; **Figure 3A**). These numbers of calls provided sufficient quantity and resolution to compare treatment groups.

To investigate the possibility that lesions in NC could induce a change in the bird's ability to produce vocal indicators of mate preference (calls), we compared the number of calls that each female produced in response to all song stimuli before and after lesioning NC. In our experimental birds (N = 12 birds, blue bar on the right in **Figure 3B**), we observed no significant change in

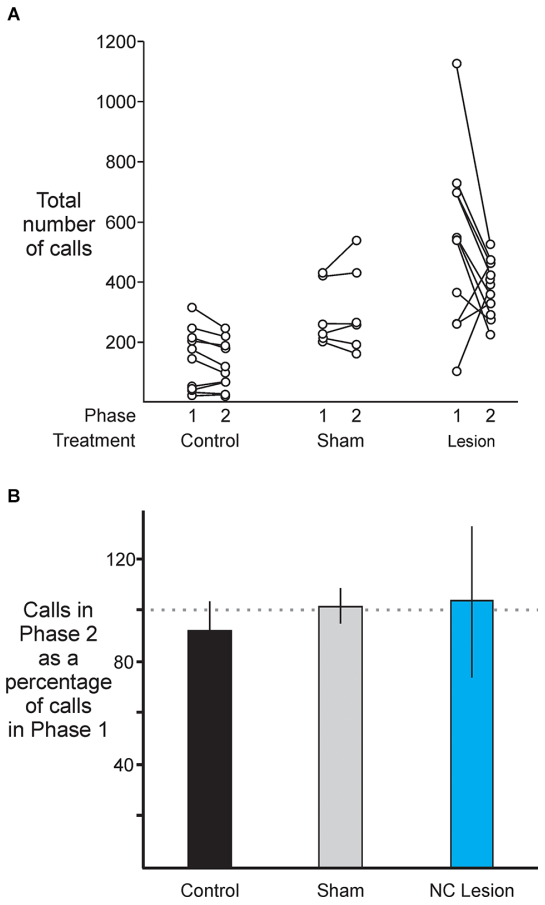

FIGURE 3
NC lesioned females were unchanged in their ability to indicate mate preference. **(A)** Females typically responded to song stimuli by producing large numbers of calls, and the numbers of calls produced varied across birds (individual data points connected by a line indicate the responses of an individual female in Phase 1 and Phase 2). **(B)** Experimental birds (blue bar, right; N = 11) expressed no significant change in their number of calls performed in Phase 2 as a percent of calls performed in Phase 1 of behavioral testing (bars and lines indicate means and SE; paired t-test, t = 0.50; p = 0.62). No change between Phase 1 and Phase 2 in the number of calls produced in response to all song stimuli was also evident for control (black bar, left; paired t-test, t = 1.01, p = 0.33, N = 10 birds) and sham conditions (gray bar, middle; paired t-test, t = 0.20, p = 0.85, N = 6 birds).

1 http://www.zebrafinchatlas.org

the number of calls evoked by male song stimuli before (Phase 1) and after lesioning (Phase 2; signed rank test, $p = 0.41$). No change from the first to second phase of behavioral testing was also evident for control birds (black bar on the left in **Figure 3B**; signed rank test, $p = 0.38$, $N = 10$ birds) and birds that received sham surgeries but had no lesions placed (gray bar in the middle in **Figure 3B**; signed rank test, $p = 0.69$, $N = 6$ birds). Together, these results indicate that lesioning NC had no significant effect on females' ability or willingness to produce calls in response to male song.

NC lesioned females were unchanged in their ability to identify songs of individual males

Lesions to NC also had no significant effect on female birds' ability to identify the songs of individual males. Comparing pre-lesion responses (solid line in **Figure 4**) to post-lesion responses (dotted line in **Figure 4**), females exhibited no significant change in the distribution of their song preferences for specific males (two sample Kolmogorov-Smirnov test, KS statistic = 0.08, $p = 0.92$, $N = 12$ birds). This absence of change between the first and second behavioral tests was also evident for control birds (two sample Kolmogorov-Smirnov test, KS statistic = 0.10, $p = 0.80$, $N = 10$ birds) and sham birds (two sample Kolmogorov-Smirnov test, KS statistic = 0.17, $p = 0.56$, $N = 6$ birds). Taken together, these results indicate that not only were females still able to hear after lesions in this auditory area, they were also still able to identify the songs of individual males.

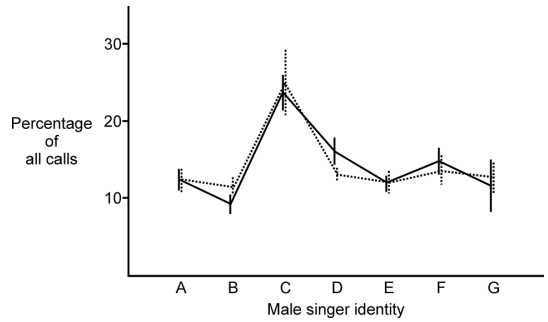

FIGURE 4
NC lesioned females were still able to identify the songs of individual males. After lesioning NC, there was no significant change in the distribution of their song preferences for specific males (two sample Kolmogorov-Smirnov test, KS statistic = 0.08, $p = 0.92$, $N = 11$ birds; solid line indicates the average percentage of calls for experimental birds in Phase 1; dotted line indicates the average percentage of calls for the same set of experimental birds in Phase 2; heterospecific song is represented by letter G). This absence of change between the first and second behavioral tests was also evident for control birds and sham birds (detailed in "Results" Section).

The conspecific song represented by letter C was generally more attractive to females than songs from other males. This pattern of one song being more broadly attractive than others has been reported previously along with an exploration of features that distinguish attractive songs from others (Dunning et al., 2020). From these data, it appears that activity in the portion of NC that we lesioned in these experiments does not play an important role in a female's ability to identify individual males based on song. As reported for many species in many studies, females generally found conspecific song more attractive than heterospecific song (reviewed in Catchpole and Slater, 2008). Prior to lesioning, 9 of 12 females found the average conspecific song more attractive than the single heterospecific stimulus, and that pattern was present in 8 of 12 females after lesioning (changes in song preference after lesioning are considered in greater detail below).

NC lesioned females were unchanged in their rank ordering of song preference

To determine if activity in NC is related to the female's ranking of preference for individual males, we analyzed each female's rank ordering of the seven male songs before and after lesions to NC (**Figure 5**). We compared the rank that each female assigned to each male prior to lesioning (Phase 1) vs. the rank that she assigned to that same male after lesioning (Phase 2). In this paradigm, no change in rank ordering of preference would be evident as data points lying along the line of identity (thin gray dashed line in **Figure 5**). Data from experimental (thick blue solid line in **Figure 5**; paired t-test, $t = 0.10$, $p = 0.92$), control (thin black solid line in **Figure 5**; paired t-test, $t = 0.48$, $p = 0.48$) and sham birds (thin black dashed line in **Figure 5**; paired t-test, $t = 0.02$, $p = 0.99$) all revealed no significant change in rank ordering of preference from the first to the second behavioral test. Thus, we detected no significant change in the rank ordering of the females' most- to least-preferred songs, indicating that NC does not play an important role in the rank ordering of song preferences.

NC lesioned females had a reduction in choosiness for male song

To investigate the degree to which activity in NC may be associated with the strength of song preference, we analyzed females' changes in preference for each song following lesioning of NC. To quantify that parameter, we computed the difference in the percentage of all calls that was produced in response to each song stimulus in Phase 2 compared to the response to the same song in Phase 1 (**Figure 6**). Using this measurement, a positive change would indicate that the bird expressed a greater preference for that song (i.e., found it more attractive)

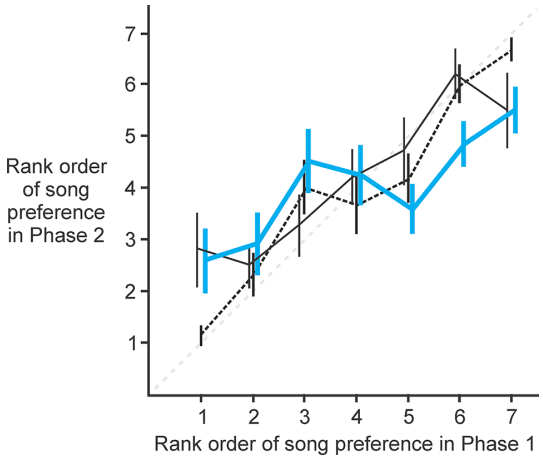

FIGURE 5
NC lesioned females were unchanged in their rank ordering of song preferences. Data from experimental (thick blue solid line; paired t-test, t = 0.10, p = 0.92), control (thin black solid line; paired t-test, t = 0.48, p = 0.48), and sham birds (thin black dashed line; paired t-test, t = 0.00, p = 1.00) all revealed no significant change in rank ordering of preference from Phase 1 to Phase 2 of behavioral testing (thin gray dashed line indicates the line of identity representing no change in rank ordering from Phase 1 to Phase 2).

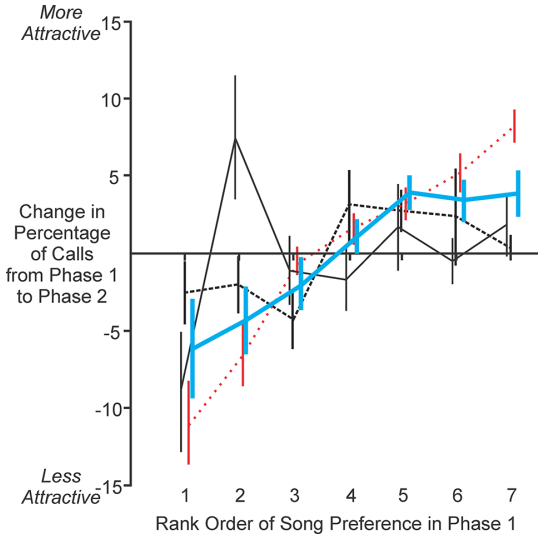

FIGURE 6
NC lesioned females expressed reduced strength of preference among songs of different males. For experimental birds (thick blue solid line), data were arranged in a linear manner with significantly positive slope (linear regression, F = 28.14, slope = 1.84, $p < 0.001$), indicating that lesioning NC caused birds to become less choosy for songs that they previously found attractive or unattractive (detailed in "Results" Section). In contrast, data from control birds (thin black solid line; linear regression, F = 1.43, p = 0.24) and sham birds (thin black dashed line; linear regression, F = 1.30, p = 0.26) had slopes that were not significantly different than zero, indicating that when NC was left unaltered, females expressed no change in choosiness for attractive vs. unattractive songs. We created a model (thin red dotted line) to simulate a scenario in which NC lesions caused preferences to become completely indistinguishable across all stimuli (i.e., one seventh of all calls produced in response to each of the seven stimuli). Data from that model yielded a slope that was significantly greater than zero (linear regression, F = 113.22, slope = 3.05, $p < 0.001$) and significantly steeper than the slope of 1.84 observed for our experimental data (linear regression of experimental data minus model data, F = 21.00, $p < 0.001$). Thus, NC lesions induced changes in preference but not a complete loss of preference, suggesting that NC plays a role in establishing a female's strength of preference among different songs.

following NC lesion, a negative change would indicate that the bird expressed a lesser preference for that song (i.e., found it less attractive) after lesioning, and no change would indicate that the bird's preference was the same in the first and second tests of song preference. Therefore, viewed in the way that the data are presented in Figure 6, a positive slope would indicate that the bird became less choosy for attractive vs. unattractive songs following lesion, a negative slope would indicate that the bird became more choosy, and a slope of zero would indicate no change in choosiness for songs that the bird found attractive vs. unattractive.

For experimental birds, the data were arranged in a linear manner with a slope that was slightly but significantly greater than zero (thick blue solid line in Figure 6; linear regression, F = 28.14, slope = 1.84, $p < 0.001$), indicating that lesioning NC caused birds to become less choosy for songs that they previously found attractive or unattractive (Figure 6). In contrast, data from control birds (thin black solid line in Figure 6; linear regression, F = 1.43, p = 0.24) and sham birds (thin black dashed line in Figure 6; linear regression, F = 1.30, p = 0.26) had slopes that were not significantly different than zero, indicating that females expressed no change in choosiness for attractive vs. unattractive songs when NC was left unchanged. These data reveal that birds express reduced choosiness in their mate preference following lesions of NC.

To investigate the possibility that NC lesions might have eliminated choosiness altogether, we created a model to simulate the scenario in which preferences were the values that we measured in the first behavioral test of preference and then became entirely uniform (went to chance) for each of the seven song stimuli in the second test (i.e., 14.3% of all calls produced in response to each stimulus). Data from that model yielded a slope that was significantly greater than zero (thin red dotted line in Figure 6; linear regression, F = 113.22, slope = 3.05, $p < 0.001$) and significantly steeper than the slope of 1.84 observed for our experimental data (linear regression of experimental data minus model data, F = 21.00, $p < 0.001$). Therefore, our experimental data for lesions of NC are intermediate between a model of no change in choosiness for attractive vs. unattractive songs (i.e., a slope of zero along the x-axis in Figure 6) and a model of complete elimination of choosiness (i.e., the red model data in Figure 6). Together, these results indicate that lesioning NC caused a reduction but not complete elimination of females'

choosiness for songs that they found attractive or unattractive prior to lesioning.

Discussion

These experiments revealed that chemically lesioning NC does not change a female's ability to perform calls. Females are also unchanged in their overall amount of call production following NC lesions, suggesting that they were also unchanged in their willingness to produce calls. It is possible that volition is affected one way by an NC lesion and general arousal is affected in another way that resulted in an overall unchanged amount of call output, but that possibility could not be addressed here. Future studies using methods such as a forced choice paradigm could yield further insight. In addition, lesioning NC does not change the bird's ability to identify the songs of individual males, nor does it alter the rank ordering of the female's preferences. However, lesioning NC does result in a statistically significant decrease in the strength of selectivity for a female's song preferences. Importantly, that decrease does not result in a complete elimination of preference, as female preferences are still evident but are not as strongly expressed after lesioning NC. Taken together, these data suggest that NC plays a role in a female's strength of preference ("choosiness") in song evaluation and mate choice.

A bird that was originally very choosy for a particular song stimulus typically became less choosy after NC was lesioned, which was evident as a reduction in the percentage of calls performed in response to that song stimulus. Additionally, a stimulus that was a female's least preferred prior to lesioning typically became more attractive (or less unattractive) after NC lesioning. Thus, NC appears to play a role in establishing the degree to which a female bird is selective in the magnitude of her responses to songs of different males. This is especially evident in the case of a female's choosiness for her most- and least-preferred song stimuli. The most attractive song became less attractive, and the least attractive (or perhaps even unattractive) song elicited more responses. These results suggest that activity in NC is closely related to the degree to which females are able to disambiguate male songs according to their subjective value.

We have previously described features of male BF song that influence female evaluation of its attractiveness (Dunning et al., 2020). A goal of future studies could be to extend those and other related studies by comparing the roles of specific brain sites in evaluating the quality of not only undirected vs. directed song performances but also familiar vs. unfamiliar and conspecific vs. heterospecific songs with a range of similarity to the songs of the female's own species. We have noted here that the calls produced by these females were of the type described as amplitude modulated calls in female Bengalese fiches (Yoneda and Okanoya, 1991). These are trills of different duration (typically 2–4 notes). Each type is performed in response to a song that a female finds attractive (Dunning et al., 2014). Additional future work could investigate the degree to which subtle differences in a female's evaluation may be evident in the degree to which she produces different proportions of different call types.

Our data reveal a role for NC in female mate preference, but NC is not alone in this functionality. It is reasonable to posit that the neural circuits underlying processes as complex as song perception and subsequent mate choice include additional selectively responsive auditory sites such as the caudal mesopallium (CM), the nucleus interfacialis (NIF), HVC shelf, and Field L because of their selective responses to auditory stimuli (Mello and Clayton, 1994; Gentner et al., 2001; Keller and Hahnloser, 2009). Among these sites, CM has been implicated in shaping female responses to songs of their own species such that birds are more responsive to heterospecific song following lesions to CM (Macdougall-Shackleton S. et al., 1998). CM is a particularly attractive candidate to shape selective expression of behavioral indicators of mate choice because its efferent pathways link sensory information to areas involved with motor production of courtship behaviors such as calls (Dunning et al., 2018).

Previous work has shown that NC is reciprocally interconnected with cells in CM (Vates et al., 1996; Dunning et al., 2018; Bloomston et al., 2022), suggesting that NC and CM may work together to control over courtship behaviors. In support of the idea that modulation of song evaluation and courtship behavior may require the coordination of activity in both of those sites, roughly half of the neurons within NC are GABAergic with projections to CM (Pinaud et al., 2008). Therefore, at least a portion of NC neurons provide inhibitory tone onto CM (Pinaud et al., 2008). Through that network, a lesion-induced decrease in inhibition between NC and CM could make CM neurons more responsive to auditory stimuli. In turn, this disinhibition could result in increased activity in sites to which CM projects. In this scenario, lesioning NC could result in disinhibition of CM projection neurons, and that could account for the observed increase in courtship behaviors in response to least preferred songs.

It could also be the case that lesioning NC could result in disinhibition of GABAergic interneurons in CM, causing less activity in CM projection neurons and resulting in lesser production of female courtship behaviors in response to songs. Within CM and NC, neurons are selective for natural vocalizations, and that selectivity may help females to assign identity to the vocalizations of specific individuals, such as songs or calls that distinguish the male that the female finds most attractive (Menardy et al., 2012). Furthermore, these neurons' response strength is different for familiar male vs. unfamiliar male and female calls (Giret et al., 2015). This level of selectivity further suggests that these neurons may contribute to recognizing the identity of the source of a vocal signal. This idea gives rise to the testable hypothesis that songs with

different degrees of subjective value drive activity in different classes of neurons (projection neurons vs. interneurons). An important goal of future experiments will be to use very precise stimulation methods to test that idea, such as optogenetic stimulation of specific subpopulations of neurons in NC and CM (Elie et al., 2019).

Two subregions of NC have been shown to play important roles that could contribute to song evaluation and mate choice. A subregion in the medial and caudal portion of NC (caudomedial nidopallium; NCM) has been associated with female preference (Tomaszycki and Blaine, 2014), and a subregion in the central and caudal portion of NC (caudocentral nidopallium; NCC) has been postulated as a center for memorization and integration of auditory experiences that impact mate preference (Van Ruijssevelt et al., 2018). Future investigations should focus on categorizing different subregions of NC. This could be done using molecular tools to identify the types of cells present and their relative prevalence across different regions of NC. Additional studies could use focal lesions and electrophysiological recordings in awake and freely behaving birds to reveal the specific roles that activity in these subregions may have in the processing of male song and production of call responses. Tract-tracing studies using precise approaches to focally apply tracer molecules or label specific cells using viral transfection should also be performed to more completely describe the circuits through which NC may play a role in processing sensory information and using that activity to direct specific motor outcomes (Bloomston et al., 2022).

Results from our group have shown that injections of anterograde tracer molecules into NC reveals clusters of axons and varicosities in the ventral portion of the intermediate arcopallium (AIV; Bloomston et al., 2022). AIV in male songbirds has been implicated in perceiving and learning vocalizations, serving as a driver of motivational state and reinforcement learning through its connections to the ventral tegmental area (VTA) and the substantia nigra pars compacta (SNc; Mandelblat-Cerf et al., 2014). Interestingly, a similar projection has been observed following anterograde tracer injections into CM (Dunning et al., 2018). Future studies of the neural basis of female mate choice should investigate the importance of this convergence from the auditory processing areas NC and CM onto AIV and this dopaminergic pathway implicated in behavioral motivation and reward. It is enticing to suspect that this network may influence female song evaluation and production of behavioral responses such as calls and CSDs.

The present results reveal that NC helps to shape female evaluation of the quality of the songs performed by different males. The significance of these findings is amplified by other results implicating CM as also playing a similar role (Macdougall-Shackleton S. A. et al., 1998) and tracing studies that reveal how activity in NC and CM can influence activation of downstream pathways implicated in motivation and production of courtship behaviors (Vates et al., 1996; Dunning et al., 2018; Bloomston et al., 2022). The link between sensory perception and selective motor activation lies at the heart of decision making, and the present results point to NC as a contributor in that process for song evaluation and mate preference. Continued study combining optogenetic, electrophysiological, and behavioral approaches will be essential to discern the degree to which activity in NC, CM, and specific downstream pathways contribute to evaluation of sensory perception, production of motor indicators of mate choice, or both. Future studies can also target different subregions of NC and use behavioral tests in addition to those used here. For example, a second means of assessing a female's song preference could be used to disambiguate a change in a female's evaluation of song quality vs. a change in her ability or desire to produce the behavioral indicator of mate preference studied here (calls). Very precisely targeting different subregions of NC (e.g., NCC, NCM, NCL) could reveal whether circuits in those subregions may contribute different facets of song evaluation and mate preference. A long term goal should be to couple these techniques with a thorough knowledge of the female's life experience. Females differ in what song they find most attractive (e.g., Dunning et al., 2014), and a female's song preference and activity in auditory processing areas such as NC and CM can be affected by experience (reviewed in Fujii et al., 2022). Coupling detailed knowledge of a female's life experience (e.g., reared in the laboratory under known acoustic and social conditions) with awake recording or optogenetic stimulation of activity in these auditory areas and their downstream targets holds the promise of revealing new insights into how this system processes sensory information in service of behavioral activation. Such studies would enable researchers to harness individual variation as a means of discovering the features that sculpt the neural basis of song evaluation and mate choice. With the present results and the insights that will emerge from those future experiments, the songbird model will continue to emerge as an especially tractable means of identifying the neural mechanisms of decision-making.

Data availability statement

Relevant data are available from the Open Science Framework at: https://osf.io/54gr8/.

Ethics statement

The animal study was reviewed and approved by the University of Wyoming Animal Care and Use Committee, and procedures were in compliance with recommendations from that group and state and federal regulations governing the housing and use of songbirds.

Author contributions

KL and JP designed, planned, oversaw the study, and wrote the first draft of the manuscript. KL, TF, EP, HH, KZ, and PS contributed to the data collection. KL, AC, and JP contributed to the data analysis. All authors provided comments on the work. All authors contributed to the article and approved the submitted version.

Funding

This work was supported by the National Science Foundation (NSF IOS CAREER 1453084 to JP). Students were supported by Wyoming NIH INBRE (NIH# 2P20GM103432; grants to TF, EP, HH, and KZ) and an NSF GRFP awarded to KL. Funding sources had no involvement in study design or any aspect of manuscript preparation.

Acknowledgments

We are also grateful to Robert Carroll for assistance with animal care.

Conflict of interest

The authors declare that the research was conducted in the absence of any commercial or financial relationships that could be construed as a potential conflict of interest.

Publisher's note

References

Banerjee, S. B., and Adkins-Regan, E. (2011). Effect of isolation and conspecific presence in a novel environment on corticosterone concentrations in a social avian species, the zebra finch (*Taeniopygia guttata*). *Horm. Behav.* 60, 233–238. doi: 10.1016/j.yhbeh.2011.05.011

Bloomston, N. A., Zaharas, K., Lawley, K., Fenn, T., Person, E., Huber, H., et al. (2022). Exploring links from sensory perception to movement and behavioral motivation in the caudal nidopallium of female songbirds. *J. Comp. Neurol.* 530, 1622–1633. doi: 10.1002/cne.25305

Byers, J., Hebets, E., and Podos, J. (2010). Female mate choice based upon male motor performance. *Anim. Behav.* 79, 771–778. doi: 10.1016/j.anbehav.2010.01.009

Candolin, U. (2003). The use of multiple cues in mate choice. *Biol. Rev. Camb. Philos. Soc.* 78, 575–595. doi: 10.1017/s1464793103006158

Catchpole, C. K. (1987). Bird song, sexual selection and female choice. *Trends Ecol. Evol.* 2, 94–97. doi: 10.1016/0169-5347(87)90165-0

Catchpole, C. K., and Slater, P. J. B. (2008). *Birdsong: Biological Themes and Variations*. Cambridge: Cambridge University Press.

Clayton, N. S. (1988). Song discrimination learning in zebra finches. *Anim. Behav.* 36, 1016–1024. doi: 10.1016/S0003-3472(88)80061-7

Cynx, J., Williams, H., and Nottebohm, F. (1990). Timbre discrimination in zebra finch (taeniopygia-guttata) song syllables. *J. Comp. Psychol.* 104, 303–308. doi: 10.1037/0735-7036.104.4.303

Dunning, J. L., Maze, S. E., Atwood, E. J., and Prather, J. F. (2018). Caudal mesopallial neurons in female songbirds bridge sensory and motor brain regions. *J. Comp. Neurol.* 526, 1703–1711. doi: 10.1002/cne.24440

Dunning, J., Pant, S., Bass, A., Coburn, Z., and Prather, J. (2014). Mate choice in adult female Bengalese finches: females express consistent preferences for individual males and prefer female-directed song performances. *PLoS One* 9:e89438. doi: 10.1371/journal.pone.0089438

Dunning, J. L., Pant, S., Murphy, K., and Prather, J. F. (2020). Female finches prefer courtship signals indicating male vigor and neuromuscular ability. *PLoS One* 15:e0226580. doi: 10.1371/journal.pone.0226580

Elie, J. E., Hoffmann, S., Dunning, J. L., Coleman, M. J., Fortune, E. S., and Prather, J. F. (2019). From perception to action: the role of auditory input in shaping vocal communication and social behaviors in birds. *Brain Behav. Evol.* 94, 51–60. doi: 10.1159/000504380

Fujii, T. G., Coulter, A., Lawley, K. S., Prather, J. F., and Okanoya, K. (2022). Song preference in female and juvenile songbirds: proximate and ultimate questions. *Front. Physiol.* 13:876205. doi: 10.3389/fphys.2022.876205

Gentner, T. Q., Hulse, S. H., and Ball, G. F. (2004). Functional differences in forebrain auditory regions during learned vocal recognition in songbirds. *J. Comp. Physiol. A Neuroethol. Sens Neural Behav. Physiol.* 190, 1001–1010. doi: 10.1007/s00359-004-0556-x

Gentner, T. Q., Hulse, S. H., Duffy, D., and Ball, G. F. (2001). Response biases in auditory forebrain regions of female songbirds following exposure to sexually relevant variation in male song. *J. Neurobiol.* 46, 48–58. doi: 10.1002/1097-4695(200101)46:1<48::aid-neu5>3.0.co;2-3

Giret, N., Menardy, F., and Del Negro, C. (2015). Sex differences in the representation of call stimuli in a songbird secondary auditory area. *Front. Behav. Neurosci.* 9:290. doi: 10.3389/fnbeh.2015.00290

Gobes, S. M. H., and Bolhuis, J. J. (2007). Birdsong memory: a neural dissociation between song recognition and production. *Curr. Biol.* 17, 789–793. doi: 10.1016/j.cub.2007.03.059

Gold, J. I., and Shadlen, M. N. (2007). The neural basis of decision making. *Annu. Rev. Neurosci.* 30, 535–574. doi: 10.1146/annurev.neuro.29.051605.113038

Jarrard, L. E. (1989). On the use of ibotenic acid to lesion selectively different components of the hippocampal formation. *J. Neurosci. Methods* 29, 251–259. doi: 10.1016/0165-0270(89)90149-0

Kable, J. W., and Glimcher, P. W. (2009). The neurobiology of decision: consensus and controversy. *Neuron* 63, 733–745. doi: 10.1016/j.neuron.2009.09.003

Keller, G. B., and Hahnloser, R. H. (2009). Neural processing of auditory feedback during vocal practice in a songbird. *Nature* 457, 187–190. doi: 10.1038/nature07467

Langmore, N. E. (2020). Female birdsong. *Curr. Biol.* 30, R789–R790. doi: 10.1016/j.cub.2020.05.042

Macdougall-Shackleton, S., Hulse, S., and Ball, G. (1998). Neural bases of song preferences in female zebra finches *(Taeniopygia guttata). Neuroreport* 9, 3047–3052. doi: 10.1097/00001756-199809140-00024

Macdougall-Shackleton, S. A., Hulse, S. H., and Ball, G. F. (1998). Neural correlates of singing behavior in male zebra finches (*Taeniopygia guttata*). *J. Neurobiol.* 36, 421–430.

Mandelblat-Cerf, Y., Las, L., Denisenko, N., and Fee, M. S. (2014). A role for descending auditory cortical projections in songbird vocal learning. *eLife* 3:e02152. doi: 10.7554/eLife.02152

Mello, C. V., and Clayton, D. F. (1994). Song-induced ZENK gene expression in auditory pathways of songbird brain and its relation to the song control system. *J. Neurosci.* 14, 6652–6666. doi: 10.1523/JNEUROSCI.14-11-06652.1994

Menardy, F., Touiki, K., Dutrieux, G., Bozon, B., Vignal, C., Mathevon, N., et al. (2012). Social experience affects neuronal responses to male calls in adult female zebra finches. *Eur. J. Neurosci.* 35, 1322–1336. doi: 10.1111/j.1460-9568.2012.08047.x

Monbureau, M., Barker, J. M., Leboucher, G., and Balthazart, J. (2015). Male song quality modulates c-Fos expression in the auditory forebrain of the female canary. *Physiol. Behav.* 147, 7–15. doi: 10.1016/j.physbeh.2015.04.005

Mooney, R., Prather, J. F., and Roberts, T. (2008). "Neurophysiology of birdsong learning," in *Learning and Memory: A Comprehensive Reference*, ed H. Eichenbaum (Oxford: Elsevier), 441–474.

Murphy, K., Lawley, K., Smith, P., and Prather, J. (2020). "New insights into the avian song system and neuronal control of learned vocalizations," in *The Neuroethology of Birdsong*, eds J. Sakata, S. Woolley and A. Popper (Cham, Switzerland: Springer Nature Publishing), 65–92.

Nowicki, S., and Searcy, W. A. (2004). Song function and the evolution of female preferences - why birds sing, why brains matter. *Ann. N Y Acad. Sci.* 1016, 704–723. doi: 10.1196/annals.1298.012

Odom, K. J., Hall, M. L., Riebel, K., Omland, K. E., and Langmore, N. E. (2014). Female song is widespread and ancestral in songbirds. *Nat. Commun.* 5:3379. doi: 10.1038/ncomms4379

Pinaud, R., Terleph, T. A., Tremere, L. A., Phan, M. L., Dagostin, A. A., Leao, R. M., et al. (2008). Inhibitory network interactions shape the auditory processing of natural communication signals in the songbird auditory forebrain. *J. Neurophysiol.* 100, 441–455. doi: 10.1152/jn.01239.2007

Prather, J. F. (2013). Auditory signal processing in communication: perception and performance of vocal sounds. *Hear. Res.* 305, 144–155. doi: 10.1016/j.heares.2013.06.007

Riebel, K. (2009). Song and female mate choice in zebra finches: a review. *Adv. Study Behav.* 40, 197–238. doi: 10.1016/s0065-3454(09)40006-8

Searcy, W. (1990). Species recognition of song by female red-winged blackbirds. *Anim. Behav.* 40, 1119–1127. doi: 10.1038/s41598-020-60231-y

Searcy, W., and Andersson, M. (1986). Sexual selection and the evolution of song. *Ann. Rev. Ecol. Syst.* 17, 507–533.

Searcy, W., and Brenowitz, E. (1988). Sexual differences in species recognition of avian song. *Nature* 332, 152–154.

Searcy, W. A., and Marler, P. (1981). A test for responsiveness to song structure and programming in female sparrows. *Science* 213, 926–928. doi: 10.1126/science.213.4510.926

Searcy, W. A., Marler, P., and Peters, S. S. (1981). Species song discrimination in adult female song and swamp sparrows. *Anim. Behav.* 29, 997–1003.

Searcy, W. A., and Yasukawa, K. (1996). The reproductive success of secondary females relative to that of monogamous and primary females in Red-winged Blackbirds. *J. Avian Biol.* 27, 225–230. doi: 10.2307/3677226

Sokal, R. R., and Rohlf, F. J. (2011). *Biometry*. New York: W.H. Freeman

Tchernichovski, O., Nottebohm, F., Ho, C. E., Pesaran, B., and Mitra, P. P. (2000). A procedure for an automated measurement of song similarity. *Anim. Behav.* 59, 1167–1176. doi: 10.1006/anbe.1999.1416

Terpstra, N. J., Bolhuis, J. J., and Den Boer-Visser, A. M. (2004). An analysis of the neural representation of birdsong memory. *J. Neurosci.* 24, 4971–4977. doi: 10.1523/JNEUROSCI.0570-04.2004

Tomaszycki, M. L., and Blaine, S. K. (2014). Temporary inactivation of NCM, an auditory region, increases social interaction and decreases song perception in female zebra finches. *Behav. Processes* 108, 65–70. doi: 10.1016/j.beproc.2014.09.031

Van Ruijssevelt, L., Chen, Y., Von Eugen, K., Hamaide, J., De Groof, G., Verhoye, M., et al. (2018). fMRI reveals a novel region for evaluating acoustic information for mate choice in a female songbird. *Curr. Biol.* 28, 711–721.e6. doi: 10.1016/j.cub.2018.01.048

Vates, G. E., Broome, B. M., Mello, C. V., and Nottebohm, F. (1996). Auditory pathways of caudal telencephalon and their relation to the song system of adult male zebra finches. *J. Comp. Neurol.* 366, 613–642. doi: 10.1002/(SICI)1096-9861(19960318)366:4<613::AID-CNE5>3.0.CO;2-7

Vernaleo, B. A., and Dooling, R. J. (2011). Relative salience of envelope and fine structure cues in zebra finch song. *J. Acoust. Soc. Am.* 129, 3373–3383. doi: 10.1121/1.3560121

Vyas, A., Harding, C., Borg, L., and Bogdan, D. (2009). Acoustic characteristics, early experience and endocrine status interact to modulate female zebra finches' behavioral responses to songs. *Horm. Behav.* 55, 50–59. doi: 10.1016/j.yhbeh.2008.08.005

Woolley, S. C., and Doupe, A. J. (2008). Social context-induced song variation affects female behavior and gene expression. *PLoS Biol.* 6:e62. doi: 10.1371/journal.pbio.0060062

Yoneda, T., and Okanoya, K. (1991). Ontogenty of sexually dimorphic distance calls in Bengalese finches (*Lunchura domestica*). *J. Ethol.* 9, 41–46.

frontiers | Frontiers in Systems Neuroscience

TYPE Review
PUBLISHED 17 November 2022
DOI 10.3389/fnsys.2022.896251

OPEN ACCESS

EDITED BY
Susanne Hoffmann,
Max Planck Institute for Ornithology, Germany

REVIEWED BY
Ronen Segev,
Ben-Gurion University of the Negev, Israel
Manu Madhav,
University of British Columbia, Canada

*CORRESPONDENCE
Kay Thurley
thurley@bio.lmu.de

RECEIVED 14 March 2022
ACCEPTED 31 October 2022
PUBLISHED 17 November 2022

CITATION
Thurley K (2022) Naturalistic neuroscience and virtual reality. *Front. Syst. Neurosci.* 16:896251. doi: 10.3389/fnsys.2022.896251

Naturalistic neuroscience and virtual reality

Kay Thurley[1,2]*

[1]Faculty of Biology, Ludwig-Maximilians-Universität München, Munich, Germany, [2]Bernstein Center for Computational Neuroscience Munich, Munich, Germany

Virtual reality (VR) is one of the techniques that became particularly popular in neuroscience over the past few decades. VR experiments feature a closed-loop between sensory stimulation and behavior. Participants interact with the stimuli and not just passively perceive them. Several senses can be stimulated at once, large-scale environments can be simulated as well as social interactions. All of this makes VR experiences more natural than those in traditional lab paradigms. Compared to the situation in field research, a VR simulation is highly controllable and reproducible, as required of a laboratory technique used in the search for neural correlates of perception and behavior. VR is therefore considered a middle ground between ecological validity and experimental control. In this review, I explore the potential of VR in eliciting naturalistic perception and behavior in humans and non-human animals. In this context, I give an overview of recent virtual reality approaches used in neuroscientific research.

KEYWORDS

virtual reality, naturalistic behavior, naturalistic neuroscience, ecological validity, animal behavior, behavioral neuroscience

1. Introduction

The arguably most important feature of natural behavior is active exploration and interrogation of the environment (Gottlieb and Oudeyer, 2018). External stimuli are not passively perceived. What is paid attention to is selected and specifically probed, reflecting the animals' motivations and needs. Moreover, natural environmental features and sensory cues are dynamic, multimodal, and complex (Sonkusare et al., 2019). This is in stark contrast to laboratory settings, which are characterized by numerous repetitions of the same imposed stimuli. These stimuli are often directed to only a single sense under simplified, artificial conditions and are disconnected from the animal's responses. Repetitions are important for behavioral modeling and the search for neural correlates and mechanisms, which both rely on trial-based averaging. It is nevertheless not surprising that results from laboratory experiments are of limited ecological validity and may not reveal the neural mechanisms underlying natural behavior (Krakauer et al., 2017; Dennis et al., 2021). Virtual reality (VR) may be part of a solution to this problem.

With VR, an artificial environment is simulated in which the user's actions determine the sensory stimulation, closing the loop between stimulation, perception, and action. A major motivation for the application of VR in neurophysiology is the desire to test behavior while recording with apparatuses that cannot be easily carried by the test subject

or that require stability that cannot be achieved during free movement. The potential of VR, however, lies beyond this simple wish to fixate a behaving subject in place.

In connection with scientific VR-use, terms like *ecological* and *ethological validity* as well as *naturalistic conditions* are frequently voiced. In this regard, VR is considered to stand above traditional laboratory methods while maintaining a similar level of experimental control (e.g., Bohil et al., 2011; Parsons, 2015; Minderer et al., 2016; Krakauer et al., 2017; Lenormand and Piolino, 2022).

In the present article, I explore the potential of VR for evoking naturalistic perception and behavior and to promote the understanding of underlying brain function. I will give an overview of current VR technologies applied in neuroscience and use cases across different species, motivate why they are used and evaluate them in view of naturalistic neuroscience. To begin, let us briefly address the question: what is VR?

2. What is VR?

In his book, LaValle (2020) defines VR as: "Inducing targeted behavior in an organism by using artificial sensory stimulation, while the organism has little or no awareness of the interference." This definition seems quite broad, but is flexible enough to embrace a variety of approaches, including those relevant to the present article. In a neuroscientific VR experiment, the participant experiences the stimulation of one or more senses to create the illusion of a "reality" that is intended by the researcher. Limited awareness seems less crucial for neuroscientific VR applications. However, one can argue that limited awareness is important for the feeling of presence in the artificial world, which as a result is treated as being natural—a basis for ecological validity.

What is missing from the above definition is that the virtual world is updated based on the user's behavior, providing an interactive experience (Bohil et al., 2011; Dombeck and Reiser, 2011; Naik et al., 2020). In terms of VR application in neuroscience, this narrowing of the definition is important because it distinguishes VR from simple sensory stimulation. The update is done in real time so that a *closed loop* is achieved between stimulation and behavior. For a real-time experience the update cycle needs to be sufficiently fast; how fast depends on the perceptual capabilities of the animal species and the sensory-motor system under investigation. Update delays can be increased parametrically depending on the research question. The most extreme case is the *open loop*, where the stimulation and the participant's actions are independent. Open loop corresponds to conventional stimulus conditions typically used in neuroscience studies.

3. Why using VR? And why for naturalistic neuroscience?

Typical motivations for using VR revolve around three different aspects: (1) multimodal stimulation with flexible and precise control, (2) interactivity instead of purely passive perception, and (3) the application of neural recording techniques that require particular mechanical stability. For naturalistic approaches, the first two points are the most important, but in a neuroscience context, the last is also relevant. I therefore discuss these three motivations next in view of their utility for naturalistic paradigms. Stimulus control and closed-loop methods have been steadily refined throughout the history of VR. For an account with regard to animal VRs and specifically rodent VRs used in research, the interested reader may be referred to Thurley and Ayaz (2017) and Naik et al. (2020). A general history of VR can be found in LaValle (2020). Finally, in this section I address the issue of *immersion*, i.e., the ability of a VR to draw the user in so that they feel present in it, which is closely related to achieving naturalistic conditions with VR.

3.1. VR provides flexible stimulus control

As a laboratory technique, VR benefits from the ability to perform experiments under precise control. This is what lets VR induce targeted behavior. Confounding and unintended influences although not completely excluded can be substantially reduced. VR is inherently flexible. It provides control over the complexity of the environment such as its size or the positioning of landmarks. Space restrictions, which can be a problem in the laboratory, do not exist in VR. Features can be easily and quickly altered without the participant noticing. One may, e.g., add or remove certain cues and test their contribution to a neural activity or a behavior. The manipulations can be done systematically and without influencing other components of the environment (Powell and Rosenthal, 2017). Also, stimuli may be provided that are unavailable in nature – although this speaks against the naturalistic use focused at in the present article. All of the above is hard to achieve in the field, where it is often less obvious which cues are attended to and which information is leveraged and which not; think, for instance, of investigating spatial navigation of primates in their natural habitat (De Lillo et al., 2014; Dolins et al., 2014, 2017; Allritz et al., 2022).

In the following, I will discuss paradigms of VR stimulus control utilized in specific areas of neuroscience research.

3.1.1. Spatial cognition and navigation

The most obvious neuroscience use of VR is in the study of spatial perception and navigation (Bohil et al., 2011;

Thurley and Ayaz, 2017). However, the advantage of VR for this purpose has been questioned since locomotion in traditional real world laboratory paradigms like foraging for food on linear tracks and in open field boxes is more natural than on a treadmill or alike (Minderer et al., 2016). In real arenas, information from the external world, e.g., from visual cues, and internally generated information, e.g., from moving body parts, are coordinated. In VR, these sources may not be aligned due to problems integrating simulation and tracking.

Such conflicts are likely the reason for the altered responses of space-encoding neurons in the rodent brain found in VR compared to real-world experiments. Head-fixed or body-fixed rodents do not receive normal vestibular input, resulting in mismatches between vestibular and visual information. Place cells in the hippocampus show altered position coding under such conditions, as confirmed by direct comparisons between virtual paradigms and their real-world counterparts (Chen et al., 2013; Ravassard et al., 2013; Aghajan et al., 2014). In VR setups that do not restrict body rotations and in which vestibular information about rotational movements is available to the animal, normal place-selective firing has been reported (Aronov and Tank, 2014; Chen et al., 2018; Haas et al., 2019). Freely-moving VRs may even better solve this problem (Del Grosso et al., 2017; Kaupert et al., 2017; Stowers et al., 2017; Madhav et al., 2022).

Thus, the design of a VR setup and the quality of a VR simulation may elicit atypical neural responses. These issues do not devalue certain VR systems—each setup may provide informative insights—but they are important indications that the suitability for understanding natural behavior and associated neural activity may be limited for some VR applications.

However, VR has advantages over traditional laboratory paradigms, which are themselves far from the situation animals face in the wild. These advantages depend on the research question. The possibility to simulate environments that are much larger than the available space in the laboratory, can increase ecological validity (Dolins et al., 2017), e.g., for the study of spatial learning in macaques (Taillade et al., 2019) and chimpanzees (Allritz et al., 2022), and fly search behavior (Kaushik et al., 2020). Specialized VR systems and paradigms can provide insights into specific topics, (e.g., path integration Petzschner and Glasauer, 2011; Lakshminarasimhan et al., 2018, 2020; Thurley and Schild, 2018; Jayakumar et al., 2019; Robinson and Wiener, 2021; Madhav et al., 2022). VR enables task standardization for cross-species comparison. For instance, spatial behavior can be tested with humans in typical rodent laboratory mazes like the Morris water maze (Laczó et al., 2010). Moreover, VR helps to overcome difficulties of testing spatial behavior and cognition in the wild as I already pointed out above.

3.1.2. (Multi-)sensory processing

In VR, several senses can be stimulated at once and in concert. Such a multimodal stimulation increases immersion and engagement. The experience will be more ecological and if natural stimuli are used more naturalistic. Already the first applications of VR, e.g., for studying sensory-motor control of flying in insects, combined visual, mechanosensory (wind source), and olfactory cues (Gray et al., 2002). In general, any VR method that connects locomotion with some type of sensory stimulation provides a multimodal experience because it inevitably encompasses sensory feedback about self-motion. In this sense, the most typical VR that uses visual stimulation with walking on a treadmill or tethered flying will always be multimodal.

In principle, unnatural stimuli may be given or the stimulation of different senses may be mismatched, allowing for experiments that are not possible in the real world. Of course, this speaks against the naturalistic principle, but let me nevertheless give a few examples for illustration. VR makes it possible to decouple stimuli that are inextricably linked in the real world. In rodent experiments, visual sensory have been dissociated from non-visual self-motion inputs to probe their differential influences on spatial responses in the hippocampal formation (Chen et al., 2013; Tennant et al., 2018; Haas et al., 2019; Jayakumar et al., 2019) or on running speed responses in visual cortex (Saleem et al., 2013). In flies, the feedback from eyes and halteres has been decoupled in simulated flight setups (Sherman and Dickinson, 2003). Also the lag between an action and the subsequent update of the virtual stimulation could be changed. For instance, positional changes could be delayed or made jump-/teleportation-like (see Domnisoru et al., 2013; Kaupert et al., 2017; Stowers et al., 2017; Tennant et al., 2018, for examples from experiments in fish and rodents). Thus, in general, sensory and motor variables can be separated in VR.

3.1.3. Social interactions

The issues of laboratory vs. field work also apply to the study of social interactions. VR can alleviate some of them. Virtual stimuli can be designed to appear more similar to real-life counterparts than stimuli used in classical ethological experiments (Naik et al., 2020). A particular advantage is that stimuli can be animated. Even under open-loop conditions, moving prey can be simulated to study prey-capture (Ioannou et al., 2012) or conspecifics to probe mate-choice (Gierszewski et al., 2017). Further examples can be found in Naik et al. (2020).

An important point for experiments on social interactions is consistency (Powell and Rosenthal, 2017). No matter if in the wild or the laboratory, the behavior of real subjects depends on their motivation and will change by their interaction with others. Simulated subjects do not change their behavior in this manner (Chouinard-Thuly et al., 2017). Alike other VR stimuli, socially-relevant ones can also be precisely controlled, held

constant or adapted, presented several times and to different subjects. Importantly, not just the static appearance is under close control but also the simulated movement patterns. In general, interaction with moving objects may sometimes be easier simulated in VR than provided in the real world, cf. e.g., the prey-capture study mentioned above (Ioannou et al., 2012).

3.2. VR goes beyond mere stimulus delivery

With VR the loop between perception and action can be closed. The participant in a VR experiment not only passively perceives the stimulation but behaves and interacts with it, which in turn changes the stimulus environment. This active engagement makes the VR experience much more reminiscent of real life and natural conditions than traditional, passive approaches.

The importance of motor actions for perception has been demonstrated, for instance, by experiments with mice moving on a treadmill while perceiving visual stimuli. Even when the treadmill is not coupled to the stimulation in such experiments, i.e., open-loop, neuronal responses in the visual cortex are substantially modulated (Niell and Stryker, 2010; Ayaz et al., 2013). More recently impacts of movement have been described not only for vision (Dadarlat and Stryker, 2017; Clancy et al., 2019) but also for audition and somatosensation (Fu et al., 2014; Schneider and Mooney, 2018). Similar dependence of sensory processing on behavioral state has also been reported in insects (Maimon et al., 2010). In zebrafish, the interaction between motor responses and visual feedback (Portugues and Engert, 2011) and related neural processing (Ahrens et al., 2012) has been investigated with closed-loop experiments as well as visually-driven swim patterns underlying natural prey capture (Trivedi and Bollmann, 2013).

Closed-loop is also helpful for decision making studies in species such as mice (Harvey et al., 2012), gerbils (Kautzky and Thurley, 2016), and zebrafish (Bahl and Engert, 2020; Dragomir et al., 2020). These studies use rather abstract visual stimuli, like random dots and stripe patterns, which are admittedly not very naturalistic. However, enabling natural motor responses, like walking and swimming, are key improvements over conventional designs that rely on nose-poking or lever-pressing.

3.3. VR enables recording of brain activity with bulky devices

One of the early motivations of using VR in neuroscience was that neural recording techniques can be used that require a high degree of mechanical stability or are too bulky and heavy to be carried by the animal (Dombeck et al., 2010; Harvey et al., 2012; Ahrens et al., 2013; Domnisoru et al., 2013; Schmidt-Hieber and Häusser, 2013; Leinweber et al., 2014). Similar reasons apply to the use of VR with fMRI or other methods for recoding human brain activity (Lenormand and Piolino, 2022). The application of VR with a focus on recording brain activity in the behaving animal has, e.g., been reviewed by Dombeck and Reiser (2011). Technological progress will increasingly weaken this motivation to use VR in the future. Miniature head-mounted systems for imaging (Yu et al., 2015) and single cell recordings (Valero and English, 2019) are under constant development and can be applied in freely moving animals.

3.4. Achieving immersion and presence in VR

Important concepts that are frequently expressed, especially in the context of human VR, are those of *immersion* and *presence*. How immersive a VR is, i.e., how strongly it draws the user in, is determined by the degree of sensory stimulation and the sensitivity to motor actions of the VR system in use. Deeper immersion leads to increased presence, i.e., the feeling of being in the virtual world (Bohil et al., 2011). For recreational or therapeutic applications with humans, high levels of immersion are surely desired and necessary. But how about scientific use?

Immersion does not seem to be the most important factor for investigating certain research questions. A VR setup could in principle only be a tool to provide some sensory stimulation and to connect it to behaviors. However, the ultimate goal of neuroscience is to investigate behavioral and brain responses that occur under natural conditions (Krakauer et al., 2017). A VR approach could only contribute to this goal if it elicits such responses. Yet, a VR that evokes responses as in real life implies deeper immersion. Thus, ecological validity and immersion are linked.

But how to determine presence and immersion? Humans can be questioned (Hofer et al., 2020), but what about animals? To determine and quantify the degree of immersion, two different types of responses seem at hand: neural and behavioral. However, not all possible types of neural activity must occur in natural behaviors, so only behavioral responses are suitable to determine proximity to natural conditions (Krakauer et al., 2017). Therefore, sufficient understanding of the behavior to be elicited in VR is required under real-world conditions.

A number of studies compared physiological and psychological reactions between real-life situations and their virtual counterparts in humans (examples are reviewed by Lenormand and Piolino, 2022). Behavioral conformity between virtual and real world is less regularly assessed with animals (Powell and Rosenthal, 2017). While it is more common in insects (see Dahmen et al., 2017 for an elegant example with ant spatial navigation) and spiders (Peckmezian and Taylor, 2015),

work with rodents on this topic is scarce (Hölscher et al., 2005). Comparisons have instead been made of neural activity between real-world and virtual conditions (e.g., for space-responses in rodent hippocampus Chen et al., 2013; Ravassard et al., 2013; Safaryan and Mehta, 2021).

Immersion is often considered in the context of the quality of the visual stimulation as it is the dominant sensory modality in primates and flying insects. For other species, however, vision is not as dominant. In these animals, immersion and ecological validity will depend more strongly on other types of perceptions, e.g., sound, touch, smell. As an example that may not seem like VR at first glance but is nonetheless consistent with the broad definition of VR favored in this article and which is ecologically valid see Faumont et al. (2011). In this study, osmo-sensitive neurons of the nematode *Caenorhabditis elegans* were optogenetically activated to simulate an aversive location in the animal's environment.

4. Technical components for naturalistic VR

Key technical components of VR are devices that provide sensory stimulation to create the virtual experience and those that keep track of the behavioral responses. How these components may promote naturalistic stimulation and behavior is discussed next.

4.1. Tracking movements and actions

In VR setups, participants are often restrained so that they can sense the stimuli appropriately while having enough freedom to move in the virtual environment. For instance, a specific position may need to be maintained in relation to a screen for visual stimulation or speakers for auditory stimulation. Other reasons are requirements on mechanical stability of neural recording devices as was already discussed above.

The type of fixation depends on the tested species. Flying insects may be tethered with their body leaving the wings free to beat (Gray et al., 2002; Sherman and Dickinson, 2003; Dombeck and Reiser, 2011). Wing motion is monitored with an optical sensor, and the difference between the amplitudes of left and right wing beats serves as an indicator of attempted body rotations (Reiser and Dickinson, 2008). In legged animals, fixation on a treadmill is the standard technique (Carrel, 1972; Dahmen, 1980; Seelig et al., 2010; Takalo et al., 2012; Peckmezian and Taylor, 2015; Thurley and Ayaz, 2017; Haberkern et al., 2019; Naik et al., 2020). Such treadmills are typically styrofoam balls on an air-cushion, cylindrical treadmills or linear belts. The animals move the treadmill with their legs, which is captured and used to update the position in the virtual world. In animals like rodents, which have a natural need for walking (Meijer and Robbers, 2014), a treadmill gives a more natural way of responding to the animals—even in non-spatial tasks (Garbers et al., 2015; Kautzky and Thurley, 2016; Henke et al., 2021, 2022). To provide a realistic, natural feeling of motion, the physical properties of the treadmill, such as its moment of inertia, must be taken into account and adapted to the animal species. For instance, treadmills for ants have particularly low friction and weight (Dahmen et al., 2017).

Any type of fixation imposes unnatural movements and disrupts sensory feedback about motor behavior. Tethered insects do not receive normal input from their balance organs (Fry et al., 2008). Head-fixed rodents do not receive natural input about rotations and linear acceleration from their vestibular organs. Also they have to make unnatural shear movements with their legs on the treadmill to make rotations in the virtual environment (Thurley and Ayaz, 2017). A similar lack of vestibular input is also found in zebrafish VRs, in which the animals' heads are immobilized (e.g., Portugues and Engert, 2011). A solution to this problem is offered by VR setups for freely flying, walking, and swimming animals (Fry et al., 2008; Del Grosso et al., 2017; Stowers et al., 2017; Ferreiro et al., 2020; Madhav et al., 2022). These setups use cameras to track the position of the animal (or only its head) and update a perspective-correct visual scenery. Alternatively, tracking information can be used to drive a motorized treadmill that compensates for the animal's movements to hold it in place with respect to the VR hardware (Kaupert et al., 2017).

Several technical considerations apply to ensure proper tracking, especially to meet the needs of the experimental animal (see Naik et al., 2020). A number of different tracking methods exist based on deep learning and other machine learning techniques (e.g., Hedrick, 2008; Robie et al., 2017; Graving et al., 2019; Mathis and Mathis, 2020; Vagvolgyi et al., 2022).

Body fixation is also not required when the stimulus display is directly attached to the sense organ and can be carried as with head-mounted displays. In VR headsets, head-mounted displays are combined with head-tracking hardware (Bohil et al., 2011; LaValle, 2020). Headsets prevail in human VR nowadays but also other tracking methods exist like treadmills for humans (examples are found in LaValle, 2020). In humans and other primates, often joysticks, game pads or keyboards are used to track motion and other responses (Washburn and Astur, 2003; Sato et al., 2004), for instance, when particular fixation is necessary like in fMRI (Lenormand and Piolino, 2022).

4.2. Displaying visual stimuli

Visual virtual worlds are the predominant type of VR. They are almost exclusively provided in first-person view, i.e., from the point of view of the participant. Compared to a third person perspective behind a visible avatar—which might be

possible with humans but is hard to imagine with animals—the first-person view enhances the experience (Dolins et al., 2017). For presentation, different types of displays are used, such as simple monitors, panoramic projection screens and head-mounted displays. Projections to the floor below the animals are also leveraged, e.g., with zebrafish (Ahrens et al., 2012; Bahl and Engert, 2020; Dragomir et al., 2020). In insects with their lower visual acuity but fast reaction times, LED displays are used (Dombeck and Reiser, 2011). For animals with eyes in the front, like primates and carnivorans, flat monitors may be sufficient. For animals with laterally positioned eyes, like rodents, only wide displays cover a sufficient part of the field of view (Dolins et al., 2017; Thurley and Ayaz, 2017). For ecological validity, the projection needs to have correct perspective and be undistorted (Dolins et al., 2017; Naik et al., 2020).

In general, it has to be kept in mind that images shown on displays are perceived differently by different animals (Chouinard-Thuly et al., 2017; Naik et al., 2020). Photoreceptor sensitivities differ across species (e.g., Osorio and Vorobyev, 2005) and the color display has to be adapted to the species' specifics to enable naturalistic stimulation. Behavioral methods can also readout animals' sensitivities (Knorr et al., 2018). Other visual capabilities like integration times and acuity also vary between species and need to be accommodated. For a detailed discussion with a focus on technical challenges see Naik et al. (2020). Similar considerations obviously apply to other sensory systems as well and have to be taken into account, especially when a naturalistic perceptual experience is intended.

Images on a screen remain 2D and natural vision is only partially achieved (Dolins et al., 2017). For instance, stereopsis is not possible with single images. Head-mounted displays in humans solve this by presenting offset images to each eye (LaValle, 2020). For an approach with insects, see Nityananda et al. (2016). Currently, there are no VR headsets for animals, although they may be in development, as they are mainly a miniaturization issue, apart from species-specific needs. Technology in this direction includes head-mounted camera systems to track eye movements (Meyer et al., 2018) and inertial sensors for head-tracking in rodents (Venkatraman et al., 2010; Fayat et al., 2021).

4.3. Sound stimulation

To simulate 3D spatial sound scenes that mimic real-life situations, virtual acoustic approaches have been developed. Human VR headsets often include headphones to provide sound stimuli in conjunction with the visual display. Alternatively, in free-field auralization, arrays of loudspeakers are placed around the user, such that sound sources can be precisely positioned in virtual space (Seeber et al., 2010). Compared to headphones, the user can listen with their own ears and the characteristics of their ears can be captured. Therefore, experiments can be also done with hearing aid wearers. A disadvantage is that the setup has to be placed in an anechoic chamber, which is demanding and expensive to construct. For correct deliverance of sound cues, the user has to be placed in a specific location with respect to the array. With such auditory VR setups, e.g., auditory motion parallax could be demonstrated in humans (Genzel et al., 2018). In rodents, virtual acoustics is done with loudspeakers placed around the treadmill (Cushman et al., 2013; Funamizu et al., 2016). Other approaches use more of an augmentation of a real arena than virtual acoustics to probe spatial localization of objects with the help of acoustic stimulation (Ferreiro et al., 2020; Amaro et al., 2021).

4.4. Tactile and haptic stimulation

In VR tactile and haptic stimulation can also be provided, simulating surfaces with different textures or the feel of forces (Bohil et al., 2011). Haptic systems for humans consist, e.g., of robotic arms with which force or pressure can be applied or pin arrays can be used to simulate surfaces (Culbertson et al., 2018; Wang et al., 2019). In tactile VR systems for rodents, the animals move through corridors simulated by movable plates (Sofroniew et al., 2014) or rotating cylinders with different textures (Ayaz et al., 2019). These "walls" are touched by the animals with their whiskers and they are adapted in closed-loop by the movements of the animal. Similar setups exist in which the animals are freely moving and that are not actually VR but still allow for simulating different tactile textures (Kerekes et al., 2017). Belt treadmills can also be equipped with tactile cues (Geiller et al., 2017).

4.5. Odors

Recently, devices have been developed to quickly and precisely deliver odorants with sufficient diffusion and clearance times for simulating spatially confined olfactory cues. Examples for use with humans are Salminen et al. (2018) and Micaroni et al. (2019). In animal studies, olfactory VR has been used with tethered rodents (Radvansky and Dombeck, 2018; Fischler-Ruiz et al., 2021; Radvansky et al., 2021) and insects (Gray et al., 2002). Precise odor delivery poses a problem for freely moving VRs, either a distribution system has to be carried on the body or, alternatively, odors could be delivered on room scale (Fry et al., 2008). However, the latter is hard to control in terms of odor concentration and distribution, preventing proper localization. Systems for humans that simulate taste are under development (Narumi et al., 2011; Vi et al., 2017; Kerruish, 2019) but have not yet been used in neuroscience as far as I know.

4.6. Rotation and gravity

VR setups that require fixation of the animals typically suffer from providing only inadequate information about rotational and linear acceleration cues. To overcome such problems, motion platforms with multiple degrees of freedom or rotating chairs providing horizontal rotations have been used for vestibular stimulation (Gu et al., 2010; Dokka et al., 2011; Genzel et al., 2016; Garzorz and MacNeilage, 2017). Similarly, rotational gimbals have been used with flies (Sherman and Dickinson, 2003). VR setups that allow for free movement do not suffer from these problems.

5. Limitations and potentials for naturalistic VR

Technical considerations for VRs with respect to species specifics and naturalistic experiments have already been discussed above. Here I address some more general issues.

5.1. Not everything can be tested in VR in terms of naturalistic experiments

There is in principle no limitation on what can be simulated with VR. For the purpose of the present article the simulation just needs to be naturalistic. We can intuitively judge how a VR simulation affects a human participant—or often simply take it for granted that we can—but this is impossible with animals. Thus, as I have argued above, naturalistic approaches must ensure that a VR simulation elicits the same behaviors that would occur in the real world counterpart (Krakauer et al., 2017; Powell and Rosenthal, 2017). This strongly constrains what can and cannot be done with VR in terms of naturalistic experiments. When a strict comparison between the real world and VR is not possible, such as with the teleportation-like position changes mentioned above, it means that the experiment is not suitable for a naturalistic VR study. Other questions may be better investigated directly in the real world, instead of investing in building a VR with all its limitations.

5.2. How natural can VR become and how natural or real does it have to be?

As pointed out by LaValle (2020), it is tempting to try to match the physical world in VR as closely as possible (*universal simulation principle*). Such a goal is inappropriate, since a simulation will never be perfect and always comprise unanticipated confounding variables. One should rather be guided by the research objective when designing the VR. A sensible design can at times mean reduction and simplification, without losing ecological validity (Bucci-Mansilla et al., 2021). Related to this is the *uncanny valley* phenomenon, in which high realism of an artificial stimulus makes observers feel uneasy (Chouinard-Thuly et al., 2017; LaValle, 2020). Among non-human animals this problem has been described with macaques (Steckenfinger and Ghazanfar, 2009).

5.3. VR sickness and fatigue

A regularly encountered problem with human VR applications is that of cyber, simulator, or *VR sickness* (Bohil et al., 2011; LaValle, 2020). Some participants experience discomfort and nausea due to latencies in the synchronization of the VR components, which results in incongruent sensory inputs. Of particular importance here is vestibular feedback from self-motion, which does not match visual input. This problem may occur due to improper tracking but also a misunderstanding and disregard of the user-perspective by the designer of the VR experience (LaValle, 2020). Related to this, *fatigue* can arise. Whereas, fatigue is certainly an issue that can be accounted for in animal studies—consider, for example, a treadmill that is too heavy or creates much friction (Dahmen et al., 2017)—analogs of VR sickness in animals may be difficult to determine. Animal VRs can suffer from unnatural feedback from different senses (Dombeck and Reiser, 2011; Thurley and Ayaz, 2017). This is exemplified by the issues of head-fixation with regard to hippocampal space-related activity in rodents discussed above.

6. Conclusions

In this article, I tried to show that VR has a multitude of applications in neuroscience that can help advancing from traditional laboratory-based to naturalistic research themes. VR can mediate between the opposing poles of ecological validity and experimental control, facilitating generalizability of laboratory results to the situation in the wild. As with any scientific approach, the means have to be adapted to the research question. A specific and maybe novel technology or method does not help with this by itself (Minderer et al., 2016; Thurley and Ayaz, 2017). When designing a VR, it is important to consider the specifics of the model species. Only then immersion can be reached, which results in a naturalistic experience and ecological validity. To determine how immersive a VR experience is, only behavioral readout is appropriate, which needs to be compared to real-world behavior. Otherwise, VR experiments will likely elicit unnatural behaviors and neural responses, which are not related to the intended research questions (Krakauer et al., 2017; Powell and Rosenthal, 2017).

Developers of VR for humans, especially for consumer applications or therapy, realized that without knowledge about

our senses, our perception and ultimately our brains, it is not possible to build VR (LaValle, 2020). This concept closes the cycle for the present article—and presents a somewhat circular argument for use of VR in naturalistic neuroscience: VR is used in neuroscience to gain insights into perception, behavior, and brain function. However, good VR experiments that are also naturalistic and ecologically valid can only be conducted if the subjects' perception, behavior, and knowledge of their physiological basis are sensibly taken into account.

Author contributions

The author confirms being the sole contributor of this work and has approved it for publication.

Acknowledgments

I wish to thank the two reviewers for their detailed comments and valuable suggestions, which contributed substantially to the improvement of the present article. I am also grateful for ongoing support from the Bernstein Center Munich.

Conflict of interest

The author declares that the research was conducted in the absence of any commercial or financial relationships that could be construed as a potential conflict of interest.

Publisher's note

All claims expressed in this article are solely those of the authors and do not necessarily represent those of their affiliated organizations, or those of the publisher, the editors and the reviewers. Any product that may be evaluated in this article, or claim that may be made by its manufacturer, is not guaranteed or endorsed by the publisher.

References

Aghajan, Z. M., Acharya, L., Moore, J. J., Cushman, J. D., Vuong, C., and Mehta, M. R. (2014). Impaired spatial selectivity and intact phase precession in two-dimensional virtual reality. *Nat Neurosci*. 18, 121–128. doi: 10.1038/nn.3884

Ahrens, M. B., Huang, K. H., Narayan, S., Mensh, B. D., and Engert, F. (2013). Two-photon calcium imaging during fictive navigation in virtual environments. *Front. Neural Circuits* 7:104. doi: 10.3389/fncir.2013.00104

Ahrens, M. B., Li, J. M., Orger, M. B., Robson, D. N., Schier, A. F., Engert, F., et al. (2012). Brain-wide neuronal dynamics during motor adaptation in zebrafish. *Nature* 485, 471–477. doi: 10.1038/nature11057

Allritz, M., Call, J., Schweller, K., McEwen, E. S., de Guinea, M., Janmaat, K. R. L., et al. (2022). Chimpanzees (*Pan troglodytes*) navigate to find hidden fruit in a virtual environment. *Sci. Adv*. 8:eabm4754. doi: 10.1126/sciadv.abm4754

Amaro, D., Ferreiro, D. N., Grothe, B., and Pecka, M. (2021). Source identity shapes spatial preference in primary auditory cortex during active navigation. *Curr. Biol*. 31, 3875–3883.e5. doi: 10.1016/j.cub.2021.06.025

Aronov, D., and Tank, D. W. (2014). Engagement of neural circuits underlying 2D spatial navigation in a rodent virtual reality system. *Neuron* 84, 442–456. doi: 10.1016/j.neuron.2014.08.042

Ayaz, A., Saleem, A. B., Schölvinck, M. L., and Carandini, M. (2013). Locomotion controls spatial integration in mouse visual cortex. *Curr. Biol*. 23, 890–894. doi: 10.1016/j.cub.2013.04.012

Ayaz, A., Stäuble, A., Hamada, M., Wulf, M.-A., Saleem, A. B., and Helmchen, F. (2019). Layer-specific integration of locomotion and sensory information in mouse barrel cortex. *Nat. Commun*. 10:2585. doi: 10.1038/s41467-019-10564-8

Bahl, A., and Engert, F. (2020). Neural circuits for evidence accumulation and decision making in larval zebrafish. *Nat. Neurosci*. 23, 94–102. doi: 10.1038/s41593-019-0534-9

Bohil, C. J., Alicea, B., and Biocca, F. A. (2011). Virtual reality in neuroscience research and therapy. *Nat. Rev. Neurosci*. 12, 752–762. doi: 10.1038/nrn3122

Bucci-Mansilla, G., Vicencio-Jimenez, S., Concha-Miranda, M., and Loyola-Navarro, R. (2021). Challenging paradigms through ecological neuroscience: Lessons from visual models. *Front. Neurosci*. 15:758388. doi: 10.3389/fnins.2021.758388

Carrel, J. S. (1972). An improved treading device for tethered insects. *Science* 175:1279. doi: 10.1126/science.175.4027.1279.b

Chen, G., King, J. A., Burgess, N., and O'Keefe, J. (2013). How vision and movement combine in the hippocampal place code. *Proc. Natl. Acad. Sci. U.S.A*. 110, 378–383. doi: 10.1073/pnas.1215834110

Chen, G., King, J. A., Lu, Y., Cacucci, F., and Burgess, N. (2018). Spatial cell firing during virtual navigation of open arenas by head-restrained mice. *eLife* 7:e26. doi: 10.7554/eLife.34789.026

Chouinard-Thuly, L., Gierszewski, S., Rosenthal, G. G., Reader, S. M., Rieucau, G., Woo, K. L., et al. (2017). Technical and conceptual considerations for using animated stimuli in studies of animal behavior. *Curr. Zool*. 63, 5–19. doi: 10.1093/cz/zow104

Clancy, K. B., Orsolic, I., and Mrsic-Flogel, T. D. (2019). Locomotion-dependent remapping of distributed cortical networks. *Nat. Neurosci*. 22, 778–786. doi: 10.1038/s41593-019-0357-8

Culbertson, H., Schorr, S. B., and Okamura, A. M. (2018). Haptics: the present and future of artificial touch sensation. *Annu. Rev. Control Robot. Auton. Syst*. 1, 385–409. doi: 10.1146/annurev-control-060117-105043

Cushman, J. D., Aharoni, D. B., Willers, B., Ravassard, P., Kees, A., Vuong, C., et al. (2013). Multisensory control of multimodal behavior: do the legs know what the tongue is doing? *PLoS ONE* 8:e80465. doi: 10.1371/journal.pone.0080465

Dadarlat, M. C., and Stryker, M. P. (2017). Locomotion enhances neural encoding of visual stimuli in mouse v1. *J. Neurosci*. 37, 3764–3775. doi: 10.1523/JNEUROSCI.2728-16.2017

Dahmen, H. (1980). A simple apparatus to investigate the orientation of walking insects. *Cell. Mol. Life Sci*. 36, 685–687. doi: 10.1007/BF01970140

Dahmen, H., Wahl, V. L., Pfeffer, S. E., Mallot, H. A., and Wittlinger, M. (2017). Naturalistic path integration of *Cataglyphis* desert ants on an air-cushioned lightweight spherical treadmill. *J. Exp. Biol*. 220, 634–644. doi: 10.1242/jeb.148213

De Lillo, C., Kirby, M., and James, F. C. (2014). Spatial working memory in immersive virtual reality foraging: path organization, traveling distance and search efficiency in humans (*Homo sapiens*). *Am. J. Primatol*. 76, 436–446. doi: 10.1002/ajp.22195

Del Grosso, N. A., Graboski, J. J., Chen, W., Blanco-Hernández, E., and Sirota, A. (2017). Virtual reality system for freely-moving rodents. *bioRxiv [preprint]*. doi: 10.1101/161232

Dennis, E. J., El Hady, A., Michaiel, A., Clemens, A., Tervo, D. R. G., Voigts, J., and Datta, S. R. (2021). Systems neuroscience of natural behaviors in rodents. *J. Neurosci.* 41, 911–919. doi: 10.1523/JNEUROSCI.1877-20.2020

Dokka, K., MacNeilage, P. R., DeAngelis, G. C., and Angelaki, D. E. (2011). Estimating distance during self-motion: a role for visual-vestibular interactions. *J. Vis.* 11, 1–16. doi: 10.1167/11.13.2

Dolins, F. L., Klimowicz, C., Kelley, J., and Menzel, C. R. (2014). Using virtual reality to investigate comparative spatial cognitive abilities in chimpanzees and humans. *Am. J. Primatol.* 76, 496–513. doi: 10.1002/ajp.22252

Dolins, F. L., Schweller, K., and Milne, S. (2017). Technology advancing the study of animal cognition: using virtual reality to present virtually simulated environments to investigate nonhuman primate spatial cognition. *Curr. Zool.* 63, 97–108. doi: 10.1093/cz/zow121

Dombeck, D. A., Harvey, C. D., Tian, L., Looger, L. L., and Tank, D. W. (2010). Functional imaging of hippocampal place cells at cellular resolution during virtual navigation. *Nat. Neurosci.* 13, 1433–1440. doi: 10.1038/nn.2648

Dombeck, D. A., and Reiser, M. B. (2011). Real neuroscience in virtual worlds. *Curr. Opin. Neurobiol.* 22, 3–10. doi: 10.1016/j.conb.2011.10.015

Domnisoru, C., Kinkhabwala, A. A., and Tank, D. W. (2013). Membrane potential dynamics of grid cells. *Nature* 495, 199–204. doi: 10.1038/nature11973

Dragomir, E. I., Štih, V., and Portugues, R. (2020). Evidence accumulation during a sensorimotor decision task revealed by whole-brain imaging. *Nat. Neurosci.* 23, 85–93. doi: 10.1038/s41593-019-0535-8

Faumont, S., Rondeau, G., Thiele, T. R., Lawton, K. J., McCormick, K. E., Sottile, M., et al. (2011). An image-free opto-mechanical system for creating virtual environments and imaging neuronal activity in freely moving *Caenorhabditis elegans*. *PLOS ONE* 6:e24666. doi: 10.1371/journal.pone.0024666

Fayat, R., Delgado Betancourt, V., Goyallon, T., Petremann, M., Liaudet, P., Descossy, V., et al. (2021). Inertial measurement of head tilt in rodents: principles and applications to vestibular research. *Sensors* 21:6318. doi: 10.3390/s21186318

Ferreiro, D. N., Amaro, D., Schmidtke, D., Sobolev, A., Gundi, P., Belliveau, L., et al. (2020). Sensory island task (sit): a new behavioral paradigm to study sensory perception and neural processing in freely moving animals. *Front. Behav. Neurosci.* 14:576154. doi: 10.3389/fnbeh.2020.576154

Fischler-Ruiz, W., Clark, D. G., Joshi, N. R., Devi-Chou, V., Kitch, L., Schnitzer, M., et al. (2021). Olfactory landmarks and path integration converge to form a cognitive spatial map. *Neuron*, 109, 4036–4049.e5. doi: 10.1016/j.neuron.2021.09.055

Fry, S. N., Rohrseitz, N., Straw, A. D., and Dickinson, M. H. (2008). Trackfly: virtual reality for a behavioral system analysis in free-flying fruit flies. *J. Neurosci. Methods* 171, 110–117. doi: 10.1016/j.jneumeth.2008.02.016

Fu, Y., Tucciarone, J. M., Espinosa, J. S., Sheng, N., Darcy, D. P., Nicoll, R. A., et al. (2014). A cortical circuit for gain control by behavioral state. *Cell* 156, 1139–1152. doi: 10.1016/j.cell.2014.01.050

Funamizu, A., Kuhn, B., and Doya, K. (2016). Neural substrate of dynamic bayesian inference in the cerebral cortex. *Nat. Neurosci.* 19, 1682–1689. doi: 10.1038/nn.4390

Garbers, C., Henke, J., Leibold, C., Wachtler, T., and Thurley, K. (2015). Contextual processing of brightness and color in *Mongolian gerbils*. *J. Vis.* 15:13. doi: 10.1167/15.1.13

Garzorz, I. T., and MacNeilage, P. R. (2017). Visual-vestibular conflict detection depends on fixation. *Curr. Biol.* 27, 2856–2861.e4. doi: 10.1016/j.cub.2017.08.011

Geiller, T., Fattahi, M., Choi, J.-S., and Royer, S. (2017). Place cells are more strongly tied to landmarks in deep than in superficial ca1. *Nat. Commun.* 8:14531. doi: 10.1038/ncomms14531

Genzel, D., Firzlaff, U., Wiegrebe, L., and MacNeilage, P. R. (2016). Dependence of auditory spatial updating on vestibular, proprioceptive, and efference copy signals. *J. Neurophysiol.* 116, 765–775. doi: 10.1152/jn.00052.2016

Genzel, D., Schutte, M., Brimijoin, W. O., MacNeilage, P. R., and Wiegrebe, L. (2018). Psychophysical evidence for auditory motion parallax. *Proc. Natl. Acad. Sci. U.S.A.* 115, 4264–4269. doi: 10.1073/pnas.1712058115

Gierszewski, S., Müller, K., Smielik, I., Hütwohl, J.-M., Kuhnert, K.-D., and Witte, K. (2017). The virtual lover: variable and easily guided 3d fish animations as an innovative tool in mate-choice experiments with Sailfin mollies-II. Validation. *Curr. Zool.* 63, 65–74. doi: 10.1093/cz/zow108

Gottlieb, J., and Oudeyer, P.-Y. (2018). Towards a neuroscience of active sampling and curiosity. *Nat. Rev. Neurosci.* 19, 758–770. doi: 10.1038/s41583-018-0078-0

Graving, J. M., Chae, D., Naik, H., Li, L., Koger, B., Costelloe, B. R., et al. (2019). Deepposekit, a software toolkit for fast and robust animal pose estimation using deep learning. *eLife* 8:e47994. doi: 10.7554/eLife.47994.sa2

Gray, J. R., Pawlowski, V., and Willis, M. A. (2002). A method for recording behavior and multineuronal CNS activity from tethered insects flying in virtual space. *J. Neurosci. Methods* 120, 211–223. doi: 10.1016/S0165-0270(02)00223-6

Gu, Y., Fetsch, C. R., Adeyemo, B., Deangelis, G. C., and Angelaki, D. E. (2010). Decoding of MSTD population activity accounts for variations in the precision of heading perception. *Neuron* 66, 596–609. doi: 10.1016/j.neuron.2010.04.026

Haas, O. V., Henke, J., Leibold, C., and Thurley, K. (2019). Modality-specific subpopulations of place fields coexist in the hippocampus. *Cereb. Cortex* 29, 1109–1120. doi: 10.1093/cercor/bhy017

Haberkern, H., Basnak, M. A., Ahanonu, B., Schauder, D., Cohen, J. D., Bolstad, M., et al. (2019). Visually guided behavior and optogenetically induced learning in head-fixed flies exploring a virtual landscape. *Curr. Biol.* 29, 1647–1659.e8. doi: 10.1016/j.cub.2019.04.033

Harvey, C. D., Coen, P., and Tank, D. W. (2012). Choice-specific sequences in parietal cortex during a virtual-navigation decision task. *Nature* 484, 62–68. doi: 10.1038/nature10918

Hedrick, T. L. (2008). Software techniques for two- and three-dimensional kinematic measurements of biological and biomimetic systems. *Bioinspir. Biomimet.* 3:034001. doi: 10.1088/1748-3182/3/3/034001

Henke, J., Bunk, D., von Werder, D., Häusler, S., Flanagin, V. L., and Thurley, K. (2021). Distributed coding of duration in rodent prefrontal cortex during time reproduction. *eLife* 10:e71612. doi: 10.7554/eLife.71612

Henke, J., Flanagin, V. L., and Thurley, K. (2022). A virtual reality time reproduction task for rodents. *Front. Behav. Neurosci.* 16:957804. doi: 10.3389/fnbeh.2022.957804

Hofer, M., Hartmann, T., Eden, A., Ratan, R., and Hahn, L. (2020). The role of plausibility in the experience of spatial presence in virtual environments. *Front. Virt. Real.* 1:2. doi: 10.3389/frvir.2020.00002

Hölscher, C., Schnee, A., Dahmen, H., Setia, L., and Mallot, H. A. (2005). Rats are able to navigate in virtual environments. *J. Exp. Biol.* 208(Pt 3), 561–569. doi: 10.1242/jeb.01371

Ioannou, C. C., Guttal, V., and Couzin, I. D. (2012). Predatory fish select for coordinated collective motion in virtual prey. *Science* 337, 1212–1215. doi: 10.1126/science.1218919

Jayakumar, R. P., Madhav, M. S., Savelli, F., Blair, H. T., Cowan, N. J., and Knierim, J. J. (2019). Recalibration of path integration in hippocampal place cells. *Nature* 566, 533–537. doi: 10.1038/s41586-019-0939-3

Kaupert, U., Thurley, K., Frei, K., Bagorda, F., Schatz, A., Tocker, G., et al. (2017). Spatial cognition in a virtual reality home-cage extension for freely moving rodents. *J. Neurophysiol.* 117, 1736–1748. doi: 10.1152/jn.00630.2016

Kaushik, P. K., Renz, M., and Olsson, S. B. (2020). Characterizing long-range search behavior in diptera using complex 3d virtual environments. *Proc. Natl. Acad. Sci. U.S.A.* 117, 12201–12207. doi: 10.1073/pnas.1912124117

Kautzky, M., and Thurley, K. (2016). Estimation of self-motion duration and distance in rodents. *R. Soc. Open Sci.* 3:160118. doi: 10.1098/rsos.160118

Kerekes, P., Daret, A., Shulz, D. E., and Ego-Stengel, V. (2017). Bilateral discrimination of tactile patterns without whisking in freely running rats. *J. Neurosci.* 37, 7567–7579. doi: 10.1523/JNEUROSCI.0528-17.2017

Kerruish, E. (2019). Arranging sensations: smell and taste in augmented and virtual reality. *Senses Soc.* 14, 31–45. doi: 10.1080/17458927.2018.1556952

Knorr, A. G., Gravot, C. M., Gordy, C., Glasauer, S., and Straka, H. (2018). I spy with my little eye: a simple behavioral assay to test color sensitivity on digital displays. *Biol. Open* 7:bio035725. doi: 10.1242/bio.035725

Krakauer, J. W., Ghazanfar, A. A., Gomez-Marin, A., MacIver, M. A., and Poeppel, D. (2017). Neuroscience needs behavior: correcting a reductionist bias. *Neuron* 93, 480–490. doi: 10.1016/j.neuron.2016.12.041

Laczó, J., Andel, R., Vyhnalek, M., Vlcek, K., Magerova, H., Varjassyova, A., et al. (2010). Human analogue of the Morris water maze for testing subjects at risk of Alzheimer's disease. *Neuro-degener. Dis.* 7, 148–152. doi: 10.1159/000289226

Lakshminarasimhan, K. J., Avila, E., Neyhart, E., DeAngelis, G. C., Pitkow, X., and Angelaki, D. E. (2020). Tracking the mind's eye: primate gaze behavior during virtual visuomotor navigation reflects belief dynamics. *Neuron* 106, 662–674.e5. doi: 10.1016/j.neuron.2020.02.023

Lakshminarasimhan, K. J., Petsalis, M., Park, H., DeAngelis, G. C., Pitkow, X., and Angelaki, D. E. (2018). A dynamic Bayesian observer model reveals origins of bias in visual path integration. *Neuron* 99, 194–206.e5. doi: 10.1016/j.neuron.2018.05.040

LaValle, S. (2020). *Virtual Reality*. Available online at: http://lavalle.pl/vr/

Leinweber, M., Zmarz, P., Buchmann, P., Argast, P., Hübener, M., Bonhoeffer, T., et al. (2014). Two-photon calcium imaging in mice navigating a virtual reality environment. *J. Vis. Exp*. 2014:e50885. doi: 10.3791/50885

Lenormand, D., and Piolino, P. (2022). In search of a naturalistic neuroimaging approach: exploration of general feasibility through the case of VR-fMRI and application in the domain of episodic memory. *Neurosci. Biobehav. Rev*. 133:104499. doi: 10.1016/j.neubiorev.2021.12.022

Madhav, M. S., Jayakumar, R. P., Lashkari, S. G., Savelli, F., Blair, H. T., Knierim, J. J., et al. (2022). The Dome: a virtual reality apparatus for freely locomoting rodents. *J. Neurosci. Methods* 368:109336. doi: 10.1016/j.jneumeth.2021.109336

Maimon, G., Straw, A. D., and Dickinson, M. H. (2010). Active flight increases the gain of visual motion processing in drosophila. *Nat. Neurosci*. 13, 393–399. doi: 10.1038/nn.2492

Mathis, M. W., and Mathis, A. (2020). Deep learning tools for the measurement of animal behavior in neuroscience. *Curr. Opin. Neurobiol*. 60, 1–11. doi: 10.1016/j.conb.2019.10.008

Meijer, J. H., and Robbers, Y. (2014). Wheel running in the wild. *Proc. R. Soc. B* 281:20140210. doi: 10.1098/rspb.2014.0210

Meyer, A. F., Poort, J., O'Keefe, J., Sahani, M., and Linden, J. F. (2018). A head-mounted camera system integrates detailed behavioral monitoring with multichannel electrophysiology in freely moving mice. *Neuron* 100, 46–60.e7. doi: 10.1016/j.neuron.2018.09.020

Micaroni, L., Carulli, M., Ferrise, F., Gallace, A., and Bordegoni, M. (2019). An olfactory display to study the integration of vision and olfaction in a virtual reality environment. *J. Comput. Inform. Sci. Eng*. 19:031015. doi: 10.1115/1.4043068

Minderer, M., Harvey, C. D., Donato, F., and Moser, E. I. (2016). Neuroscience: virtual reality explored. *Nature* 533, 324–325. doi: 10.1038/nature17899

Naik, H., Bastien, R., Navab, N., and Couzin, I. D. (2020). Animals in virtual environments. *IEEE Trans. Visual. Comput. Graph*. 26, 2073–2083. doi: 10.1109/TVCG.2020.2973063

Narumi, T., Nishizaka, S., Kajinami, T., Tanikawa, T., and Hirose, M. (2011). "Augmented reality flavors: gustatory display based on edible marker and cross-modal interaction," in *Proceedings of the SIGCHI Conference on Human Factors in Computing Systems, CHI '11* (New York, NY: Association for Computing Machinery), 93–102. doi: 10.1145/1978942.1978957

Niell, C. M., and Stryker, M. P. (2010). Modulation of visual responses by behavioral state in mouse visual cortex. *Neuron* 65, 472–479. doi: 10.1016/j.neuron.2010.01.033

Nityananda, V., Tarawneh, G., Rosner, R., Nicolas, J., Crichton, S., and Read, J. (2016). Insect stereopsis demonstrated using a 3D insect cinema. *Sci. Rep*. 6:18718. doi: 10.1038/srep18718

Osorio, D., and Vorobyev, M. (2005). Photoreceptor sectral sensitivities in terrestrial animals: adaptations for luminance and colour vision. *Proc. R. Soc. B Biol. Sci*. 272, 1745–1752. doi: 10.1098/rspb.2005.3156

Parsons, T. D. (2015). Virtual reality for enhanced ecological validity and experimental control in the clinical, affective and social neurosciences. *Front. Hum. Neurosci*. 9:660. doi: 10.3389/fnhum.2015.00660

Peckmezian, T., and Taylor, P. W. (2015). A virtual reality paradigm for the study of visually mediated behaviour and cognition in spiders. *Anim. Behav*. 107, 87–95. doi: 10.1016/j.anbehav.2015.06.018

Petzschner, F. H., and Glasauer, S. (2011). Iterative Bayesian estimation as an explanation for range and regression effects: a study on human path integration. *J. Neurosci*. 31, 17220–17229. doi: 10.1523/JNEUROSCI.2028-11.2011

Portugues, R., and Engert, F. (2011). Adaptive locomotor behavior in larval Zebrafish. *Front. Syst. Neurosci*. 5:72. doi: 10.3389/fnsys.2011.00072

Powell, D. L., and Rosenthal, G. G. (2017). What artifice can and cannot tell us about animal behavior. *Curr. Zool*. 63, 21–26. doi: 10.1093/cz/zow091

Radvansky, B. A., and Dombeck, D. A. (2018). An olfactory virtual reality system for mice. *Nat. Commun*. 9:839. doi: 10.1038/s41467-018-03262-4

Radvansky, B. A., Oh, J. Y., Climer, J. R., and Dombeck, D. A. (2021). Behavior determines the hippocampal spatial mapping of a multisensory environment. *Cell Rep*. 36:109444. doi: 10.1016/j.celrep.2021.109444

Ravassard, P., Kees, A., Willers, B., Ho, D., Aharoni, D., Cushman, J., et al. (2013). Multisensory control of hippocampal spatiotemporal selectivity. *Science* 340, 1342–1346. doi: 10.1126/science.1232655

Reiser, M. B., and Dickinson, M. H. (2008). A modular display system for insect behavioral neuroscience. *J. Neurosci. Methods* 167, 127–139. doi: 10.1016/j.jneumeth.2007.07.019

Robie, A. A., Seagraves, K. M., Egnor, S. E. R., Branson, K., Levine, J. D., Kronauer, D. J. C., et al. (2017). Machine vision methods for analyzing social interactions. *J. Exp. Biol*. 220, 25–34. doi: 10.1242/jeb.142281

Robinson, E. M., and Wiener, M. (2021). Dissociable neural indices for time and space estimates during virtual distance reproduction. *NeuroImage* 226:117607. doi: 10.1016/j.neuroimage.2020.117607

Safaryan, K., and Mehta, M. R. (2021). Enhanced hippocampal theta rhythmicity and emergence of eta oscillation in virtual reality. *Nat. Neurosci*. 24, 1065–1070. doi: 10.1038/s41593-021-00871-z

Saleem, A. B., Ayaz, A., Jeffery, K. J., Harris, K. D., and Carandini, M. (2013). Integration of visual motion and locomotion in mouse visual cortex. *Nat. Neurosci*. 16, 1864–1869. doi: 10.1038/nn.3567

Salminen, K., Rantala, J., Isokoski, P., Lehtonen, M., Müller, P., Karjalainen, M., et al. (2018). "Olfactory display prototype for presenting and sensing authentic and synthetic odors," in *Proceedings of the 20th ACM International Conference on Multimodal Interaction, ICMI '18* (New York, NY: Association for Computing Machinery), 73–77. doi: 10.1145/3242969.3242999

Sato, N., Sakata, H., Tanaka, Y., and Taira, M. (2004). Navigation in virtual environment by the macaque monkey. *Behav. Brain Res*. 153, 287–291. doi: 10.1016/j.bbr.2003.10.026

Schmidt-Hieber, C., and Häusser, M. (2013). Cellular mechanisms of spatial navigation in the medial entorhinal cortex. *Nat. Neurosci*. 16, 325–331. doi: 10.1038/nn.3340

Schneider, D. M., and Mooney, R. (2018). How movement modulates hearing. *Annu. Rev. Neurosci*. 41, 553–572. doi: 10.1146/annurev-neuro-072116-031215

Seeber, B. U., Kerber, S., and Hafter, E. R. (2010). A system to simulate and reproduce audio-visual environments for spatial hearing research. *Hear. Res*. 260, 1–10. doi: 10.1016/j.heares.2009.11.004

Seelig, J. D., Chiappe, M. E., Lott, G. K., Dutta, A., Osborne, J. E., Reiser, M. B., et al. (2010). Two-photon calcium imaging from head-fixed drosophila during optomotor walking behavior. *Nat. Methods* 7, 535–540. doi: 10.1038/nmeth.1468

Sherman, A., and Dickinson, M. H. (2003). A comparison of visual and haltere-mediated equilibrium reflexes in the fruit fly drosophila melanogaster. *J. Exp. Biol*. 206, 295–302. doi: 10.1242/jeb.00075

Sofroniew, N. J., Cohen, J. D., Lee, A. K., and Svoboda, K. (2014). Natural whisker-guided behavior by head-fixed mice in tactile virtual reality. *J. Neurosci*. 34, 9537–9550. doi: 10.1523/JNEUROSCI.0712-14.2014

Sonkusare, S., Breakspear, M., and Guo, C. (2019). Naturalistic stimuli in neuroscience: critically acclaimed. *Trends Cogn. Sci*. 23, 699–714. doi: 10.1016/j.tics.2019.05.004

Steckenfinger, S. A., and Ghazanfar, A. A. (2009). Monkey visual behavior falls into the uncanny valley. *Proc. Natl. Acad. Sci. U.S.A*. 106, 18362–18366. doi: 10.1073/pnas.0910063106

Stowers, J. R., Hofbauer, M., Bastien, R., Griessner, J., Higgins, P., Farooqui, S., et al. (2017). Virtual reality for freely moving animals. *Nat. Methods* 14, 995–1002. doi: 10.1038/nmeth.4399

Taillade, M., N'Kaoua, B., and Gross, C. (2019). Navigation strategy in macaque monkeys: an exploratory experiment in virtual reality. *J. Neurosci. Methods* 326:108336. doi: 10.1016/j.jneumeth.2019.108336

Takalo, J., Piironen, A., Honkanen, A., Lempeä, M., Aikio, M., Tuukkanen, T., et al. (2012). A fast and flexible panoramic virtual reality system for behavioural and electrophysiological experiments. *Sci. Rep*. 2:324. doi: 10.1038/srep00324

Tennant, S. A., Fischer, L., Garden, D. L. F., Gerlei, K. Z., Martinez-Gonzalez, C., McClure, C., et al. (2018). Stellate cells in the medial entorhinal cortex are required for spatial learning. *Cell Rep*. 22, 1313–1324. doi: 10.1016/j.celrep.2018.01.005

Thurley, K., and Ayaz, A. (2017). Virtual reality systems for rodents. *Curr. Zool*. 63, 109–119. doi: 10.1093/cz/zow070

Thurley, K., and Schild, U. (2018). Time and distance estimation in children using an egocentric navigation task. *Sci. Rep*. 8:18001. doi: 10.1038/s41598-018-36234-1

Trivedi, C. A., and Bollmann, J. H. (2013). Visually driven chaining of elementary swim patterns into a goal-directed motor sequence: a virtual reality study of zebrafish prey capture. *Front. Neural Circuits* 7:86. doi: 10.3389/fncir.2013.00086

Vagvolgyi, B. P., Jayakumar, R. P., Madhav, M. S., Knierim, J. J., and Cowan, N. J. (2022). Wide-angle, monocular head tracking using passive markers. *J. Neurosci. Methods* 368:109453. doi: 10.1016/j.jneumeth.2021.109453

Valero, M., and English, D. F. (2019). Head-mounted approaches for targeting single-cells in freely moving animals. *J. Neurosci. Methods* 326:108397. doi: 10.1016/j.jneumeth.2019.108397

Venkatraman, S., Jin, X., Costa, R. M., and Carmena, J. M. (2010). Investigating neural correlates of behavior in freely behaving rodents using inertial sensors. *J. Neurophysiol.* 104, 569–575. doi: 10.1152/jn.00121.2010

Vi, C. T., Ablart, D., Arthur, D., and Obrist, M. (2017). "Gustatory interface: the challenges of 'how' to stimulate the sense of taste," in *Proceedings of the 2nd ACM SIGCHI International Workshop on Multisensory Approaches to Human-Food Interaction, MHFI 2017* (New York, NY: Association for Computing Machinery), 29–33. doi: 10.1145/3141788.3141794

Wang, D., Guo, Y., Liu, S., Zhang, Y., Xu, W., and Xiao, J. (2019). Haptic display for virtual reality: progress and challenges. *Virt. Real. Intell. Hardw.* 1, 136–162. doi: 10.3724/SP.J.2096-5796.2019.0008

Washburn, D. A., and Astur, R. S. (2003). Exploration of virtual mazes by rhesus monkeys (*Macaca mulatta*). *Anim. Cogn.* 6, 161–168. doi: 10.1007/s10071-003-0173-z

Yu, H., Senarathna, J., Tyler, B. M., Thakor, N. V., and Pathak, A. P. (2015). Miniaturized optical neuroimaging in unrestrained animals. *NeuroImage* 113, 397–406. doi: 10.1016/j.neuroimage.2015.02.070

Frontiers in
Neural Circuits

Explores the emergent properties of neural circuits - the brain's elementary modules

Part of the most cited neuroscience journal series, focuses on the anatomy, physiology, development and function of neural circuitry, exploring how plasticity shapes the architecture of the brain's elementary modules.

Discover the latest Research Topics

See more →

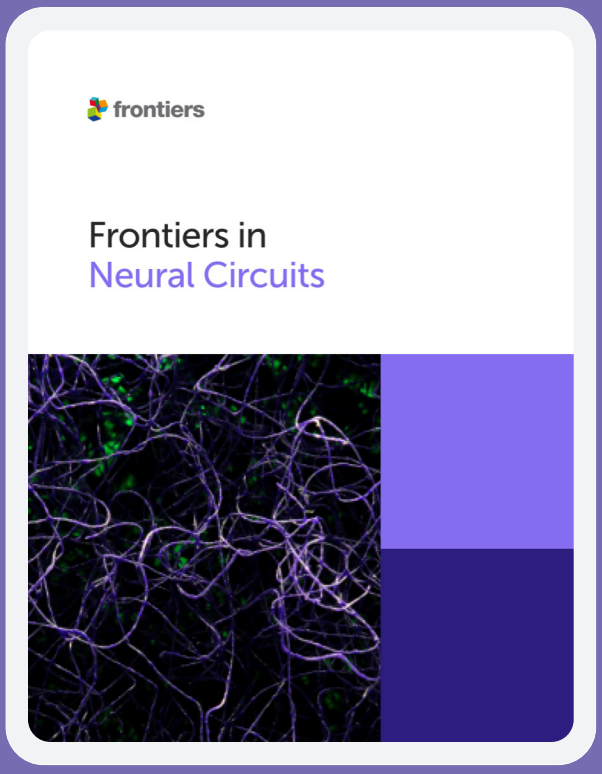

Frontiers

Avenue du Tribunal-Fédéral 34
1005 Lausanne, Switzerland
frontiersin.org

Contact us

+41 (0)21 510 17 00
frontiersin.org/about/contact